

Special Issue Reprint

Modeling of Liquids Behavior

Experiments, Theory and Simulations

Edited by
William E. Acree, Jr. and Juan Ortega Saavedra

www.mdpi.com/journal/liquids

Modeling of Liquids Behavior: Experiments, Theory and Simulations

Modeling of Liquids Behavior: Experiments, Theory and Simulations

Editors

William E. Acree, Jr.

Juan Ortega Saavedra

MDPI • Basel • Beijing • Wuhan • Barcelona • Belgrade • Manchester • Tokyo • Cluj • Tianjin



Editors

William E. Acree, Jr.
University of North Texas
Denton, TX, USA

Juan Ortega Saavedra
University of Las Palmas de
Gran Canaria
Las Palmas de Gran Canaria,
Spain

Editorial Office

MDPI
St. Alban-Anlage 66
4052 Basel, Switzerland

This is a reprint of articles from the Special Issue published online in the open access journal *Liquids* (ISSN 2673-8015) (available at: https://www.mdpi.com/journal/liquids/special_issues/modeling-liquids).

For citation purposes, cite each article independently as indicated on the article page online and as indicated below:

LastName, A.A.; LastName, B.B.; LastName, C.C. Article Title. *Journal Name* **Year**, *Volume Number*, Page Range.

ISBN 978-3-0365-8008-1 (Hbk)

ISBN 978-3-0365-8009-8 (PDF)

© 2023 by the authors. Articles in this book are Open Access and distributed under the Creative Commons Attribution (CC BY) license, which allows users to download, copy and build upon published articles, as long as the author and publisher are properly credited, which ensures maximum dissemination and a wider impact of our publications.

The book as a whole is distributed by MDPI under the terms and conditions of the Creative Commons license CC BY-NC-ND.

Contents

About the Editors	vii
Preface to "Modeling of Liquids Behavior: Experiments, Theory and Simulations"	ix
Darío A. Tinjacá, Fleming Martínez, Ovidio A. Almanza, M. Ángeles Peña, Abolghasem Jouyban and William E. Acree, Jr. Increasing the Equilibrium Solubility of Meloxicam in Aqueous Media by Using Dimethyl Sulfoxide as a Cosolvent: Correlation, Dissolution Thermodynamics and Preferential Solvation Reprinted from: <i>Liquids</i> 2022 , 2, 11, doi:10.3390/liquids2030011	1
Laine Longacre, Emily Wu, Chelsea Yang, Miles Zhang, Sneha Sinha, Advika Varadharajan and William E. Acree, Jr. Development of Abraham Model Correlations for Solute Transfer into the <i>tert</i> -Butyl Acetate Mono-Solvent and Updated Equations for Both Ethyl Acetate and Butyl Acetate Reprinted from: <i>Liquids</i> 2022 , 2, 16, doi:10.3390/liquids2040016	23
Derek M. Hall, Serguei N. Lvov and Isaac K. Gamwo Thermodynamic Modeling of Mineral Scaling in High-Temperature and High-Pressure Aqueous Environments Reprinted from: <i>Liquids</i> 2022 , 2, 18, doi:10.3390/liquids2040018	55
William E. Acree, Jr., Wei-Khiong Chong, Andrew S.I.D. Lang and Hamed Mozafari Estimating Equivalent Alkane Carbon Number Using Abraham Solute Parameters Reprinted from: <i>Liquids</i> 2022 , 2, 19, doi:10.3390/liquids2040019	71
Rudolf Naef and William E. Acree, Jr. Revision and Extension of a Generally Applicable Group Additivity Method for the Calculation of the Refractivity and Polarizability of Organic Molecules at 298.15 K Reprinted from: <i>Liquids</i> 2022 , 2, 20, doi:10.3390/liquids2040020	81
Navid Kabudi, Ali Shayanfar, William E. Acree, Jr. and Abolghasem Jouyban Correlation of Surface Tension of Mono-Solvents at Various Temperatures Reprinted from: <i>Liquids</i> 2022 , 2, 21, doi:10.3390/liquids2040021	133
Cunbin Du The Solubility of Ethyl Candesartan in Mono Solvents and Investigation of Intermolecular Interactions Reprinted from: <i>Liquids</i> 2022 , 2, 23, doi:10.3390/liquids2040023	143
Luis Fernández, Juan Ortega, Leandro Domínguez, David Lorenzo, Aurora Santos and Arturo Romero Using Two Group-Contribution Methods to Calculate Properties of Liquid Compounds Involved in the Cyclohexanone Production Operations Reprinted from: <i>Liquids</i> 2022 , 2, 24, doi:10.3390/liquids2040024	153
G. Reza Vakili-Nezhaad, Morteza Mohammadzaheri, Farzaneh Mohammadi and Mohammed Humaid Density and Refractive Index of Binary Ionic Liquid Mixtures with Common Cations/Anions, along with ANFIS Modelling Reprinted from: <i>Liquids</i> 2022 , 2, 25, doi:10.3390/liquids2040025	173

Mikhail I. Yagofarov, Ilya S. Balakhontsev, Andrey A. Sokolov and Boris N. Solomonov Application of Solution Calorimetry to Determining the Fusion Enthalpy of an Arylaliphatic Compound at 298.15 K: <i>n</i> -Octadecanophenone Reprinted from: <i>Liquids</i> 2023 , 3, 1, doi:10.3390/liquids3010001	187
Carlos Francisco Trujillo-Trujillo, Fredy Angarita-Reina, Mauricio Herrera, Claudia Patria Ortiz, Rossember Edén Cardenas-Torres, Fleming Marínez and Daniel Ricardo Delgado Thermodynamic Analysis of the Solubility of Sulfadiazine in (Acetonitrile + 1-Propanol) Cosolvent Mixtures from 278.15 K to 318.15 K Reprinted from: <i>Liquids</i> 2023 , 3, 2, doi:10.3390/liquids3010002	193
Deepika and Siddharth Pandey Density and Dynamic Viscosity of Perfluorodecalin-Added <i>n</i> -Hexane Mixtures: Deciphering the Role of Fluorous Liquids Reprinted from: <i>Liquids</i> 2023 , 3, 5, doi:10.3390/liquids3010005	205
Giuseppe Graziano The Relevance of Cavity Creation for Several Phenomena Occurring in Water Reprinted from: <i>Liquids</i> 2023 , 3, 6, doi:10.3390/liquids3010006	215
Costas Panayiotou, Ioannis Zuburtikudis, Hadil Abu Khalifeh and Vassily Hatzimanikatis Linear Solvation–Energy Relationships (LSER) and Equation-of-State Thermodynamics: On the Extraction of Thermodynamic Information from the LSER Database Reprinted from: <i>Liquids</i> 2023 , 3, 7, doi:10.3390/liquids3010007	225

About the Editors

William E. Acree, Jr.

William E. Acree, Jr. received his bachelor's degree (1975), master's degree (1977), and doctorate degree (1981) in Chemistry from the University of Missouri at Rolla. He taught at Kent State University from September 1982 to August 1988 before moving to the University of North Texas, where he is currently a Professor in the Chemistry Department. His research interests encompass the broad areas of chemical and solution thermodynamics, spectrofluorometric probe studies, and the development of linear free energy relationships to describe mathematically solute transfer processes. To date, his research has resulted in the publication of more than 1,030 peer-refereed research articles, one research monograph on solution thermodynamic properties of nonelectrolyte solutions, six volumes in the IUPAC-NIST Solubility Data Series, as well as several encyclopedia articles, book chapters and educational articles in the *Journal of Chemical Education*.

Juan Ortega Saavedra

Juan Ortega Saavedra graduated in industrial engineering (1976) and received his PhD in 1979, being the first doctor from the University of Las Palmas de Gran Canaria (Canary Islands, Spain), where he has always worked as a Professor of Thermodynamics in the High School of Engineering. He directed a research team working on phase equilibrium of solutions with young PhD students. He has contributed to a number of papers and has published almost 300 research articles including book chapters, divulgation articles, contributions to databases, etc. Currently, he is Professor Emeritus of the University, where he teaches and carries out his research, which is now directed towards modeling.

Preface to "Modeling of Liquids Behavior: Experiments, Theory and Simulations"

The subject of this Special Issue is the determination and modeling of the physical and thermodynamic properties of both pure liquids, as well as binary and ternary liquid mixtures containing organic and inorganic materials using modern experimental and computational methods. Special emphasis is given to studies that report the latest technical and theoretical results concerning the properties and processes of industrial significance.

The authors of the fourteen papers contained in this Special Issue are experts in their respective fields of solution thermodynamics and computational chemistry, and they have made significant contributions to the understanding of solute–solvent and solvent–solvent molecular interactions in liquid solutions. They have collaborated to create an informative and valuable scientific resource for academicians, as well as scientists and engineers working in the chemical and pharmaceutical manufacturing sectors.

Specific topics covered in the Special Issue include the prediction of drug molecules in both neat and binary solvent mixtures; preferential solvation of solvent molecules around a dissolved solute; the development of Abraham model correlations for describing solute transfer into three alkyl acetate mono-solvents; an atom additivity model to estimate molar refractivity and polarizability of organic compounds; a novel solution calorimetric method for determining enthalpies of fusion; deciphering the role of fluoruous liquids through density and dynamic viscosity measurements; the extraction of valuable thermodynamic information from published databases using linear free energy relationships and equation-of-state thermodynamic models; estimation of surface tension and equivalent carbon atom number using solvation parameters; an artificial intelligence model and an adaptive neuro-fuzzy inference system for calculating the densities and refractive indices of binary ionic liquid mixtures containing common cations/anions; application of group contribution methods to calculate thermodynamic properties pertaining to the industrial cyclohexanone production; the importance of cavity creation for processes occurring in water; and thermodynamic modeling of mineral scaling in both high-temperature and high-pressure aqueous environments. Each paper provides valuable insight into the underlying fundamental principles that govern the studied processes. The predictive expressions and models presented in the published papers will enable practicing scientists and engineers to estimate physical and thermodynamic properties needed in industrial process design calculations.

William E. Acree, Jr. and Juan Ortega Saavedra
Editors

Article

Increasing the Equilibrium Solubility of Meloxicam in Aqueous Media by Using Dimethyl Sulfoxide as a Cosolvent: Correlation, Dissolution Thermodynamics and Preferential Solvation

Darío A. Tinjacá¹, Fleming Martínez^{2,*}, Ovidio A. Almanza³, M. Ángeles Peña⁴, Abolghasem Jouyban^{5,6} and William E. Acree, Jr.⁷

¹ Facultad de Ciencias, Universidad El Bosque, Av. Cra. 9 No. 131A-02, Bogotá 110911, Colombia

² Grupo de Investigaciones Farmacéutico-Físicoquímicas, Departamento de Farmacia, Facultad de Ciencias, Universidad Nacional de Colombia, Sede Bogotá, Cra. 30 No. 45-03, Bogotá 111321, Colombia

³ Grupo de Física Aplicada, Departamento de Física, Facultad de Ciencias, Universidad Nacional de Colombia, Sede Bogotá, Cra. 30 No. 45-03, Bogotá 111321, Colombia

⁴ Departamento de Ciencias Biomédicas, Facultad de Farmacia, Universidad de Alcalá, Alcalá de Henares, 28801 Madrid, Spain

⁵ Pharmaceutical Analysis Research Center, Faculty of Pharmacy, Tabriz University of Medical Sciences, Tabriz 5165665931, Iran

⁶ Faculty of Pharmacy, Near East University, 99138 Nicosia, Turkey

⁷ Department of Chemistry, University of North Texas, Denton, TX 76203, USA

* Correspondence: fmartinezr@unal.edu.co; Tel.: +571-3165000 (ext. 14608)

Citation: Tinjacá, D.A.; Martínez, F.; Almanza, O.A.; Peña, M.Á.; Jouyban, A.; Acree, W.E., Jr. Increasing the Equilibrium Solubility of Meloxicam in Aqueous Media by Using Dimethyl Sulfoxide as a Cosolvent: Correlation, Dissolution Thermodynamics and Preferential Solvation. *Liquids* **2022**, *2*, 161–182. <https://doi.org/10.3390/liquids2030011>

Academic Editor: Urban Bren

Received: 14 July 2022

Accepted: 9 August 2022

Published: 12 August 2022

Publisher's Note: MDPI stays neutral with regard to jurisdictional claims in published maps and institutional affiliations.



Copyright: © 2022 by the authors. Licensee MDPI, Basel, Switzerland. This article is an open access article distributed under the terms and conditions of the Creative Commons Attribution (CC BY) license (<https://creativecommons.org/licenses/by/4.0/>).

Abstract: Meloxicam is widely prescribed as an analgesic and anti-inflammatory drug in human therapeutics. Owing to the very low aqueous solubility of meloxicam, this property has been studied in dimethyl sulfoxide (DMSO)-aqueous solvent systems at several temperatures from 273.15 to 313.15 K to expand the solubility database about analgesic drugs in mixed solvents. The flask shake method followed by ultraviolet-visible (UV-vis) spectrophotometry analysis were used for meloxicam solubility determinations. A number of cosolvency models, including the Jouyban–Acree model, were challenged for solubility correlation/prediction of this drug in these mixtures. The van't Hoff and Gibbs equations were employed to calculate the apparent standard thermodynamic quantities relative to dissolution and mixing processes. The inverse Kirkwood–Buff integral method was employed for calculating the preferential solvation parameters of meloxicam by DMSO in the mixtures. Meloxicam solubility increases with increasing temperature and maximum solubilities are observed in neat DMSO at all temperatures studied. Dissolution processes were endothermic in all cases and entropy-driven in the composition interval of $0.40 \leq x_1 \leq 1.00$. A nonlinear enthalpy–entropy relationship was observed in the plot of enthalpy vs. Gibbs energy for drug transfer processes. Meloxicam is preferentially solvated by water in water-rich mixtures but preferentially solvated by DMSO in the composition interval of $0.21 < x_1 < 1.00$.

Keywords: meloxicam; [DMSO (1) + water (2)] mixtures; cosolvency; Jouyban–Acree model; dissolution thermodynamics; preferential solvation; IKBI

1. Introduction

Meloxicam (molecular structure shown in Figure 1, IUPAC name: 4-hydroxy-2-methyl-N-(5-methyl-2-thiazolyl)-2H-1,2-benzothiazine-3-carboxamide-1,1-dioxide, molar mass 351.40 g·mol⁻¹, CAS number: 71125-38-7, PubChem CID: 54677470) is a non-steroidal anti-inflammatory drug used commonly for pain and inflammatory treatments [1–5]. From a physicochemical point of view, meloxicam exhibits very low aqueous solubility, which influences negatively in vivo dissolution rates, affecting its biological performance. Otherwise, because of the very low aqueous solubility of this drug, all the duties relative

to research and development of homogeneous liquid dosage forms, such as peroral or injectable products, based on this drug, are very long and hard at an industrial pharmaceutical level. In order to overcome the drawbacks mentioned above, some investigations have been intended to increase the aqueous equilibrium solubility of meloxicam. These investigations were mainly based in the evaluation of the solubilizing effect of some common pharmaceutical cosolvents, as has recently been summarized in a previous communication of our research group [6]. More recently, some other aqueous mixtures involving different cosolvents, including choline-based deep eutectic solvents, have also been studied and reported [7–11]. It is noteworthy that very good meloxicam solubility-increasing has been reported, reaching more than 1000-fold in some cases, as follows: 1144 with Carbitol® [9], 1399 with *N*-methylformamide [6], and 11,233 with *N,N*-dimethylformamide [6].

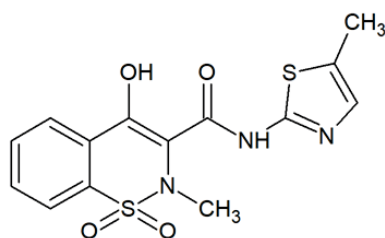


Figure 1. Molecular structure of meloxicam.

Dimethyl sulfoxide (molar mass: 78.13 g·mol⁻¹, CAS number: 67-68-5, PubChem CID 679) is a polar, aprotic solvent, miscible with water and with a wide range of organic solvents in all possible compositions, which makes it adequate for dissolving substances of both polar and nonpolar nature [1,12]. It exhibits less toxicity than *N*-methylformamide and *N*-methyl-2-pyrrolidone and has been reported about its good power of penetrating the skin and other membranes without damaging them. This is the reason why it has a high potential to increase the penetration of less soluble active ingredients. Otherwise, DMSO exhibits by itself some analgesic and anti-inflammatory properties [13]. Indeed, there are some references in the literature that suggest the potential use of DMSO as a possible pharmacotherapeutic agent in the management of pain and other conditions [14]. Moreover, owing its high solubilizing power for different active pharmaceutical ingredients, it has been used as an excipient in topical and parenteral medications for human and veterinary use [15]. On the other hand, DMSO has also been considered as solvent model in medicinal chemistry for studying intermolecular effects of different drugs [16]. In this way, aqueous mixtures of DMSO have been studied for solubilizing several drugs, drug-alike compounds, and other organic chemicals, including bergenin [17], *N*-guanyurea dinitramide [18], naringin [19], sinapic acid [20], *p*-nitrobenzamide [21], *d*-histidine [22], micoflavin [23], phenformin [24], baricitinib [25], a pyridazinone derivative [26], and nicotinamide [27], among others.

As it is well-described in the specialized chemical and pharmaceutical literature, all the physicochemical data about the equilibrium solubility of drugs or drug-alike compounds in aqueous cosolvent mixtures, as well, as the deep understanding of the respective dissolution mechanisms, are very important for both theoretical and practical points of view in pharmaceutical and chemical sciences. This is because the measured, reported, and analyzed solubility values expand the respective solubility databases, which is very useful for theoretical and practical purposes in both the pharmaceutical and chemical industries, as indicated above [28–31].

Therefore, the main aims of this research were as follows: (i) to determine and analyze the effects of both mixtures' composition and temperature on the solubility of meloxicam in [DMSO (1) + water (2)] mixtures; (ii) to correlate equilibrium solubility data with several well-known thermodynamic models; (iii) to calculate the apparent standard dissolution and mixing thermodynamic parameters; and (iv) to study the preferential solvation parameters

of meloxicam in binary mixtures conformed by DMSO and water. Therefore, this research is a continuation of some other similar ones reported earlier in the literature [6–9,11,32] about the meloxicam equilibrium solubility in other aqueous cosolvent systems of pharmaceutical interest for design of dosage forms and its quality control analysis, but using another commonly used cosolvent because of its high solubilizing power.

2. Materials and Methods

2.1. Materials and Reagents

Meloxicam (Technodrugs & Intermediates PVT LTD, component 3, purity > 0.995 in mass fraction), DMSO (Panreac, component 1, purity > 0.995 in mass fraction), and distilled water with conductivity < 2 $\mu\text{S}\cdot\text{cm}^{-1}$ (component 2), were used. Purities of meloxicam and DMSO were reported by the suppliers, as determined by high-performance liquid chromatography and gas chromatography, respectively.

2.2. Preparation of Solvent Mixtures

All the {DMSO (1) + water (2)} binary solvent mixtures were prepared gravimetrically by using an Ohaus Pioneer TM PA214 analytical balance (USA, sensitivity ± 0.1 mg), in quantities of 50.00 g. The mole fractions of DMSO of the nine mixtures prepared, varied by 0.10 in steps from $x_1 = 0.10$ to $x_1 = 0.90$.

2.3. Solubility Determinations

Equilibrium meloxicam solubilities were determined by using the shake-flask method [33], followed by UV-spectrophotometric analysis, as follows: an excess amount of meloxicam was added to 50.00 g of each binary solvent mixture or neat DMSO in dark glass pharmaceutical flasks. The stoppered flasks were putted in an ultrasonic bath (Elma[®] E60H Elmasonic, Fremont, CA, USA) during 15 min and were later transferred to thermostatic mechanical shakers (Julabo SW23, Seelbach, Germany) or re-circulating thermostatic baths (Neslab RTE 10 Digital One Thermo Electron Company, Waltham, MA, USA) and kept at 313.15 K for at least four days to ensure that the drug saturation had been achieved. After that, the supernatant solutions were isothermally filtered (Millipore Corp. Swinnex[®]-13, Burlington, MA, USA) to remove undissolved solid particles before sampling. Meloxicam concentrations were determined after appropriate gravimetric dilution with a 0.10 mol·dm⁻³ NaOH solution, by measuring the UV light absorbance at the maximum absorbance wavelength, $\lambda_{\text{max}} = 361$ nm (UV/VIS BioMate 3 Thermo Electron Company spectrophotometer, USA), followed by interpolation from a previously validated UV spectrophotometric gravimetric calibration curve prepared in NaOH 0.10 mol·dm⁻³. The respective equation was: Absorbance = 0.0073 + 52.508·C, with C expressed as $\mu\text{g}\cdot\text{g}^{-1}$. Later, the thermostatic baths temperature was decreased from 313.15 K to 308.15 K allowing the meloxicam excess precipitation during two days, following with the same procedures mentioned above to determine the new meloxicam concentrations at saturation. All these procedures were performed successively until solid-liquid equilibrium was achieved at 293.15 K. All the solubility experiments were performed at least three times and the respective results were averaged. The density of the saturated solutions was measured by using a digital density meter (DMA 45 Anton Paar, Graz, Austria) connected to a re-circulating thermostatic bath (Neslab RTE 10 Digital One Thermo Electron Company, USA) in order to transform the obtained gravimetric solubility values into volumetric concentration scales. The density meter was calibrated at every temperature by using air and water as standards as indicated in the respective instruction manuals [34].

2.4. Solid Phase Analyses

2.4.1. X-ray Diffraction (XRD) Analysis

To determine the crystal nature of the solid meloxicam samples both before and after the saturation in neat water, in the mixture of $x_1 = 0.50$, and in neat DMSO, the respective X-ray powder diffraction analyses were performed by using a PANalytical Xpert Pro X-ray

diffractometer. The equipment is provided with $\text{CuK}\alpha$ radiation $\lambda = 1.5418 \text{ \AA}$. Generator setting: 40 kV and 40 mA and Bragg–Brentano geometry. Data were collected at 2θ from 5° to 70° and angle variation of 0.02° with detector data acquisition time of 9.46 min operating under room temperature.

2.4.2. Fourier Transform Infrared (FTIR) Analysis

In addition to XRD analyses, in order to confirm the nature of the solid meloxicam samples, both before and after the saturation in neat water, in the mixture of $x_1 = 0.50$, and in neat DMSO, FTIR analyses were also performed. The meloxicam solid samples were ground with quantities from 10 to 100 times its bulk of pure potassium bromide and the resulting mixtures were pressed into discs by using a special mold and a manual hydraulic press (Specac[®], Fort Washington, PA, USA). The respective spectra were obtained in an FTIR spectrophotometer (IRAffinity-1, Shimadzu, Kyoto, Japan).

3. Results and Discussion

3.1. Experimental Mole Fraction and Molarity Solubility

Tables 1 and 2 summarize the experimental equilibrium solubilities of meloxicam in all {DMSO (1) + water (2)} solvent systems at $293.15 \leq T/\text{K} \leq 313.15$, as expressed in mole fraction and molarity ($\text{mol}\cdot\text{dm}^{-3}$), respectively. The studied temperature interval includes what is commonly known as “room temperature” for products storage, as well as, the normal human body temperature. It is worth mentioning that all solubility values in neat water were taken from reference [32]. The average relative uncertainty obtained in the reported solubility values was 2.4%, which is in agreement with that commonly observed in this kind of experiments. If the mole fraction scale is considered, at $T = 298.15 \text{ K}$, Table 1 shows that the meloxicam solubility increased 6956 times from $x_3 = 1.137 \times 10^{-6}$ in neat water to $x_3 = 7.909 \times 10^{-3}$ in neat DMSO, where maximum solubility is obtained. A deep comparison about the meloxicam solubility in neat water has been reported and discussed earlier in one of our previous communications [6]. Regarding the meloxicam mole fraction equilibrium solubility in neat DMSO Sathesh-Babu et al. reported a value of $x_3 = 5.496 \times 10^{-3}$ at $T = 298.15 \text{ K}$ [35], which is in good agreement with the one obtained in this research (i.e., $x_3 = 7.909 \times 10^{-2}$, Table 1). Moreover, when considering the molarity scale, a value of $C = 1.516 \times 10^{-2} \text{ mol}\cdot\text{dm}^{-3}$ was reported by Castro et al. at $T = 298.15 \text{ K}$ [36], which differs in almost one order of magnitude regarding our value (i.e., $C = 0.1089 \text{ mol}\cdot\text{dm}^{-3}$, Table 2). The observed differences in solubility values could be attributed to several reasons such as different polymorphic states, different saturation times, or different analytical procedures, among others, as described earlier [31]. Up to the best of our knowledge, no solubility values of meloxicam in aqueous mixtures of DMSO have been reported and no more comparisons are possible.

Figure 2 depicts the meloxicam solubility profiles as function of the Hildebrand solubility parameters (δ_{1+2}) of {DMSO (1) + water (2)} mixtures at $T = 298.15 \text{ K}$. As widely described, δ_{1+2} is a very important polarity descriptor of cosolvent mixtures [28–31]. This descriptor was calculated considering the Hildebrand solubility parameter of both pure solvents ($\delta_1 = 26.6 \text{ MPa}^{1/2}$ for DMSO and $\delta_2 = 47.8 \text{ MPa}^{1/2}$ for water [37,38]), and the volume fraction (f_i) of each solvent, as [29,39]:

$$\delta_{1+2} = \sum_{i=1}^2 f_i \delta_i \quad (1)$$

Table 1. Experimental mole fraction solubility (x_3) of meloxicam in {DMSO (1) + water (2)} mixtures at several temperatures and $p = 96$ kPa ^{a,b}.

x_1 ^{a,b}	T/K ^b				
	293.15	298.15	303.15	308.15	313.15
0.000 ^c	1.088×10^{-6}	1.137×10^{-6}	1.187×10^{-6}	1.262×10^{-6}	1.329×10^{-6}
0.100	3.394×10^{-6}	3.497×10^{-6}	3.656×10^{-6}	3.800×10^{-6}	3.909×10^{-6}
0.200	7.879×10^{-6}	8.835×10^{-6}	9.860×10^{-6}	1.067×10^{-5}	1.182×10^{-5}
0.300	2.303×10^{-5}	2.705×10^{-5}	3.104×10^{-5}	3.777×10^{-5}	4.406×10^{-5}
0.400	9.685×10^{-5}	1.124×10^{-4}	1.355×10^{-4}	1.567×10^{-4}	1.892×10^{-4}
0.500	3.461×10^{-4}	3.972×10^{-4}	4.788×10^{-4}	5.510×10^{-4}	6.719×10^{-4}
0.600	7.750×10^{-4}	9.861×10^{-4}	1.303×10^{-3}	1.643×10^{-3}	2.012×10^{-3}
0.700	1.509×10^{-3}	1.878×10^{-3}	2.260×10^{-3}	2.885×10^{-3}	3.655×10^{-3}
0.800	2.739×10^{-3}	3.339×10^{-3}	3.954×10^{-3}	4.996×10^{-3}	6.230×10^{-3}
0.900	4.337×10^{-3}	5.298×10^{-3}	6.245×10^{-3}	7.742×10^{-3}	9.553×10^{-3}
1.000	6.624×10^{-3}	7.909×10^{-3}	9.187×10^{-3}	1.135×10^{-2}	1.381×10^{-2}
Ideal ^c	2.607×10^{-3}	3.079×10^{-3}	3.627×10^{-3}	4.260×10^{-3}	4.991×10^{-3}

^a p is the atmospheric pressure in Bogotá, Colombia. x_1 is the mole fraction of DMSO (1) in the {DMSO (1) + water (2)} mixtures free of meloxicam (3). Mean uncertainty in x_1 , $u(x_1) = 0.0005$. ^b Standard uncertainty in p is $u(p) = 3.0$ kPa. Average relative uncertainty in x_3 , $u_r(x_3) = 0.024$. Standard uncertainty in T is $u(T) = 0.10$ K. ^c Data taken from Delgado et al. [32].

Table 2. Experimental molar solubility (C , mol·dm⁻³) of meloxicam in {DMSO (1) + water (2)} mixtures at several temperatures and $p = 96$ kPa. ^{a,b}

x_1 ^{a,b}	T/K ^b				
	293.15	298.15	303.15	308.15	313.15
0.000 ^c	6.025×10^{-5}	6.290×10^{-5}	6.557×10^{-5}	6.962×10^{-5}	7.319×10^{-5}
0.100	1.475×10^{-4}	1.516×10^{-4}	1.582×10^{-4}	1.640×10^{-4}	1.683×10^{-4}
0.200	2.818×10^{-4}	3.150×10^{-4}	3.506×10^{-4}	3.780×10^{-4}	4.176×10^{-4}
0.300	6.963×10^{-4}	8.153×10^{-4}	9.328×10^{-4}	1.131×10^{-3}	1.315×10^{-3}
0.400	2.525×10^{-3}	2.923×10^{-3}	3.512×10^{-3}	4.043×10^{-3}	4.864×10^{-3}
0.500	7.909×10^{-3}	9.034×10^{-3}	1.087×10^{-2}	1.245×10^{-2}	1.512×10^{-2}
0.600	1.575×10^{-2}	1.992×10^{-2}	2.622×10^{-2}	3.288×10^{-2}	4.006×10^{-2}
0.700	2.753×10^{-2}	3.409×10^{-2}	4.081×10^{-2}	5.176×10^{-2}	6.522×10^{-2}
0.800	4.531×10^{-2}	5.485×10^{-2}	6.459×10^{-2}	8.099×10^{-2}	0.1002
0.900	6.552×10^{-2}	7.942×10^{-2}	9.297×10^{-2}	0.1144	0.1398
1.000	9.195×10^{-2}	0.1089	0.1255	0.1536	0.1851

^a p is the atmospheric pressure in Bogotá, Colombia. x_1 is the mole fraction of DMSO (1) in the {DMSO (1) + water (2)} mixtures free of meloxicam (3). Mean uncertainty in x_1 , $u(x_1) = 0.0005$. ^b Standard uncertainty in p is $u(p) = 3.0$ kPa. Average relative uncertainty in C , $u_r(C) = 0.024$. Standard uncertainty in T is $u(T) = 0.10$ K. ^c Data taken from Delgado et al. [32].

As observed, the solubility curve exhibited maximum in neat DMSO, where δ_1 is 26.6 MPa^{1/2}. Because solutes normally reach their maximum solubilities in solvent systems exhibiting similar polarity [28,29], it is expected that the meloxicam δ_3 value would be lower than 26.6 MPa^{1/2} at 298.15 K. However, this δ_3 value is lower compared with the one reported earlier ($\delta_3 = 32.1$ MPa^{1/2}) [6] calculated by means of the Fedors method [40]. This high discrepancy could be mainly attributed to specific drug solvation processes by DMSO or water, which are not considered in Fedors' calculations, in particular, if considering the structural effects

described for aqueous mixtures of DMSO [41,42]. Otherwise, Figure 2 also compares the logarithmic solubility of meloxicam as function of the Hildebrand solubility parameter in some aqueous-aprotic cosolvent mixtures, namely, {DMSO (1) + water (2)}, {dimethyl formamide (1) + water (2)} [6], and {acetonitrile (1) + water (2)} [7], mixtures at 298.15 K. It is noteworthy that meloxicam solubilities are highest in {dimethyl formamide (1) + water (2)} mixtures followed by {DMSO (1) + water (2)} mixtures of $\delta_{1+2} < 34.0 \text{ MPa}^{1/2}$ and lowest in {acetonitrile (1) + water (2)} mixtures of $\delta_{1+2} < 34.0 \text{ MPa}^{1/2}$. Otherwise, in mixtures of $\delta_{1+2} > 34.0 \text{ MPa}^{1/2}$, the solubilities in aqueous mixtures of DMSO and acetonitrile are similar. This result shows that meloxicam solubility depends not only on the polarity but also on some other physicochemical properties of solute and solvent systems.

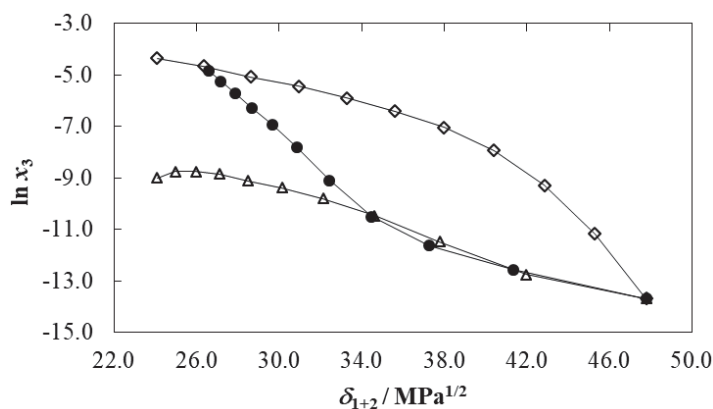


Figure 2. Logarithmic mole fraction solubility of meloxicam ($\ln x_3$) as function of the Hildebrand solubility parameter in some {cosolvent (1) + water (2)} mixtures at 298.15 K. ●: DMSO (1) + water (2), ◇: Dimethylformamide (1) + water (2) [6], △: acetonitrile (1) + water (2) [7].

3.2. Solid Phases' Analyses

X-ray diffraction (XRD) spectra for meloxicam of the original untreated sample and after its saturation in neat water, neat DMSO, and the aqueous-DMSO mixture of $x_1 = 0.50$ are shown in Figure 3. Because of the high similarity among all obtained spectra, it could be concluded that changes of the crystalline form of meloxicam are not observed after its dissolution and saturation in these four solvent systems. Moreover, Table 3 summarizes the position, 2θ spacing, peak height (in counts), and the relative intensity of peaks exhibiting values higher than 10% for the original untreated meloxicam sample. These values are in good coincidence with those reported by Wu et al. [43]. Moreover, all the obtained XRD spectra of this research are very similar to that reported earlier for the polymorph I of meloxicam [32,44–47]. Finally, the FTIR spectra of all solid meloxicam samples shown in Figure 4 are also coincident with those reported in the literature, which allows to indicate that the three bottom-solid phases, obtained after drug saturation, have the same nature as the original untreated sample [47–49]. Therefore, meloxicam did not suffer crystal polymorphic transitions or solvates formation after saturation in these dissolution experiments.

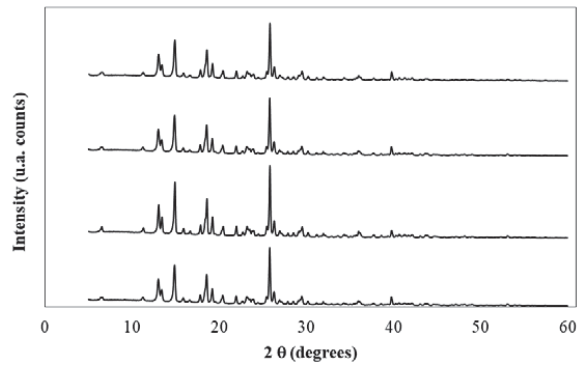


Figure 3. X-ray diffraction spectra of meloxicam. From top to bottom: crystallized in water, crystallized in {DMSO (1) + water (2)} ($x_1 = 0.50$) mixture, crystallized in DMSO, original sample.

Table 3. X-ray diffraction analysis of the original untreated meloxicam sample: position, 2θ spacing, peak height (in counts) and relative intensity of peaks with values higher than 10%.

Peak	2θ	d-Spacing/Å	Height/Counts	Relative Intensity (%)
1	12.98	6.81	3752.7	34.0
2	13.41	6.60	1909.4	17.3
3	14.89	5.95	6361.9	57.7
4	17.80	4.98	1376.8	12.5
5	18.57	4.77	4630.4	42.0
6	19.20	4.62	2633.3	23.9
7	20.39	4.35	1483.6	13.5
8	21.93	4.05	1346.4	12.2
9	23.11	3.85	1185.2	10.8
10	25.40	3.50	1325.3	12.0
11	25.79	3.45	11,029.5	100.0
12	26.27	3.39	2203.8	20.0
13	29.47	3.03	1585.0	14.4
14	39.75	2.27	1853.3	16.8

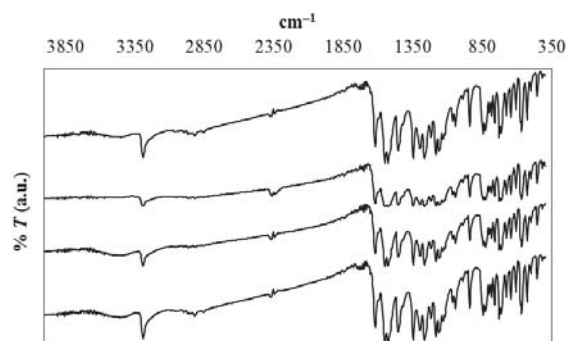


Figure 4. FTIR spectra of meloxicam. From top to bottom: original sample, crystallized in DMSO, crystallized in {DMSO (1) + water (2)} ($x_1 = 0.50$) mixture, crystallized in water.

3.3. Activity Coefficients in Mixed Solvents

Table 4 summarizes the asymmetrical activity coefficients (γ_3) of meloxicam in all the {DMSO (1) + water (2)} solvent systems. These values were calculated as the quotient x_3^{id}/x_3 from the ideal (x_3^{id}) and experimental solubilities of meloxicam summarized in Table 1. It is noteworthy that ideal solubilities were taken from the literature [32]. As observed, the γ_3 values vary from 2708 in neat water (where the lower drug solubilities are observed) to 0.389 in neat DMSO at $T = 298.15$ K, where the maximum drug solubility is observed at this temperature. At all temperatures, meloxicam exhibits γ_3 values higher than unity in neat water and the mixtures of $x_1 \leq 0.70$, but lower than unity in DMSO-rich mixtures and neat DMSO. On the other hand, in neat water and the mixtures of $x_1 = 0.10$ and 0.20, the γ_3 values increase with an increase in temperature. This implies some distancing from the ideal dissolution behavior with increasing temperature. In mixtures of $0.30 \leq x_1 \leq 0.50$, the γ_3 values are almost independent on temperature. On the contrary, in mixtures of $x_1 \geq 0.60$ and neat DMSO, the γ_3 values decrease with the increase in temperature.

Table 4. Activity coefficients of meloxicam in {DMSO (1) + water (2)} mixtures at several temperatures and $p = 96$ kPa ^{a,b}.

x_1 ^{a,b}	T/K ^b				
	293.15	298.15	303.15	308.15	313.15
0.000 ^c	2396	2708	3055	3376	3755
0.100	768	881	992	1121	1277
0.200	331	349	368	399	422
0.300	113	114	117	113	113
0.400	26.9	27.4	26.8	27.2	26.4
0.500	7.53	7.75	7.57	7.73	7.43
0.600	3.36	3.12	2.78	2.59	2.48
0.700	1.73	1.64	1.60	1.48	1.37
0.800	0.952	0.922	0.917	0.853	0.801
0.900	0.601	0.581	0.581	0.550	0.522
1.000	0.394	0.389	0.395	0.375	0.361

^a p is the atmospheric pressure in Bogotá, Colombia. x_1 is the mole fraction of DMSO (1) in the {DMSO (1) + water (2)} mixtures free of meloxicam (3). Mean uncertainty in x_1 , $u(x_1) = 0.0005$. ^b Standard uncertainty in p is $u(p) = 3.0$ kPa. Average relative uncertainty in γ_3 is $u_r(\gamma_3) = 0.027$. Standard uncertainty in T is $u(T) = 0.10$ K. ^c Data taken from Delgado et al. [32].

Moreover, Equation (2) allows a rough estimate of the magnitudes of solute–solvent intermolecular interactions from γ_3 values [50].

$$\ln \gamma_3 = (e_{ss} + e_{33} - 2e_{s3}) \frac{V_3 \varphi_s^2}{RT} \quad (2)$$

where subscript 1 stands for the solvent system that here corresponds to neat solvents or aqueous DMSO binary mixtures, e_{ss} , e_{33} , and e_{s3} represent the magnitudes of solvent–solvent, solute–solute, and solvent–solute interaction energies, respectively. However, it is important to keep in mind that in the case of ternary systems, such as DMSO–water–meloxicam studied here, some water–cosolvent interactions are present, which could also play an important role in drug solubilities and dissolution rates. V_3 denotes the molar volume of the super-cooled liquid meloxicam, whereas, φ_s denotes the volume fraction of every solvent system. For low x_3 solubility values, $V_3 \varphi_s^2/RT$ may be considered as constant despite of the solvent system. Hence, γ_3 values would depend mainly on e_{ss} , e_{33} , and e_{s3} [50]. As is well-known, e_{ss} and e_{33} are unfavorable for drug solubility and dissolution, whereas e_{s3} favors the respective drug solubility and dissolution rate increasing.

The contribution of e_{33} could be considered as constant in the different solvent systems studied. Thus, from a qualitative viewpoint, based on the energetic quantities described in Equation (2), the following analysis could be established: because e_{ss} is highest in neat water ($\delta_2 = 47.8 \text{ MPa}^{1/2}$) and lowest in neat DMSO ($\delta_1 = 26.6 \text{ MPa}^{1/2}$) [37,38], neat water and water-rich mixtures (exhibiting γ_3 values higher than 2300) would imply high e_{ss} and low e_{s3} values, whereas, in DMSO-rich mixtures (exhibiting γ_3 values near the unity), the e_{ss} values are relatively low, and therefore, the e_{s3} values would be high. In this way, a higher solvation of meloxicam by DMSO in DMSO-rich mixtures is expected.

3.4. Solubility Modeling

Among the available cosolvency models presented for calculation of drug solubilities in mixed solvents at isothermal condition or at various temperatures [51,52], the Yalkowsky model is the simplest one [53] and requires only two experimental solubility determinations (in neat solvents) to predict the solubility at other solvent compositions. The Yalkowsky model is commonly represented as:

$$\ln x_{3-(1+2)} = x_1 \ln x_{3(1)} + x_2 \ln x_{3(2)} \quad (3)$$

where $x_{3-(1+2)}$ denotes the mole fraction solubility of meloxicam in the aqueous-cosolvent mixtures, $x_{3(1)}$ denotes the mole fraction solubility in neat DMSO (component 1), $x_{3(2)}$ denotes the mole fraction solubility in neat water (component 2), and x_1 and x_2 are the mole fractions of DMSO (1) and water (2) in the cosolvent mixtures in the absence of meloxicam (3). Thus, the obtained mean percentage deviation (*MPD*) values after calculation of the solubility of meloxicam in {DMSO (1) + water (2)} mixtures at $T = (293.15, 298.15, 303.15, 308.15, \text{ and } 313.15) \text{ K}$ by means of this model were (41.3, 42.9, 44.8, 45.6, and 46.7)%, respectively, with the overall *MPD* of 44.2%. The numerical values of the *MPD* were computed using:

$$MPD = \frac{100}{N} \sum \frac{|x_3^{calc} - x_3|}{x_3} \quad (4)$$

where N is the number of experimental data points.

As mentioned above, Equation (3) is capable of estimating drug solubility in cosolvent mixtures at individual T using only the drug solubility data in the mono-solvents at this T . However, it could be extended to obtain:

$$\ln x_{3(1+2),T} = x_1 \left(A_1 + \frac{B_1}{T} \right) + x_2 \left(A_2 + \frac{B_2}{T} \right) \quad (5)$$

to be applied at various temperatures ($x_{3(1+2),T}$) using a single equation. In Equation (5), A and B terms are the model constants [54]. The trained model for solubility of meloxicam in {DMSO (1) + water (2)} mixtures is:

$$\ln x_{3(1+2),T} = x_1 \left(6.419 - \frac{3357.251}{T} \right) + x_2 \left(-10.582 - \frac{924.993}{T} \right) \quad (6)$$

which resulted in the *MPD* of 44.4%.

The main limitation of the Yalkowsky model is that it does not consider any more interaction term after mixing the solutions and considers the mixing behavior as an ideal one. The Jouyban–Acree model includes as many as required interaction terms (J_i terms) to describe the non-ideality of the mixing and produced the most accurate results in correlating drug solubility data in binary solvent mixtures at various temperatures. The model is presented as [51]:

$$\ln x_{3(1+2),T} = x_1 \ln x_{3(1),T} + x_2 \ln x_{3(2),T} + \left(\frac{x_1 x_2}{T} \right) \sum_{i=0}^2 J_i (x_1 - x_2)^i \quad (7)$$

where J_i terms are the respective model constants that are computed by using a non-intercept least square analysis [31]. Accordingly, the generated solubility values of meloxicam in {DMSO (1) + water (2)} were fitted to Equation (7) and the obtained trained model was:

$$\ln x_{3(1+2),T} = x_1 \ln x_{3(1),T} + x_2 \ln x_{3(2),T} + \left(\frac{x_1 x_2}{T}\right) [1707.481 + 1045.950(x_1 - x_2) - 1264.920(x_1 - x_2)^2] \quad (8)$$

The F value of Equation (8) was 791 and the adjusted correlation coefficient (R) was 0.979, whereas the correlation and the model constants were significant with $p < 0.0005$. Equation (8) is valid for calculating the solubility of meloxicam in different {DMSO (1) + water (2)} mixtures at various temperatures or mixtures-composition of interest, by employing the solubility data of meloxicam in neat DMSO and neat water at each temperature. The obtained MPD for the back-calculated solubility data of meloxicam when using Equation (8) was 9.6%.

Although Equation (8) provided an accurate correlation for the solubility of meloxicam in these {DMSO (1) + water (2)} mixtures, it requires the experimental solubility data in mono-solvents (i.e., $x_{3(1),T}$ and $x_{3(2),T}$) at any temperature of interest to calculate the solubility of meloxicam in the required binary solvent mixtures. However, one may combine the trained version of Equation (5) with Equation (7) to provide a full predictive model, obtaining the following:

$$\begin{aligned} \ln x_{3(1+2),T} = & x_1 \left(6.419 - \frac{3357.251}{T}\right) + x_2 \left(-10.582 - \frac{924.993}{T}\right) \\ & + \left(\frac{x_1 x_2}{T}\right) [1707.332 + 1046.323(x_1 - x_2) - 1265.293(x_1 - x_2)^2] \end{aligned} \quad (9)$$

Equation (9) allows to calculate the solubilities of meloxicam in all these binary mixtures at various temperatures with an MPD of 9.9% and it does not require any experimental input data. The F and R values for Equation (9) were 787 and 0.978, respectively. For practical applications of Equation (9), one may train the model using the minimum number of seven experimental solubility points, and then, predict the rest of required data in any aqueous-DMSO mixture composition and temperature of interest, as has been exemplified in the literature [55]. When the model was trained with the solubility data in DMSO and water at $T = (293.15$ and $313.15)$ K (i.e., the lowest and highest temperatures) and in $x_1 = 0.3, 0.5$ and 0.7 at $T = 298.15$ K (total 7 data points), the rest of the data points were predicted with the MPD of 18.7% ($N = 48$).

In a previous work [56], generally trained version of the Jouyban–Acree–Abraham and Jouyban–Acree–Hansen models were presented for predicting the solubility of meloxicam in various binary solvent mixtures. These models are:

$$\begin{aligned} \ln x_{m,T} = & w_1 \ln x_{1,T} + w_2 \ln x_{2,T} \\ & + \left(\frac{x_1 x_2}{T}\right) \left[\begin{aligned} & 1285.932 + 1413.305(c_1 - c_2)^2 + 5976.117(e_1 - e_2)^2 \\ & - 148.762(s_1 - s_2)^2 - 230.735(a_1 - a_2)^2 \\ & - 50.130(b_1 - b_2)^2 + 243.383(v_1 - v_2)^2 \end{aligned} \right] \\ & + \left(\frac{w_1 w_2 (w_1 - w_2)}{T}\right) \left[\begin{aligned} & -238.740 + 1753.598(c_1 - c_2)^2 - 5123.773(e_1 - e_2)^2 \\ & - 114.361(s_1 - s_2)^2 + 46.071(a_1 - a_2)^2 \\ & + 43.967(b_1 - b_2)^2 - 163.838(v_1 - v_2)^2 \end{aligned} \right] \\ & + \left(\frac{w_1 w_2 (w_1 - w_2)^2}{T}\right) \left[\begin{aligned} & 358.925 - 862.281(c_1 - c_2)^2 + 6965.842(e_1 - e_2)^2 \\ & + 383.849(s_1 - s_2)^2 + 97.860(a_1 - a_2)^2 - 44.224(b_1 - b_2)^2 \\ & + 162.067(v_1 - v_2)^2 - 13.147(a_1 b_1 - a_2 b_2)^2 \end{aligned} \right] \end{aligned} \quad (10)$$

and

$$\begin{aligned} \ln x_{m,T} = & w_1 \ln x_{1,T} + w_2 \ln x_{2,T} \\ & + \left(\frac{x_1 x_2}{T}\right) \left[\begin{aligned} & 1027.586 - 116.816(\delta_{d1} - \delta_{d2})^2 \\ & - 6.910(\delta_{p1} - \delta_{p2})^2 + 1.168(\delta_{h1} - \delta_{h2})^2 \end{aligned} \right] \\ & + \left(\frac{w_1 w_2 (w_1 - w_2)}{T}\right) \left[-717.903 + 11.233(\delta_{p1} - \delta_{p2})^2 \right] \end{aligned} \quad (11)$$

The c , e , s , a , b , and v are Abraham solvent's coefficients and δ_{d1} , δ_{p1} , δ_{h1} , and δ_{d2} , δ_{p2} , and δ_{h2} are the Hansen parameters for solvents 1 and 2, respectively [56]. Equations (10) and (11) predicted the solubility of meloxicam in (DMSO + water) mixtures with the MPDs of 74.3 and 35.6%. Although the prediction errors are relatively large, these equations only require the solubility data in the neat solvent.

3.5. Apparent Thermodynamic Functions of Dissolution

All the apparent standard thermodynamic quantities relative to meloxicam dissolution processes were calculated at the mean harmonic temperature, $T_{\text{hm}} = 303.0$ K, which was calculated by using Equation (12) [57].

$$T_{\text{hm}} = \frac{n}{\sum_{i=1}^n \left(\frac{1}{T}\right)} \quad (12)$$

where n is the number of temperatures under study (i.e., 5 in this case). Hence, all the apparent standard enthalpy changes relative to dissolution processes ($\Delta_{\text{soln}}H^\circ$) were obtained by means of the modified van't Hoff equation, as shown in Equation (13) [58]:

$$\left(\frac{\partial \ln x_3}{\partial(1/T - 1/T_{\text{hm}})}\right)_p = -\frac{\Delta_{\text{soln}}H^\circ}{R} \quad (13)$$

The apparent standard Gibbs energy changes relative to all the meloxicam dissolution processes ($\Delta_{\text{soln}}G^\circ$) were calculated by means of [58–60]:

$$\Delta_{\text{soln}}G^\circ = -RT \cdot \text{intercept} \quad (14)$$

The intercepts used in Equation (14) were those obtained as the result of the linear regressions of $\ln x_3$ as function of $(1/T - 1/T_{\text{hm}})$. Therefore, Figure 5 depicts the meloxicam solubility linear van't Hoff behavior in all the {DMSO (1) + water (2)} mixtures, as well as in both neat solvents. It is noteworthy that linear regressions with $r^2 > 0.993$ were observed in all the solvent systems [61–63].

Finally, the apparent standard changes in entropy, for all the studied meloxicam dissolution processes ($\Delta_{\text{soln}}S^\circ$) were calculated based on the respective $\Delta_{\text{soln}}H^\circ$ and $\Delta_{\text{soln}}G^\circ$ values by using [59,60]:

$$\Delta_{\text{soln}}S^\circ = \frac{(\Delta_{\text{soln}}H^\circ - \Delta_{\text{soln}}G^\circ)}{T_{\text{hm}}} \quad (15)$$

Table 5 summarizes all the apparent standard thermodynamic quantities for the dissolution processes of meloxicam in all the {DMSO (1) + water (2)} mixtures at $T_{\text{hm}} = 303.0$ K, including those corresponding to dissolution processes in neat water and DMSO. It is notable that all apparent standard dissolution thermodynamic quantities for neat water were taken from previous research results [32]. As expected, all the apparent standard Gibbs energies and apparent enthalpies of dissolution of meloxicam are positive in every case in these DMSO-aqueous systems. Otherwise, the apparent standard entropies of dissolution were negative in neat water, as well as in the mixtures of $x_1 \leq 0.30$ but positive from the mixture of $x_1 = 0.40$ to neat DMSO. Thus, the global dissolution processes of meloxicam are always endothermic in nature and entropy-driven for those occurring in the composition interval of $0.40 \leq x_1 \leq 1.00$; whereas, in neat water and the mixtures of $x_1 \leq 0.30$, neither

entropy or enthalpy-driving are observed because $\Delta_{\text{soln}}H^\circ > 0$ and $\Delta_{\text{soln}}S^\circ < 0$). All $\Delta_{\text{soln}}G^\circ$ values decrease continuously from neat water (where highest $\Delta_{\text{soln}}G^\circ$ value is obtained) to reach the lowest value in neat DMSO. Otherwise, $\Delta_{\text{soln}}H^\circ$ decreases from neat water to reach the lowest value in the mixture of $x_1 = 0.10$, and later, it increases with the DMSO proportion to reach a quasi-plateau in the mixtures of $x_1 = 0.30, 0.40,$ and 0.50 to increase again, reaching the highest value in the mixture of $x_1 = 0.60$; after, it decreases to reach a new minimum in neat DMSO. The $\Delta_{\text{soln}}S^\circ$ values increase from a lowest negative value in neat water ($-87.99 \text{ J}\cdot\text{mol}^{-1}\cdot\text{K}^{-1}$) to reach the maximum positive value in the mixture of $x_1 = 0.60$ ($66.49 \text{ J}\cdot\text{mol}^{-1}\cdot\text{K}^{-1}$), and later, they decrease continuously with the DMSO proportion to reach a lower value in neat DMSO ($53.35 \text{ J}\cdot\text{mol}^{-1}\cdot\text{K}^{-1}$). As observed, the lowest $\Delta_{\text{soln}}H^\circ$ and $\Delta_{\text{soln}}S^\circ$ values are observed in neat water or in the mixture of $x_1 = 0.00$. The negative apparent dissolution entropies observed in neat water and the mixtures of composition $x_1 = 0.10, 0.20,$ and 0.30 could be a consequence of the possible hydrophobic hydration around the methyl and phenylene groups of meloxicam (Figure 1).

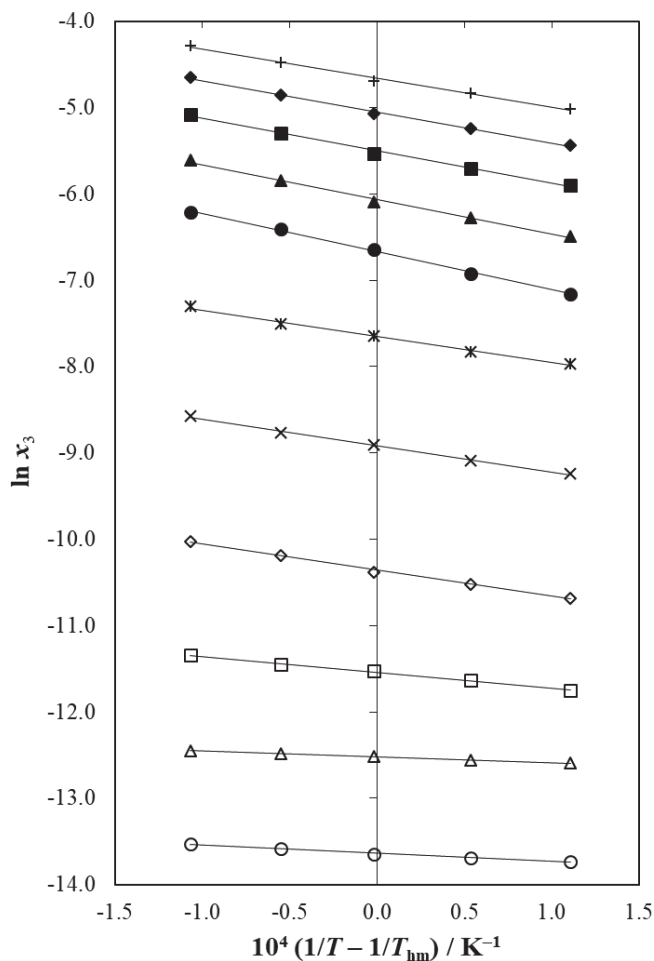


Figure 5. Van't Hoff plot of the solubility of meloxicam (3) in {DMSO (1) + water (2)} solvent systems. ○: $x_1 = 0.00$ (neat water), △: $x_1 = 0.10$, □: $x_1 = 0.20$, ◇: $x_1 = 0.30$, ×: $x_1 = 0.40$, *: $x_1 = 0.50$, ●: $x_1 = 0.60$, ▲: $x_1 = 0.70$, ■: $x_1 = 0.80$, ◆: $x_1 = 0.90$, +: $x_1 = 0.10$ (neat DMSO).

Table 5. Apparent thermodynamic functions relative to dissolution processes of meloxicam (3) in {DMSO (1) + water (2)} mixtures at $T_{\text{hm}} = 303.0$ K and $p = 96$ kPa ^{a,b}.

x_1 ^{a,b}	$\Delta_{\text{soln}}G^\circ / \text{kJ}\cdot\text{mol}^{-1}$ ^b	$\Delta_{\text{soln}}H^\circ / \text{kJ}\cdot\text{mol}^{-1}$ ^b	$\Delta_{\text{soln}}S^\circ / \text{J}\cdot\text{mol}^{-1}\cdot\text{K}^{-1}$ ^b	$T\Delta_{\text{soln}}S^\circ / \text{kJ}\cdot\text{mol}^{-1}$ ^b	ζ_H ^c	ζ_{TS} ^c
0.000 ^d	34.35	7.69	−87.99	−26.66	0.224	0.776
0.100	31.55	5.59	−85.68	−25.96	0.177	0.823
0.200	29.08	15.27	−45.55	−13.80	0.525	0.475
0.300	26.09	24.89	−3.96	−1.20	0.954	0.046
0.400	22.46	25.49	9.99	3.03	0.894	0.106
0.500	19.27	25.23	19.65	5.96	0.809	0.191
0.600	16.80	36.95	66.49	20.15	0.647	0.353
0.700	15.28	33.53	60.23	18.25	0.648	0.352
0.800	13.86	31.20	57.24	17.34	0.643	0.357
0.900	12.73	29.87	56.58	17.14	0.635	0.365
1.000	11.74	27.91	53.35	16.16	0.633	0.367
Ideal ^d	14.16	24.78	35.03	10.61	0.700	0.300

^a p is the atmospheric pressure in Bogotá, Colombia. x_1 is the mole fraction of DMSO (1) in the {DMSO (1) + water (2)} mixtures free of meloxicam (3). Mean uncertainty in x_1 , $u(x_1) = 0.0005$. ^b Standard uncertainty in T_{hm} is $u(T_{\text{hm}}) = 0.13$ K. Standard uncertainty in p is $u(p) = 3.0$ kPa. Average relative standard uncertainty in apparent thermodynamic quantities of real dissolution processes are $u_r(\Delta_{\text{soln}}G^\circ) = 0.027$, $u_r(\Delta_{\text{soln}}H^\circ) = 0.035$, $u_r(\Delta_{\text{soln}}S^\circ) = 0.045$, $u_r(T\Delta_{\text{soln}}S^\circ) = 0.045$. ^c ζ_H and ζ_{TS} are the relative contributions by enthalpy and entropy toward apparent Gibbs energy of dissolution. ^d Data taken from Delgado et al. [32].

Moreover, to calculate the magnitude contributions by enthalpy (ζ_H) and entropy (ζ_{TS}) toward the dissolution processes, the following equations were used [64]:

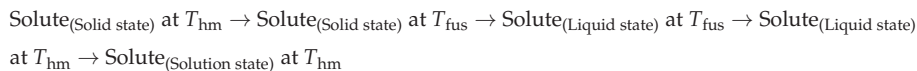
$$\zeta_H = \frac{|\Delta_{\text{soln}}H^\circ|}{|\Delta_{\text{soln}}H^\circ| + |T\Delta_{\text{soln}}S^\circ|} \quad (16)$$

$$\zeta_{TS} = \frac{|T\Delta_{\text{soln}}S^\circ|}{|\Delta_{\text{soln}}H^\circ| + |T\Delta_{\text{soln}}S^\circ|} \quad (17)$$

As observed in Table 5, the higher contribution to the positive apparent standard molar Gibbs energies of meloxicam dissolution is given by the positive enthalpy. This demonstrates that in almost all the mixtures, the main contributor to this positive standard molar Gibbs energy of solution of meloxicam (reflected in the low meloxicam solubility) is the enthalpy except for neat water and the mixture of $x_1 = 0.10$, where $\zeta_H = 0.224$ and 0.177 , respectively, and thus, entropy is the dominant function in these two cases.

3.6. Apparent Thermodynamic Quantities of Mixing

The overall dissolution processes of meloxicam in all {DMSO (1) + water (2)} solvent systems may be represented with the following hypothetical stages:



Here, the hypothetical stages are considered as follows: (i) the heating and fusion of meloxicam at $T_{\text{fus}} = 536.7$ K, (ii) the cooling of the liquid fused meloxicam to the considered temperature (i.e., $T_{\text{hm}} = 303.0$ K), and (iii) the subsequent mixing of both the hypothetical super-cooled liquid meloxicam and the liquid aqueous-DMSO solvent system

at $T_{\text{hm}} = 303.0 \text{ K}$ [65]. This treatment allowed us to calculate every individual thermodynamic contribution toward the overall meloxicam dissolution processes by means of:

$$\Delta_{\text{soln}}H^\circ = \Delta_{\text{fus}}H^{T_{\text{hm}}} + \Delta_{\text{mix}}H^\circ \quad (18)$$

$$\Delta_{\text{soln}}S^\circ = \Delta_{\text{fus}}S^{T_{\text{hm}}} + \Delta_{\text{mix}}S^\circ \quad (19)$$

where $\Delta_{\text{fus}}H^{T_{\text{hm}}}$ and $\Delta_{\text{fus}}S^{T_{\text{hm}}}$ represent the thermodynamic quantities relative to meloxicam melting and its cooling at $T_{\text{hm}} = 303.0 \text{ K}$, which, in turn, are calculated by means of [66]:

$$\Delta_{\text{fus}}H^{T_{\text{hm}}} = \Delta_{\text{fus}}H^{T_{\text{fus}}} - \Delta C_p(T_{\text{fus}} - T_{\text{hm}}) \quad (20)$$

$$\Delta_{\text{fus}}S^{T_{\text{hm}}} = \Delta_{\text{fus}}S^{T_{\text{fus}}} - \Delta C_p \ln\left(\frac{T_{\text{fus}}}{T_{\text{hm}}}\right) \quad (21)$$

where ΔC_p denotes the difference of heat capacities of liquid and solid states at the temperature of melting. Owing the difficulties in ΔC_p experimental determinations, the entropy of fusion (ΔS_f) is used instead [66]. Table 6 summarizes all the apparent standard thermodynamic quantities of mixing of the hypothetical super-cooled liquid meloxicam with all the studied aqueous-DMSO mixtures and the neat solvents, water, and DMSO, as calculated at $T_{\text{hm}} = 303.0 \text{ K}$. As observed, the Gibbs energies of mixing are positive from neat water to the mixture of $x_1 = 0.70$ because the experimental drug solubilities are lower than ideal solubilities; on the contrary, they are negative from the mixture of $x_1 = 0.80$ to neat DMSO, because the experimental solubilities are higher than the ideal ones. The contributions by the thermodynamic quantities of mixing subprocesses to the overall dissolution processes of meloxicam are variable and depend on the aqueous-DMSO mixtures' composition. Thus, $\Delta_{\text{mix}}H^\circ$ values are negative in neat water and the mixtures of $x_1 = 0.10$ and 0.20 but positive in the solvent systems in the interval of $0.30 \leq x_1 \leq 1.00$. Moreover, $\Delta_{\text{mix}}S^\circ$ values are negative in the interval $0.00 \leq x_1 \leq 0.50$ but positive in the other cases. Thus, the mixing processes in neat water and the mixture of $x_1 = 0.10$ and 0.20 are enthalpy-driven because of the exothermic character exhibited. In the mixtures $0.30 \leq x_1 \leq 0.50$, neither enthalpy nor entropy-driving is observed for mixing. Finally, in the interval of $0.60 \leq x_1 \leq 1.00$, entropy-driven is observed. Furthermore, in order to evaluate the relative contributions by enthalpy (ζ_H) and entropy (ζ_{TS}) to the mixing processes in all these solvent systems, two equations analogous to Equations (16) and (17) were also employed. As observed, in water-rich and DMSO-rich mixtures, the main contributor to Gibbs energies of mixing is the entropy, but in the mixtures' composition interval of $0.30 \leq x_1 \leq 0.70$, it is the enthalpy.

As described earlier in the literature, the net variation of $\Delta_{\text{mix}}H^\circ$ values regarding the aqueous-cosolvent mixtures' composition depends on the contribution of different kinds of intermolecular interactions. Hence, the cavity formation in the solvent system, required for the solute accommodation, is endothermic because some quantity of energy must be supplied against the respective cohesive forces of the solvent. This contribution diminishes the drug solubility as mentioned above. Oppositely, the solvent-solute interactions, resulting mainly from van der Waals and Lewis acid-base interactions, such as hydrogen bonding, are clearly exothermic in nature. This effect increases the drug solubility and dissolution rate as also indicated before. Even more, the structuring of water molecules around the phenylene ring and the methyl group of meloxicam structure (Figure 1) would be contributing to diminish the net $\Delta_{\text{mix}}H^\circ$ quantity to small or even negative values in water-rich mixtures [67]. This event is clearly observed with meloxicam in aqueous-DMSO mixtures as indicated in Table 5 for solvent systems from neat water to the mixture of $x_1 = 0.50$.

Table 6. Apparent thermodynamic functions relative to mixing processes of meloxicam (3) in (DMSO (1) + water (2)) mixtures at $T_{\text{hm}} = 303.0$ K and $p = 96$ kPa ^{a,b}.

x_1 ^{a,b}	$\Delta_{\text{mix}}G^\circ / \text{kJ}\cdot\text{mol}^{-1}$ ^b	$\Delta_{\text{mix}}H^\circ / \text{kJ}\cdot\text{mol}^{-1}$ ^b	$\Delta_{\text{mix}}S^\circ / \text{J}\cdot\text{mol}^{-1}\cdot\text{K}^{-1}$ ^b	$T\Delta_{\text{mix}}S^\circ / \text{kJ}\cdot\text{mol}^{-1}$ ^b	ζ_H ^c	ζ_{TS} ^c
0.000	20.19	−17.09	−123.02	−37.27	0.314	0.686
0.100	17.38	−19.19	−120.71	−36.57	0.344	0.656
0.200	14.91	−9.50	−80.58	−24.42	0.280	0.720
0.300	11.93	0.12	−38.99	−11.81	0.010	0.990
0.400	8.30	0.71	−25.03	−7.59	0.086	0.914
0.500	5.11	0.45	−15.38	−4.66	0.088	0.912
0.600	2.64	12.17	31.46	9.53	0.561	0.439
0.700	1.12	8.75	25.20	7.63	0.534	0.466
0.800	−0.30	6.43	22.21	6.73	0.489	0.511
0.900	−1.43	5.10	21.55	6.53	0.438	0.562
1.000	−2.42	3.13	18.32	5.55	0.361	0.639

^a p is the atmospheric pressure in Bogotá, Colombia. x_1 is the mole fraction of DMSO (1) in the (DMSO (1) + water (2)) mixtures free of meloxicam (3). Mean uncertainty in x_1 , $u(x_1) = 0.0005$. ^b Standard uncertainty in T_{hm} is $u(T_{\text{hm}}) = 0.13$ K. Standard uncertainty in p is $u(p) = 3.0$ kPa. Average relative standard uncertainty in apparent thermodynamic quantities of mixing processes are $u_r(\Delta_{\text{mix}}G^\circ) = 0.030$, $u_r(\Delta_{\text{mix}}H^\circ) = 0.040$, $u_r(\Delta_{\text{mix}}S^\circ) = 0.050$, $u_r(T\Delta_{\text{mix}}S^\circ) = 0.050$. ^c ζ_H and ζ_{TS} are the relative contributions by enthalpy and entropy toward apparent Gibbs energy of mixing.

3.7. Enthalpy–Entropy Compensation Analysis

Classical extra-thermodynamic studies, in particular those based on the enthalpy–entropy compensation analyses, provide a powerful physicochemical tool to find or identify similar mechanisms responsible for some physical and chemical processes involving organic compounds [68,69]. Some well-known literature reports demonstrated the presence of nonlinear-enthalpy–entropy compensation effects in the dissolution processes of many drugs and drug-alike compounds in different aqueous cosolvent binary systems. These extra-thermodynamic studies have usually been performed by different research groups to identify the main mechanisms involved in the cosolvent action for solubility increasing or decreasing, depending on the mixtures' composition [70–72]. As shown in Figure 6, meloxicam exhibits a nonlinear $\Delta_{\text{soln}}H^\circ$ vs. $\Delta_{\text{soln}}G^\circ$ trend with negative slopes from neat water to the mixture of $x_1 = 0.10$ and from the mixture of $x_1 = 0.60$ to neat DMSO, whereas, in the interval of $0.10 \leq x_1 \leq 0.30$ and from $x_1 = 0.50$ to $x_1 = 0.60$, positive slopes are observed; finally, in the interval of $0.30 \leq x_1 \leq 0.50$, a plateau is observed. In the first cases, the driving mechanism for transferring meloxicam from the most polar solvent systems to less polar solvent systems is the entropy. For the intervals exhibiting positive slopes, the drug transfer is driven by the enthalpy. Otherwise, in the interval of $0.30 \leq x_1 \leq 0.50$, the function driving the transfer is not clear. Nevertheless, it is not easy to identify the molecular effects involved, owing the complexity of aqueous–DMSO mixtures as indicated earlier [41,42].

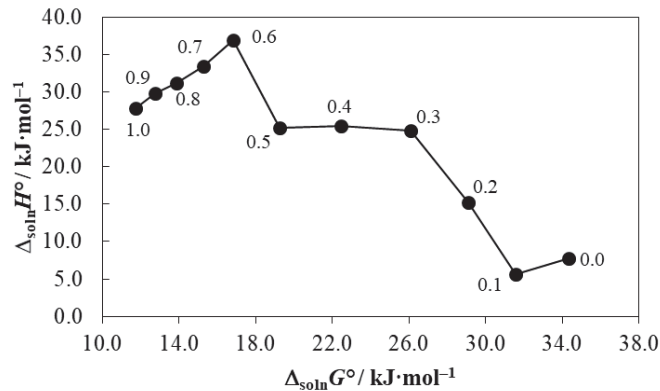


Figure 6. $\Delta_{\text{soln}}H^\circ$ vs. $\Delta_{\text{soln}}G^\circ$ enthalpy–entropy compensation plot for the solubility of meloxicam (3) in {DMSO (1) + water (2)} mixtures at $T_{\text{hm}} = 303.0$ K. The points represent the mole fraction of DMSO (1) in the {DMSO (1) + water (2)} mixtures in the absence of meloxicam (3).

3.8. Preferential Solvation Analysis

The preferential solvation parameter of meloxicam (component 3) by DMSO (component 1) in the {DMSO (1) + water (2)} mixtures at saturation is defined as:

$$\delta x_{1,3} = x_{1,3}^L - x_1 = -\delta x_{2,3} \quad (22)$$

where $x_{1,3}^L$ is the local mole fraction of DMSO in the molecular environment around meloxicam and x_1 is the bulk mole fraction of DMSO in the initial aqueous–DMSO mixture in the absence of meloxicam. If $\delta x_{1,3}$ values were positive, meloxicam would be preferentially solvated by DMSO, but if they were negative, meloxicam would be preferentially solvated by water. Thus, the respective $\delta x_{1,3}$ values were obtained by means of the inverse Kirkwood–Buff integrals (IKBI) for the solvent components based on [73–75]:

$$\delta x_{1,3} = \frac{x_1 x_2 (G_{1,3} - G_{2,3})}{x_1 G_{1,3} + x_2 G_{2,3} + V_{\text{cor}}} \quad (23)$$

with,

$$G_{1,3} = RT\kappa_T - \bar{V}_3 + x_2 \bar{V}_2 \left(\frac{D}{Q} \right) \quad (24)$$

$$G_{2,3} = RT\kappa_T - \bar{V}_3 + x_1 \bar{V}_1 \left(\frac{D}{Q} \right) \quad (25)$$

$$V_{\text{cor}} = 2522.5 \cdot \left\{ r_3 + 0.1363 \cdot \left(x_{1,3}^L \bar{V}_1 + x_{2,3}^L \bar{V}_2 \right)^{1/3} - 0.085 \right\}^3 \quad (26)$$

Here, κ_T represents the isothermal compressibility of every {DMSO (1) + water (2)} mixture. \bar{V}_1 and \bar{V}_2 denote the partial molar volumes of DMSO and water in the aqueous–DMSO mixtures. \bar{V}_3 denotes the partial molar volume of meloxicam. The function D corresponds to the first derivative of the variation of standard molar Gibbs energies of transfer of meloxicam from neat water to {DMSO (1) + water (2)} mixtures regarding the DMSO-proportion in the mixtures free of solute, as shown in Equation (27). The function Q involves the second derivative of the variation of excess molar Gibbs energy of mixing of DMSO and water (G_{1+2}^{Ex}) regarding the water-proportion in the aqueous–DMSO mixtures, as shown in Equation (28). V_{cor} is the correlation volume and r_3 is the hydrodynamic

molecular radius of meloxicam, which is commonly calculated by means of Equation (29), where N_{Av} is the number of Avogadro.

$$D = \left(\frac{\partial \Delta_{tr} G_{3,2 \rightarrow 1+2}^{\circ}}{\partial x_1} \right)_{T,p} \quad (27)$$

$$Q = RT + x_1 x_2 \left(\frac{\partial^2 G_{1+2}^{Exc}}{\partial x_2^2} \right)_{T,p} \quad (28)$$

$$r_3 = \left(\frac{3 \cdot 10^{21} V_3}{4\pi N_{Av}} \right)^{1/3} \quad (29)$$

As exposed in the literature, the definitive V_{cor} values require iteration because they depend on the local mole fractions of DMSO and water around the meloxicam molecules in the equilibrated solutions. Hence, these iterations are performed by substituting $\delta x_{1,3}$ and V_{cor} values in Equations (22), (23), and (26) in order to recalculate the $x_{1,3}^L$ value until almost invariant values of V_{cor} are obtained.

Figure 7 depicts the apparent Gibbs energies of transfer of meloxicam from neat water to {DMSO (1) + water (2)} mixtures ($\Delta_{tr} G_{3,2 \rightarrow 1+2}^{\circ}$) at $T = 298.15$ K. These $\Delta_{tr} G_{3,2 \rightarrow 1+2}^{\circ}$ values were calculated from the mole fraction solubilities shown Table 1, by using:

$$\Delta_{tr} G_{3,2 \rightarrow 1+2}^{\circ} = RT \ln \left(\frac{x_{3,2}}{x_{3,1+2}} \right) \quad (30)$$

$\Delta_{tr} G_{3,2 \rightarrow 1+2}^{\circ}$ values were correlated according to the regular fourth degree polynomial presented as Equation (31), with adjusted $r^2 = 0.998$, typical error = 0.317, and F value = 1484.

$$\Delta_{tr} G_{3,2 \rightarrow 1+2}^{\circ} = -0.19(\pm 0.30) - 15.72(\pm 4.68)x_1 - 63.14(\pm 20.49)x_1^2 + 96.50(\pm 31.53)x_1^3 - 39.34(\pm 15.64)x_1^4 \quad (31)$$

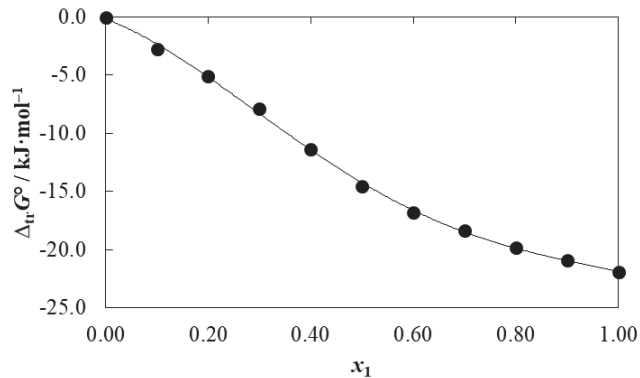


Figure 7. Gibbs energy of transfer of meloxicam (3) from neat water (2) to {DMSO (1) + water (2)} mixtures at $T = 298.15$ K.

In this way, the D values shown in Table 7 were calculated from the first derivative of Equation (31) by considering the variation of aqueous-DMSO mixtures composition in incremental $x_1 = 0.05$ steps through all the mixtures' composition interval. Otherwise, the required Q , $RT\kappa_T$, \bar{V}_1 , and \bar{V}_2 values corresponding to {DMSO (1) + water (2)} mixtures were taken from the literature [76].

Table 7. Some properties associated to preferential solvation of meloxicam (3) in {DMSO (1) + water (2)} mixtures at $T = 298.15$ K.

x_1^a	$D/$ $\text{kJ}\cdot\text{mol}^{-1}$	$G_{1,3}/$ $\text{cm}^3\cdot\text{mol}^{-1}$	$G_{2,3}/$ $\text{cm}^3\cdot\text{mol}^{-1}$	$V_{\text{cor}}/$ $\text{cm}^3\cdot\text{mol}^{-1}$	$100 \delta x_{1,3}$
0.00	−15.72	−297.0	−182.2	830	0.00
0.05	−21.33	−335.5	−212.0	876	−0.89
0.10	−25.61	−353.3	−253.3	926	−1.36
0.15	−28.68	−352.2	−296.1	984	−1.05
0.20	−30.65	−338.1	−332.4	1047	−0.13
0.25	−31.65	−317.6	−358.6	1111	1.01
0.30	−31.80	−295.3	−374.6	1173	2.03
0.35	−31.20	−274.2	−381.9	1231	2.76
0.40	−29.98	−255.5	−382.3	1286	3.19
0.45	−28.26	−239.7	−377.7	1337	3.34
0.50	−26.16	−226.6	−369.7	1386	3.29
0.55	−23.78	−216.1	−359.4	1433	3.08
0.60	−21.26	−207.7	−348.1	1478	2.78
0.65	−18.70	−201.1	−336.5	1522	2.42
0.70	−16.24	−196.0	−325.7	1566	2.05
0.75	−13.97	−192.1	−316.8	1610	1.69
0.80	−12.03	−189.2	−311.5	1654	1.36
0.85	−10.54	−187.1	−312.5	1697	1.07
0.90	−9.60	−185.5	−325.1	1741	0.82
0.95	−9.33	−184.1	−362.4	1783	0.53
1.00	−9.86	−182.0	−465.7	1823	0.00

^a x_1 is the mole fraction of DMSO (1) in the {DMSO (1) + water (2)} mixtures free of meloxicam (3).

Because \bar{V}_3 values are not available for meloxicam in {DMSO (1) + water (2)} mixtures, these values were considered as the one calculated based on Fedors' method, i.e., $183.3 \text{ cm}^3\cdot\text{mol}^{-1}$ [6]. $G_{1,3}$ and $G_{2,3}$ shown in Table 7 are negative in all cases, indicating the affinity of meloxicam by DMSO and water. The approximated hydrodynamic radius of meloxicam (r_3) was calculated as 0.417 nm by means of Equation (29). In turn, the preferential solvation parameters of meloxicam by DMSO molecules are also summarized in Table 7. According to Figure 8, initially adding of DMSO to water makes the $\delta x_{1,3}$ values of meloxicam negative in the interval from neat water to the mixture of $x_1 = 0.21$. The maximum negative value of this parameter is obtained in the mixture of $x_1 = 0.10$, with $\delta x_{1,3} = -1.36 \times 10^{-2}$, which is higher than 1.00×10^{-2} if the absolute value is considered; therefore, it could be a consequence of real preferential solvation effects by water on meloxicam, rather than a consequence of the uncertainty propagation in the respective IKBI calculations [77,78]. The cosolvent action of DMSO for increasing the meloxicam solubility in these water-rich mixtures could be associated to the breaking of the ordered structure exhibited by water molecules, such as "icebergs", around the non-polar moieties of meloxicam, which, in turn, would be increasing the meloxicam solubility and solvation.

In mixtures of $0.21 < x_1 < 1.00$, the $\delta x_{1,3}$ values are positive indicating preferential solvation of meloxicam by DMSO. Maximum $\delta x_{1,3}$ value was obtained in the mixture of $x_1 = 0.45$ ($\delta x_{1,3} = 3.34 \times 10^{-2}$). This maximum positive $\delta x_{1,3}$ value is also higher than $|1.00 \times 10^{-2}|$ being a consequence of real preferential solvation effects by DMSO [77,78]. From a mechanistic viewpoint, in the mixtures' composition region of $0.19 < x_1 < 1.00$, it is adequately conjecturable that meloxicam could be acting as a Lewis acid in front of

the DMSO molecules owing the unshared electrons of the sulfoxide oxygen atom of this cosolvent. Notably, this cosolvent is more basic than water, as remarkable by the magnitude of their Kamlet–Taft hydrogen bond acceptor parameters, namely $\beta = 0.76$ for DMSO and 0.47 for water [38]. Moreover, Figure 8 allows the comparison of preferential solvation of meloxicam by DMSO and *N,N*-dimethylformamide in their respective aqueous mixtures [6]. As observed, the cosolvent regions of preferential solvation are similar, as well as the magnitudes of preferential solvation by both cosolvents. Nevertheless, preferential hydration of meloxicam is higher with *N,N*-dimethylformamide, which could be a consequence of its lower polarity ($\delta_1 = 24.1 \text{ MPa}^{1/2}$) regarding DMSO ($\delta_1 = 26.6 \text{ MPa}^{1/2}$) [37,38]. These interesting behaviors could be a consequence of the high water-association effects around the non-polar groups of this drug, which could be favored by the more hydrophobic moieties present in the cosolvents, as they exhibit less polar nature. In turn, the hydrophobic groups present in the cosolvents could also be acting as water-association promoters depending on their respective molecular sizes [11]. Finally, from all the physicochemical analyses reported, it is noteworthy to mention that this investigation expands the equilibrium solubility database about non-steroidal anti-inflammatory drugs in commonly used aqueous cosolvent mixtures [79].

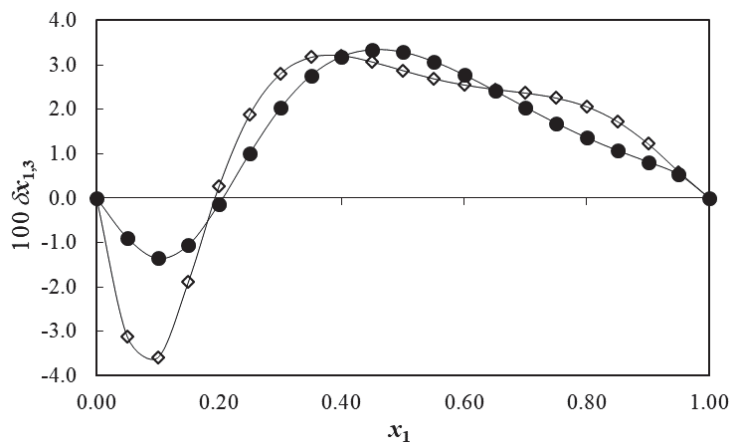


Figure 8. Preferential solvation parameters of meloxicam (3) in some [cosolvent (1) + water (2)] mixtures at $T = 298.15 \text{ K}$. ●: DMSO (1) + water (2), ◇: Dimethylformamide (1) + water (2) [6].

4. Conclusions

Equilibrium molar and mole fraction solubilities of analgesic drug meloxicam in different {DMSO (1) + water (2)} mixtures at five temperatures from 293.15 to 313.15 K were determined by using the shake flask method followed by UV-vis drug quantification, reported and analyzed. Meloxicam mole fraction solubility in these mixtures was adequately correlated with some well-known correlation models obtaining mean percentage deviations (MPDs) of 9.6 to 9.9%. In addition, a number of predictive models which were already trained using published datasets and by employing the minimum number of measured experimental data from this project were produced with MPDs of 35.6 to 74.3%. Apparent standard thermodynamic quantities of dissolution and mixing processes were calculated observing endothermic dissolution processes in all cases and favored in DMSO-rich mixtures. Nonlinear enthalpy-entropy compensation was observed indicating different mechanisms for the cosolvent action. IKBI treatment demonstrated preferential hydration of meloxicam in water-rich mixtures but preferential solvation by DMSO in mixtures of $0.21 < x_1 < 1.00$.

Author Contributions: Conceptualization, D.A.T., F.M., O.A.A., M.Á.P., A.J. and W.E.A.J.; methodology, D.A.T., F.M. and O.A.A.; software, D.A.T., F.M., M.Á.P. and A.J.; validation, D.A.T., F.M., A.J. and W.E.A.J.; formal analysis, D.A.T., F.M., O.A.A., M.Á.P., A.J. and W.E.A.J.; investigation, D.A.T., F.M., O.A.A., M.Á.P., A.J. and W.E.A.J.; resources, D.A.T., F.M. and O.A.A.; data curation, D.A.T. and F.M.; writing—original draft preparation, D.A.T., F.M., M.Á.P. and A.J.; writing—review and editing, D.A.T., F.M., O.A.A., M.Á.P., A.J. and W.E.A.J.; visualization, D.A.T., F.M., O.A.A., M.Á.P., A.J. and W.E.A.J.; supervision, F.M., M.Á.P., A.J. and W.E.A.J.; project administration, D.A.T., F.M., A.J. and W.E.A.J.; funding acquisition, D.A.T., F.M. and O.A.A. All authors have read and agreed to the published version of the manuscript.

Funding: This research was funded by Minciencias (formerly Colciencias), grant number 785-2019.

Data Availability Statement: Not applicable.

Acknowledgments: We thank the Departments of Pharmacy and Physics of the Universidad Nacional de Colombia for facilitating the equipment and laboratories used. Financial support of Minciencias (formerly Colciencias) is also highly appreciated.

Conflicts of Interest: The authors declare no conflict of interest.

References

- Budavari, S.; O'Neil, M.J.; Smith, A.; Heckelman, P.E.; Obenchain, J.R., Jr.; Gallipeau, J.A.R.; D'Arecca, M.A. *The Merck Index: An Encyclopedia of Chemicals, Drugs, and Biologicals*, 13th ed.; Merck & Co., Inc.: Whitehouse Station, NJ, USA, 2001.
- Brooks, P.M.; Day, R.O. Non steroidal anti-inflammatory drugs—differences and similarities. *N. Engl. J. Med.* **1991**, *324*, 1716–1725. [[CrossRef](#)] [[PubMed](#)]
- Engelhardt, G.; Homma, D.; Schlegel, K.; Utzmann, R.; Schnitzler, C. Anti-inflammatory, analgesic, antipyretic and related properties of meloxicam, a new non-steroidal anti-inflammatory agent with favourable gastrointestinal tolerance. *Inflamm. Res.* **1995**, *44*, 423–433. [[CrossRef](#)]
- Türk, D.; Roth, W.; Busch, U. A review of the clinical pharmacokinetics of meloxicam. *British J. Rheumatol.* **1996**, *35*, 13–16. [[CrossRef](#)] [[PubMed](#)]
- Sweetman, S.C. *Martindale: The Complete Drug Reference*, 36th ed.; Pharmaceutical Press: London, UK, 2009.
- Tinjacá, D.A.; Martínez, F.; Almanza, O.A.; Jouyban, A.; Acree, W.E., Jr. Solubility of meloxicam in aqueous binary mixtures of formamide, N-methylformamide and N,N-dimethylformamide: Determination, correlation, thermodynamics and preferential solvation. *J. Chem. Thermodyn.* **2021**, *154*, 106332. [[CrossRef](#)]
- Tinjacá, D.A.; Martínez, F.; Almanza, O.A.; Jouyban, A.; Acree, W.E., Jr. Dissolution thermodynamics and preferential solvation of meloxicam in (acetonitrile + water) mixtures. *Phys. Chem. Liq.* **2021**, *59*, 733–752. [[CrossRef](#)]
- Tinjacá, D.A.; Martínez, F.; Almanza, O.A.; Jouyban, A.; Acree, W.E., Jr. Solubility, dissolution thermodynamics and preferential solvation of meloxicam in (methanol + water) mixtures. *J. Solution Chem.* **2021**, *50*, 667–689. [[CrossRef](#)]
- Tinjacá, D.A.; Martínez, F.; Almanza, O.A.; Jouyban, A.; Acree, W.E., Jr. Solubility of meloxicam in (Carbitol[®] + water) mixtures: Determination, correlation, dissolution thermodynamics and preferential solvation. *J. Mol. Liq.* **2021**, *324*, 114671. [[CrossRef](#)]
- Golgoun, S.; Mokhtarpour, M.; Shekaari, H. Solubility enhancement of betamethasone, meloxicam and piroxicam by use of choline-based deep eutectic solvents. *Pharm. Sci.* **2021**, *27*, 86–101. [[CrossRef](#)]
- Tinjacá, D.A.; Martínez, F.; Almanza, O.A.; Jouyban, A.; Acree, W.E., Jr. Solubility, correlation, dissolution thermodynamics and preferential solvation of meloxicam in aqueous mixtures of 2-propanol. *Pharm. Sci.* **2022**, *28*, 130–144. [[CrossRef](#)]
- Rowe, R.C.; Sheskey, P.J.; Quinn, M.E. *Handbook of Pharmaceutical Excipients*, 6th ed.; American Pharmacists Association and Pharmaceutical Press: London, UK, 2009.
- Shirley, S.W.; Stewart, B.H.; Mirelman, S. Dimethyl sulfoxide in treatment of inflammatory genitourinary disorders. *Urology* **1978**, *11*, 215–220. [[CrossRef](#)]
- Jacob, S.W.; De la Torre, J.C. *Dimethyl Sulfoxide (DMSO) in Trauma and Disease*; CRC Press: Boca Raton, FL, USA, 2015.
- Jacob, S.W.; Herschler, R. Introductory remarks: Dimethyl sulfoxide after twenty years. *Ann. N. Y. Acad. Sci.* **1983**, *411*, 13–17. [[CrossRef](#)] [[PubMed](#)]
- Lipinski, C. Drug solubility in water and dimethylsulfoxide. In *Molecular Drug Properties: Measurement and Prediction*; Mannhold, R., Ed.; Wiley: Weinheim, Germany, 2007; pp. 257–282.
- Shakeel, F.; Mothana, R.A.; Haq, N.; Siddiqui, N.A.; Al-Oqail, M.M.; Al-Rehaily, A.J. Solubility and thermodynamic function of bergenin in different (DMSO + water) mixtures at different temperatures. *J. Mol. Liq.* **2016**, *220*, 823–828. [[CrossRef](#)]
- Manh, T.N.; Kim, K.-J. Solubility of N-guanylurea dinitramide in binary solvent mixtures. *Propellants Explos. Pyrotech.* **2016**, *41*, 709–712. [[CrossRef](#)]
- Jabbari, M.; Khosravi, N.; Feizabadi, M.; Ajloo, D. Solubility temperature and solvent dependence and preferential solvation of citrus flavonoid naringin in aqueous DMSO mixtures: An experimental and molecular dynamics simulation study. *RSC Adv.* **2017**, *7*, 14776–14789. [[CrossRef](#)]

20. Shakeel, F.; Haq, N.; Salem-Bekhit, M.M.; Raish, M. Solubility and dissolution thermodynamics of sinapic acid in (DMSO + water) binary solvent mixtures at different temperatures. *J. Mol. Liq.* **2017**, *225*, 833–839. [[CrossRef](#)]
21. Yuan, Y.; Farajtabar, A.; Kong, L.; Zhao, H. Thermodynamic solubility modelling, solvent effect and preferential solvation of p-nitrobenzamide in aqueous co-solvent mixtures of dimethyl sulfoxide, ethanol, isopropanol and ethylene glycol. *J. Chem. Thermodyn.* **2019**, *136*, 123–131. [[CrossRef](#)]
22. Li, W.; Farajtabar, A.; Xing, R.; Zhu, Y.; Zhao, H. Solubility of d-histidine in aqueous cosolvent mixtures of N,N-dimethylformamide, ethanol, dimethyl sulfoxide, and N-methyl-2-pyrrolidone: Determination, preferential solvation, and solvent effect. *J. Chem. Eng. Data* **2020**, *65*, 1695–1704. [[CrossRef](#)]
23. Li, X.; Zhu, Y.; Zhang, X.; Farajtabar, A.; Zhao, H. Solubility, preferential solvation, and solvent effect of microflavin in aqueous mixtures of dimethylsulfoxide, isopropanol, propylene glycol, and ethanol. *J. Chem. Eng. Data* **2020**, *65*, 1976–1985. [[CrossRef](#)]
24. Zhao, X.; Farajtabar, A.; Han, G.; Zhao, H. Phenformin in aqueous co-solvent mixtures of N,N-dimethylformamide, ethanol, N-methylpyrrolidone and dimethyl sulfoxide: Solubility, solvent effect and preferential solvation. *J. Chem. Thermodyn.* **2020**, *144*, 106085. [[CrossRef](#)]
25. Alshahrani, S.M.; Shakeel, F. Solubility data and computational modeling of baricitinib in various (DMSO +Water) mixtures. *Molecules* **2020**, *25*, 2124. [[CrossRef](#)] [[PubMed](#)]
26. Shakeel, F.; Alshehri, S.; Imran, M.; Haq, N.; Alanazi, A.; Anwer, M.K. Experimental and computational approaches for solubility measurement of pyridazinone derivative in binary (DMSO +water) systems. *Molecules* **2020**, *25*, 171. [[CrossRef](#)] [[PubMed](#)]
27. Cysewski, P.; Przybyłek, M.; Kowalska, A.; Tymorek, N. Thermodynamics and intermolecular interactions of nicotinamide in neat and binary solutions: Experimental measurements and COSMO-RS concentration dependent reactions investigations. *Int. J. Mol. Sci.* **2021**, *22*, 7365. [[CrossRef](#)] [[PubMed](#)]
28. Rubino, J.T. Cosolvents and cosolvency. In *Encyclopedia of Pharmaceutical Technology*; Swarbrick, J., Boylan, J.C., Eds.; Marcel Dekker, Inc.: New York, NY, USA, 1988; Volume 3, pp. 375–398.
29. Martin, A.; Bustamante, P.; Chun, A.H.C. *Physical Pharmacy: Physical Chemical Principles in the Pharmaceutical Sciences*, 4th ed.; Lea & Febiger: Philadelphia, PA, USA, 1993.
30. Yalkowsky, S.H. *Solubility and Solubilization in Aqueous Media*; American Chemical Society and Oxford University Press: New York, NY, USA, 1999.
31. Jouyban, A. *Handbook of Solubility Data for Pharmaceutical*; CRC Press: Boca Raton, FL, USA, 2010.
32. Delgado, D.R.; Holguin, A.R.; Almanza, O.A.; Martinez, F.; Marcus, Y. Solubility and preferential solvation of meloxicam in ethanol + water mixtures. *Fluid Phase Equilib.* **2011**, *305*, 88–95. [[CrossRef](#)]
33. Higuchi, T.; Connors, K.A. Phase solubility techniques. *Adv. Anal. Chem. Instrum.* **1965**, *4*, 117–212.
34. Kratky, O.; Leopold, H.; Stabinger, H. *DMA45 Calculating Digital Density Meter, Instruction Manual*; Anton Paar, K.G.: Graz, Austria, 1980.
35. Sathesh-Babu, P.R.; Subrahmanyam, C.V.S.; Thimmasetty, J.; Manavalan, R.; Valliappan, K. Extended Hansen’s solubility approach: Meloxicam in individual solvents. *Pak. J. Pharm. Sci.* **2007**, *20*, 311–316.
36. Castro, G.T.; Filippa, M.A.; Sancho, M.I.; Gasull, E.I.; Almandoz, M.C. Solvent effect on the solubility and absorption spectra of meloxicam: Experimental and theoretical calculations. *Phys. Chem. Liq.* **2020**, *58*, 337–348. [[CrossRef](#)]
37. Barton, A.F.M. *Handbook of Solubility Parameters and Other Cohesion Parameters*, 2nd ed.; CRC Press: Boca Raton, FL, USA, 1991.
38. Marcus, Y. *The Properties of Solvents*; John Wiley & Sons: Chichester, UK, 1998.
39. Connors, K.A. *Thermodynamics of Pharmaceutical Systems: An Introduction for Students of Pharmacy*; Wiley–Interscience: Hoboken, NJ, USA, 2002.
40. Fedors, R.F. A method for estimating both the solubility parameters and molar volumes of liquids. *Polym. Eng. Sci.* **1974**, *14*, 147–154. [[CrossRef](#)]
41. Kirchner, B.; Reiher, M. The secret of dimethyl sulfoxide–water mixtures. A quantum chemical study of 1DMSO–*n*-water clusters. *J. Am. Chem. Soc.* **2002**, *124*, 6206–6215. [[CrossRef](#)] [[PubMed](#)]
42. Lu, Z.; Manias, E.; Macdonald, D.D.; Lanagan, M. Dielectric relaxation in dimethyl sulfoxide/water mixtures studied by microwave dielectric relaxation spectroscopy. *J. Phys. Chem. A* **2009**, *113*, 12207–12214. [[CrossRef](#)] [[PubMed](#)]
43. Wu, X.Q.; Tang, P.X.; Li, S.S.; Zhang, L.L.; Li, H. X-ray powder diffraction data for meloxicam, C₁₄H₁₃N₃O₄S₂. *Powder Diffr.* **2014**, *29*, 196–198. [[CrossRef](#)]
44. Freitas, J.T.J.; Santos-Viana, O.M.M.; Bonfilio, R.; Doriguetto, A.C.; Benjamim de Araújo, M. Analysis of polymorphic contamination in meloxicam raw materials and its effects on the physicochemical quality of drug product. *Eur. J. Pharm. Sci.* **2017**, *109*, 347–358. [[CrossRef](#)] [[PubMed](#)]
45. Banerjee, R.; Sarkar, M. Spectroscopic studies of microenvironment dictated structural forms of piroxicam and meloxicam. *J. Lumin.* **2002**, *99*, 255–263. [[CrossRef](#)]
46. Luger, P.; Daneck, K.; Engel, W.; Trummlitz, G.; Wagner, K. Structure and physicochemical properties of meloxicam, a new NSAID. *Eur. J. Pharm. Sci.* **1996**, *4*, 175–187. [[CrossRef](#)]
47. Noolkar, S.B.; Jadhav, N.R.; Bhende, S.A.; Killedar, S.G. Solid-state characterization and dissolution properties of meloxicam–moringa coagulant–PVP ternary solid dispersions. *AAPS PharmSciTech* **2013**, *14*, 569–577. [[CrossRef](#)] [[PubMed](#)]
48. Sirisolla, J. Solubility enhancement of meloxicam by liquisolid technique and its characterization. *Int. J. Pharm. Sci. Res.* **2015**, *6*, 835–840. [[CrossRef](#)]

49. Alnaief, M.; Obaidat, R.; Mashaqbeh, H. Loading and evaluation of meloxicam and atorvastatin in carrageenan microspherical aerogels particles. *J. Appl. Pharm. Sci.* **2019**, *9*, 83–88. [[CrossRef](#)]
50. Kristl, A.; Vesnaver, G. Thermodynamic investigation of the effect of octanol–water mutual miscibility on the partitioning and solubility of some guanine derivatives. *J. Chem. Soc. Faraday Trans.* **1995**, *91*, 995–998. [[CrossRef](#)]
51. Jouyban, A.; Acree, W.E., Jr. Mathematical derivation of the Jouyban-Acree model to represent solute solubility data in mixed solvents at various temperatures. *J. Mol. Liq.* **2018**, *256*, 541–547. [[CrossRef](#)]
52. Jouyban-Gharamaleki, A.; Valaee, L.; Barzegar-Jalali, M.; Clark, B.J.; Acree, W.E., Jr. Comparison of various cosolvency models for calculating solute solubility in water-cosolvent mixtures. *Int. J. Pharm.* **1999**, *177*, 93–101. [[CrossRef](#)]
53. Yalkowsky, S.H.; Roseman, T.J. Solubilization of drugs by cosolvents. In *Techniques of Solubilization of Drugs*; Yalkowsky, S.H., Ed.; Marcel Dekker: New York, NY, USA, 1981; pp. 91–134.
54. Jouyban, A.; Romero, S.; Chan, H.K.; Clark, B.J.; Bustamante, P. A cosolvency model to predict solubility of drugs at several temperatures from a limited number of solubility measurements. *Chem. Pharm. Bull.* **2002**, *50*, 594–599. [[CrossRef](#)] [[PubMed](#)]
55. Dadmand, S.; Kamari, F.; Acree, W.E., Jr.; Jouyban, A. Solubility prediction of drugs in binary solvent mixtures at various temperatures using a minimum number of experimental data points. *AAPS PharmSciTech* **2019**, *20*, 10. [[CrossRef](#)]
56. Rahimpour, E.; Jouyban, A. Utilizing Abraham and Hansen solvation parameters for solubility prediction of meloxicam in cosolvency systems. *J. Mol. Liq.* **2021**, *328*, 115400. [[CrossRef](#)]
57. Krug, R.R.; Hunter, W.G.; Grieger, R.A. Enthalpy-entropy compensation. 1. Some fundamental statistical problems associated with the analysis of van't Hoff and Arrhenius data. *J. Phys. Chem.* **1976**, *80*, 2335–2341. [[CrossRef](#)]
58. Krug, R.R.; Hunter, W.G.; Grieger, R.A. Enthalpy-entropy compensation. 2. Separation of the chemical from the statistical effect. *J. Phys. Chem.* **1976**, *80*, 2341–2351. [[CrossRef](#)]
59. Ruidiaz, M.A.; Delgado, D.R.; Martínez, F.; Marcus, Y. Solubility and preferential solvation of indomethacin in 1,4-dioxane + water solvent mixtures. *Fluid Phase Equilib.* **2010**, *299*, 259–265. [[CrossRef](#)]
60. Aydi, A.; Dali, I.; Ghachem, K.; Al-Khazaal, A.Z.; Delgado, D.R.; Kolsi, L. Solubility of Hydroxytyrosol in binary mixture of ethanol + water from (293.15 to 318.15) K: Measurement, correlation, dissolution thermodynamics and preferential solvation. *Alex. Eng. J.* **2021**, *60*, 905–914. [[CrossRef](#)]
61. Bevington, P.R. *Data Reduction and Error Analysis for the Physical Sciences*; McGraw-Hill Book, Co.: New York, NY, USA, 1969; pp. 56–65.
62. Carstensen, J.T. *Modeling and Data Treatment in the Pharmaceutical Sciences*; Technomic Publishing Co., Inc.: Lancaster, PA, USA, 1996; pp. 127–159.
63. Barranté, J.R. *Applied Mathematics for Physical Chemistry*, 2nd ed.; Prentice Hall, Inc.: Upper Saddle River, NJ, USA, 1998; 227p.
64. Perlovich, G.L.; Kurkov, S.V.; Kinchin, A.N.; Bauer-Brandl, A. Thermodynamics of solutions III: Comparison of the solvation of (+)-naproxen with other NSAIDs. *Eur. J. Pharm. Biopharm.* **2004**, *57*, 411–420. [[CrossRef](#)] [[PubMed](#)]
65. Delgado, D.R.; Almanza, O.A.; Martínez, F.; Peña, M.A.; Jouyban, A.; Acree, W.E., Jr. Solution thermodynamics and preferential solvation of sulfamethazine in (methanol + water) mixtures. *J. Chem. Thermodyn.* **2016**, *97*, 264–276. [[CrossRef](#)]
66. Jouyban, K.; Agha, E.M.H.; Hemmati, S.; Martínez, F.; Kuentz, M.; Jouyban, A. Solubility of 5-aminosalicylic acid in N-methyl-2-pyrrolidone + water mixtures at various temperatures. *J. Mol. Liq.* **2020**, *310*, 113143. [[CrossRef](#)]
67. Romero, S.; Reillo, A.; Escalera, B.; Bustamante, P. The behaviour of paracetamol in mixtures of aprotic and amphiprotic-protic solvents. Relationship of solubility curves to specific and nonspecific interactions. *Chem. Pharm. Bull.* **1996**, *44*, 1061–1066. [[CrossRef](#)]
68. Tomlinson, E. Enthalpy-entropy compensation analysis of pharmaceutical, biochemical and biological systems. *Int. J. Pharm.* **1983**, *13*, 115–144. [[CrossRef](#)]
69. Leffler, J.E.; Grunwald, E. *Rates and Equilibria of Organic Reactions: As Treated by Statistical, Thermodynamic and Extrathermodynamic Methods*; Dover Publications Inc.: New York, NY, USA, 1989.
70. Bustamante, P.; Romero, S.; Reillo, A. Thermodynamics of paracetamol in amphiprotic and amphiprotic-protic solvent mixtures. *Pharm. Pharmacol. Commun.* **1995**, *1*, 505–507. [[CrossRef](#)]
71. Bustamante, P.; Romero, S.; Peña, A.; Escalera, B.; Reillo, A. Nonlinear enthalpy-entropy compensation for the solubility of drugs in solvent mixtures: Paracetamol, acetanilide and nalidixic acid in dioxane-water. *J. Pharm. Sci.* **1998**, *87*, 1590–1596. [[CrossRef](#)] [[PubMed](#)]
72. Martínez, F.; Peña, M.A.; Bustamante, P. Thermodynamic analysis and enthalpy-entropy compensation for the solubility of indomethacin in aqueous and non-aqueous mixtures. *Fluid Phase Equilib.* **2011**, *308*, 98–106. [[CrossRef](#)]
73. Marcus, Y. *Solvent Mixtures: Properties and Selective Solvation*; Marcel Dekker, Inc.: New York, NY, USA, 2002.
74. Marcus, Y. On the preferential solvation of drugs and PAHs in binary solvent mixtures. *J. Mol. Liq.* **2008**, *140*, 61–67. [[CrossRef](#)]
75. Marcus, Y. Preferential solvation of drugs in binary solvent mixtures. *Pharm. Anal. Acta* **2017**, *8*, 1000537. [[CrossRef](#)]
76. Martínez, F.; Jouyban, A.; Acree, W.E., Jr. Modelling the solubility and preferential solvation of bergenin in DMSO + water mixtures. *Lat. Am. J. Pharm.* **2016**, *35*, 2185–2190.
77. Ben-Naim, A. Preferential solvation in two- and in three-component systems. *Pure Appl. Chem.* **1990**, *62*, 25–34. [[CrossRef](#)]
78. Marcus, Y. Solubility and solvation in mixed solvent systems. *Pure Appl. Chem.* **1990**, *62*, 2069–2076. [[CrossRef](#)]
79. Acree, W.E., Jr. IUPAC-NIST Solubility Data Series. 102. Solubility of nonsteroidal anti-inflammatory drugs (NSAIDs) in neat organic solvents and organic solvent mixtures. *J. Phys. Chem. Ref. Data* **2014**, *43*, 023102. [[CrossRef](#)]

Article

Development of Abraham Model Correlations for Solute Transfer into the *tert*-Butyl Acetate Mono-Solvent and Updated Equations for Both Ethyl Acetate and Butyl Acetate

Laine Longacre, Emily Wu, Chelsea Yang, Miles Zhang, Sneha Sinha, Advika Varadharajan and William E. Acree, Jr. *

Department of Chemistry, University of North Texas, Denton, TX 76203, USA

* Correspondence: bill.acree@unt.edu

Abstract: Experimental solubilities were determined for 31 solid nonelectrolyte organic compounds dissolved in *tert*-butyl acetate at 298.15 K. Results of the experimental measurements were combined with published mole fraction solubility data for two lipid-lowering medicinal compounds (lovastatin and simvastatin) in order to derive Abraham model expressions for solute transfer into the *tert*-butyl acetate mono-solvent. The derived correlations provided an accurate mathematical description of the observed experimental data. As part of the current study, previously published Abraham model solvent correlations for both ethyl acetate and butyl acetate were updated using much larger datasets that contained an additional 64 and 35 experimental data points, respectively. The mathematical correlations presented in the current study describe the observed solubility ratios of solutes dissolved in *tert*-butyl acetate, ethyl acetate, and butyl acetate to within an overall standard deviation of 0.15 log units or less.

Keywords: Abraham model correlations; molar solubility ratios; *tert*-Butyl acetate solvent; ethyl acetate; butyl acetate solvent

Citation: Longacre, L.; Wu, E.; Yang, C.; Zhang, M.; Sinha, S.; Varadharajan, A.; Acree, W.E., Jr. Development of Abraham Model Correlations for Solute Transfer into the *tert*-Butyl Acetate Mono-Solvent and Updated Equations for Both Ethyl Acetate and Butyl Acetate. *Liquids* **2022**, *2*, 258–288. <https://doi.org/10.3390/liquids2040016>

Academic Editor: Cory Pye

Received: 8 September 2022

Accepted: 19 September 2022

Published: 22 September 2022

Publisher's Note: MDPI stays neutral with regard to jurisdictional claims in published maps and institutional affiliations.



Copyright: © 2022 by the authors. Licensee MDPI, Basel, Switzerland. This article is an open access article distributed under the terms and conditions of the Creative Commons Attribution (CC BY) license (<https://creativecommons.org/licenses/by/4.0/>).

1. Introduction

Individuals employed by the chemical manufacturing sector handle and are exposed to organic solvents on a daily basis. Organic solvents serve as the solubilizing reaction media in the preparation of new chemical products, as cleansing and degreasing agents for chemical glassware and industrial machinery, as components of aqueous–organic biphasic extraction systems used in the removal of unwanted impurities from synthesized chemical materials, and as dispersing agents in paint and cosmetic products. Organic solvents have also been used to extract biochemical materials from plants and to preconcentrate and remove trace organic analytes from chemical samples prior to gas–liquid and high-performance chromatographic analyses. Several million tons of petroleum-based organic solvents are purchased and discarded on an annual basis. Governmental regulations pertaining to chemical waste disposal have encouraged the manufacturing sector to utilize more environmentally compatible organic solvents, to search for solvent-free synthetic processes, and to design effective solvent recovery methods in order to reduce the quantity of hazardous materials that are released into the natural environment.

Replacing hazardous organic solvents with safer chemical alternatives is not an easy task. Industrial processes are often designed around the specific solvent that is currently being used. Altering an existing process can be an expensive endeavor, even if one has identified a safer solvent which possesses suitable physical and chemical properties. Our contribution in the solvent selection and replacement process has been to develop mathematical Abraham model expressions [1–4] that enable process design engineers to predict molar solubilities of chemical reactants, synthesized chemical products, and reaction by-products in a wide range of organic solvents of varying polarity and hydrogen-bonding

character. Unlike physical properties such as density, viscosity, and vapor pressure, one cannot easily locate needed solubility data in the published chemical and engineering literature. Solubility data is solute-solvent specific in nature, and it is not feasible to determine solubilities for every possible combination of chemical compounds. Currently there are more than 60 million known chemical compounds [5], and the number continually increases with each newly synthesized organic/inorganic molecule.

The Abraham model is among the simplest and most versatile predictive solubility expressions that have been developed in the past 30 years. The basic model [6–9] describes solute transfer, which, in the current study, is given by the logarithm of molar solubility ratios, $\log(C_{S,\text{organic}}/C_{S,\text{water}})$, and $\log(C_{S,\text{organic}}/C_{S,\text{gas}})$, in terms of:

$$\log(C_{S,\text{organic}}/C_{S,\text{water}}) = e_{\text{eq}1} \times \mathbf{E} + s_{\text{eq}1} \times \mathbf{S} + a_{\text{eq}1} \times \mathbf{A} + b_{\text{eq}1} \times \mathbf{B} + v_{\text{eq}1} \times \mathbf{V} + c_{\text{eq}1} \quad (1)$$

$$\log(C_{S,\text{organic}}/C_{S,\text{gas}}) = e_{\text{eq}2} \times \mathbf{E} + s_{\text{eq}2} \times \mathbf{S} + a_{\text{eq}2} \times \mathbf{A} + b_{\text{eq}2} \times \mathbf{B} + l_{\text{eq}2} \times \mathbf{L} + c_{\text{eq}2} \quad (2)$$

the molecular solute–solvent interactions that govern the dissolution process. The subscripts “organic”, “water”, and “gas” on solubility ratios denote the phase to which the molar solute concentration pertains. Each molecular interaction is quantified as the product of a solute property multiplied by the complimentary solvent property. Solute properties (also called solute descriptors) are denoted by the capitalized alphabetical characters on the right-hand side of Equations (1) and (2) and are defined as follows: **A** and **B** refer to the respective overall hydrogen-bond donating and accepting capacities of the dissolved solute; **E** corresponds the molar refraction of the given solute (in units of $(\text{cm}^3 \text{ mol}^{-1})/10$) in excess of that of a linear alkane having a comparable molecular size; **L** is the logarithm of the solute’s gas-to-hexadecane partition coefficient determined at 298.15 K; **S** represents a combination of the electrostatic polarity and polarizability of the solute; **V** denotes the McGowan molecular volume of the solute (in units of $(\text{cm}^3 \text{ mol}^{-1})/100$) calculated from atomic sizes and chemical bond numbers. The complimentary solvent properties in Equations (1) and (2) are given by the lowercase alphabetical characters ($c_{\text{eq}1}$, $e_{\text{eq}1}$, $s_{\text{eq}1}$, $a_{\text{eq}1}$, $b_{\text{eq}1}$, $v_{\text{eq}1}$, $c_{\text{eq}2}$, $e_{\text{eq}2}$, $s_{\text{eq}2}$, $a_{\text{eq}2}$, $b_{\text{eq}2}$, and $l_{\text{eq}2}$). Numerical values of the solvent properties are determined by regressing measured molar solubility ratio data in accordance with Equations (1) and (2). Once determined, the lowercase alphabetical characters allow one to predict the molar solubilities of additional solutes in the given organic solvent, provided, of course, that the solute descriptors are known. Currently, equation coefficients are known for slightly more than 130 different organic solvents and binary aqueous-organic solvent mixtures [10]. This represents only a small fraction of the organic solvents currently used in industrial manufacturing processes and consumer product formulations. Less than half of the solvents for which equation coefficients have been obtained fall into the classification of “preferred” and/or “recommended” on the solvent selection guide developed by pharmaceutical companies [11–13].

In the current study, we extend our earlier considerations to include the *tert*-butyl acetate mono-solvent, which is on the list of “recommended” organic solvents [14], along with several other alkyl acetates like ethyl acetate, propyl acetate, isopropyl acetate, and butyl acetate [11,15–17]. Alkyl acetates and other esters score well on published solvent selection guides because of their low toxicity and preparation from biomass materials [18]. Abraham predictive expressions are reported for *tert*-butyl acetate based on our measured solubility data for acenaphthene, acetylsalicylic acid, anthracene, benzil, benzoic acid, benzoin, 4-*tert*-butylbenzoic acid, 1-chloroanthraquinone, 3-chlorobenzoic acid, 4-chlorobenzoic acid, 2-chloro-5-nitrobenzoic acid, 4-chloro-3-nitrobenzoic acid, 3,4-dichlorobenzoic acid, 3,4-dimethoxybenzoic acid, 3,5-dinitrobenzoic acid, diphenyl sulfone, 2-ethylanthraquinone, hippuric acid, 2-hydroxybenzoic acid, 2-methoxybenzoic acid, 4-methoxybenzoic acid, 2-methylbenzoic acid, 3-methylbenzoic acid, 2-methyl-3-nitrobenzoic acid, 3-methyl-4-nitrobenzoic acid, 4-methyl-3-nitrobenzoic acid, 3-nitrobenzoic acid, 4-nitrobenzoic acid, salicylamide, 3,4,5-trimethoxybenzoic acid, and xanthene. In total, mole fraction solubilities

have been determined for 31 crystalline organic compounds dissolved in *tert*-butyl acetate at 298.15 K.

As part of the current study, we are also revising our existing Abraham model mathematical correlations for both ethyl acetate (dry, anhydrous) [19]:

$$\log P \text{ and } \log (C_{S,\text{organic}}/C_{S,\text{water}}) = 0.328(0.034) + 0.369(0.057)\mathbf{E} - 0.446(0.080)\mathbf{S} \\ - 0.700(0.069)\mathbf{A} - 4.904(0.113)\mathbf{B} + 4.150(0.033)\mathbf{V} \quad (3) \\ (N = 106, SD = 0.165, R^2 = 0.996, F = 4475.1)$$

$$\log K \text{ and } \log (C_{S,\text{organic}}/C_{S,\text{gas}}) = 0.182(0.026) - 0.352(0.048)\mathbf{E} + 1.316(0.050)\mathbf{S} \\ + 2.891(0.061)\mathbf{A} + 0.916(0.008)\mathbf{L} \quad (4) \\ (N = 106, SD = 0.148, R^2 = 0.998, F = 15,635.1)$$

and butyl acetate (dry, anhydrous) [19]:

$$\log P \text{ and } \log (C_{S,\text{organic}}/C_{S,\text{water}}) = 0.248(0.047) + 0.356(0.065)\mathbf{E} - 0.501(0.082)\mathbf{S} \\ - 0.867(0.096)\mathbf{A} - 4.973(0.100)\mathbf{B} + 4.281(0.027)\mathbf{V} \quad (5) \\ (N = 73, SD = 0.160, R^2 = 0.998, F = 7380)$$

$$\log K \text{ and } \log (C_{S,\text{organic}}/C_{S,\text{gas}}) = 0.147(0.040) - 0.414(0.064)\mathbf{E} + 1.212(0.077)\mathbf{S} \\ + 2.623(0.086)\mathbf{A} + 0.954(0.007)\mathbf{L} \quad (6) \\ (N = 73, SD = 0.157, R^2 = 0.998, F = 6174.7)$$

as there has been sufficient new experimental data [19–88] published since 2008, when the earlier correlations first appeared, to merit a redetermination of the equation coefficients. Equations (3)–(6) are based on 106 and 73 experimental molar solubility ratios; indirect water-to-alkyl acetate transfer coefficients, *P*; and gas-to-alkyl acetate partition coefficients, *K*, respectively. The updated correlations reported in the current study are based on much larger, more chemically diverse data sets, which include 170 (ethyl acetate) and 108 (butyl acetate) solutes. It is the chemical diversity, as reflected by the solute descriptor values, that defines the area of predictive chemical space over which a derived Abraham correlation can be used. One should not use a mathematical correlation to make predictions for solutes whose descriptor values fall too far outside of the range of values used in determining the equation coefficients.

The words ‘dry, anhydrous’ after the solvent name indicate that the organic solvent was not in direct contact with water, as would be the case for practical partitioning processes involving the removal of the solute from water with ethyl acetate or butyl acetate as the extracting organic solvent. Abraham model correlations have been published for “wet” ethyl acetate and “wet” butyl acetate in an earlier paper [19]; however, there has not been sufficient new experimental water-to-ethyl acetate and water-to-butyl acetate partition coefficient data to merit updating these existing “wet” Abraham model correlations.

The statistical information associated with Equations (3)–(6) appears immediately below the equation itself and includes the number of experimental data points used in the regression analysis, *N*; the standard deviation, *SD*; the squared correlation coefficient, *R*²; and the Fisher *F*-statistic, *F*. The numerical values contained within parenthesis that immediately follow each equation coefficient are the standard error in the respective calculated coefficient. As an informational item, the *b* × **B** term is missing in Equations (4) and (6), because both ethyl acetate and butyl acetate lack an acidic hydrogen, and thus, they cannot act as an H-bond donor. The term does appear in Equations (3) and (5), as here, the *b*-coefficients represent the difference in the H-bond acidity of the alkyl acetate solvent(s) and water. Water does possess an H-bond donor character.

2. Experimental Methodology

The crystalline organic solutes selected for the solubility study include 22 carboxylic acids as well as 9 noncarboxylic acid solutes possessing relatedly large **E** and **S** descriptor values. All chemicals used in the current study were purchased from commercial sources

in the highest purity available. Several of the compounds were further purified by recrystallization from either acetone or anhydrous methanol prior to performing the solubility measurements. All solid compounds were dried for two days at 333 K. Purification details and chemical suppliers are given in Table 1, along with the final purities as determined by either a gas–liquid chromatographic analysis (noncarboxylic acid solutes, flame ionization detector) or the non-aqueous acid–base titrimetric method based on a modified procedure recommended by Fritz and Lisicki [89]. Our modified titration procedure replaced benzene with toluene as a component in the titration solvent for health reasons.

Table 1. Chemical sources and final mass fraction purities of chemicals used in the solubility studies.

Chemical	Supplier	Purification Method	Purity (Mass Fraction)
<i>tert</i> -Butyl acetate	TCI America, Portland, OR, USA	Stored over activated molecular sieves and distilled	0.997
1-Chloroanthraquinone	Aldrich Chemical Company, Milwaukee, WI, USA	Recrystallized from anhydrous methanol	0.997
2-Ethylanthraquinone	Aldrich Chemical Company	Recrystallized from anhydrous methanol	0.996
Acenaphthene	Aldrich Chemical Company	Recrystallized from anhydrous methanol	0.997
Benzil	Aldrich Chemical Company	Recrystallized from anhydrous methanol	0.997
Anthracene	Aldrich Chemical Company	Recrystallized from anhydrous acetone	0.997
Acetylsalicylic acid	Aldrich Chemical Company	Dried for two days at 333 K	0.998
Diphenyl sulfone	Aldrich Chemical Company	Recrystallized from anhydrous methanol	0.996
Salicylamide	Aldrich Chemical Company	Recrystallized from anhydrous methanol	0.997
Benzoin	Aldrich Chemical Company	Recrystallized from anhydrous methanol	0.997
Xanthene	Aldrich Chemical Company	Recrystallized from anhydrous methanol	0.996
Benzoic acid	Aldrich Chemical Company	Dried for two days at 333 K	0.998
4- <i>tert</i> -Butylbenzoic acid	TCI America Chemical Company	Dried for two days at 333 K	0.998
3-Chlorobenzoic acid	Aldrich Chemical Company	Dried for two days at 333 K	0.997
4-Chlorobenzoic acid	Acros Organics, Morris Plains, NJ, USA	Dried for two days at 333 K	0.996
2-Chloro-5-nitrobenzoic acid	Acros Organics	Dried for two days at 333 K	0.998
4-Chloro-3-nitrobenzoic acid	Acros Organics	Dried for two days at 333 K	0.998
3,4-Dichlorobenzoic acid	Aldrich Chemical Company	Dried for two days at 333 K	0.998
Hippuric acid	TCI America	Dried for two days at 333 K	0.997
2-Hydroxybenzoic acid	Aldrich Chemical Company	Dried for two days at 333 K	0.997
2-Methoxybenzoic acid	Aldrich Chemical Company	Dried for two days at 333 K	0.998
4-Methoxybenzoic acid	Aldrich Chemical Company	Dried for two days at 333 K	0.998
3,4-Dimethoxybenzoic acid	Acros Organics	Dried for two days at 333 K	0.998
3,4,5-Trimethoxybenzoic acid	Aldrich Chemical Company	Dried for two days at 333 K	0.998
2-Methylbenzoic acid	Aldrich Chemical Company	Dried for two days at 333 K	0.998
3-Methylbenzoic acid	Aldrich Chemical Company	Dried for two days at 333 K	0.998
2-Methyl-3-nitrobenzoic acid	Aldrich Chemical Company	Dried for two days at 333 K	0.997
3-Methyl-4-nitrobenzoic acid	Aldrich Chemical Company	Dried for two days at 333 K	0.997
4-Methyl-3-nitrobenzoic acid	Aldrich Chemical Company	Dried for two days at 333 K	0.998
3-Nitrobenzoic acid	Aldrich Chemical Company	Dried for two days at 333 K	0.996
4-Nitrobenzoic acid	Acros Organics	Dried for two days at 333 K	0.998
3,5-Dinitrobenzoic acid	Aldrich Chemical Company	Dried for two days at 333 K	0.997
Toluene	Aldrich Chemical Company	None	0.998, anhydrous
Sodium methoxide, 25 mass % solution in methanol	Aldrich Chemical Company	None	
2-Propanol	Aldrich Chemical Company	None	0.99

Solubilities of the organic compounds, except for 2-hydroxybenzoic acid and 2-methyl-3-nitrobenzoic acid, were determined using a well-established spectrophotometric method of chemical analysis. Solubilities of 2-hydroxybenzoic acid and 2-methyl-3-nitrobenzoic acid were measured by volumetric acid–base titrations to the phenolphthalein endpoint using a standardized aqueous-sodium hydroxide titrant. In both analytical methods, weighed

aliquots of the saturated solutions were transferred into volumetric (for spectrophotometric method) or Erlenmeyer (for titrimetric method) flasks after an initial three-day equilibration in constant-temperature water at 298.15 ± 0.05 K. The samples were periodically shaken to facilitate mixing and dissolution of the solid solute. In the case of the spectrophotometric determinations, the transferred aliquot was quantitatively diluted with 2-propanol. Additional dilutions were performed if necessary in order for the samples' absorbencies to fall on the Beer–Lambert Law calibration curve, established by graphing the measured absorbances versus the molar concentrations of the nine standard solutions having a known molar solute concentration. All absorbance measurements were recorded on a Milton Roy Spectronic 1000 Plus spectrophotometer. The analysis wavelengths and molar concentration ranges of the standard solutions are reported in Table 2 for each of the analytes, whose solubility was determined by the spectrophotometric method. Attainment of equilibrium was established by performing replicate measurements on the equilibrated samples after two (and in some cases three) additional days of equilibrium. In all instances, the replicate measurements confirmed that equilibrium had been obtained after the initial three-day equilibrium period.

Table 2. Analysis wavelengths and concentration ranges of standard solutions used in the spectrophotometric determination of solubility.

Chemical	Analysis Wavelength	Molar Concentration Range
1-Chloroanthraquinone	337 (nm)	8.79×10^{-5} to 2.93×10^{-4}
2-Ethylantraquinone	325 (nm)	1.21×10^{-4} to 4.04×10^{-4}
Acenaphthene	289 (nm)	8.05×10^{-5} to 2.68×10^{-4}
Benzil	390 (nm)	5.49×10^{-3} to 1.83×10^{-2}
Anthracene	356 (nm)	6.76×10^{-5} to 2.25×10^{-4}
Acetylsalicylic acid	272 (nm)	4.19×10^{-4} to 1.40×10^{-3}
Diphenyl sulfone	267 (nm)	2.71×10^{-4} to 9.03×10^{-4}
Salicylamide	300 (nm)	1.06×10^{-4} to 3.55×10^{-4}
Benzoin	313 (nm)	1.11×10^{-3} to 3.71×10^{-3}
Xanthene	280 (nm)	1.79×10^{-4} to 5.95×10^{-4}
Benzoic acid	275 (nm)	4.88×10^{-4} to 1.63×10^{-3}
4- <i>tert</i> -Butylbenzoic acid	275 (nm)	2.86×10^{-4} to 9.54×10^{-4}
3-Chlorobenzoic acid	280 (nm)	4.99×10^{-4} to 1.66×10^{-3}
4-Chlorobenzoic acid	272 (nm)	4.60×10^{-4} to 1.53×10^{-3}
2-Chloro-5-nitrobenzoic acid	280 (nm)	8.79×10^{-5} to 2.93×10^{-4}
4-Chloro-3-nitrobenzoic acid	292 (nm)	3.72×10^{-4} to 1.34×10^{-3}
3,4-Dichlorobenzoic acid	280 (nm)	4.60×10^{-4} to 1.53×10^{-3}
Hippuric acid	269 (nm)	6.74×10^{-4} to 2.25×10^{-3}
2-Methoxybenzoic acid	295 (nm)	1.61×10^{-4} to 5.37×10^{-4}
4-Methoxybenzoic acid	273 (nm)	9.72×10^{-5} to 3.24×10^{-4}
3,4-Dimethoxybenzoic acid	286 (nm)	9.23×10^{-5} to 3.08×10^{-4}
3,4,5-Trimethoxybenzoic acid	289 (nm)	1.35×10^{-4} to 4.49×10^{-4}
2-Methylbenzoic acid	279 (nm)	4.49×10^{-4} to 1.50×10^{-3}
3-Methylbenzoic acid	280 (nm)	3.97×10^{-4} to 1.32×10^{-3}
3-Methyl-4-nitrobenzoic acid	295 (nm)	1.73×10^{-4} to 5.78×10^{-4}
4-Methyl-3-nitrobenzoic acid	295 (nm)	3.29×10^{-4} to 1.10×10^{-3}
3-Nitrobenzoic acid	280 (nm)	1.51×10^{-4} to 5.06×10^{-4}
4-Nitrobenzoic acid	272 (nm)	4.51×10^{-5} to 1.50×10^{-4}
3,5-Dinitrobenzoic acid	267 (nm)	6.35×10^{-5} to 2.12×10^{-4}

To check for possible solid–solvate formation and/or possible solid-to-solid phase transition during the solution equilibration time, we did determine the melting point temperature of the solid material recovered from each saturated solution after the solubility measurements were performed. As shown in Table 3, the measured point temperature was within experimental error of the melting point temperature of the purchased commercial sample or the recrystallized compound prior to being placed in contact with the *tert*-butyl acetate mono-solvent. No indication of solid–solvate formation or polymorphism was observed.

Table 3. Comparison of the melting point temperatures of the crystalline solutes prior to contact with *tert*-butyl acetate, $T_{mp,initial}$, and of the recovered crystalline solute in equilibrium with the saturated solution, $T_{mp,equilibrated}$.

Solute	$T_{mp,initial}/K$	$T_{mp,equilibrated}/K$
Benzil	368.5 ± 0.5	368.2 ± 0.4
Anthracene	490.3 ± 0.4	490.0 ± 0.5
Acenaphthene	367.0 ± 0.4	367.2 ± 0.5
Xanthene	374.6 ± 0.5	374.3 ± 0.5
1-Chloroanthraquinone	435.4 ± 0.5	435.2 ± 0.4
Benzoic acid	395.6 ± 0.4	395.8 ± 0.4
4- <i>tert</i> -Butylbenzoic acid	441.7 ± 0.6	441.6 ± 0.4
3-Chlorobenzoic acid	427.9 ± 0.4	428.1 ± 0.3
4-Chlorobenzoic acid	512.5 ± 0.3	512.8 ± 0.4
3,4-Dichlorobenzoic acid	479.2 ± 0.5	479.1 ± 0.4
3,4-Dimethoxybenzoic acid	454.3 ± 0.4	454.5 ± 0.5
3,4,5-Trimethoxybenzoic acid	445.6 ± 0.6	445.8 ± 0.5
2-Hydroxybenzoic acid	432.7 ± 0.5	432.9 ± 0.5
2-Methoxybenzoic acid	374.7 ± 0.5	374.8 ± 0.4
4-Methoxybenzoic acid	456.6 ± 0.5	456.3 ± 0.4
2-Methylbenzoic acid	376.5 ± 0.4	376.7 ± 0.4
3-Methylbenzoic acid	382.4 ± 0.4	382.5 ± 0.4
2-Methyl-3-nitrobenzoic acid	455.5 ± 0.4	455.2 ± 0.5
3-Methyl-4-nitrobenzoic acid	490.7 ± 0.5	491.0 ± 0.5
4-Methyl-3-nitrobenzoic acid	461.2 ± 0.6	461.6 ± 0.6
3-Nitrobenzoic acid	414.7 ± 0.4	414.4 ± 0.5
4-Nitrobenzoic acid	512.6 ± 0.5	512.5 ± 0.4
3,5-Dinitrobenzoic acid	481.4 ± 0.5	481.3 ± 0.4
2-Chloro-5-nitrobenzoic acid	440.1 ± 0.5	440.4 ± 0.5
4-Chloro-3-nitrobenzoic acid	456.3 ± 0.5	456.5 ± 0.5
2-Ethylanthraquinone	383.9 ± 0.5	384.2 ± 0.5
Diphenyl sulfone	398.2 ± 0.4	397.9 ± 0.5
Acetylsalicylic acid	413.7 ± 0.5	413.3 ± 0.6
Salicylamide	413.2 ± 0.5	413.4 ± 0.4
Benzoin	410.4 ± 0.4	410.7 ± 0.5
Hippuric acid	463.2 ± 0.5	462.8 ± 0.5

3. Results and Discussion

The experimental mole fraction solubilities, $X_{S,\text{organic}}$, of the 31 different crystalline organic solutes dissolved in *tert*-butyl acetate are tabulated in the second and fourth columns of Table 4. The numerical values represent the average of 4–7 independent experimental determinations, which were reproducible to within $\pm 2.5\%$ (relative error). We were not able to find, in the published chemical and engineering literature, solubility data for these organic solutes in *tert*-butyl acetate that we could compare our experimental values against. The only published experimental solubility data that we found was for lovastatin. Nti-Gyabaah and coworkers previously had measured the solubility of lovastatin [23] and simvastatin [88] in seven alkyl acetates between 285 K and 313 K using a high-performance liquid chromatographic method of chemical analysis. The solubility data for both lipid-lowering drug molecules will be used in our determination of the Abraham model equation coefficients for *tert*-butyl acetate. Both lovastatin ($S = 2.730$, $B = 1.760$, $V = 3.2853$, and $L = 15.459$) and simvastatin ($S = 2.550$, $B = 1.860$, $V = 3.4628$, and $L = 15.551$) possess large numerical values for several solute descriptors.

Development of a meaningful Abraham model correlation generally requires somewhere between 30 to 40 experimental values [90,91] that cover a sufficient range of solute descriptor values to enable one to make predictions for a large number of additional solutes. In the case of *tert*-butyl acetate, we have the 31 experimental mole fraction solubilities tabulated in Table 3, as well as the mole fraction solubility data for lovastatin [23] and simvastatin [88], which were retrieved from our search of the published literature. There were two additional experimental values that could be used in our regression analysis, and those were the gas-to-*tert*-butyl acetate partition coefficient and water-to-*tert*-butyl acetate transfer coefficient derived from the vapor pressure of *tert*-butyl acetate and the Raoult's law infinite dilution activity coefficient of *tert*-butyl acetate dissolved in itself. By definition, the Raoult's Law infinite dilution activity coefficient of a compound dissolved in itself is unity. The calculation of $\log K$ and $\log P$ from activity coefficients is described in greater detail in the published paper [19] that reported the existing Abraham model correlations for ethyl acetate and butyl acetate. In total, we have experimental solubilities and partition coefficients/transfer coefficients for 34 different solutes.

The Abraham model correlates the logarithms of molar solubility ratios, $\log(C_{S,\text{organic}}/C_{S,\text{water}})$ and $\log(C_{S,\text{organic}}/C_{S,\text{gas}})$, and not the mole fraction solubilities, as with our measured data given in Table 4. The tabulated mole fraction solubility data in Table 4 is converted into molar solubilities by dividing $X_{S,\text{organic}}$ by the ideal molar volume of the saturated solution (i.e., $C_{S,\text{organic}} \approx X_{S,\text{organic}}/[X_{S,\text{organic}}V_{\text{Solute}} + (1 - X_{S,\text{organic}})V_{\text{Solvent}}]$). A numerical value of $V_{\text{solvent}} = 0.13550 \text{ L mol}^{-1}$ was used for the molar volume of *tert*-butyl acetate. The numerical values of the molar volumes of the hypothetical subcooled liquid solutes were given in our earlier publications [24,40–42,53–57,92–107], along with the aqueous molar solubilities, $C_{S,\text{water}}$, and solute molar gas concentrations, $C_{S,\text{gas}}$, needed in obtaining the two molar solubility ratios. Published mole fraction solubilities of lovastatin and simvastatin were converted to molar solubility ratios in a similar fashion. The experimental $\log(C_{S,\text{organic}}/C_{S,\text{gas}})$ and $\log(C_{S,\text{organic}}/C_{S,\text{water}})$ values at 298.15 K for 33 solutes dissolved in *tert*-butyl acetate are listed in Table 5. Also included in Table 5 is the logarithm of the water-to-*tert*-butyl acetate transfer coefficient, $\log P$, and gas-to-*tert*-butyl acetate partition coefficient, $\log K$, for the solute *tert*-butyl acetate itself.

Once both sets of molar solubility ratios were calculated, we constructed a series of Abraham model $\log(C_{S,\text{organic}}/C_{S,\text{water}})$ and $\log(C_{S,\text{organic}}/C_{S,\text{gas}})$ equations by substituting the numerical solubility ratios and solute descriptors into Equations (1) and (2). Solute descriptors needed in constructing the Abraham model equations are given in Table 6. As an informational note, several of the compounds listed in Table 6 used the alternant hydrogen-bond basicity descriptor, B° , in “wet” water-organic solvents when the wet organic solvent contained appreciable quantities of water. For most solutes, B and B° were numerically equal but did differ mainly for alkylanilines, alkyipyridines, and sulfoxides.

Table 4. Mole fraction solubilities, $X_{S,organic}$, of select crystalline nonelectrolyte organic compounds dissolved in *tert*-butyl acetate at a temperature of 298.15 K and ambient atmospheric pressure of 101 kPa ^a.

Chemical Name	$X_{S,organic}$	Chemical Name	$X_{S,organic}$
1-Chloroanthraquinone	0.003494	3,4-Dichlorobenzoic acid	0.01216
2-Ethylanthraquinone	0.02086	2-Hydroxybenzoic acid	0.1187
Acenaphthene	0.09654	Hippuric acid	0.0005241
Benzil	0.09184	2-Methoxybenzoic acid	0.02938
Anthracene	0.003755	4-Methoxybenzoic acid	0.006635
Acetylsalicylic acid	0.02041	3,4-Dimethoxybenzoic acid	0.003625
Diphenyl sulfone	0.02108	3,4,5-Trimethoxybenzoic acid	0.007172
Salicylamide	0.04114	2-Methylbenzoic acid	0.1170
Benzoïn	0.006353	3-Methylbenzoic acid	0.1114
Xanthene	0.08530	2-Methyl-3-nitrobenzoic acid	0.02141
Benzoic acid	0.1295	3-Methyl-4-nitrobenzoic acid	0.008034
4- <i>tert</i> -Butylbenzoic acid	0.06369	4-Methyl-3-nitrobenzoic acid	0.01549
3-Chlorobenzoic acid	0.04934	3-Nitrobenzoic acid	0.07749
4-Chlorobenzoic acid	0.007404	4-Nitrobenzoic acid	0.006436
2-Chloro-5-nitrobenzoic acid	0.03879	3,5-Dinitrobenzoic acid	0.02331
4-Chloro-3-nitrobenzoic acid	0.01991		

^a Standard uncertainties and relative uncertainties are $u(T) = 0.05$ K; $u(p) = 5$ kPa; and $u_r(x) = 0.025$.

Table 5. Experimental logarithms of molar solubility ratios; water-to-*tert*-butyl acetate transfer coefficients, $\log P$; and gas-to-*tert*-butyl acetate partition coefficients, $\log K$, at 298.15 K.

Solute	$\log K^a$	$\log P^b$
<i>tert</i> -Butyl acetate	3.53 ^c	2.09
Benzil	8.74	3.87
Anthracene	7.90	4.87
Acenaphthene	6.75	4.39
Xanthene	7.51	5.01
1-Chloroanthraquinone	9.99	3.95
Benzoic acid	6.68	1.54
4- <i>tert</i> -Butylbenzoic acid	8.79	3.56
3-Chlorobenzoic acid	7.36	2.22
4-Chlorobenzoic acid	7.10	2.30
3,4-Dichlorobenzoic acid	7.67	2.93
3,4-Dimethoxybenzoic acid	9.37	0.92
3,4,5-Trimethoxybenzoic acid	10.53	1.27
2-Hydroxybenzoic acid	7.23	1.87
2-Methoxybenzoic acid	7.69	0.89
4-Methoxybenzoic acid	8.19	1.49
2-Methylbenzoic acid	6.30	2.00
3-Methylbenzoic acid	7.04	2.06

Table 5. Cont.

Solute	Log K ^a	Log P ^b
2-Methyl-3-nitrobenzoic acid	8.65	1.91
3-Methyl-4-nitrobenzoic acid	8.37	2.00
4-Methyl-3-nitrobenzoic acid	9.03	1.72
3-Nitrobenzoic acid	8.37	1.44
4-Nitrobenzoic acid	8.56	1.66
3,5-Dinitrobenzoic acid	9.95	1.65
2-Chloro-5-nitrobenzoic acid	9.00	2.05
4-Chloro-3-nitrobenzoic acid	9.38	2.17
2-Ethylantraquinone	9.53	4.71
Diphenyl sulfone	10.22	2.83
Acetylsalicylic acid	9.36	0.86
Salicylamide	8.92	1.24
Benzoin	11.07	2.34
Hippuric acid	11.72	−0.55
Lovastatin	18.10	4.09
Simvastatin	18.17	4.23

^a For the crystalline solutes, the experimental value was $\log(C_{S,organic}/C_{S,gas})$. The estimated uncertainty in $\log(C_{S,organic}/C_{S,water})$ was 0.02, based on uncertainties in the mole fraction solubilities. ^b For the crystalline solutes the experimental value was $\log(C_{S,organic}/C_{S,water})$. The estimated uncertainty in $\log(C_{S,organic}/C_{S,water})$ was 0.02, based on uncertainties in the mole fraction solubilities. ^c Log K was calculated based on an activity coefficient of unity for *tert*-butyl acetate dissolved in *tert*-butyl acetate.

Table 6. Solute descriptors of the compounds used in the regression analysis for determining the Abraham model correlations for *tert*-butyl acetate, ethyl acetate, and butyl acetate.

Solute	E	S	A	B	L	V
Radon	0.000	0.000	0.000	0.000	0.877	0.3840
Hydrogen	0.000	0.000	0.000	0.000	−1.200	0.1086
Oxygen	0.000	0.000	0.000	0.000	−0.723	0.1830
Nitrogen	0.000	0.000	0.000	0.000	−0.978	0.2222
Carbon monoxide	0.000	0.000	0.000	0.040	−0.836	0.2220
Sulfur dioxide	0.370	0.660	0.240	0.190	0.778	0.3465
Ethane	0.000	0.000	0.000	0.000	0.492	0.3904
2-Methylpropane	0.000	0.000	0.000	0.000	1.409	0.6722
Pentane	0.000	0.000	0.000	0.000	2.162	0.8131
Hexane	0.000	0.000	0.000	0.000	2.668	0.9540
Heptane	0.000	0.000	0.000	0.000	3.173	1.0949
Octane	0.000	0.000	0.000	0.000	3.677	1.2358
Nonane	0.000	0.000	0.000	0.000	4.182	1.3767
Octadecane	0.000	0.000	0.000	0.000	8.722	2.6448
Nonadecane	0.000	0.000	0.000	0.000	9.226	2.7857
Eicosane	0.000	0.000	0.000	0.000	9.731	2.9266

Table 6. Cont.

Solute	E	S	A	B	L	V
Docosane	0.000	0.000	0.000	0.000	10.740	3.2084
Tricosane	0.000	0.000	0.000	0.000	11.252	3.3493
Tetracosane	0.000	0.000	0.000	0.000	11.758	3.4902
Octacosane	0.000	0.000	0.000	0.000	13.780	4.0538
2-Methylpentane	0.000	0.000	0.000	0.000	2.503	0.9540
2,4-Dimethylpentane	0.000	0.000	0.000	0.000	2.809	1.0949
2,5-Dimethylhexane	0.000	0.000	0.000	0.000	3.308	1.2358
2,3,4-Trimethylpentane	0.000	0.000	0.000	0.000	3.481	1.2358
Cyclohexane	0.305	0.100	0.000	0.000	2.964	0.8454
Ethylcyclohexane	0.263	0.100	0.000	0.000	3.877	1.1272
Propene	0.103	0.080	0.000	0.070	0.946	0.4883
<i>trans</i> -But-2-ene	0.126	0.080	0.000	0.050	1.664	0.6292
Pent-1-ene	0.093	0.080	0.000	0.070	2.047	0.7701
2-Methylprop-1-ene	0.120	0.080	0.000	0.080	1.579	0.6292
3-Methylbut-1-ene	0.063	0.060	0.000	0.050	1.933	0.7701
Hept-1-ene	0.092	0.080	0.000	0.070	3.063	1.0519
Buta-1,2-diene	0.320	0.230	0.000	0.100	1.543	0.5862
2-Methylbuta-1,3-diene	0.313	0.230	0.000	0.100	2.101	0.7271
Hepta-1,6-diene	0.189	0.200	0.000	0.100	3.028	1.0089
Dichloromethane	0.387	0.570	0.100	0.050	2.019	0.4943
Trichloromethane	0.425	0.490	0.150	0.020	2.480	0.6167
Tetrachloromethane	0.458	0.380	0.000	0.000	2.823	0.7391
1,2-Dichloroethane	0.416	0.640	0.100	0.110	2.573	0.6352
1-Chloropropane	0.216	0.400	0.000	0.100	2.202	0.6537
1-Chlorobutane	0.210	0.400	0.000	0.100	2.722	0.7946
2-Chloro-2-methylpropane	0.142	0.300	0.000	0.030	2.273	0.7946
Bromoethane	0.366	0.400	0.000	0.120	2.120	0.5654
2-Bromo-2-methylpropane	0.305	0.290	0.000	0.070	2.609	0.8472
Iodomethane	0.676	0.430	0.000	0.120	2.106	0.5077
Iodoethane	0.640	0.400	0.000	0.140	2.573	0.6486
1,1,2-Trifluorotrichloroethane	0.010	0.130	0.000	0.000	2.210	0.8107
1,2-Difluorotetrachloroethane	0.227	0.330	0.000	0.020	3.034	0.9154
Tetrahydrofuran	0.289	0.520	0.000	0.480	2.636	0.6223
1,4-Dioxane	0.329	0.750	0.000	0.640	2.892	0.6810
2-Methylpropionaldehyde	0.144	0.620	0.000	0.450	2.120	0.6879
Propanone	0.179	0.700	0.040	0.490	1.696	0.5470
Butanone	0.166	0.700	0.000	0.510	2.287	0.6879
Ethyl acetate	0.106	0.620	0.000	0.450	2.314	0.7466
Butyl acetate	0.071	0.600	0.000	0.450	3.353	1.0284

Table 6. Cont.

Solute	E	S	A	B	L	V
Acetonitrile	0.237	0.900	0.070	0.320	1.739	0.4042
Propionitrile	0.162	0.900	0.020	0.360	2.082	0.5450
Diethylamine	0.154	0.300	0.080	0.690	2.395	0.7220
Triethylamine	0.101	0.150	0.000	0.790	3.040	1.0538
Nitromethane	0.313	0.950	0.060	0.310	1.892	0.4237
<i>N,N</i> -Dimethylformamide	0.367	1.310	0.000	0.740	3.173	0.6468
Methanol	0.278	0.440	0.430	0.470	0.970	0.3082
Ethanol	0.246	0.420	0.370	0.480	1.485	0.4491
1-Propanol	0.236	0.420	0.370	0.480	2.031	0.5900
1-Pentanol	0.219	0.420	0.370	0.480	3.106	0.8718
1-Hexanol	0.210	0.420	0.370	0.480	3.610	1.0127
2-Propanol	0.212	0.360	0.330	0.560	1.764	0.5900
2-Butanol	0.217	0.360	0.330	0.560	2.338	0.7309
2-Methyl-1-propanol	0.217	0.390	0.370	0.480	2.413	0.7309
3-Methyl-1-butanol	0.192	0.390	0.370	0.480	3.011	0.8718
Cyclohexanol	0.460	0.540	0.320	0.570	3.758	0.9040
1,3-Dichloro-2-propanol	0.546	0.930	0.420	0.540	3.650	0.8348
Dimethyl sulfoxide	0.522	1.720	0.000	0.970	3.401	0.6126
Carbon disulfide	0.876	0.260	0.000	0.030	2.370	0.4905
Tetramethyltin	0.324	0.110	0.000	0.100	2.651	1.0431
Benzene	0.610	0.520	0.000	0.140	2.786	0.7164
Toluene	0.601	0.520	0.000	0.140	3.325	0.8573
<i>o</i> -Xylene	0.663	0.560	0.000	0.160	3.939	0.9982
<i>m</i> -Xylene	0.623	0.520	0.000	0.160	3.839	0.9982
<i>p</i> -Xylene	0.613	0.520	0.000	0.160	3.839	0.9982
<i>trans</i> -Stilbene	1.350	1.210	0.000	0.230	7.456	1.5630
Acenaphthene	1.604	1.050	0.000	0.220	6.469	1.2586
Anthracene	2.290	1.340	0.000	0.280	7.568	1.4544
Phenanthrene	2.055	1.290	0.000	0.290	7.632	1.4544
Fluoranthene	2.377	1.550	0.000	0.240	8.827	1.5846
Pyrene	2.808	1.710	0.000	0.280	8.833	1.5846
Chlorobenzene	0.718	0.650	0.000	0.070	3.657	0.8388
Aniline	0.955	0.960	0.260	0.410	3.934	0.8162
Benzoic acid	0.730	0.900	0.590	0.400	4.657	0.9317
2-Hydroxybenzoic acid	0.900	0.850	0.730	0.370	4.732	0.9904
4-Hydroxybenzoic acid	0.930	0.900	0.810	0.560	4.867	0.9904
Methyl 4-hydroxybenzoate	0.900	1.370	0.690	0.450	5.665	1.1313
2-Methylpyridine	0.598	0.750	0.000	0.580	3.422	0.8162
2-Furaldehyde	0.690	1.130	0.000	0.450	3.318	0.6929
Phenylacetic acid	0.730	1.080	0.660	0.570	4.962	1.0726

Table 6. Cont.

Solute	E	S	A	B	L	V
4-Hydroxyphenylacetic acid	1.030	1.450	0.940	0.740	5.902	1.1313
4-Ethoxyacetanilide	0.940	1.480	0.480	0.860	6.893	1.4542
Betulin	1.790	2.120	0.700	1.140	17.470	3.8670
3-Nitrophthalic acid	1.360	2.010	1.200	0.890	7.780	1.3212
Acetylsalicylic acid	0.781	1.690	0.710	0.670	6.279	1.2879
3-Chlorobenzoic acid	0.840	0.950	0.630	0.320	5.197	1.0541
4-Chlorobenzoic acid	0.840	1.020	0.630	0.270	4.947	1.0541
3-Nitrobenzoic acid	0.990	1.180	0.730	0.520	5.601	1.1059
4-Nitrobenzoic acid	0.990	1.520	0.680	0.400	5.770	1.1059
3,5-Dinitrobenzoic acid	1.250	1.630	0.700	0.590	6.984	1.2801
4-Chloro-3-nitrobenzoic acid	1.250	1.470	0.700	0.440	6.685	1.2283
2-Chloro-5-nitrobenzoic acid	1.250	1.400	0.670	0.460	6.513	1.2283
2-Methoxybenzoic acid	0.899	1.410	0.450	0.620	5.636	1.1313
4-Methoxybenzoic acid	0.899	1.250	0.620	0.520	5.741	1.1313
2-Methylbenzoic acid	0.730	0.840	0.420	0.440	4.677	1.0726
3-Methylbenzoic acid	0.730	0.890	0.600	0.400	4.819	1.0726
Ketoprofen	1.650	2.260	0.550	0.890	10.527	1.9779
Naproxen	1.510	2.020	0.600	0.670	9.207	1.7821
Haloperidol	1.900	1.390	0.400	1.760	12.819	2.7980
Paracetamol	1.060	1.630	1.040	0.860	6.430	1.1724
4-Nitrobenzyl chloride	1.080	1.350	0.000	0.350	5.806	1.1539
Salicylamide	1.160	1.580	0.610	0.510	5.818	1.0315
Benzil	1.445	1.590	0.000	0.620	7.611	1.6374
1-Chloroanthraquinone	1.900	1.790	0.000	0.570	9.171	1.6512
Monuron	1.140	1.500	0.470	0.780	7.180	1.4768
Diuron	1.280	1.600	0.570	0.700	8.060	1.5992
Ferrocene	1.350	0.850	0.000	0.200	5.622	1.1209
Diphenyl sulfone	1.570	2.150	0.000	0.700	8.902	1.6051
Hexachlorobenzene	1.490	0.990	0.000	0.000	7.390	1.4508
Hydroquinone	1.063	1.270	1.060	0.570	4.827	0.8338
1,3-Dicyanobenzene	0.890	1.639	0.000	0.561	5.372	1.0258
1,4-Dicyanobenzene	0.870	1.602	0.000	0.470	5.330	1.0258
Benzenesulfonamide	1.130	2.137	0.651	0.647	6.524	1.0971
2-Chlorobenzenesulfonamide	1.220	2.310	0.660	0.623	7.291	1.2195
<i>o</i> -Toluenesulfonamide	1.130	2.157	0.692	0.595	7.076	1.2380
<i>p</i> -Toluenesulfonamide	1.130	2.203	0.680	0.679	7.108	1.2380
Methyl 2-Sulfamoylbenzoate	1.170	2.813	0.664	0.928	8.476	1.4533
2-Chlorothioxanthone	2.226	1.394	0.000	0.556	9.319	1.6581
2-Mercapto-1,3,4-thiadiazole	1.166	1.066	0.365	0.457	4.285	0.7224
Dapsone	2.210	3.370	0.800	1.080	11.716	1.8047

Table 6. Cont.

Solute	E	S	A	B	L	V
Salicylanilide	1.868	2.161	0.895	0.361	8.915	1.4436
Dimethyl terephthalate	0.788	1.426	0.000	0.567	6.519	1.4288
5,6-Dimethoxy-1-indanone	1.037	1.211	0.000	0.785	6.703	1.4454
Pyrazinamide	1.030	1.458	0.331	0.856	4.976	0.8106
3-Methyl-4-nitrophenol	1.070	1.300	0.740	0.320	5.731	1.0902
2-Ethoxybenzamide	0.910	1.406	0.377	0.952	6.297	1.3133
Chloropropanamide	1.224	2.234	0.734	0.988	9.712	1.8986
Thioxanthen-9-one	1.940	1.441	0.000	0.557	8.436	1.5357
2-Iodoaniline	1.530	1.096	0.130	0.426	5.818	1.0744
4-Iodoaniline	1.530	1.342	0.225	0.400	6.031	1.0744
Nicotinamide	1.010	1.277	0.621	0.958	5.067	0.9317
2-Phenylindole	1.990	1.880	0.420	0.360	9.051	1.5542
Syringic acid	1.070	1.790	0.820	0.900	7.269	1.3896
Kojic acid	1.130	1.589	0.706	0.939	5.594	0.9512
Pyrimethamine	2.230	1.863	0.392	1.101	10.508	1.8458
2-Bromodibenzofuran	2.340	1.778	0.000	0.612	10.781	1.9218
<i>p</i> -Coumaric acid	1.330	1.453	0.841	0.674	6.795	1.2292
2,4-Dinitroaniline	1.430	2.197	0.554	0.310	7.259	1.1646
Terephthaldehyde	1.030	1.235	0.000	0.566	5.235	1.0296
2-Methoxy-4-nitroaniline	1.220	1.680	0.170	0.460	6.474	1.1900
2-Chloro-5-nitroaniline	1.290	1.564	0.268	0.358	6.238	1.1128
1-Methyl-4-(methylsulfonyl)benzene	0.792	1.573	0.000	0.788	6.034	1.2791
1,3-Diphenylguanidine	1.540	1.974	0.585	0.767	9.216	1.7215
Tinidazole	1.400	2.768	0.000	1.348	9.402	1.6959
Sorafenib	2.460	2.913	0.574	1.494	15.998	3.0195
3,4-Dichlorobenzoic acid	0.950	0.920	0.670	0.260	5.623	1.1766
3,4-Dimethoxybenzoic acid	0.950	1.646	0.570	0.755	6.746	1.3309
3,4,5-Trimethoxybenzoic acid	1.001	1.760	0.603	0.850	7.711	1.5309
4- <i>tert</i> -Butylbenzoic acid	0.730	1.111	0.551	0.443	6.547	1.4953
Vanillin	0.990	1.336	0.321	0.662	5.703	1.1313
Isovanillin	1.040	1.477	0.308	0.681	5.868	1.1313
2-Ethylanthraquinone	1.410	1.545	0.000	0.557	8.781	1.8106
Benzoin	1.587	2.115	0.196	0.847	9.159	1.6804
Hippuric acid	1.170	1.839	1.207	0.918	7.375	1.3290
2-Methyl-3-nitrobenzoic acid	1.040	1.396	0.541	0.532	6.332	1.2468
3-Methyl-4-nitrobenzoic acid	1.040	1.336	0.525	0.500	6.266	1.2468
4-Methyl-3-nitrobenzoic acid	1.040	1.461	0.659	0.521	6.434	1.2468
Sorbic acid	0.480	0.904	0.528	0.432	4.047	0.9424
Maltol	0.888	1.152	0.212	0.763	4.510	0.8925
<i>o</i> -Acetoacetanilide	1.190	2.333	0.264	1.025	8.563	1.6108

Table 6. Cont.

Solute	E	S	A	B	L	V
Isophthalic acid	1.100	1.210	0.960	0.590	5.988	1.1470
Vanillyl alcohol	1.053	1.817	0.755	0.890	6.464	1.1743
Ethyl vanillin	1.040	1.587	0.411	0.664	6.544	1.2722
Vanillic acid	1.144	1.476	0.826	0.639	6.407	1.1900
3,4-Dichloro-1-nitrobenzene	1.100	1.333	0.000	0.141	5.782	1.1354
2,3-Dichloro-1-nitrobenzene	1.100	1.563	0.000	0.098	6.001	1.1354
3,5-Dinitro-2-methylbenzoic acid	1.310	2.120	0.750	0.650	8.040	1.4210
Xanthone	1.640	1.173	0.000	0.563	7.466	1.4309
Lovastatin	1.230	2.730	0.310	1.760	15.459	3.2853
Simvastatin	1.350	2.550	0.320	1.860	15.551	3.4268
2-Bromo-9-fluorenone	1.840	1.425	0.000	0.399	8.415	1.5472
Benorilate	1.897	2.916	0.484	1.364	12.564	2.2930
Probenecid	1.206	1.951	0.701	1.080	10.369	2.1578
3-Methylflavone-8-carboxylic acid	2.050	1.929	0.485	1.034	10.969	2.0259
Metamitron	1.650	2.248	0.395	1.032	6.777	1.5003

Once the numerical values had been inserted into the equations, the only quantities left without numerical values were the two sets of equation coefficients (c_{eq1} , e_{eq1} , s_{eq1} , a_{eq1} , b_{eq1} , v_{eq1}) and (c_{eq2} , e_{eq2} , s_{eq2} , a_{eq2} , b_{eq2} , l_{eq2}) for the *tert*-butyl acetate mono-solvent. The 34 $\log(C_{S,organic}/C_{S,water})$ equations and 34 $\log(C_{S,organic}/C_{S,gas})$ equations were solved simultaneously to yield:

$$\begin{aligned} \text{Log}(C_{S,organic}/C_{S,water}) &= 0.456(0.110) + 0.324(0.090) \mathbf{E} - 0.661(0.111) \mathbf{S} \\ &- 1.068(0.084) \mathbf{A} - 4.680(0.228) \mathbf{B} + 4.101(0.115) \mathbf{V} \end{aligned} \quad (7)$$

(with $N = 34$, $SD = 0.100$, $R^2 = 0.994$, $F = 990.6$)

$$\begin{aligned} \text{Log}(C_{S,organic}/C_{S,gas}) &= 0.178(0.088) - 0.444(0.061) \mathbf{E} + 1.045(0.090) \mathbf{S} \\ &+ 2.522(0.077) \mathbf{A} + 0.964(0.017) \mathbf{L} \end{aligned} \quad (8)$$

(with $N = 34$, $SD = 0.103$, $R^2 = 0.999$, $F = 5319$),

the values of the respective equation coefficients that best describe the logarithms of the observed molar solubility ratios. The $b \times \mathbf{B}$ term is missing in Equation (8), because *tert*-butyl acetate lacks an acidic hydrogen, and thus, it cannot act as an H-bond donor. Both correlations were obtained using the IBM SPSS Statistical 22 commercial software.

The two Abraham model correlations provided a very accurate mathematical description of the observed molar solubility ratios, as evidenced by the near-unity squared correlation coefficients ($R^2 = 0.994$ for Equation (7) and $R^2 = 0.999$ for Equation (8)) and low standard deviations ($SD = 0.100$ log units for Equation (7) and $SD = 0.103$ log units for Equation (8)). Figures 1 and 2 provide a graphical comparison of the experimental data versus back-calculated values based on Equations (8) and (7), respectively. The experimental $\log(C_{S,organic}/C_{S,gas})$ values spanned a range of approximately 14.6 log units. A slightly smaller range of approximately 5.6 log units was spanned by the $\log(C_{S,organic}/C_{S,water})$ values. As an informational note, Equations (7) and (8) were built using a small dataset containing only 34 compounds. Several of the compounds in the dataset were structurally similar to each other, so there would have been some intercorrelation between their descriptor values. In the case of Equation (8), strong correlations were found between the \mathbf{B} and \mathbf{S} , \mathbf{B} and \mathbf{L} , and \mathbf{S} and \mathbf{L} descriptors. For Equation (7), strong correlations were noted between \mathbf{B} and \mathbf{S} ,

B and V, and S and V. Intercorrelations would diminish as more experimental values were added to the datasets.

The existing Abraham model correlations for both ethyl acetate and butyl acetate were published in 2008, based on the experimental solubility and infinite dilution activity coefficient data that were available at the time. During the last 10 years, there has been an enormous quantity of experimental solubility data reported for new pharmaceutical compounds, pesticides and herbicides, and important chemical reactants used in industrial manufacturing processes. A recent search of the published chemical literature managed to find experimental mole fraction solubility data for an additional 64 and 35 organic compounds dissolved in ethyl acetate and butyl acetate, respectively. The additional solubility data represent an approximate 50% increase in the number of experimental data points that are now available to update the earlier 2008 correlations. The additional compounds include not only important medicinal compounds (simvastatin, lovastatin, sorafenib, tinidazole, dapson, chlorpropanamide, benorilate, probenecid), flavoring agents (vanillin, vanillic acid, vanillyl alcohol, ethyl vanillin), and substituted benzoic acid derivatives, but also a wide range of multi-functional organic compounds of varying shapes and sizes. The entire ethyl acetate and butyl acetate datasets are given in Tables 6 and 7, respectively, along with the references from which the data were taken. In order to conserve journal space, the experimental values used in deriving the earlier correlations are referenced to the earlier paper [19] in which Equations (3)–(6) first appeared. Experimental-based solute descriptors of several of the additional compounds are reported for the first time in Table 6. As an additional note, the datasets associated with the Abraham model solvent equations have been used by several research groups [108–114] in developing group contribution approaches, machine learning models, quantitative structure-property relationships, and quantum-mechanical methods for predicting Gibbs energies of solvation and Gibbs energies of transfer for describing the equilibrium partitioning of solutes between two phases. Tables 7 and 8 provide enlarged ethyl acetate and butyl acetate datasets to use in future modelling endeavors.

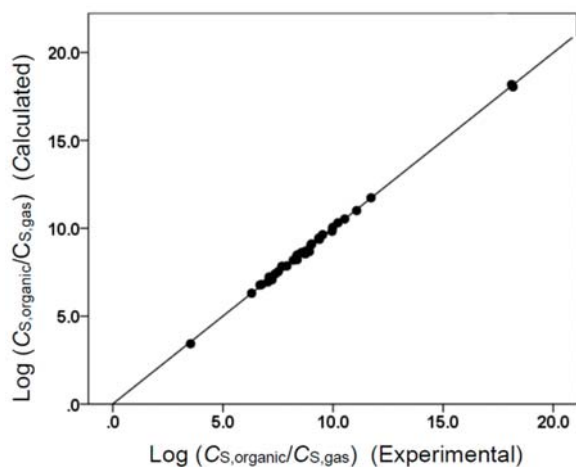


Figure 1. Comparison of observed $\log (C_{S,\text{organic}}/C_{S,\text{gas}})$ data versus back-calculated values based on Equation (8) for *tert*-butyl acetate. The straight line that is drawn corresponds to $\log (C_{S,\text{organic}}/C_{S,\text{gas}})$ (Calculated) = $\log (C_{S,\text{organic}}/C_{S,\text{gas}})$ (Experimental).

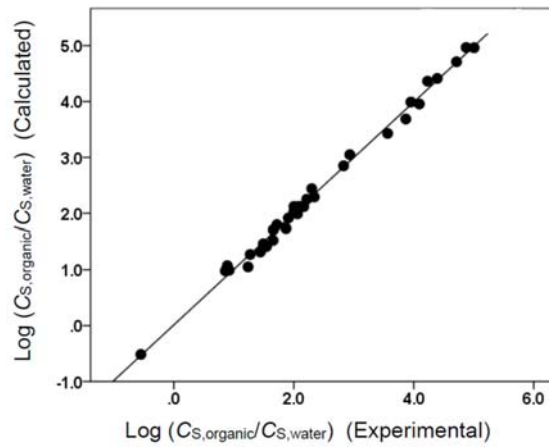


Figure 2. Comparison of observed $\log (C_{S,organic}/C_{S,water})$ data versus back-calculated values based on Equation (7) for *tert*-butyl acetate. The straight line that is drawn corresponds to $\log (C_{S,organic}/C_{S,water})$ (Calculated) = $\log (C_{S,organic}/C_{S,water})$ (Experimental).

Table 7. Experimental logarithms of molar solubility ratios; water-to-ethyl acetate transfer coefficients, $\log P$; and gas-to-ethyl acetate partition coefficients, $\log K$, at 298.15 K.

Solute	$\log K^a$	$\log P^b$	Ref.
Radon	0.810	1.460	[19]
Hydrogen	−1.070	0.650	[19]
Oxygen	−0.660	0.850	[19]
Nitrogen	−0.760	1.040	[19]
Carbon monoxide	−0.600	1.020	[19]
Sulfur dioxide	2.360	0.830	[19]
Ethane	0.490	1.830	[19]
2-Methylpropane	1.580	3.280	[19]
Pentane	2.090	3.790	[19]
Hexane	2.540	4.360	[19]
Heptane	2.980	4.940	[19]
Octane	3.450	5.560	[19]
Nonane	3.910	6.060	[19]
2-Methylpentane	2.410	4.250	[19]
2,4-Dimethylpentane	2.700	4.780	[19]
2,5-Dimethylhexane	3.160	5.180	[19]
2,3,4-Trimethylpentane	3.230	5.110	[19]
Cyclohexane	2.760	3.660	[19]
Ethylcyclohexane	3.540	5.120	[19]
Propene	1.110	2.080	[19]
<i>trans</i> -But-2-ene	2.030	3.140	[19]

Table 7. Cont.

Solute	Log K^a	Log P^b	Ref.
Pent-1-ene	2.170	3.400	[19]
2-Methylprop-1-ene	1.870	2.730	[19]
3-Methylbut-1-ene	2.010	3.350	[19]
Hept-1-ene	2.980	4.300	[19]
Buta-1,2-diene	2.080	2.530	[19]
2-Methylbuta-1,3-diene	2.410	2.910	[19]
Hepta-1,6-diene	3.370	4.220	[19]
Dichloromethane	2.960	2.000	[19]
Trichloromethane	3.380	2.590	[19]
Tetrachloromethane	3.100	3.290	[19]
1,2-Dichloroethane	3.460	2.190	[19]
1-Chloropropane	2.700	2.460	[19]
1-Chlorobutane	3.160	3.040	[19]
2-Chloro-2-methylpropane	2.610	3.410	[19]
Bromoethane	2.590	2.050	[19]
2-Bromo-2-methylpropane	2.970	3.570	[19]
Iodomethane	2.540	1.890	[19]
Iodoethane	2.960	2.420	[19]
1,1,2-Trifluorotrichloroethane	2.490	3.790	[19]
1,2-Difluorotetrachloroethane	3.390	4.030	[19]
Tetrahydrofuran	3.010	0.460	[19]
1,4-Dioxane	3.670	−0.040	[19]
2-Methylpropionaldehyde	2.970	0.870	[19]
Propanone	2.860	0.030	[19]
Butanone	3.260	0.540	[19]
Ethyl acetate	3.300	1.140	[19]
Acetonitrile	3.070	0.220	[19]
Propionitrile	3.430	0.610	[19]
Diethylamine	2.750	−0.240	[19]
Triethylamine	3.130	0.770	[19]
Nitromethane	3.610	0.660	[19]
<i>N,N</i> -Dimethylformamide	4.470	−1.260	[19]
Methanol	2.700	−1.040	[19]
Ethanol	3.020	−0.650	[19]
2-Propanol	3.030	−0.450	[19]
Dimethyl sulfoxide	4.880	−2.980	[19]
Carbon disulfide	2.290	2.440	[19]
Tetramethyltin	2.640	4.170	[19]
Benzene	3.240	2.610	[19]
Toluene	3.690	3.040	[19]
<i>trans</i> -Stilbene	8.240	5.720	[85]

Table 7. Cont.

Solute	Log K^a	Log P^b	Ref.
Acenaphthene	6.920	4.560	[19]
Anthracene	8.150	5.120	[19]
Phenanthrene	8.120	5.320	[19]
Fluoranthene	9.280	5.840	[19]
Pyrene	9.280	5.780	[19]
Chlorobenzene	4.150	3.330	[19]
Aniline	5.490	1.190	[19]
Benzoic acid	6.910	1.790	[19]
2-Hydroxybenzoic acid	7.410	2.020	[19]
4-Hydroxybenzoic acid	8.110	1.330	[19]
Methyl 4-hydroxybenzoate	8.750	1.900	[19]
2-Methylpyridine	4.160	0.760	[19]
2-Furaldehyde	4.620	0.790	[19]
Phenylacetic acid	8.140	1.670	[19]
4-Hydroxyphenylacetic acid	9.950	0.440	[19]
4-Ethoxyacetanilide	9.420	1.420	[19]
Betulin	20.410	10.020	[19]
3-Nitrophthalic acid	12.680	0.010	[19]
Acetylsalicylic acid	9.900	1.330	[19]
3-Chlorobenzoic acid	7.610	2.460	[19]
4-Chlorobenzoic acid	7.410	2.610	[19]
3-Nitrobenzoic acid	8.750	1.820	[19]
4-Nitrobenzoic acid	8.980	2.080	[19]
3,5-Dinitrobenzoic acid	10.410	2.110	[19]
4-Chloro-3-nitrobenzoic acid	9.760	2.550	[19]
2-Chloro-5-nitrobenzoic acid	9.410	2.460	[19]
2-Methoxybenzoic acid	8.180	1.370	[19]
4-Methoxybenzoic acid	8.620	1.920	[19]
2-Methylbenzoic acid	6.530	2.230	[19]
3-Methylbenzoic acid	7.260	2.280	[19]
Ketoprofen	13.760	3.300	[19]
Naproxen	12.500	3.700	[19]
Salicylamide	9.230	1.630	[19]
Benzil	9.040	4.170	[19]
1-Chloroanthraquinone	10.410	4.380	[19]
Monuron	9.580	1.950	[19]
Diuron	10.700	2.700	[19]
Ferrocene	6.020	4.100	[19]
Diphenyl sulfone	10.670	3.280	[19]
Hexachlorobenzene	7.510	6.100	[19]
Docosane	10.010	13.580	[19]

Table 7. Cont.

Solute	Log K^a	Log P^b	Ref.
Tricosane	10.540	14.260	[19]
Hydroquinone	9.050	0.180	[19]
1,3-Dicyanobenzene	7.209	1.670	[39]
1,4-Dicyanobenzene	7.062	2.055	[34]
Benzenesulfonamide	10.581	0.811	[78]
2-Chlorobenzenesulfonamide	11.478	1.368	[33]
<i>o</i> -Toluenesulfonamide	11.189	1.574	[28]
<i>p</i> -Toluenesulfonamide	11.252	1.163	[74]
Methyl 2-Sulfamoylbenzoate	13.433	0.757	[77]
2-Chlorothioxanthone	9.878	4.789	[35]
2-Mercapto-1,3,4-thiadizole	6.127	0.780	[37]
Dapsone	16.998	1.408	[68]
Salicylanilide	13.001	3.502	[31]
Dimethyl terephthalate	8.015	3.373	[29]
5,6-Dimethoxy-1-indanone	7.722	2.487	[48]
Pyrazinamide	7.348	−0.569	[65]
3-Methyl-4-nitrophenol	8.881	2.550	[81]
2-Ethoxybenzamide	8.405	0.409	[82]
Chloropropanamide	13.734	2.351	[30]
Thioxanthen-9-one	9.155	4.087	[58]
2-Iodoaniline	6.792	2.623	[46]
4-Iodoaniline	7.513	2.498	[46]
Nicotinamide	7.874	−1.148	[22]
2-Phenylindole	11.533	4.638	[44]
Syringic acid	11.199	0.700	[80]
Kojic acid	8.951	−1.167	[64]
Pyrimethamine	12.767	2.501	[47]
2-Bromodibenzofuran	11.704	5.505	[50]
<i>p</i> -Coumaric acid	10.061	1.187	[21]
2,4-Dinitroaniline	10.930	2.868	[51]
Terephthaldehyde	6.294	1.703	[52]
2-Methoxy-4-nitroaniline	8.569	2.742	[25]
2-Chloro-5-nitroaniline	8.427	2.912	[20]
1-Methyl-4-(methylsulfonyl)benzene	7.731	1.549	[79]
1,3-Diphenylguanidine	12.388	2.986	[45]
Tinidazole	12.262	0.329	[38]
Sorafenib	19.501	4.760	[36]

Table 7. Cont.

Solute	Log K^a	Log P^b	Ref.
3,4-Dichlorobenzoic acid	7.939	3.199	[40]
3,4-Dimethoxybenzoic acid	9.680	1.410	[41]
3,4,5-Trimethoxybenzoic acid	11.012	1.757	[42]
4- <i>tert</i> -Butylbenzoic acid	8.951	3.726	[53]
Vanillin	7.739	1.311	[65]
Isovanillin	7.995	1.157	[86]
2-Ethylanthraquinone	9.925	5.111	[24]
Benzoin	11.512	2.781	[57]
Hippuric acid	12.276	0.001	[49]
2-Methyl-3-nitrobenzoic acid	8.951	2.214	[54]
3-Methyl-4-nitrobenzoic acid	8.743	2.379	[55]
4-Methyl-3-nitrobenzoic acid	9.485	2.173	[56]
Sorbic acid	6.340	1.429	[60]
Maltol	6.129	−0.045	[75]
<i>o</i> -Acetoacetanisidide	11.661	1.427	[63]
Isophthalic acid	9.193	0.933	[69]
Vanillyl alcohol	10.308	−0.114	[73]
Ethyl vanillin	9.075	1.734	[72]
Vanillic acid	9.983	1.317	[70]
3,4-Dichloro-1-nitrobenzene	6.712	4.006	[61]
2,3-Dichloro-1-nitrobenzene	7.280	4.187	[61]
3,5-Dinitro-2-methylbenzoic acid	12.058	2.102	[59]
Xanthone	8.034	3.624	[43]
Lovastatin	18.336	4.424	[23]
Simvastatin	18.400	4.749	[88]
2-Bromo-9-fluorenone	9.139	4.841	[67]
Benorilate	16.329	2.278	[32]
Probenecid	13.750	2.976	[76]
3-Methylflavone-8-carboxylic acid	13.426	3.198	[84]
Metamitron	11.823	0.916	[87]

^a For the crystalline solutes, the experimental value is $\log(C_{S,organic}/C_{S,water})$. ^b For the crystalline solutes, the experimental value is $\log(C_{S,organic}/C_{S,gas})$.

Analysis of the experimental values in Tables 6 and 7 in accordance with the Abraham general solvation model yielded the following mathematical correlations:

For Ethyl Acetate:

$$\begin{aligned} \log(C_{S,organic}/C_{S,water}) &= 0.328(0.025) + 0.314(0.033) \mathbf{E} - 0.348(0.039) \mathbf{S} \\ &\quad - 0.847(0.043) \mathbf{A} - 4.899(0.058) \mathbf{B} + 4.142(0.025) \mathbf{V} \\ &\quad (\text{with } N = 170, SD = 0.144, R^2 = 0.996, F = 7548) \end{aligned} \quad (9)$$

$$\begin{aligned} \log(C_{S,organic}/C_{S,gas}) &= 0.171(0.020) - 0.403(0.030) \mathbf{E} + 1.428(0.028) \mathbf{S} \\ &\quad + 2.726(0.038) \mathbf{A} + 0.914(0.006) \mathbf{L} \\ &\quad (\text{with } N = 170, SD = 0.131, R^2 = 0.999, F = 42942) \end{aligned} \quad (10)$$

For Butyl Acetate:

$$\begin{aligned} \text{Log}(C_{S,\text{organic}}/C_{S,\text{water}}) &= 0.289(0.037) + 0.336(0.041) \mathbf{E} - 0.501(0.050) \mathbf{S} \\ &- 0.913(0.054) \mathbf{A} - 4.964(0.063) \mathbf{B} + 4.262(0.021) \mathbf{V} \end{aligned} \quad (11)$$

(with $N = 108$, $SD = 0.140$, $R^2 = 0.998$, $F = 11519$)

$$\begin{aligned} \text{Log}(C_{S,\text{organic}}/C_{S,\text{gas}}) &= 0.154(0.034) - 0.439(0.041) \mathbf{E} + 1.223(0.041) \mathbf{S} \\ &+ 2.586(0.056) \mathbf{A} + 0.953(0.006) \mathbf{L} \end{aligned} \quad (12)$$

(with $N = 108$, $SD = 0.148$, $R^2 = 0.999$, $F = 17169$)

As, before, the $b \times \mathbf{B}$ term was missing in Equations (10) and (12), neither ethyl acetate nor butyl acetate could act as an H-bond donor. Neither solvent molecule possesses an acidic hydrogen. All four derived correlations provided a reasonably accurate description of the observed solubility and partition coefficient data, as numerically reflected by the near unity squared correlation coefficient and the relatively small standard deviations. The descriptive ability is further illustrated in Figures 3–6. For most of the solute molecules considered, the graphed points fell near the drawn straight line, indicating a near-perfect back-calculation.

Table 8. Experimental logarithms of molar solubility ratios; water-to-butyl acetate transfer coefficients, $\log P$; and gas-to-butyl acetate partition coefficients, $\log K$, at 298.15 K.

Solute	Log K^a	Log P^b	Ref.
Hydrogen	−1.100	0.620	[19]
Nitrogen	−0.800	1.000	[19]
Nitrous oxide	0.720	0.950	[19]
Carbon monoxide	−0.640	0.980	[19]
Pentane	2.150	3.850	[19]
Hexane	2.630	4.450	[19]
Heptane	3.100	5.060	[19]
Octane	3.560	5.670	[19]
Nonane	4.020	6.170	[19]
2-Methylpentane	2.490	4.330	[19]
2,4-Dimethylpentane	2.790	4.870	[19]
2,5-Dimethylhexane	3.270	5.290	[19]
2,3,4-Trimethylpentane	3.340	5.220	[19]
Cyclohexane	2.870	3.770	[19]
Ethylcyclohexane	3.660	5.240	[19]
1-Heptene	3.140	4.360	[19]
1,6-Heptadiene	3.240	4.090	[19]
Carbon tetrachloride	3.120	3.310	[19]
Butyl acetate	4.090	2.150	[19]
2-Butanol	3.590	0.200	[19]
2-Methyl-1-propanol	3.550	0.250	[19]
1-Propanol	3.410	0.150	[19]
1-Pentanol	4.600	1.250	[19]
3-Methyl-1-butanol	4.240	1.000	[19]

Table 8. Cont.

Solute	Log K^a	Log P^b	Ref.
1-Hexanol	5.010	1.780	[19]
Cyclohexanol	5.180	1.170	[19]
1,3-Dichloro-2-propanol	5.560	0.380	[19]
Benzene	2.840	2.210	[19]
Toluene	4.030	3.380	[19]
<i>o</i> -Xylene	4.560	3.820	[19]
<i>m</i> -Xylene	4.440	3.830	[19]
<i>p</i> -Xylene	4.470	3.880	[19]
Octadecane	8.750	11.790	[19]
Nonadecane	9.280	12.490	[19]
Eicosane	9.470	12.780	[19]
Docosane	10.360	13.930	[19]
Tricosane	10.930	14.650	[19]
Tetracosane	11.260	15.100	[19]
Octacosane	13.090	17.430	[19]
Anthracene	8.160	5.130	[19]
Pyrene	9.290	5.790	[19]
Fluoranthene	9.270	5.830	[19]
Acenaphthene	6.910	4.550	[19]
Phenanthrene	8.090	5.290	[19]
Methyl 4-hydroxybenzoate	8.680	1.840	[19]
Benzoic acid	6.810	1.710	[19]
2-Hydroxybenzoic acid	7.340	1.950	[19]
4-Hydroxybenzoic acid	7.890	1.110	[19]
<i>trans</i> -Stilbene	8.210	5.690	[85]
Diuron	10.610	2.610	[19]
Monouron	9.390	1.760	[19]
Hexachlorobenzene	7.620	6.120	[19]
Diphenyl sulfone	10.440	3.050	[19]
4-Nitrobenzyl chloride	7.090	3.320	[19]
Paracetamol	10.380	−0.520	[19]
Ferrocene	6.010	4.243	[27]
3-Chlorobenzoic acid	7.500	2.350	[19]
4-Chlorobenzoic acid	7.210	2.410	[19]
3,4-Dichlorobenzoic acid	7.911	3.171	[40]
3-Nitrobenzoic acid	8.530	1.600	[19]
4-Nitrobenzoic acid	8.760	1.860	[19]
3,5-Dinitrobenzoic acid	10.180	1.880	[19]
3,5-Dinitro-2-methylbenzoic acid	11.853	1.897	[59]
2-Methylbenzoic acid	6.420	2.120	[19]

Table 8. Cont.

Solute	Log K^a	Log P^b	Ref.
3-Methylbenzoic acid	7.100	2.120	[19]
3-Methyl-4-nitrobenzoic acid	8.635	2.271	[55]
Naproxen	12.200	3.400	[19]
Acetylsalicylic acid	9.580	1.080	[19]
2-Methoxybenzoic acid	7.880	1.080	[19]
4-Methoxybenzoic acid	8.410	1.710	[19]
3,4-Dimethoxybenzoic acid	9.462	1.192	[41]
3,4,5-Trimethoxybenzoic acid	10.757	1.501	[42]
Benzil	8.930	4.060	[19]
4-Nitroaniline	9.290	2.100	[19]
Haloperidol	14.320	3.020	[19]
Hydroquinone	8.960	0.140	[19]
1-Chloroanthraquinone	10.290	4.260	[19]
Salicylamide	9.010	1.410	[19]
4-Chloro-3-nitrobenzoic acid	9.390	2.360	[20]
2-Chloro-5-nitrobenzoic acid	9.130	2.180	[20]
Lovastatin	18.279	4.267	[23]
2-Ethylanthraquinone	9.865	5.042	[24]
Simvastatin	18.677	4.678	[88]
Thioxanthen-9-one	9.335	4.051	[58]
Benzoin	11.305	2.574	[57]
Maltol	6.033	-0.156	[75]
Nicotinamide	7.727	-1.295	[26]
2-Methyl-3-nitrobenzoic acid	8.847	2.110	[54]
4- <i>tert</i> -Butylbenzoic acid	8.825	3.600	[53]
<i>o</i> -Acetoacetanisidide	11.407	1.173	[63]
Xanthone	7.940	3.530	[43]
Vanillyl alcohol	9.948	-0.474	[73]
Hippuric acid	12.082	-0.193	[49]
2-Ethoxybenzamide	8.310	0.314	[83]
Chloropropanamide	13.479	2.096	[30]
4-Methyl-3-nitrobenzoic acid	9.342	2.063	[56]
Dapsone	16.416	0.826	[68]
Salicylanilide	12.785	3.286	[31]
Dimethyl terephthalate	7.867	3.225	[29]
5,6-Dimethoxy-1-indanone	7.398	2.163	[48]
Pyrazinamide	7.108	-0.809	[65]
3-Methyl-4-nitrophenol	8.746	2.415	[81]
Tinidazole	11.922	-0.011	[38]
2-Bromo-9-fluorenone	9.134	4.836	[67]
Benorilate	15.974	1.925	[32]

Table 8. Cont.

Solute	Log K^a	Log P^b	Ref.
Probenecid	13.554	2.780	[76]
3-Methylflavone-8-carboxylic acid	13.151	2.923	[84]
Metamitron	11.593	0.686	[87]

^a For the crystalline solutes, the experimental value is $\log(C_{S,organic}/C_{S,gas})$. ^b For the crystalline solutes, the experimental value is $\log(C_{S,organic}/C_{S,water})$.

We further note that the numerical values of the equation coefficients changed slightly from the values given in the earlier 2008 correlations (See Equations (3)–(6)). The change is likely reflected by the addition of several large, highly basic molecules (sorafenib, $B = 1.494$, $V = 3.0195$; lovastatin, $B = 1.760$, $V = 3.2853$; simvastatin, $B = 1.860$, $V = 3.4268$) to the datasets. Prior to the inclusion of an additional 64 compounds, betulin ($B = 1.140$) was the only compound in the ethyl acetate dataset having a B-solute descriptor that exceeded unity. It is important to periodically update existing correlations as new experimental data become available in order to expand the predictive area of chemical space. Ethyl acetate and, to a lesser extent, butyl acetate are solvents that researchers use in performing solubility studies on new drug molecules. These are also two organic solvents that we routinely use in calculating solute descriptor values. Datasets used in determining the Abraham model correlations need to contain solutes that possess the molecular size, polarity, and lipophilicity common to the newly approved medicinal compounds, if the correlations are to be used in calculating solute descriptors of these compounds. Newer drug molecules tend to be larger and more lipophilic and possess a greater H-bond acceptor capability than older drugs [115]. The predictive area of chemical space covered by the Abraham model correlations needs to keep pace with the molecular properties of today's modern drug molecules.

Many of the compounds used in chemical manufacturing processes will have solute descriptors that fall within these ranges. Currently solute descriptors are readily available on the UFZ-LSER internet website [116] for more than 8500 different organic compounds. If not available, there are group contribution methods [117,118], as well as machine learning models [108,119], that can be used to estimate the desired descriptor values. The estimation requires simply inputting the canonical SMILES code of the desired solute into the software program found at either the UFZ-LSER website or at the RMG-MIT website link embedded in [89] in the published paper [108].

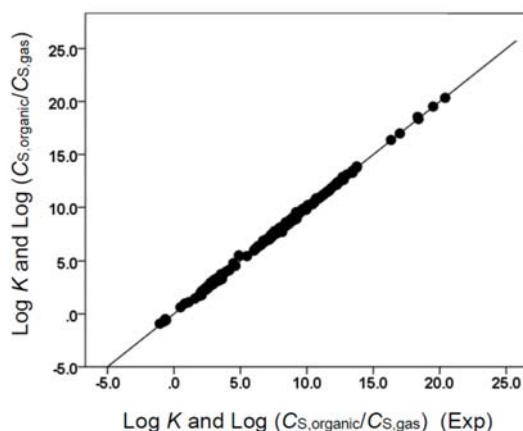


Figure 3. Comparison of observed $\log K$ and $\log(C_{S,organic}/C_{S,gas})$ data versus back-calculated values based on Equation (10) for ethyl acetate. The straight line that is drawn corresponds to $\log K$ and $\log(C_{S,organic}/C_{S,gas})$ (Calc) = $\log K$ and $\log(C_{S,organic}/C_{S,gas})$ (Exp).

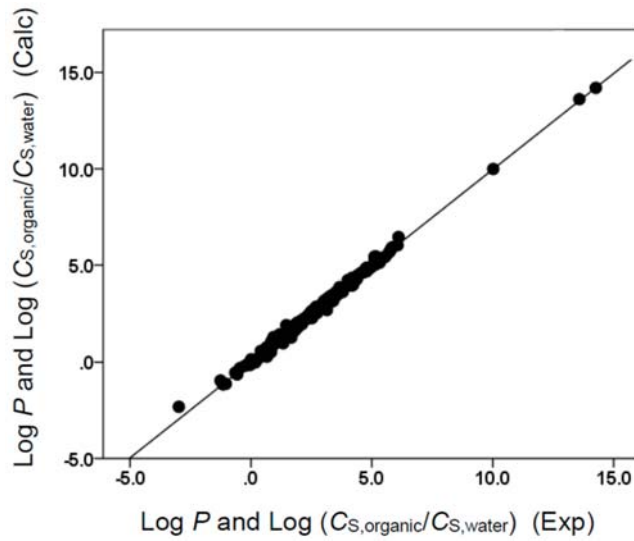


Figure 4. Comparison of observed $\log P$ and $\log (C_{S,organic}/C_{S,water})$ data versus back-calculated values based on Equation (9) for ethyl acetate. The straight line that is drawn corresponds to $\log P$ and $\log (C_{S,organic}/C_{S,water})$ (Calc) = $\log P$ and $\log (C_{S,organic}/C_{S,water})$ (Exp).

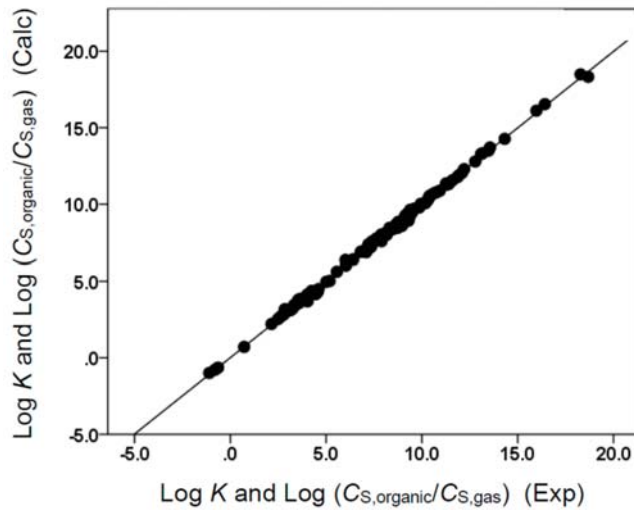


Figure 5. Comparison of observed $\log K$ and $\log (C_{S,organic}/C_{S,gas})$ data versus back-calculated values based on Equation (12) for butyl acetate. The straight line that is drawn corresponds to $\log K$ and $\log (C_{S,organic}/C_{S,gas})$ (Calc) = $\log K$ and $\log (C_{S,organic}/C_{S,gas})$ (Exp).

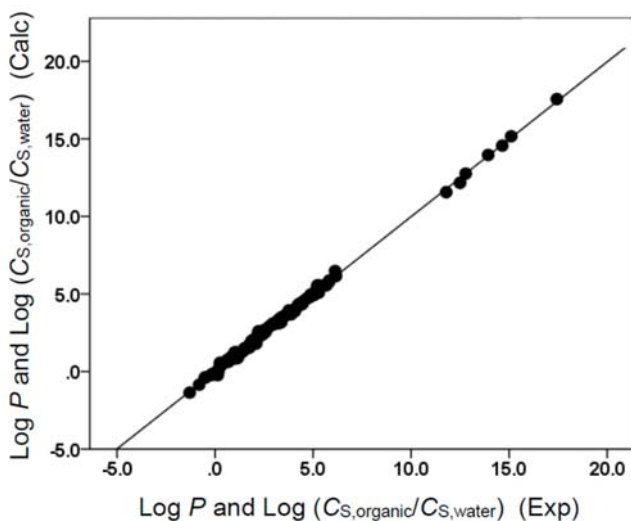


Figure 6. Comparison of observed $\log P$ and $\log (C_{S,organic}/C_{S,water})$ data versus back-calculated values based on Equation (11) for butyl acetate. The straight line that is drawn corresponds to $\log P$ and $\log (C_{S,organic}/C_{S,water})$ (Calc) = $\log P$ and $\log (C_{S,organic}/C_{S,water})$ (Exp).

4. Conclusions

Mathematical expressions based upon the Abraham general solvation parameter model were obtained for predicting the solute transfer of molecular organic compounds and inorganic gases into three alkyl acetate mono-solvents (*tert*-butyl acetate, ethyl acetate, and butyl acetate). The predictive expressions for the three alkyl acetate solvents were determined using chemically diverse datasets, which contained 34, 170, and 108 solutes of various molecular sizes and shapes, polarities, and hydrogen-bonding characteristics. The mathematical correlations presented in the current study describe the observed solubility ratios of solutes dissolved in *tert*-butyl acetate, ethyl acetate, and butyl acetate to within an overall standard deviation of 0.15 log units or less. Based on our past experience using the Abraham model, we fully expect the derived mathematical expressions to provide comparable predictions for the solubility and partitioning behavior of additional organic solutes in the three fore-mentioned solvents, provided, of course, that the descriptor values of the additional solutes fall within the range of values used in deriving the respective predictive expression. Many of the compounds used in chemical manufacturing processes will have solute descriptors that fall within these ranges.

Author Contributions: Conceptualization and writing—original draft preparation, W.E.A.J.; formal data analysis, L.L., E.W., C.Y., M.Z., S.S. and A.V.; writing—review and editing, L.L., E.W., C.Y., M.Z., S.S. and A.V. All authors have read and agreed to the published version of the manuscript.

Funding: This research received no external funding.

Data Availability Statement: Data are contained within the article.

Acknowledgments: Emily Wu, Chelsea Yang, Miles Zhang, and Sneha Sinha thank the University of North Texas's Texas Academy of Mathematics & Science (TAMS) program for providing a summer research scholarship to each student.

Conflicts of Interest: The authors declare no conflict of interest.

References

1. Xu, A.; Varadharajan, A.; Shanmugam, N.; Kim, K.; Huang, E.; Cai, S.K.; Acree, W.E., Jr. Abraham model description of the solubilising properties of the isopropyl acetate organic mono-solvent. *Phys. Chem. Liq.* **2022**, *60*, 312–324. [[CrossRef](#)]
2. Kim, K.; Shanmugam, N.; Xu, A.; Varadharajan, A.; Cai, S.K.; Huang, E.; Acree, W.E., Jr. Abraham model correlations for describing solute transfer into anisole based on measured activity coefficients and molar solubilities. *Phys. Chem. Liq.* **2022**, *60*, 452–462. [[CrossRef](#)]
3. Cai, S.K.; Huang, E.; Kim, K.; Shanmugam, N.; Varadharajan, A.; Xu, A.; Acree, W.E., Jr. Development of Abraham model correlations for solute transfer into cyclopentanol from both water and the gas phase based on measured solubility ratios. *Phys. Chem. Liq.* **2022**, *60*, 287–296. [[CrossRef](#)]
4. Strickland, S.; Ocon, L.; Zhang, A.; Wang, S.; Eddula, S.; Liu, G.; Tirumala, P.; Huang, J.; Dai, J.; Jiang, C.; et al. Abraham model correlations for describing dissolution of organic solutes and inorganic gases in dimethyl carbonate. *Phys. Chem. Liq.* **2021**, *59*, 181–195. [[CrossRef](#)]
5. Ruddigkeit, L.; van Deursen, R.; Blum, L.C.; Reymond, J.-L. Enumeration of 166 billion organic small molecules in the Chemical Universe Database GDB-17. *J. Chem. Inf. Model.* **2012**, *52*, 2864–2875. [[CrossRef](#)] [[PubMed](#)]
6. Abraham, M.H. Scales of solute hydrogen-bonding: Their construction and application to physicochemical and biochemical processes. *Chem. Soc. Rev.* **1993**, *22*, 73–83. [[CrossRef](#)]
7. Abraham, M.H.; Ibrahim, A.; Zissimos, A.M. Determination of sets of solute descriptors from chromatographic measurements. *J. Chromatogr. A* **2004**, *1037*, 29–47. [[CrossRef](#)]
8. Abraham, M.H.; Smith, R.E.; Luchtefeld, R.; Boorem, A.J.; Luo, R.; Acree, W.E., Jr. Prediction of solubility of drugs and other compounds in organic solvents. *J. Pharm. Sci.* **2010**, *99*, 1500–1515. [[CrossRef](#)]
9. Abraham, M.H.; Acree, W.E., Jr. Descriptors for the prediction of partition coefficients of 8-hydroxyquinoline and its derivatives. *Sep. Sci. Technol.* **2014**, *49*, 2135–2141. [[CrossRef](#)]
10. Sinha, S.; Yang, C.; Wu, E.; Acree, W.E., Jr. Abraham solvation parameter model: Examination of possible intramolecular hydrogen-bonding using calculated solute descriptors. *Liquids* **2022**, *2*, 131–146. [[CrossRef](#)]
11. Byrne, F.P.; Jin, S.; Paggiola, G.; Petchey, T.H.M.; Clark, J.H.; Farmer, T.J.; Hunt, A.J.; McElroy, C.R.; Sherwood, J. Tools and techniques for solvent selection: Green solvent selection guides. *Sustain. Chem. Process.* **2016**, *4*, 1–24. [[CrossRef](#)]
12. Henderson, R.K.; Jimenez-Gonzalez, C.; Constable, D.J.C.; Alston, S.R.; Inglis, G.G.A.; Fisher, G.; Sherwood, J.; Binks, S.P.; Curzons, A.D. Expanding GSK's solvent selection guide-embedding sustainability into solvent selection starting at medicinal chemistry. *Green Chem.* **2011**, *13*, 854–862. [[CrossRef](#)]
13. Jimenez-Gonzalez, C.; Curzons, A.D.; Constable, D.J.C.; Cunningham, V.L. Expanding GSK's solvent selection guide-application of life cycle assessment to enhance solvent selections. *Clean Technol. Environ. Policy.* **2005**, *7*, 42–50. [[CrossRef](#)]
14. Welton, T. Solvents and sustainable chemistry. *Proc. R. Soc. A.* **2015**, *471*, 20150502. [[CrossRef](#)]
15. Duereh, A.; Sato, Y.; Smith, R.L., Jr.; Inomata, H. Methodology for replacing dipolar aprotic solvents used in API processing with safe hydrogen-bond donor and acceptor solvent-pair mixtures. *Org. Process Res. Dev.* **2017**, *21*, 114–124. [[CrossRef](#)]
16. Joshi, D.R.; Adhikari, N. An overview on common organic solvents and their toxicity. *J. Pharm. Res. Int.* **2019**, *28*, JPRI.49840. [[CrossRef](#)]
17. Prat, D.; Hayler, J.; Wells, A. A survey of solvent selection guides. *Green Chem.* **2014**, *16*, 4546–4551. [[CrossRef](#)]
18. Byrne, F.P.; Forier, B.; Bossaert, G.; Hoebers, C.; Farmer, T.J.; Hunt, A.J. A methodical selection process for the development of ketones and esters as bio-based replacements for traditional hydrocarbon solvents. *Green Chem.* **2018**, *20*, 4003–4011. [[CrossRef](#)]
19. Sprunger, L.M.; Proctor, A.; Acree, W.E., Jr.; Abraham, M.H.; Benjelloun-Dakhama, N. Correlation and prediction of partition coefficient between the gas phase and water, and the solvents dry methyl acetate, dry and wet ethyl acetate, and dry and wet butyl acetate. *Fluid Phase Equilib.* **2008**, *270*, 30–44. [[CrossRef](#)]
20. Xu, R.; Wang, J. Solubility measurement and thermodynamic model correlation and evaluation of 2-chloro-5-nitroaniline in 12 pure solvents. *J. Chem. Eng. Data.* **2019**, *64*, 1357–1365. [[CrossRef](#)]
21. Ji, W.; Meng, Q.; Li, P.; Yang, B.; Wang, F.; Ding, L.; Wang, B. Measurement and correlation of the solubility of p-coumaric acid in nine pure and water + ethanol mixed solvents at temperatures from 293.15 to 333.15 K. *J. Chem. Eng. Data.* **2016**, *61*, 3457–3465. [[CrossRef](#)]
22. Wu, H.; Dang, L.; Wei, H. Solid-liquid phase equilibrium of nicotinamide in different pure solvents: Measurements and thermodynamic modeling. *Ind. Eng. Chem. Res.* **2014**, *53*, 1707–1711. [[CrossRef](#)]
23. Nti-Gyabaah, J.; Chiew, Y.C. Solubility of lovastatin in ethyl acetate, propyl acetate, isopropyl acetate, butyl acetate, sec-butyl acetate, isobutyl acetate, tert-butyl acetate, and 2-butanone, between (285 and 313) K. *J. Chem. Eng. Data.* **2008**, *53*, 2060–2065. [[CrossRef](#)]
24. Holley, K.; Acree, W.E., Jr.; Abraham, M.H. Determination of Abraham model solute descriptors for 2-ethylanthraquinone based on measured solubility ratios. *Phys. Chem. Liq.* **2011**, *49*, 355–365. [[CrossRef](#)]
25. Bao, Y.; Wu, J.; Zhao, X.; Zhao, H. 2-Methoxy-4-nitroaniline solubility in several monosolvents: Measurement, correlation, and solvent effect analysis. *J. Chem. Eng. Data.* **2020**, *65*, 757–765. [[CrossRef](#)]
26. Ouyang, J.; Zhang, Y.; Na, B.; Liu, Z.; Zhou, L.; Hao, H. Solubility determination of nicotinamide and its application for the cocrystallization with benzoic acid. *J. Chem. Eng. Data.* **2018**, *63*, 4157–4165. [[CrossRef](#)]

27. Abraham, M.H.; Acree, W.E., Jr. Descriptors for ferrocene and some substituted ferrocenes. *J. Mol. Liq.* **2017**, *232*, 325–331. [[CrossRef](#)]
28. Wu, K.; Li, Y. Solubility Measurement and thermodynamic modeling for o-toluenesulfonamide in 16 solvents from T = 273.15 to 323.85 K. *J. Chem. Eng. Data.* **2019**, *64*, 5238–5247. [[CrossRef](#)]
29. Zhang, Z.; Qu, Y.; Li, M.; Wang, S.; Wang, J. Solubility and thermodynamic modeling of dimethyl terephthalate in pure solvents and the evaluation of the mixing properties of the solutions. *J. Chem. Eng. Data.* **2019**, *64*, 4565–4579. [[CrossRef](#)]
30. Liu, H.; Wang, S.; Qu, C.; Li, M.; Qu, Y. Solid-liquid equilibrium of chlorpropamide in 14 pure solvents at temperature of 283.15 to 323.15 K. *J. Chem. Eng. Data.* **2020**, *65*, 2859–2871. [[CrossRef](#)]
31. Peng, H.; Liu, Y.; Yan, H.; Yu, C.; Feng, S.; Yin, H.; Chen, M. Solubility measurement and data correlation of salicylanilide in 12 pure solvents at temperatures ranging from 283.15 to 323.15 K. *J. Chem. Eng. Data.* **2021**, *66*, 1501–1507. [[CrossRef](#)]
32. Hu, W.; Shang, Z.; Wei, N.; Hou, B.; Gong, J.; Wang, Y. Solubility of benorilate in twelve monosolvents: Determination, correlation and COSMO-RS analysis. *J. Chem. Thermodyn.* **2021**, *152*, 106272/1–106272/10. [[CrossRef](#)]
33. Wu, K.; Li, Y. Solid-liquid phase equilibrium and solution thermodynamics of 2-chlorobenzenesulfonamide in 16 mono solvents at temperature ranging from 273.15 K to 324.65 K. *J. Mol. Liq.* **2020**, *304*, 112795/1–112795/11. [[CrossRef](#)]
34. Li, Y.; Lu, C.; Chen, R.; Wu, K. Determination, correlation, and thermodynamic analysis of the solid-liquid phase equilibrium of 1,4-dicyanobenzene in pure solvents at various temperatures. *J. Chem. Eng. Data.* **2020**, *65*, 4991–5002. [[CrossRef](#)]
35. Liu, J.-Q.; Zhang, Y.; Wang, W. Solubility measurement and correlation of 2-chlorothioxanthone (CTX) in twelve mono organic solvents. *J. Mol. Liq.* **2022**, *360*, 119503/1–119503/11. [[CrossRef](#)]
36. Wu, Y.; Guo, Q.; Bai, J.; Guo, C. Solubility determination, solute-solvent interactions, and model correlation of sorafenib in twelve pure organic solvents between T = 273.15 and 313.15 K. *J. Chem. Eng. Data.* **2021**, *66*, 4286–4292. [[CrossRef](#)]
37. Gao, X.; Yu, S.; Wu, G.; Cheng, Y.; Xue, F. Solid-liquid phase equilibrium of 2-mercapto-1,3,4-thiadiazol in pure organic solvents. *J. Chem. Eng. Data.* **2021**, *66*, 4706–4713. [[CrossRef](#)]
38. Li, T.; Zhu, L.; Li, J.; Cao, Z.; Sha, J.; Li, Y.; Ren, B. Solubility, thermodynamic properties and molecular simulation of tinidazole in fourteen mono-solvents at different temperatures. *J. Chem. Thermodyn.* **2022**, *170*, 106767/1–106767/14. [[CrossRef](#)]
39. Wu, K.; Guan, Y.; Yang, Z.; Ji, H. Solid-liquid phase equilibrium of isophthalonitrile in 16 solvents from T = 273.15 to 324.75 K and mixing properties of solutions. *J. Chem. Eng. Data.* **2021**, *66*, 4442–4452. [[CrossRef](#)]
40. Wilson, A.; Tian, A.; Chou, V.; Quay, A.N.; Acree, W.E., Jr.; Abraham, M.H. Experimental and predicted solubilities of 3,4-dichlorobenzoic acid in select organic solvents and in binary aqueous-ethanol mixtures. *Phys. Chem. Liq.* **2012**, *50*, 324–335. [[CrossRef](#)]
41. Bowen, K.R.; Stephens, T.W.; Lu, H.; Satish, K.; Shan, D.; Acree, W.E., Jr.; Abraham, M.H. Experimental and predicted solubilities of 3,4-dimethoxybenzoic acid in select organic solvents of varying polarity and hydrogen-bonding character. *Eur. Chem. Bull.* **2013**, *2*, 577–583.
42. Hart, E.; Klein, A.; Zha, O.; Wadawadigi, A.; Qian, E.; Dunn, S.; Herron, J.; Kankolongo, K.; Ryan, S.; Acree, W.E., Jr.; et al. Determination of Abraham model solute descriptors for monomeric 3,4,5-trimethoxybenzoic acid from experimental solubility data in organic solvents measured at 298.2 K. *Phys. Chem. Liq.* **2018**, *56*, 381–390. [[CrossRef](#)]
43. Qian, E.; Lee, G.; Che, M.; Wang, L.; Yue, D.; Fischer, R.; Jodray, M.; Gupta, A.; Neal, R.; Liu, Y.; et al. Determination of Abraham model solute descriptors for xanthone based on experimental solubility measurements at 298.2 K. *Phys. Chem. Liq.* **2020**, *58*, 214–221. [[CrossRef](#)]
44. Liu, J.-Q.; Chen, H.; An, S.-F.; Li, T.-T. Solubility measurement and correlation of 2-phenyl-1H-indole in fourteen mono organic solvents from 289.05 K to 338.55 K. *J. Mol. Liq.* **2020**, *302*, 112491/1–112491/11. [[CrossRef](#)]
45. Xu, R.; Wang, J.; Du, C.; Han, S.; Meng, L.; Zhao, H. Solubility determination and thermodynamic dissolution functions of 1,3-diphenylguanidine in nine organic solvents at evaluated temperatures. *J. Chem. Thermodyn.* **2016**, *99*, 86–95. [[CrossRef](#)]
46. Xu, K.; Zhu, J.; Li, T. Measurement and correlation of the dissolution equilibria of o-iodoaniline and p-iodoaniline in pure solvents. *J. Chem. Eng. Data.* **2018**, *63*, 217–224. [[CrossRef](#)]
47. Song, T.; Xiao, Y.; Shi, K.; Bai, Y.; Li, J.; Qi, L.; Xie, C. Solubility measurement and data correlation of pyrimethamine in 13 pure solvents at temperatures from 278.15 to 318.15 K. *J. Chem. Eng. Data.* **2022**, *67*, 28–36. [[CrossRef](#)]
48. Li, J.; Yao, M.; Kang, X.; Yu, C.; Liu, Y.; Yan, H.; Yin, H.; Chen, M. Equilibrium solubility determination and dissolution property analysis of 5,6-dimethoxy-1-indanone in 15 pure solvents from 283.15 to 323.15 K. *J. Chem. Eng. Data.* **2021**, *66*, 1813–1820. [[CrossRef](#)]
49. Sinha, S.; Varadharajan, A.; Xu, A.; Wu, E.; Acree, W.E., Jr. Determination of Abraham model solute descriptors for hippuric acid from measured molar solubilities in several organic mono-solvents of varying polarity and hydrogen-bonding ability. *Phys. Chem. Liq.* **2022**, *60*, 563–571. [[CrossRef](#)]
50. Xu, S.; Cao, T.; Ma, M.; Wang, Y. Uncover the effect of solvent and temperature on solid-liquid equilibrium behavior of 2-bromodibenzofuran. *J. Chem. Thermodyn.* **2022**, *171*, 106813. [[CrossRef](#)]
51. Xu, R.; Xu, A.; Du, C.; Cong, Y.; Wang, J. Solubility determination and thermodynamic modeling of 2,4-dinitroaniline in nine organic solvents from T = (278.15 to 318.15) K and mixing properties of solutions. *J. Chem. Thermodyn.* **2016**, *102*, 178–187.
52. Wang, J.; Xu, A.; Xu, R. Determination and correlation of terephthalaldehyde solubility in (ethanol, isopropanol, ethyl acetate, isopentanol) + N,N-dimethylformamide mixed solvents at temperatures from 273.15 K to 318.15 K. *J. Chem. Thermodyn.* **2017**, *105*, 327–336. [[CrossRef](#)]

53. Hart, E.; Lee, G.; Qian, E.; Jodray, M.; Barrera, M.; Fischer, R.; Che, M.; Liu, Y.; Zha, O.; Woods, D.; et al. Determination of Abraham model solute descriptors for 4-tert-butylbenzoic acid from experimental solubility data in organic mono-solvents. *Phys. Chem. Liq.* **2019**, *57*, 445–452. [[CrossRef](#)]
54. Hart, E.; Ramirez, A.M.; Cheeran, S.; Barrera, M.; Horton, M.Y.; Wadawadigi, A.; Acree, W.E., Jr.; Abraham, M.H. Determination of Abraham model solute descriptors for 2-methyl-3-nitrobenzoic acid from measured solubility data in alcohol, alkyl ether, alkyl acetate and 2-alkoxyalcohol mono-solvents. *Phys. Chem. Liq.* **2017**, *55*, 796–804. [[CrossRef](#)]
55. Acree, W.E., Jr.; Bowen, K.R.; Horton, M.Y.; Abraham, M.H. Computation of Abraham model solute descriptors for 3-methyl-4-nitrobenzoic acid from measured solubility data. *Phys. Chem. Liq.* **2017**, *55*, 482–491. [[CrossRef](#)]
56. Wang, S.; Liu, K.; Zhang, A.; Dai, J.; Gupta, A.; Zhu, S.; Eddula, S.; Jiang, C.; Acree, W.E., Jr.; Abraham, M.H. Solubility of 4-methyl-3-nitrobenzoic acid in organic mono-solvents: Calculation of Abraham model solute descriptors. *Phys. Chem. Liq.* **2020**, *58*, 782–791. [[CrossRef](#)]
57. Stephens, T.W.; Loera, M.; Calderas, M.; Diaz, R.; Montney, N.; Acree, W.E., Jr.; Abraham, M.H. Determination of Abraham model solute descriptors for benzoic acid based on measured solubility ratios. *Phys. Chem. Liq.* **2012**, *50*, 254–265. [[CrossRef](#)]
58. Fletcher, K.A.; Coym, K.S.; Roy, L.E.; Hernandez, C.E.; McHale, M.E.R.; Acree, W.E., Jr. Solubility of thioxanthene-9-one in organic nonelectrolyte solvents. Comparison of observed versus predicted values based upon mobile order theory (MOT). *Phys. Chem. Liq.* **1998**, *35*, 243–252. [[CrossRef](#)]
59. Ye, S.; Saifullah, M.; Grubbs, L.M.; McMillan-Wiggins, M.C.; Acosta, P.; Mejorado, D.; Flores, I.; Acree, W.E., Jr.; Abraham, M.H. Determination of the Abraham model solute descriptors for 3,5-dinitro-2-methylbenzoic acid from measured solubility data in organic solvents. *Phys. Chem. Liq.* **2011**, *49*, 821–829. [[CrossRef](#)]
60. Fang, J.; Zhang, M.; Zhu, P.; Ouyanga, J.; Gong, J.; Chen, W.; Xu, F. Solubility and solution thermodynamics of sorbic acid in eight pure organic solvents. *J. Chem. Thermodyn.* **2015**, *85*, 202–209. [[CrossRef](#)]
61. Xu, H.; Zhang, B.; Yang, Z.; Yao, G.; Zhao, H. Solubility of dichloronitrobenzene in eight organic solvents from T = (278.15 to 303.15) K: Measurement and thermodynamic modeling. *J. Chem. Eng. Data.* **2014**, *59*, 1281–1287. [[CrossRef](#)]
62. Zhao, H.; Xu, H.; Yang, Z.; Li, R. Solubility of 3,4-dichloronitrobenzene in methanol, ethanol, and liquid mixtures (methanol + water, ethanol + water): Experimental measurement and thermodynamic modeling. *J. Chem. Eng. Data.* **2013**, *58*, 3061–3068. [[CrossRef](#)]
63. Lee, G.; Che, M.; Qian, E.; Wang, L.; Gupta, A.; Neal, R.; Yue, D.; Downs, S.; Mayes, T.; Rose, O.; et al. Determination of Abraham model solute descriptors for o-acetoacetanilide based on experimental solubility data in organic mono-solvents. *Phys. Chem. Liq.* **2019**, *57*, 528–535. [[CrossRef](#)]
64. Sun, R.; He, H.; Wan, Y.; Li, L.; Sha, J.; Jiang, G.; Li, Y.; Li, T.; Ren, B. Kojic acid in fourteen mono-solvents: Solubility data, Hansen solubility parameter and thermodynamic properties. *J. Chem. Thermodyn.* **2021**, *152*, 106280/1–116280/13. [[CrossRef](#)]
65. Zhang, K.; Shen, H.; Xu, S.; Zhang, H.; Zhu, M.; Shi, P.; Fu, X.; Yang, Y.; Gong, J. Thermodynamic study of solubility for pyrazinamide in ten solvents from T = (283.15 to 323.15) K. *J. Chem. Thermodyn.* **2017**, *112*, 204–212. [[CrossRef](#)]
66. Jia, S.; Zhang, K.; Wan, X.; Gao, Z.; Gong, J.; Rohani, S. Effects of temperature and solvent properties on the liquid-solid phase equilibrium of γ -pyrazinamide. *J. Chem. Eng. Data.* **2020**, *65*, 3667–3678. [[CrossRef](#)]
67. Peng, Y.; Wang, Z.; Jiao, W.; Cheng, X.; Yang, J.; Hu, Y.; Mi, L. Determination and analysis of solubility of 2-bromo-9-fluorenone in 10 different organic solvents and three binary solvent mixtures at different temperatures (T = 278.15–323.15 K). *J. Chem. Eng. Data* **2022**, *in press*. [[CrossRef](#)]
68. Li, W.; Ma, Y.; Yang, Y.; Xu, S.; Shi, P.; Wu, S. Solubility measurement, correlation and mixing thermodynamics properties of dapson in twelve mono solvents. *J. Mol. Liq.* **2019**, *280*, 175–181. [[CrossRef](#)]
69. Long, B.; Yang, Z. Measurements of the solubilities of m-phthalic acid in acetone, ethanol and acetic ether. *Fluid Phase Equilib.* **2008**, *266*, 38–41. [[CrossRef](#)]
70. Noubigh, A.; Abderrabba, M. Solid-liquid phase equilibrium and thermodynamic properties of vanillic acid in different pure solvents. *J. Mol. Liq.* **2016**, *223*, 261–266. [[CrossRef](#)]
71. Shakeel, F.; Haq, N.; Siddiqui, N.A. Solubility and thermodynamic function of vanillin in ten different environmentally benign solvents. *Food Chem.* **2015**, *180*, 244–248. [[CrossRef](#)] [[PubMed](#)]
72. Wu, H.; Wang, J.; Zhou, Y.; Guo, N.; Liu, Q.; Zong, S.; Bao, Y.; Hao, H. Solid-liquid phase equilibrium and dissolution properties of ethyl vanillin in pure solvents. *J. Chem. Thermodyn.* **2017**, *105*, 345–351. [[CrossRef](#)]
73. Guo, Y.; Hao, Y.; Zhou, Y.; Han, Z.; Xie, C.; Su, W.; Hao, H. Solubility and thermodynamic properties of vanillyl alcohol in some pure solvents. *J. Chem. Thermodyn.* **2017**, *106*, 276–284. [[CrossRef](#)]
74. Wu, K.; Li, Y. Solubility and solution thermodynamics of p-toluenesulfonamide in 16 solvents from T = 273.15 to 324.75 K. *J. Mol. Liq.* **2019**, *293*, 111577. [[CrossRef](#)]
75. Li, J.; Hao, H.; Guo, N.; Wang, N.; Hao, Y.; Luan, Y.; Chen, K.; Huang, X. Solubility and thermodynamic properties of maltol in different pure solvents. *J. Mol. Liq.* **2017**, *243*, 313–323. [[CrossRef](#)]
76. Shi, J.; Liu, L.; Wang, L.; Ding, Z.; Wu, S. Solubility measurement and correlation of probenecid in 12 pure organic solvents and thermodynamic properties of mixing of solutions. *J. Chem. Eng. Data.* **2019**, *64*, 624–631. [[CrossRef](#)]
77. Wu, K.; Han, R.; Xu, L.; Li, X.; Li, Y. Thermodynamic modelling for solubility of methyl 2-sulfamoylbenzoate in sixteen organic solvents from T (272.15–324.15 K) and dissolution properties. *J. Mol. Liq.* **2021**, *337*, 116618. [[CrossRef](#)]

78. Li, Y.; Wu, K.; Liang, L. Solubility determination, modeling, and thermodynamic dissolution properties of benzenesulfonamide in 16 neat solvents from 273.15 to 324.45 K. *J. Chem. Eng. Data*. **2019**, *64*, 3606–3616. [[CrossRef](#)]
79. Xu, J.; Han, S.; Cong, Y.; Du, C.; Cheng, C.; Wang, J.; Zhao, H. Thermodynamic functions of 1-methyl-4-(methylsulfonyl)benzene solubility in nine organic solvents from T = (278.15 to 318.15) K. *J. Chem. Thermodyn.* **2016**, *103*, 234–243. [[CrossRef](#)]
80. Vilas-Boas, S.M.; Vieira, V.; Brandao, P.; Alves, R.S.; Coutinho, J.A.P.; Pinho, S.P.; Ferreira, O. Solvent and temperature effects on the solubility of syringic, vanillic or veratric acids: Experimental, modeling and solid phase studies. *J. Mol. Liq.* **2019**, *289*, 111089. [[CrossRef](#)]
81. Buchowski, H.; Jodzewicz, W.; Milek, R.; Ufnalski, W.; Maczynski, A. Solubility and hydrogen bonding. I. Solubility of 4-nitro-5-methylphenol in one-component solvents. *Roczniki Chemii*. **1975**, *49*, 1879–1887. [[CrossRef](#)]
82. Tong, Y.; Wang, Z.; Yang, E.; Pan, B.; Jiang, J.; Dang, L.; Wei, H. Determination and correlation of solubility and solution thermodynamics of ethenzamide in different pure solvents. *Fluid Phase Equilib.* **2016**, *427*, 549–556. [[CrossRef](#)]
83. Wang, K.; Shang, Z.; Zhang, J.; Liu, Y.; Han, J.; Tang, W. Solubility determination and thermodynamic correlation of 2-ethoxybenzamide in 12 pure solvents from 288.15 to 328.15 K. *J. Chem. Eng. Data*. **2021**, *66*, 1508–1514. [[CrossRef](#)]
84. Wang, Z.; Peng, Y.; Cheng, X.; Yang, J.; Zhou, B.; Mi, L.; Hu, Y. Investigation on Hansen solubility parameter, solvent effect and thermodynamic properties of 3-methylflavone-8-carboxylic acid dissolved in different solvents. *J. Mol. Liq.* **2022**, *356*, 119017. [[CrossRef](#)]
85. Abraham, M.H.; Acree, W.E., Jr. Gas-solvent and water-solvent partition of trans-stilbene at 298 K. *J. Mol. Liq.* **2017**, *238*, 58–61. [[CrossRef](#)]
86. Zhang, S.; Wang, H.; Dai, J.; Niu, Y.; Yin, Q.; Zhou, L. Solubility determination, model evaluation and solution thermodynamics of isovanillin in 15 pure solvents and 4 binary solvents. *J. Mol. Liq.* **2021**, *340*, 116847. [[CrossRef](#)]
87. Xiao, Y.; Wu, C.; Zhao, C.; Qi, L.; Bao, Y.; Zhou, L.; Yin, Q. Analysis of solid-liquid equilibrium behavior of highly water-soluble beet herbicide metamitron in thirteen pure solvents using experiments and molecular simulations. *J. Mol. Liq.* **2022**, in press. [[CrossRef](#)]
88. Nti-Gyabaah, J.; Chan, V.; Chiew, Y.C. Solubility and limiting activity coefficient of simvastatin in different organic solvents. *Fluid Phase Equilib.* **2009**, *280*, 35–41. [[CrossRef](#)]
89. Fritz, J.S.; Lisicki, N.M. Titration of acids in nonaqueous solvents. *Anal. Chem.* **1951**, *23*, 589–591. [[CrossRef](#)]
90. Knofczynski, G.T.; Daniel Mundfrom, D. Sample sizes when using multiple linear regression for prediction. *Educ. Psychol. Meas.* **2008**, *68*, 431–442. [[CrossRef](#)]
91. Austin, P.C.; Steyerberg, E.W. The number of subjects per variable required in linear regression analyses. *J. Clin. Epidemiol.* **2015**, *68*, 627–636. [[CrossRef](#)] [[PubMed](#)]
92. Charlton, A.K.; Daniels, C.R.; Acree, W.E., Jr.; Abraham, M.H. solubility of crystalline nonelectrolyte solutes in organic solvents: Mathematical correlation of acetylsalicylic acid solubilities with the Abraham general solvation model. *J. Solution Chem.* **2003**, *32*, 1087–1102. [[CrossRef](#)]
93. Abraham, M.H.; Zissimos, A.M.; Acree, W.E., Jr. Partition of solutes into wet and dry ethers; an LFER analysis. *New J. Chem.* **2003**, *27*, 1041–1044. [[CrossRef](#)]
94. Blake-Taylor, B.H.; Deleon, V.H.; Acree, W.E., Jr.; Abraham, M.H. Mathematical correlation of salicylamide solubilities in organic solvents with the Abraham solvation parameter model. *Phys. Chem. Liq.* **2007**, *45*, 389–398. [[CrossRef](#)]
95. Flanagan, K.B.; Hoover, K.R.; Garza, O.; Hizon, A.; Soto, T.; Villegas, N.; Acree, W.E., Jr.; Abraham, M.H. Mathematical correlation of 1-chloroanthraquinone solubilities in organic solvents with the Abraham solvation parameter model. *Phys. Chem. Liq.* **2006**, *44*, 377–386. [[CrossRef](#)]
96. Stovall, D.M.; Givens, C.; Keown, S.; Hoover, K.R.; Barnes, R.; Harris, C.; Lozano, J.; Nguyen, M.; Rodriguez, E.; Acree, W.E., Jr.; et al. Solubility of crystalline nonelectrolyte solutes in organic solvents: Mathematical correlation of 4-chloro-3-nitrobenzoic acid and 2-chloro-5-nitrobenzoic acid solubilities with the Abraham solvation parameter model. *Phys. Chem. Liq.* **2005**, *43*, 351–360. [[CrossRef](#)]
97. Stovall, D.M.; Acree, W.E., Jr.; Abraham, M.H. Solubility of 9-fluorenone, thianthrene and xanthene in organic solvents. *Fluid Phase Equilib.* **2005**, *232*, 113–121. [[CrossRef](#)]
98. Hoover, K.R.; Pop, K.; Acree, W.E., Jr.; Abraham, M.H. Solubility of crystalline nonelectrolyte solutes in organic solvents: Mathematical correlation of 3-chlorobenzoic acid solubilities with the Abraham solvation parameter model. *S. Afr. J. Chem.* **2005**, *58*, 25–29.
99. Hoover, K.R.; Stovall, D.M.; Pustejovsky, E.; Coaxum, R.; Pop, K.; Acree, W.E., Jr.; Abraham, M.H. Solubility of crystalline nonelectrolyte solutes in organic solvents—Mathematical correlation of 2-methoxybenzoic acid and 4-methoxybenzoic acid solubilities with the Abraham solvation parameter model. *Can. J. Chem.* **2004**, *82*, 1353–1360. [[CrossRef](#)]
100. Charlton, A.K.; Daniels, C.R.; Wold, R.M.; Pustejovsky, E.; Acree, W.E., Jr.; Abraham, M.H. Solubility of crystalline nonelectrolyte solutes in organic solvents: Mathematical correlation of 3-nitrobenzoic acid solubilities with the Abraham general solvation model. *J. Mol. Liq.* **2004**, *116*, 19–28. [[CrossRef](#)]
101. Hoover, K.R.; Coaxum, R.; Pustejovsky, E.; Acree, W.E., Jr.; Abraham, M.H. Thermochemical behavior of dissolved carboxylic acid solutes: Part 5-mathematical correlation of 3,5-dinitrobenzoic acid solubilities with the Abraham solvation parameter model. *Phys. Chem. Liq.* **2004**, *42*, 457–466. [[CrossRef](#)]

102. Hoover, K.R.; Coaxum, R.; Pustejovsky, E.; Stovall, D.M.; Acree, W.E., Jr.; Abraham, M.H. Thermochemical behavior of dissolved carboxylic acid solutes: Part 4—Mathematical correlation of 4-nitrobenzoic acid solubilities with the Abraham solvation parameter model. *Phys. Chem. Liq.* **2004**, *42*, 339–347. [CrossRef]
103. Coaxum, R.; Hoover, K.R.; Pustejovsky, E.; Stovall, D.M.; Acree, W.E., Jr.; Abraham, M.H. Thermochemical behavior of dissolved carboxylic acid solutes: Part 3—MATHEMATICAL correlation of 2-methylbenzoic acid solubilities with the Abraham solvation parameter model. *Phys. Chem. Liq.* **2004**, *42*, 313–322. [CrossRef]
104. Daniels, C.R.; Charlton, A.K.; Wold, R.M.; Acree, W.E., Jr.; Abraham, M.H. Thermochemical behavior of dissolved carboxylic acid solutes: Solubilities of 3-methylbenzoic acid and 4-chlorobenzoic acid in organic solvents. *Can. J. Chem.* **2003**, *81*, 1492–1501. [CrossRef]
105. Acree, W.E., Jr.; Abraham, M.H. Solubility of crystalline nonelectrolyte solutes in organic solvents: Mathematical correlation of benzil solubilities with the Abraham general solvation model. *J. Solution Chem.* **2002**, *31*, 293–303. [CrossRef]
106. Acree, W.E., Jr.; Abraham, M.H. Solubility predictions for crystalline nonelectrolyte solutes dissolved in organic solvents based upon the Abraham general solvation model. *Can. J. Chem.* **2001**, *79*, 1466–1476. [CrossRef]
107. Acree, W.E., Jr.; Abraham, M.H. Solubility predictions for crystalline polycyclic aromatic hydrocarbons (PAHs) dissolved in organic solvents based upon the Abraham general solvation model. *Fluid Phase Equilib.* **2002**, *201*, 245–258. [CrossRef]
108. Chung, Y.; Vermeire, F.H.; Wu, H.; Walker, P.J.; Abraham, M.H.; Green, W.H. Group contribution and machine learning approaches to predict Abraham solute parameters, solvation free energy, and solvation enthalpy. *J. Chem. Inf. Model.* **2022**, *62*, 433–446. [CrossRef]
109. Brown, T.N. Empirical regressions between system parameters and solute descriptors of polyparameter linear free energy relationships (PPLFERs) for predicting solvent-air partitioning. *Fluid Phase Equilib.* **2021**, *540*, 113035. [CrossRef]
110. Hille, C.; Ringe, S.; Deimel, M.; Kunkel, C.; Acree, W.E.; Reuter, K.; Oberhofer, H. Generalized molecular solvation in non-aqueous solutions by a single parameter implicit solvation scheme. *J. Chem. Phys.* **2019**, *150*, 041710. [CrossRef]
111. Kashefogheta, S.; Oliveira, M.P.; Rieder, S.R.; Horta, B.A.C.; Acree, W.E., Jr.; Hunenberger, P.H. Evaluating classical force fields against experimental cross-solvation free energies. *J. Chem. Theory Comput.* **2020**, *16*, 7556–7580. [CrossRef]
112. Kashefogheta, S.; Wang, S.; Acree, W.E.; Hunenberger, P.H. Evaluation of nine condensed-phase force fields of the GROMOS, CHARMM, OPLS, AMBER, and OpenFF families against experimental cross-solvation free energies. *Phys. Chem. Chem. Phys.* **2021**, *23*, 13055–13074. [CrossRef]
113. Lee, S.; Cho, K.-H.; Acree, W.E., Jr.; No, K.T. Development of surface-SFED models for polar solvents. *J. Chem. Inf. Model.* **2012**, *52*, 440–448. [CrossRef]
114. Ma, S.; Hwang, S.; Lee, S.; Acree, W.E.; No, K.T. Incorporation of hydrogen bond angle dependency into the generalized solvation free energy density model. *J. Chem. Inf. Model.* **2018**, *58*, 761–772. [CrossRef]
115. Avdeef, A.; Kansy, M. Predicting solubility of newly-approved drugs (2016–2020) with a simple ABSOLV and GSE(flexible-acceptor) consensus model outperforming Random Forest regression. *J. Solut. Chem.* **2022**, *51*, 1020–1055. [CrossRef]
116. Ulrich, N.; Endo, S.; Brown, T.N.; Watanabe, N.; Bronner, G.; Abraham, M.H.; Goss, K.-U. UFZ-LSER Database v 3.2.1 [Internet], Leipzig, Germany, Helmholtz Centre for Environmental Research-UFZ. 2017. Available online: <http://www.ufz.de/lserd> (accessed on 1 September 2022).
117. Platts, J.A.; Butina, D.; Abraham, M.H.; Hersey, A. Estimation of molecular linear free energy relation descriptors using a group contribution approach. *J. Chem. Inf. Comput. Sci.* **1999**, *39*, 835–845. [CrossRef]
118. Platts, J.A.; Abraham, M.H.; Butina, D.; Hersey, A. Estimation of molecular linear free energy relationship descriptors by a group contribution approach. 2. Prediction of partition coefficients. *J. Chem. Inf. Comput. Sci.* **2000**, *40*, 71–80. [CrossRef] [PubMed]
119. Ulrich, N.; Ebert, A. Can deep learning algorithms enhance the prediction of solute descriptors for linear solvation energy relationship approaches? *Fluid Phase Equilib.* **2022**, *555*, 113349. [CrossRef]

Review

Thermodynamic Modeling of Mineral Scaling in High-Temperature and High-Pressure Aqueous Environments

Derek M. Hall ^{1,2}, Serguei N. Lvov ^{1,2,3} and Isaac K. Gamwo ^{1,*}

¹ National Energy Technology Laboratory (NETL), Research and Innovation Center, U.S. Department of Energy, Pittsburgh, PA 152356, USA

² Department of Energy and Mineral Engineering, The Pennsylvania State University, University Park, PA 16802, USA

³ Department of Materials Science and Engineering, The Pennsylvania State University, University Park, PA 16802, USA

* Correspondence: isaac.gamwo@netl.doe.gov

Abstract: Methods of predicting mineral scale formation have evolved over the years from simple empirical fittings to sophisticated computational programs. Though best practices can now solve complex multi-phase, multi-component systems, they are largely restricted to temperatures below 300 °C. This review examines critical gaps in existing mineral scale modeling approaches as well as strategies to overcome them. Above 300 °C, the most widely used model of standard thermodynamic functions for aqueous species fails when fluid densities are below 0.7 g cm⁻³. This failure occurs due to the model's reliance on an empirical form of the Born equation which is unable to capture the trends observed in these high temperature, low density regimes. However, new models based on molecular solvent-solute interactions offer a pathway to overcome some of the deficiencies currently limiting high-temperature and high-pressure mineral scale predictions. Examples of the most common scale prediction methods are presented, and their advantages and disadvantages are discussed.

Keywords: mineral scale; high temperature; high pressure; review scaling models; aqueous species; partial molar Gibbs energy; equilibrium constants; Gibbs energy minimization

Citation: Hall, D.M.; Lvov, S.N.; Gamwo, I.K. Thermodynamic Modeling of Mineral Scaling in High-Temperature and High-Pressure Aqueous Environments. *Liquids* **2022**, *2*, 303–317. <https://doi.org/10.3390/liquids2040018>

Academic Editors: Juan Ortega Saavedra and William E. Acree, Jr.

Received: 13 August 2022
Accepted: 20 September 2022
Published: 28 September 2022

Publisher's Note: MDPI stays neutral with regard to jurisdictional claims in published maps and institutional affiliations.



Copyright: © 2022 by the authors. Licensee MDPI, Basel, Switzerland. This article is an open access article distributed under the terms and conditions of the Creative Commons Attribution (CC BY) license (<https://creativecommons.org/licenses/by/4.0/>).

1. Introduction

The safety and reliance of many engineering applications rely on the prediction of operating scenarios that lead to severe mineral scale formation events. A classic example of the immediate and dramatic effects of scale formation is an event that occurred during early production from the Miller oil field which brought production of 30,000 barrels a day to zero in 24 h [1]. Knowledge of scaling conditions inform operating decisions that directly affect lifetime and safety [2]. As such, methods of modeling mineral solubility, which is the driving force for scale formation, date back to the early 1900s and are still being improved today. When available, mineral scale models can be used to (i) avoid mixing of incompatible brines, (ii) determine if scale inhibitors are needed and (iii) predict when scale removal maintenance is required [2,3]. Some common mineral scales are sulfate-based (Ba, Sr, Ca), oxides/hydroxide-based (Fe, Mg), and carbonate-based (Ca, Mg, Fe) [2]. However, the development of models to predict the formation of all these possibilities is an ongoing effort with many challenges due to the number of possible conditions that lead to mineral scale formation.

Determining the thermodynamic favorability of mineral scale formation is the first and most important step in combating mineral scaling. Thermodynamic favorability is governed by a mineral's solubility limit (b_{sat}) and whether a particular fluid is above or below that limit. As such, knowing b_{sat} is paramount to effective mineral scale control. To better predict b_{sat} , the modeling of how it changes with system conditions has evolved from simple polynomials [4,5] to sophisticated thermodynamic programs [6–9] containing

computational algorithms and thermodynamic databases [10–12]. This progression was a necessary response to the increasing complexity and diversity of how different mineral solubility limits change with the composition, temperature and pressure of fluids observed in applications which now range from low-temperature, low-pressure (LTLP) to high-temperature, high-pressure (HTHP) conditions [2,3]. Though complex, it is vital that thermodynamic models reliably capture these trends because system properties (temperature, pressure, etc.) vary dramatically within a system which can promote scaling in different regions (see Figure 1).

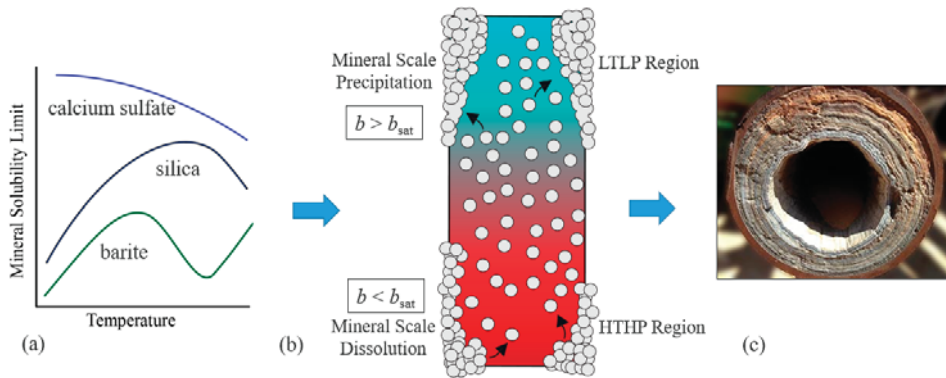


Figure 1. (a) A generic demonstration of how mineral solubility limits (b_{sat}) can vary with temperature for three different minerals (not to scale), (b) an example of how temperature and pressure gradients can promote mineral scale formation (without considering the scaling kinetics), and (c) an image capturing the possible consequences of mineral scale formation [13]. Figure 1c is reprinted with permission from [13]. Copyright 2022 FQE Chemicals.

The solubility limits of a mineral depend strongly on the capacity of a solution to solubilize the solute species needed to form that mineral. This capacity is called the ion activity product (*IAP*), and it is used with a solubility product (K_{sp}) to assess a fluid's tendency for scale formation [14,15]. This tendency is quantified with what is known as the scale saturation ratio (*SR*),

$$SR = \frac{IAP}{K_{sp}} \quad (1)$$

which is a ratio of the *IAP* to K_{sp} for a given mineral [14,15].

For barite, a common scale in oil and gas applications, the *SR* is determined as follows:

$$SR(\text{Barite}) = \frac{a_{\text{Ba}^{2+}(\text{aq})} a_{\text{SO}_4^{2-}(\text{aq})}}{K_{sp, \text{BaSO}_4(\text{s})}} \quad (2)$$

where $a_{\text{Ba}^{2+}(\text{aq})}$ is the activity of barium ions and $a_{\text{SO}_4^{2-}(\text{aq})}$ is the activity of sulfate ions within the solution. The *IAP* value represents the activities of species present in the solution, which can deviate from what is thermodynamically stable, and is affected by side reactions with other chemical species also within the solution [14]. Setting aside the non-thermodynamic contributions (e.g., kinetics of scaling), the influence of possible side reactions with additional chemical species is no trivial matter and a primary driver of the steady evolution of models to predict the solubility limit of minerals that account for multi-phase, multi-component contributions.

Many publications address the modeling of mineral solubility limits; all of which can be sub-divided into three distinct strategies that have certain advantages and disadvantages. However, the option to use a particular method depends strongly on the availability of specific datasets. Over the last 40 years, the three options most frequently used are

(i) empirical data fits of experimental data from solubility experiments, (ii) thermodynamic calculation of solubility products from thermodynamic databases, and (iii) multi-phase, multi-component computational thermodynamic programs. The first approach requires experimental solubility limit data for the system of interest, whereas the last two approaches leverage databases and publications that provide standard partial molar Gibbs energy values for the species of interest to these models. Each method can be further sub-divided to differentiate the range of sub-techniques used to obtain solubility limits of scaling minerals (see Figure 2).

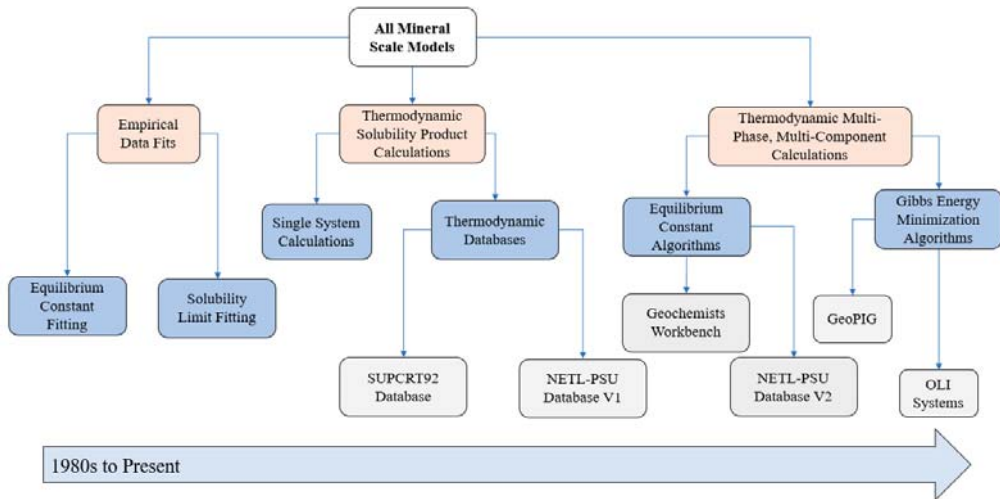


Figure 2. Model evolution tree of mineral scale solubility models from the 1980s to today. The grey boxes are examples of the different techniques.

Though empirical fits are often the easiest to apply and the most readily available for simple systems, they have been steadily phased out from use for multi-phase, multi-component environments.

Because a number of reviews have already been conducted on mineral scale modeling strategies, we will briefly draw attention to some of their main findings to emphasize how this review differs. A few recent publications have identified important deficiencies in scale modeling methods for the petroleum and natural gas industry up to 200 °C. They found that the availability of experimental data [16,17] and shortcomings in activity coefficient modeling databases are both impeding reliable mineral scale modeling efforts [16,18]. A few studies have also stressed the need to incorporate multi-phase, multicomponent features into scale modeling practices given their significant impact to several important mineral scale chemistries [16,18]. Other studies have focused on the role of scale mitigation strategies through the use of inhibitors [17,19,20]. However, none of these works discuss the underlying model limitations for the standard thermodynamic functions that underpin many of these modeling methods if extended to temperatures above 300 °C. Likewise, the internal consistency and viability of available standard Gibbs energy and equilibrium constant data used by many scale modeling programs are rarely discussed. Here, we provide a general overview of basic scale modeling methods, discuss overlooked technical gaps still present in commonly used standard thermodynamic functions and highlight strategies to overcome them.

2. Empirical Fitting Methods

One of the earliest methods for modeling the solubility limits of mineral scale were basic empirical fits of solubility data. Prior to the early 1980s, the partial molar standard

Gibbs energy data required to determine the thermodynamic driving force for mineral scale deposition reactions were not readily accessible or known for many conditions [21]. A good example of this method is calcium carbonate mineral scale in pure water and saltwater environments [5,22]. These empirical fits were used to model solubility limits for specific systems with known compositions, temperatures, and pressures. As such, they were frequently updated as more experimental data became available; in many instances, this approach remains the best way to compile data from multiple experimental studies.

Most empirical solubility models are basic polynomials with the minimum number of parameters needed to get a satisfactory fit (i.e., a high R^2 value). These models either fit an equilibrium constant for a mineral precipitation reaction (solubility product) or a solubility limit concentration itself [4,5,22–24]. The choice of solubility product over solubility limit was often based on the desired use of the final fitting. Earlier works often focused on obtaining the solubility products, since these were not known for many mineral reactions, whereas later works focused on the solubility limits since these values are often used to validate new thermodynamic models for predicting mineral precipitation conditions.

A notable example of the simple empirical method for solubility limits was demonstrated by Krumgalz [4,23,24]. His three-part publication series analyzed over a thousand publications with mineral solubility data to formulate empirical fits of the solubility limits for alkaline and alkaline earth sulfates, chlorides and bromides at elevated temperatures. The cations examined in each publication were sodium, potassium, magnesium, calcium, strontium and barium, and the anions were chlorides, bromides, and sulfates. The temperature range varied from mineral to mineral because they were limited by the availability of experimental data. Generally, several of the minerals were fit for a range of 0 to 300 °C. The systems analyzed were the mineral of interest in pure water for a series of different temperatures. Each of these minerals were fit to a polynomial that had up to six of the following terms:

$$b_{\text{sat}} = a_0 + a_1t + a_2t^2 + a_3t^3 + a_4t^4 + a_5t^5 + a_6t^6 \quad (3)$$

where t is the temperature in Celsius, and a_0 – a_6 are empirical constants used to fit the experimental data. As such, this empirical model provides reliable mineral solubility limits for the water-mineral system over a given temperature range. The work by Krumgalz demonstrates both the impact of temperature on the solubility of common minerals, and how they can vary dramatically between minerals for the same set of conditions (see Figure 3).

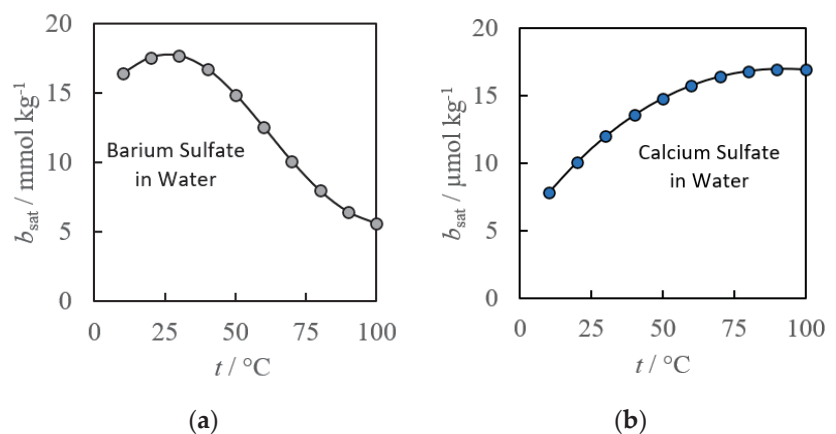


Figure 3. Calcium sulfate (a) and barium sulfate (b) empirical fits of mineral solubility limits in pure water as a function of temperature [4].

Of the minerals analyzed, most fits obtained had an R^2 of 0.98 or better, with only three of the six empirical constants, but the number of constants required typically increased

with the temperature range. Three to six terms are required for simple systems over small temperature ranges, it becomes increasingly difficult to accommodate additional dependences such as composition and pressure changes without a model being inundated by empirical constants.

Though less common now, this empirical approach has been used to capture the impact of more than one independent variable. Examples can be found as far back as the early 1980s, when scientists were documenting the solubility product (K_{sp}) of calcium carbonate minerals in different seawater salinities for a range of temperatures [5,22]. Their goal was to model both the temperature and salinity dependences of calcium carbonate. The resulting model to capture temperature and salinity trends are as follows:

$$\log_{10}K_{sp} = a_0 + a_1T + a_2T^{-1} + a_3\log_{10}(T) + (b_0 + b_1T + b_2T^{-1})S^{0.5} + c_0S + d_0S^{1.5} \quad (4)$$

where a_0 – a_3 , b_0 – b_2 , c_0 and d_0 are all the empirical constants needed to model the dependence of the solubility product on salinity (S), (from 5 to 44 ppt), and temperature (T), (from 278.15 to 313.15 K). Note that K_{sp} can be converted to b_{sat} through the following expression:

$$b_{sat} = K_{sp}^{0.5} \quad (5)$$

Using Equation (5), the impact of salinity on the solubility limit of calcite is clear (see Figure 4). Increasing salinity results in an order of magnitude increase in the solubility limit for the range of temperatures observed.

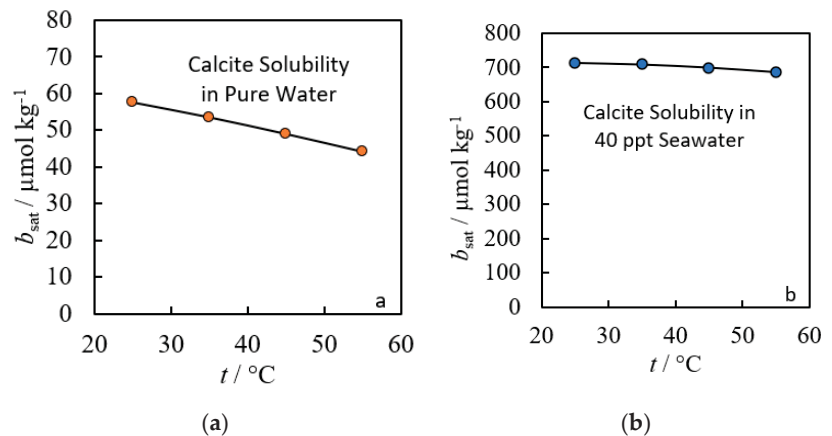


Figure 4. Modeled calcite solubility limits in pure water (a) versus in 40 ppt salinity seawater (b) both from 20 to 60 $^{\circ}\text{C}$ at atmospheric pressure [5,22].

Though good agreement can be obtained between experimental data and the resulting solubility models [4,5,22–25], the added complexity required to capture such a limited range of conditions highlights the limitations of this approach. Extending the range and properties covered by an empirical fit requires an ever-growing number of experimental data and empirical constants. In short, though this approach is the easiest model to implement, it only works for systems with available solubility data and a viable fit. Due to the strong temperature and compositional dependences of solubility, larger data sets require more empirical parameters and more empirical fits. These constraints limit the applicability of this approach to simple systems and are typically of little value to the energy industry beyond model validation.

3. Solubility Product Methods

In the 1990s, the introduction of comprehensive thermodynamic databases for minerals and aqueous species allowed for direct calculation of solubility products without fitting experimental solubility data [6,26,27]. This was accomplished with knowledge of standard Gibbs energy of formation ($\Delta_f G^0$) data for species participating in mineral scale reactions. These values can be used to calculate the standard Gibbs energy of reaction ($\Delta_r G^0$), and by extension the solubility products shown in Section 2. Unlike the empirical approaches in Section 2, this method leverages shared thermodynamic values for aqueous and solid species that can be determined by experiments not directly involving solubility measurements. This both reduces the number of empirical parameters required and expands the data available for use in mineral scale predictions. The central link between these so-called thermodynamic databases and mineral solubility limits is through the relationship between K_{sp} and the $\Delta_r G^0$:

$$\ln(K_{sp}) = -\Delta_r G^0 (RT^{-1}) \quad (6)$$

where R is the molar gas constant (in $\text{J mol}^{-1} \text{K}^{-1}$) and T is the thermodynamic temperature (in K). Despite the apparent simplicity of this approach, the underlying equations used to determine the necessary Gibbs energy data can be quite involved but they are able to capture an extraordinary range of temperatures and pressures.

One prominent example of this approach is the prediction of barite solubility between 0 and 300 °C in pure water using just standard Gibbs energy of formation values. For these conditions, the $\Delta_r G^0$ can be calculated using the following relation which requires the partial molar Gibbs energy of formation for each aqueous species as well as the molar Gibbs energy of formation of barite at the temperature of interest:

$$\Delta_r G_T^0 = \Delta_f G_{\text{Ba}^{2+}(\text{aq}),T}^0 + \Delta_f G_{\text{SO}_4^{2-}(\text{aq}),T}^0 - \Delta_f G_{\text{BaSO}_4(\text{s}),T}^0 \quad (7)$$

The molar Gibbs energies of formation obtained from the SUPCRT database of minerals and aqueous species [8] required by Equation (7) results in predictions that are in excellent agreement with experimental solubility data up to 300 °C (see Figure 5).

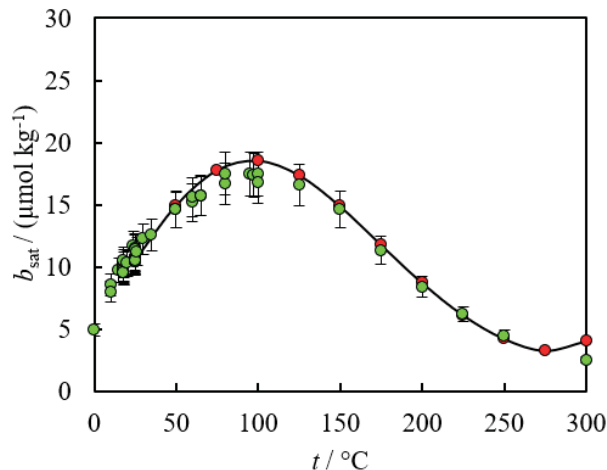


Figure 5. Comparison between experimental data (green) [4] and model predictions (red) using Equations (5)–(7). All calculations were performed assuming negligible solution non-ideality.

Though effective for simple systems, this approach requires self-consistent thermodynamic databases which necessitate considerable work to develop. Through great efforts in the 1980s to the 1990s, a few notable databases were established and enabled solubility

product calculations over a wide range of conditions for hundreds of minerals. However, due to the considerable efforts required in building these databases, many technical gaps [6,8] have gone unaddressed in the decades since.

One of the most notable thermodynamic databases for minerals was first published by the U.S. Geological Bulletin in 1978 with revisions ending in 1984 [28]. This massive database covered thermodynamic properties of 133 metal oxides and 212 other minerals [28]. Gibbs energy values were tabulated in 100 K intervals up to 1800 K provided no phase changes were expected [28]. Temperature dependences of all mineral species were captured using a polynomial to express enthalpy at a given temperature (H_T) relative to its enthalpy at a reference temperature (H_{298}) [28]:

$$H_T - H_{298} = A + BT + CT^2 + DT^{-1} + ET^{1/2} + FT^3 \quad (8)$$

where A , B , C , D , E , and F are specific to each mineral empirical constants which are fitted using available data across the temperature range. A derivation of this relationship can provide values of $\Delta_f G_T^0$ for over 300 minerals using the following equation [28]:

$$\Delta_f G_T^0 = H_{298} + \Delta T \left[\frac{H_T - H_{298}}{T} - S_T^0 \right] \quad (9)$$

where S_T^0 is the standard molar entropy of the mineral at temperature T . Applying this approach enabled the use of a broader range of experiments beyond solubility and mineral scale tests to fit model parameters relating to the solid phase. Shortly after the introduction of this massive mineral database, the underlying equations were also published [8] for one of the most comprehensive aqueous species thermodynamic databases.

Unlike gas and mineral phases, thermodynamic models for species in aqueous phases took much longer to create due to the complexities of solvent–solute interactions. It was not until the early 1990s that scientific literature contained a critical mass of thermodynamic properties for aqueous species at elevated temperatures and pressures required to make a comprehensive database. Much of the credit is due to a few scientists who developed the robust model underpinning most modern databases, now known as the Helgeson–Kirkham–Flowers (HKF) model, and the subsequent fitting of more than a hundred species over the next 10 years [21]. The HKF model predicts the standard partial molar Gibbs energy values of aqueous species based on the Born equation for solvation with seven empirical parameters. The HKF model works over a remarkable range of pressures (1–5000 bar) and temperatures (0–1000 °C) but only at relatively high density $\rho > 0.7 \text{ g cm}^{-3}$ [8]. This density limitation excludes a sizable range of conditions of interest to petroleum and natural gas extraction [29] and some other important applications such as high-enthalpy supercritical geothermal technology [30] and supercritical water gasification of biomass [31] (see Figure 6).

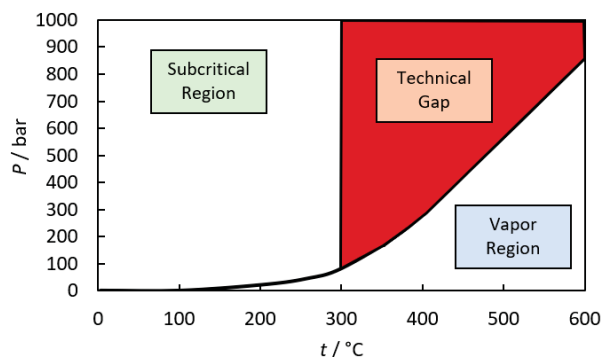


Figure 6. Temperature and pressure ranges (shown in red) where the HKF model has been observed to fail due to model limitations and insufficient experimental data.

Several studies [32–37] fit available data to extend the HKF model and provide reliable predictions for multiple species that were used to form the SUPCRT database. The primary equation within the HKF model is as follows:

$$\begin{aligned} \Delta G_{P,T}^0 = & \Delta_f G_{Pr,Tr}^0 - S_{Pr,Tr}^0 (T - T_r) - c_1 \left[T \ln \left(\frac{T}{T_r} \right) - T + T_r \right] + a_1 (P - P_r) \\ & + a_2 \ln \left(\frac{\Psi + P}{\Psi + P_r} \right) \left(\frac{\Psi + P}{\Psi + P_r} \right) \\ & + \left[a_3 (P - P_r) + a_4 \ln \left(\frac{\Psi + P}{\Psi + P_r} \right) \right] \left(\frac{1}{T - \Theta} \right) \\ & - c_2 \left[\left(\left(\frac{1}{T - \Theta} \right) - \left(\frac{1}{T_r - \Theta} \right) \right) \left(\frac{\Theta - T}{\Theta} \right) - \frac{T}{\Theta^2} \ln \left(\frac{T_r (T - \Theta)}{T (T_r - \Theta)} \right) \right] \\ & + \omega \left(\frac{1}{\varepsilon} - 1 \right) - \omega_{Pr,Tr} \left(\frac{1}{\varepsilon_{Pr,Tr}} - 1 \right) + \omega_{Pr,Tr} Y_{Pr,Tr} (T - T_r) \end{aligned} \quad (10)$$

where a_1 – a_4 , c_1 – c_2 and ω are the seven empirical constants specific to each species. In Equation (10) $\Theta = 228$ K and $\Psi = 2600$ bar are constant values within the model. $\Omega_{Pr,Tr}$ is the conventional born coefficient, ε is the relative permittivity of the solvent, and $Y_{Pr,Tr}$ is a constant based on of the relative permittivity of the solvent at 25 °C and 1 bar.

To calculate a reliable solubility product using these databases, both the empirical constants for the participating species and the underlying model equations must be valid for the conditions of interest. However, in practice one or both conditions may not be satisfied. Recent works by the authors of this review have demonstrated the failures of the HKF model in predicting the solubility of silica (see Figure 7) and barite (see Figure 8) in HTHP conditions [6,38].

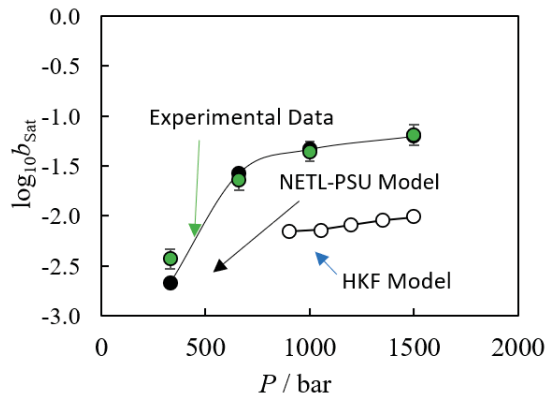


Figure 7. Observed (●) solubility of quartz in supercritical water at $t = 500$ °C as a function of pressure [39] compared to NETL-PSU model [6] calculations (●) and HKF results which failed due to model limitations (○) [6]. The authors generated these plots assuming negligible activity coefficient contributions.

Models of some aqueous species were extended into the critical technical gap shown in Figure 6 by leveraging advances in molecular statistical thermodynamics [6,38]. This approach decreased the number of empirical constants from seven (aka. The HKF model) to four for ionic species or five for species with a dipole moment. It also expanded the Born equation to a more correct form that treats the solvent molecules like a particle rather than a dielectric continuum, thereby accounting for the ion-dipole and dipole–dipole interactions based on the molecular statistical theory with the mean spherical approximation (MSA). The basic thermodynamic equation in this approach for calculating the molar Gibbs energy of formation of an aqueous species is as follows [6,38]:

$$\Delta_f G_{T,P}^0 = \Delta_f G_{T_r,P_r}^0 - \left\{ \left[-S_{T_r,P_r}^0 + \sum_k S_{T_r,P_r}^k \right] (T - T_r) + a_1 (P - P_r) - c_1 \left(T \ln \frac{T}{T_r} + T_r - T \right) \right\} + \left(\sum_k G_{T,P}^k - \sum_k G_{T_r,P_r}^k \right) \quad (11)$$

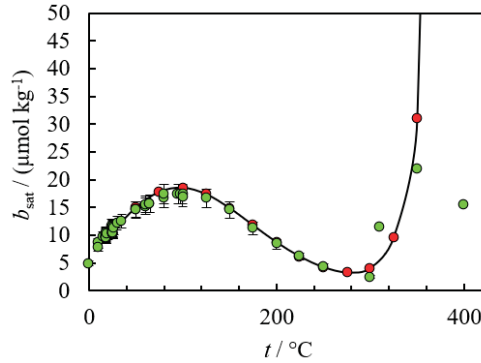


Figure 8. Comparison between HKF model (red) predictions to experimental data (green), (2700% deviations at 400 °C due to invalid empirical parameters and model limitations) [38]. The authors generated these plots assuming negligible activity coefficient contributions.

where $\Delta_f G_{T_r,P_r}^0$ is the molar Gibbs energy of formation of an aqueous species at $T_r = 298.15$ K and $P_r = 1$ bar, a_1 and c_1 are empirical parameters responsible for all short range interactions and $G_{T,P}^k$ and S_{T_r,P_r}^k are the contributions of specific molecular statistical interactions that account for hard sphere interactions [40] and electrostatic interactions [41–43]. Additionally, the standard state contributions are included to $G_{T,P}^k$ and S_{T_r,P_r}^k [44]. Within these expressions empirical diameters of the solute (σ_i) and solvent (σ_w) and dipole moment of a molecule/ion pair (p_j) are the three parameters that are fit for an ionic species with or without a dipole [6].

The hard sphere contribution, G_j^{HS} , is determined as [40]:

$$\frac{G_j^{\text{HS}}}{RT} = -\ln(1 - \eta) + 3D \left(\frac{\eta}{1 - \eta} \right) + 3D^2 \left(\frac{\eta}{(1 - \eta)^2} + \frac{\eta}{(1 - \eta)} + \ln(1 - \eta) \right) - D^3 \left(\frac{3\eta^3 - 6\eta^2 + \beta\eta}{(1 - \eta)^3} + 2 \ln(1 - \eta) \right) \quad (12)$$

where R is the molar gas constant = $8.3145 \text{ J K}^{-1} \text{ mol}^{-1}$, $\eta = \pi N_A \rho \sigma_w^3 / 6$, ρ is the molecular density, $D = \sigma_i / \sigma_w$, N_A is the Avogadro number = $6.0221 \cdot 10^{23} \text{ mol}^{-1}$, $\beta = 1 / (kT)$ where k is the Boltzmann constant = $1.3806 \cdot 10^{-23} \text{ J K}^{-1}$. The mean spherical approximation (MSA) for an ion-dipole interaction was determined as [42]:

$$\frac{G_j^{\text{ID}}}{RT} = -N_A e^2 z_j^2 \frac{(1 - 1/\epsilon)}{\sigma_j + \sigma_w (\beta_6 / \beta_3)} \quad (13)$$

where z_j is the charge number of the ionic species, e is the elementary charge = $1.602 \cdot 10^{-19} \text{ C}$, ϵ is the permittivity of the pure solvent. ϵ is related to β_6 and β_3 through the well-known Wertheim equation given as:

$$\epsilon = \frac{\beta_4^2 \beta_3^2}{\beta_6^2} = \frac{(1 + b_2/12)^4 (1 + b_2/3)^2}{(1 - b_2/6)^6} \quad (14)$$

where b_2 is a parameter of the MSA theory. The dipole–dipole electrostatic term, G_j^{DD} , is calculated as [43]:

$$\frac{G_j^{DD}}{RT} = \frac{-8N_A p_j^2 (\epsilon - 1)}{2\sigma_w^3 \left(1 - \frac{\beta_{12}}{\beta_3}\right) \left(\frac{\beta_{12}}{\beta_6}\right)^3 + 2\epsilon \left(\sigma_j + \sigma_w \frac{\beta_6}{\beta_3}\right)^3 + \left(\sigma_j + \sigma_w \frac{\beta_{12}}{\beta_6}\right)^3} \quad (15)$$

The Gibbs energy contribution due to the change in the standard state density is given as [6]:

$$\frac{G_j^{SS}}{RT} = -RT \ln(\rho RT / P^*) \quad (16)$$

where $P^* = 1$ bar is the pressure of the ideal gas reference state. Lastly, the Gibbs energy that determines the difference in unit mol fraction and unit molality reference states is given as [6]:

$$\frac{G_j^{MS}}{RT} = -RT \ln(M_s / b^0) \quad (17)$$

where M_s is the molar mass of the solvent = $18.015 \cdot 10^{-3}$ kg/mol and $b^0 = 1$ mol/kg is the standard molality. While this approach has been more successful than the HKF model, it has only been applied to a few dozen species and not the hundreds currently covered by the SUPCRT database.

Limitations in the HKF model and the fitted parameters can result in errors in excess of 1000% [38] when $\rho < 0.7$ g cm⁻³ or prohibit calculations entirely [8,10]. As such, this approach to mineral scale modeling is only valid if (i) the reaction of interest is known, (ii) the database models are valid for the conditions of interest and (iii) the species of interest have available empirical constants for the conditions of interest. For these reasons, the multi-phase, multi-component systems, encountered in the applications mentioned earlier, require computational software beyond the basic solubility product methods for predicting the solubility limit of scaling minerals.

4. Speciation Model Methods

The coupled phase and thermochemistry requirements to model mineral scaling are examples of thermodynamic problems best solved using computational thermodynamics. Both empirical fits and solubility product methods are limited in their ability to predict the diverse impacts of composition-based and phase-based influences on mineral scale formation. This is in large part due to the multi-phase and multi-component nature of the scaling process. As a classical example, the impact of solution pH and CO₂ partial pressure on calcium carbonate scaling are well-known [9,15,45–47], and require more complex methods to predict the extent of scaling [9,48,49]. Likewise, the advent of ion-pairs at elevated temperatures and pressures [26,50–52], complicate the identification of the correct solubility product limiting mineral solubility.

By the 1990s, speciation and phase equilibria software provided a means to leverage the thermodynamic databases with the increasing availability and computation power of computers. Phase equilibria and speciation calculations provide detailed predictions of how the solution composition changes, in addition to phase changes such as scale deposition. The impact of pH and its influence on some mineral solubility is a common example (see Figure 9).

Though many software options are available, each employs one of two methods, Gibbs energy minimization (GEM) or iteratively solving a system of equilibrium constants [10,55–57]. The most notable examples of the equilibrium constant approach are the Geochemist's workbench [58–60] and PHREEQC. It leverages the thermodynamic databases of Unitherm [10,61] and others described previously developed to solve complex speciation problems. Notable examples of the GEM approach are OLI Studio:Scalechem [12,62,63], HCh [10,61,64,65], and Thermo-Calc [57].

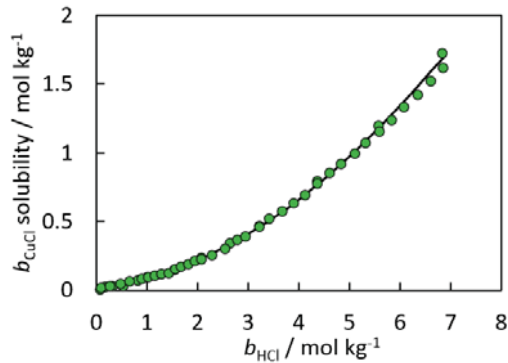


Figure 9. Comparison of speciation model predictions (black line) to experimental data (green circles) [28,53,54] for CuCl(s) over a range of HCl concentrations. The authors used mean activity coefficient data obtained for concentrated HCl solutions at 25 °C and 1 bar.

The equilibrium constant method requires the assembly of a systems of equations connecting species interest to potentially relevant reactions. The first step is to express each of these reactions as equilibrium constants that can be calculated using standard Gibbs energy of reactions [14]. Next, mass and charge balance equations [14] must be formulated. The resulting equations can be solved to determine the resulting speciation from known inputs.

By comparison, the GEM approach formulates an equation to calculate the total Gibbs energy of a system and minimizes the function under mass balance and charge balance constraints using Lagrangian functions [55,57]. A general description of the Gibbs energy of a system is as follows:

$$G = \sum_p \Delta_f G_{T,p}^0 \sum_k n_k^p \quad (18)$$

where G is the Gibbs energy of the system and n_k^p are the molar amount of substance, k in phase, p [66]. Using the expression for the Gibbs energy of the system and equations for all necessary mass balance and charge balance constraints, a Lagrangian function, L can be formulated to minimize the Gibbs energy of the system as follows [13]:

$$L = G - \sum_{i=1}^j \lambda_i \Phi_i \quad (19)$$

where λ_i are the Lagrangian factors corresponding to each constraint function, Φ_i [13]. By solving these series of equations, these programs provide the molar amounts of species in each phase that result in the lowest Gibbs energy for the constraints provided.

Regardless of the method, these computational thermodynamic programs permit the prediction of transitions from one predominant scaling reaction to another, which was otherwise difficult to accomplish without prior knowledge. One such example is the transition observed with barite at temperatures above 300 °C due to the thermodynamically favored formation of an ion pair between barium and sulfate ions (see Figure 10) [38].

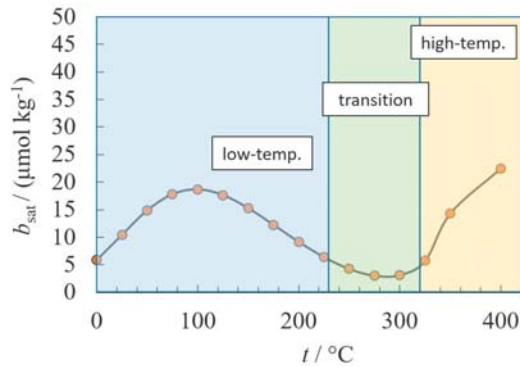


Figure 10. The effect of forming an ion pair on the solubility of barite at high temperatures [38]. The computation program predicts that mineral solubility limit is limited by the formation of ionic species at low temperatures and the ionic pair at high temperatures. The authors generated these plots assuming negligible activity coefficient contributions.

The introduction of speciation models provides a means to resolve composition dependences on mineral scaling that limited empirical and solubility product approaches. However, it is important to note that these speciation programs are still limited by the shortcomings of the thermodynamic databases used within these programs. Therefore, technical gaps in the underlying models and limited speciation databases will impact these approaches as significantly as the solubility product method.

5. Conclusions

Multiple approaches have been developed to predict the thermodynamic favorability of mineral scale formation in aqueous systems at high-temperature, high-pressure conditions. Table 1 provides a final summary of the benefits and limitations to each method covered in this review.

Table 1. Overview of Mineral Scale Modeling Techniques.

Method	Empirical Fits	Solubility Product	Speciation Models
Benefits	Easy to implement	Easy to implement Predictive capabilities	Predictive capabilities Works with multiphase systems Provides solution compositions
Limitations	No predictive capabilities Requires system-specific solubility data Limited to the temperature and pressure range of the fit	Requires a thermodynamic database Limited to the temperature and pressure range of the database Limited to simple systems	Requires a thermodynamic database Limited to the temperature and pressure range of the database

Early methods were restricted to empirical fits of experimental data collected from the mineral scaling system. After the emergence of the HKF model, researchers developed thermodynamic databases able to predict the standard partial molar Gibbs energy of formation values for aqueous species over a considerable range of temperatures and pressures. Access to thermodynamic databases permitted the prediction of solubility limits for hundreds of simple mineral scale systems. Now, computational thermodynamic programs can provide solubility limits for multi-phase, multi-component systems within the confines of pre-existing database limitations.

Though many works now focus on activity coefficient models and increasing the pool of available experimental data, a third equally important factor also needs to be addressed before mineral scale modeling can be successful above 300 °C. As of now, almost all standard thermodynamic databases are not reliable in high temperature (>300 °C), low

density ($<0.7 \text{ g cm}^{-3}$) regions. This issue stems from inherent flaws in the empirical models used to build these databases. Though models of new standard thermodynamic functions have proved to be successful, they still cover a very small number of species needed by the growing number of industrial applications in this space. Therefore, future efforts are needed to recreate these self-consistent databases which have underpinned so much recent growth in aqueous-based mineral scale modeling.

Author Contributions: Conceptualization, I.K.G., D.M.H., S.N.L.; writing—original draft preparation, D.M.H., I.K.G.; writing—review and editing, S.N.L., I.K.G.; visualization, D.M.H., I.K.G. All authors have read and agreed to the published version of the manuscript.

Funding: This research was funded by the U.S. Department of Energy, National Energy Technology Laboratory's ongoing research under the Advanced Offshore Research Field Work Proposal, DE-FE-FE1610260.

Conflicts of Interest: The authors declare no conflict of interest. This project was funded by the United States Department of Energy, National Energy Technology Laboratory, in part, through ORISE. Neither the United States Government nor any agency thereof, nor any of their employees, nor the support contractor, nor any of their employees, makes any warranty, express or implied, or assumes any legal liability or responsibility for the accuracy, completeness, or usefulness of any information, apparatus, product, or process disclosed, or represents that its use would not infringe privately owned rights. Reference herein to any specific commercial product, process, or service by trade name, trademark, manufacturer, or otherwise does not necessarily constitute or imply its endorsement, recommendation, or favoring by the United States Government or any agency thereof. The views and opinions of authors expressed herein do not necessarily state or reflect those of the United States Government or any agency thereof.

References

1. Brown, M. Full Scale Attack. *Review* **1998**, *30*, 30–32.
2. Kamal, M.S.; Hussein, I.; Mahmoud, M.; Sultan, A.S.; Saad, M.A.S. Oilfield Scale Formation and Chemical Removal: A Review. *J. Pet. Sci. Eng.* **2018**, *171*, 127–139. [CrossRef]
3. Olajire, A.A. A Review of Oilfield Scale Management Technology for Oil and Gas Production. *J. Pet. Sci. Eng.* **2015**, *135*, 723–737. [CrossRef]
4. Krumgalz, B.S. Temperature Dependence of Mineral Solubility in Water. Part 3. Alkaline and Alkaline Earth Sulfates. *J. Phys. Chem. Ref. Data* **2018**, *47*, 023101. [CrossRef]
5. Mucci, A. The Solubility of Calcite and Aragonite in Seawater at Various Salinities, Temperatures, and One Atmosphere Total Pressure. *Am. J. Sci.* **1983**, *283*, 780–799. [CrossRef]
6. Lvov, S.N.; Hall, D.M.; Bandura, A.V.; Gamwo, I.K. A Semi-Empirical Molecular Statistical Thermodynamic Model for Calculating Standard Molar Gibbs Energies of Aqueous Species above and below the Critical Point of Water. *J. Mol. Liq.* **2018**, *270*, 62–73. [CrossRef]
7. Helgeson, H.C. Thermodynamics of Hydrothermal Systems at Elevated Temperatures and Pressures. *Am. J. Sci.* **1969**, *267*, 729–804. [CrossRef]
8. Johnson, J.W.; Oelkers, E.H.; Helgeson, H.C. SUPCRT92: A Software Package for Calculating the Standard Molal Thermodynamic Properties of Minerals, Gases, Aqueous Species, and Reactions from 1 to 5000 Bars and 0 to 1000 °C. *Comput. Geosci.* **1992**, *18*, 899–947. [CrossRef]
9. Kan, A.T.; Dai, J.Z.; Deng, G.; Ruan, G.; Li, W.; Harouaka, K.; Lu, Y.T.; Wang, X.; Zhao, Y.; Tomson, M.B. Recent Advances in Scale Prediction, Approach, and Limitations. *SPE J.* **2019**, *24*, 2209–2220. [CrossRef]
10. Shvarov, Y.V. HCh: New Potentialities for the Thermodynamic Simulation of Geochemical Systems Offered by Windows. *Geochem. Int.* **2008**, *46*, 834–839. [CrossRef]
11. OLI Systems Inc. *Selecting AQ, MSE or MSE-SRK for Your Scaling Calculation*; OLI Systems Inc.: Parsippany, NJ, USA, 2017.
12. Wang, P.; Springer, R.D.; Anderko, A.; Young, R.D. Modeling Phase Equilibria and Speciation in Mixed-Solvent Electrolyte Systems. *Fluid Phase Equilib.* **2004**, *222–223*, 11–17. [CrossRef]
13. FQE Chemicals. Pipe contaminated with Barium Sulfate and NORM scale. Available online: <https://fqechemicals.com/contaminants/barium-sulfate-scale/> (accessed on 10 August 2022).
14. Greg Anderson Rock-Water Systems. In *Thermodynamics of Natural Systems*; Cambridge University Press: Cambridge, UK, 2005; pp. 473–497.
15. Zhang, P.; Kan, A.T.; Tomson, M.B. Oil Field Mineral Scale Control. In *Mineral Scales and Deposits*; Elsevier: Amsterdam, The Netherlands, 2015; pp. 603–617. ISBN 9780444627520.
16. Kan, A.T.; Tomson, M.B. Scale Prediction for Oil and Gas Production. *SPE J.* **2012**, *17*, 362–378. [CrossRef]

17. Fan, C.; Kan, A.T.; Zhang, P.; Lu, H.; Work, S.; Yu, J.; Tomson, M.B. Scale Prediction and Inhibition for Oil and Gas Production at High Temperature/High Pressure. *SPE J.* **2012**, *17*, 379–392. [[CrossRef](#)]
18. Kan, A.T.; Dai, Z.; Tomson, M.B. The State of the Art in Scale Inhibitor Squeeze Treatment. *Pet. Sci.* **2020**, *17*, 1579–1601. [[CrossRef](#)]
19. Mpelwa, M.; Tang, S.F. State of the Art of Synthetic Threshold Scale Inhibitors for Mineral Scaling in the Petroleum Industry: A Review. *Pet. Sci.* **2019**, *16*, 830–849. [[CrossRef](#)]
20. Helgeson, H.C.; Kirkham, D.H.; Flowers, G.C. Theoretical Prediction of the Thermodynamic Behavior of Aqueous Electrolytes at High Pressures and Temperatures: Calculation of Activity Coefficients, Osmotic Coefficients, and Apparent Molal and Standard and Relative Partial Molal Properties to 600 °C And. *Am. J. Sci.* **1981**, *281*, 1249–1516. [[CrossRef](#)]
21. Plummer, N.; Busenberg, E. The Solubilities of Calcite, Aragonite and Vaterite in CO₂-H₂O Solutions between 0 and 90 C, and an Evaluation of the Aqueous Model for the System CaCO₃-CO₂-H₂O. *Geochim. Cosmochim. Acta* **1981**, *46*, 1011–1040. [[CrossRef](#)]
22. Krumgalz, B.S. Temperature Dependence of Mineral Solubility in Water. Part I. Alkaline and Alkaline Earth Chlorides. *J. Phys. Chem. Ref. Data* **2017**, *46*, 043101. [[CrossRef](#)]
23. Krumgalz, B.S. Temperature Dependence of Mineral Solubility in Water. Part 2. Alkaline and Alkaline Earth Bromides. *J. Phys. Chem. Ref. Data* **2018**, *47*, 013101. [[CrossRef](#)]
24. Marion, G.M.; Millero, F.J.; Feistel, R. Precipitation of Solid Phase Calcium Carbonates and Their Effect on Application of Seawater SA-T-P Models. *Ocean Sci.* **2009**, *5*, 285–291. [[CrossRef](#)]
25. Djamali, E.; Chapman, W.G.; Cox, K.R. A Systematic Investigation of the Thermodynamic Properties of Aqueous Barium Sulfate up to High Temperatures and High Pressures. *J. Chem. Eng. Data* **2016**, *61*, 3585–3594. [[CrossRef](#)]
26. Monnin, C. A Thermodynamic Model for the Solubility of Barite and Celestite in Electrolyte Solutions and Seawater to 200 °C and to 1 Kbar. *Chem. Geol.* **1999**, *153*, 187–209. [[CrossRef](#)]
27. Robie, R.; Hemingway, B.; Fisher, J. Thermodynamic Properties of Minerals and Related Substances at 298.15 K and 1 bar Pressure and at Higher Temperatures. *US Geol. Surv. Bull.* **1984**, *1452*. [[CrossRef](#)]
28. Phi, T.; Elgaddafi, R.; Al Ramadan, M.; Fahd, K.; Ahmed, R.; Teodoriu, C. Well Integrity Issues: Extreme High-Pressure High-Temperature Wells and Geothermal Wells a Review. In *SPE Thermal Well Integrity and Design Symposium*; OnePetro: Richardson, TX, USA, 2019. [[CrossRef](#)]
29. Friðleifsson, G.; Elders, W.A.; Zierenberg, R.A.; Fowler, A.P.G.; Weisenberger, T.B.; Mesfin, K.G.; Sigurðsson, Ó.; Nielsson, S.; Einarsson, G.; Óskarsson, F.; et al. The Iceland Deep Drilling Project at Reykjanes: Drilling into the Root Zone of a Black Smoker Analog. *J. Volcanol. Geotherm. Res.* **2020**, *391*, 106435. [[CrossRef](#)]
30. Su, H.; Yan, M.; Wang, S. Recent Advances in Supercritical Water Gasification of Biowaste Catalyzed by Transition Metal-Based Catalysts for Hydrogen Production. *Renew. Sustain. Energy Rev.* **2022**, *154*, 111831. [[CrossRef](#)]
31. Shock, E.L.; Helgeson, H.C. Calculation of the Thermodynamic and Transport Properties of Aqueous Species at High Pressures and Temperatures: Correlation Algorithms for Ionic Species and Equation of State Predictions to 5 Kb and 1000 °C. *Geochim. Cosmochim. Acta* **1988**, *52*, 2009–2036. [[CrossRef](#)]
32. Haas, J.R.; Shock, E.L.; Sassani, D.C. Rare-Earth Elements in Hydrothermal Systems—Estimates of Standard Partial Molal Thermodynamic Properties of Aqueous Complexes of the Rare-Earth Elements at High-Pressures and Temperatures. *Geochim. Cosmochim. Acta* **1995**, *59*, 4329–4350. [[CrossRef](#)]
33. Sverjensky, D.A.; Shock, E.L.; Helgeson, H.C. Prediction of the Thermodynamic Properties of Aqueous Metal Complexes to 1000 Degrees C and 5 Kb. *Geochim. Cosmochim. Acta* **1997**, *61*, 1359–1412. [[CrossRef](#)]
34. Shock, E.L.L.; Sassani, D.C.; Willis, M.; Sverjensky, D.A. Inorganic Species in Geologic Fluids: Correlations among Standard Molal Thermodynamic Properties of Aqueous Ions and Hydroxide Complexes. *Geochim. Cosmochim. Acta* **1997**, *61*, 907–950. [[CrossRef](#)]
35. Shock, E.L.; Helgeson, H.C. Calculation of the Thermodynamic and Transport Properties of Aqueous Species at High Pressures and Temperatures: Standard Partial Molal Properties of Organic Species. *Geochim. Cosmochim. Acta* **1990**, *54*, 915–945. [[CrossRef](#)]
36. Pokrovskii, V.A.; Helgeson, H.C. Calculation of the Standard Partial Molal Thermodynamic and Activity Coefficients of Aqueous KCl at Temperatures and Pressures. *Geochim. Cosmochim. Acta* **1997**, *61*, 2175–2183. [[CrossRef](#)]
37. Hall, D.M.; Lvov, S.N.; Gamwo, I.K. Prediction of Barium Sulfate Deposition in Petroleum and Hydrothermal Systems. In *Solid-Liquid Separation Technologies: Applications for Produced Water*; CRC Press Taylor & Francis: Boca Raton, FL, USA, 2022.
38. Morey, G.W.; Hesselgesser, J.M. The Solubility of Some Minerals in Superheated Steam at High Pressures. *Econ. Geol.* **1951**, *46*, 821–835. [[CrossRef](#)]
39. Mansoori, G.A.; Carnahan, N.F.; Starling, K.E.; Leland, T.W., Jr. Equilibrium Thermodynamic Properties of the Mixture of Hard Spheres. *J. Chem. Phys.* **1971**, *54*, 1523–1525. [[CrossRef](#)]
40. Triolo, R.; Grigera, J.; Blum, L. Simple Electrolytes in the Mean Spherical Approximation. *J. Phys. Chem.* **1976**, *80*, 1858–1861. [[CrossRef](#)]
41. Blum, L. Solution of a Model for the Solvent-Electrolyte Interactions in the Mean Spherical Approximation. *J. Chem. Phys.* **1974**, *61*, 2129. [[CrossRef](#)]
42. Bandura, A.V.; Holovko, M.F.; Lvov, S.N. The Chemical Potential of a Dipole in Dipolar Solvent at Infinite Dilution: Mean Spherical Approximation and Monte Carlo Simulation. *J. Mol. Liq.* **2018**, *270*, 52–61. [[CrossRef](#)]
43. Lvov, S.N.; Wood, R.H. Equation of State of Aqueous NaCl Solutions over a Wide Range of Temperatures, Pressures and Concentrations. *Fluid Phase Equilib.* **1990**, *60*, 273–287. [[CrossRef](#)]

44. Heberling, F.; Trainor, T.P.; Lützenkirchen, J.; Eng, P.; Denecke, M.A.; Bosbach, D. Structure and Reactivity of the Calcite-Water Interface. *J. Colloid Interface Sci.* **2011**, *354*, 843–857. [[CrossRef](#)]
45. García, A.V.; Thomsen, K.; Stenby, E.H. Prediction of Mineral Scale Formation in Geothermal and Oilfield Operations Using the Extended UNIQUAC Model. Part II. Carbonate-Scaling Minerals. *Geothermics* **2006**, *35*, 239–284. [[CrossRef](#)]
46. Li, J.; Duan, Z. A Thermodynamic Model for the Prediction of Phase Equilibria and Speciation in the H₂O-CO₂-NaCl-CaCO₃-CaSO₄ System from 0 to 250 °C, 1 to 1000 Bar with NaCl Concentrations up to Halite Saturation. *Geochim. Cosmochim. Acta* **2011**, *75*, 4351–4376. [[CrossRef](#)]
47. Amiri, M.; Moghadasi, J. The Effect of Temperature on Calcium Carbonate Scale Formation in Iranian Oil Reservoirs Using OLI ScaleChem Software. *Pet. Sci. Technol.* **2012**, *30*, 453–466. [[CrossRef](#)]
48. Hajirezaie, S.; Wu, X.; Soltanian, M.R.; Sakha, S. Numerical Simulation of Mineral Precipitation in Hydrocarbon Reservoirs and Wellbores. *Fuel* **2019**, *238*, 462–472. [[CrossRef](#)]
49. Ho, P.C.; Palmer, D.A. Ion Association of Dilute Aqueous Potassium Chloride and Potassium Hydroxide Solutions to 600 °C and 300 MPa Determined by Electrical Conductance Measurements. *Geochim. Cosmochim. Acta* **1997**, *61*, 3027–3040. [[CrossRef](#)]
50. Ho, P.C.; Bianchi, H.; Palmer, D.A.; Wood, R.H. Conductivity of Dilute Aqueous Electrolyte Solutions at High Temperatures and Pressures Using a Flow Cell. *J. Solution Chem.* **2000**, *29*, 217–235. [[CrossRef](#)]
51. Ho, P.; Palmer, D. Ion Association of Dilute Aqueous Sodium Hydroxide Solutions to 600 C and 300 MPa by Conductance Measurements. *J. Solution Chem.* **1996**, *25*, 711–729. [[CrossRef](#)]
52. Fritz, J.J. Chloride Complexes of CuCl in Aqueous Solution. *J. Phys. Chem.* **1980**, *84*, 2241–2246. [[CrossRef](#)]
53. Balashov, V.N.; Schatz, R.S.; Chalkova, E.; Akinfiev, N.N.; Fedkin, M.V.; Lvov, S.N. CuCl Electrolysis for Hydrogen Production in the Cu–Cl Thermochemical Cycle. *J. Electrochem. Soc.* **2011**, *158*, B266–B275. [[CrossRef](#)]
54. Lvov, S.N.; Akinfiev, N.N.; Bandura, A.V.; Sigon, F.; Perboni, G. Multisys: Computer Code for Calculating Multicomponent Equilibria in High-Temperature Subcritical and Supercritical Aqueous Systems. In *Steam, Water, and Hydrothermal Systems: Physics and Chemistry Meeting the Needs of Industry*; Tremaine, P.R., Hill, P.G., Irish, D.E., Palakrishnan, P.V., Eds.; NRC Press: Ottawa, ON, USA, 2000; pp. 866–873.
55. Du, P.C.; Mansoori, G.A. Phase Equilibrium of Multicomponent Mixtures: Continuous Mixture Gibbs Free Energy Minimization and Phase Rule. *Chem. Eng. Commun.* **1987**, *54*, 139–148. [[CrossRef](#)]
56. Shobu, K.; Tabaru, T. Development of New Equilibrium Calculation Software: CaTCalc. *Mater. Trans.* **2005**, *46*, 1175–1179. [[CrossRef](#)]
57. Bethke, C.M. *Geochemical Reaction Modelling: Concepts and Applications*; Oxford University Press: New York, NY, USA, 1996.
58. Bethke, C.M. *The Geochemists Workbench Version 4.0: A User's Guide*; University of Illinois: Urbana, IL, USA, 2002.
59. Cleverley, J.S.; Bastrakov, E.N. K2GWB: Utility for Generating Thermodynamic Data Files for The Geochemist's Workbench@at 0–1000 °C and 1–5000 Bar from UT2K and the UNITHERM Database. *Comput. Geosci.* **2005**, *31*, 756–767. [[CrossRef](#)]
60. Shvarov, Y. A Suite of Programs, OptimA, OptimB, OptimC, and OptimS Compatible with the Unitherm Database, for Deriving the Thermodynamic Properties of Aqueous Species from Solubility, Potentiometry and Spectroscopy Measurements. *Appl. Geochem.* **2015**, *55*, 17–27. [[CrossRef](#)]
61. OLI Systems. *OLI Studio Stream Analyzer User Guide. V 9.5*; OLI Systems: Parsippany, NJ, USA, 2018.
62. Lencka, M.M.; Springer, R.D.; Wang, P.; Anderko, A. Modeling Mineral Scaling in Oil and Gas Environments up to Ultra High Pressures and Temperatures: Paper No. C2018-10828. In *CORROSION*; OnePetro: Richardson, TX, USA, 2018; pp. 1–15.
63. Shvarov, Y.V. A General Equilibrium Criterion for an Isobaric-Isothermal Model of a Chemical System. *Geochem. Int.* **1981**, *18*, 38–45.
64. Shvarov, Y.V. Algorithmization of the Numeric Equilibrium Modeling of Dynamic Geochemical Processes. *Geochem. Int.* **1999**, *37*, 571–576.
65. Hall, D.M.; Akinfiev, N.N.; LaRow, E.G.; Schatz, R.S.; Lvov, S.N. Thermodynamics and Efficiency of a CuCl(Aq)/HCl(Aq) Electrolyzer. *Electrochim. Acta* **2014**, *143*, 70–82. [[CrossRef](#)]
66. Koukkari, P.; Pajarre, R. Calculation of Constrained Equilibria by Gibbs Energy Minimization. *Comput. Coupling Phase Diagr. Thermochem.* **2006**, *30*, 18–26. [[CrossRef](#)]

Article

Estimating Equivalent Alkane Carbon Number Using Abraham Solute Parameters

William E. Acree, Jr.¹, Wei-Khiong Chong², Andrew S.I.D. Lang^{3,*} and Hamed Mozafari³¹ Department of Chemistry, University of North Texas, Denton, TX 76203, USA² Advent Polytech Co., Ltd., Taipao City 61249, Taiwan³ Department of Computing & Mathematics, Oral Roberts University, Tulsa, OK 74136, USA

* Correspondence: alang@oru.edu

Abstract: The use of equivalent alkane carbon numbers (EACN) to characterize oils is important in surfactant-oil-water (SOW) systems. However, the measurement of EACN values is non-trivial and thus it becomes desirable to predict EACN values from structure. In this work, we present a simple linear model that can be used to estimate the EACN value of oils with known Abraham solute parameters. We used linear regression with leave-one-out cross validation on a dataset of $N = 80$ oils with known Abraham solute parameters to derive a general model that can reliably estimate EACN values based upon the Abraham solute parameters: E (the measured liquid or gas molar refraction at 20 °C minus that of a hypothetical alkane of identical volume), S (dipolarity/polarizability), A (hydrogen bond acidity), B (hydrogen bond basicity), and V (McGowan characteristic volume) with good accuracy within the chemical space studied ($N = 80$, $R^2 = 0.92$, $RMSE = 1.16$, $MAE = 0.90$, $p < 2.2 \times 10^{-16}$). These parameters are consistent with those in other models found in the literature and are available for a wide range of compounds.

Keywords: equivalent alkane carbon number (EACN); Abraham solute parameters; hydrophobicity; oils

Citation: Acree, W.E., Jr.; Chong, W.-K.; Lang, A.S.I.D.; Mozafari, H. Estimating Equivalent Alkane Carbon Number Using Abraham Solute Parameters. *Liquids* **2022**, *2*, 318–326. <https://doi.org/10.3390/liquids2040019>

Academic Editor: Slobodan Žumer

Received: 19 August 2022

Accepted: 26 September 2022

Published: 2 October 2022

Publisher's Note: MDPI stays neutral with regard to jurisdictional claims in published maps and institutional affiliations.



Copyright: © 2022 by the authors. Licensee MDPI, Basel, Switzerland. This article is an open access article distributed under the terms and conditions of the Creative Commons Attribution (CC BY) license (<https://creativecommons.org/licenses/by/4.0/>).

1. Introduction

Considerable attention has been given in recent years to development of better surfactant-based microemulsions and foam systems for enhanced oil recovery in petroleum processes, for removal of oil from contaminated soil and industrial machinery surfaces, and for the solubilization of fragrances in water-based formulations. Many factors including the temperature, electrolyte concentration, and the hydrophobicities of both the surfactant and oil contribute to the overall efficiency of the extraction system. Experimental determination of the optimum set of conditions for a given surfactant-oil-water system is both expensive and very time-consuming. Fortunately, empirical equations have been proposed to describe how the various factors affect microemulsion formation. One such expression is based on the hydrophilic-lipophilic difference (HLD) framework [1,2].

$$\text{Ionic surfactant: HLD} = \ln(S) - k \cdot \text{EACN} + C_c - \alpha \cdot (T - T_{\text{ref}}) \quad (1)$$

$$\text{Nonionic surfactant: HLD} = b \cdot S - K \cdot \text{EACN} + C_c + CT \cdot (T - T_{\text{ref}}) \quad (2)$$

where S is the salinity (not to be confused with Abraham's S parameter) and the terms $\ln(S)$ and $b \cdot S$ take into account the electrolyte concentration (usually in grams per 100 mL) of the system, b is electrolyte and surfactant specific, EACN is the equivalent alkane carbon number of the oil phase, C_c represents the hydrophilicity of the surfactant, and the last two terms, $\alpha \cdot (T - T_{\text{ref}})$ and $CT \cdot (T - T_{\text{ref}})$ are related to the temperature effect. The application of HLD in predicting the type and microemulsion phase behavior is described in greater detail elsewhere [1–3].

Our interest in the current study is in developing a predictive method for the equivalent alkane carbon number (EACN), which for simple alkanes is numerically equal to the number of carbons (ACN), and for other liquids it is equal to the number of carbons of the n-alkane exhibiting a similar phase behavior in a reference surfactant-oil-water (SOW) system. EACNs can be determined by comparing the oil's fish-tail-temperature (T^*) in a reference SOW to standard calibration curves for n-alkanes [4]. The experimental determination of EACN values for novel oils may be time consuming and the ability to predict EACN values is advantageous. Bouton et al. [5] have developed a two-descriptor model based upon experimental data for 43 oils using the proprietary Molecular Operating Environment (MOE) software:

$$\text{EACN} = -19.84 + 2.88 \cdot \text{average negative softness} + 0.88 \cdot \text{KierA3} \quad (3)$$

where KierA3 is the third alpha modified shape index and "average negative softness"—which is related to polarizability. Lukowicz et al. [6] have developed a three-descriptor model based upon 70 oils using COSMO-RS σ -moments:

$$\text{EACN} = -4.85 - 0.23 \cdot M_2 - 0.33 \cdot M_{\text{acc}} + 0.06 \cdot M_0, \quad (4)$$

where M_2 is molecular polarity, M_{acc} is hydrogen bond basicity, and M_0 is total molecular surface area. This extends previous work in this area [7]. Most recently, Delforce et al. [8] have developed both a graph machine model using SMILES codes and a neural network model using COSMO-RS-computed σ -moments based on reliable EACN values for 111 molecules.

This work develops a model for EACN based upon experimental EACN values for 80 liquids using the five Abraham solute parameters E, S, A, B, and V which encode physicochemical properties related to those already found to be important—namely size and shape, polarizability, and hydrogen bond basicity, i.e., we propose the following model:

$$\text{EACN} = c + e \cdot E + s \cdot S + a \cdot A + b \cdot B + v \cdot V \quad (5)$$

where E is the solute excess molar refractivity—the measured liquid or gas molar refraction at 20 °C minus that of a hypothetical alkane of identical volume—in units of (cm³/mol)/10, S is the solute dipolarity/polarizability, A and B are the overall or summation hydrogen bond acidity and basicity, and V is the McGowan characteristic volume in units of (cm³/mol)/100.

2. Materials and Methods

Experimentally measured EACN values, collected by Aubry et al. [4,8], were combined with their experimentally determined Abraham solute parameters, primarily from the UFZ-LSER database [9], with the values for decylcyclohexane taken from a paper by Chung et al. [10], and the values for dodecylcyclohexane and bis(2-ethylhexyl) adipate new to this work (from an unpublished database of measured Abraham parameters original to Professor Abraham dated December 2020 shared with one of the authors before Professor Abraham's passing on the 19 January 2021), see Table 1. A modeling dataset was created from these data by: 1. Using median EACN values for compounds with multiple experimental measurements. 2. Only keeping compounds with all 5 Abraham parameters available (measured, not predicted) [9]. This dataset of $N = 86$ compounds with EACN values and Abraham parameters is available under a CC0 license from figshare [11]. Modeling was performed using R v4.2.0 (R Core Team, Vienna, Austria) [12].

Table 1. Measured EACN values with available Abraham Solute Parameters.

Compound	EACN	E	S	A	B	V	EACN Ref.
Branched and cyclic alkanes							
Cyclohexane	2.4	0.305	0.10	0.00	0.00	0.8454	[13]
Cyclohexane	1.7	0.305	0.10	0.00	0.00	0.8454	[13]
Cyclohexane	1.8	0.305	0.10	0.00	0.00	0.8454	[14]
Cyclohexane	2.5	0.305	0.10	0.00	0.00	0.8454	[15]
Methylcyclohexane	3.5	0.244	0.06	0.00	0.00	0.9863	[13]
Methylcyclohexane	2.8	0.244	0.06	0.00	0.00	0.9863	[13]
1,4-Dimethylcyclohexane	4.6	0.191	0.17	0.00	0.00	1.1272	[13]
1,4-Dimethylcyclohexane	4.5	0.191	0.17	0.00	0.00	1.1272	[13]
Ethylcyclohexane	4.5	0.263	0.10	0.00	0.00	1.1272	[13]
Ethylcyclohexane	4.5	0.263	0.10	0.00	0.00	1.1272	[13]
Ethylcyclohexane	3.7	0.263	0.10	0.00	0.00	1.1272	[16]
Cyclooctane	4.1	0.409	0.10	0.00	0.00	1.1272	[6]
1,2-Dimethylcyclohexane	3.9	0.320	0.23	0.00	0.00	1.1272	[16]
1,2-Dimethylcyclohexane	2.6	0.320	0.23	0.00	0.00	1.1272	[13]
Propylcyclohexane	5.8	0.257	0.14	0.00	0.00	1.2681	[13]
Propylcyclohexane	6.3	0.257	0.14	0.00	0.00	1.2681	[13]
Propylcyclohexane	5.5	0.257	0.14	0.00	0.00	1.2681	[16]
Isopropylcyclohexane	5.6	0.283	0.07	0.00	0.00	1.2681	[13]
Isopropylcyclohexane	5.7	0.283	0.07	0.00	0.00	1.2681	[13]
Isopropylcyclohexane	4.5	0.283	0.07	0.00	0.00	1.2681	[13]
Butylcyclohexane	7.2	0.255	0.14	0.00	0.00	1.4090	[13]
Butylcyclohexane	7.9	0.255	0.14	0.00	0.00	1.4090	[17]
Butylcyclohexane	6.9	0.255	0.14	0.00	0.00	1.4090	[16]
Cyclodecane	5.6	0.474	0.10	0.00	0.00	1.4090	[18]
cis-Decalin	5.3	0.544	0.25	0.00	0.00	1.3004	[18]
Myrcane	10.0	0.000	0.00	0.00	0.00	1.5176	[5,19]
Myrcane	11.2	0.000	0.00	0.00	0.00	1.5176	[6,20]
Myrcane	10.1	0.000	0.00	0.00	0.00	1.5176	[13]
Pinane	4.3	0.421	0.12	0.00	0.13	1.3004	[6,20]
Pinane	3.9	0.421	0.12	0.00	0.13	1.3004	[6,20]
p-Menthane	6.3	0.270	0.07	0.00	0.00	1.4090	[6,20]
p-Menthane	6.7	0.270	0.07	0.00	0.00	1.4090	[6,20]
p-Menthane	4.6	0.270	0.07	0.00	0.00	1.4090	[6,20]
Decylcyclohexane	14.4	0.243	0.23	0.00	0.00	2.2544	[21]
Dodecylcyclohexane	17.5	0.300	0.23	0.00	0.00	2.5362	[16]
Isododecane	11.7	0.000	0.00	0.00	0.00	1.7994	[7]
Hemisqualene	14.8	0.000	0.00	0.00	0.00	2.2221	[7]
Squalane	24.5	-	-	-	-	-	[21]
Squalene	13.8	-	-	-	-	-	[22]
Halogenated alkanes							
1-Bromo-2-methylpropane	-3.4	0.340	0.37	0.00	0.12	0.8472	[18]
1-Chlorooctane	1.0	0.191	0.40	0.00	0.09	1.3582	[23]
1-Chlorodecane	3.5	0.185	0.40	0.00	0.09	1.6400	[18]
1,10-Dichlorodecane	6.3	0.366	-	0.00	-	1.7624	[24]
1-Chlorododecane	5.6	0.181	0.40	0.00	0.10	1.9218	[18]
1-Chlorododecane	5.8	0.181	0.40	0.00	0.10	1.9218	[23]
1-Chlorotetradecane	8.0	0.176	0.41	0.00	0.10	2.2036	[18]
1-Chlorotetradecane	7.3	0.176	0.41	0.00	0.10	2.2036	[23]
1-Chlorohexadecane	9.8	0.173	0.42	0.00	0.10	2.4854	[18]
1-Chlorohexadecane	9.0	0.173	0.42	0.00	0.10	2.4854	[23]

Table 1. Cont.

Compound	EACN	E	S	A	B	V	EACN Ref.
Alkenes, terpenes, alkynes and aromatics							
Cyclohexene	-1.2	0.395	0.28	0.00	0.09	0.8024	[13]
1,3-Cyclohexadiene	-3.1	0.515	0.38	0.00	0.12	0.7594	[13]
1,4-Cyclohexadiene	-4.1	0.501	0.46	0.00	0.16	0.7594	[13]
1-Methyl-1-cyclohexene	0.8	0.391	0.18	0.00	0.10	0.9433	[13]
1-Methyl-1-cyclohexene	-0.8	0.391	0.18	0.00	0.10	0.9433	[13]
4-Methyl-1-cyclohexene	0.6	0.347	0.22	0.00	0.10	0.9433	[13]
4-Methyl-1-cyclohexene	-0.5	0.347	0.22	0.00	0.10	0.9433	[13]
3-Methyl-1-cyclohexene	0.4	0.360	0.20	0.00	0.10	0.9433	[13]
3-Methyl-1-cyclohexene	-1.4	0.360	0.20	0.00	0.10	0.9433	[13]
2,5-Norbornadiene	-3.2	0.495	0.32	0.00	0.11	0.7919	[13]
1-Octene	3.9	0.094	0.08	0.00	0.07	1.1928	[18]
cis-Cycloctene	1.5	0.460	0.24	0.00	0.10	1.0842	[18]
1-Octyne	-1.8	0.155	0.22	0.09	0.10	1.1498	[18]
p-Xylene	-2.4	0.613	0.52	0.00	0.16	0.9982	[18]
1-Decene	5.5	0.093	0.08	0.00	0.07	1.4746	[18]
1-Decyne	0.1	0.143	0.22	0.09	0.10	1.4316	[18]
Butylbenzene	0.4	0.600	0.51	0.00	0.15	1.2800	[18]
Phenyl-1-butyne	-3.3	-	-	-	-	-	[18]
alpha-Pinene	3.6	0.438	0.20	0.00	0.14	1.2574	[6,20]
alpha-Pinene	3.4	0.438	0.20	0.00	0.14	1.2574	[6,20]
p-Menth-2-ene	3.1	0.350	0.12	0.00	0.07	1.3660	[19]
p-Menth-2-ene	3.6	0.350	0.12	0.00	0.07	1.3660	[6,20]
Delta-3-carene	2.9	0.492	0.22	0.00	0.14	1.2574	[6,20]
Delta-3-carene	2.0	0.492	0.22	0.00	0.14	1.2574	[6,20]
beta-Pinene	2.3	0.515	0.19	0.00	0.15	1.2574	[6,20]
beta-Pinene	2.0	0.515	0.19	0.00	0.15	1.2574	[6,20]
Limonene	2.0	0.501	0.31	0.00	0.23	1.3230	[6,20]
Limonene	1.6	0.501	0.31	0.00	0.23	1.3230	[6,20]
gamma-Terpinene	1.9	0.522	0.29	0.00	0.22	1.3230	[6,20]
gamma-Terpinene	1.4	0.522	0.29	0.00	0.22	1.3230	[6,20]
alpha-Terpinene	1.5	0.526	0.25	0.00	0.23	1.3230	[6,20]
alpha-Terpinene	0.8	0.526	0.25	0.00	0.23	1.3230	[6,20]
Terpinolene	1.3	0.590	0.31	0.00	0.20	1.3230	[6,20]
Terpinolene	0.1	0.590	0.31	0.00	0.20	1.3230	[6,20]
p-Cymene	-0.3	0.607	0.49	0.00	0.19	1.2800	[6,20]
p-Cymene	-1.3	0.607	0.49	0.00	0.19	1.2800	[6,20]
1-Dodecene	8.1	0.089	0.08	0.00	0.07	1.7564	[18]
1-Dodecyne	2.0	0.133	0.22	0.09	0.10	1.7134	[18]
1-Tetradecyne	3.9	-	-	-	-	-	[18]
Octylbenzene	4.0	0.579	0.48	0.00	0.15	1.8436	[16]
2,6,10-Trimethylundecane-2,6-diene	10.3	-	-	-	-	-	[6,20]
Longifolene	6.6	0.757	0.20	0.00	0.22	1.8533	[20]
Longifolene	7.3	0.757	0.20	0.00	0.22	1.8533	[6,20]
Caryophyllene	5.7	0.720	0.15	0.00	0.25	1.9189	[6,20]
Caryophyllene	6.2	0.720	0.15	0.00	0.25	1.9189	[6,20]
Decylbenzene	6.0	0.579	0.47	0.00	0.15	2.1254	[25]
1-Octadecene	14.4	0.079	0.08	0.00	0.07	2.6018	[18]
Dodecylbenzene	7.8	0.571	0.47	0.00	0.15	2.4072	[25]

Table 1. Cont.

Compound	EACN	E	S	A	B	V	EACN Ref.
Ethers, esters, nitriles and ketones							
Diisopropyl ether	2.2	−0.063	0.17	0.00	0.57	1.0127	[26]
Dibutyl ether	2.4	0.000	0.25	0.00	0.45	1.2945	[22]
Dibutyl ether	3.3	0.000	0.25	0.00	0.45	1.2945	[25]
Dibutyl ether	3.2	0.000	0.25	0.00	0.45	1.2945	[27]
2-Octanone	−3.4	0.108	0.68	0.00	0.51	1.2515	[22]
Octanenitrile	−1.7	0.162	0.90	0.00	0.36	1.2500	[22]
Dipentyl ether	4.2	0.000	0.25	0.00	0.45	1.5763	[22]
C3-O-C4-O-C3	1.9	-	-	-	-	-	[27]
C4-O-C2-O-C4	1.7	-	0.51	0.00	-	1.6350	[27]
2-Decanone	−2.1	0.108	0.68	0.00	0.51	1.5333	[22]
Decanenitrile	−0.6	0.156	0.90	0.00	0.36	1.5320	[22]
2-Undecanone	−1.3	0.101	0.68	0.00	0.51	1.6742	[22]
Ethyl decanoate	1.8	0.013	0.58	0.00	0.45	1.8738	[17]
Ethyl decanoate	2.3	0.013	0.58	0.00	0.45	1.8738	[20]
Ethyl decanoate	2.2	0.013	0.58	0.00	0.45	1.8738	[18]
Dihexyl ether	6.2	0.000	0.25	0.00	0.45	1.8581	[22]
2-Dodecanone	−0.6	0.103	0.68	0.00	0.51	1.8151	[22]
Dodecanenitrile	0.3	0.132	0.90	0.00	0.36	1.8132	[22]
Ethyl dodecanoate	3.8	0.002	0.58	0.00	0.45	2.1556	[6]
Decyl butyrate	5.0	-	-	-	-	-	[6]
Hexyl octanoate	6.2	0.002	0.56	0.00	0.45	2.1556	[6]
Diheptyl ether	8.0	-	-	-	-	-	[22]
Ethyl myristate	5.2	0.000	0.58	0.00	0.45	2.4374	[6]
Butyl dodecanoate	7.2	-	-	-	-	-	[6]
Octyl octanoate	8.1	−0.010	0.06	0.00	0.45	2.4374	[6]
Dioctyl ether	10.3	0.000	0.25	0.00	0.45	2.4217	[22]
Myristyl propionate	6.8	-	-	-	-	-	[6]
Isopropyl myristate	7.2	−0.062	0.53	0.00	0.45	2.5783	[6]
Isopropyl myristate	7.3	−0.062	0.53	0.00	0.45	2.5783	[25]
Ethyl palmitate	6.8	0.000	0.58	0.00	0.45	2.7192	[6]
Hexyl dodecanoate	9.3	-	-	-	-	-	[20]
Ethyl oleate	7.3	-	-	-	-	-	[6]
Ethyl oleate	7.1	-	-	-	-	-	[28]
Bis(2-ethylhexyl) adipate	9.7	−0.010	1.10	0.00	1.13	3.3572	[6]
Tricaprilin	12.2	-	-	-	-	-	[6]
Tricaprin	13.8	-	-	-	-	-	[6]
Tricaprin	13.0	-	-	-	-	-	[25]
Trilaurin	15.7	-	-	-	-	-	[5]
Trimyristin	18.5	-	-	-	-	-	[5]
Tripalmitin	21.2	-	-	-	-	-	[5]
Tristearin	23.9	−0.040	1.25	0.00	1.28	8.3631	[5]
Triolein	21.2	-	-	-	-	-	[5]
Fragrances, acrylates and miscellaneous							
Menthone	−1.5	0.322	0.61	0.00	0.62	1.4247	[21]
Eucalyptol	−1.6	0.380	0.33	0.00	0.76	1.3591	[21]
Rose oxide	−1.7	-	-	-	-	-	[21]
D-Carvone	−3.1	0.674	0.86	0.00	0.57	1.3390	[21]
Hexyl methacrylate	0.4	0.154	0.49	0.00	0.45	1.5490	[29]
Hexyl methacrylate	−0.2	0.154	0.49	0.00	0.45	1.5490	[29]
Hexyl methacrylate	−0.1	0.154	0.49	0.00	0.45	1.5490	[29]
Hexyl methacrylate	0.8	0.154	0.49	0.00	0.45	1.5490	[29]

Table 1. Cont.

Compound	EACN	E	S	A	B	V	EACN Ref.
Fragrances, acrylates and miscellaneous							
Hexyl methacrylate	0.7	0.154	0.49	0.00	0.45	1.5490	[29]
Hexyl methacrylate	−0.2	0.154	0.49	0.00	0.45	1.5490	[29]
Hexyl methacrylate	1.5	0.154	0.49	0.00	0.45	1.5490	[29]
Hexyl methacrylate	0.2	0.154	0.49	0.00	0.45	1.5490	[29]
Hexyl methacrylate	−0.4	0.154	0.49	0.00	0.45	1.5490	[29]
Menthyl acetate	−0.1	0.243	0.65	0.00	0.54	1.7652	[6,20]
Citronellyl acetate	−0.2	0.198	0.59	0.00	0.64	1.8308	[21,22]
Geranyl acetate	−0.6	0.368	0.65	0.00	0.68	1.7878	[21,22]
Linalyl acetate	−0.9	0.331	0.65	0.00	0.65	1.7878	[21,22]
alpha-Damascone	−1.3	-	-	-	-	-	[21]
Methyl dihydrojasmonate	−1.7	0.340	1.53	0.00	0.97	1.9218	[21]
beta-Ionone	−1.9	0.892	0.78	0.00	0.76	1.7614	[17]
Ethylene brassylate	−1.1	-	-	-	-	-	[21]
Methyl cedryl ether	3.5	-	-	-	-	-	[21]
Ambrettolide	1.0	-	-	-	-	-	[21]

3. Results

The standard Abraham solute descriptor-based model is represented by Equation (6), where c is the intercept, E , S , A , B , and V are the Abraham solute descriptors, and e , s , a , b , v are their coefficients obtained by linear regression:

$$\text{EACN} = c + e \cdot E + s \cdot S + a \cdot A + b \cdot B + v \cdot V \quad (6)$$

When using all the data, we found a moderate correlation ($R^2 = 0.61$) between S and B . Removing S -parameter outliers bis(2-ethylhexyl) adipate, tristearin, and methyl dihydrojasmonate ($S > 1$) resulted in a dataset where all pairwise correlations had coefficients of determination lower than 0.50 and the coefficients of determination of each parameter against all others was lower than 0.80. Removing S -parameter outliers provides a greater reliability to the model, but may limit its application to a smaller chemical space.

Performing linear regression with leave-out-out (LOO) cross-validation showed that dodecylcyclohexane, decylcyclohexane, and octyl octanoate were clear outliers. Removing the three outliers, and again using LOO linear regression, we found that EACN can be estimated with similar accuracy (LOO measures) using Abraham solute parameters ($N = 80$, $R^2 = 0.92$, $\text{RMSE} = 1.16$, $\text{MAE} = 0.90$, $p < 2.2 \times 10^{-16}$) as compared to previous models [5–8], at least within the chemical space represented in the study:

$$\text{EACN} = -2.16 - 2.08 \cdot E - 9.51 \cdot S - 50.91 \cdot A - 5.41 \cdot B + 6.83 \cdot V \quad (7)$$

Analyzing the EACN estimates for each compound type, we see that the model performs the best for alkenes, terpenes, alkynes, and aromatics ($N = 31$, $\text{ME} = 0.37$, $\text{MAE} = 0.57$, $\text{RMSE} = 0.76$). Good performance is seen for the four other types: branched and cyclic alkanes ($N = 16$, $\text{ME} = -0.81$, $\text{MAE} = 0.85$, $\text{RMSE} = 1.11$); halogenated alkanes ($N = 6$, $\text{ME} = 0.99$, $\text{MAE} = 0.99$, $\text{RMSE} = 1.16$); fragrances, acrylates, and miscellaneous ($N = 9$, $\text{ME} = -0.16$, $\text{MAE} = 0.94$, $\text{RMSE} = 1.18$); and ethers, esters, nitriles, and ketones ($N = 18$, $\text{ME} = -0.17$, $\text{MAE} = 1.16$, $\text{RMSE} = 1.32$)—with consistent over-prediction for halogenated alkanes and consistent under-prediction for branched and cyclic alkanes, see Figure 1.

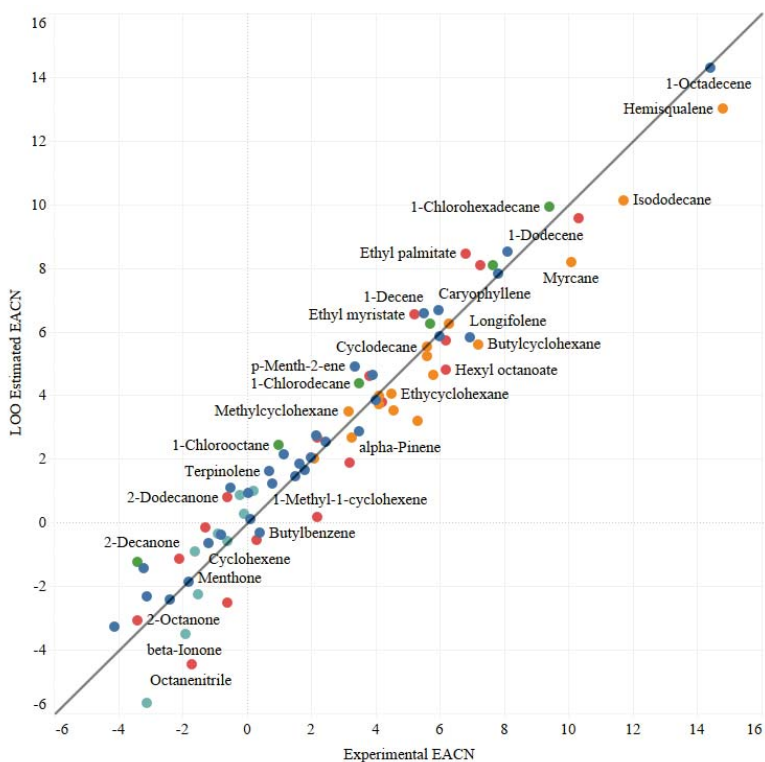


Figure 1. Estimated vs. Measured EACN values colored by type: alkenes, terpenes, alkynes, and aromatics (dark blue); branched and cyclic alkanes (orange); ethers, nitriles, and ketones (red); fragrances, acrylates, and miscellaneous (light blue); and halogenated alkanes (green).

4. Discussion

We have demonstrated that EACN can be estimated using the standard Abraham solute parameter model, see Equation (7). The first four parameters all have negative coefficients where E is the solute excess molar refractivity—the measured liquid or gas molar refraction at 20 °C minus that of a hypothetical alkane of identical volume—in units of $(\text{cm}^3/\text{mol})/10$, S is the solute dipolarity/polarizability, A and B are the overall or summation hydrogen bond acidity and basicity, and V is the McGowan characteristic volume in units of $(\text{cm}^3/\text{mol})/100$. These results align with previous results [5–8], using different parameter systems, but showing similar accuracy and that EACN has contributions from shape (size and branching) [5–8], polarity/polarizability [5–8], and hydrogen bond basicity [6–8]. Our addition of hydrogen bond acidity, represented by the A descriptor, leads to superior estimation of EACN values for alkynes something not seen in previous models.

We began with a dataset of $N = 86$ oils with both measured EACN values and measured Abraham solute descriptors. During modeling we removed six compounds: bis(2-ethylhexyl) adipate, tristearin, methyl dihydrojasmonate, decylcyclohexane, dodecylcyclohexane, and octyl octanoate.

The first three compounds were removed because they had large S -values which resulted in an artificially high collinearity with the B parameter. The second set of three compounds were removed as outliers from a first LOO cross-validation analysis. Even so, Equation (7)-predicted EACN values for these compounds are generally of the right order, see the predicted values in the open dataset [11]. The utility of Equation (7) can also be seen by using it to predict EACN values of compounds that have measured EACN values but

that do not have measured Abraham solute parameters. Using predicted Abraham solute parameters [9], we predicted the EACN values of several of these compounds without measured Abraham solute parameters from Table 1, see Table 2. For the compounds listed in Table 2, Equation (7) performs relatively well, with statistics similar to those found for the estimated EACN results above, specifically: $N = 11$, $ME = 0.17$, $MAE = 1.13$, $RMSE = 1.61$.

Table 2. Equation (7)-predicted EACN values using predicted Abraham solute parameters.

Compound	EACN	E	S	A	B	V	Predicted EACN
1-Tetradecyne	3.9	0.150	0.24	0.05	0.12	1.9952	5.7
2,6,10-Trimethylundecane-2,6-diene	10.3	0.350	0.23	0.00	0.34	2.1361	7.7
Decyl butyrate	5.0	0.000	0.56	0.00	0.55	2.1556	4.3
Butyl dodecanoate	7.2	0.010	0.56	0.00	0.52	2.4374	6.3
Myristyl propionate	6.8	0.050	0.56	0.00	0.53	2.5783	7.2
Diheptyl ether	8.0	0.000	0.18	0.00	0.46	2.1399	8.3
Hexyl dodecanoate	9.3	0.010	0.56	0.00	0.52	2.7192	8.3
Ethyl oleate	7.1	0.130	0.72	0.00	0.68	2.9580	7.2
Ethyl oleate	7.3	0.130	0.72	0.00	0.68	2.9580	7.2
Methyl cedryl ether	3.5	0.650	0.23	0.00	0.22	2.0959	7.4
Ambrettolide	1.0	0.540	0.68	0.00	0.76	2.2858	1.8
alpha-Damascone	-1.3	0.680	0.71	0.00	0.54	1.7614	-1.2

The most recent paper by Delforce et al. [8] notes that the measured EACN of 2.2 for diisopropyl ether reported previously [26] is an outlier for their model. Our model estimates the EACN value of diisopropyl ether to be 0.2 which is in line with their newly measured EACN value of 0.6.

Our approach provides a useful tool for estimating equivalent alkane carbon numbers as Abraham solute parameters are available for a significant number of compounds [9,10]. While a general model is presented, models for specific families of compounds can be easily created using our open dataset [11]. We also note that the estimated EACN values of individual hydrocarbons from Equation (7) will allow estimation of EACN values of heavy hydrocarbon mixtures, $EACN_{mix}$, using the mathematical expression proposed by Cayias et al. [30] and Cash et al. [31]:

$$EACN_{mix} = \sum_{i=1}^N x_i EACN_i \quad (8)$$

where x_i and $EACN_i$ denote the mole fraction and numerical EACN value of the individual hydrocarbon component i , respectively.

Future research directions include measuring the EACN values of more diverse compounds, especially those with known non-zero A-parameter values.

Author Contributions: Conceptualization, W.-K.C.; methodology, W.E.A.J., A.S.I.D.L. and H.M.; data collection and curation, A.S.I.D.L. and H.M.; writing—original draft preparation, W.E.A.J., W.-K.C., A.S.I.D.L. and H.M.; writing—review and editing, W.E.A.J., W.-K.C., A.S.I.D.L. and H.M. All authors have read and agreed to the published version of the manuscript.

Funding: This research received no external funding.

Data Availability Statement: Data used in this study is available from figshare under a CC0 license [11].

Conflicts of Interest: The authors declare no conflict of interest.

References

- Salager, J.L.; Morgan, J.C.; Schechter, R.S.; Wade, W.H.; Spe-Aime, M.; Vasquez, E. Optimum formulation of surfactant/water/oil systems for minimum interfacial tension or phase behavior. *Soc. Pet. Eng. AIME J.* **1979**, *19*, 107–115. [CrossRef]
- Ghayour, A.; Acosta, E. Characterizing the oil-like and surfactant-like behavior of polar oils. *Langmuir* **2019**, *35*, 15038–15050. [CrossRef] [PubMed]

3. Virin Kittithammavong, V.; Charoensang, A.; Khaodhiar, S. A Normalized HLD (HLD_N) tool for optimal salt-concentration prediction of microemulsions. *Appl. Sci.* **2021**, *11*, 9151. [CrossRef]
4. Aubry, J.-M.; Ontiveros, J.F.; Salager, J.L.; Nardello-Rataj, V. Use of the normalized hydrophilic-lipophilic-deviation (HLDN) equation for determining the equivalent alkane carbon number (EACN) of oils and the preferred alkane carbon number (PACN) of nonionic surfactants by the fish-tail method (FTM). *Adv. Colloid Interface Sci.* **2020**, *276*, 102099. [CrossRef]
5. Bouton, F.; Durand, M.; Nardello-Rataj, V.; Borosy, A.P.; Quillet, C.; Aubry, J.M. A QSPR model for the prediction of the “fish-tail” temperature of C₁₀E₄/water/polar hydrocarbon oil systems. *Langmuir* **2010**, *26*, 7962–7970. [CrossRef]
6. Lukowicz, T.; Illous, E.; Nardello-Rataj, V.; Aubry, J.M. Prediction of the equivalent alkane carbon number (EACN) of aprotic polar oils with COSMO-RS sigma-moments. *Colloids Surf. A Physicochem. Eng. Asp.* **2018**, *536*, 53–59. [CrossRef]
7. Lukowicz, T.; Benazzouz, A.; Nardello-Rataj, V.; Aubry, J.-M. Rationalization and Prediction of the Equivalent Alkane Carbon Number (EACN) of Polar Hydrocarbon Oils with COSMO-RS σ -Moments. *Langmuir* **2015**, *31*, 11220–11226. [CrossRef]
8. Delforce, L.; Duprat, F.; Ploix, J.-L.; Ontiveros, J.F.; Goussard, V.; Nardello-Rataj, V.; Aubry, J.-M. Fast Prediction of the Equivalent Alkane Carbon Number Using Graph Machines and Neural Networks. *ACS Omega* **2022**, *in press*.
9. Ulrich, N.; Endo, S.; Brown, T.N.; Watanabe, N.; Bronner, G.; Abraham, M.H.; Goss, K.-U. UFZ-LSER Database v 3.2.1 [Internet], Leipzig, Germany, Helmholtz Centre for Environmental Research-UFZ. 2017. Available online: <http://www.ufz.de/lserd> (accessed on 31 December 2021).
10. Chung, Y.; Vermeire, F.H.; Wu, H.; Walker, P.J.; Abraham, M.H.; Green, W.H. Group Contribution and Machine Learning Approaches to Predict Abraham Solute Parameters, Solvation Free Energy, and Solvation Enthalpy. *J. Chem. Inf. Modeling* **2022**, *62*, 433–446. [CrossRef]
11. Acree, W.E.; Chong, W.; Lang, A.S.I.D.; Mozafari, H. Dataset: EACN and Abraham Parameter Values. Figshare. *Dataset* **2022**. [CrossRef]
12. R Core Team. R: A Language and Environment for Statistical Computing. R Foundation for Statistical Computing, Vienna, Austria. 2022. Available online: <https://www.R-project.org/> (accessed on 31 December 2021).
13. Bouton, F. Influence of Terpenes and Terpenoids on the Phase Behavior of Micro-and Macro-Emulsions. Ph.D. Thesis, University of Lille, Lille, France, 2010.
14. Kahlweit, M.; Strey, R.; Busse, G. Effect of alcohols on the phase behavior of microemulsions. *J. Phys. Chem.* **1991**, *95*, 5344–5352. [CrossRef]
15. Burauer, S.; Sottmann, T.; Strey, R. Nonionic microemulsions with cyclic oils—Oil penetration, efficiency and monomeric solubility. *Tenside Surfactants Deterg.* **2000**, *37*, 8–16.
16. Queste, S.; Salager, J.L.; Strey, R.; Aubry, J.M. The EACN scale for oil classification revisited thanks to fish diagrams. *J. Colloid Interface Sci.* **2007**, *312*, 98–107. [CrossRef] [PubMed]
17. Lukowicz, T. Synergistic Solubilisation of Fragrances in Binary Surfactant Systems and Prediction of Their EACN Value with COSMO-RS. Ph.D. Thesis, Université Lille, Lille, France, 2015.
18. Tchakalova, V.; Testard, F.; Wong, K.; Parker, A.; Benzédi, D.; Zemb, T. Solubilization and interfacial curvature in microemulsions: I. Interfacial expansion and co-extraction of oil. *Colloids Surf. A Physicochem. Eng. Asp.* **2008**, *331*, 31–39. [CrossRef]
19. Bouton, F.; Durand, M.; Nardello-Rataj, V.; Serry, M.; Aubry, J.M. Classification of terpene oils using the fish diagrams and the Equivalent Alkane Carbon (EACN) scale. *Colloids Surf. A Physicochem. Eng. Asp.* **2009**, *338*, 142–147. [CrossRef]
20. Ontiveros, J.F.; Pierlot, C.; Catté, M.; Molinier, V.; Pizzino, A.; Salager, J.L.; Aubry, J.M. Classification of ester oils according to their Equivalent Alkane Carbon Number (EACN) and asymmetry of fish diagrams of C₁₀E₄/ester oil/water systems. *J. Colloid Interface Sci.* **2013**, *403*, 67–76. [CrossRef]
21. Gradziński, M.; Langevin, D.; Sottmann, T.; Strey, R. Droplet microemulsions at the emulsification boundary: The influence of the surfactant structure on the elastic constants of the amphiphilic film. *J. Chem. Phys.* **1997**, *106*, 8232–8238. [CrossRef]
22. Tchakalova, V.; Testard, F.; Wong, K.; Parker, A.; Benzédi, D.; Zemb, T. Solubilization and interfacial curvature in microemulsions: II. Surfactant efficiency and PIT. *Colloids Surf. A Physicochem. Eng. Asp.* **2008**, *331*, 40–47. [CrossRef]
23. Israelachvili, J.N.; Mitchell, D.J.; Ninham, B.W. Theory of self-assembly of hydrocarbon amphiphiles into micelles and bilayers. *J. Chem. Soc. Faraday Trans. 2 Mol. Chem. Phys.* **1976**, *72*, 1525–1568. [CrossRef]
24. Deen, G.R.; Pedersen, J.S. Phase behavior and microstructure of C₁₂E₅ nonionic microemulsions with chlorinated oils. *Langmuir* **2008**, *24*, 3111–3117. [CrossRef]
25. Engelskirchen, S.; Elsner, N.; Sottmann, T.; Strey, R. Triacylglycerol microemulsions stabilized by alkyl ethoxylate surfactants—A basic study: Phase behavior, interfacial tension and microstructure. *J. Colloid Interface Sci.* **2007**, *312*, 114–121. [CrossRef] [PubMed]
26. Wormuth, K.R.; Kaler, E.W. Microemulsifying polar oils. *J. Phys. Chem.* **1989**, *93*, 4855–4861. [CrossRef]
27. Tanford, C. *The Hydrophobic Effect: Formation of Micelles and Biological Membranes*, 2nd ed.; J. Wiley: Hoboken, NJ, USA, 1980.
28. Kahlweit, M.; Busse, G.; Faulhaber, B.; Eibl, H. Preparing nontoxic microemulsions. *Langmuir* **1995**, *11*, 4185–4187. [CrossRef]
29. van Os, N.M.; Haak, J.R.; Rupert, L.A.M. *Physico-Chemical Properties of Selected Anionic, Cationic and Nonionic Surfactants*; Elsevier: Amsterdam, The Netherlands, 2012.
30. Cayias, J.L.; Schechter, R.S.; Wade, W.H. Modeling crude oils for low interfacial tension. *Soc. Pet. Eng. J.* **1976**, *16*, 351–357. [CrossRef]
31. Cash, L.; Cayias, J.L.; Fournier, G.; Macallister, D.; Schares, T.; Schechter, R.S.; Wade, W.H. The application of low interfacial tension scaling rules to binary hydrocarbon mixtures. *J. Colloid Interface Sci.* **1976**, *59*, 39–44. [CrossRef]

Article

Revision and Extension of a Generally Applicable Group Additivity Method for the Calculation of the Refractivity and Polarizability of Organic Molecules at 298.15 K

Rudolf Naef ^{1,*} and William E. Acree, Jr. ²¹ Department of Chemistry, University of Basel, 4003 Basel, Switzerland² Department of Chemistry, University of North Texas, Denton, TX 76203, USA

* Correspondence: rudolf.naef@unibas.ch; Tel.: +41-619-119-273

Abstract: In a continuation and extension of an earlier publication, the calculation of the refractivity and polarizability of organic molecules at standard conditions is presented, applying a commonly applicable computer algorithm based on an atom group additivity method, where the molecules are broken down into their constituting atoms, these again being further characterized by their immediate neighbor atoms. The calculation of their group contributions, carried out by means of a fast Gauss–Seidel fitting calculus, used the experimental data of 5988 molecules from literature. An immediate subsequent ten-fold cross-validation test confirmed the extraordinary accuracy of the prediction of the molar refractivity, indicated by a correlation coefficient R^2 and a cross-validated analog Q^2 of 0.9997, a standard deviation σ of 0.38, a cross-validated analog S of 0.41, and a mean absolute deviation of 0.76%. The high reliability of the predictions was exemplified with three classes of molecules: ionic liquids and silicon- and boron-containing compounds. The corresponding molecular polarizabilities were calculated indirectly from the refractivity using the inverse Lorentz–Lorenz relation. In addition, it could be shown that there is a close relationship between the “true” volume and the refractivity of a molecule, revealing an excellent correlation coefficient R^2 of 0.9645 and a mean absolute deviation of 7.53%.

Keywords: group additivity method; Gauss–Seidel diagonalization; refractivity; polarizability; ionic liquids; silanes; boranes

Citation: Naef, R.; Acree, W.E., Jr. Revision and Extension of a Generally Applicable Group Additivity Method for the Calculation of the Refractivity and Polarizability of Organic Molecules at 298.15 K. *Liquids* **2022**, *2*, 327–377. <https://doi.org/10.3390/liquids2040020>

Academic Editor: Enrico Bodo

Received: 30 August 2022

Accepted: 7 October 2022

Published: 13 October 2022

Publisher’s Note: MDPI stays neutral with regard to jurisdictional claims in published maps and institutional affiliations.



Copyright: © 2022 by the authors. Licensee MDPI, Basel, Switzerland. This article is an open access article distributed under the terms and conditions of the Creative Commons Attribution (CC BY) license (<https://creativecommons.org/licenses/by/4.0/>).

1. Introduction

In continuation of an earlier paper [1], which used a generally applicable atom groups additivity method for the prediction of various molecular descriptors including the refractivity and the polarizability of molecules, the present work puts the focus on the latter two descriptors, for which on the one hand, an extended number of further experimental refractivity data has been included in the atom group parameters calculation, and on the other hand, a different method for the prediction of the polarizability has been introduced, this time based on the former descriptor. The main goal of the present work was to not only increase the reliability of the atom group parameters already published in [1], but in particular to extend the number of atom groups for which as yet no parameter values have been available, with the main interest aimed at atom groups found in ionic liquids. In addition to these, parameters for a large number of additional groups with boron and silicon as central atom could be generated, thus enabling the prediction of the refractivities and polarizabilities of many boranes and silanes.

Earlier calculations of the refractivity and polarizability have been based on the bond refraction and bond polarizability, respectively, on the assumption that the molar refraction and polarizability is the sum of all the bonds in the molecule [2]. The average error between experiment and calculation was 0.7% over a number of less than 100 sample molecules. Later on, Ghose and Crippen [3] developed a method based on 110 atom types,

characterized by the polarizing effect of the heteroatoms and the effect of overlapping with non-hydrogen atoms, again assuming that the sum of all the atom parameters defines the molecular descriptor value. Applying a quadratic, constrained least squares technique for the evaluation of the atom type parameters for 504 molecules, they reported a correlation coefficient of 0.994 and a standard deviation of 1.269. Except for the parameters calculation approach, Ghose and Crippen's method compares closely with the present one, since their atom types follow a similar principle and therefore the present results may best be compared with theirs. Another group additivity approach was chosen by Miller [4,5] for the calculation of the molecular polarizability, whereby the atoms are defined by their state of hybridization, neglecting their neighbor atoms.

The importance of the knowledge of the refractivity and polarizability for the modeling of the dispersive and hydrophobic interactions was outlined in detail by Ghose and Crippen [3]. The attractive forces between nonpolar compounds, also known as dispersive forces, are the result of the correlated motions of their electrons. These forces are evidently closely related to the polarizability of the molecules. Their polarizability again is linearly proportional to their refractivity, given by the Lorentz–Lorenz relation $R = 4/3\pi N\alpha$, where R is the molar refractivity, N is Avogadro's constant, and α is the polarizability. Accordingly, and in contrast to our earlier calculations of the polarizability by means of the group additivity method in [1], the present polarizabilities are directly evaluated from the molar refractivities, with the added bonus that the amount of experimental refractivity data is much larger than that of the polarity, thus enabling the prediction of molecular polarities for which in its atom groups parameter set in [1], no atom groups are defined. It has also been shown that the molecular polarizability is directly proportional to the molecular volume [6]. Hence, on combining the polarizability/volume and polarizability/refractivity correlations, there should be a direct correlation of the refractivity with the molecular volume as postulated by Ghose and Crippen [3]. It would therefore be interesting to see if there is indeed a direct correlation of the refractivity with the "true" molecular volume as applied for the prediction of the heat capacity of solids and liquids in an earlier paper [7].

2. Method

The calculations were carried out on a set of 5988 compounds for which the experimental refractivity or polarizability data have been published, collected from a database of at present 35,952 molecules in their geometry-optimized 3D conformation, encompassing pharmaceuticals, plant protectors, dyes, ionic liquids, liquid crystals, metal-organics, intermediates, and many more, including many further experimentally determined and calculated molecular descriptors. The structural presentations were standardized before storage by a special algorithm, ensuring that all six-membered aromatic ring systems are defined by six aromatic bonds in order to avoid structural ambiguities. In addition and for the same reason, the positive charge in amidinium, pyrazolium, and guanidinium fragments of the ionic liquids was manually positioned on the carbon atom between the nitrogen atoms and their C(+)-N bonds were assumed to be aromatic, which incidentally is in better conformance with the true charge distribution in these cations, as exemplified in, e.g., Figure 1 in [8]. The analogous treatment of the carboxylate and nitro groups is not necessary, as within the present concept of atom groups definitions, they are unambiguously defined.

2.1. Definition of the Atom Groups

Details of the definition of the atom groups for use in a computer-readable form were outlined in [1]. In Table 1 of [1], their namings and meanings were explained; they have been retained in all the subsequent papers including the present one. However, in order to cover the successively increasing amount of additional, structurally variable molecules, several further atom groups had to be added to the parameters list. In particular, the inclusion of ordinary salts and ionic liquids as well as a number of boron- and silicon-containing molecules required the corresponding atom groups listed and explained in Table 1 on some examples. These new atom groups were interpreted and processed by the

computer algorithm in the same way as the remaining ones. In fact, some of these have already been applied in the calculation of the liquid viscosity of molecules in [8].

Table 1. Examples of charged or boron- or silicon-containing atom groups and their meaning.

No	Atom Type	Neighbors	Meaning	Example
1	B	HN2	HBN ₂	Bis(butylamino)borane
7	B	CO2	CBO ₂	Phenyl dimethoxyborane
21	B	O3	BO ₃	Triethoxyborane
25	B(-)	C4	BC ₄ ⁻	Tetracyanoborate
152	C(-) sp3	C3	C-C ⁻ (C)-C	Tricyanomethanide
245	C aromatic	H:C:N(+)	C:CH:N ⁺	C2 in pyridinium
272	C(+) aromatic	H:N2	N:C ⁺ (H):N	C2 in imidazolium
280	C sp	C#N(-)	N#C-C ⁻	Tricyanomethanide
290	C sp	N#N(-)	N#C-N ⁻	Dicyanoamide
295	C sp	=N=S(-)	N=C=S ⁻	Thiocyanate
316	N sp3	HSi2	HNSi ₂	Bis(trimethoxysilyl)amine
352	N(+ sp3)	C4	NC ₄ ⁺	Tetraalkylammonium
359	N(+ sp2)	O2=O(-)	NO ₃ ⁻	Nitrate
363	N aromatic	C2:C(+)	C-N(C):C ⁺	N1 in 1-alkylimidazolium
365	N(+ aromatic)	C:C2	C:N ⁺ (C):C	N in 1-alkylpyridinium
370	N(-)	C2	C-N ⁻ -C	Dicyanoamide
398	O	CSi	COSi	Bis(trimethoxysilyl)amine
502	S4	CO=O2(-)	C-SO ₃ ⁻	Methylsulfonate
512	S4	O2=O2(-)	SO ₄ ⁻	Hydrosulfate
533	Si	C3O	C ₃ SiO	Methoxytrimethylsilane
539	Si	C2N2	C ₂ SiN ₂	Diethyldiisothiocyanatosilane
554	Si	NO3	NSiO ₃	Bis(trimethoxysilyl)amine

2.2. Calculation of the Atom Group Contributions

As outlined in [1], the parameter values of the atom groups are evaluated in four steps: in the first step, those compounds for which the experimental refractivities are known are stored in a temporarily generated help list. In the second step, each molecule in the help list is broken down into its constituting “backbone” atoms (i.e., atoms bound to at least two directly bound neighbor atoms), their atom types and neighbor terms defined according to the rules detailed in [1], and then their occurrences counted. The third step involves the generation of an $M \times (N + 1)$ matrix, wherein M is the number of molecules, $N + 1$ is the complete number of atom groups occurring plus the molecules’ refractivity value, and where each matrix element (i, j) receives the number of occurrences of the j th atom group in the i th molecule. The final step comprises the normalization of this matrix into an $Ax = B$ matrix and its subsequent balancing by means of a fast Gauss–Seidel calculus [9] to receive the atom group contributions x , which are stored and shown in Table 2, together with the corresponding statistics data at the bottom in lines A to H.

Table 2. Atom groups and their contribution in refractivity calculations.

Entry	Atom Type	Neighbors	Contribution	Occurrences	Molecules
1	B	HN2	39.13	15	11
2	B	HNS	46.42	2	2
3	B	HO2	28.1	1	1
4	B	HS2	52.49	5	5
5	B	C3	66.64	4	4
6	B	C2N	62.25	8	8
7	B	C2O	64.24	22	15
8	B	C2S	69.73	10	10
9	B	CN2	58.53	2	2
10	B	CNO	59.28	1	1

Table 2. Cont.

Entry	Atom Type	Neighbors	Contribution	Occurrences	Molecules
11	B	CNS	65.63	1	1
12	B	CO2	61.69	31	26
13	B	COCl	48.7	4	4
14	B	CS2	72.57	8	8
15	B	CSCl	53.86	2	2
16	B	CSBr	56.93	4	4
17	B	CCl2	36.22	8	6
18	B	N3	54.93	4	2
19	B	N2O	56.24	4	2
20	B	NO2	58.3	1	1
21	B	O3	59.3	21	21
22	B	O2Cl	46.04	8	8
23	B	OCl2	33.44	6	6
24	B	S3	75.69	3	3
25	B(−)	C4	74.59	5	5
26	B(−)	O2F2	63.86	4	4
27	B(−)	F4	−2.41	18	18
28	C sp3	H3C	5.7	9421	4296
29	C sp3	H3C(+)	58.97	3	3
30	C sp3	H3N	12.24	387	246
31	C sp3	H3N(+)	19.98	76	55
32	C sp3	H3O	11.65	505	359
33	C sp3	H3S	11.49	79	55
34	C sp3	H3S(+)	16.94	2	2
35	C sp3	H3P	14.04	17	16
36	C sp3	H3P(+)	11.23	2	2
37	C sp3	H3Si	10.79	626	180
38	C sp3	H2BC	−16.41	97	53
39	C sp3	H2C2	4.63	15,752	3454
40	C sp3	H2CN	11.13	1078	561
41	C sp3	H2CN(+)	18.6	223	129
42	C sp3	H2CO	10.61	2562	1560
43	C sp3	H2CS	10.63	395	253
44	C sp3	H2CS(+)	15.8	13	5
45	C sp3	H2CP	12.84	239	171
46	C sp3	H2CP(+)	12.03	46	12
47	C sp3	H2CF	5.62	33	28
48	C sp3	H2CCl	10.5	229	190
49	C sp3	H2CBr	13.44	144	127
50	C sp3	H2CJ	18.58	39	35
51	C sp3	H2CSi	9.66	345	154
52	C sp3	H2N2	17.9	2	2
53	C sp3	H2NO	18.9	1	1
54	C sp3	H2NS	17.11	1	1
55	C sp3	H2O2	16.37	19	18
56	C sp3	H2OCl	16.45	8	7
57	C sp3	H2OBr	20.6	7	7
58	C sp3	H2S2	16.43	10	5
59	C sp3	H2SCl	16.52	4	4
60	C sp3	H2SJ	21.65	2	2
61	C sp3	H2SiCl	15.47	6	5
62	C sp3	H2SiBr	18.54	4	3
63	C sp3	H2Si2	14.42	5	3
64	C sp3	HBC2	−17.46	10	7
65	C sp3	HC3	3.52	1516	1044
66	C sp3	HC2N	9.99	135	114
67	C sp3	HC2N(+)	17.27	13	13

Table 2. Cont.

Entry	Atom Type	Neighbors	Contribution	Occurrences	Molecules
68	C sp3	HC2O	9.55	561	462
69	C sp3	HC2P	11.84	23	21
70	C sp3	HC2S	9.55	75	53
71	C sp3	HC2F	8.42	2	2
72	C sp3	HC2Cl	9.39	84	74
73	C sp3	HC2Br	12.42	80	70
74	C sp3	HC2J	17.84	7	7
75	C sp3	HC2Si	8.64	29	15
76	C sp3	HCN2(+)	31.68	1	1
77	C sp3	HCNCl(+)	23.09	2	2
78	C sp3	HCO2	15.36	53	45
79	C sp3	HCOF	11.6	2	2
80	C sp3	HCOC1	15.53	14	9
81	C sp3	HCOBr	20.2	1	1
82	C sp3	HCS2	15.5	11	11
83	C sp3	HCSC1	14.69	1	1
84	C sp3	HCF2	5.59	29	19
85	C sp3	HCFCl	10.61	7	6
86	C sp3	HCFBr	13.45	1	1
87	C sp3	HCCl2	15.36	33	32
88	C sp3	HCClBr	18.18	5	5
89	C sp3	HCClJ	22.97	2	2
90	C sp3	HCB2	20.98	13	12
91	C sp3	HCB2J	25.95	1	1
92	C sp3	HCJ2	31.39	2	2
93	C sp3	HNO2	21.67	2	2
94	C sp3	HO3	21.51	9	9
95	C sp3	HOF2	11.17	1	1
96	C sp3	HOCl2	21.99	1	1
97	C sp3	HS3	22.99	2	2
98	C sp3	HSiCl2	20.41	5	4
99	C sp3	C4	2.47	299	251
100	C sp3	C3N	8.92	25	21
101	C sp3	C3N(+)	16.1	2	2
102	C sp3	C3O	8.42	125	113
103	C sp3	C3S	8.86	21	14
104	C sp3	C3P	11.38	1	1
105	C sp3	C3F	3.41	5	4
106	C sp3	C3Cl	8.47	7	7
107	C sp3	C3Br	11.46	7	7
108	C sp3	C3J	16.82	3	3
109	C sp3	C3Si	8.05	1	1
110	C sp3	C2NCl(+)	22.78	1	1
111	C sp3	C2O2	14.18	15	15
112	C sp3	C2OCl	14.76	4	4
113	C sp3	C2OS	14	1	1
114	C sp3	C2OP	17.43	3	3
115	C sp3	C2S2	14.73	14	14
116	C sp3	C2Si2	10.98	1	1
117	C sp3	C2F2	5.01	145	40
118	C sp3	C2FC1	9.6	3	3
119	C sp3	C2Cl2	14.26	29	26
120	C sp3	C2ClBr	17.66	3	3
121	C sp3	C2Br2	20.24	6	6
122	C sp3	C2J2	30.57	1	1
123	C sp3	CNF2	11.26	8	3
124	C sp3	CNF2(+)	19.26	2	1
125	C sp3	CO3	19.63	7	7

Table 2. Cont.

Entry	Atom Type	Neighbors	Contribution	Occurrences	Molecules
126	C sp3	CO2Si	17.49	1	1
127	C sp3	COF2	11.48	9	8
128	C sp3	COFCl	16.44	1	1
129	C sp3	CS3	25.53	2	2
130	C sp3	CSF2	10.98	4	3
131	C sp3	CSCI2	22.95	1	1
132	C sp3	CSiBr2	32.18	1	1
133	C sp3	CF3	5.98	98	75
134	C sp3	CF2Cl	10.67	16	14
135	C sp3	CF2Br	13.41	6	5
136	C sp3	CF2J	18.51	4	3
137	C sp3	CPF2(-)	8.9	6	2
138	C sp3	CFCl2	15.39	8	6
139	C sp3	CCl3	20.42	34	31
140	C sp3	CCl2Br	23.23	3	3
141	C sp3	CBr3	29.63	4	3
142	C sp3	N2F2(+)	32.23	1	1
143	C sp3	O4	25.69	3	3
144	C sp3	OSCl2	28.62	3	3
145	C sp3	OF3	11.23	7	7
146	C sp3	OF2Cl	16.36	1	1
147	C sp3	OCl3	26.18	5	5
148	C sp3	SF3	11.78	134	72
149	C sp3	SCl3	28.7	1	1
150	C sp3	SiCl3	25.66	1	1
151	C(-) sp3	HC2	8.26	2	2
152	C(-) sp3	C3	24.54	5	5
153	C sp2	H2=C	5.49	497	428
154	C sp2	HC=C	4.53	1415	860
155	C sp2	HC=N	8.09	22	21
156	C sp2	HC=N(+)	16.04	1	1
157	C sp2	H=CN	9.75	238	132
158	C sp2	H=CN(+)	17.95	3	3
159	C sp2	H=CN(-)	-7.22	4	4
160	C sp2	HC=O	6.22	99	97
161	C sp2	H=CO	3.36	131	120
162	C sp2	H=CP	14.75	25	25
163	C sp2	H=CS	10.03	79	72
164	C sp2	H=CF	5.13	1	1
165	C sp2	H=CCL	10.29	26	23
166	C sp2	H=CBr	13.14	15	13
167	C sp2	H=CJ	18.02	2	2
168	C sp2	H=CSi	9.49	21	15
169	C sp2	HN=N	13.1	7	7
170	C sp2	HN=N(-)	5.23	2	2
171	C sp2	HN=O	11.36	11	11
172	C sp2	H=NO	6.76	3	3
173	C sp2	H=NS	13.17	2	2
174	C sp2	H=NS(+)	-1.5	11	11
175	C sp2	HN=S	20.09	1	1
176	C sp2	HO=O	5.11	25	23
177	C sp2	HO=O(-)	-0.62	4	4
178	C sp2	H=OS	12.42	2	2
179	C sp2	C2=C	3.53	377	295
180	C sp2	C2=N	6.82	41	34
181	C sp2	C2=N(+)	25.75	5	5
182	C sp2	C2=O	4.9	341	330

Table 2. Cont.

Entry	Atom Type	Neighbors	Contribution	Occurrences	Molecules
183	C sp2	C2=O(−)	0	4	2
184	C sp2	C2=S	11.71	1	1
185	C sp2	C=CN	8.66	44	33
186	C sp2	C=CN(+)	16.87	3	3
187	C sp2	C=CO	2.4	94	88
188	C sp2	C=CS	9.32	40	39
189	C sp2	C=CF	4.43	6	4
190	C sp2	C=CCl	9.45	51	39
191	C sp2	C=CBr	11.94	15	15
192	C sp2	C=CJ	18.24	1	1
193	C sp2	CN=N	12.41	3	3
194	C sp2	CN=N(+)	−2.61	4	4
195	C sp2	CN=O	10.15	76	71
196	C sp2	C=NO	5.46	11	11
197	C sp2	CN=O(+)	22.4	3	3
198	C sp2	=CNO(+)	18.51	1	1
199	C sp2	C=NS	12.19	3	3
200	C sp2	CO=O	3.91	1115	877
201	C sp2	CO=O(−)	−2.03	50	50
202	C sp2	C=OP	13.82	1	1
203	C sp2	C=OS	10.82	8	8
204	C sp2	C=OF	4.46	2	2
205	C sp2	C=OCl	11.16	64	55
206	C sp2	C=OBr	14.11	4	4
207	C sp2	C=OJ	20.45	1	1
208	C sp2	CS=S	19.39	1	1
209	C sp2	=CO2	1.21	2	2
210	C sp2	=COS	8	3	3
211	C sp2	=COCl	7.75	1	1
212	C sp2	=COBr	10.45	1	1
213	C sp2	=COJ	15.61	1	1
214	C sp2	=CSCl	14.74	6	4
215	C sp2	=CSBr	17.68	4	3
216	C sp2	=CSJ	22.25	1	1
217	C sp2	=CSiBr	17.13	1	1
218	C sp2	=CF2	5.09	7	7
219	C sp2	=CFCl	10.2	3	2
220	C sp2	=CCL2	15.3	15	13
221	C sp2	=CClJ	22.87	1	1
222	C sp2	=CBr2	20.76	7	7
223	C sp2	=CBrJ	25.82	1	1
224	C sp2	=CJ2	30.75	1	1
225	C sp2	N2=N	16.88	2	2
226	C sp2	N2=O	14.77	10	10
227	C sp2	N2=S	21.5	2	2
228	C sp2	NO=O	9.3	19	16
229	C sp2	NO=S	18.4	1	1
230	C sp2	N=OS	17.32	2	2
231	C sp2	N=OCl	16.29	1	1
232	C sp2	=NOCl	10.4	1	1
233	C sp2	=NS2	20.87	3	3
234	C sp2	=NSCl	17.86	1	1
235	C sp2	=NSBr	21.65	1	1
236	C sp2	O2=O	2.9	21	20
237	C sp2	O=OS	−14.19	1	1
238	C sp2	O=OCl	10	13	12
239	C sp2	=OS2	17.71	1	1
240	C sp2	OS=S	18.21	8	8

Table 2. Cont.

Entry	Atom Type	Neighbors	Contribution	Occurrences	Molecules
241	C sp2	S2=S	26.78	2	2
242	C sp2	=OSCl	17.33	1	1
243	C aromatic	H:C2	4.42	6519	1357
244	C aromatic	H:C:N	6.45	139	92
245	C aromatic	H:C:N(+)	3.24	62	33
246	C aromatic	H:N2	7.84	3	3
247	C aromatic	B:C2	-16.99	46	37
248	C aromatic	:C3	4.56	251	119
249	C aromatic	C:C2	3.53	1300	909
250	C aromatic	C:C:N	5.73	52	43
251	C aromatic	C:C:N(+)	2.09	6	5
252	C aromatic	:C2N	9.79	158	143
253	C aromatic	:C2N(+)	18.25	40	35
254	C aromatic	:C2:N	6.2	11	11
255	C aromatic	:C2O	2.8	359	287
256	C aromatic	:C2P	11.21	35	34
257	C aromatic	:C2S	9.77	43	40
258	C aromatic	:C2F	4.32	119	64
259	C aromatic	:C2Cl	9.24	123	99
260	C aromatic	:C2Br	12.01	60	54
261	C aromatic	:C2J	16.99	19	18
262	C aromatic	:C2Si	8.57	79	52
263	C aromatic	:CN:N	11.15	3	2
264	C aromatic	C:N2	8.01	4	2
265	C aromatic	:C:NO	5.39	4	4
266	C aromatic	:C:NF	6.07	5	4
267	C aromatic	:C:NCl	11.5	3	3
268	C aromatic	:C:NBr	13.99	2	2
269	C aromatic	:C:NJ	20.37	1	1
270	C aromatic	N:N2	15.39	5	2
271	C aromatic	:N2Cl	12.28	1	1
272	C(+) aromatic	H:N2	-10.11	95	95
273	C(+) aromatic	C:N2	-64.74	3	3
274	C(+) aromatic	:N3	-8.28	5	5
275	C sp	B#N(-)	-14.24	20	5
276	C sp	H#C	4.41	84	77
277	C sp	=C2	4.9	9	9
278	C sp	C#C	3.88	200	138
279	C sp	C#N	5.49	149	132
280	C sp	C#N(-)	-3.13	15	5
281	C sp	=C=O	5.84	4	3
282	C sp	#CO	3.2	6	6
283	C sp	#CS	9.65	1	1
284	C sp	#CSi	8.08	6	3
285	C sp	#CCl	10.37	3	3
286	C sp	#CBr	12.31	4	4
287	C sp	#CJ	17.16	6	6
288	C sp	=N2	11.03	1	1
289	C sp	N#N	10.62	3	3
290	C sp	N#N(-)	1.34	26	13
291	C sp	=N=O	8.24	18	14
292	C sp	#NO	5.66	1	1
293	C sp	#NP	-2.29	1	1
294	C sp	=N=S	15.8	34	20
295	C sp	=N=S(-)	7.85	4	4
296	C sp	#NS	11.5	12	12
297	N sp3	H2B	-12.94	1	1

Table 2. Cont.

Entry	Atom Type	Neighbors	Contribution	Occurrences	Molecules
298	N sp3	H2C	−2	148	133
299	N sp3	H2C(pi)	−1.3	77	69
300	N sp3	H2N	−5.01	13	13
301	N sp3	H2Si	1.97	4	4
302	N sp3	HC2	−9.63	110	108
303	N sp3	HBC	−20.05	18	11
304	N sp3	HBC(pi)	−18.67	6	5
305	N sp3	HC2(pi)	−8.63	54	53
306	N sp3	HC2(2pi)	−7.37	37	34
307	N sp3	HCN	−2.94	9	5
308	N sp3	HCN(pi)	−1.31	2	2
309	N sp3	HCN(+)(pi)	4.48	2	2
310	N sp3	HCN(2pi)	−3.61	3	3
311	N sp3	HCO	−2.67	2	2
312	N sp3	HCP	0.72	3	3
313	N sp3	HCSi	−5.5	6	6
314	N sp3	HCSi(pi)	−4.28	1	1
315	N sp3	HNSi	−8.36	34	19
316	N sp3	HSi2	−1.34	19	15
317	N sp3	B2C	−38.6	12	4
318	N sp3	BC2	−27.51	16	11
319	N sp3	BC2(pi)	−26.43	2	1
320	N sp3	C3	−16.75	123	110
321	N sp3	C3(pi)	−15.83	67	61
322	N sp3	C3(2pi)	−14.97	22	22
323	N sp3	C3(3pi)	−15.13	3	3
324	N sp3	C2N	−0.73	45	30
325	N sp3	C2N(pi)	−0.19	14	14
326	N sp3	C2N(2pi)	−10.64	4	4
327	N sp3	C2N(3pi)	−9.23	2	2
328	N sp3	C2N(+)(pi)	−2.99	2	2
329	N sp3	C2N(+)(2pi)	−1.57	2	2
330	N sp3	C2N(+)(3pi)	−40.57	5	5
331	N sp3	C2O	−10.11	4	4
332	N sp3	C2P	−6.55	86	54
333	N sp3	C2Si	−12.89	27	12
334	N sp3	CCl2(pi)	11.05	1	1
335	N sp2	H=C	1.03	8	8
336	N sp2	C=C	−6.59	63	58
337	N sp2	C=N	−2.23	11	6
338	N sp2	C=N(+)	0.41	5	5
339	N sp2	=CN	−0.2	19	13
340	N sp2	=CN(−)	13.22	2	2
341	N sp2	=CO	−2.21	34	33
342	N sp2	=CP	2.65	1	1
343	N sp2	=CS	4.72	3	2
344	N sp2	=CSi	−2.01	26	12
345	N sp2	N=N	3.04	1	1
346	N sp2	N=O	−4.93	12	12
347	N sp2	O=O	3.41	18	15
348	N sp2	P=P	4.02	9	3
349	N(+) sp3	H3C	−0.39	13	13
350	N(+) sp3	H2C2	−15.27	4	4
351	N(+) sp3	HC3	−30.15	8	8
352	N(+) sp3	C4	−47.94	46	46
353	N(+) sp2	HC=C	12.52	4	4
354	N(+) sp2	C2=C	−5.91	11	11
355	N(+) sp2	C=CN	0	5	5

Table 2. Cont.

Entry	Atom Type	Neighbors	Contribution	Occurrences	Molecules
356	N(+) sp2	C=NO(-)	-4.48	2	2
357	N(+) sp2	CO=O(-)	-7.16	75	65
358	N(+) sp2	NO=O(-)	0	6	6
359	N(+) sp2	O2=O(-)	0.2	27	20
360	N aromatic	H2:C(+)	0	5	5
361	N aromatic	HC:C(+)	10.05	1	1
362	N aromatic	:C2	-1.94	120	105
363	N aromatic	C2:C(+)	1.26	205	103
364	N aromatic	:C:N	0.2	6	3
365	N(+) aromatic	C:C2	-1.86	33	33
366	N(+) aromatic	:C2O(-)	8.85	1	1
367	N(+) sp	C#C(-)	-7.99	3	3
368	N(+) sp	=C=N(-)	-3.91	1	1
369	N(+) sp	=N2(-)	2.99	3	3
370	N(-)	C2	4.69	15	15
371	N(-)	CN	-12.52	2	2
372	N(-)	S2	1.69	69	69
373	O	HB	-17.09	3	3
374	O	B2	-35.49	6	6
375	O	HC	-3.5	602	527
376	O	HC(pi)	3.39	266	250
377	O	HN	2.35	4	4
378	O	HN(pi)	4.33	14	14
379	O	HO	2.75	15	15
380	O	HS	7.17	5	4
381	O	HP	5.14	26	23
382	O	HSi	0.8	7	7
383	O	BC	-23.16	165	75
384	O	BC(pi)	-11.65	2	1
385	O	BC(-)(pi)	-31.4	8	4
386	O	C2	-10.27	617	420
387	O	C2(pi)	-3.51	1209	958
388	O	C2(2pi)	3.23	137	135
389	O	CN	-4.7	2	2
390	O	CN(pi)	-2.22	31	28
391	O	CN(+)(pi)	2.51	24	17
392	O	CN(2pi)	3.03	5	5
393	O	CO	-3.92	31	23
394	O	CO(pi)	3.65	2	2
395	O	CP	-1.46	471	249
396	O	CP(pi)	4.87	50	30
397	O	CS	-0.98	48	37
398	O	CSi	-6.31	244	103
399	O	CSi(pi)	0.28	29	19
400	O	CCL	2.14	1	1
401	O	N2(2pi)	3.14	1	1
402	O	P2	7.2	23	19
403	O	Si2	-2.39	116	35
404	P3	H2C	2.85	17	17
405	P3	HC2	-6.24	3	3
406	P3	C3	-15.17	18	18
407	P3	C2O	-10.92	10	10
408	P3	C2S	-3.08	3	3
409	P3	C2Cl	-6.82	16	16
410	P3	CO2	-6.82	15	15
411	P3	COCl	-2.2	6	6
412	P3	CS2	17.67	1	1
413	P3	CCL2	12.05	8	8

Table 2. Cont.

Entry	Atom Type	Neighbors	Contribution	Occurrences	Molecules
414	P3	N3	-4.26	1	1
415	P3	N2O	-2.29	3	3
416	P3	NO2	-1.46	3	3
417	P3	O3	-1.41	26	26
418	P3	O2Cl	6.11	1	1
419	P3	OCI2	16.38	1	1
420	P3	S3	21.45	4	4
421	P4	HC2=O	-7.52	2	2
422	P4	HO2=O	2.18	17	17
423	P4	HO2=S	8.79	3	3
424	P4	C3=O	-17.18	3	3
425	P4	C3=S	-8.85	3	3
426	P4	C2O=O	-12.11	10	10
427	P4	C2O=O(-)	-15.97	1	1
428	P4	C2=OS	-4.17	1	1
429	P4	C2O=S	-4.41	1	1
430	P4	C2S=S	-0.38	1	1
431	P4	C2=SCl	5.18	1	1
432	P4	CN2=O	-10.68	10	10
433	P4	CNO=O	8.01	1	1
434	P4	CN=OF	-5.4	4	4
435	P4	CN=OCl	0.56	5	5
436	P4	CO2=O	-7.79	42	42
437	P4	CO2=O(-)	-10.36	1	1
438	P4	CO2=S	0.26	8	8
439	P4	C=OS2	8.61	2	2
440	P4	COS=S	7.49	30	30
441	P4	C=OF2	0.52	5	5
442	P4	C=OCI2	11.1	9	9
443	P4	CS2=S	16.66	6	3
444	P4	C=SCl2	19.41	5	5
445	P4	N3=O	-6.3	1	1
446	P4	N2O=O	-5	5	5
447	P4	N=NO2	-3.25	6	2
448	P4	N2O=S	3.2	2	2
449	P4	N2=OF	-0.37	1	1
450	P4	N=NS2	12.33	3	1
451	P4	NO2=O	-4.03	3	3
452	P4	NO2=S	4.11	6	6
453	P4	NO=OF	0.12	7	6
454	P4	NO=SF	7.56	5	4
455	P4	N=OF2	4.05	1	1
456	P4	N=OFCl	9.6	2	2
457	P4	N=OFBr	12.55	1	1
458	P4	N=OCI2	14.9	1	1
459	P4	N=SFCl	17.24	1	1
460	P4	N=SFBr	20.83	1	1
461	P4	N=SCl2	22.78	1	1
462	P4	O3=O	-2.5	33	26
463	P4	O3=O(-)	-6.33	3	3
464	P4	O3=S	5.03	16	14
465	P4	O2=OS	15.08	4	4
466	P4	O2=OF	1.56	16	12
467	P4	O2=OCl	6.38	2	2
468	P4	O2S=S	12.87	2	2
469	P4	O2=SF	9.65	2	1
470	P4	O2=SCl	14.28	3	3

Table 2. Cont.

Entry	Atom Type	Neighbors	Contribution	Occurrences	Molecules
471	P4	O=OF2	5.45	1	1
472	P4	O=OFCl	10.51	7	6
473	P4	O=OFBr	13.17	1	1
474	P4	O=OC12	15.86	1	1
475	P4	O=SF2	12.58	1	1
476	P4	O=SFCl	18.16	1	1
477	P4	O=SFBr	21.4	1	1
478	P4	O=SCl2	23.03	1	1
479	P(-)	C3F3	-11.9	2	2
480	P(-)	F6	1.32	6	6
481	P(+)	C4	-14.3	12	12
482	S2	HC	2.74	78	58
483	S2	HC(pi)	2.64	8	7
484	S2	HP	5.84	27	27
485	S2	BC	-21.7	51	32
486	S2	BC(pi)	-21.88	3	3
487	S2	C2	-4.08	157	98
488	S2	C2(pi)	-3.93	77	73
489	S2	C2(2pi)	-4.31	70	70
490	S2	CP	-1.63	34	18
491	S2	CS	2.06	38	21
492	S2	CS(pi)	-12.06	2	1
493	S2	CCl	6.16	5	5
494	S2	N2(2pi)	-5.14	1	1
495	S2	PCl	0	4	4
496	S2	P2	0	6	3
497	S2	S2	8.87	6	5
498	S4	C2=O	-3.2	4	4
499	S4	C2=O2	-3.24	12	12
500	S4	CN=O2(-)	-0.22	126	63
501	S4	CO=O2	-1.48	11	11
502	S4	CO=O2(-)	-3.78	24	24
503	S4	C=OCl	9.42	6	6
504	S4	C=OS	3.69	4	4
505	S4	C=O2F	4.69	8	8
506	S4	C=O2Cl	8.91	8	8
507	S4	N=O2F(-)	5.76	12	6
508	S4	N=O2Cl	10.28	1	1
509	S4	O=OCl	11.86	1	1
510	S4	O2=O	1.31	7	7
511	S4	O2=O2	1.17	4	4
512	S4	O2=O2(-)	-2.26	16	16
513	S4	O=O2Cl	11.45	2	2
514	S4	O=O2F	5.93	1	1
515	S(+)	C3	-19.18	5	5
516	Si	H3C	6.42	8	7
517	Si	H3Si	12.32	19	8
518	Si	H2C2	0.06	12	10
519	Si	H2CN	6.65	1	1
520	Si	H2CCl	10.82	1	1
521	Si	H2Si2	12.04	18	7
522	Si	HC3	-6.7	14	14
523	Si	HC2N	0.57	5	4
524	Si	HC2O	-0.27	11	7
525	Si	HC2Cl	3.98	4	4
526	Si	HCN2	7.39	6	6
527	Si	HCO2	5.89	18	9
528	Si	HCOCl	10.13	1	1

Table 2. Cont.

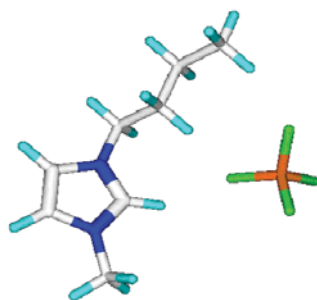
Entry	Atom Type	Neighbors	Contribution	Occurrences	Molecules
529	Si	HN3	14.51	1	1
530	Si	HSi3	12.05	3	3
531	Si	C4	-12.83	49	40
532	Si	C3N	-6.05	42	32
533	Si	C3O	-6.7	84	61
534	Si	C3F	-7.57	5	5
535	Si	C3Cl	-2.55	12	12
536	Si	C3Br	0.52	3	3
537	Si	C3J	6.46	2	2
538	Si	C3Si	-6.69	6	3
539	Si	C2N2	1.02	12	10
540	Si	C2O2	-0.54	100	39
541	Si	C2Si2	-0.39	3	2
542	Si	C2SiCl	3.56	2	1
543	Si	C2F2	-2.89	6	6
544	Si	C2Cl2	8.03	13	13
545	Si	C2Br2	14.34	1	1
546	Si	C2J2	26	1	1
547	Si	CN3	7.74	6	6
548	Si	CN2Cl	11.22	2	2
549	Si	CO3	5.81	30	30
550	Si	COCl2	14.59	4	4
551	Si	CF3	2.56	3	3
552	Si	CCl3	18.65	17	16
553	Si	CBr3	27.76	1	1
554	Si	NO3	12.84	6	4
555	Si	N2O2	4.42	1	1
556	Si	N3O	0.43	1	1
557	Si	N4	14.64	4	4
558	Si	O4	12.5	15	15
559	Si	O3Cl	16.78	1	1
560	Si	OCl3	25.14	2	2
561	Chloride		-1	7	7
562	Bromide		3.11	3	3
A	Based on	Valid groups	382		5988
B	Goodness of fit	R ²	0.9997		5763
C	Deviation	Average	0.29		5763
D	Deviation	Standard	0.38		5763
E	K-fold cv	K	10		5572
F	Goodness of fit	Q ²	0.9997		5572
G	Deviation	Average (cv)	0.31		5572
H	Deviation	Standard (cv)	0.41		5572

2.3. Calculation of the Refractivity

The calculation of the refractivity of a molecule, based on the atom group parameters compiled in Table 2, is a simple summing up of the contribution of each atom group found in a molecule, as exemplified in Table 3 for 1-butyl-3-methylimidazolium tetrafluoroborate (Figure 1), for which the experimentally evaluated refractivity value was 47.81 [10]. The parameters for the monoatomic anions found among some ILs are given under the respective “group” names “Chloride” and “Bromide”. Any further halogenide anion can be taken into account analogously as soon as the experimental data of at least three representative compounds are available.

Table 3. Example calculation of the refractivity of 1-butyl-3-methylimidazolium tetrafluoroborate.

Atom Type Neighbors	B(-) F4	C sp3 H3C	C sp3 H3N	C sp3 H2C2	C sp3 H2CN	C sp2 H=CN	C(+) Aromatic HN2	N Aromatic C2:C(+)	Sum
Contribution	-2.41	5.7	12.24	4.63	11.13	9.75	-10.11	1.26	
n Groups	1	1	1	2	1	2	1	2	
n × Contribution	-2.41	5.7	12.24	9.26	11.13	19.5	-10.11	2.52	47.83

**Figure 1.** 1-Butyl-3-methylimidazolium tetrafluoroborate.

It goes without saying that this calculation method is limited to compounds for which each atom group is defined by a parameter value in Table 2. In addition, as the reliability of these parameter values increases with the number of independent molecules upon which they are based, only atom groups should be considered for which the number of molecules in the rightmost column of Table 2 is three or more, which are henceforth called “valid”. (It could be shown by means of several cross-validation calculations that the decrease of the cross-validated standard deviation on going from three to four molecules per atom group is insignificant compared with the decrease observed when going from two to three molecules per atom group.) Consequently, the number of molecules for which the refractivity values have been calculated (lines B, C, and D in Table 2) is necessarily smaller than the number upon which the calculation of the complete set of parameters is based (line A in Table 2).

2.4. Cross-Validation Calculations

The calculations of the atom group parameters are immediately followed by a plausibility test applying a 10-fold cross-validation algorithm comprising 10 recalculations omitting in each case a different tenth of the complete set of compounds, ensuring that each compound has been used once as a test sample. The resulting training and test data are added to the molecule’s datafiles. Finally, the corresponding statistics data are evaluated and collected at the bottom of Table 2. Due to the smaller number of training molecules in the cross-validation calculations and the condition that only atom group parameters should be considered in the calculation of the individual refractivities for which the number of molecules in the rightmost column is three or more, the number of molecules with calculated refractivities (lines E, F, G, and H) is again lower in the test set than in the training set (lines B, C, and D). Atom group parameters with molecule numbers below three in the rightmost column, which are accordingly at present not applicable for refractivity calculations, have deliberately been left in Table 2 for future use in this continuing project and not least in the hope that interested scientists may assist in increasing the number of “valid” groups in this parameters list by compounds carrying the underrepresented atom groups. At present, the list of elements for refractivity/polarizability calculations is limited to H, B, C, N, O, P, S, Si, and/or halogen, but is easily extendable to enable the parametrization of atom groups containing additional elements for which experimental densities and refractive indices are available.

2.5. Calculation of the Polarizability

According to the Lorentz–Lorenz relation $R = 4/3\pi N\alpha$, N being Avogadro’s number, the refractivity R of a molecule can be translated into its polarizability α by simply multiplying its refractivity value with the reciprocal value of $4/3\pi N$, which is 0.3964, if the refractivity is expressed in mL and the polarizability in Å^3 . Therefore, in this study, for each input experimental refractivity value, the corresponding polarizability value was also evaluated and stored as experimental value in the database, and vice versa. The latter is all the more justified as in many (if not most) cases, the polarizability value was evaluated via the refractivity value. Accordingly, the number of experimental data for these two descriptors is identical, and so is their list of atom group parameters. As a consequence, calculation of a molecule’s refractivity value by means of the group additivity method, based on the refractivity parameters in Table 2, immediately enabled the calculation of its polarizability value by simply multiplying it by 0.3964.

3. Sources of Refractivity and Polarizability Data

In most cases, it was not the refractivity value itself that was published in the following references but the refractive index (n_d) and the density (d) of the molecules, which then had to be translated into the refractivity (R) according to the equation $R = (n_d^2 - 1)/(n_d^2 + 2) \times (M/d)$, where M is the molecular weight. The primary sources of the refractivity data for the earlier [1] as well as the present study were the comprehensive CRC Handbook of Chemistry and Physics [11] and the collective work of Ghose and Crippen [12]. Within the last 7 years since the first publication dealing with the present subject however, a large number of further papers has been collected producing additional refractivity and polarizability data which helped to extend the scope of applicability of the atom group additivity method, particularly for boron- and silicon-containing compounds and ionic liquids. In the following, they have been sorted by their dominant functional features. Within the last ca. 85 years, many papers have been published producing the refractive indices and densities to characterize various hydrocarbons [13–34], alcohols [35–42], ethers [43–47], acids [48], (ortho)esters and carbonates [49–62], acetals [63,64], ketones [65,66], peroxides [67–71], amines, hydrazines, nitriles, and nitro compounds [72–78], and various boron- [79–96], phosphorus- [97–136], and sulfur-containing compounds [137–160]. Many of the compounds mentioned so far also carried halogens [161–182,182–196]. An interesting extension to the parameters database was provided by papers presenting results of silicon-containing compounds [197–240]. Beyond the refractivity data of the various mentioned functional groups, those for a number of heteroarenes and heterocycles have been published [241–260]. Another important extension that was not covered in the earlier paper [1] is the class of ionic liquids [10,261–366]. In addition, several papers have been added which contributed various subjects that could not be assigned to any specific subject of the aforementioned ones [2,367–385]. Finally, a number of papers published experimental data of the polarizability of molecules, in many cases derived from their refractivity values [6,386–395].

4. Results

4.1. Refractivity

In the paper of Ghose and Crippen [3] mentioned earlier, it was stated that the molar refractivity is directly related to the molecule’s volume, expressed in the refractivity’s unit “mL”, their atom group parameters accordingly being associated with the volume of the molecule’s constituting atoms. The present approach, on the other hand, does not care about the theoretical background of the refractivity as it is a purely mathematical method to adjust the calculated to the experimental data, and therefore the resulting atom group parameters must not be assigned with any physical meaning. Consequently, as can be seen in Tables 2 and 3, negative parameter values are not unusual.

While in the earlier paper [1], generally no limit was given concerning the deviation of the experimental data from the calculated ones for the evaluation of the atom group parameters, in the present work, the atom group parameters in Table 2 and the statistics

data at its bottom (Lines A to H) are the result after a stepwise elimination of outliers, defined as their experimental value deviating from the calculated one by more than three times the cross-validated standard error Q^2 . The final list of discarded outliers is available in the Supplementary Materials. As a consequence, 5988 of the originally 6501 compounds with experimental data remained for the evaluation of said parameters, leaving ca. 7.9% as outliers. Due to the elimination of the outliers, the statistical data significantly improved in comparison with those in the earlier paper: not only is the present set of parameters based on a significantly larger number of molecules (5988 vs. 4300, rows A in present Table 2 vs. corresponding Table 13 of [1]) and a larger number of atom groups (562 vs. 364), but also their standard deviation (0.38 vs. 0.66, rows D) and the cross-validated deviation (0.41 vs. 0.7, rows H) drastically improved. Together with the corresponding correlation coefficients R^2 and Q^2 of 0.9997 (rows B and F in Table 2) in the present work, they compare very favorably with the correlation coefficient of 0.994 and the standard deviation of 1.269 published by Ghose and Crippen [3]. The mean absolute percentage deviation (MAPD) of the finally calculated refractivities from the experimental values of 5988 molecules is 0.76%. The increased number of “valid” atom group parameters enabled the calculation of the refractivities and polarizabilities of ca. 80% of the close to 36,000 molecules in the present database, which can be viewed as representative for the entire chemical realm. The excellent correlation between experiment and prediction is visualized in the correlation diagram of Figure 2. The corresponding histogram in Figure 3 confirms the uniform distribution of the deviations between the experimental and calculated refractivities, their experimental values ranging from 8.23 (methanol) to 271.13 (glycerol tristearate). The complete set of compounds with experimental refractivities used for the atom group parameters of Table 2 are available in the Supplementary Materials.

An interesting observation can be made with respect to the outliers in that many of them are solids. Cao et al. [396] showed that solid compounds can exhibit up to three differing refractive indices, depending on their crystal symmetry. A typical example is Ibuprofen, a non-steroidal anti-inflammatory, which shows the three refractive index values 1.522, 1.572, and 1.644. With its reported density of 1.119 g/cm³ and a refractivity of 60.95, calculated by means of our group additivity model, we calculated a refractive index of 1.575, which is pretty close to the mean of the three experimental values. Analogous results have been found with several other outliers, confirming the assessment that in cases where the experimental refractive index strongly deviates from the predicted one, the reason might be that a specific crystal form of the compound was examined. Since these mean refractive index values usually do not represent real crystalline forms, they were not included in the group parameters optimization procedure.

Since the last paper [1] of 2015, the systematic screening of the chemical literature has provided a number of refractivities data of previously under-represented classes of molecules enabling, as mentioned earlier, a substantial increase of the number of atom group parameters in the present Table 2 compared with the one of Table 13 in [1]. In particular, three classes of compounds have experienced an extended representation and will in the following be discussed in more detail: ionic liquids and silicon- and boron-containing compounds.

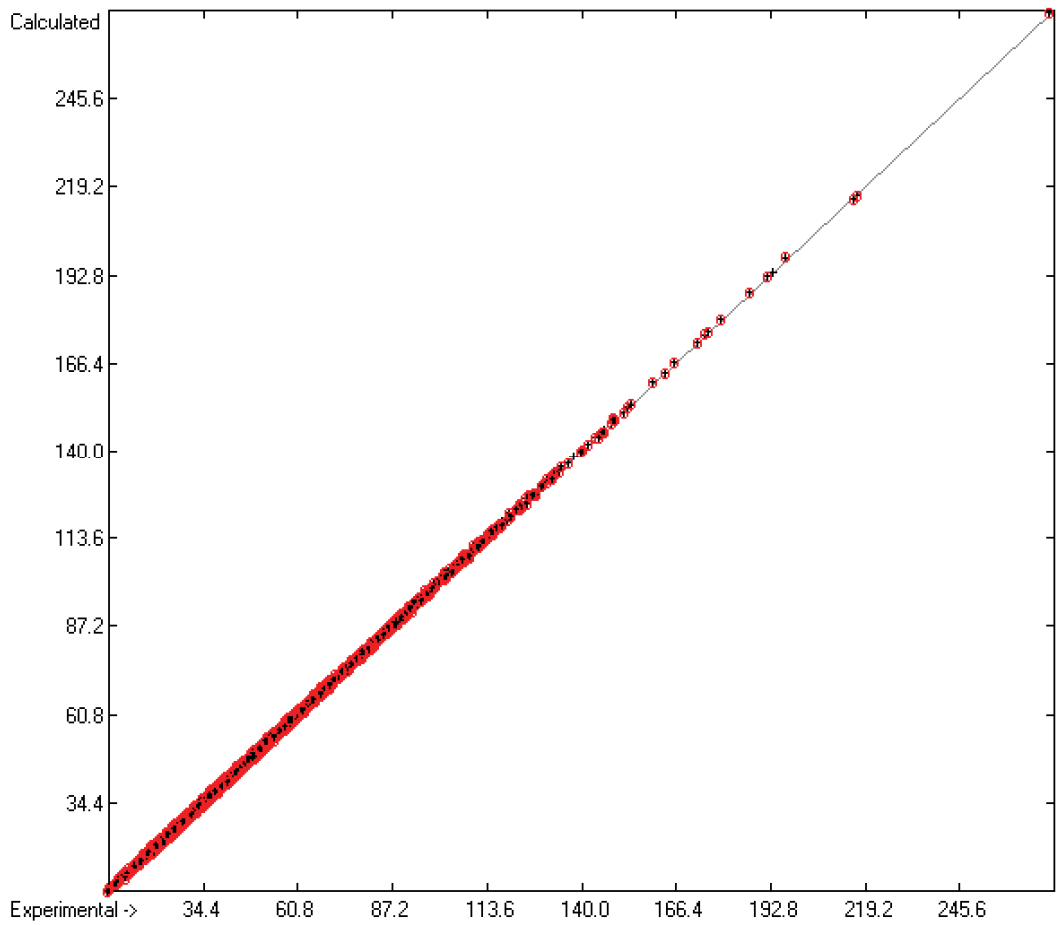


Figure 2. Correlation diagram of the refractivity data. Cross-validation data are superpositioned as red circles. (10-fold cross-valid.: $N = 5763$, $Q^2 = 0.9997$, regression line: intercept = 0.0292; slope = 0.9995, MAPD = 0.76%).

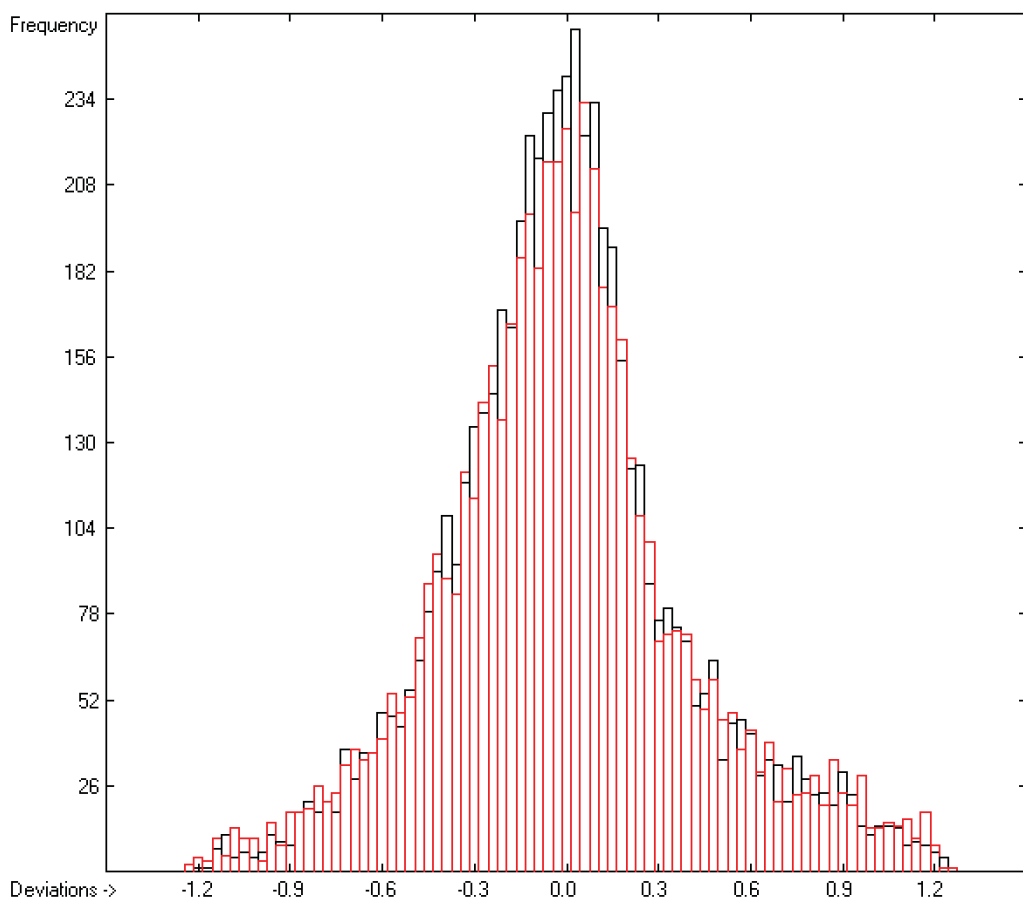


Figure 3. Histogram of the refractivity data. Cross-validation data are superpositioned as red bars. ($\sigma = 0.38$; $S = 0.41$; experimental values range from 8.23 to 271.13).

4.1.1. Ionic Liquids

In the last ca. 25 years, ionic liquids (ILs) have experienced increasing attention as potential replacements for volatile solvents as they are non-volatile, non-inflammable, and can easily be recycled. Their physical properties are easily tunable by suitable choice of their cation and anion, making them favorable candidates as media for chemical syntheses. The enormous variety of potential cation–anion combinations, however, obliges one to put the focus on those candidates with the most promising properties. In the last few years, a substantial number of ILs have been synthesized and their physical properties have been examined. Based on these results, few attempts have been made so far to utilize these results for the prediction of the physical properties of as yet unknown cation–anion combinations, and if yes, then for a narrow scope within the scientists’ range of experience (see, e.g., Almeida et al. [317]), or as in other cases, as in the papers of Sattari et al. [335] or of Venkatraman et al. [359], for the prediction of a specific property based on a fairly large range of ILs by either applying quantitative structure–property relationship (QSPR) technique or machine learning. The present atom group additivity approach, on the other hand, has proven its versatility in that it is able to predict a number of properties of nearly any type of compound by means of an identical algorithm, simply using the appropriate atom group parameters tables. Accordingly, based on the updated parameters tables in

this ongoing project, we have been able to calculate the heat of combustion [397] for 30 ILs with a correlation coefficient R^2 of 1.0 and a mean average percentage deviation from experimental values (MAPD) of 0.21% and a standard deviation σ of 17.75 kJ/mol, the heat of vaporization [398] of 61 ILs ($R^2 = 0.9615$, MAPD = 2.12%, $\sigma = 4.22$ kJ/mol), the liquid viscosity [8] for 113 ILs ($R^2 = 0.9830$, MAPD = 3.43%, $\sigma = 0.11$ J/mol/K), the surface tension [399] of 161 ILs ($R^2 = 0.8413$, MAPD = 5.17%, $\sigma = 2.40$ dyn/cm), and the liquid heat capacity at 298 K [400] of 140 ILs ($R^2 = 0.9986$, MAPD = 1.05%, $\sigma = 7.50$ J/mol/K). In analogy to these results, the refractivity values of 228 ILs calculated by means of the atom group parameters of Table 2 were compared with their experimental data and collected alphabetically in Table 4, revealing a MAPD of only 0.44% and a σ of 0.38. For comparison: the statistics for the 203 ILs for which, while serving as test samples in the cross-validation calculations, the test results could be calculated, yielded an only slightly inferior MAPD of 0.51% and a σ of 0.44.

Table 4. Calculated and experimental refractivity of ionic liquids.

Molecule Name	Refractivity Exp.	Refractivity Calc.	Deviation	Dev. in %
1-(2-Cyanoethyl)-3-(2-hydroxyethyl)-imidazolium chloride	51.06	50.40	0.66	1.29
1-(2-Cyanoethyl)-3-(2-propen-1-yl)-imidazolium chloride	53.46	53.31	0.15	0.28
1-(2-Cyanoethyl)-3-octylimidazolium 3-sulfobenzoate	111.59	112.27	-0.68	-0.61
1-(2-Hydroxyethyl)-3-methylimidazolium perfluoropentanoate	62.30	61.37	0.93	1.49
1-(3-Cyanopropyl)-3-methylimidazolium bis(trifluoromethylsulfonyl) amide	74.64	74.84	-0.20	-0.27
1-(3-Cyanopropyl)-3-methylimidazolium dicyanamide	56.96	57.40	-0.44	-0.77
1-(3-Cyanopropyl)-3-methylimidazolium tetrafluoroborate	46.88	47.62	-0.74	-1.58
1-(3-Cyanopropyl)-pyridinium bis(trifluoromethylsulfonyl) amide	75.74	76.04	-0.30	-0.40
1-(3-Cyanopropyl)-pyridinium dicyanamide	57.75	58.60	-0.85	-1.47
1,1,3,3-Tetramethylguanidinium butanoate	56.23	56.13	0.10	0.18
1,1,3,3-Tetramethylguanidinium heptanoate	70.63	70.02	0.61	0.86
1,1,3,3-Tetramethylguanidinium hexanoate	64.74	65.39	-0.65	-1.00
1,1,3,3-Tetramethylguanidinium octanoate	74.36	74.65	-0.29	-0.39
1,1,3,3-Tetramethylguanidinium pentanoate	60.85	60.76	0.09	0.15
1,2-Diethylpyridinium ethylsulfate	64.48	64.43	0.05	0.08
1,3-Diethylimidazolium bis(trifluoromethylsulfonyl) amide	70.29	70.38	-0.09	-0.13
1,3-Dimethylimidazolium bis(trifluoromethylsulfonyl) amide	60.56	61.20	-0.64	-1.06
1,3-Dimethylimidazolium methosulfate	44.78	44.80	-0.02	-0.04
1,3-Dipropylimidazolium bis(trifluoromethylsulfonyl) amide	79.71	79.64	0.07	0.09
1-Benzyl-3-methylimidazolium bis(trifluoromethylsulfonyl) amide	85.86	85.72	0.14	0.16
1-Butyl-1-methylpiperidinium bis(trifluoromethylsulfonyl)amide	81.48	81.50	-0.02	-0.02
1-Butyl-1-methylpyrrolidinium 2-acryloamido-2-methylpropanesulfonate	91.47	90.77	0.70	0.77
1-Butyl-1-methylpyrrolidinium acetate	55.00	55.73	-0.73	-1.33
1-Butyl-1-methylpyrrolidinium bis(trifluoromethylsulfonyl)amide	76.89	76.87	0.02	0.03
1-Butyl-1-methylpyrrolidinium dicyanamide	60.12	59.43	0.69	1.15
1-Butyl-1-methylpyrrolidinium methylsulfate	60.93	60.47	0.46	0.75
1-Butyl-1-methylpyrrolidinium trifluoromethanesulfonate	60.44	60.06	0.38	0.63
1-Butyl-2,3-dimethylimidazolium bis(trifluoromethanesulfonyl) amide	79.33	79.39	-0.06	-0.08
1-Butyl-2,3-dimethylimidazolium tetrafluoroborate	52.38	52.17	0.21	0.40
1-Butyl-2-methylpyridinium tetrafluoroborate	53.45	53.58	-0.13	-0.24
1-Butyl-3-(2-cyanoethyl)-imidazolium chloride	57.93	58.25	-0.32	-0.55
1-Butyl-3-(2-cyanoethyl)imidazolium thiocyanate	67.06	67.10	-0.04	-0.06
1-Butyl-3-ethylimidazolium bis(trifluoromethylsulfonyl) amide	79.44	79.64	-0.20	-0.25
1-Butyl-3-ethylimidazolium triflate	63.01	62.83	0.18	0.29
1-Butyl-3-methylimidazolium 2-acryloamido-2-methylpropanesulfonate	88.52	88.95	-0.43	-0.49
1-Butyl-3-methylimidazolium acetate	54.18	53.91	0.27	0.50
1-Butyl-3-methylimidazolium bis(perfluorobutanesulfonyl) amide	105.39	105.45	-0.06	-0.06
1-Butyl-3-methylimidazolium bis(trifluoromethanesulfonyl) amide	74.99	75.05	-0.06	-0.08
1-Butyl-3-methylimidazolium dicyanoamide	57.80	57.61	0.19	0.33
1-Butyl-3-methylimidazolium glycine	58.39	57.34	1.05	1.80
1-Butyl-3-methylimidazolium hexafluorophosphate	51.46	51.56	-0.10	-0.19
1-Butyl-3-methylimidazolium methosulfate	58.58	58.65	-0.07	-0.12
1-Butyl-3-methylimidazolium octylsulfate	91.49	91.09	0.40	0.44

Table 4. Cont.

Molecule Name	Refractivity Exp.	Refractivity Calc.	Deviation	Dev. in %
1-Butyl-3-methylimidazolium perfluorobutylsulfonate	73.34	73.44	−0.10	−0.14
1-Butyl-3-methylimidazolium tetracyanoborate	67.83	67.87	−0.04	−0.06
1-Butyl-3-methylimidazolium tetrafluoroborate	47.81	47.83	−0.02	−0.04
1-Butyl-3-methylimidazolium thiocyanate	57.79	58.09	−0.30	−0.52
1-Butyl-3-methylimidazolium threoninate	68.48	67.95	0.53	0.77
1-Butyl-3-methylimidazolium tricyanomethanide	65.33	65.39	−0.06	−0.09
1-Butyl-3-methylimidazolium trifluoromethylsulfonate	57.91	58.24	−0.33	−0.57
1-Butyl-4-methylpyridinium tetrafluoroborate	54.00	53.84	0.16	0.30
1-Butylpyridinium 2-acryloamido-2-methylpropanesulfonate	91.01	90.15	0.86	0.94
1-Butylpyridinium bis(fluorosulfonyl) amide	64.60	64.65	−0.05	−0.08
1-Butylpyridinium dicyanamide	58.87	58.81	0.06	0.10
1-Butylpyridinium tetrafluoroborate	48.99	49.03	−0.04	−0.08
1-Butyltetrahydrothiophenium dicyanamide	59.59	59.81	−0.22	−0.37
1-Decyl-3-methylimidazolium bis(trifluoromethanesulfonyl) amide	102.90	102.83	0.07	0.07
1-Decyl-3-methylimidazolium tetracyanoborate	95.66	95.65	0.01	0.01
1-Decyl-3-methylimidazolium tricyanomethanide	93.23	93.17	0.06	0.06
1-Dodecyl-3-methylimidazolium bis(trifluoromethanesulfonyl) amide	112.08	112.09	−0.01	−0.01
1-Ethyl-2,3-dimethylimidazolium bis(trifluoromethanesulfonyl) amide	69.94	70.13	−0.19	−0.27
1-Ethyl-3-methylimidazolium 1,1,2,2-tetrafluoroethanesulfonate	53.91	53.77	0.14	0.26
1-Ethyl-3-methylimidazolium acetate	44.95	44.65	0.30	0.67
1-Ethyl-3-methylimidazolium aminoacetate	47.68	48.08	−0.40	−0.84
1-Ethyl-3-methylimidazolium bis(trifluoromethanesulfonyl) amide	65.77	65.79	−0.02	−0.03
1-Ethyl-3-methylimidazolium dicyanamide	48.35	48.35	0.00	0.00
1-Ethyl-3-methylimidazolium diethylphosphate	64.56	64.35	0.21	0.33
1-Ethyl-3-methylimidazolium dimethylphosphate	55.17	55.03	0.14	0.25
1-Ethyl-3-methylimidazolium ethosulfate	54.16	54.05	0.11	0.20
1-Ethyl-3-methylimidazolium imidodisulfurylfluoride	54.05	54.19	−0.14	−0.26
1-Ethyl-3-methylimidazolium L-alanine	52.10	52.64	−0.54	−1.04
1-Ethyl-3-methylimidazolium L-proline	58.84	59.70	−0.86	−1.46
1-Ethyl-3-methylimidazolium L-serine	54.05	54.05	0.00	0.00
1-Ethyl-3-methylimidazolium methanesulfonate	48.45	48.69	−0.24	−0.50
1-Ethyl-3-methylimidazolium methylsulfate	48.62	49.39	−0.77	−1.58
1-Ethyl-3-methylimidazolium taurinate	56.41	56.96	−0.55	−0.98
1-Ethyl-3-methylimidazolium tetracyanoborate	58.77	58.61	0.16	0.27
1-Ethyl-3-methylimidazolium tetrafluoroborate	38.70	38.57	0.13	0.34
1-Ethyl-3-methylimidazolium thiocyanate	48.31	48.83	−0.52	−1.08
1-Ethyl-3-methylimidazolium threoninate	58.86	58.69	0.17	0.29
1-Ethyl-3-methylimidazolium tricyanomethide	55.87	56.13	−0.26	−0.47
1-Ethyl-3-methylimidazolium trifluoromethylsulfonate	48.91	48.98	−0.07	−0.14
1-Ethyl-3-methylpyridinium bis(fluorosulfonyl) amide	60.16	60.20	−0.04	−0.07
1-Ethyl-3-methylpyridinium ethylsulfate	60.18	60.06	0.12	0.20
1-Ethyl-3-propylimidazolium bis(trifluoromethanesulfonyl) amide	74.95	75.01	−0.06	−0.08
1-Ethylmorpholinium tetrafluoroborate	40.81	39.89	0.92	2.25
1-Ethylpyridinium bis(fluorosulfonyl) amide	55.18	55.39	−0.21	−0.38
1-Ethylpyridinium ethylsulfate	55.29	55.25	0.04	0.07
1-Ethylpyridinium triflate	50.05	50.18	−0.13	−0.26
1-Ethyltetrahydrothiophenium dicyanamide	50.87	50.55	0.32	0.63
1-Heptyl-3-methylimidazolium bis(trifluoromethanesulfonyl) amide	88.14	88.94	−0.80	−0.91
1-Heptyl-3-methylimidazolium hexafluorophosphate	65.44	65.45	−0.01	−0.02
1-Hexyl-1-methylpyrrolidinium bis(trifluoromethanesulfonyl) amide	87.26	86.13	1.13	1.29
1-Hexyl-3,5-dimethylpyridinium bis(trifluoromethylsulfonyl)amide	95.56	95.13	0.43	0.45
1-Hexyl-3-methylimidazolium acetate	63.54	63.17	0.37	0.58
1-Hexyl-3-methylimidazolium bis(trifluoromethanesulfonyl) amide	84.23	84.31	−0.08	−0.09
1-Hexyl-3-methylimidazolium chloride	58.80	58.50	0.30	0.51
1-Hexyl-3-methylimidazolium dicyanoamide	67.19	66.87	0.32	0.48
1-Hexyl-3-methylimidazolium hexafluorophosphate	60.69	60.82	−0.13	−0.21
1-Hexyl-3-methylimidazolium tetracyanoborate	76.88	77.13	−0.25	−0.33
1-Hexyl-3-methylimidazolium tetrafluoroborate	56.91	57.09	−0.18	−0.32
1-Hexyl-3-methylimidazolium thiocyanate	68.17	67.35	0.82	1.20
1-Hexyl-3-methylimidazolium tricyanomethanide	74.67	74.65	0.02	0.03
1-Hexylpyridinium bis(fluorosulfonyl) amide	73.94	73.91	0.03	0.04
1-Isobutyl-1-methylpyrrolidinium bis(trifluoromethylsulfonyl)amide	77.02	76.83	0.19	0.25
1-Isobutyl-3-methylimidazolium bis(trifluoromethanesulfonyl) amide	74.92	75.01	−0.09	−0.12
1-Isobutyl-3-methylpyridinium bis(trifluoromethylsulfonyl)amide	81.23	81.02	0.21	0.26
1-Methyl-1-(2',3'-epoxypropyl)-2-oxopyrrolidinium chloride	49.38	49.79	−0.41	−0.83

Table 4. Cont.

Molecule Name	Refractivity Exp.	Refractivity Calc.	Deviation	Dev. in %
1-Methyl-1-decylpyrrolidinium bis(trifluoromethanesulfonyl) amide	104.90	104.65	0.25	0.24
1-Methyl-1-propylpiperidinium bis(trifluoromethylsulfonyl)amide	76.90	76.87	0.03	0.04
1-Methyl-1-propylpyrrolidinium bis(fluorosulfonyl) amide	61.04	60.64	0.40	0.66
1-Methyl-1-propylpyrrolidinium bis(trifluoromethanesulfonyl) amide	72.50	72.24	0.26	0.36
1-Methyl-2-pyrrolidonium tetrafluoroborate	37.04	37.68	−0.64	−1.73
1-Methyl-3-hexylimidazolium threoninate	77.73	77.21	0.52	0.67
1-Methyl-3-pentylimidazolium threoninate	73.07	72.58	0.49	0.67
1-Methyl-3-propylimidazolium threoninate	63.75	63.32	0.43	0.67
1-Methylmorpholinium tetrafluoroborate	35.90	35.57	0.33	0.92
1-Methylpiperidinium tetrafluoroborate	37.84	38.51	−0.67	−1.77
1-Methylpyridinium methylsulfate	46.05	46.27	−0.22	−0.48
1-Methylpyrrolidinium tetrafluoroborate	34.55	33.88	0.67	1.94
1-Nonyl-3-methylimidazolium bis(trifluoromethanesulfonyl) amide	98.06	98.20	−0.14	−0.14
1-Nonyl-3-methylimidazolium hexafluorophosphate	74.74	74.71	0.03	0.04
1-Octyl-3-methylimidazolium bis(trifluoromethanesulfonyl) amide	93.61	93.57	0.04	0.04
1-Octyl-3-methylimidazolium chloride	67.80	67.76	0.04	0.06
1-Octyl-3-methylimidazolium hexafluorophosphate	70.30	70.08	0.22	0.31
1-Octyl-3-methylimidazolium tetracyanoborate	86.41	86.39	0.02	0.02
1-Octyl-3-methylimidazolium tetrafluoroborate	66.24	66.35	−0.11	−0.17
1-Octyl-3-methylimidazolium tricyanomethanide	84.09	83.91	0.18	0.21
1-Octyl-3-methylpyridinium tetrafluoroborate	72.74	72.36	0.38	0.52
1-Octylpyridinium bis(trifluoromethylsulfonyl)amide	95.19	94.77	0.42	0.44
1-Pentyl-3-methylimidazolium acetate	59.01	58.54	0.47	0.80
1-Pentyl-3-methylimidazolium bis(trifluoromethanesulfonyl) amide	79.57	79.58	−0.11	−0.14
1-Pentyl-3-methylimidazolium hexafluorophosphate	56.11	56.19	−0.08	−0.14
1-Pentyl-3-methylimidazolium tetrafluoroborate	52.25	52.46	−0.21	−0.40
1-Pentylpyridinium dicyanamide	63.44	63.44	0.00	0.00
1-Phenyl-2,3,5-trimethylpyrazolium methylsulfonate	68.77	69.35	−0.58	−0.84
1-Phenyl-2-butyl-3,5-dimethylpyrazolium methylsulfonate	82.67	82.93	−0.26	−0.31
1-Phenyl-2-heptyl-3,5-dimethylpyrazolium methylsulfonate	97.61	96.82	0.79	0.81
1-Phenyl-2-hexyl-3,5-dimethylpyrazolium methylsulfonate	92.64	92.19	0.45	0.49
1-Phenyl-2-pentyl-3,5-dimethylpyrazolium methylsulfonate	87.17	87.56	−0.39	−0.45
1-Propyl-3-methylimidazolium acetate	49.37	49.28	0.09	0.18
1-Propyl-3-methylimidazolium bis(trifluoromethanesulfonyl) amide	70.48	70.42	0.06	0.09
1-Propyl-3-methylimidazolium tetrafluoroborate	43.09	43.20	−0.11	−0.26
1-Propylpyridinium dicyanamide	54.24	54.18	0.06	0.11
1-Propylpyridinium tetrafluoroborate	44.35	44.40	−0.05	−0.11
1-Propyronitrile-3-butylimidazolium bromide	62.60	62.36	0.24	0.38
1-Propyronitrile-3-hexylimidazolium bromide	71.74	71.62	0.12	0.17
1-Propyronitrile-3-octylimidazolium bromide	80.51	80.88	−0.37	−0.46
2-Hydroxyethylammonium acetate	29.31	28.99	0.32	1.09
2-hydroxyethylammonium butanoate	38.53	38.25	0.28	0.73
2-Hydroxyethylammonium formate	24.85	24.70	0.15	0.60
2-Hydroxyethylammonium hexanoate	47.80	47.51	0.29	0.61
2-Hydroxyethylammonium lactate	34.69	35.04	−0.35	−1.01
2-Hydroxyethylammonium pentanoate	43.12	42.88	0.24	0.56
2-Hydroxyethylammonium propionate	33.29	33.62	−0.33	−0.99
3-Methyl-1-propylpyridinium bis(trifluoromethylsulfonyl)amide	76.40	76.43	−0.03	−0.04
Bis(2-hydroxyethyl)ammonium hexanoate	58.49	58.34	0.15	0.26
Butylammonium nitrate	33.34	33.37	−0.03	−0.09
Dimethyl butyl isopropylammonium bis(trifluoromethylsulfonyl)amide	78.81	79.06	−0.25	−0.32
Dimethyl hexyl isopropylammonium bis(trifluoromethylsulfonyl)amide	89.14	88.32	0.82	0.92
Dimethylpropylisopropylammonium bis(trifluoromethylsulfonyl)amide	73.56	74.43	−0.87	−1.18
Ethylammonium nitrate	24.14	24.11	0.03	0.12
L-Alanine 1-methylethyl ester dodecyl sulfate	102.88	103.30	−0.42	−0.41
L-Alanine 2-methylpropyl ester dodecyl sulfate	107.40	107.88	−0.48	−0.45
L-Proline 1-methylethyl ester dodecyl sulfate	110.32	110.58	−0.26	−0.24
L-Valine 1-methylethyl ester dodecyl sulfate	112.65	112.52	0.13	0.12
Morpholinium formate	32.20	32.26	−0.06	−0.19
N-(2',3'-Epoxypropyl)-N-methylpyrrolidonium acetate	55.50	54.46	1.04	1.87
N-Butyl-3-methylpyridinium bis(trifluoromethylsulfonyl)amide	80.49	81.06	−0.57	−0.71

Table 4. Cont.

Molecule Name	Refractivity Exp.	Refractivity Calc.	Deviation	Dev. in %
N-Butyl-3-methylpyridinium trifluoromethanesulfonate	64.26	64.25	0.01	0.02
N-Butyl-4-methylthiazolium bis(trifluoromethylsulfonyl) amide	78.68	79.25	-0.57	-0.72
N-Butyl-4-methylthiazolium difluoro(oxalato)borate	63.24	63.32	-0.08	-0.13
N-Butyl-N-methylmorpholinium N-acetylanilate	74.32	74.63	-0.31	-0.42
N-Butyl-N-methylmorpholinium N-acetylleucinate	88.43	88.48	-0.05	-0.06
N-Butyl-N-methylmorpholinium N-acetylvalinate	83.98	83.85	0.13	0.15
N-Butylpyridinium bis(trifluoromethanesulfonyl) amide	76.22	76.25	-0.03	-0.04
N-Butylpyridinium triflate	59.25	59.44	-0.19	-0.32
N-Butylpyridinium trifluoroacetate	54.87	55.39	-0.52	-0.95
N-Butylthiazolium bis(trifluoromethylsulfonyl) amide	73.89	74.63	-0.74	-1.00
N-Butylthiazolium difluoro(oxalato)borate	58.43	58.70	-0.27	-0.46
N-Decylpyridinium bis(trifluoromethanesulfonyl) amide	104.52	104.03	0.49	0.47
N-Dodecylpyridinium bis(trifluoromethanesulfonyl) amide	113.68	113.29	0.39	0.34
N-Ethyl-2-methylpyridinium bis(trifluoromethylsulfonyl)amide	71.54	71.54	0.00	0.00
N-Ethylmorpholinium formate	41.07	41.68	-0.61	-1.49
N-Ethyl-N-methylmorpholinium N-acetylanilate	65.23	65.37	-0.14	-0.21
N-Ethyl-N-methylmorpholinium N-acetylsoleucinate	78.62	79.22	-0.60	-0.76
N-Ethyl-N-methylmorpholinium N-acetylleucinate	78.65	79.22	-0.57	-0.72
N-Ethyl-N-methylmorpholinium N-acetylvalinate	74.01	74.59	-0.58	-0.78
N-Hexyl-N-methylmorpholinium N-acetylanilate	83.42	83.89	-0.47	-0.56
N-Hexyl-N-methylmorpholinium N-acetylleucinate	97.24	97.74	-0.50	-0.51
N-Hexyl-N-methylmorpholinium N-acetylvalinate	92.26	93.11	-0.85	-0.92
N-Isobutyl-3-sulfoopropan-1-aminium hydrogen sulfate	62.85	62.71	0.14	0.22
N-Methyl-N-(2,3-dihydroxypropyl)pyrrolidinium bis(trifluoromethanesulfonyl) amide	74.88	75.07	-0.19	-0.25
N-Octyl-N-methylmorpholinium N-acetylanilate	92.82	93.15	-0.33	-0.36
N-Octyl-N-methylmorpholinium N-acetylvalinate	102.12	102.37	-0.25	-0.24
N-Propyl-2-methylpyridinium bis(trifluoromethylsulfonyl)amide	76.28	76.17	0.11	0.14
N-Propyl-N-methylmorpholinium N-acetylanilate	69.57	70.00	-0.43	-0.62
N-Propyl-N-methylmorpholinium N-acetylleucinate	83.88	83.85	0.03	0.04
N-Propyl-N-methylmorpholinium N-acetylvalinate	79.02	79.22	-0.20	-0.25
Propylammonium nitrate	28.78	28.74	0.04	0.14
S-Butyl-dimethylthioformamidium bis(trifluoromethylsulfonyl) amide	79.26	79.02	0.24	0.30
S-Butyl-dimethylthioformamidium difluoro(oxalato)borate	63.42	63.09	0.33	0.52
S-Ethyl-dimethylthioformamidium bis(trifluoromethylsulfonyl) amide	69.84	69.76	0.08	0.11
S-Ethyl-dimethylthioformamidium difluoro(oxalato)borate	53.86	53.83	0.03	0.06
S-Ethyl-dimethylthioformamidium trifluoromethylsulfonate	53.62	52.95	0.67	1.25
S-Methyl-dimethylthioformamidium bis(trifluoromethylsulfonyl) amide	64.95	64.92	0.03	0.05
S-Methyl-dimethylthioformamidium trifluoromethylsulfonate	48.32	48.11	0.21	0.43
Tetrabutylphosphonium acetate	97.22	97.33	-0.11	-0.11
Tetrabutylphosphonium formate	93.57	93.04	0.53	0.57
Tetrabutylphosphonium propanoate	102.16	101.96	0.20	0.20
Tetradecyl trihexylphosphonium bis(trifluoromethylsulfonyl)amide	192.57	192.55	0.02	0.01
Tetradecyl trihexylphosphonium chloride	166.32	166.74	-0.42	-0.25
Tributylmethylammonium bis(trifluoromethylsulfonyl)amide	97.59	97.53	0.06	0.06
Triethylammonium acetate	46.76	46.42	0.34	0.73
Triethyldecylammonium bis(trifluoromethylsulfonyl) amide	111.38	111.11	0.27	0.24
Triethyldodecylammonium bis(trifluoromethylsulfonyl) amide	120.72	120.37	0.35	0.29
Triethylheptylammonium bis(trifluoromethylsulfonyl) amide	97.05	97.22	-0.17	-0.18
Triethylhexylammonium bis(trifluoromethylsulfonyl) amide	92.72	92.59	0.13	0.14
Triethyloctylammonium bis(trifluoromethylsulfonyl) amide	101.96	101.85	0.11	0.11
Triethylsulfonium bis(trifluoromethylsulfonyl) amide	70.04	70.13	-0.09	-0.13
Triethyltetradecylammonium bis(trifluoromethylsulfonyl) amide	129.84	129.63	0.21	0.16
Trihexyl tetradecyl phosphonium dicyanamide	174.84	175.11	-0.27	-0.15
Trihexyl tetradecyl phosphonium trifluoromethylsulfonate	175.69	175.74	-0.05	-0.03
Trimethyl butylammonium bis(trifluoromethylsulfonyl)amide	70.29	70.37	-0.08	-0.11
Trimethyl hexylammonium bis(trifluoromethylsulfonyl)amide	79.64	79.63	0.01	0.01
Trimethyl octylammonium bis(trifluoromethylsulfonyl)amide	88.97	88.89	0.08	0.09
Trimethyl pentylammonium bis(trifluoromethylsulfonyl)amide	75.01	75.00	0.01	0.01
Trimethyl propylammonium bis(trifluoromethylsulfonyl)amide	65.65	65.74	-0.09	-0.14

4.1.2. Silanes, Silanols, Siloxanes, Silazanes, and Silicates

Silicon-containing compounds have found use in synthetic processes as intermediates as well as in commercial products, e.g., in detergents, cosmetics, deodorants, soaps,

as water-resistant coatings, as defoaming agents, or as coolants. Despite the large variety of applications, the number of physico-chemical data for this class of molecules is fairly limited within the chemical realm. Nevertheless, a thorough scan of the literature of the last ca. 80 years delivered a sufficient number of data to enable the creation of a basis for the prediction of several chemical descriptors of interest based on the present atom group additivity principle. Accordingly, in analogy to the previous section, the updated parameters tables provided the group parameters for the heat of combustion [397], enabling its calculation for 99 silicon compounds with a correlation coefficient R^2 of 1.0, a MAPD of 0.19% and a σ of 17.67 kJ/mol, for the heat of vaporization [398] for 106 ($R^2 = 0.7936$, MAPD = 10.91%, $\sigma = 6.17$ kJ/mol), for the surface tension [399] of 18 ($R^2 = 0.9835$, MAPD = 2.62%, $\sigma = 0.66$ dyn/cm), for the liquid heat capacity at 298 K [400] of 26 ($R^2 = 0.9981$, MAPD = 2.32%, $\sigma = 9.02$ J/mol/K), for the solid heat capacity at 298 K [400] of 14 ($R^2 = 0.9925$, MAPD = 2.77%, $\sigma = 18.35$ J/mol/K), for the standard entropy of fusion [398] of 45 ($R^2 = 0.7251$, MAPD = 15.09%, $\sigma = 15.56$ J/mol/K), and even for the vapor pressure at 298 K [401] of 9 silicon compounds ($R^2 = 0.9897$, MAPD = 7.92%, $\sigma = 0.16$). In addition to these descriptors, the present work now provides the refractivity data for 351 silicon derivatives, alphabetically sampled in Table 5. They prove the reliability of the calculated values with a MAPD of only 0.39% and a standard deviation σ of 0.31, compared with their experimental values. Analogously, when used as test samples in the cv calculations, 324 of these silicon compounds yielded a MAPD of 0.47% and a σ of 0.37.

Table 5. Calculated and experimental refractivity of silicon-containing compounds.

Molecule Name	Refractivity Exp.	Refractivity Calc.	Deviation	Dev. in %
(2-Phenylethyl)trichlorosilane	58.62	58.57	0.05	0.09
(3-Chloropropyl)trichlorosilane	43.26	43.44	-0.18	-0.42
(3-Chloropropyl)trimethoxysilane	46.53	46.62	-0.09	-0.19
(3-Chloropropyl)trimethylsilane	44.47	44.33	0.14	0.31
(4-Bromophenoxy)trimethylsilane	58.55	58.44	0.11	0.19
(4-Chlorophenyl)trichlorosilane	55.04	54.14	0.90	1.64
(4-Methoxyphenyl)trimethylsilane	56.94	56.73	0.21	0.37
(4-Methylphenyl)trimethylsilane	54.82	55.02	-0.20	-0.36
(Bromomethyl)chlorodimethylsilane	37.57	37.57	0.00	0.00
(Bromomethyl)trimethylsilane	38.09	38.08	0.01	0.03
(Chloromethyl)trichlorosilane	34.10	34.12	-0.02	-0.06
(Chloromethyl)trimethylsilane	35.13	35.01	0.12	0.34
(Dichloromethyl)trichlorosilane	39.36	39.06	0.30	0.76
(Diethylamino)trimethylsilane	47.33	47.09	0.24	0.51
1,1,1,3,5,5,5-Heptamethyltrisiloxane	63.17	63.24	-0.07	-0.11
1,1,1,3,5,7,7,7-Octamethyltetrasiloxane	77.46	77.53	-0.07	-0.09
1,1,3,3-Tetramethyl-1,3-diphenyldisiloxane	88.87	88.71	0.16	0.18
1,1,3,3-Tetramethyldisiloxane	40.19	40.23	-0.04	-0.10
1,2-Bis(tributylsilyl)acetylene	138.06	138.22	-0.16	-0.12
1,2-Bis(triethylsilyl)ethane	85.59	85.82	-0.23	-0.27
1,2-Bis(trimethylsilyl)acetylene	55.18	55.24	-0.06	-0.11
1,2-Dis(trimethylsilyl)-ethylene	58.50	58.06	0.44	0.75
1,3,5-Trisilacyclohexane	43.69	43.44	0.25	0.57
1,3-Bis(bromomethyl)tetramethyldisiloxane	64.41	64.45	-0.04	-0.06
1,3-Bis(chloromethyl)tetramethyldisiloxane	58.30	58.31	-0.01	-0.02
1,3-Bis(dichloromethyl)tetramethyldisiloxane	68.07	68.19	-0.12	-0.18
1,3-Bis(trimethylsiloxy)benzene	75.39	75.18	0.21	0.28
1,3-Divinyl-1,1,3,3-tetramethyldisiloxane	57.23	57.33	-0.10	-0.17
1-Heptyltrifluorosilane	41.32	41.07	0.25	0.61
2,2,4,4,6,6-Hexamethylcyclotrisilazane	63.90	63.78	0.12	0.19
2,4,6,8,10,12-Hexamethylcyclohexasiloxane	85.86	85.74	0.12	0.14
2,4,6,8-Tetramethylcyclotetrasiloxane	57.13	57.16	-0.03	-0.05
2,4,6-Trimethyl-2,4,6-triphenylcyclotrisiloxane	115.86	115.59	0.27	0.23

Table 5. Cont.

Molecule Name	Refractivity Exp.	Refractivity Calc.	Deviation	Dev. in %
2-Butylsilane	31.02	31.09	−0.07	−0.23
2-Pentyloxytrimethylsilane	49.75	49.57	0.18	0.36
2-Silylpentasilane	73.17	73.09	0.08	0.11
2-Silyltetrasilane	61.12	61.05	0.07	0.11
2-Silyltrisilane	48.88	49.01	−0.13	−0.27
3-(Triethoxysilyl)-1-propanamine	59.24	59.23	0.01	0.02
3-(Trimethylsilyl)-1-propanol	41.55	40.94	0.61	1.47
3-Mercaptopropyl-trimethoxysilane	49.46	49.49	−0.03	−0.06
4-Bromophenyltrimethylsilane	57.19	57.80	−0.61	−1.07
4-Chlorophenoxytriethylsilane	69.66	69.38	0.28	0.40
4-Fluorophenyltrimethylsilane	50.34	50.11	0.23	0.46
4-Trifluoromethylphenyltrimethylsilane	54.63	55.30	−0.67	−1.23
4-Trimethylsiloxyphenyltrimethylsilane	74.63	74.54	0.09	0.12
Allylchlorodimethylsilane	37.98	38.71	−0.73	−1.92
Allylmethyldichlorosilane	38.14	38.50	−0.36	−0.94
Allyltrichlorosilane	38.97	38.33	0.64	1.64
Allyltriethoxysilane	55.73	55.49	0.24	0.43
Allyltrimethylsilane	39.14	39.22	−0.08	−0.20
Amylsilane	35.64	35.67	−0.03	−0.08
Benzyltrimethylsilane	55.11	54.83	0.28	0.51
Bis(butylthio) 2-(diethylmethylsilyl)ethyl borane	101.77	102.28	−0.51	−0.50
Bis(diethyl)disiloxane	58.54	58.51	0.03	0.05
Bis(diethylmethylsilyl)amine	69.24	69.58	−0.34	−0.49
Bis(diethylsilyl)amine	61.40	61.24	0.16	0.26
Bis(dimethylamino)bis(diethylamino)silane	79.50	79.36	0.14	0.18
Bis(dimethylphenylsilyl)amine	91.08	91.06	0.02	0.02
Bis(ethyl)dimethylsilyl)amine	61.01	60.44	0.57	0.93
Bis(ethylisobutyl)disiloxane	76.95	76.95	0.00	0.00
Bis(ethylphenyl)disiloxane	88.84	89.13	−0.29	−0.33
Bis(trichlorosilyl)methane	51.08	51.72	−0.64	−1.25
Bis(triethylsilyl)amine	78.33	78.72	−0.39	−0.50
Bis(trihexylsilyl)acetylene	193.90	193.78	0.12	0.06
Bis(trimethoxysilyl)amine	56.30	56.38	−0.08	−0.14
Bis(trimethoxysilylamino)dimethylsilane	77.61	77.64	−0.03	−0.04
Bis(trimethylsilylamino)dimethylsilane	71.81	72.56	−0.75	−1.04
Bromotriethylsilane	46.44	46.60	−0.16	−0.34
Bromotrimethylsilane	32.92	32.89	0.03	0.09
Butoxytrimethylsilane	44.88	44.93	−0.05	−0.11
Butylsilane	30.90	31.04	−0.14	−0.45
Butyltrichlorosilane	43.18	43.27	−0.09	−0.21
Butyltriisothiocyanatosilane	73.92	73.73	0.19	0.26
Chloro(chloromethyl)dimethylsilane	34.43	34.50	−0.07	−0.20
Chloro(dichloromethyl)dimethylsilane	39.39	39.44	−0.05	−0.13
Chlorodiethylsilane	34.92	34.70	0.22	0.63
Chlorodimethylphenylsilane	49.33	49.70	−0.37	−0.75
Chlorodimethylsilane	25.90	25.56	0.34	1.31
Chloroethyl)dimethylsilane	35.15	34.39	0.76	2.16
Chloromethylphenylsilane	45.46	45.44	0.02	0.04
Chlorotriethylsilane	43.54	43.53	0.01	0.02
Chlorotrimethylsilane	29.88	29.82	0.06	0.20
Chlorovinyl)dimethylsilane	34.49	34.01	0.48	1.39
cis-1,2-Bis(trimethylsilyl)-3,3-dichlorocyclopropane	71.37	70.62	0.75	1.05
cis-1,2-Dis(trimethylsilyl)-ethylene	57.88	58.06	−0.18	−0.31
Cyclohexyloxytrimethylsilane	52.12	52.06	0.06	0.12
Cyclohexyltrifluorosilane	34.26	34.35	−0.09	−0.26
Decamethylcyclopentasiloxane	93.33	93.25	0.08	0.09
Decamethyltetrasiloxane	86.18	86.25	−0.07	−0.08

Table 5. Cont.

Molecule Name	Refractivity Exp.	Refractivity Calc.	Deviation	Dev. in %
Decyldiphenylnonylsilane	148.69	148.68	0.01	0.01
Decyldiphenylsilane	106.74	107.04	-0.30	-0.28
Decyloxytrimethylsilane	72.71	72.71	0.00	0.00
Di(cyclohexyloxy)dimethylsilane	74.01	73.82	0.19	0.26
Diallyldimethylsilane	48.34	48.11	0.23	0.48
Diamylsilane	58.60	58.56	0.04	0.07
Dibutyl-diisothiocyanatosilane	77.77	77.84	-0.07	-0.09
Dibutyl-dinonylsilane	131.54	131.95	-0.41	-0.31
Dibutylmethylsilyl bromide	60.64	60.55	0.09	0.15
Dibutyl-nonylsilane	90.16	90.31	-0.15	-0.17
Dibutylsilane	49.39	49.30	0.09	0.18
Dichloro(chloromethyl)methylsilane	34.17	34.29	-0.12	-0.35
Dichloro(dichloromethyl)methylsilane	39.13	39.23	-0.10	-0.26
Dichlorodiethylsilane	38.71	38.75	-0.04	-0.10
Dichlorodimethylsilane	29.65	29.61	0.04	0.13
Dichlorodiphenylsilane	69.99	69.37	0.62	0.89
Dichloromethylphenylsilane	48.81	49.49	-0.68	-1.39
Dicosamethyldecasiloxane	197.51	198.15	-0.64	-0.32
Didecyldiphenylsilane	153.40	153.31	0.09	0.06
Diethoxydimethylsilane	40.99	41.04	-0.05	-0.12
Diethoxydiphenylsilane	81.07	80.80	0.27	0.33
Diethoxymethylphenylsilane	60.85	60.92	-0.07	-0.12
Diethoxymethylsilane	36.84	36.68	0.16	0.43
Diethyl 2,2-diethylhydrazinosilane	55.43	55.86	-0.43	-0.78
Diethyl 2,2-dimethylhydrazinosilane	46.39	46.68	-0.29	-0.63
Diethyl bis(2,2-diethylhydrazino)silane	81.18	80.88	0.30	0.37
Diethyl bis(2,2-dimethylhydrazino)silane	62.47	62.52	-0.05	-0.08
Diethyl diethylaminosilane	52.34	52.06	0.28	0.53
Diethyl difluorosilane	27.74	27.83	-0.09	-0.32
Diethyl-diisothiocyanatosilane	59.55	59.32	0.23	0.39
Diethylmethylchlorosilane	38.62	38.96	-0.34	-0.88
Diethylmethylsilanol	35.43	35.61	-0.18	-0.51
Diethylnonylsilane	71.60	71.79	-0.19	-0.27
Diethyloctylsilane	67.23	67.16	0.07	0.10
Diethylphenyl 1-isopropoxyethoxysilane	80.26	80.12	0.14	0.17
Diethylsilane	30.71	30.78	-0.07	-0.23
Diethylsilanol	31.62	31.25	0.37	1.17
Difluorodiphenylsilane	58.69	58.45	0.24	0.41
Dimethoxydiphenylsilane	71.70	71.48	0.22	0.31
Dimethyl bis(2,2-diethylhydrazino)silane	71.55	71.74	-0.19	-0.27
Dimethyl bis(2,2-dimethylhydrazino)silane	53.54	53.38	0.16	0.30
Dimethyl bis(2-chloropropoxy)silane	59.83	59.82	0.01	0.02
Dimethyl di(2-ethylbutoxy)silane	78.27	78.00	0.27	0.34
Dimethyl di(2-octyloxy)silane	96.44	96.62	-0.18	-0.19
Dimethyl di-2-butoxysilane	59.68	59.58	0.10	0.17
Dimethyl di-2-pentoxysilane	68.61	68.84	-0.23	-0.34
Dimethyl diacetoxysilane	40.81	40.82	-0.01	-0.02
Dimethyl dibutoxysilane	59.63	59.56	0.07	0.12
Dimethyl didodecyloxysilane	133.43	133.64	-0.21	-0.16
Dimethyl diheptoxysilane	87.25	87.34	-0.09	-0.10
Dimethyl dihexoxysilane	77.46	78.08	-0.62	-0.80
Dimethyl diisopropoxysilane	49.53	50.32	-0.79	-1.59
Dimethyl diisothiocyanatosilane	49.92	50.18	-0.26	-0.52
Dimethyl dimethoxysilane	31.51	31.72	-0.21	-0.67
Dimethyl dinonyloxysilane	105.67	105.86	-0.19	-0.18
Dimethyl dioctoxysilane	96.50	96.60	-0.10	-0.10
Dimethyl dipentoxysilane	68.38	68.82	-0.44	-0.64

Table 5. Cont.

Molecule Name	Refractivity Exp.	Refractivity Calc.	Deviation	Dev. in %
Dimethyldiphenoxysilane	71.56	71.40	0.16	0.22
Dimethyldiphenylsilane	70.04	70.09	-0.05	-0.07
Dimethyldipropoxysilane	50.94	50.30	0.64	1.26
Dimethylethylsilanol	30.79	31.04	-0.25	-0.81
Dimethylphenylsilane	45.04	45.55	-0.51	-1.13
Dimethylvinylethoxysilane	39.82	39.86	-0.04	-0.10
Dinonyldiphenylsilane	144.50	144.05	0.45	0.31
Diphenylmethylsilane	65.28	65.43	-0.15	-0.23
Diphenylmethylsilylamine	68.03	68.05	-0.02	-0.03
Diphenylnonylsilane	102.30	102.41	-0.11	-0.11
Diphenylsilane	61.53	61.40	0.13	0.21
Dipropyldifluorosilane	37.24	37.09	0.15	0.40
Dipropylsilane	40.08	40.04	0.04	0.10
Disilanomethane	27.16	27.26	-0.10	-0.37
Dodecamethylcyclohexasiloxane	111.89	111.90	-0.01	-0.01
Dodecamethylpentasiloxane	104.79	104.90	-0.11	-0.10
Eicosamethylnonasiloxane	179.30	179.50	-0.20	-0.11
Ethoxytriethylsilane	49.10	49.38	-0.28	-0.57
Ethoxytriethylsilane	105.58	104.94	0.64	0.61
Ethoxytrimethylsilane	35.67	35.67	0.00	0.00
Ethyl bis(2,2-diethylhydrazino)silane	71.76	71.89	-0.13	-0.18
Ethyl bis(2,2-dimethylhydrazino)silane	53.67	53.53	0.14	0.26
Ethyl bis(2-chloropropoxy)silane	59.73	60.03	-0.30	-0.50
Ethyl bis(diethylamino)silane	64.26	64.29	-0.03	-0.05
Ethyl isobutyl 2-chloropropoxysilane	59.24	59.06	0.18	0.30
Ethyl tris(2,2-diethylhydrazino)silane	96.93	96.81	0.12	0.12
Ethylaminotriethylsilane	51.46	51.36	0.10	0.19
Ethylcyclohexyldifluorosilane	44.31	44.26	0.05	0.11
Ethyl dibutoxysilane	59.63	59.77	-0.14	-0.23
Ethyl dimethyl 1-(3-pentoxo)ethoxysilane	64.89	64.93	-0.04	-0.06
Ethyl isobutylsilanol	40.40	40.47	-0.07	-0.17
Ethyl phenylchlorosilane	49.44	50.01	-0.57	-1.15
Ethyl tributoxysilane	78.67	78.95	-0.28	-0.36
Ethyl trichlorosilane	33.83	34.01	-0.18	-0.53
Ethyl triethoxysilane	51.50	51.17	0.33	0.64
Ethyl triisothiocyanatosilane	64.17	64.47	-0.30	-0.47
Ethyl trimethoxysilane	37.01	37.19	-0.18	-0.49
Fluoroethyl diisopropylsilane	47.71	47.87	-0.16	-0.34
Fluoro tributylsilane	66.71	66.29	0.42	0.63
Fluoro triethylsilane	38.10	38.51	-0.41	-1.08
Fluoro triphenylsilane	80.30	80.18	0.12	0.15
Fluoro tripropylsilane	52.33	52.40	-0.07	-0.13
Heptasilane	84.77	84.84	-0.07	-0.08
Heptyloxytrimethylsilane	58.80	58.82	-0.02	-0.03
Hexadecamethylheptasiloxane	142.31	142.20	0.11	0.08
Hexaethyl disiloxane	75.92	76.37	-0.45	-0.59
Hexamethyl disilane	51.42	51.36	0.06	0.12
Hexamethyl disiloxane	48.94	48.95	-0.01	-0.02
Hexapropyl disiloxane	104.05	104.15	-0.10	-0.10
Hexasilane	72.78	72.80	-0.02	-0.03
Hexyloxytrimethylsilane	54.16	54.19	-0.03	-0.06
Hexylsilane	40.34	40.30	0.04	0.10
HMDS	51.55	51.30	0.25	0.48
iso-Butylsilane	31.05	31.00	0.05	0.16
Isopentyloxytrimethylsilane	49.54	49.52	0.02	0.04
Isopropylmethylsilane	30.66	30.89	-0.23	-0.75
Isopropyl triisothiocyanatosilane	69.52	69.15	0.37	0.53

Table 5. Cont.

Molecule Name	Refractivity Exp.	Refractivity Calc.	Deviation	Dev. in %
Isopropyltrimethylsilane	38.47	39.58	−1.11	−2.89
Methoxytriethylsilane	44.49	44.72	−0.23	−0.52
Methoxytrimethylsilane	30.80	31.01	−0.21	−0.68
Methoxytripropylsilane	58.64	58.61	0.03	0.05
Methyl bis(2,2-diethylhydrazino)silane	67.18	67.32	−0.14	−0.21
Methyl bis(2,2-dimethylhydrazino)silane	48.80	48.96	−0.16	−0.33
Methyl bis(2-chloropropoxy)silane	55.37	55.46	−0.09	−0.16
Methyl bis(diethylamino)silane	59.99	59.72	0.27	0.45
Methyl tris(2,2-diethylhydrazino)silane	92.26	92.24	0.02	0.02
Methylcyclohexyldifluorosilane	39.68	39.69	−0.01	−0.03
Methyl dibutoxysilane	54.87	55.20	−0.33	−0.60
Methyldichloro-2-(2,4-dichlorophenoxy)ethylsilane	70.31	70.12	0.19	0.27
Methyldichloro-2-(4-chlorophenoxy)ethylsilane	65.49	65.30	0.19	0.29
Methyldichloro-2,4-dichlorophenoxyethylsilane	60.94	60.20	0.74	1.21
Methyldichloro-2-butoxyethylsilane	55.11	54.39	0.72	1.31
Methyldichloro-2-isobutoxyethylsilane	54.52	54.35	0.17	0.31
Methyldichloro-2-phenoxyethylsilane	60.39	60.48	−0.09	−0.15
Methyldichloro-4-chlorophenoxyethylsilane	55.08	55.38	−0.30	−0.54
Methyldichlorobutoxysilane	44.66	44.64	0.02	0.04
Methyldichlorophenoxyethylsilane	50.14	50.56	−0.42	−0.84
Methyldiethyl-2-phenoxyethylsilane	70.07	70.34	−0.27	−0.39
Methyldiethylphenoxyethylsilane	60.29	59.99	0.30	0.50
Methylnonylphenylsilane	82.90	82.53	0.37	0.45
Methyloctylphenylsilane	78.18	77.90	0.28	0.36
Methylphenyldifluorosilane	38.26	38.57	−0.31	−0.81
Methylphenylsilane	40.82	41.52	−0.70	−1.71
Methylpropylsilane	30.73	30.84	−0.11	−0.36
Methylsilanetriol triacetate	46.27	46.27	0.00	0.00
Methyltri(2-octyloxy)silane	129.85	129.97	−0.12	−0.09
Methyltributoxysilane	74.39	74.38	0.01	0.01
Methyltrichlorosilane	29.13	29.44	−0.31	−1.06
Methyltriheptyloxysilane	116.01	116.05	−0.04	−0.03
Methyltriheptyloxysilane	102.11	102.16	−0.05	−0.05
Methyltriisopentylloxysilane	88.26	88.15	0.11	0.12
Methyltripentylloxysilane	88.20	88.27	−0.07	−0.08
Methyltriphenoxysilane	91.85	92.14	−0.29	−0.32
Methylvinylchlorosilane	33.33	33.80	−0.47	−1.41
N-(1,1-Dimethylpropyl)aminotriethylsilane	64.79	65.18	−0.39	−0.60
N-(3-(Trimethoxysilyl)propyl)-1,2-ethanediamine	58.21	57.88	0.33	0.57
N,N-Dibutylaminotriethylsilane	78.65	79.32	−0.67	−0.85
N,N-Diethylaminotriethylsilane	60.99	60.80	0.19	0.31
N,N-Diisobutylaminotriethylsilane	78.67	79.24	−0.57	−0.72
N-Fenchylaminotriethylsilane	83.74	83.97	−0.23	−0.27
N-Isopropylaminotriethylsilane	56.05	55.92	0.13	0.23
Nonyloxytrimethylsilane	68.07	68.08	−0.01	−0.01
N-Propylaminotriethylsilane	56.11	55.99	0.12	0.21
N-t-Butylaminotriethylsilane	60.63	60.55	0.08	0.13
Octadecamethyloctasiloxane	160.19	160.85	−0.66	−0.41
Octadecyltrichlorosilane	108.02	108.09	−0.07	−0.06
Octamethylcyclotetrasiloxane	74.68	74.60	0.08	0.11
Octamethyltrisiloxane	67.44	67.60	−0.16	−0.24
Octyloxytrimethylsilane	63.43	63.45	−0.02	−0.03
Pentasilane	60.80	60.76	0.04	0.07
Pentylxytrimethylsilane	49.52	49.56	−0.04	−0.08
Pentyltrichlorosilane	48.79	47.90	0.89	1.82
Phenoxytriethylsilane	64.47	64.56	−0.09	−0.14
Phenoxytrimethylsilane	51.17	50.85	0.32	0.63

Table 5. Cont.

Molecule Name	Refractivity Exp.	Refractivity Calc.	Deviation	Dev. in %
Phenoxytripropylsilane	78.41	78.45	−0.04	−0.05
Phenylsilane	37.44	37.09	0.35	0.93
Phenyltri(2-octyloxy)silane	149.82	149.85	−0.03	−0.02
Phenyltri(cyclohexyloxy)silane	115.70	115.65	0.05	0.04
Phenyltrichlorosilane	48.92	49.32	−0.40	−0.82
Phenyltrifluorosilane	33.09	33.23	−0.14	−0.42
Phenyltriisopentylloxysilane	108.25	108.03	0.22	0.20
Phenyltrimethylsilane	49.88	50.21	−0.33	−0.66
Propyltrichlorosilane	38.46	38.64	−0.18	−0.47
Propyltriisothiocyanatosilane	68.69	69.10	−0.41	−0.60
t-Butoxytriethylsilane	58.54	58.59	−0.05	−0.09
t-Butoxytrimethylsilane	44.98	44.88	0.10	0.22
t-Butoxytripropylsilane	72.68	72.48	0.20	0.28
Tetra(1H,1H,3H-perfluoropropyl)silicate	72.19	72.10	0.09	0.12
Tetra(1H,1H,5H-perfluoropentyl)silicate	111.97	112.18	−0.21	−0.19
Tetra(2-ethylbutyl) silicate	125.53	126.42	−0.89	−0.71
Tetra(diethylamino)silane	97.33	97.72	−0.39	−0.40
Tetra(dimethylamino)silane	61.29	61.00	0.29	0.47
Tetra-2-butoxysilane	90.48	89.58	0.90	0.99
Tetra-2-methyl-1-propoxysilane	88.88	89.38	−0.50	−0.56
Tetra-2-pentoxysilane	108.98	108.10	0.88	0.81
Tetra-3-methyl-1-butoxysilane	107.23	107.90	−0.67	−0.62
Tetrabutoxysilane	88.88	89.54	−0.66	−0.74
Tetracosamethylhendecasiloxane	217.25	216.80	0.45	0.21
Tetradecamethylcycloheptasiloxane	130.84	130.55	0.29	0.22
Tetradecamethylhexasiloxane	123.45	123.55	−0.10	−0.08
Tetraethoxysilane	53.33	52.50	0.83	1.56
Tetraethylsilane	48.37	48.61	−0.24	−0.50
Tetrahexoxysilane	127.50	126.58	0.92	0.72
Tetraisobutylsilane	86.00	85.49	0.51	0.59
Tetraisopropoxysilane	70.82	71.06	−0.24	−0.34
Tetraisopropylsilane	66.92	67.33	−0.41	−0.61
Tetramethylsilane	29.95	30.33	−0.38	−1.27
Tetramethyltetraphenylcyclotetrasiloxane	154.31	154.12	0.19	0.12
Tetramethoxysilane	33.51	33.86	−0.35	−1.04
Tetraoctoxysilane	163.90	163.62	0.28	0.17
Tetrapentoxysilane	107.38	108.06	−0.68	−0.63
Tetrapropoxysilane	70.65	71.02	−0.37	−0.52
Tetrasilane	48.89	48.72	0.17	0.35
Tetravinylsilane	46.88	47.09	−0.21	−0.45
trans-1,2-Bis(trimethylsilyl)-3,3-dichlorocyclopropane	71.02	70.62	0.40	0.56
Tributylisothiocyanatosilane	82.05	81.60	0.45	0.55
Tributylsilane	67.51	67.16	0.35	0.52
Tributylsilanol	67.79	67.96	−0.17	−0.25
Tributylsilylamine	69.61	69.78	−0.17	−0.24
Trichloro-2-phenoxyethylsilane	60.44	60.31	0.13	0.22
Trichlorovinylsilane	33.54	33.63	−0.09	−0.27
Triethoxymethylsilane	46.50	46.60	−0.10	−0.22
Triethoxypentylsilane	64.96	65.06	−0.10	−0.15
Triethoxyphenylsilane	66.15	66.48	−0.33	−0.50
Triethyl 1-propoxyethoxysilane	65.15	64.80	0.35	0.54
Triethyl 2,2-diethylhydrazinosilane	64.50	64.60	−0.10	−0.16
Triethyl 2,2-dimethylhydrazinosilane	55.48	55.42	0.06	0.11
Triethylisothiocyanatosilane	53.85	53.82	0.03	0.06
Triethylsilane	39.60	39.38	0.22	0.56
Triethylsilanol	40.59	40.18	0.41	1.01
Triethylsilylamine	42.07	42.00	0.07	0.17

Table 5. Cont.

Molecule Name	Refractivity Exp.	Refractivity Calc.	Deviation	Dev. in %
Triethylsilyloxytripropylsilane	90.19	90.26	−0.07	−0.08
Triethyltriphenylcyclotrisiloxane	129.17	129.30	−0.13	−0.10
Triisopropoxyvinylsilane	65.03	64.71	0.32	0.49
Triisopropylethoxysilane	63.56	63.42	0.14	0.22
Triisopropylphenylsilane	77.50	77.96	−0.46	−0.59
Triisopropylsilane	53.57	53.42	0.15	0.28
Triisopropylsilyl chloride	57.72	57.57	0.15	0.26
Trimethoxymethylsilane	32.24	32.62	−0.38	−1.18
Trimethoxyphenylsilane	52.32	52.50	−0.18	−0.34
Trimethoxysilylamine	30.95	30.83	0.12	0.39
Trimethyl 1-ethoxyethoxysilane	46.52	46.46	0.06	0.13
Trimethyl 1-isopropoxyethoxysilane	51.15	51.10	0.05	0.10
Trimethyl 2,2-diethylhydrazinosilane	50.99	50.89	0.10	0.20
Trimethyl 2,2-dimethylhydrazinosilane	41.77	41.71	0.06	0.14
Trimethylisothiocyanatosilane	40.13	40.11	0.02	0.05
Trimethylsilanol	26.22	26.47	−0.25	−0.95
Trimethylsilylaminodimethylphenylsilane	71.09	71.18	−0.09	−0.13
Trimethylsilylaminodiphenylmethylsilane	91.05	91.06	−0.01	−0.01
Trimethylsilylaminotriethylsilane	65.00	65.01	−0.01	−0.02
Trimethylsilylaminotrimethoxysilane	53.70	53.84	−0.14	−0.26
Trimethylsilylaminotriphenylsilane	111.69	110.94	0.75	0.67
Trimethylsilyloxytriethylsilane	62.45	62.66	−0.21	−0.34
Trimethylsilyloxytripropylsilane	76.55	76.55	0.00	0.00
Trimethylvinylsilane	34.55	34.52	0.03	0.09
Tripentylsilane	81.54	81.05	0.49	0.60
Tripropylsilane	52.75	53.27	−0.52	−0.99
Tris(dimethylamino)dibutylaminosilane	88.58	88.70	−0.12	−0.14
Trisilane	36.61	36.68	−0.07	−0.19
Vinyl tris(2-chloropropoxy)silane	79.31	78.96	0.35	0.44
Vinyldiethoxymethylsilane	45.09	45.23	−0.14	−0.31
Vinyltriacetoxysilane	50.55	50.46	0.09	0.18
Vinyltriethoxysilane	50.75	50.79	−0.04	−0.08
Vinyltrimethoxysilane	36.41	36.81	−0.40	−1.10

4.1.3. Boranes, Borines, Borazines, Boronates, and Borates

In contrast to the prior two sections, boron-containing compounds are essentially important intermediates in chemical syntheses, and therefore experimental physico-chemical data are scarce. The large number of refractivity data, on the other hand, is primarily owed to the need to characterize the newly synthesized molecules by some easily accessible physical data, such as elemental analysis, melting point, density, and refractive index. With a few exceptions (e.g., Christopher et al. [80]) however, most authors have not shown any interest in using the latter two values for the calculation of the molecules' refractivity or polarizability. The present collection of refractivity data for 137 boron compounds listed in Table 6, although perhaps of merely academic interest, nevertheless confirms—by the strong linearity over the complete set—the overall correctness of the experimental data and at the same time proves the versatility of the present group additivity approach, revealing a MAPD of just 0.46% and a σ of 0.37. Similarly, the test data of 127 of these boron derivatives, when applied as test samples in the cv calculations, resulted in a MAPD of 0.54% and a σ of 0.45.

Table 6. Calculated and experimental refractivity of boron-containing compounds.

Molecule Name	Refractivity Exp.	Refractivity Calc.	Deviation	Dev. in %
1,2-Bis(dipentylborinoxy)ethane	116.12	116.10	0.02	0.02
1,3,5-Tributylborazine	79.59	79.86	-0.27	-0.34
1,3,5-Triethylborazine	52.48	52.08	0.40	0.76
1,3-Bis(dibutoxyboryl)propane	104.73	104.83	-0.10	-0.10
1,3-Bis(dichloroboryl)propane	44.12	44.25	-0.13	-0.29
1,3-Bis(dimethoxyboryl)propane	48.96	49.15	-0.19	-0.39
1,4-Bis(dichloroboryl)butane	48.79	48.88	-0.09	-0.18
1,4-Bis(diethoxyboryl)butane	73.12	72.42	0.70	0.96
1,5-Bis(diethoxyboryl)pentane	77.13	77.05	0.08	0.10
1,6-Bis(diethoxyboryl)hexane	81.81	81.68	0.13	0.16
2-Butoxy-2-bora-1,3-dioxacyclopentane	37.13	36.61	0.52	1.40
2-Tolyl 3-tolyl propoxyborine	82.11	81.86	0.25	0.30
2-Tolyl 4-tolyl propoxyborine	82.26	81.86	0.40	0.49
2-Tolyl dibutoxyborine	76.18	76.43	-0.25	-0.33
2-Tolyl diethoxyborine	57.69	57.91	-0.22	-0.38
2-Tolyl dimethoxyborine	48.14	48.59	-0.45	-0.93
2-Tolyl dipropoxyborine	66.97	67.17	-0.20	-0.30
3-Tolyl dibutoxyborine	76.48	76.43	0.05	0.07
3-Tolyl diethoxyborine	58.08	57.91	0.17	0.29
3-Tolyl dimethoxyborine	48.38	48.59	-0.21	-0.43
3-Tolyl dipropoxyborine	67.26	67.17	0.09	0.13
4-Tolyl dibutoxyborine	76.67	76.43	0.24	0.31
4-Tolyl diethoxyborine	58.04	57.91	0.13	0.22
4-Tolyl dimethoxyborine	48.49	48.59	-0.10	-0.21
4-Tolyl dipropoxyborine	67.42	67.17	0.25	0.37
Bis(2-tolyl)-N-ethylaminoborane	79.12	78.87	0.25	0.32
Bis(2-tolyl)-N-isobutylaminoborane	88.08	88.09	-0.01	-0.01
Bis(2-tolyl)-N-methylaminoborane	74.00	74.28	-0.28	-0.38
Bis(allylamino)borane	40.89	41.33	-0.44	-1.08
Bis(butylamino)borane	51.24	51.21	0.03	0.06
Bis(butylthio) 2-(diethylmethylsilyl)ethyl borane	101.77	102.28	-0.51	-0.50
Bis(butylthio) hexyl borane	88.58	88.16	0.42	0.47
Bis(butylthio) octyl borane	98.30	97.42	0.88	0.90
Bis(butylthio)borane	60.17	60.27	-0.10	-0.17
Bis(diallylamino)borane	67.84	68.71	-0.87	-1.28
Bis(diethylamino)borane	51.54	51.43	0.11	0.21
Bis(di-isoamylamino)borane	107.11	106.83	0.28	0.26
Bis(diisobutylamino)borane	88.26	88.31	-0.05	-0.06
Bis(ethylthio) butylborane	60.19	60.38	-0.19	-0.32
Bis(ethylthio) isobutylborane	60.30	60.34	-0.04	-0.07
Bis(ethylthio) isopropylborane	55.34	55.77	-0.43	-0.78
Bis(ethylthio) octyl borane	78.77	78.90	-0.13	-0.17
Bis(ethylthio) propylborane	55.66	55.75	-0.09	-0.16
Bis(ethylthio)borane	41.16	41.75	-0.59	-1.43
Bis(isobutyl) cyclohexylboronate	72.44	72.12	0.32	0.44
Bis(isopropylthio)borane	51.08	50.99	0.09	0.18
Bis(propylthio)borane	50.77	51.01	-0.24	-0.47
Bis(t-butylthio)borane	61.77	61.01	0.76	1.23
Bromo butylthio isopentylborane	64.00	63.96	0.04	0.06
Bromo ethylthio isopentylborane	54.51	54.70	-0.19	-0.35
Bromo ethylthio isopropylborane	45.04	45.50	-0.46	-1.02
Bromo ethylthio phenylborane	57.27	56.67	0.60	1.05
Butoxy chloro phenylborine	56.56	56.22	0.34	0.60
Butyl butoxy chloroborine	49.43	49.66	-0.23	-0.47
Butyl dibutoxyborine	64.87	65.06	-0.19	-0.29
Butylphenylboronic acid	50.06	50.81	-0.75	-1.50
Butylthiodiethylborane	52.20	52.20	0.00	0.00

Table 6. Cont.

Molecule Name	Refractivity Exp.	Refractivity Calc.	Deviation	Dev. in %
Chloro 2-octoxy phenylborine	74.42	74.75	−0.33	−0.44
Chloro di(1,2,2-trimethylpropoxy)borine	69.31	69.36	−0.05	−0.07
Chloro di(2-octoxy)borine	87.34	87.92	−0.58	−0.66
Chloro di(sec-butoxy)borine	50.69	50.88	−0.19	−0.37
Chloro dibutoxyborine	51.03	50.86	0.17	0.33
Chloro diisobutoxyborine	50.35	50.78	−0.43	−0.85
Chloro dineopentoxyborine	60.34	60.08	0.26	0.43
Chloro dioctoxyborine	88.29	87.90	0.39	0.44
Chloro dipropoxyborine	41.83	41.60	0.23	0.55
Cyclohexyldichloroborane	41.98	41.91	0.07	0.17
Dibutoxy 2-hydroxyethoxy borine	59.48	58.68	0.80	1.34
Dibutylboronic anhydride	86.44	87.19	−0.75	−0.87
Dibutylbutylaminoborane	65.68	65.39	0.29	0.44
Dibutylethylthioborane	61.49	61.46	0.03	0.05
Dibutylphenylaminoborane	72.53	72.57	−0.04	−0.06
Dibutylphenylthioborane	76.46	76.82	−0.36	−0.47
Dichloro 4-chlorobutoxyborine	40.73	40.65	0.08	0.20
Dichloro butoxyborine	36.03	35.85	0.18	0.50
Dichloro isobutoxyborine	36.55	35.81	0.74	2.02
Dichloro neopentoxyborine	40.51	40.46	0.05	0.12
Dichloro octoxyborine	53.85	54.37	−0.52	−0.97
Dichloro propoxyborine	30.62	31.22	−0.60	−1.96
Diisoamylbutylthioborane	79.99	79.90	0.09	0.11
Diisobutylboronic anhydride	87.73	87.03	0.70	0.80
Diisobutylbutylthioborane	71.06	70.64	0.42	0.59
Diisopentylboronic anhydride	105.56	105.55	0.01	0.01
Diisopropylboronic anhydride	68.78	68.75	0.03	0.04
Diocetyl butoxyborine	100.02	100.79	−0.77	−0.77
Dipropylbutylthioborane	61.51	61.46	0.05	0.08
Dipropylethylthioborane	52.48	52.20	0.28	0.53
Dipropylisobutylaminoborane	55.99	56.09	−0.10	−0.18
Dipropylphenylaminoborane	63.31	63.31	0.00	0.00
Dipropylphenylthioborane	67.67	67.56	0.11	0.16
Ethyl phenyl butoxyborine	61.09	61.05	0.04	0.07
Ethylphenylboronic acid	42.13	41.55	0.58	1.38
Ethylphenylboronic anhydride	82.57	81.79	0.78	0.94
Ethylthio dioctyl borane	98.03	98.50	−0.47	−0.48
Ethylthiodiethylborane	42.82	42.94	−0.12	−0.28
Hexyldichloroborane	44.07	44.03	0.04	0.09
Isobutyl cyclohexylchloroboronate	56.96	56.76	0.20	0.35
o-Tolylamino(diethylamino)borane	63.48	63.31	0.17	0.27
Pentylchloroborane	39.49	39.40	0.09	0.23
Phenyl 2-tolyl propoxyborine	77.12	77.05	0.07	0.09
Phenyl di(sec-butoxy)borine	71.45	71.64	−0.19	−0.27
Phenyl di(sec-octoxy)borine	108.55	108.68	−0.13	−0.12
Phenyl dibutoxyborine	71.32	71.62	−0.30	−0.42
Phenyl diethoxyborine	52.87	53.10	−0.23	−0.44
Phenyl diisobutoxyborine	71.44	71.54	−0.10	−0.14
Phenyl dimethoxyborine	43.45	43.78	−0.33	−0.76
Phenyl dipropoxyborine	62.40	62.36	0.04	0.06
Phenylamino(diethylamino)borane	58.85	58.50	0.35	0.59
Phenylboron dichloride	41.64	41.33	0.31	0.74
Phenylpropylboronic acid	46.40	46.18	0.22	0.47
Phenylpropylboronic anhydride	90.30	91.05	−0.75	−0.83
Tri(1,2,2-trimethylpropoxy)borine	93.61	94.28	−0.67	−0.72
Tri(1,3-dichloro-2-propoxy)borine	81.12	81.47	−0.35	−0.43

Table 6. Cont.

Molecule Name	Refractivity Exp.	Refractivity Calc.	Deviation	Dev. in %
Tri(1-chloroethoxy)borine	52.99	53.51	−0.52	−0.98
Tri(1-ethoxycarbonylethoxy)borine	85.93	85.70	0.23	0.27
Tri(1-methoxyethoxy)borine	57.42	57.14	0.28	0.49
Tri(2-ethoxycarbonylethoxy)borine	84.97	85.67	−0.70	−0.82
Tri(2-pentoxy)borine	80.11	80.45	−0.34	−0.42
Tri(butylthio)borane	87.47	87.36	0.11	0.13
Tri(ethoxycarbonylmethoxy)borine	71.14	71.78	−0.64	−0.90
Tri(propylthio)borane	73.47	73.47	0.00	0.00
Tri(<i>t</i> -butoxy)borine	66.77	66.38	0.39	0.58
Tributyl borate	66.65	66.53	0.12	0.18
Tridecyl borate	149.41	149.87	−0.46	−0.31
Triethyl borate	38.69	38.75	−0.06	−0.16
Triethylborane	33.72	34.51	−0.79	−2.34
Triheptyl borate	109.18	108.20	0.98	0.90
Triisobutylborane	62.31	62.17	0.14	0.22
Triisopentoxyborine	80.14	80.30	−0.16	−0.20
Triisopentylborane	76.54	76.06	0.48	0.63
Triisopropyl borate	52.52	52.67	−0.15	−0.29
Trimethoxyborine	24.86	24.77	0.09	0.36
Trioctyl borate	122.30	122.09	0.21	0.17
Tripenoxyborine	80.42	80.42	0.00	0.00
Tripropyl borate	52.55	52.64	−0.09	−0.17
Tripropylborane	48.54	48.40	0.14	0.29
Tris(ethylthio)borane	59.41	59.58	−0.17	−0.29

4.2. Polarizability

The calculation of the molecular polarizabilities was carried out indirectly via the calculated refractivities applying the inverse Lorentz–Lorenz relation. In order to include the relatively limited number of experimentally determined polarizability data in the atom group parameters and any further calculations, they were translated into the corresponding refractivity values and henceforth treated just like the remaining experimental refractivities. Conversely, all the experimental refractivity values were analogously converted into “experimental” polarizabilities. The complete set of true and indirectly determined experimental polarizability values is compared in Figure 4 with the indirectly calculated polarizability values, mirroring the excellent correlation of Figure 2, which at first sight is not surprising as both value sets are multiplied with the same factor. However, we should not forget that the truly experimentally determined polarizability values were evaluated by various methods that differ from those for the experimental determination of the refractivity. In fact, as the histogram in Figure 5 reveals, it turned out that 23 compounds should be viewed as outliers because their experimental refractivity values deviated by more than three times the standard deviation σ of 0.15 \AA^3 from calculations. They are collected in a separate list, available in the Supplementary Materials, together with the complete set of compounds with experimental and calculated polarizabilities.

In a paper by Tariq et al. [273], the applicability of the Lorentz–Lorenz relation was questioned for ILs because it is based on the assumption of the compounds being “isotropic fluids composed of spherical and non-interacting particles” which is not given with this class of salts, since at least one of its ions is non-spherical, and they are clearly non-isotropic fluids as they consist of polar centers surrounded by non-polar moieties. These considerations are certainly justified with respect to the relationship between refractivity and polarizability of ILs. In the following section, however, we will demonstrate that the non-spherical character of the ILs is no obstacle for a reasonable correlation between molecular volume and refractivity.

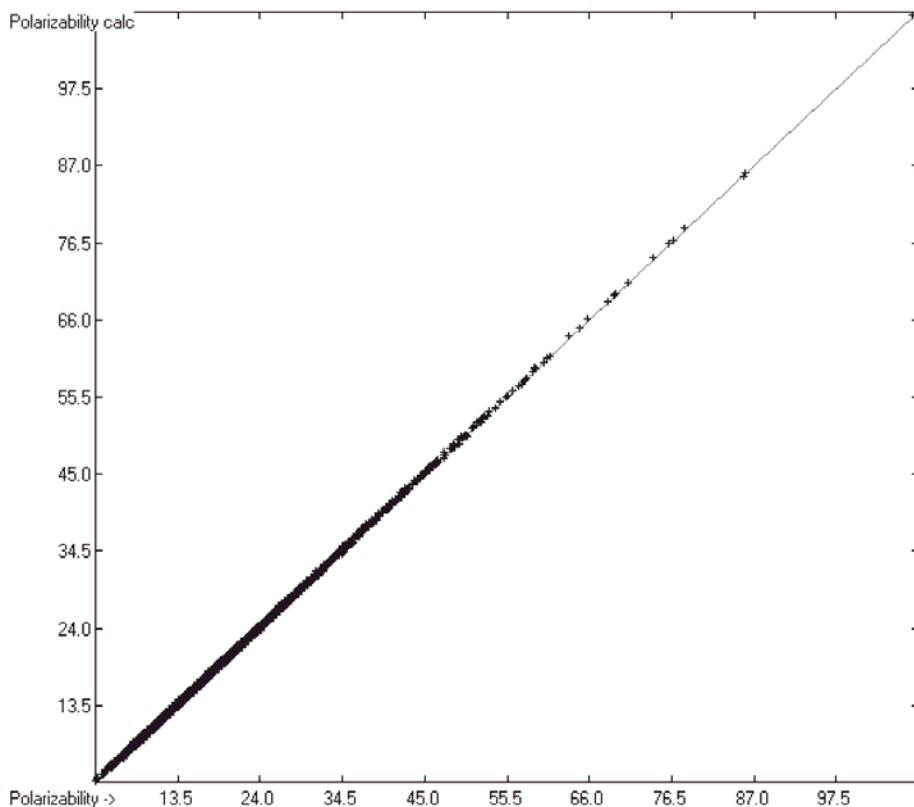


Figure 4. Correlation diagram of the polarizability data (in Å³). (N = 5763, R² = 0.9997, regression line: intercept = 0.0115; slope = 0.9995, MAPD = 0.72%).

4.3. Refractivity/Polarizability and Molecular Volume

A paper of Brinck et al. [6] discussed the relationship between the polarizability of a molecule and its volume, arguing that physically “the polarizability α of a conducting sphere of radius R is equal to R^3 ”, its relation expressed by the equation $\alpha = 3V/4\pi$, where V is the volume. This relation is true on condition that the electrostatic potential is uniform within this sphere, which is certainly not the case in a molecule. An approximate equation, known as the Clausius–Mossotti equation, proposes for nonpolar molecules the polarizability as being directly proportional to their volume and a function of their dielectric constant. Several approaches for the calculation of the molecular volumes have been chosen in order to assess their applicability for polarizability predictions. Gough [402], Laidig and Bader [403], and Brinck et al. [6] used various Hartree–Fock self-consistent field methods to compute the volumes of a limited number of small molecules and achieved good linearity with their polarizability, depending on the size of the contour of the electronic density defining the molecule’s surface. In an earlier paper [7], we presented a fast numerical method for the calculation of the “true” molecular volume (in Å³) of molecules of any size and type, including ILs, based on the atoms’ Van-der-Waals radii. Since these “true” (elsewhere also called “hardcore”) volumes are automatically generated on entering a new compound to the database, it was obvious to examine their potential linearity with their experimental polarizability or refractivity as far as available. In Figure 6, the correlation between the “true” molecular volume and the experimental refractivity of 6069 molecules is shown, revealing an excellent correlation coefficient R² of 0.9645 and a MAPD of 7.53%.

Figure 7 presents the same correlation diagram, but restricted to the class of ILs, indicating that the path of prediction of their refractivity R via their molecular volume V as calculated in [7] and applying the simple linear equation $R = \text{intercept} + (V \times \text{slope})$ provides a reliable refractivity value with a MAPD of little more than 5% within the ILs class over a large range of molecular volumes, if the atom group additivity method does not allow a calculation due to the limitations mentioned earlier. The complete list of molecules with their “true” molecular volume and experimental and volume-derived refractivity is available in the Supplementary Materials.

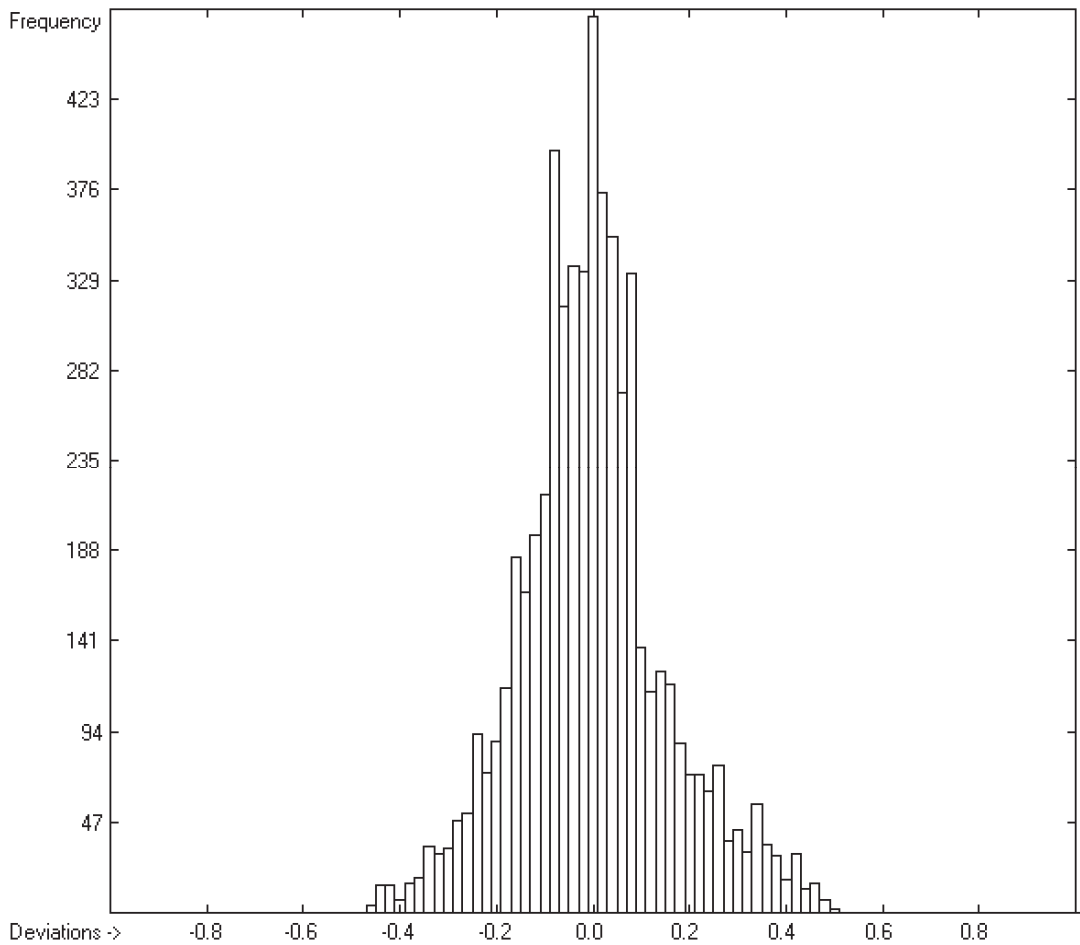


Figure 5. Histogram of the polarizability data ($\sigma = 0.15 \text{ \AA}^3$; exp. values range from 3.23 to 107.53 \AA^3).

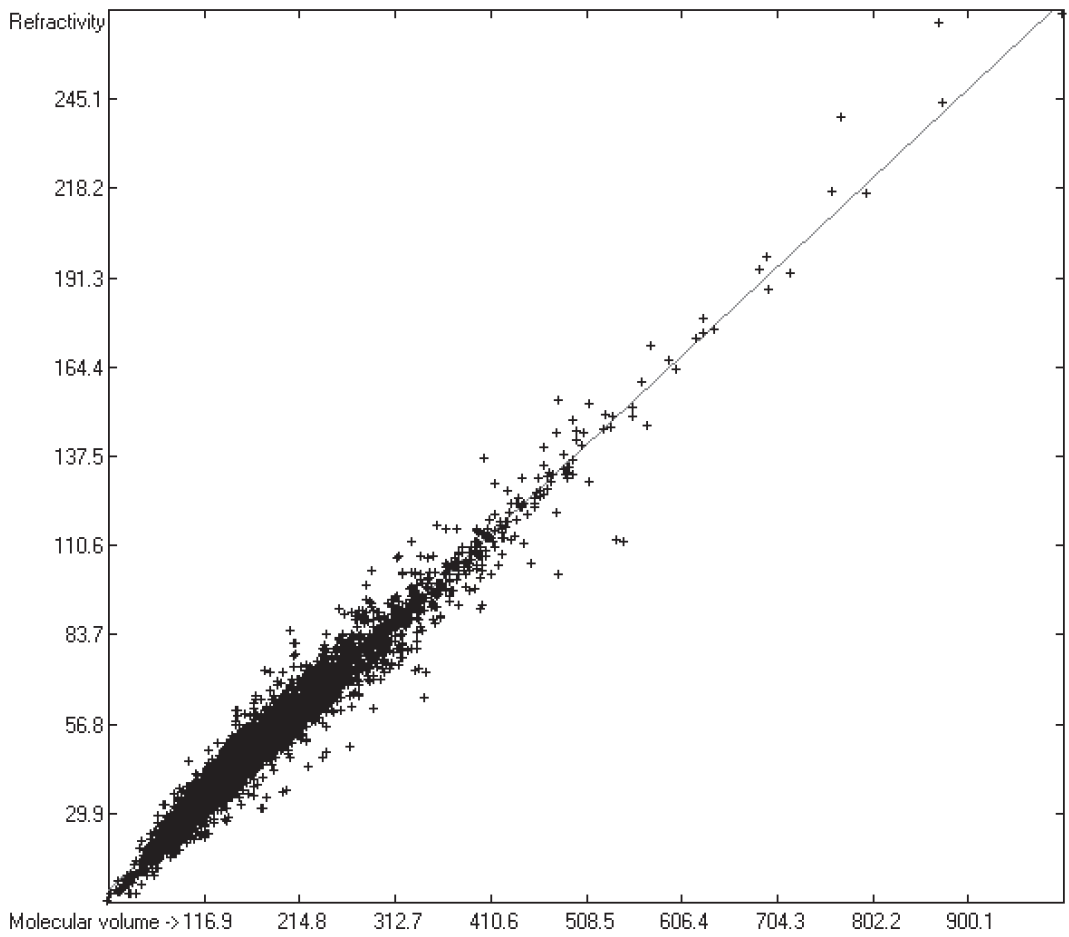


Figure 6. Correlation diagram of “true” molecular volume (in Å³) [7] vs. experimental refractivity. (N = 6069, R² = 0.9645, regression line: intercept = 1.4354; slope = 0.2743, MAPD = 7.53%).

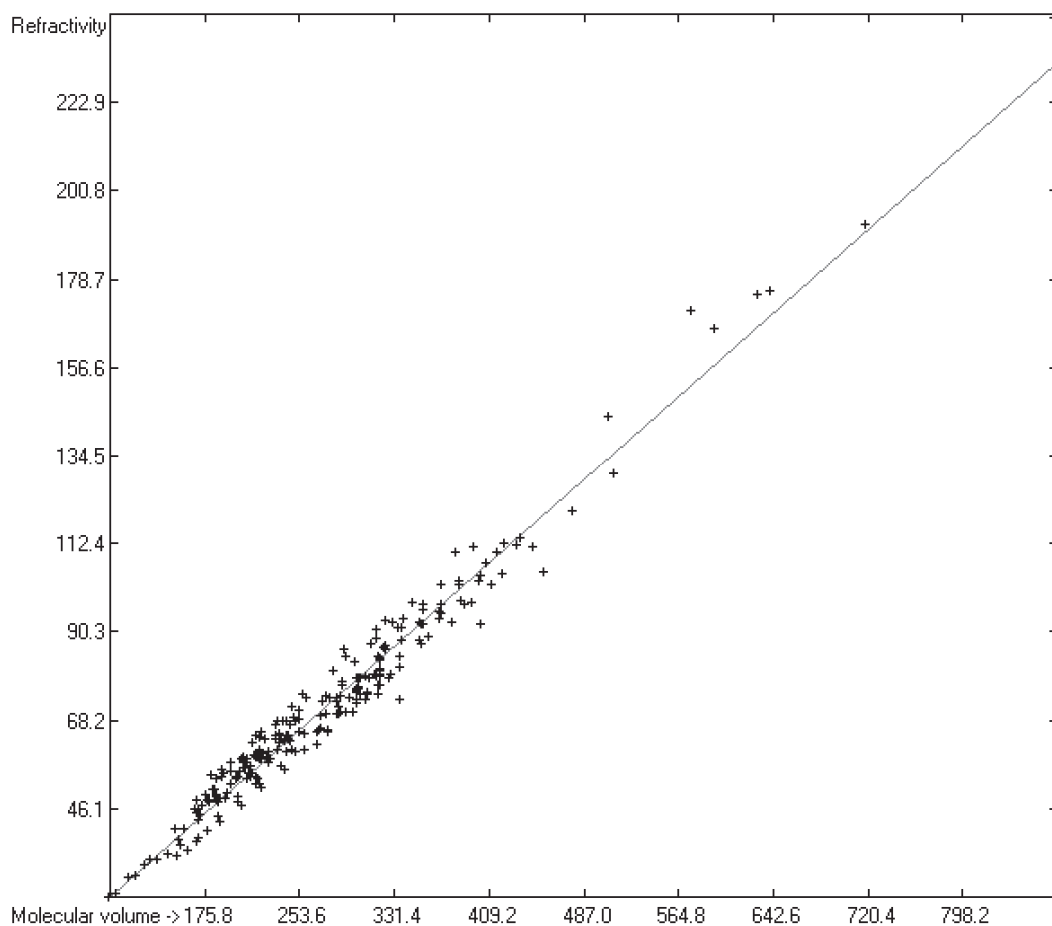


Figure 7. Correlation diagram of “true” molecular volume (in Å³) [7] vs. experimental refractivity of ILs. (N = 247, R² = 0.9700, regression line: intercept = −2.4557; slope = 0.2686, MAPD = 5.35%).

5. Conclusions

In several earlier papers [1,7,8,397–401], the present atom groups additivity algorithm, outlined in [1], proved its formidable versatility for the reliable prediction of up to 17 physical, thermodynamic, solubility-, optics-, charge-, and environment-related descriptors. In the present work, which is part of an ongoing project, the results of the present refractivity/polarizability calculations again demonstrate its as-yet unsurpassed accuracy and easy expandability. The nearly 6000 molecules providing their experimental refractivity or polarizability values, either directly or via their refractive index and density, enabled the calculation of a large set of atom group parameters allowing the refractivity/polarizability of nearly 80% of the compounds listed in a database of presently approaching 36,000 of nearly any molecular structure, size, and application. The big advantage of the present method is the basic possibility to calculate the refractivity simply by means of paper and pencil applying the parameters set listed in Table 2. In addition, we have shown that optional refractivity/polarizability calculations are possible via the molecular volume route—although with lower accuracy—in cases where the group additivity method is disabled.

The mentioned project's software is called ChemBrain IXL, available from Neuronix Software (www.neuronix.ch, 1.1.2015, Rudolf Naef, Lupsingen, Switzerland).

Supplementary Materials: The following supporting information can be downloaded at: <https://www.mdpi.com/article/10.3390/liquids2040020/s1>, The list of compounds used in the present work, their experimental data, and 3D structures are available online as standard SDF files, accessible for external chemistry software, under the name of "S01. Compounds List for Refractivity-Parameters Calculations.sdf". The list of the compounds used in the correlation diagrams and histograms containing their names and their experimental and calculated values are available under the corresponding names of "S02. Experimental vs. Calculated Refractivities.doc", "S03. Experimental vs. Calculated Polarizabilities.doc" and "S04. Molecular Volume vs. Refractivity Data Table.doc". Separate analogous lists are available for ionic liquids under the name of "S05. Experimental vs. Calculated Refractivities of Ionic Liquids.doc", for silicon compounds under the name of "S06. Experimental vs. Calculated Refractivities of Silicon Compounds.doc", and for boron compounds under the name of "S07. Experimental vs. Calculated Refractivities of Boron Compounds.doc". In addition, two lists containing the outliers in the calculations of the refractivity and polarizability of molecules are available under the names of "S08. Refractivity Outliers.doc" and "S09. Polarizability outliers.doc". Finally, the figures are available as .tif files and the tables as .doc files under the names given in the text.

Author Contributions: R.N. developed project ChemBrain and its software upon which this paper is based, and also fed the database, calculated, and analyzed the results, and wrote the paper. W.E.A.J. suggested the extension of ChemBrain's tool and contributed experimental data and the great majority of the literature references. Beyond this, R.N. is indebted to W.E.A.J. for the many valuable discussions. All authors have read and agreed to the published version of the manuscript.

Funding: This research received no external funding.

Data Availability Statement: The data presented in this study are available in Supplementary Material.

Acknowledgments: R.N. is indebted to the library of the University of Basel for allowing him full and free access to the electronic literature database.

Conflicts of Interest: The authors declare no conflict of interest.

References

- Naef, R. A Generally Applicable Computer Algorithm Based on the Group Additivity Method for the Calculation of Seven Molecular Descriptors: Heat of Combustion, LogPO/W, LogS, Refractivity, Polarizability, Toxicity and LogBB of Organic Compounds; Scope and Limits of Applicability. *Molecules* **2015**, *20*, 18279–18351. [[CrossRef](#)] [[PubMed](#)]
- Denbigh, K.G. The Polarizabilities of Bonds—I. *Trans. Faraday Soc.* **1940**, *36*, 936–948. [[CrossRef](#)]
- Ghose, A.K.; Crippen, G.M. Atomic physicochemical parameters for three-dimensional structure-directed quantitative structure-activity relationships I. Partition coefficients as a measure of hydrophobicity. *J. Comput. Chem.* **1986**, *7*, 565–577. [[CrossRef](#)]
- Miller, K.J.; Savchik, J.A. A new empirical Method to calculate Average Molecular Polarizabilities. *J. Am. Chem. Soc.* **1979**, *101*, 7206–7213. [[CrossRef](#)]
- Miller, K.J. Additivity methods in molecular polarizability. *J. Am. Chem. Soc.* **1990**, *112*, 8533–8542. [[CrossRef](#)]
- Brink, T.; Murray, J.S.; Politzer, P. Polarizability and volume. *J. Chem. Phys.* **1993**, *98*, 4305–4306. [[CrossRef](#)]
- Naef, R. Calculation of the isobaric heat capacities of the liquid and solid phase of organic compounds at and around 298.15 K based on their "True" molecular volume. *Molecules* **2019**, *24*, 1626. [[CrossRef](#)] [[PubMed](#)]
- Naef, R.; Acree, W.E. Application of a General Computer Algorithm Based on the Group-Additivity Method for the Calculation of Two Molecular Descriptors at Both Ends of Dilution: Liquid Viscosity and Activity Coefficient in Water at Infinite Dilution. *Molecules* **2018**, *23*, 5. [[CrossRef](#)] [[PubMed](#)]
- Hardtwig, E. *Fehler- Und Ausgleichsrechnung*; Bibliographisches Institut AG: Mannheim, Germany, 1968.
- Kim, K.-S.; Shin, B.-K.; Lee, H.; Ziegler, F. Refractive index and heat capacity of 1-butyl-3-methylimidazolium bromide and 1-butyl-3-methylimidazolium tetrafluoroborate, and vapor pressure of binary systems for 1-butyl-3-methylimidazolium bromide + trifluoroethanol and 1-butyl-3-methylimidazolium tetrafluoroborate + trifluoroethanol. *Fluid Phase Equil.* **2004**, *218*, 215–220. [[CrossRef](#)]
- Lide, D.R. (Ed.) Physical Constants of Organic Compounds. In *CRC Handbook of Chemistry and Physics*; CRC Press: Boca Raton, FL, USA, 2005; pp. 3-1–3-740.

12. Ghose, A.K.; Crippen, G.M. Atomic Physicochemical Parameters for Three-Dimensional-Structure-Directed Quantitative Structure-Activity Relationships. 2. Modeling Dispersive and Hydrophobic Interactions. *J. Chem. Inf. Comput. Sci.* **1987**, *27*, 21–35. [[CrossRef](#)] [[PubMed](#)]
13. Perlman, D.; Davidson, D.; Bogert, M.T. The Synthesis of Phenanthrenes from Hydroxyl Derivatives of beta-Phenylethylcyclohexanes and the Nature of the By-Product. *J. Org. Chem.* **1936**, *01*, 288–299. [[CrossRef](#)]
14. Drake, N.L.; Welsh, L.H. 2,2,3,4-Tetramethylhexane and 3,3,5-trimethylheptane. *J. Am. Chem. Soc.* **1938**, *60*, 488–489. [[CrossRef](#)]
15. Petrov, A.D.; Baidanov, A.P.; Zakotin, N.N.; Suntsov, P.I. The synthesis and properties of α -methylheptylbenzene, α -butylamylbenzene and α -hexylheptylbenzene. *Zh. Obsh. Khim.* **1939**, *9*, 509–512.
16. Matui, E. Styrene substitutes and their polymers. II. p-Ethylstyrene and its polymers. *Kogyo Kagaku Zasshi* **1941**, *44*, 107–108.
17. Matui, E. Substituted styrenes and their polymers. III. p-Isopropylstyrene and its polymer. *Kogyo Kagaku Zasshi* **1941**, *44*, 284–286.
18. Petrov, A.D.; Pavlov, A.M.; Makarov, Y.A. Synthesis of 3-ethyldecane and of 2,5-dimethylhendecane. *Zh. Obsh. Khim.* **1941**, *2*, 1104–1106.
19. Petrov, A.D.; Chel'tsova, M.A. Synthesis and properties of hydrocarbons of aromatic and naphthenic series of the composition C_{19} – C_{26} . II. *Zh. Obsh. Khim.* **1942**, *12*, 87–94.
20. Petrov, A.D.; Kaplan, E.P. Synthesis and properties of isoparaffin hydrocarbons of the composition C_{12} – C_{22} . II. *Zh. Obsh. Khim.* **1942**, *12*, 99–103.
21. Petrov, A.D.; Shchupina, Z.K.; Ol'dekop, Y.A. Synthesis of 9,10-dimethyloctadecane and 9,10-di-propyloctadecane. *Zh. Obsh. Khim.* **1944**, *14*, 490–500.
22. Petrov, A.D.; Vittikh, M.V. Synthesis and properties of isoparaffinic hydrocarbons of the composition C_{13} – C_{24} . *Izvest. Akad. Nauk SSSR Ser. Khim.* **1944**, 238–242.
23. Petrov, A.D.; Krutov, K.M.; Khrenov, I.M. Synthesis and properties of cyclohexylhexylmethanol and 3-cyclohexyl-2-methylnonane. *Zh. Obsh. Khim.* **1945**, *15*, 799–801.
24. Lunshof, H.J.; van Stenis, J.; Waterman, H.I. Preparation of some Physical Constants of 2-Methyltetradecane and 3-Methylpentadecane. *Rec. Trav. Chim. Pays Bas* **1947**, *66*, 348–352. [[CrossRef](#)]
25. Petrov, A.D.; Ol'dekop, Y.A. Synthesis and properties of higher isoparaffin hydrocarbons of composition C_{20} – C_{34} (7,8-diisopropyltetradecane, 7,8-diisoamyltetradecane, 10,11-dipropyleicosane, 11,12-dipropyldocosane, 9,10-dioctyloctadecane, and 9,10,11,12-tetrapropyleicosane). *Zh. Obsh. Khim.* **1948**, *18*, 859–864.
26. Petrov, A.D.; Kaplan, E.P. The synthesis and the physical properties of C_{22} -branched hydrocarbons. *Izvest. Akad. Nauk SSSR Ser. Khim.* **1949**, 539–544.
27. Romadane, I. Alkylation of naphthalene with iso alcohols in the presence of boron trifluoride. *Zh. Obsh. Khim.* **1957**, *27*, 1939–1941.
28. Petrov, A.A.; Mingaleva, K.S.; Kupin, B.S. Dipole moments and reactivity of vinylacetylenic hydrocarbons. *Dokl. Akad. Nauk SSSR* **1958**, *123*, 298–300.
29. Terres, E.; Brinkmann, L.; Fischer, D.; Hüllstrung, D.; Lorz, W.; Weisbrod, G. Synthese und physikalische Daten einiger Isoparaffinreihen mit 11 bis 24 C-Atomen. *Brennstoff Chem.* **1959**, *40*, 279–280.
30. Petrov, A.A.; Sergienko, S.R.; Nechitailo, N.A.; Tsedilina, A.L. Synthesis and properties of C_{12} – C_{16} monomethylalkanes. *Russ. Chem. Bull.* **1959**, *8*, 1091–1097. [[CrossRef](#)]
31. Leibnitz, E.; Hager, W.; Winkler, R. Studien zur Chemie der Paraffine und Paraffingatsche. V. Synthese und physikalische Eigenschaften einiger 4n-Propyl- und 2-Methyl-3-isopropyl-Alkane mit mehr als 10 C-Atomen. *J. Prakt. Chem.* **1959**, *9*, 275–288. [[CrossRef](#)]
32. Levina, R.Y.; Kostin, V.N.; Gembitskii, P.A.; Treshchova, E.G. Cyclopropanes and cyclobutanes. XVII. Reduction of arylcyclopropanes with metals in liquid ammonia and with methyl alcohol. *Zh. Obsh. Khim.* **1960**, *31*, 829–836.
33. Terres, E.; Paulsen, S.R.; Huellstrung, D. Isoparaffins. *Erdoel Kohle* **1960**, *13*, 323–325.
34. Xiaomei, Q.; Xiaofang, C.; Yongsheng, G.; Li, X.; Shenlin, H.; Wenjun, F. Density, Viscosity, Surface Tension, and Refractive Index for Binary Mixtures of 1,3-Dimethyladamantane with Four C_{10} Alkanes. *J. Chem. Eng. Data* **2014**, *59*, 775–783.
35. Skita, A.; Faust, W. Velocities of formation of the stereomeric methylcyclohexanols. *Ber. Dt. Chem. Ges.* **1931**, *64B*, 2878–2892. [[CrossRef](#)]
36. Viktorova, E.A.; Shuikin, N.I.; Karakhanov, E.A. Catalytic alkylation of p-cresol by dipropenyl. *Izvest. Akad. Nauk SSSR Ser. Khim.* **1963**, *12*, 2226–2227. [[CrossRef](#)]
37. Viktorova, E.A.; Karakhanov, E.A.; Shuikin, A.N.; Shuikin, N.I. Alkylation of phenols by compounds with two functions. II. Alkylation of p-cresol by diene hydrocarbons with isolated double bonds. *Izvest. Akad. Nauk SSSR Ser. Khim.* **1966**, *3*, 523–527.
38. Viktorova, E.A.; Shuikin, N.I.; Karakhanov, E.A. Alkylation of phenols with bifunctional compounds. XII. Catalytic alkenylation of o- and p-cresols with butadiene. *Izvest. Akad. Nauk SSSR Ser. Khim.* **1966**, *5*, 915–918.
39. Mori, S. Response Correction of Differential Refractometer for Polyethylene Glycols in Size Exclusion Chromatography. *Anal. Chem.* **1978**, *50*, 1639–1643. [[CrossRef](#)]
40. Teregulova, G.T. Synthesis of 1,3-dioxolanes containing aromatic fragments. *Zh. Priklad Khim.* **1990**, *63*, 1383–1386.
41. Crespo, E.A.; Costa, J.M.L.; Hanafiah, Z.B.M.A.; Kurnia, K.A.; Oliveira, M.B.; Lovell, F.; Vega, L.F.; Carvalho, P.J.; Coutinho, J.A.P. New measurements and modeling of high pressure thermodynamic properties of glycols. *Fluid Phase Equil.* **2017**, *436*, 113–123. [[CrossRef](#)]

42. Chaudhary, N.; Nain, A.K. Densities, speeds of sound, refractive indices, excess and partial molar properties of polyethylene glycol 200 + benzyl methacrylate binary mixtures at temperatures from 293.15 to 318.15 K. *J. Mol. Liq.* **2021**, *346*, 117923. [[CrossRef](#)]
43. Mottier, M. Sur La Méthylene-Pyrocatechine. *Arch. Sci. Phys. Nat.* **1935**, *17*, 289–291.
44. Jacobs, T.L.; Cramer, R.; Hanson, J.E. Acetylenic ethers. II. Ethoxy- and butoxyacetylene. *J. Am. Chem. Soc.* **1942**, *64*, 223–226. [[CrossRef](#)]
45. Dandegaonker, S.H.; Gerrard, W.; Lappert, M.F. Reactions of phenylboron dichloride with ethers. *J. Chem. Soc.* **1957**, 2893–2897. [[CrossRef](#)]
46. Kalabina, A.V.; Shergina, S.I.; Shergina, N.I. Synthesis and properties of the cis and trans isomers of β -bromo vinyl aryl ethers. *Izvest. Vysssnikh Ucheb. Zavedenii Khim Khim. Tekhnol.* **1959**, *2*, 545–549.
47. Dai, F.; Xin, K.; Song, Y.; Shi, M.; Yu, Y.; Li, Q. Liquid-liquid equilibria for the ternary system containing 1-Butanol + methoxy-(methoxymethoxy)methane + water at temperatures of 303.15, 323.15 and 343.15 K. *Fluid Phase Equil.* **2016**, *409*, 466–471. [[CrossRef](#)]
48. Berinde, Z.M. QSPR Models for the Molar Refraction, Polarizability and Refractive Index of Aliphatic Carboxylic Acids Using the ZEP Topological Index. *Symmetry* **2021**, *13*, 2359. [[CrossRef](#)]
49. West, C.D. Crystal Form of Sucrose Octaacetate. *J. Am. Chem. Soc.* **1941**, *63*, 630. [[CrossRef](#)]
50. Rehberg, C.E.; Faucette, W.A. Preparation and Polymerization of Cycloalkyl Acrylates. *J. Am. Chem. Soc.* **1950**, *72*, 4307. [[CrossRef](#)]
51. Alexander, E.R.; Busch, H.M. A convenient synthesis of orthoformic esters. *J. Am. Chem. Soc.* **1952**, *74*, 554–555. [[CrossRef](#)]
52. Satta, V.; Fein, M.L.; Filachtone, E.M. Some Esters of Unsaturated Acids. *J. Am. Chem. Soc.* **1953**, *75*, 4101. [[CrossRef](#)]
53. Arbuzov, B.A.; Shavsha-Tolkacheva, T.G. Dipole moments of esters of orthopropionic and orthoformic acids. *Russ. Chem. Bull.* **1954**, *3*, 525–530. [[CrossRef](#)]
54. Shigley, J.W.; Bonhorst, C.W.; Liang, C.C.; Althouse, P.M.; Triebold, H.O. Physical Characterization of a) a Series of Ethyl Esters and b) a Series of Ethanoate Esters. *J. Am. Oil Chem. Soc.* **1955**, *32*, 213–215. [[CrossRef](#)]
55. Grzeskowiak, R.; Jeffrey, G.H.; Vogel, A.I. Physical Properties and Chemical Constitution. Part XXIX. Acetylenic Compounds. *J. Chem. Soc.* **1960**, 4719–4722. [[CrossRef](#)]
56. Mekhtiev, S.D.; Sharifova, S.M.; Smirnova, V.P. Esterification of terephthalic and isophthalic acids by aliphatic alcohols. *Azerbaij. Khim. Zh.* **1965**, *3*, 67–72.
57. Freidlin, G.N.; Bushinskii, V.I. Physical Properties of Monoalkyl Esters of Adipic Acid. *Zh. Prikl. Khim.* **1971**, *44*, 944–945.
58. Ortega, J. Measurements of Excess Enthalpies of [a Methyl n-Alkanoate (from n-Hexanoate to n-Pentadecanoate) + n-Pentadecane] at 298.15 K. *J. Chem. Thermodyn.* **1990**, *22*, 1165–1170. [[CrossRef](#)]
59. De Lorenzi, L.; Fermeglia, M.; Torriani, G. Density, Refractive Index, and Kinematic Viscosity of Diesters and Triesters. *J. Chem. Eng. Data* **1997**, *42*, 919–923. [[CrossRef](#)]
60. De Lorenzi, L.; Fermeglia, M.; Torriani, G. Density, Kinematic Viscosity, and Refractive Index for Bis(2-ethylhexyl) Adipate, Tris(2-ethylhexyl) Trimellitate, and Diisononyl Phthalate. *J. Chem. Eng. Data* **1998**, *43*, 183–186. [[CrossRef](#)]
61. Oswal, S.L.; Oswal, P.; Modi, P.S.; Dave, J.P.; Gardas, R.L. Acoustic, volumetric, compressibility and refractivity properties and Flory's reduction parameters of some homologous series of alkyl alkanoates from 298.15 to 333.15 K. *Thermochim. Acta* **2004**, *410*, 1–14. [[CrossRef](#)]
62. Anton, V.; Munoz-Embid, J.; Gascon, I.; Artal, M.; Lafuente, C. Thermophysical Characterization of Furfuryl Esters: Experimental and Modeling. *Energy Fuels* **2017**, *31*, 4143–4154. [[CrossRef](#)]
63. Bogdanova, A.V.; Shostakovskii, M.F.; Plotnikova, G.I. Synthesis of unsaturated ether acetals, thioether acetals, and mercaptals. *Dokl Akad. Nauk SSSR* **1960**, *134*, 587–590.
64. Makin, S.M.; Sudakova, V.S. Telomerization of vinyl ethyl ether with acetaldehyde acetal. Synthesis of 1-alkoxypolyenes. *Zh. Obsh. Khim.* **1962**, *32*, 3161–3166.
65. Vogel, A.I. Physical Properties and Chemical Constitution. Part XI. Ketones. *J. Chem. Soc.* **1948**, 610–615. [[CrossRef](#)]
66. Overberger, C.G.; Frazier, C.; Mandelman, J.; Smith, H.F. The Preparation and Polymerization of p-Alkylstyrenes. Effect of Structure on the Transition Temperatures of the Polymers. *J. Am. Chem. Soc.* **1953**, *75*, 3326–3330. [[CrossRef](#)]
67. Medwedew, S.S.; Alexejewa, E.N.; Organische Peroxyde, I. Mitteil.: Propyl- und Isopropyl-hydroperoxyd. *Ber. Dt. Chem. Ges.* **1932**, *65*, 133–137. [[CrossRef](#)]
68. Harris, E.J. Decomposition of alkyl peroxides: Propyl peroxide, ethyl hydrogen peroxide and propyl hydrogen peroxide. *Proc. R. Soc. A* **1939**, *173*, 126–146. [[CrossRef](#)]
69. Milas, N.A.; Surgenor, D.M. Organic peroxides. X. t-Amyl hydroperoxide and di-t-amyl peroxide. *J. Am. Chem. Soc.* **1946**, *68*, 643–644. [[CrossRef](#)]
70. Lindstrom, E.G. Preparation of normal and secondary butyl hydroperoxides. *J. Am. Chem. Soc.* **1953**, *75*, 5123–5124. [[CrossRef](#)]
71. Williams, H.R.; Mosher, H.S. Peroxides. I. n-Alkyl Hydroperoxides. *J. Am. Chem. Soc.* **1954**, *76*, 2984–2987. [[CrossRef](#)]
72. Sanz, L.F.; Gonzalez, J.A.; de la Garcia Fuente, I.; Cobos, J.C. Thermodynamics of mixtures with strongly negative deviations from Raoult's law. XII. Densities, viscosities and refractive indices at T = (293.15 to 303.15) K for (1-heptanol, or 1-decanol + cyclohexylamine) systems. Application of the ERAS model to (1-alkanol + cyclohexylamine) mixtures. *J. Chem. Thermodyn.* **2015**, *80*, 161–171. [[CrossRef](#)]
73. Ioffe, B.V. Synthesis of unsymmetric dialkylhydrazines. *Zh. Obsh. Khim.* **1958**, *28*, 1296–1302.
74. Legrand, R. Dimethylaminobenzylidenemalononitrile. *Bull. Soc. Chim. Belges* **1944**, *53*, 166–177.

75. Paul, R.; Tchelitcheff, S. Synthesis of w-dinitriles and w-chlorinated nitriles from acetonitrile. *Bull. Soc. Chim. Fr.* **1949**, *16*, 470–475.
76. Kuhn, L.P.; DeAngelis, L. The thermal decomposition of dinitrites. I. Vicinal dinitrites. *J. Am. Chem. Soc.* **1954**, *76*, 328–329. [[CrossRef](#)]
77. Toops, E.E., Jr. Physical Properties of Eight High-Purity Nitroparaffins. *J. Phys. Chem.* **1956**, *60*, 304–306. [[CrossRef](#)]
78. Oswal, S.L.; Oswal, P.; Gardas, R.L.; Patel, S.G.; Shinde, R.G. Acoustic, volumetric, compressibility and refractivity properties and reduction parameters for the ERAS and Flory models of some homologous series of amines from 298.15 to 328.15 K. *Fluid Phase Equil.* **2004**, *216*, 33–45. [[CrossRef](#)]
79. McCusker, P.A.; Ashby, E.C.; Makowski, H.S. Organoboron compounds. III. Preparation and properties of alkylchloroboranes. *J. Am. Chem. Soc.* **1957**, *79*, 5182–5184. [[CrossRef](#)]
80. Christopher, P.M.; Tully, T.J. Some Octet and Bond Refractivities Involving Boron. *J. Am. Chem. Soc.* **1958**, *80*, 6516–6519. [[CrossRef](#)]
81. Aubrey, D.W.; Lappert, M.F. 586. Cyclic organic boron compounds. Part IV. B-amino- and B-alkoxy-borazoles and their precursors the tris(primary amino)borons and (primary amino)boron alkoxides. *J. Chem. Soc.* **1959**, 2927–2931. [[CrossRef](#)]
82. Mikhailov, B.M.; Bazhenova, A.V. Organoboron compounds. 29. Cyclohexaneboronic acid and its derivatives. *Russ. Chem. Bull.* **1959**, *8*, 68–71. [[CrossRef](#)]
83. Mikhailov, B.M.; Bubnov, Y.N. Organoboron compounds. XXXVIII. Reaction of trialkylboron with sulfur. Synthesis of esters of dialkylthioboronic acids. *Zh. Obsh. Khim.* **1959**, *29*, 1648–1650.
84. Mikhailov, B.M.; Aronovich, P.M. Organoboron compounds. XXXV. Alkylphenylboronic acids and their anhydrides. *Zh. Obsh. Khim.* **1959**, *29*, 1257–1262.
85. Mikhailov, B.M.; Shchegoleva, T.A. Synthesis of bis(alkylthio) boranes and trialkyl thioborates. *Izvest. Akad. Nauk SSSR Ser. Khim.* **1959**, *8*, 1868.
86. Mikhailov, B.M.; Shchegoleva, T.A.; Blokhina, A.N. Reaction of tetra-n-butylmercaptodiborane with unsaturated compounds. *Russ. Chem. Bull.* **1960**, *9*, 1218–1219. [[CrossRef](#)]
87. Mikhailov, B.M.; Shchegoleva, T.A. Synthesis and some transformations of alkylthiodiboranes. *Dokl. Akad. Nauk SSSR* **1960**, *131*, 834–836.
88. Mikhailov, B.M.; Dorokhov, V.A. Organoboron compounds. LXXXVI. Alkylthio(diethylamino) boranes. *Zh. Obsh. Khim.* **1961**, *31*, 3750–3756.
89. Mikhailov, B.M.; Bubnov, Y.N. Organoboron compounds. LXV. Synthesis of esters of dialkylthioboronic acids by the action of mercaptans on trialkylboron. *Zh. Obsh. Khim.* **1961**, *31*, 160–166.
90. Shchegoleva, T.A.; Belyavskaya, E.M. Organoboron compounds. Synthesis and some properties of tris(ethylthio) diborane. *Dokl. Akad. Nauk SSSR* **1961**, *136*, 638–641.
91. Mikhailov, B.M.; Shchegoleva, T.A.; Shashkova, E.M. The synthesis of esters of alkyl thioboronic acids from trialkylboron and thioborates. *Russ. Chem. Bull.* **1961**, *10*, 845–847. [[CrossRef](#)]
92. Mikhailov, B.M.; Kozminskaya, T.K. Organoboron Compounds. 90. Alkanethioboronic esters. *Russ. Chem. Bull.* **1962**, *11*, 234–237. [[CrossRef](#)]
93. Mikhailov, B.M.; Dorokhov, V.A. Organoboron compounds. XCIV. Bis(dialkylamino) boranes, and bis(monoalkylamino) boranes. *Zh. Obsh. Khim.* **1962**, *32*, 1511–1514.
94. Mikhailov, B.M.; Fedotov, N.S. The mechanism of nucleophilic substitution at the boron atom in organoboron compounds. *Dokl. Akad. Nauk SSSR* **1964**, *154*, 1128–1131.
95. Mikhailov, B.M.; Vasil'ev, L.S. Organoboron compounds. CLII. Mutual exchange of alkoxy and alkylthio groups in organoboron compounds. *Zh. Obsh. Khim.* **1965**, *35*, 1073–1078.
96. Zakharkin, L.L.; Kovredov, A.I. Compounds produced from products of 1,3-butadiene hydroboration. *Zh. Obsh. Khim.* **1966**, *36*, 2153–2170.
97. Jackson, I.K.; Davies, W.C.; Jones, W.J. Tertiary arylalkylphosphines. I. *J. Chem. Soc.* **1930**, 2298–2301. [[CrossRef](#)]
98. Kosolapoff, G.M. Isomerization of alkyl phosphites. III. Synthesis of alkylphosphonic acids. *J. Am. Chem. Soc.* **1945**, *67*, 1180–1182. [[CrossRef](#)]
99. Jones, W.J.; Davies, W.C.; Bowden, S.T.; Edwards, C.; Davis, V.E.; Thomas, L.H. Preparation and properties of allyl phosphines, arsines, and stannanes. *J. Chem. Soc.* **1947**, 1446–1450. [[CrossRef](#)]
100. Knunyants, I.L.; Sterlin, R.N. Reactions between organic oxides and phosphine. *Comptes Rendus (Dokl.) Acad. Des Sci. URSS* **1947**, *56*, 49–52.
101. Fox, R.B. Organophosphorus compounds. Alkylchlorophosphines. *J. Am. Chem. Soc.* **1950**, *72*, 4147–4149. [[CrossRef](#)]
102. Razumov, A.I.; Mukhacheva, O.A.; Khen, S.-D. Certain alkylphosphonothionic, alkylphosphonoselenonic, dialkylphosphinic, and alkylphosphonous esters, and the mechanism of addition to alkylphosphonous esters. *Russ. Chem. Bull.* **1952**, *1*, 797–802. [[CrossRef](#)]
103. Pudovik, A.N.; Yarmukhametova, D.K. New synthesis of esters of phosphonic and thiophosphonic acids. XV. Addition of esters of phenyl- and alkylphosphonous acids to esters of methacrylic and acrylic acids. *Izvest. Akad. Nauk SSSR Ser. Khim.* **1952**, 902–907.
104. Yakubovich, A.Y.; Motsarev, G.V. Synthesis of hetero-organic compounds of the aromatic series by the reaction of arylsilanes with aluminum chloride and halides of various elements. I. Organophosphorus compounds. *Zh. Obsh. Khim.* **1953**, *23*, 1547–1552.

105. Arbuzov, B.A.; Rizpolozhenskii, N.I. Esters of diethylphosphinous acid. *Dokl. Akad. Nauk SSSR* **1953**, *89*, 291–292.
106. Anisimov, K.N.; Nesmeyanov, A.N. Derivatives of unsaturated phosphonic acids. *Russ. Chem. Bull.* **1955**, *4*, 915–917. [[CrossRef](#)]
107. Anisimov, K.N.; Kolobova, N.E.; Nesmeyanov, A.N. Derivatives of unsaturated phosphonic acids. IX. Neutral esters of 2-alkoxy (or phenoxy)vinylthiophosphonic acids. *Izvest. Akad. Nauk SSSR Ser. Khim.* **1955**, 669–671.
108. Razumov, A.I.; Mukhacheva, O.A. Derivatives of alkylphosphonous and dialkylphosphinic acids. III. Atomic refraction of phosphorus in esters of alkylphosphonous acids. *Zh. Obsh. Khim.* **1956**, *26*, 1436–1440.
109. Razumov, A.I.; Mukhacheva, O.A. Derivatives of alkylphosphonous and dialkylphosphinic acids. IV. Reactions of addition and isomerization of esters of alkylphosphonous acids. *Zh. Obsh. Khim.* **1956**, *26*, 2463–2468.
110. Anisimov, K.N.; Nesmeyanov, A.N. Derivatives of unsaturated phosphonic acids. XVII. Derivatives of β -phenylvinylphosphonic acid. *Izvest. Akad. Nauk SSSR Ser. Khim.* **1956**, 19–22.
111. Anisimov, K.N.; Kolobova, N.E.; Nesmeyanov, A.N. Derivatives of unsaturated phosphonic acids. XVIII. Chlorides of alkylthiovinylphosphonic acids and their derivatives. *Izvest. Akad. Nauk SSSR Ser. Khim.* **1956**, 23–26.
112. Lenard-Borecka, B.; Michalski, J. Organophosphorus compounds of sulfur and selenium. VII. Dialkoxyposphinylsulfenyl chlorides. *Rocz. Chem.* **1957**, *31*, 1167–1176.
113. Razumov, A.I.; Mukhacheva, O.A.; Markovich, E.A. Derivatives of alkylphosphonous and phosphonic acids. VIII. Synthesis and properties of some alkylated amides of alkylphosphonic chlorides. *Zh. Obsh. Khim.* **1958**, *28*, 194–197.
114. Yamasaki, T. Preparation and properties of alkyl phosphonothionates, $(RO)_2P(S)H$. *Sci. Repts. Res. Insts. Tohoku Univ. Ser. A* **1959**, *11*, 73–79.
115. Kukhtin, V.A.; Abramov, V.S.; Orekhova, K.M. Rearrangement of esters of α -hydroxyalkylphosphonic acids into isomeric phosphates. *Dokl. Akad. Nauk SSSR* **1959**, *128*, 1198–1200.
116. Grechkin, N.P.; Shagidullin, R.R. Organophosphorus derivatives of ethylenimine. *Russ. Chem. Bull.* **1960**, *9*, 1978–1982. [[CrossRef](#)]
117. Grechkin, N.P.; Shagidullin, R.R. Organophosphorus derivatives of ethylenimine. III. Addition of acids to ethylenamides of phosphorus acids. *Izvest. Akad. Nauk SSSR Ser. Khim.* **1960**, 2135–2139.
118. Stolzer, C.; Simon, A. Fluorophosphorus compounds. III. Symmetrical diphosphoryl difluoride dichloride, $P_2O_3Cl_2F_2$. *Chem. Ber.* **1961**, *94*, 1976–1979. [[CrossRef](#)]
119. Pass, F.; Steininger, E.; Zorn, H. Organic phosphorus compounds III. A new method for the preparation of primary phosphines. *Monats. Chem.* **1962**, *93*, 230–236. [[CrossRef](#)]
120. Pass, F.; Steininger, E.; Zorn, H. Eine neue Methode zur Darstellung primärer Phosphine. *Mon. Chem. Und Verwandte Teile And. Wiss.* **1962**, *93*, 230–236. [[CrossRef](#)]
121. Kabachnik, M.I.; Tsvetkov, E.N. Lower dialkylphosphinous acids (secondary phosphine oxides) and some of their properties. *Russ. Chem. Bull.* **1963**, *12*, 1120–1124. [[CrossRef](#)]
122. Boerner, K.B.; Stoelzer, C.; Simon, A. Fluorophosphorus compounds. IX. The catalytic hydrogenation of fluorophosphoric acid phenyl esters. *Chem. Ber.* **1963**, *96*, 1328–1334.
123. Stoelzer, C.; Simon, A. Fluorophosphorus compounds. VI. Alkylamides of fluorodiphosphoric acids. *Chem. Ber.* **1963**, *96*, 881–895.
124. Stoelzer, C.; Simon, A. Fluorophosphorus compounds. X. Results of refractometric investigations of fluorophosphoric acid derivatives. *Chem. Ber.* **1963**, *96*, 1335–1340.
125. Arbuzov, B.A.; Vinokurova, G.M. Synthesis of bifunctional organophosphorus compounds. II. Addition of butylphosphine to unsaturated compounds. *Izvest. Akad. Nauk SSSR Ser. Khim.* **1963**, *3*, 502–506.
126. Voigt, D.; Labarre, M.C. Synthesis and magneto-optical study of some trialkylated trithiophosphites. *Compt. Rend.* **1964**, *259*, 4632–4634.
127. Zhmurova, I.N.; Voitsekhovskaya, I.Y. Alkyltetrachlorophosphoranes. *Zh. Obsh. Khim.* **1965**, *35*, 2197–2200.
128. Grishina, O.N.; Bezzubova, L.M. Alkylthiophosphine sulfides. III. O-Alkyl alkylphosphonodithioates. *Izvest. Akad. Nauk SSSR Ser. Khim.* **1966**, *9*, 1617–1620.
129. Neimysheva, A.A.; Knunyants, I.L. Nucleophilic displacement in the series of derivatives of acids of phosphorus. I. Kinetics of hydrolysis of chlorides of di-alkylphosphinic acids. *Zh. Obsh. Khim.* **1966**, *36*, 1090–1098.
130. Foxton, A.A.; Jeffrey, G.H.; Vogel, A.I. Physical properties and chemical constitution. Part XLIX. The refractivities, densities, and surface tensions of some organophosphorus compounds. *J. Chem. Soc. A* **1966**, 249–253. [[CrossRef](#)]
131. Akamsin, V.D.; Rizpolozhenskii, N.I. Esters of phosphorus(III) thioacids. V. New method for preparation of thiophosphinous acid esters. *Izvest. Akad. Nauk SSSR Ser. Khim.* **1967**, *9*, 1987–1989.
132. Buina, N.A.; Nuretdinov, I.A.; Grechkin, N.P. Ethylenimides of arylphosphorous and thiophosphoric acids. *Izvest. Akad. Nauk SSSR Ser. Khim.* **1967**, *1*, 217–220. [[CrossRef](#)]
133. Voigt, D.; Turpin, R.; Torres, M. Magneto-optical study of some dialkylphosphines. *Comptes Rendus. Seances Acad. Sci. Ser. C Sc. Chim.* **1967**, *265*, 884–887.
134. Grishina, O.N.; Potekhina, M.I. Synthesis of O-alkylalkylidithiophosphinic acids from products of oxidative phosphorylation of hydrocarbons of petroleum fractions. *Neftekhim* **1968**, *8*, 111–117.
135. Kas'yanova, E.F.; Gurvich, S.M. Synthesis of some derivatives of monothiophosphoric acid for the flotation of ores of heavy nonferrous metals. *Zh. Obsh. Khim.* **1969**, *39*, 365–366.
136. Fushimi, T.; Allcock, H.R. Cyclotriphosphazenes with sulfur-containing side groups: Refractive index and optical dispersion. *Dalton Trans.* **2009**, *14*, 2477–2481. [[CrossRef](#)]

137. Noller, C.R.; Gordon, J.J. The Preparation of Some Higher Aliphatic Sulfonic Acids. *J. Am. Chem. Soc.* **1933**, *55*, 1090–1094. [[CrossRef](#)]
138. Allen, P., Jr. The Preparation of Some Normal Aliphatic Thiocyanates. *J. Am. Chem. Soc.* **1935**, *57*, 198–199. [[CrossRef](#)]
139. Post, H.W. The reaction of certain orthoesters with aldehydes. *J. Org. Chem.* **1940**, *5*, 244–249. [[CrossRef](#)]
140. Hall, W.P.; Reid, E.E. A Series of α,ω -Dimercaptans. *J. Am. Chem. Soc.* **1943**, *65*, 1466–1468. [[CrossRef](#)]
141. Whitehead, E.V.; Dean, R.A.; Fidler, F.A. The preparation and properties of sulfur compounds related to petroleum. II. Cyclic sulfides. *J. Am. Chem. Soc.* **1951**, *73*, 3632–3635. [[CrossRef](#)]
142. Cairns, T.L.; Evans, G.L.; Larchar, A.W.; McKusick, B.C. Gem-Dithiols. *J. Am. Chem. Soc.* **1952**, *74*, 3982–3989. [[CrossRef](#)]
143. Birch, S.F.; Cullum, T.V.; Dean, R.A. The preparation and properties of dialkyl di- and polysulfides. Some disproportionation reactions. *J. Inst. Pet.* **1953**, *39*, 206–219.
144. Cope, A.C.; Farkas, E. Cleavage of carbon-sulfur bonds by catalytic hydrogenation. *J. Org. Chem.* **1954**, *19*, 385–390. [[CrossRef](#)]
145. Backer, H.J.; Kloosterziel, H. Thiolsulfinic esters. *Rec. Trav. Chim. Pays Bas Belg.* **1954**, *73*, 129–139. [[CrossRef](#)]
146. Kabachnik, M.I.; Golubeva, E.I. Addition of sulfur to dialkyl phosphites. *Dokl. Akad. Nauk SSSR* **1955**, *105*, 1258–1261.
147. Haines, W.E.; Helm, B.V.; Cook, G.L.; Ball, J.S. Purification and Properties of Ten Organic Sulfur Compounds—Second Series. *Phys. Chem.* **1956**, *60*, 549–555. [[CrossRef](#)]
148. Freidlina, R.K.; Chukovskaya, E.T. Reaction of mercuric acetate with esters of xanthic acids. *Izvest. Akad. Nauk SSSR Ser. Khim.* **1957**, *6*, 187–193.
149. Boonstra, H.J.; Brandsma, L.; Wiegman, A.M.; Arens, J.F. Chemistry of acetylenic ethers. XXXVI. Preparation and properties of some 1-alkylthio-1-alkynes. *Rec. Trav. Chim. Pays Bas Belg.* **1959**, *78*, 252–264. [[CrossRef](#)]
150. Jeffrey, G.H.; Parker, R.; Vogel, A.I. 113. Physical properties and chemical constitution. Part XXXII. Thiophen compounds. *J. Chem. Soc.* **1961**, 570–575. [[CrossRef](#)]
151. Mathias, S.; de Carvalho, E., Jr.; Cecchini, R.G. The Dipole Moments of Cyclohexanethiol, *a*-Toluenethiol and Benzenethiol. *J. Phys. Chem.* **1961**, *65*, 425–427. [[CrossRef](#)]
152. Hine, J.; Bayer, R.P.; Hammer, G.G. Formation of Bis-(Methylthio)-Methylene from Methyl Orthothioformate and Potassium Amide. *J. Am. Chem. Soc.* **1962**, *84*, 1751–1752. [[CrossRef](#)]
153. Volynskii, N.P.; Gal'pern, G.D.; Smolyaninov, V.V. Synthesis of 2-substituted thiacyclohexanes. *Neftekhim* **1963**, *3*, 482–487. [[CrossRef](#)]
154. Shostakovskii, M.F.; Atavin, A.S.; Dmitrieva, L.P.; Vasil'ev, N.P.; Gladkova, G.A. Reaction of 2,2-dialkyl-4-vinylloxymethyl-1,3-dioxolanes with thiols. *Zh. Obshch. Khim.* **1966**, *2*, 209–212.
155. Shostakovskii, M.F.; Atabin, A.S.; Mikhaleva, A.I.; Vasil'ev, N.P.; Dmitrieva, L.P. Synthesis of 2,2-bis(alkthio)propyl vinyl ethers. *Russ. Chem. Bull.* **1967**, *16*, 1337–1338. [[CrossRef](#)]
156. Nakhmanovich, A.S.; Skvortsova, G.G.; Shostakovskii, M.F.; Shulyak, L.A. Synthesis of vinyl esters of α -thienylcarbinols. *Khim. Atset. Dokl. Vsesoyuz. Nauch. Konf. Khim. Atset. Ego Proiz.* **1968**, 256–259.
157. Bittell, J.E.; Speier, J.L. Synthesis of Thiols and Polysulfides from Alkyl Halides, Hydrogen Sulfide, Ammonia, and Sulfur. *J. Org. Chem.* **1978**, *43*, 1687–1689. [[CrossRef](#)]
158. Taganliev, A.; Rol'nik, L.Z.; Lapuka, L.F.; Rol'nik, L.Z.; Kirilyuk, G.G.; Pastushchenko, E.V.; Khekimov, Y.K. Structure and physicochemical properties of thioorthoformates. *Izvest Akad. Nauk Turkm. SSR Ser. Fiz. Tekhn. Khim. Geolog. Nauk* **1986**, *1*, 60–64.
159. Khekimov, Y.K.; Taganlyev, A.; Kurbanov, D.; Khodzhalayev, T.K.; Kurbanov, I. Homolytic isomerization of 1,1,1-tris(ethylthio) ethane. *Izvest Akad. Nauk Turkm. SSR Ser. Fiz. Tekhn. Khim. Geolog. Nauk* **1987**, *4*, 105–106.
160. Gilani, H.G.; Gilani, A.G.; Shekarsaree, S. Solubility and tie line data of the water–phosphoric acid–solvents at T = 303.2, 313.2, and 323.2 K: An experimental and correlational study. *Thermochim. Acta* **2013**, *558*, 36–45. [[CrossRef](#)]
161. Vaughn, T.H. 1-Propyl-2-iodoacetylene. *J. Am. Chem. Soc.* **1933**, *55*, 1293. [[CrossRef](#)]
162. Vaughn, T.H. Direct iodination of monosubstituted acetylenes. *J. Am. Chem. Soc.* **1933**, *55*, 2150–2153. [[CrossRef](#)]
163. Bachman, G.B. Dehalogenation of aliphatic bromo acids. The bromo- and dibromo iefins. *J. Am. Chem. Soc.* **1933**, *55*, 4279–4284. [[CrossRef](#)]
164. Vaughn, T.H.; Nieuwland, J.A. Synthesis and properties of 2-iodo-1-vinylacetylene. *J. Chem. Soc.* **1933**, 741–743. [[CrossRef](#)]
165. Desreux, V. Further study of alkyl fluorides. *Bull. Cl. Sci. Acad. Royale Belg.* **1934**, *20*, 457–476.
166. Audsley, A.; Goss, F.R. The magnitude of the solvent effect in dipole-moment measurements. V. The solvent-effect constant and the moments of alkyl iodides. *J. Chem. Soc.* **1942**, 358, 358–366. [[CrossRef](#)]
167. Schmerling, L. Condensation of saturated halides with unsaturated compounds. II. Condensation of alkyl halides with monohaloalofins. *J. Am. Chem. Soc.* **1946**, *68*, 1650–1654. [[CrossRef](#)]
168. Mousseron, M.; Winternitz, F.; Jacquier, R. Some alicyclic chloro epoxides. *Compt. Rend.* **1946**, *223*, 1014–1015.
169. Luciens, H.W.; Mason, C.T. The Preparation and Properties of Some Branched-Chain Alkyl Bromomethyl Ethers. *J. Am. Chem. Soc.* **1949**, *71*, 258–260. [[CrossRef](#)]
170. Hoffmann, F.W. Aliphatic fluorides. I. ω , ω' -Difluoroalkanes. *J. Org. Chem.* **1949**, *14*, 105–110. [[CrossRef](#)]
171. Coffman, D.D.; Raasch, M.S.; Rigby, G.W.; Barrick, P.L.; Hanford, W.E. Addition reactions of tetrafluoroethylene. *J. Org. Chem.* **1949**, *14*, 747–753. [[CrossRef](#)]
172. Roe, A.; Cheek, P.H.; Hawkins, G.F. The Synthesis of 2-Fluoro-4- and 2-Fluoro-6-pyridinecarboxylic Acid and Derivatives. *J. Am. Chem. Soc.* **1949**, *71*, 4152–4153. [[CrossRef](#)]

173. Stone, H.; Shechter, H. A new method for the preparation of organic iodides. *J. Org. Chem.* **1950**, *15*, 491–495. [[CrossRef](#)]
174. Norton, T.R. New synthesis of ethyl trifluoroacetate. *J. Am. Chem. Soc.* **1950**, *72*, 3527–3528. [[CrossRef](#)]
175. Hauptschein, M.; Grosse, A.V. Perfluoroalkyl Halides Prepared from Silver Perfluoro-fatty Acid Salts. I. Perfluoroalkyl Iodides. *J. Am. Chem. Soc.* **1951**, *73*, 2461–2463. [[CrossRef](#)]
176. Douglass, I.B.; Martin, F.T.; Addor, R. Sulfenyl Chloride Studies. II. Mono-, Di-, and Tri-Chloromethanesulfenyl Chlorides and Certain of their Derivatives. *J. Org. Chem.* **1951**, *16*, 1297–1302. [[CrossRef](#)]
177. Hauptschein, M.; Stokes, C.S.; Grosse, A.V. The properties and reactions of perfluorobutyrolactone. *J. Am. Chem. Soc.* **1952**, *74*, 1974–1976. [[CrossRef](#)]
178. Douglass, I.B.; Osborne, C.E. The anhydrous chlorination of thioesters and related compounds. *J. Am. Chem. Soc.* **1953**, *75*, 4582–4583. [[CrossRef](#)]
179. Yagupol'skii, L.M. Synthesis of derivatives of phenyl trifluoromethyl ether. *Dokl. Akad. Nauk SSSR* **1955**, *105*, 100–102.
180. Stevens, C.L.; Mukherjee, T.K.; Traynelis, V. gem-Dihalides from the Hofmann degradation of α -haloamides. *J. Am. Chem. Soc.* **1956**, *78*, 2264–2267. [[CrossRef](#)]
181. Douglass, I.B.; Warner, G.H. Methyl and ethyl trichloromethyl ethers. *J. Am. Chem. Soc.* **1956**, *78*, 6070–6071. [[CrossRef](#)]
182. Douglass, I.B.; Poole, D.R. A New Method for the Preparation of Sulfinyl Chlorides. *J. Org. Chem.* **1957**, *22*, 536–537. [[CrossRef](#)]
183. Yarovenko, N.N.; Vasil'eva, A.S. New method of introduction of the trihalomethyl group into organic compounds. *Zh. Obshh. Khim.* **1958**, *28*, 2502–2504.
184. Soborovskii, L.Z.; Gladstein, B.M.; Kiseleva, M.I.; Chernetskii, V.N. Organic compounds of sulfur. I. Synthesis of fluorides of alkanesulfonic acids and their halogen derivatives. *Zh. Obshh. Khim.* **1958**, *28*, 1866–1870.
185. Bissell, E.R.; Spengler, R.E. Styrene-p-carboxylic acid. *J. Org. Chem.* **1959**, *24*, 1146–1147. [[CrossRef](#)]
186. Macey, W.A.T. The Physical Properties of Certain Organic Fluorides. *J. Phys. Chem.* **1960**, *64*, 254–257. [[CrossRef](#)]
187. Sadykh-Zade, S.I.; Sultanov, N.T. A new synthesis of α - and β -chlorostyrenes by direct chlorination of styrene. *Azerbaid. Khim. Zh.* **1960**, *5*, 33–36.
188. Stolzer, C.; Simon, A. Fluorophosphorus compounds. I. *Chem. Ber.* **1960**, *93*, 1323–1331.
189. Stolzer, C.; Simon, A. Fluorophosphorus compounds. II. Esters of fluorodiphosphoric acids. *Chem. Ber.* **1960**, *93*, 2578–2590.
190. Bergel'son, L.D. Stereochemistry of addition reactions at a triple bond. VII. Stereochemistry of hydrobromination of bromoacetylenes under radical conditions. *Izvest. Akad. Nauk SSSR Ser. Khim.* **1960**, *9*, 1235–1240.
191. Kost, V.N.; Freidlina, R.K. Telomerization of ethylene with polychloroalkanes containing the CCl_2Br group. *Izvest. Akad. Nauk SSSR Ser. Khim.* **1961**, *10*, 1252–1256. [[CrossRef](#)]
192. Gubanov, V.A.; Tumanova, A.V.; Dolgopolskii, I.M.; Shcherbakov, V.A. Reaction of perfluoromethyl perfluorovinyl ether with hydrogen halides. *Zh. Obshh. Khim.* **1964**, *34*, 2802–2803.
193. Ol'dekop, Y.A.; Kaberdin, R.V. Acyl peroxides. IX. Reaction of acetyl peroxide with cis-1,2-dichloroethylene. *Zh. Organ. Khim.* **1965**, *1*, 873–876.
194. Knunyants, I.L.; Krasuskaya, M.P.; Del'tsova, D.P. Di (1, 2, 4-oxadiazolyl) polydifluoromethylenes. *Izvest. Akad. Nauk SSSR Ser. Khim.* **1966**, 577–579.
195. Tataurov, G.P.; Sokolov, S.V. Synthesis and properties of octafluoroanisole. *Zh. Obshh. Khim.* **1966**, *36*, 537–540.
196. Vipinchandra, A.R.; Hemalkumar, P.V.; Hemant, A.C. Static Permittivity and Refractive Index of Binary Mixtures of 3-Bromoanisole and 1-Propanol at Different Temperatures. *J. Chem. Eng. Data* **2015**, *60*, 3113–3119. [[CrossRef](#)]
197. Gierut, J.A.; Sowa, F.J.; Nieuwland, J.A. Organic reactions with silicon compounds. II. The reaction of silicon tetrafluoride with the Grignard reagent. *J. Am. Chem. Soc.* **1936**, *58*, 897–898. [[CrossRef](#)]
198. Gilman, H.; Clark, R.N. Some steric effects of the isopropyl group in organosilicon compounds. *J. Am. Chem. Soc.* **1947**, *69*, 1499–1500. [[CrossRef](#)]
199. Petrov, A.D.; Shchukovskaya, L.L. Synthesis and properties of symmetric acetylenic disilanes. *Dokl. Akad. Nauk SSSR* **1952**, *86*, 551–553.
200. Takatani, T. Silicic acid esters. V. Some physical properties of the silicates of aliphatic alcohols. *Nippon Kagaku Zasshi* **1953**, *74*, 948–950. [[CrossRef](#)]
201. Petrov, A.D.; Ponomarenko, V.A. Synthesis and properties of disilylmethane, 1,2-disilylethane, 1,3-disilylpropane, and 1,3,5-trisilylcyclohexane. *Dokl. Akad. Nauk SSSR* **1953**, *90*, 387–390.
202. Zimmermann, W. Stability of chlorinated methylchlorosilane and chlorinated methylsiloxanes. *Chem. Ber.* **1954**, *87*, 887–891. [[CrossRef](#)]
203. Batuev, M.I.; Shostakovskii, M.F.; Belyaev, V.I.; Matveeva, A.D.; Dubrova, E.V. Chemical and physical properties of the hydroxyl group in trimethylsilanol. *Dokl. Akad. Nauk SSSR* **1954**, *95*, 531–534.
204. Dolgov, B.N.; Kharitonov, N.P.; Voronkov, M.G. Reaction of triethylsilane with ammonia and amines. *Zh. Obshh. Khim.* **1954**, *24*, 678–683.
205. Voronkov, M.G.; Dolgov, B.N. Isothiocyno-substituted silanes. *Zh. Obshh. Khim.* **1954**, *24*, 1082–1087.
206. Petrov, A.D.; Chernysheva, T.I. Synthesis of tetraisobutyl, tetraisopropyl, tetracyclohexyl, and tetra-1-naphthylsilanes. *Zh. Obshh. Khim.* **1954**, *24*, 1189–1192.
207. Shostakovskii, M.F.; Shikhiev, I.A.; Kochkin, D.A.; Belyaev, V.I. Oxygen-containing organosilicon compounds. III. Preparation of trimethyl- and triethylsilanols and their transformations. *Zh. Obshh. Khim.* **1954**, *24*, 2202–2206.

208. Petrov, A.D.; Shchukovskaya, L.L. Behavior toward chemical reagents of the silicon-carbon bond in α -alkynyl- and β -alkenylsilanes. *Zh. Obsh. Khim.* **1955**, *25*, 1128–1136.
209. Shostakovskii, M.F.; Malinovskii, M.S.; Romantsevich, M.K.; Kochkin, D.A. Synthesis and transformations of oxygen-containing organosilicon compounds. III. Reactions of propylene oxide with alkyl(aryl)chlorosilanes. *Izvest. Akad. Nauk SSSR Ser. Khim.* **1956**, 632–634.
210. Voronkov, M.G.; Khudobin, Y.I. Reaction of trialkylsilanes with iodine and hydrogen iodide. *Akad. Nauk SSSR Ser. Khim.* **1956**, *5*, 805–810. [[CrossRef](#)]
211. Shostakovskii, M.F.; Kochkin, D.A.; Rogov, V.M. 102. Synthesis and transformation of oxygen-containing organosilicon compounds. VI. Preparation of secondary dialkyl(aryl)chlorosilanes, dialkyl(aryl)silanol, and some of their transformations. *Akad. Nauk SSSR Ser. Khim.* **1956**, 1062–1069.
212. Shostakovskii, M.F.; Kochkin, D.A.; Vinogradov, V.L.; Neterman, V.A. Synthesis and transformation of oxygen-containing organosilicon compounds. VI. Reaction of hydrogen containing alkyl(aryl)dichlorosilanes with alcohols. *Akad. Nauk SSSR Ser. Khim.* **1956**, 1269–1271.
213. Dolgov, B.N.; Borisov, S.N.; Voronkov, M.G. Reaction of alkylhalosilanes with trialkylsilanes. *Zh. Obsh. Khim.* **1957**, *27*, 2692–2697.
214. Kaufman, H.C.; Douthett, O.R. Preparation and Comparison of the Physical Properties of Alkyl and Alkylaryl Silicates. *Ind. Eng. Chem.* **1958**, *3*, 324–327.
215. Voronkov, M.G.; Shabarova, Z.I. Alkoxysilanes. XIV. Cleavage of organosiloxanes by alcohols as a method of synthesis of organoalkoxysilanes. *Zh. Obsh. Khim.* **1959**, *29*, 1528–1534.
216. Duffaut, N.; Calas, R.; Mace, J.C. The oxidation of trialkyl and triaryl silanes by oxygen containing silver compounds. *Bull. Soc. Chim. Fr.* **1959**, 1971–1973.
217. Wilson, G.R.; Smith, A.G. Preparation of Decamethyltetrasilane and Its Lower Homologs. *J. Org. Chem.* **1961**, *26*, 557–559. [[CrossRef](#)]
218. Sergeeva, S.I.; Chien, H.-C.; Tsitovich, D.D. Synthesis of alkyl- and dialkylbis(1,1-dialkylhydrazino)silane. *Zh. Obsh. Khim.* **1960**, *30*, 694–695.
219. Voronkov, M.G.; Rabkina, S.M. Alkoxysilanes. XVI. Reaction of tetraalkoxysilanes with ketones. *Zh. Obsh. Khim.* **1961**, *31*, 1259–1265.
220. Sergeeva, Z.I.; Hsieh, C.-L. A new method of synthesis of organosilicon hydrazines. *Zh. Obsh. Khim.* **1962**, *32*, 1987–1993.
221. Stolberg, U.G. Octamethyltrisilane and decamethyltetrasilane. *Angew. Chem.* **1962**, *74*, 696.
222. Sergeeva, Z.I.; Hsieh, C.-L. Reaction of nonsymmetric dialkylhydrazines with alkylchlorosilanes. *Zh. Obsh. Khim.* **1963**, *33*, 1874–1878.
223. Shostakovskii, M.F.; Sokolov, B.A.; Dmitrieva, G.V.; Alekseeva, G.M. Addition reaction of hydrosilanes with vinyl ethers. *Zh. Obsh. Khim.* **1964**, *34*, 2839–2842.
224. Cudlin, J.; Schraml, J.; Chvalovsky, V. Organosilicon compounds. XXXV. Addition of dichloromethylene to isomeric bis(trimethylsilyl) ethylenes. *Coll. Czech. Chem. Comm.* **1964**, *29*, 1476–1483. [[CrossRef](#)]
225. Voronkov, M.G.; Skorik, Y.I. Synthesis of organofluorosilanes. *Akad. Nauk SSSR Ser. Khim.* **1964**, *7*, 1215–1221. [[CrossRef](#)]
226. Giao, D.-H. New cleavage method for tetrabutylated derivatives of Si, Ge, and Sn. *Compt. Rend.* **1965**, *260*, 6937–6938.
227. Prejzner, J. Organoxycyanatosilanes. I. Preparation and properties of phenoxyisocyanatosilanes. *Rocz. Chem.* **1965**, *39*, 747–753.
228. Bolotov, B.A.; Kharitonov, N.P.; Bataev, E.A.; Romyantseva, E.G. Destructive hydrogenation of trialkylalkoxysilanes. *Zh. Obsh. Khim.* **1967**, *37*, 2113–2117.
229. Cer, L.; Vaisarova, V.; Chvalovsky, V. Organosilicon compounds. LIII. Dipole moments of benzylmethylethoxysilanes. *Coll. Czech. Chem. Comm.* **1967**, *32*, 3784–3786. [[CrossRef](#)]
230. Kannengiesser, G.; Damm, F. Preparation of some tetrakis(dialkylamino)silanes. *Bull. Soc. Chim. Fr.* **1967**, *7*, 2492–2495.
231. Khudobin, Y.I.; Voronkov, M.G.; Kharitonov, N.P. Trialkyl(aryl)bromosilanes. *Lav. PSR Zinat. Akad. Vest. Kim. Ser.* **1967**, *5*, 595–600.
232. Zhinkin, D.Y.; Mal'nova, G.N.; Gorislavskaya, Z.V. Ammonolysis of triorganochlorosilanes, their coammonolysis with trimethylchlorosilane, and coammonolysis of some tri- and diorganochlorosilanes. *Zh. Obsh. Khim.* **1968**, *38*, 2800–2807.
233. Feher, F.; Hädicke, P.; Frings, H. Beiträge zur Chemie des Siliciums und Germaniums, XXIII (1) Physikalisch-Chemische Eigenschaften der Silane von Trisilan bis Heptasilan. *Inorg. Nucl. Chem. Lett.* **1973**, *9*, 931–936. [[CrossRef](#)]
234. Boredau, M.; Dédir, J.; Fraignet, E. Etude Structurale d'Hexaalkyldisiloxanes et de Trialkylalkoxy- ou Aryloxysilanes. I. Détermination par Dipolemetrie d'Angles SiOC et SiOSi. *J. Organomet. Chem.* **1973**, *59*, 125–139.
235. Moerlein, S.M. Synthesis and Spectroscopic Characteristics of Aryltrimethyl-Silicon, -Germanium, and Tin Compounds. *J. Organomet. Chem.* **1987**, *319*, 29–39. [[CrossRef](#)]
236. Alagar, M.; Krishnasami, V. Ultrasonic Properties of Tetraalkoxysilanes. *Ultrasonics* **1987**, *25*, 283–287. [[CrossRef](#)]
237. Alagar, M.; Ponnusamy, M.; Amsavel, A. Studies on Dielectric Behaviour of Dimethyldialkoxysilanes. *Hung. J. Ind. Chem.* **1993**, *21*, 19–22.
238. Yu, L.; Hu, Y.; Dong, H.; Wu, C. The physicochemical properties of 1,3,5-trimethyl-1,3,5-tris(3,3,3-trifluoropropyl)cyclotrisiloxane with various aromatic hydrocarbons at T = (308.15 to 323.15) K. *J. Chem. Thermodyn.* **2016**, *96*, 117–126. [[CrossRef](#)]

239. Hu, Y.; Zhang, C.; Dong, H.; Wu, C. Excess molar volume along with refractive index for binary systems of dimethoxymethylphenylsilane with dimethyldimethoxysilane, dimethyldiethoxysilane, methylvinyl-diethoxysilane and ethenyltrimethoxysilane. *J. Chem. Thermodyn.* **2017**, *109*, 82–90. [CrossRef]
240. Jin, J.; Shao, F.; Dong, H.; Wu, C. Volumetric and Optical Properties of Dimethylvinylethoxysilane with n-Alkanes (C₇ to C₁₀) at Temperatures in the Range (298.15 to 318.15) K. *J. Sol. Chem.* **2019**, *48*, 82–103. [CrossRef]
241. Terent'ev, A.P.; Yanovskaya, L.A. Sulfonation and sulfonic acids of acidophobic substances. XVI. Sulfonation of some indole derivatives. *Zh. Obshch. Khim.* **1951**, *21*, 1295–1297.
242. Leonard, N.J.; Ryder, B.L. The stereoisomers of vic-dialkylpiperidines. The 2-butyl-3-methylpiperidines. *J. Org. Chem.* **1953**, *18*, 598–608. [CrossRef]
243. Mikhailov, G.I. 2-Bromopyridine. *Zh. Prikl. Khim.* **1954**, *27*, 349–351.
244. Shuikin, N.I.; Bel'skii, I.F.; Skobtsova, G.E. Catalytic synthesis of higher homologs of pyrrole and pyrrolidine from α -furylalkylamines. *Izvest. Akad. Nauk SSSR Ser. Khim.* **1963**, *9*, 1678–1680. [CrossRef]
245. Bel'skii, I.F.; Shuikin, N.I.; Skobtsova, G.E. Conjugated hydrogenolysis in the synthesis of pyrrolidine homologs. *Izvest. Akad. Nauk SSSR Ser. Khim.* **1963**, *9*, 1675–1678. [CrossRef]
246. Shuikin, N.I.; Bel'skii, I.F.; Karakhanov, R.A.; Kozma, B.; Bartok, M. Investigations in the field of diols and cyclic ethers. V. Preparation of 2-monosubstituted derivatives of tetrahydropyran. *Acta Phys. Chem.* **1963**, *9*, 37–42.
247. Bel'skii, I.F.; Shuikin, N.I.; Skobtsova, G.E. Catalytic conversion of furan amines into 2,4-dialkylpyrroles. *Izvest. Akad. Nauk SSSR Ser. Khim.* **1964**, *6*, 1118–1120.
248. Shuikin, N.I.; Bel'skii, I.F.; Karakhanov, R.A.; Kozma, B.; Bartok, M. Isomerization of tetrahydropyrans. *Izvest. Akad. Nauk SSSR Ser. Khim.* **1964**, *4*, 747–750. [CrossRef]
249. Shuikin, N.I.; Bel'skii, I.F.; Barkovskaya, L.Y.; Dronov, V.I.; Alalykina, L.A. Synthesis of 2,4- and 2,5-dialkylthiophanes. *Khim. Sera Organ. Soedin. Soderzhshch. Neff. Nefteprod. Akad. Nauk SSSR Bashkirsk. Filial* **1964**, *6*, 197–200.
250. Shuikin, N.I.; Bel'skii, I.F.; Barkovskaya, L.Y.; Gerasimov, M.M. Synthesis of some cyclic sulfides. *Khim. Sera Organ. Soedin. Soderzhshch. Neff. Nefteprod. Akad. Nauk SSSR Bashkirsk. Filial* **1964**, *7*, 58–60.
251. Bel'skii, I.F.; Shuikin, N.I.; Karakhanov, R.A. Synthesis of γ -oxo alcohols and dihydrofurans from 1-furyl-3alkanols. *Izvest. Akad. Nauk SSSR Ser. Khim.* **1964**, *2*, 326–331.
252. Bel'skii, I.F.; Shuikin, N.I.; Skobtsova, G.E. Catalytic synthesis of pyrrole and pyrrolidine homologs. *Probl. Organ. Sintez Akad. Nauk SSSR Otd. Obshch. Tekhn. Khim.* **1965**, 186–189.
253. Shuikin, N.I.; Bel'skii, I.F.; Abgaforova, G.E. Conjugated hydrogenolysis in the synthesis of 2,5-dialkylpyrroles. *Izvest. Akad. Nauk SSSR Ser. Khim.* **1965**, *1*, 163–165.
254. Bel'skii, I.F.; Khar'kov, S.N.; Shuikin, N.I. Synthesis of homologs of 1,4-dioxane and 1,4-dioxene. *Dokl. Akad. Nauk SSSR* **1965**, *165*, 821–823.
255. Abgaforova, G.E.; Shuikin, N.I.; Bel'skii, I.F. Synthesis of trialkyl derivatives of pyrrole and pyrrolidine. *Izvest. Akad. Nauk SSSR Ser. Khim.* **1965**, *4*, 734–736. [CrossRef]
256. Shuikin, N.I.; Lebedev, B.L. Alkylation of thiophene by isobutylene. *Izvest. Akad. Nauk SSSR Ser. Khim.* **1967**, *5*, 1154–1155. [CrossRef]
257. Shuikin, N.I.; Lebedev, B.L.; Nikol'skii, V.G.; Korytina, O.A.; Kessenikh, A.V.; Prokof'ev, E.P. Direction of furan alkylation with isobutylene. *Izvest. Akad. Nauk SSSR Ser. Khim.* **1967**, *7*, 1618–1620.
258. Fedorov, E.I.; Mikhant'ev, B.I. Crotylation of sodium 2-pyridinolate. *Khim. Geterotsikl. Soedin.* **1969**, *6*, 1022–1023.
259. Anton, V.; Munoz-Embid, J.; Artigas, H.; Artal, M.; Lafuente, C. Thermophysical properties of oxygenated thiophene derivatives: Experimental data and modelling. *J. Chem. Thermodyn.* **2017**, *113*, 330–339. [CrossRef]
260. Baird, Z.S.; Dahlberg, A.; Uusi-Kyyny, P.; Osmanbegovic, N.; Witos, J.; Helminen, J.; Cederkrantz, D.; Hyväri, P.; Alopaeus, V.; Kilpeläinen, I.; et al. Physical Properties of 7-Methyl-1,5,7-triazabicyclo[4.4.0]dec-5-ene (mTBD). *Int. J. Thermophys.* **2019**, *40*, 71. [CrossRef]
261. Gomez, E.; Gonzalez, B.; Dominguez, A.; Tojo, E.; Tojo, J. Dynamic Viscosities of a Series of 1-Alkyl-3-methylimidazolium Chloride Ionic Liquids and Their Binary Mixtures with Water at Several Temperatures. *J. Chem. Eng. Data* **2006**, *51*, 696–701. [CrossRef]
262. Pereiro, A.B.; Tojo, E.; Rodriguez, A.; Canosa, J.; Tojo, J. Properties of ionic liquid HMIMPF₆ with carbonates, ketones and alkyl acetates. *J. Chem. Thermodyn.* **2006**, *38*, 651–661. [CrossRef]
263. Pereiro, A.B.; Santamarta, F.; Tojo, E.; Rodriguez, A.; Tojo, J. Temperature Dependence of Physical Properties of Ionic Liquid 1,3-Dimethylimidazolium Methyl Sulfate. *J. Chem. Eng. Data* **2006**, *51*, 952–954. [CrossRef]
264. Pereiro, A.B.; Verdia, P.; Tojo, E.; Rodriguez, A. Physical Properties of 1-Butyl-3-methylimidazolium Methyl Sulfate as a Function of Temperature. *J. Chem. Eng. Data* **2007**, *52*, 377–380. [CrossRef]
265. Pereiro, A.B.; Legido, J.L.; Rodriguez, A. Physical properties of ionic liquids based on 1-alkyl-3-methylimidazolium cation and hexafluorophosphate as anion and temperature dependence. *J. Chem. Thermodyn.* **2007**, *39*, 1168–1175. [CrossRef]
266. Zhang, Q.; Li, Z.; Zhang, J.; Zhang, S.; Zhu, L.; Yang, J.; Zhang, X.; Deng, Y. Physicochemical Properties of Nitrile-Functionalized Ionic Liquids. *J. Phys. Chem. B* **2007**, *111*, 2864–2872. [CrossRef]
267. Pereiro, A.B.; Rodriguez, A. Thermodynamic Properties of Ionic Liquids in Organic Solvents from (293.15 to 303.15) K. *J. Chem. Eng. Data* **2007**, *52*, 600–608. [CrossRef]

268. Mokhtarin, B.; Mojtahedi, M.M.; Mortaheb, H.R.; Mafi, M.; Yazdani, F.; Sadeghian, F. Densities, Refractive Indices, and Viscosities of the Ionic Liquids 1-Methyl-3-octylimidazolium Tetrafluoroborate and 1-Methyl-3-butylimidazolium Perchlorate and Their Binary Mixtures with Ethanol at Several Temperatures. *J. Chem. Eng. Data* **2008**, *53*, 677–682. [CrossRef]
269. Ortega, J.; Vreekamp, R.; Penco, E.; Marrero, E. Mixing thermodynamic properties of 1-butyl-4-methylpyridinium tetrafluoroborate [b4mpy][BF₄] with water and with an alkan-1-ol (methanol to pentanol). *J. Chem. Thermodyn.* **2008**, *40*, 1087–1094. [CrossRef]
270. Gonzalez, B.; Calvar, N.; Gomez, E.; Macedo, E.A.; Dominguez, A. Synthesis and Physical Properties of 1-Ethyl 3-methylpyridinium Ethylsulfate and Its Binary Mixtures with Ethanol and Water at Several Temperatures. *J. Chem. Eng. Data* **2008**, *53*, 1824–1828. [CrossRef]
271. Muhammad, A.; Mutalib, M.I.A.; Wilfred, C.D.; Murugesan, T.; Shafeeq, A. Thermophysical properties of 1-hexyl-3-methyl imidazolium based ionic liquids with tetrafluoroborate, hexafluorophosphate and bis(trifluoromethylsulfonyl)imide anions. *J. Chem. Thermodyn.* **2008**, *40*, 1433–1438. [CrossRef]
272. Malham, I.B.; Turmine, M. Viscosities and refractive indices of binary mixtures of 1-butyl-3-methylimidazolium tetrafluoroborate and 1-butyl-2,3-dimethylimidazolium tetrafluoroborate with water at 298 K. *J. Chem. Thermodyn.* **2008**, *40*, 718–723. [CrossRef]
273. Tariq, M.; Forte, P.A.S.; Gomes, M.F.C.; Lopes, J.N.C.; Rebelo, L.P.N. Densities and refractive indices of imidazolium- and phosphonium-based ionic liquids: Effect of temperature, alkyl chain length, and anion. *J. Chem. Thermodyn.* **2009**, *41*, 790–798. [CrossRef]
274. Torrecilla, J.S.; Palomar, J.; Garcia, J.; Rodriguez, F. Effect of Cationic and Anionic Chain Lengths on Volumetric, Transport, and Surface Properties of 1-Alkyl-3-methylimidazolium Alkylsulfate Ionic Liquids at (298.15 and 313.15) K. *J. Chem. Eng. Data* **2009**, *54*, 1297–1301. [CrossRef]
275. Pereiro, A.B.; Veiga, H.I.M.; Esperanca, J.M.S.S.; Rodriguez, A. Effect of temperature on the physical properties of two ionic liquids. *J. Chem. Thermodyn.* **2009**, *41*, 1419–1423. [CrossRef]
276. Calvar, N.; Gomez, E.; Gonzalez, B.; Dominguez, A. Experimental Determination, Correlation, and Prediction of Physical Properties of the Ternary Mixtures Ethanol and 1-Propanol + Water + 1-Ethyl-3-methylpyridinium Ethylsulfate at 298.15 K. *J. Chem. Eng. Data* **2009**, *54*, 2229–2234. [CrossRef]
277. Navas, A.; Ortega, J.; Vreekamp, R.; Marrero, E.; Palomar, J. Experimental Thermodynamic Properties of 1-Butyl-2-methylpyridinium Tetrafluoroborate [b2mpy][BF₄] with Water and with Alkan-1-ol and Their Interpretation with the COSMO-RS Methodology. *Ind. Eng. Chem. Res.* **2009**, *48*, 2678–2690. [CrossRef]
278. Soriano, A.N.; Doma, B.T., Jr.; Li, M.-H. Measurements of the density and refractive index for 1-n-butyl-3-methylimidazolium-based ionic liquids. *J. Chem. Thermodyn.* **2009**, *41*, 301–307. [CrossRef]
279. Zhang, Q.; Liu, S.; Li, Z.; Li, J.; Chen, Z.; Wang, R.; Lu, L.; Deng, Y. Novel Cyclic Sulfonium-Based Ionic Liquids: Synthesis, Characterization, and Physicochemical Properties. *Chem. Eur. J.* **2009**, *15*, 765–778. [CrossRef]
280. Pereiro, A.B.; Rodriguez, A. Separation of Ethanol-Heptane Azeotropic Mixtures by Solvent Extraction with an Ionic Liquid. *Ind. Eng. Chem. Res.* **2009**, *48*, 1579–1585. [CrossRef]
281. Gonzalez, R.; Calvar, N.; Gomez, E.; Dominguez, I.; Dominguez, A. Synthesis and Physical Properties of 1-Ethylpyridinium Ethylsulfate and its Binary Mixtures with Ethanol and 1-Propanol at Several Temperatures. *J. Chem. Eng. Data* **2009**, *54*, 1353–1358. [CrossRef]
282. Singh, T.; Kumar, A. Temperature Dependence of Physical Properties of Imidazolium Based Ionic Liquids: Internal Pressure and Molar Refraction. *J. Solut. Chem.* **2009**, *38*, 1043–1053. [CrossRef]
283. Bandres, I.; Giner, B.; Artigas, H.; Lafuente, C.; Royo, F.M. Thermophysical Properties of N-Octyl-3-methylpyridinium Tetrafluoroborate. *J. Chem. Eng. Data* **2009**, *54*, 236–240. [CrossRef]
284. Bandres, I.; Pera, G.; Martin, S.; Castro, M.; Lafuente, C. Thermophysical Study of 1-Butyl-2-Methylpyridinium Tetrafluoroborate Ionic Liquid. *J. Phys. Chem. B* **2009**, *113*, 11936–11942. [CrossRef] [PubMed]
285. Bandres, I.; Royo, F.; Gascon, I.; Castro, M.; Lafuente, C. Anion Influence on Thermophysical Properties of Ionic Liquids: 1-Butylpyridinium Tetrafluoroborate and 1-Butylpyridinium Triflate. *J. Phys. Chem. B* **2010**, *114*, 3601–3607. [CrossRef] [PubMed]
286. Arce, A.; Francisco, M.; Soto, A. Evaluation of the polysubstituted pyridinium ionic liquid [hmpy][Ntf₂] as a suitable solvent for desulfurization: Phase equilibria. *J. Chem. Thermodyn.* **2010**, *42*, 712–718. [CrossRef]
287. Shekaari, H.; Armanfar, E. Physical Properties of Aqueous Solutions of Ionic Liquid, 1-Propyl-3-methylimidazolium Methyl Sulfate, at T) (298.15 to 328.15) K. *J. Chem. Eng. Data* **2010**, *55*, 765–772. [CrossRef]
288. Brigouleix, C.; Arnouti, M.; Jacquemin, J.; Caillon-Caravanier, M.; Galiano, H.; Lemordant, D. Physicochemical Characterization of Morpholinium Cation Based Protic Ionic Liquids Used As Electrolytes. *J. Phys. Chem. B* **2010**, *114*, 1757–1766. [CrossRef]
289. Alvarez, V.H.; Mattedi, S.; Martin-Pastor, M.; Aznar, M.; Iglesias, M. Synthesis and thermophysical properties of two new protic long-chain ionic liquids with the oleate anion. *Fluid Phase Equil.* **2010**, *299*, 42–50. [CrossRef]
290. Yunus, N.M.; Mutalib, M.I.A.; Man, Z.; Bustam, M.A.; Murugesan, T. Thermophysical properties of 1-alkylpyridinium bis(trifluoromethylsulfonyl)imide ionic liquids. *J. Chem. Thermodyn.* **2010**, *42*, 491–495. [CrossRef]
291. Ziyada, A.K.; Wilfred, C.D.; Bustam, M.A.; Man, Z.; Murugesan, T. Thermophysical Properties of 1-Propyl-3-methylimidazolium Bromide Ionic Liquids at Temperatures from (293.15 to 353.15) K. *J. Chem. Eng. Data* **2010**, *55*, 3886–3890. [CrossRef]

292. Yu, Z.; Gao, H.; Wang, H.; Chen, L. Densities, Excess Molar Volumes, and Refractive Properties of the Binary Mixtures of the Amino Acid Ionic Liquid [bmim][Gly] with 1-Butanol or Isopropanol at T = (298.15 to 313.15) K. *J. Chem. Eng. Data* **2011**, *56*, 4295–4300. [[CrossRef](#)]
293. Kurnia, K.A.; Taib, M.M.; Mutalib, M.I.A.; Murugesan, T. Densities, refractive indices and excess molar volumes for binary mixtures of protic ionic liquids with methanol at T = 293.15 to 313.15 K. *J. Mol. Liq.* **2011**, *159*, 211–219. [[CrossRef](#)]
294. Ziyada, A.K.; Bustam, M.A.; Wilfred, C.D.; Murugesan, T. Densities, Viscosities, and Refractive Indices of 1-Hexyl-3-propanenitrile Imidazolium Ionic Liquids Incorporated with Sulfonate-Based Anions. *J. Chem. Eng. Data* **2011**, *56*, 2343–2348. [[CrossRef](#)]
295. Yu, Z.; Gao, H.; Wang, H.; Chen, L. Densities, Viscosities, and Refractive Properties of the Binary Mixtures of the Amino Acid Ionic Liquid [bmim][Ala] with Methanol or Benzylalcohol at T = (298.15 to 313.15) K. *J. Chem. Eng. Data* **2011**, *56*, 2877–2883. [[CrossRef](#)]
296. Taib, M.M.; Murugesan, T. Density, Refractive Index, and Excess Properties of 1-Butyl-3-methylimidazolium Tetrafluoroborate with Water and Monoethanolamine. *J. Chem. Eng. Data* **2012**, *57*, 120–126. [[CrossRef](#)]
297. Zhang, Q.; Ma, X.; Liu, S.; Yang, B.; Lu, L.; He, Y.; Deng, Y. Hydrophobic 1-allyl-3-alkylimidazolium dicyanamide ionic liquids with low densities. *J. Mater. Chem.* **2011**, *21*, 6864–6868. [[CrossRef](#)]
298. de Hadlich Oliveira, L.; Aznar, M. Liquid-Liquid Equilibria for {1-Ethyl-3-methylimidazolium Diethylphosphate or 1-Ethyl-3-methylimidazolium Ethylsulfate} + 4,6-Dimethyldibenzothiophene + Dodecane Systems at 298.2 K and 313.2 K. *J. Chem. Eng. Data* **2011**, *56*, 2005–2012. [[CrossRef](#)]
299. Tsunashima, K.; Kawabata, A.; Matsumiya, M.; Kodama, S.; Enomoto, R.; Sugiya, M.; Kunugi, Y. Low viscous and highly conductive phosphonium ionic liquids based on bis(fluorosulfonyl)amide anion as potential electrolytes. *Electrochem. Comm.* **2011**, *13*, 178–181. [[CrossRef](#)]
300. Gonzalez, B.; Gomez, E.; Dominguez, A.; Vilas, M.; Tojo, E. Physicochemical Characterization of New Sulfate Ionic Liquids. *J. Chem. Eng. Data* **2011**, *56*, 14–20. [[CrossRef](#)]
301. Vercher, E.; Llopis, F.J.; Gonzalez-Alfaro, V.; Miguel, P.J.; Martinez-Andreu, A. Refractive Indices and Deviations in Refractive Indices of Trifluoromethanesulfonate-Based Ionic Liquids in Water. *J. Chem. Eng. Data* **2011**, *56*, 4499–4504. [[CrossRef](#)]
302. Wu, T.Y.; Su, S.G.; Gung, S.T.; Lin, M.W.; Ouyang, W.C.; Sun, I.W.; Lai, C.A. Synthesis and Characterization of Protic Ionic Liquids Containing Cyclic Amine Cations and Tetrafluoroborate Anion. *J. Iran. Chem. Soc.* **2011**, *8*, 149–165. [[CrossRef](#)]
303. Muhammad, N.; Man, Z.B.; Bustam, M.A.; Mutalib, M.I.A.; Wilfred, C.D.; Rafiq, S. Synthesis and Thermophysical Properties of Low Viscosity Amino Acid-Based Ionic Liquids. *J. Chem. Eng. Data* **2011**, *56*, 3157–3162. [[CrossRef](#)]
304. Hossain, M.I.; Babaa, M.-R.; El-Harbawi, M.; Man, Z.; Hefter, G.; Yin, C.-Y. Synthesis, Characterization, Physical Properties, and Cytotoxicities of 1-(6-Hydroxyhexyl)-3-alkylimidazolium Chloride Ionic Liquids. *J. Chem. Eng. Data* **2011**, *56*, 4188–4193. [[CrossRef](#)]
305. Freire, M.G.; Teles, A.R.R.; Rocha, M.A.A.; Schröder, B.; Neves, C.M.S.S.; Carvalho, P.J.; Evtuguin, D.V.; Santos, L.M.N.B.F.; Coutinho, J.A.P. Thermophysical Characterization of Ionic Liquids Able To Dissolve Biomass. *J. Chem. Eng. Data* **2011**, *56*, 4813–4822. [[CrossRef](#)]
306. Larriba, M.; Garcia, S.; Garcia, J.; Torrecilla, J.S.; Rodriguez, F. Thermophysical Properties of 1-Ethyl-3-methylimidazolium 1,1,2,2-Tetrafluoroethanesulfonate and 1-Ethyl-3-methylimidazolium Ethylsulfate Ionic Liquids as a Function of Temperature. *J. Chem. Eng. Data* **2011**, *56*, 3589–3597. [[CrossRef](#)]
307. Deive, F.J.; Rivas, M.A.; Rodriguez, A. Thermophysical properties of two ionic liquids based on benzyl imidazolium cation. *J. Chem. Thermodyn.* **2011**, *43*, 487–491. [[CrossRef](#)]
308. Seki, S.; Tsuzuki, S.; Hayamizu, K.; Umebayashi, Y.; Serizawa, N.; Takei, K.; Miyashiro, H. Comprehensive Refractive Index Property for Room-Temperature Ionic Liquids. *J. Chem. Eng. Data* **2012**, *57*, 2211–2216. [[CrossRef](#)]
309. Xu, W.-G.; Li, L.; Ma, X.-X.; Wei, J.; Duan, W.-B.; Guan, W.; Yang, J.-Z. Density, Surface Tension, and Refractive Index of Ionic Liquids Homologue of 1-Alkyl-3-methylimidazolium Tetrafluoroborate [Cnmim][BF₄] (n = 2,3,4,5,6). *J. Chem. Eng. Data* **2012**, *57*, 2177–2184. [[CrossRef](#)]
310. Gomez, E.; Calvar, N.; Macedo, E.A.; Dominguez, A. Effect of the temperature on the physical properties of pure 1-propyl-3-methylimidazolium bis(trifluoromethylsulfonyl)imide and characterization of its binary mixtures with alcohols. *J. Chem. Thermodyn.* **2012**, *45*, 9–15. [[CrossRef](#)]
311. Gonzalez, E.J.; Dominguez, A.; Macedo, E.A. Physical and Excess Properties of Eight Binary Mixtures Containing Water and Ionic Liquids. *J. Chem. Eng. Data* **2012**, *57*, 2165–2176. [[CrossRef](#)]
312. Larriba, M.; Garcia, S.; Navarro, P.; Garcia, J.; Rodriguez, F. Physical Properties of N-Butylpyridinium Tetrafluoroborate and N-Butylpyridinium Bis(trifluoromethylsulfonyl)imide Binary Ionic Liquid Mixtures. *J. Chem. Eng. Data* **2012**, *57*, 1318–1325. [[CrossRef](#)]
313. Trivedi, T.J.; Bharmoria, P.; Singh, T.; Kumar, A. Temperature Dependence of Physical Properties of Amino Acid Ionic Liquid Surfactants. *J. Chem. Eng. Data* **2012**, *57*, 317–323. [[CrossRef](#)]
314. Bandres, I.; Lopez, M.C.; Castro, M.; Barbera, J.; Lafuente, C. Thermophysical properties of 1-propylpyridinium tetrafluoroborate. *J. Chem. Thermodyn.* **2012**, *44*, 148–153. [[CrossRef](#)]
315. Machanova, K.; Boisset, A.; Sedlakova, Z.; Anouti, M.; Bendova, M.; Jacquemin, J. Thermophysical Properties of Ammonium-Based Bis(trifluoromethylsulfonyl)imide Ionic Liquids: Volumetric and Transport Properties. *J. Chem. Eng. Data* **2012**, *57*, 2227–2235. [[CrossRef](#)]

316. Muhammad, N.; Man, Z.; Ziyada, A.K.; Bustam, M.A.; Mutalib, M.I.A.; Wilfred, C.D.; Rafiq, S.; Tan, I.M. Thermophysical Properties of Dual Functionalized Imidazolium-Based Ionic Liquids. *J. Chem. Eng. Data* **2012**, *57*, 737–743. [\[CrossRef\]](#)
317. Almeida, H.F.D.; Passos, H.; Lopes-da-Silva, J.A.; Fernandes, A.M.; Freire, M.G.; Coutinho, J.A.P. Thermophysical Properties of Five Acetate-Based Ionic Liquids. *J. Chem. Eng. Data* **2012**, *57*, 3005–3013. [\[CrossRef\]](#)
318. Reddy, P.; Siddiqi, M.A.; Atakan, B.; Diedenhofen, M.; Ramjugernath, D. Activity coefficients at infinite dilution of organic solutes in the ionic liquid PEG-5 cocomonium methylsulfate at T = (313.15, 323.15, 333.15, and 343.15) K: Experimental results and COSMO-RS predictions. *J. Chem. Thermodyn.* **2013**, *58*, 322–329. [\[CrossRef\]](#)
319. Ma, X.-X.; Wei, J.; Zhang, Q.-B.; Tian, F.; Feng, Y.-Y.; Guan, W. Prediction of Thermophysical Properties of Acetate-Based Ionic Liquids Using Semiempirical Methods. *Ind. Eng. Chem. Res.* **2013**, *52*, 9490–9496. [\[CrossRef\]](#)
320. Neves, C.M.S.S.; Kurnia, K.A.; Coutinho, J.A.P.; Marrucho, I.M.; Lopes, J.N.C.; Freire, M.G.; Rebelo, L.P.N. Systematic Study of the Thermophysical Properties of Imidazolium-Based Ionic Liquids with Cyano-Functionalized Anions. *J. Phys. Chem. B* **2013**, *117*, 10271–10283. [\[CrossRef\]](#)
321. Rocha, M.A.A.; Ribeiro, F.M.S.; Loobo Ferreira, A.I.M.C.; Coutinho, J.A.P.; Santos, L.M.N.B.F. Thermophysical properties of [C_{N-1}C₁m][PF₆] ionic liquids. *J. Mol. Liq.* **2013**, *188*, 196–202. [\[CrossRef\]](#)
322. Koller, T.M.; Rausch, M.H.; Ramos, J.; Schulz, P.S.; Wasserscheid, P.; Economou, I.G.; Fröba, A.P. Thermophysical Properties of the Ionic Liquids [EMIM][B(CN)₄] and [HMIM][B(CN)₄]. *J. Phys. Chem. B* **2013**, *117*, 8512–8523. [\[CrossRef\]](#)
323. Koller, T.M.; Schmid, S.R.; Sachnov, S.J.; Rausch, M.H.; Wasserscheid, P.; Fröba, A.P. Measurement and Prediction of the Thermal Conductivity of Tricyanomethanide- and Tetracyanoborate-Based Imidazolium Ionic Liquids. *Int. J. Thermophys.* **2014**, *35*, 195–217. [\[CrossRef\]](#)
324. Oezdemir, M.C.; Oezgün, B. Phenyl/alkyl-substituted-3,5-dimethylpyrazolium ionic liquids. *J. Mol. Liq.* **2014**, *200*, 129–135. [\[CrossRef\]](#)
325. Seki, S.; Tsuzuki, S.; Hayamizu, K.; Serizawa, N.; Ono, S.; Takei, K.; Doi, H.; Umebayashi, Y. Static and Transport Properties of Alkyltrimethylammonium Cation-Based Room-Temperature Ionic Liquids. *J. Phys. Chem. B* **2014**, *118*, 4590–4599. [\[CrossRef\]](#) [\[PubMed\]](#)
326. Wei, J.; Ma, T.; Ma, X.; Guan, W.; Liu, Q.; Yang, J. Study on thermodynamic properties and estimation of polarity of ionic liquids {[C_nmim][NTf₂] (n = 2, 4)}. *RSC Adv.* **2014**, *4*, 30725–30732. [\[CrossRef\]](#)
327. Meng, Y.; Liu, J.; Li, Z.; Wei, H. Synthesis and Physicochemical Properties of Two SO₃H-Functionalized Ionic Liquids with Hydrogen Sulfate Anion. *J. Chem. Eng. Data* **2014**, *59*, 2186–2195. [\[CrossRef\]](#)
328. Bhattacharjee, A.; Carvalho, P.J.; Coutinho, J.A.P. The effect of the cation aromaticity upon the thermophysical properties of piperidinium- and pyridinium-based ionic liquids. *Fluid Phase Equil.* **2014**, *375*, 80–88. [\[CrossRef\]](#)
329. Umapathi, R.; Attri, P.; Venkatesu, P. Thermophysical Properties of Aqueous Solution of Ammonium-Based Ionic Liquids. *J. Phys. Chem. B* **2014**, *118*, 5971–5982. [\[CrossRef\]](#)
330. Bhattacharjee, A.; Luis, A.; Santos, J.H.; Lopes-da-Silva, J.A.; Freire, M.G.; Carvalho, P.J.; Coutinho, J.A.P. Thermophysical properties of sulfonium- and ammonium-based ionic liquids. *Fluid Phase Equil.* **2014**, *381*, 36–45. [\[CrossRef\]](#)
331. Pinto, R.R.; Santos, D.; Mattedi, S.; Aznar, M. Density, refractive index, apparent volumes and excess molar Volumes of four protic ionic liquids + water at T = 298.15 and 323.15 K. *Braz. J. Chem. Eng.* **2015**, *32*, 671–682. [\[CrossRef\]](#)
332. Rodriguez, A.S.M.C.; Rocha, M.A.A.; Almeida, H.F.D.; Neves, C.M.S.S.; Lopes-da-Silva, J.A.; Freire, M.G.; Coutinho, J.A.P.; Santos, L.M.N.B.F. Effect of the Methylation and N–H Acidic Group on the Physicochemical Properties of Imidazolium-Based Ionic Liquids. *J. Phys. Chem. B* **2015**, *119*, 8781–8792. [\[CrossRef\]](#)
333. Gonfa, G.; Bustam, M.A.; Muhammad, N.; Khan, A.S. Evaluation of Thermophysical Properties of Functionalized Imidazolium Thiocyanate Based Ionic Liquids. *Ind. Eng. Chem. Res.* **2015**, *54*, 12428–12437. [\[CrossRef\]](#)
334. Rao, S.G.; Mohan, T.M.; Krishna, T.V.; Raju, K.T.S.S.; Rao, B.S. Excess thermodynamic properties of ionic liquid 1-butyl-3-methylimidazolium tetrafluoroborate and N-octyl-2-pyrrolidone from T = (298.15 to 323.15) K at atmospheric pressure. *J. Chem. Thermodyn.* **2015**, *89*, 286–295.
335. Sattari, M.; Kamari, A.; Mohammadi, A.H.; Ramjugernath, D. Prediction of refractive indices of ionic liquids—A quantitative structure-property relationship based model. *J. Taiwan Inst. Chem. Eng.* **2015**, *52*, 165–180. [\[CrossRef\]](#)
336. Soucknova, M.; Klomfar, J.; Patek, J. Surface tension and 0.1 MPa density data for 1-C_n-3-methylimidazolium iodides with n = 3, 4, and 6, validated using a parachor and group contribution model. *J. Chem. Thermodyn.* **2015**, *83*, 52–60. [\[CrossRef\]](#)
337. Vatasin, E.; Dohnal, V. Thermophysical properties of aqueous solutions of the 1-ethyl-3-methylimidazolium tricyanomethanide ionic liquid. *J. Chem. Thermodyn.* **2015**, *89*, 169–176. [\[CrossRef\]](#)
338. Bhattacharjee, A.; Lopes-da-Silva, J.A.; Freire, M.G.; Coutinho, J.A.P.; Carvalho, P.J. Thermophysical properties of phosphonium-based ionic liquids. *Fluid Phase Equil.* **2015**, *400*, 103–113. [\[CrossRef\]](#)
339. Bhattacharjee, A.; Coutinho, J.A.P.; Freire, M.G.; Carvalho, P.J. Thermophysical Properties of Two Ammonium-Based Protic Ionic Liquids. *J. Solut. Chem.* **2015**, *44*, 703–717. [\[CrossRef\]](#)
340. Akbar, M.M.; Chemat, F.; Arunagiri, A.; Murugesan, T. Density and excess properties of N-methyldiethanolamine (MDEA) with 1-hexyl-3-methylimidazolium tris(pentafluoroethyl)trifluorophosphate [hmim][FAP]. *J. Therm. Anal. Calorim.* **2016**, *123*, 785–791. [\[CrossRef\]](#)
341. Gouveia, A.S.L.; Tome, L.C.; Marrucho, I.M. Density, Viscosity, and Refractive Index of Ionic Liquid Mixtures Containing Cyano and Amino Acid-Based Anions. *J. Chem. Eng. Data* **2016**, *61*, 83–93. [\[CrossRef\]](#)

342. Xue, L.; Gurung, E.; Tamas, G.; Koh, Y.P.; Shadeck, M.; Simon, S.I.; Maroncelli, M.; Quitevis, E.L. Effect of Alkyl Chain Branching on Physicochemical Properties of Imidazolium-Based Ionic Liquids. *J. Chem. Eng. Data* **2016**, *61*, 1078–1091. [CrossRef]
343. Kumar, A.V.; Redhi, G.G.; Gengan, R.M. Influence of Epoxy Group in 2-Pyrrolidonium Ionic Liquid Interactions and Thermo-Physical Properties with Ethanoic or Propanoic Acid at Various Temperatures. *ACS Sustain. Chem. Eng.* **2016**, *4*, 4951–4964. [CrossRef]
344. Chen, F.-F.; Dong, Y.; Sang, X.-Y.; Zhou, Y.; Tao, D.-J. Physicochemical Properties and CO₂ Solubility of Tetrabutylphosphonium Carboxylate Ionic Liquids. *Acta Phys. Chim. Sin.* **2016**, *32*, 605–610. [CrossRef]
345. Ye, F.; Zhu, J.; Yu, K.; Zhu, R.; Xu, Y.; Chen, J.; Chen, L. Physicochemical properties of binary mixtures of 1,1,3,3-tetramethylguanidine imidazolide ionic liquid with water and alcohols. *J. Chem. Thermodyn.* **2016**, *97*, 39–47. [CrossRef]
346. Segade, L.; Cabanas, M.; Dominguez-Perez, M.; Rilo, E.; Garcia-Garabal, S.; Turmine, M.; Varela, L.M.; Gomez-Gonzalez, V.; Docampo-Alvarez, B.; Cabeza, O. Surface and bulk characterisation of mixtures containing alkylammonium nitrates and water or ethanol: Experimental and simulated properties at 298.15 K. *J. Mol. Liq.* **2016**, *222*, 663–670. [CrossRef]
347. Rodrigues, A.S.M.C.; Almeida, H.F.D.; Freire, M.G.; Lopes-da-Silva, J.A.; Coutinho, J.A.P.; Santos, L.M.N.B.F. The effect of n vs. iso isomerization on the thermophysical properties of aromatic and non-aromatic ionic liquids. *Fluid Phase Equil.* **2016**, *423*, 190–202. [CrossRef]
348. Xing, N.; Dai, B.; Ma, X.; Wei, J.; Pan, Y.; Guan, W. The molar surface Gibbs energy and prediction of surface tension of [Cnpy][DCA] (n = 3,4,5). *J. Chem. Thermodyn.* **2016**, *95*, 21–25. [CrossRef]
349. Shekaari, H.; Zafarani-Moattar, M.T.; Niknam, M. Thermodynamic evaluation of imidazolium based ionic liquids with thiocyanate anion as effective solvent to thiophene extraction. *J. Mol. Liq.* **2016**, *219*, 975–984. [CrossRef]
350. Garcia-Andreu, M.; Castro, M.; Gascon, I.; Lafuente, C. Thermophysical characterization of 1-ethylpyridinium triflate and comparison with similar ionic liquids. *J. Chem. Thermodyn.* **2016**, *103*, 395–402. [CrossRef]
351. Xu, Y. CO₂ absorption behavior of azole-based protic ionic liquids: Influence of the alkalinity and physicochemical properties. *J. CO₂ Utiliz.* **2017**, *19*, 1–8. [CrossRef]
352. Nazet, A.; Sokolov, S.; Sonnleitner, T.; Friesen, S.; Buchner, R. Densities, Refractive Indices, Viscosities, and Conductivities of Non-Imidazolium Ionic Liquids [Et₃S][TFSI], [Et₂MeS][TFSI], [BuPy][TFSI], [N₈₈₈₁][TFA], and [P₁₄][DCA]. *J. Chem. Eng. Data* **2017**, *62*, 2549–2561. [CrossRef]
353. Lee, K.-H.; Park, S.-J.; Choi, Y.-Y. Density, refractive index and kinematic viscosity of MIPK, MEK and phosphonium-based ionic liquids and the excess and deviation properties of their binary systems. *Korean J. Chem. Eng.* **2017**, *34*, 214–224. [CrossRef]
354. Sardar, S.; Wilfred, C.D.; Mumtaz, A.; Leveque, J.-M. Investigation of the Thermophysical Properties of AMPS-Based Aprotic Ionic Liquids for Potential Application in CO₂ Sorption Processes. *J. Chem. Eng. Data* **2017**, *62*, 4160–4168. [CrossRef]
355. Zhang, D.; Gong, Y.-Y.; Tong, J.; Fang, D.-W.; Tong, J. Physicochemical properties of [C n mim][Thr](n = 3,5,6) amino acid ionic liquids. *J. Chem. Thermodyn.* **2017**, *115*, 47–51. [CrossRef]
356. Arosa, Y.; Fernandez, C.D.R.; Lago, E.L.; Amigo, A.; Varela, L.M.; Cabeza, O.; de la Fuente, R. Refractive index measurement of imidazolium based ionic liquids in the Vis-NIR. *Opt. Mat.* **2017**, *73*, 647–657. [CrossRef]
357. Arumugam, V.; Redhi, G.G.; Gengan, R.M. Synthesis, characterization and thermophysical properties of novel 2',3'-N-epoxypropyl-N-methyl-2-oxopyrrolidinium acetate ionic liquid and their binary mixture with water or methanol. *J. Mol. Liq.* **2017**, *242*, 1215–1227. [CrossRef]
358. Pereiro, A.B.; Llovel, F.; Araujo, J.M.M.; Santos, A.S.S.; Rebelo, L.P.N.; Pineiro, M.M.; Vega, L.F. Thermophysical Characterization of Ionic Liquids Based on the Perfluorobutanesulfonate Anion: Experimental and Soft-SAFT Modeling Results. *ChemPhysChem* **2017**, *18*, 2012–2023. [CrossRef]
359. Venkatraman, V.; Raj, J.J.; Evjen, S.; Lethesh, K.C.; Fiksdahl, A. In silico prediction and experimental verification of ionic liquid refractive indices. *J. Mol. Liq.* **2018**, *264*, 563–570. [CrossRef]
360. Marcinkowski, L.; Szepeński, E.; Milewska, M.J.; Kloskowski, A. Density, sound velocity, viscosity, and refractive index of new morpholinium ionic liquids with amino acid-based anions: Effect of temperature, alkyl chain length, and anion. *J. Mol. Liq.* **2019**, *284*, 557–568. [CrossRef]
361. Ferreira, M.L.; Araújo, J.M.M.; Vega, L.F.; Llovel, F.; Pereiro, A.B. Functionalization of fluorinated ionic liquids: A combined experimental-theoretical study. *J. Mol. Liq.* **2020**, *302*, 112489. [CrossRef]
362. Wu, X.-L.; Sang, X.-Y.; Li, Z.-M.; Tao, D.-J. Study on physicochemical properties and basicity of carbanionfunctionalized ionic liquids. *J. Mol. Liq.* **2020**, *312*, 113405. [CrossRef]
363. Song, Z.; Yan, Q.; Xia, M.; Qi, X.; Zhang, Z.; Wei, J.; Fang, D.; Ma, X. Physicochemical properties of N-alkylpyridine trifluoroacetate ionic liquids [Cn Py][TFA] (n = 2–6). *J. Chem. Thermodyn.* **2021**, *155*, 106366. [CrossRef]
364. Fei, Y.; Chen, Z.; Zhang, J.; Yu, M.; Kong, J.; Wu, Z.; Cao, J.; Zhang, J. Thiazolium-based ionic liquids: Synthesis, characterization and physicochemical properties. *J. Mol. Liq.* **2021**, *342*, 117553. [CrossRef]
365. Aljasmí, A.; Aljímaz, A.S.; Alkhalidi, K.H.A.E.; AlTuwaim, M.S. Dependency of Physicochemical Properties of Imidazolium Bis(Trifluoromethylsulfonyl)Imide-Based Ionic Liquids on Temperature and Alkyl Chain. *J. Chem. Eng. Data* **2022**, *67*, 858–868. [CrossRef]
366. Kong, J.; Liu, L.; Li, X.; Yang, Y.; Chen, X.; Fei, Y.; Xu, L.; Chen, Z. Dimethylthioformamide-derived ionic liquids: Synthesis, characterization and application as supercapacitor electrolyte. *J. Mol. Liq.* **2022**, *365*, 120114. [CrossRef]

367. Vogel, A.I. 369. Physical properties and chemical constitution. Part XXIII. Miscellaneous compounds. Investigation of the so-called co-ordinate or dative link in esters of oxy-acids and in nitro-paraffins by molecular refractivity determinations, atomic, structural, and group parachors and refractivities. *J. Chem. Soc.* **1948**, 1833–1855. [[CrossRef](#)]
368. Vogel, A.I.; Cresswell, W.T.; Jeffrey, G.H.; Leicester, J. 98. Physical properties and chemical constitution. Part XXIV. Aliphatic aldoximes, ketoximes, and ketoxime O-alkyl ethers, NN-dialkylhydrazines, aliphatic ketazines, mono- and dialkylaminopropionitriles, alkoxypropionitriles, dialkyl azodiformates, and dialkyl carbonates. Bond parachors, bond refractions, and bond refraction coefficients. *J. Chem. Soc.* **1952**, 514–549. [[CrossRef](#)]
369. Shuikin, N.I.; Bel'skii, I.F. Catalytic hydrogenolysis in the series of furan compounds. *Zh. Obshch. Khim.* **1957**, *27*, 402–406.
370. Yur'ev, Y.K.; Novitskii, K.Y.; Bolesov, I.G. Furan series. I. Synthesis of N-(β -hydroxyalkyl)furfurylamines. *Zh. Obshch. Khim.* **1959**, *29*, 2951–2954.
371. Petrov, A.A.; Mingaleva, K.S.; Zavgorodnii, V.S. Chemistry of unsaturated stannyl hydrocarbons. IV. Dipole moments of alkyl-, alkenyl-, and phenylacetylenic stannyl hydrocarbons. *Zh. Obshch. Khim.* **1964**, *34*, 533–535.
372. Bel'skii, I.F.; Shuikin, N.I.; Vol'nova, Z. K Synthesis and isomerization of 2,2-dialkyl-5-propyltetrahydrofurans. *Izvest Akad. Nauk SSSR Ser Khim.* **1964**, *2*, 369–371. [[CrossRef](#)]
373. Shuikin, N.I.; Lebedev, B.L.; Nikol'skii, V.G. Vinylation of cyclanes and cyclic ethers. *Dokl. Akad. Nauk SSSR* **1964**, *158*, 692–693.
374. Arrowsmith, G.B.; Jeffery, G.H. Vogel, Physical Properties and Chemical Constitution. Part XLI. Naphthalene Compounds. *J. Chem. Soc.* **1965**, 2072–2078. [[CrossRef](#)]
375. Bel'skii, I.F.; Khar'kov, S.N.; Shuikin, N.I. Synthesis of 3-oxa-5-oxo alcohols and a study of their tautomeric transformations to form dioxenes. *Dokl. Akad. Nauk SSSR* **1965**, *165*, 1071–1074.
376. Wiswanadhan, V.N.; Ghose, A.K.; Revankar, G.R.; Robins, R.K. Atomic Physicochemical Parameters for Three Dimensional Structure Directed Quantitative Structure-Activity Relationships. 4. Additional Parameters for Hydrophobic and Dispersive Interactions and Their Application for an Automated Superposition of Certain Naturally Occurring Nucleoside Antibiotics. *J. Chem. Inf. Comput. Sci.* **1989**, *29*, 163–172.
377. Pacak, P. Refractivity and density of some organic solvents. *Chem. Pap.* **1991**, *45*, 227–232.
378. Oswal, S.; Patel, A.T. Speeds of Sound, Isentropic Compressibilities, and Excess Volumes of Binary Mixtures. 1. Tri-n-alkylamines with Cyclohexane and Benzene. *J. Chem. Eng. Data* **1994**, *39*, 366–371. [[CrossRef](#)]
379. Gao, D.; Zhu, D.; Zhang, L.; Guan, H.; Sun, H.; Chen, H.; Si, J. Isobaric Vapor-Liquid Equilibria for Binary and Ternary Mixtures of Propanal, Propanol, and Propanoic Acid. *J. Chem. Eng. Data* **2010**, *55*, 5887–5895. [[CrossRef](#)]
380. Chen, K.-D.; Lin, Y.-F.; Tu, C.-H. Densities, Viscosities, Refractive Indices, and Surface Tensions for Mixtures of Ethanol, Benzyl Acetate, and Benzyl Alcohol. *J. Chem. Eng. Data* **2012**, *57*, 1118–1127. [[CrossRef](#)]
381. Kumar, S.; Jeevanandham, P. Densities, viscosities, refractive indices and excess properties of aniline and o-anisidine with 2-alkoxyethanols at 303.15 K. *J. Mol. Liq.* **2012**, *174*, 34–41. [[CrossRef](#)]
382. Jeevanandham, P.; Kumar, S.; Periyasamy, P. Densities, viscosities, refractive indices and excess properties of ortho- and meta-chloroaniline with 2-alkoxyethanols at 303.15 K. *J. Mol. Liq.* **2013**, *188*, 203–209. [[CrossRef](#)]
383. Cai, C.; Marsh, A.; Zhang, Y.-H.; Reid, J.P. Group Contribution Approach To Predict the Refractive Index of Pure Organic Components in Ambient Organic Aerosol. *Environ. Sci. Technol.* **2017**, *51*, 9683–9690. [[CrossRef](#)] [[PubMed](#)]
384. Dantas, C.E.S.; Ceriani, R. Liquid–Liquid Equilibria of Ternary Mixtures Containing n-Tetradecane + γ -Valerolactone + Aldehyde [Butanal or Pentanal or (E)-2-Undecenal] at 298.15 K. *J. Chem. Eng. Data* **2022**, *67*, 393–403. [[CrossRef](#)]
385. Sema, T.; Gao, H.; Liang, Z.; Tontiwachwuthikul, P.; Idem, R.O. New Insights and Updated Correlations for Density, Viscosity, Refractive Index, and Associated Properties of Aqueous 4-Diethyl-Amino-2-Butanol Solution. *Fluid Phase Equil.* **2022**, *562*, 113565. [[CrossRef](#)]
386. Applequist, J.; Carl, J.R.; Fung, K.-K. An Atom Dipole Interaction Model for Molecular Polarizability. Application to Polyatomic Molecules and Determination of Atom Polarizabilities. *J. Am. Chem. Soc.* **1972**, *94*, 2952–2960. [[CrossRef](#)]
387. Thole, B.T. Molecular polarizabilities calculated with a modified dipole interaction. *Chem. Phys.* **1981**, *59*, 341–350. [[CrossRef](#)]
388. Nagle, J.K. Atomic Polarizability and Electronegativity. *J. Am. Chem. Soc.* **1990**, *112*, 4741–4747. [[CrossRef](#)]
389. Miller, K.J. Calculation of the Molecular Polarizability Tensor. *J. Am. Chem. Soc.* **1990**, *112*, 8543–8551. [[CrossRef](#)]
390. Cheng, L.-T.; Tam, W.; Stevenson, S.H.; Meredith, G.R.; Rikken, G.; Marder, S.R. Experimental Investigations of Organic Molecular Nonlinear Optical Polarizabilities. 1. Methods and Results on Benzene and Stilbene Derivatives. *J. Phys. Chem.* **1991**, *95*, 10631–10643. [[CrossRef](#)]
391. Lu, Y.-J.; Lee, S.-L. Semi-empirical calculations of the nonlinear optical properties of polycyclic aromatic compounds. *Chem. Phys.* **1994**, *179*, 431–444. [[CrossRef](#)]
392. Schürer, G.; Geddeck, P.; Gottschalk, M.; Clark, T. Accurate Parametrized Variational Calculations of the Molecular Electronic Polarizability by NDDO-Based Methods. *Intern. J. Quantum Chem.* **1999**, *75*, 17–31. [[CrossRef](#)]
393. Bosque, R.; Sales, J. Polarizabilities of Solvents from the Chemical Composition. *J. Chem. Inf. Comput. Sci.* **2002**, *42*, 1154–1163. [[CrossRef](#)] [[PubMed](#)]
394. Wang, J.; Xie, X.-Q.; Hou, T.; Xu, X. Fast Approaches for Molecular Polarizability Calculations. *Phys. Chem. A* **2007**, *111*, 4443–4448. [[CrossRef](#)] [[PubMed](#)]
395. Murthy, A.R.; Giridhar, G.; Rangacharyulu, M. Molecular Polarizabilities of Some Liquid Crystal Compounds. *Chin. J. Phys.* **2008**, *46*, 54–62.

396. Cao, X.; Hancock, B.C.; Leyva, N.; Becker, J.; Yu, W.; Masterson, V.M. Estimating the refractive index of pharmaceutical solids using predictive methods. *Int. J. Pharm.* **2009**, *368*, 16–23. [[CrossRef](#)] [[PubMed](#)]
397. Naef, R.; Acree, W.E., Jr. Revision and Extension of a Generally Applicable Group-Additivity Method for the Calculation of the Standard Heat of Combustion and Formation of Organic Molecules. *Molecules* **2021**, *26*, 6101. [[CrossRef](#)] [[PubMed](#)]
398. Naef, R.; Acree, W.E., Jr. Calculation of Five Thermodynamic Molecular Descriptors by Means of a General Computer Algorithm Based on the Group-Additivity Method: Standard Enthalpies of Vaporization, Sublimation and Solvation, and Entropy of Fusion of Ordinary Organic Molecules and Total Phase-Change Entropy of Liquid Crystals. *Molecules* **2017**, *22*, 1059. [[CrossRef](#)]
399. Naef, R.; Acree, W.E., Jr. Calculation of the Surface Tension of Ordinary Organic and Ionic Liquids by Means of a Generally Applicable Computer Algorithm Based on the Group-Additivity Method. *Molecules* **2018**, *23*, 1224. [[CrossRef](#)]
400. Naef, R. Calculation of the Isobaric Heat Capacities of the Liquid and Solid Phase of Organic Compounds at 298.15K by Means of the Group-Additivity Method. *Molecules* **2020**, *25*, 1147. [[CrossRef](#)]
401. Naef, R.; Acree, W.E., Jr. Calculation of the Vapour Pressure of Organic Molecules by Means of a Group-Additivity Method and Their Resultant Gibbs Free Energy and Entropy of Vaporization at 298.15 K. *Molecules* **2021**, *26*, 1045. [[CrossRef](#)]
402. Gough, K.M. Theoretical analysis of molecular polarizabilities and polarizability derivatives in hydrocarbons. *J. Chem. Phys.* **1989**, *91*, 2424. [[CrossRef](#)]
403. Laidig, K.E.; Bader, R.F.W. Properties of atoms in molecules: Atomic polarizabilities. *J. Chem. Phys.* **1990**, *93*, 7213. [[CrossRef](#)]

Article

Correlation of Surface Tension of Mono-Solvents at Various Temperatures

Navid Kabudi ¹, Ali Shayanfar ², William E. Acree, Jr. ³ and Abolghasem Jouyban ^{2,4,*}

¹ Student Research Committee, Faculty of Pharmacy, Tabriz University of Medical Sciences, Tabriz 5165665811, Iran

² Pharmaceutical Analysis Research Center and Faculty of Pharmacy, Tabriz University of Medical Sciences, Tabriz 5165665811, Iran

³ Department of Chemistry, University of North Texas, Denton, TX 76203-5070, USA

⁴ Faculty of Pharmacy, Near East University, North Cyprus Via Mersin 10, Nicosia 99138, Turkey

* Correspondence: ajouyban@hotmail.com or ghasemjouyban@gmail.com

Abstract: Surface tension is among the most important factors in chemical and pharmaceutical processes. Modeling the surface tension of solvents at different temperatures helps to optimize the type of solvent and temperature. The surface tension of solvents at different temperatures with their solvation parameters was used in this study to develop a model based on the van't Hoff equation by multiple linear regression. Abraham solvation parameters, Hansen solubility parameters, and Catalan parameters are among the most discriminating descriptors. The overall MPD of the model was 3.48%, with a minimum and maximum MPD of 0.04% and 11.62%, respectively. The model proposed in this study could be useful for predicting the surface tension of mono-solvents at different temperatures.

Keywords: surface tension; solvation parameters; model; predict

Citation: Kabudi, N.; Shayanfar, A.; Acree, W.E., Jr.; Jouyban, A. Correlation of Surface Tension of Mono-Solvents at Various Temperatures. *Liquids* **2022**, *2*, 378–387. <https://doi.org/10.3390/liquids2040021>

Academic Editor: Enrico Bodo

Received: 13 October 2022

Accepted: 20 October 2022

Published: 26 October 2022

Publisher's Note: MDPI stays neutral with regard to jurisdictional claims in published maps and institutional affiliations.



Copyright: © 2022 by the authors. Licensee MDPI, Basel, Switzerland. This article is an open access article distributed under the terms and conditions of the Creative Commons Attribution (CC BY) license (<https://creativecommons.org/licenses/by/4.0/>).

1. Introduction

Surface activity is one of the main physico-chemical properties of liquids. Surface and/or interfacial tension represents the surface and/or interfacial activity of a liquid. Surface tension data is required in many industrial applications, including wettability, dispersibility, and deflocculation of the solid particles in liquids; emulsification of immiscible liquids in emulsion and microemulsion formulations; detergency in sanitary; adsorption of gases and solutes from solutions; solubilization of insoluble drugs in liquid dosage forms; biological activity of drugs and drug absorption from mucosa [1]. Surface tension affects the transformation of heat and mass in solutions which influences many chemical processes [2]. It is a vital step in drug formulation. For example, granulation is a method to improve the falling ability of a powder by adding a binder to the active pharmaceutical ingredient. A crucial step in optimizing granulation performance is wetting the substrate with the binder and spreading the binder over the substrate. Surface tension also acts as an important parameter in controlling the coating process. Suspensions are a dosage form with many pros and cons compared to other dosage forms. One of the disadvantages is related to its instability and cake formation, which could be modified by surface tension control. A comprehensive review of the applications of surface tension in the pharmaceutical sciences was provided in an earlier review paper [3]. Many biological reactions occur at the surface but not in solution. For proper absorption of a drug and efficient function on its active site, it needs to be dissolved properly in the gastric fluids. Surface tension plays a vital role in the function of the respiratory system. A mixture of surface active agents, such as dipalmitoyl lecithin, causes a reduction in the surface tension of alveoli fluid. Increasing the surface tension of alveoli lining fluid results in respiratory distress syndrome and atelectasis, which are two major respiratory disorders. The most important roles of surface tension in clinical sciences have been summarized in a review work [4].

Surface tension reflects the intermolecular interactions and forces between a liquid molecule and the air and depends on many different variables, including viscosity, the existence of ionized compounds in the solution, and temperature [5].

There are various methods for measuring surface tension, including the Du Noüy ring method, Wilhelmy plate method, and spinning drop method, but they all require a lot of cost and energy, and they require an expert to perform the laboratory work. Numerical methods to predict the surface tension of mixed solvents have been proposed, but there are few studies on computational modeling for surface tension prediction of mono-solvents at different temperatures [5].

The aim of this study is to propose a mathematical model for calculating the surface tension of mono-solvents at various temperatures by combining an adopted van't Hoff model with the solvation parameters, including Abraham solvation parameters, Hansen solubility parameters, and Catalan parameters. The applicability of the proposed model is evaluated by using the published surface tension data of several different mono-solvents at various temperatures.

2. Computational Methods

The surface tension of a liquid is decreased by an increase in temperature. An adapted version of the van't Hoff equation is used to represent the temperature effects on the surface tension data ($\sigma_{i,T}$). The van't Hoff type model is:

$$\log \sigma_{i,T} = \alpha_i + \frac{\beta_i}{T} \quad (1)$$

in which α_i and β_i are the model constants [6]. It has been shown that α_i and β_i terms could represent the effects of the physico-chemical properties (PCP) of a given solvent at various temperatures. It is possible to include Abraham solvation parameters (AP_i) [7], Hansen solubility parameters (HP_i) [8], and Catalan parameters (CP_i) [9] to represent the effects of solvent's PCPs on surface tension. To do this, we combined these PCPs with the van't Hoff type model as:

$$\log \sigma_{i,T} = \left(\alpha_0 + \sum_{i=1}^5 \alpha_{i,AP} AP_i + \sum_{i=1}^3 \alpha_{i,HP} HP_i + \sum_{i=1}^4 \alpha_{i,CP} CP_i \right) + \left(\frac{\beta_0 + \sum_{i=1}^5 \beta_{i,AP} AP_i + \sum_{i=1}^3 \beta_{i,HP} HP_i + \sum_{i=1}^4 \beta_{i,CP} CP_i}{T} \right) \quad (2)$$

where α and β terms are the model constants.

Thirty-two solvents with their numerical surface tension ($\sigma_{i,T}$) values at different temperatures were obtained from the literature (Table 1) [10–33]. The tabulated numerical values pertain to a homogeneous liquid system at the specified temperature in equilibrium with its own vapor pressure. The solvents considered in the study contain a wide range of functional groups, and they cannot be classified as belonging to a single type of chemical compound. For each solvent, Abraham solvation parameters [7,34,35], Catalan parameters [9], and Hansen solubility parameters [8] were gathered from different sources. Details of the parameters with their references are listed in Tables 2–4. Parameters for each solvent were divided by temperature to differentiate between the descriptor's numerical values at different temperatures. Repeated data were excluded from the final analyses, and for the data with close reported surface tension data, the average numerical value of surface tension was used for further analysis.

Table 1. Experimental ($\sigma_{i,T}^{Exp}$) and calculated ($\sigma_{i,T}^{Calc}$) surface tension values of the studied mono-solvents at different temperatures (T), the mean percentage deviation (MPD), and the references for $\sigma_{i,T}^{Exp}$ data.

Solvent	T (K)	$\sigma_{i,T}^{Exp}$	$\sigma_{i,T}^{Calc}$	MPD	Ref.
1,4-dioxane	288	33.98	32.40	4.74	[10]
1,4-dioxane	293	33.58	31.70	5.51	[10]
1,4-dioxane	298	32.69	31.10	4.80	[10]
1,4-dioxane	303	32.15	30.50	5.01	[10]
1,4-dioxane	308	31.42	30.00	4.52	[10]
1-butanol	288	24.68	24.80	0.28	[11]
1-butanol	293	24.21	24.20	0.04	[11]
1-butanol	298	24.10	23.70	1.70	[11,12]
1-butanol	303	23.34	23.20	0.60	[11]
1-butanol	308	22.79	22.70	0.26	[11]
1-hexanol	288	26.08	26.40	1.23	[11]
1-hexanol	293	25.61	25.90	1.09	[11]
1-hexanol	298	25.43	25.40	0.08	[11,12]
1-hexanol	303	24.74	25.00	0.89	[11]
1-hexanol	308	24.19	24.50	1.41	[11]
1-octanol	288	27.41	26.80	2.12	[11]
1-octanol	293	26.94	26.30	2.26	[11]
1-octanol	298	26.90	25.90	3.90	[11,12]
1-octanol	303	26.07	25.40	2.57	[11]
1-octanol	308	25.52	25.00	2.16	[11]
1-pentanol	293	25.69	25.50	1.09	[13,14]
1-pentanol	298	25.00	25.00	0.12	[12,14]
1-pentanol	318	23.67	23.30	1.44	[13,14]
1-propanol	293	23.69	24.20	2.11	[13,14]
1-propanol	298	23.34	23.70	1.37	[12,14]
1-propanol	303	22.89	23.20	1.22	[14]
1-propanol	308	22.51	22.70	0.84	[14]
1-propanol	313	22.11	22.30	0.68	[14]
1-propanol	318	21.69	21.80	0.69	[13,14]
1-propanol	323	21.31	21.40	0.56	[14]
2-butanol	298	23.01	23.70	2.78	[13]
2-butanone	293	24.70	22.80	7.61	[15]
2-butanone	298	24.00	22.20	7.38	[15]
2-methyl-1-propanol	298	22.34	23.40	4.52	[16]
2-pentanol	293	23.70	24.20	2.24	[13]
2-pentanol	298	23.28	23.70	1.89	[13]
2-pentanol	315	21.60	22.20	2.69	[13]
2-propanol	293	21.74	22.10	1.66	[14]
2-propanol	298	21.03	21.60	2.57	[14]
2-propanol	303	20.72	21.10	1.64	[14]
2-propanol	308	20.23	20.60	1.73	[14]
2-propanol	313	19.71	20.10	2.13	[14]
2-propanol	318	19.21	19.70	2.55	[14]
2-propanol	323	18.69	19.30	3.26	[14]
acetone	273	25.17	25.50	1.47	[17]
acetone	287	24.70	23.40	5.22	[17]
acetone	288	23.37	23.30	0.39	[17]
acetone	293	23.03	22.60	1.78	[18]
acetone	298	22.50	22.00	2.22	[18]
acetone	303	21.80	21.40	1.79	[17]
acetone	308	21.20	20.90	1.60	[17]
acetone	313	20.80	20.30	2.21	[18]
acetone	318	19.78	19.90	0.35	[17]

Table 1. Cont.

Solvent	T (K)	$\sigma_{i,T}^{Exp}$	$\sigma_{i,T}^{Calc}$	MPD	Ref.
acetone	323	19.51	19.40	0.62	[18]
acetone	328	18.60	19.00	1.88	[17]
acetonitrile	298	28.41	28.40	0.21	[19]
acetonitrile	303	28.03	27.50	2.07	[19]
acetonitrile	308	27.40	26.60	2.88	[19]
acetonitrile	313	26.76	25.80	3.55	[19]
acetonitrile	318	26.13	25.10	4.06	[19]
benzene	293	28.85	32.20	11.61	[20]
benzene	303	27.55	30.80	11.62	[20]
butyl acetate	298	24.88	22.80	8.32	[21]
cyclohexane	288	25.34	24.30	4.18	[22]
cyclohexane	293	25.00	23.40	6.28	[23]
cyclohexane	298	24.20	22.60	6.49	[23]
cyclohexane	303	23.85	21.90	8.22	[23]
cyclohexane	308	23.02	21.20	7.91	[22,23]
cyclohexane	318	21.84	19.90	8.70	[22,23]
cyclohexane	328	20.71	18.80	9.13	[22,23]
dimethylsulfoxide	288	43.68	45.40	3.94	[24]
dimethylsulfoxide	298	42.18	43.90	4.10	[24]
dimethylsulfoxide	308	41.11	42.60	3.55	[24]
dimethylsulfoxide	318	39.99	41.40	3.40	[24]
dimethylsulfoxide	328	38.72	40.20	3.93	[24]
ethanol	288	22.68	24.70	8.86	[14,25]
ethanol	293	22.28	24.10	8.17	[25]
ethanol	298	21.78	23.60	8.13	[12,25]
ethanol	303	21.40	23.00	7.62	[25]
ethanol	308	21.04	22.50	7.13	[25]
ethanol	313	20.66	22.10	6.82	[25]
ethanol	318	20.36	21.60	6.24	[25]
ethanol	323	19.91	21.20	6.53	[25]
ethyl acetate	298	23.93	21.90	8.32	[20]
ethylene glycol	283	49.76	46.70	6.25	[26,27]
ethylene glycol	293	49.02	45.60	7.04	[26,27]
ethylene glycol	298	48.24	45.10	6.59	[26,27]
ethylene glycol	303	47.67	44.60	6.48	[26,27]
ethylene glycol	308	47.50	44.10	7.14	[26,27]
ethylene glycol	313	47.58	43.70	8.22	[26,27]
ethylene glycol	318	46.40	43.30	6.79	[26,27]
ethylene glycol	323	46.68	42.80	8.23	[26,27]
heptane	288	20.73	22.20	6.90	[11,22]
heptane	293	20.40	21.30	4.56	[11,28]
heptane	298	19.64	20.60	4.74	[11,22]
heptane	303	19.34	19.90	2.69	[11,22]
heptane	308	18.80	19.20	2.07	[11,22]
heptane	313	18.46	18.60	0.60	[28]
heptane	318	17.76	18.00	1.24	[22]
heptane	323	17.42	17.40	0.06	[28]
heptane	328	16.68	16.90	1.44	[22]
heptane	333	16.46	16.40	0.18	[28]
heptane	343	15.32	15.50	1.44	[28]
methanol	293	22.80	22.80	0.18	[14]
methanol	298	22.27	22.30	0.09	[14]
methanol	303	21.79	21.70	0.46	[14]
methanol	308	21.52	21.20	1.67	[14]
methanol	313	21.13	20.70	2.22	[14]
methanol	318	20.61	20.20	2.04	[14]

Table 1. Cont.

Solvent	T (K)	$\sigma_{i,T}^{Exp}$	$\sigma_{i,T}^{Calc}$	MPD	Ref.
methanol	323	19.86	19.80	0.55	[14]
methyl acetate	298	24.79	22.90	7.62	[29]
N,N-dimethylformamide	288	36.96	36.40	1.41	[22]
N,N-dimethylformamide	298	35.83	35.30	1.40	[22]
N,N-dimethylformamide	308	34.65	34.30	0.95	[22]
N,N-dimethylformamide	318	33.37	33.40	0.12	[22]
N,N-dimethylformamide	328	32.03	32.60	1.69	[22]
N-methyl-2-pyrrolidone	239	41.13	44.30	7.80	[22]
N-methyl-2-pyrrolidone	278	42.60	40.80	4.18	[22]
N-methyl-2-pyrrolidone	288	41.35	40.10	3.00	[22]
N-methyl-2-pyrrolidone	298	40.25	39.50	1.99	[22]
N-methyl-2-pyrrolidone	303	40.38	39.10	3.12	[30]
N-methyl-2-pyrrolidone	308	39.10	38.80	0.66	[22]
N-methyl-2-pyrrolidone	313	39.99	38.50	3.63	[30]
N-methyl-2-pyrrolidone	318	37.91	38.30	0.98	[22]
N-methyl-2-pyrrolidone	328	36.80	37.80	2.61	[22]
N-methyl-2-pyrrolidone	333	35.90	37.50	4.46	[30]
N-methyl-2-pyrrolidone	338	35.66	37.30	4.54	[22]
propylene glycol	298	35.80	36.30	1.51	[31]
propylene glycol	303	35.70	35.80	0.34	[31]
propylene glycol	313	35.00	34.90	0.40	[31]
propylene glycol	323	34.10	34.00	0.35	[31]
toluene	288	28.93	31.90	10.40	[22]
toluene	298	27.76	30.50	9.69	[22]
toluene	308	26.60	29.10	9.47	[22]
toluene	318	25.46	27.90	9.66	[22]
toluene	328	24.29	26.80	10.50	[22]
water	283	74.27	77.60	4.42	[32]
water	293	72.72	74.80	2.83	[32]
water	298	71.92	73.50	2.18	[16,32,33]
water	303	71.18	72.30	1.53	[32,33]
water	308	70.35	71.10	1.08	[32,33]
water	311	69.91	70.40	0.76	[32]
water	313	69.49	70.00	0.73	[32]
water	318	68.67	69.00	0.41	[32,33]
water	323	67.78	67.90	0.24	[32,33]
water	328	66.60	67.00	0.57	[32,33]

Table 2. Applied solvation parameters of studied solvents for modeling.

Descriptor	Definition
Abraham solvent parameters [7,34,35]	
c	The intercept value in Abraham's solvation model
e	Excess molar refraction
s	Polarity/polarizability
a	Hydrogen-bond acidity
b	Hydrogen-bond basicity
v	McGowan volume characteristic
Hansen solubility parameters [8]	
δ_D	The energy from dispersion forces between molecules
δ_P	The energy from dipolar intermolecular force between molecules
δ_H	The energy from hydrogen bonds between molecules
Catalan parameters [9]	
SdP	Solvent dipolarity
SP	Solvent polarizability
SA	Solvent acidity
SB	Solvent basicity

Table 3. Numerical values of the Abraham solvent parameters.

Solvent	<i>c</i>	<i>e</i>	<i>s</i>	<i>a</i>	<i>b</i>	<i>v</i>
1-butanol	0.17	0.40	−1.01	0.06	−3.96	4.04
1-hexanol	0.12	0.49	−1.16	0.05	−3.98	4.13
1-octanol	−0.03	0.49	−1.04	−0.02	−4.24	4.22
1-pentanol	0.15	0.54	−1.23	0.14	−3.86	4.08
1-propanol	0.14	0.41	−1.03	0.25	−3.77	3.99
1,4-dioxane	0.10	0.35	−0.08	−0.56	−4.83	4.17
2-butanol	0.19	0.35	−1.13	0.02	−3.57	3.97
2-butanone	0.25	0.26	−0.08	−0.77	−4.86	4.15
2-methyl−1-propanol	0.13	0.25	−0.98	0.16	−3.88	4.11
2-pentanol	0.12	0.46	−1.33	0.21	−3.75	4.20
2-propanol	0.10	0.34	−1.05	0.41	−3.83	4.03
acetone	0.31	0.31	−0.12	−0.61	−4.75	3.94
acetonitrile	0.41	0.08	0.33	−1.57	4.39	3.36
benzene	0.14	0.46	−0.59	−3.10	−4.63	4.49
butyl acetate	0.25	0.36	−0.50	−0.87	−4.97	4.28
cyclohexane	0.16	0.78	−1.68	−3.74	−4.93	4.58
dimethylsulfoxide	−0.19	0.33	0.79	−1.26	−4.54	3.36
ethanol	0.22	0.47	−1.04	0.33	−3.60	3.86
ethyl acetate	0.33	0.37	−0.45	−0.70	−4.90	4.15
ethylene glycol	−0.27	0.58	−0.51	0.72	−2.62	2.73
heptane	0.33	0.67	−2.06	−3.32	−4.73	4.54
methanol	0.28	0.33	−0.71	0.24	−3.32	3.55
methyl acetate	0.35	0.22	−0.15	−1.04	−4.53	3.97
<i>N</i> -methyl−2-pyrrolidone	0.15	0.53	0.23	0.84	−4.79	3.67
<i>N,N</i> -dimethylformamide	−0.31	−0.06	0.34	0.36	−4.87	4.49
propylene glycol	−0.15	0.75	−0.97	0.68	−3.13	3.25
toluene	0.14	0.53	−0.72	−3.01	−4.82	4.55
water	−0.99	0.58	2.55	3.81	4.84	−0.87

Multiple linear regression was used in this study to develop a model to calculate the surface tension of different solvents at various temperatures based on the parameters mentioned in Table 1. Surface tension was set as the dependent variable, and solubility parameters as independent variables. Descriptors with *p*-value >0.1 were excluded from the model. The *p*-value shows the statistical significance of the coefficients of each independent variable assessed employing the *t*-test.

The results of the correlations with the proposed model were compared with those of the previously reported model by Freitas et al. [36], which calculates the surface tension of liquids at 20 °C ($\sigma_{i,20\text{ }^\circ\text{C}}$):

$$\sigma_{i,20\text{ }^\circ\text{C}} = 14.9 + 4.35A_i^{\text{Exp}} - 1.3B_i^{\text{Exp}} + 11.3S_i^{\text{Exp}} + 10.9E_i + 3.0V_i + 0.8N_C \quad (3)$$

and a model based on Abraham solute parameters [37] to compute the surface tensions at various temperatures ($\sigma_{i,T}$):

$$\log \sigma_{i,T} = 1.245E_i + 0.344A_i + 0.542V_i + \frac{1}{T}(384.020 - 305.012E_i + 22.350S_i - 101.827A_i + 16.608B_i - 152.522V_i) \quad (4)$$

where A_i^{Exp} , B_i^{Exp} , S_i^{Exp} , E_i and V_i are the Abraham solute parameters of the liquids. The numerical values of A_i^{Exp} , B_i^{Exp} and S_i^{Exp} were derived from experimental solubility data of the compounds dissolved in a number of organic solvents with known Abraham solvent parameters [37], E_i was calculated from refractive index data [38] and V_i was computed using a group contribution method of McGowan and Abraham [39]. N_C is the number of carbons in n-alkanes minus six, i.e., $N_C = 0$ for n-alkanes up to hexane and 1 for heptane [36]. As an informational note, the Abraham solute descriptors used in Equations (3) and (4) are

denoted by capitalized alphabetical characters. These solute descriptors could either be determined from experimental solubility data (denoted by *Exp* as superscript in this work) or could be computed using available software [40]. Abraham solvent parameters, which will be used in later equations, will be denoted by lowercase alphabetical characters.

The accuracy of the models was investigated by computing *MPD* (mean percentage deviation) as follows:

$$MPD = \frac{100}{N} \sum \left(\frac{|\sigma_{i,T}^{Calc} - \sigma_{i,T}^{Exp}|}{\sigma_{i,T}^{Exp}} \right) \quad (5)$$

where *N* is the number of data points used in the regression analyses.

Table 4. Numerical values of the Hansen and Catalan parameters for the solvents investigated in this work.

solvent	Hansen Parameters				Catalan Parameters		
	δ_D	δ_P	δ_H	<i>SP</i>	<i>SdP</i>	<i>SA</i>	<i>SB</i>
1-butanol	16.00	5.70	15.80	0.67	0.66	0.34	0.81
1-hexanol	15.90	5.80	12.50	0.70	0.55	0.32	0.88
1-octanol	17.00	3.30	11.90	0.71	0.45	0.30	0.92
1-pentanol	13.83	8.82	13.80	0.69	0.59	0.32	0.86
1-propanol	16.00	6.80	17.40	0.66	0.75	0.37	0.78
1,4-dioxane	19.00	1.80	7.40	0.74	0.31	0.00	0.44
2-butanol	13.38	9.53	14.08	0.66	0.71	0.22	0.89
2-butanone	16.00	9.00	5.10	0.67	0.87	0.00	0.52
2-methyl-1-propanol	13.38	9.53	14.08	0.66	0.68	0.31	0.83
2-pentanol	13.65	8.87	12.95	0.67	0.67	0.20	0.92
2-propanol	12.97	10.35	15.68	0.63	0.81	0.28	0.83
acetone	15.50	10.40	7.00	0.65	0.91	0.00	0.48
acetonitrile	11.59	12.95	16.34	0.65	0.97	0.04	0.29
benzene	18.40	0.00	2.00	0.79	0.27	0.00	0.12
butyl acetate	14.49	7.74	6.53	0.67	0.54	0.00	0.53
cyclohexane	16.80	0.00	0.20	0.68	0.00	0.00	0.07
dimethylsulfoxide	18.40	16.40	10.20	0.83	1.00	0.07	0.65
ethanol	15.80	8.80	19.40	0.64	0.78	0.40	0.66
ethyl acetate	15.80	5.30	7.20	0.66	0.60	0.00	0.54
ethylene glycol	17.00	11.00	26.00	0.78	0.91	0.72	0.53
heptane	15.30	0.00	0.00	0.64	0.00	0.00	0.08
methanol	15.10	12.30	22.30	0.61	0.90	0.61	0.55
methyl acetate	12.68	11.42	11.79	0.65	0.64	0.00	0.53
<i>N</i> -methyl-2-pyrrolidone	18.00	12.30	7.20	0.81	0.96	0.02	0.61
<i>N,N</i> -dimethylformamide	17.40	13.70	11.30	0.76	0.98	0.03	0.61
propylene glycol	12.75	14.23	27.95	0.73	0.89	0.48	0.60
toluene	18.00	1.40	2.00	0.78	0.28	0.00	0.13
water	15.50	16.00	42.30	0.68	1.00	1.06	0.03

3. Results and Discussion

The collected surface tension data of the mono-solvents at various temperatures were correlated with three sets of solvation parameters, and the obtained model after excluding non-significant parameters ($p > 0.05$) is:

$$\log \sigma_T = \left(\begin{array}{l} -1.713 - 0.037s + 0.118a + 0.008b + 0.008\delta_D \\ + 0.006\delta_P + 0.003\delta_H + 3.636SP - 0.087SdP - 0.089SB \\ + \left(\frac{729.913 - 16.509c - 23.369e - 29.450g - 19.611v - 687.1555P - 35.2115A}{T} \right) \end{array} \right) \quad (6)$$

The correlation coefficient of this equation is 0.992, the *F* value is 503, and the correlation is statistically significant with a *p*-value of <0.0005. The *F* value is the Fischer test value revealing the statistical significance of the overall correlation. The minimum and maximum

MPD values for the back-calculated surface tensions belong to 1-butanol at temperature 293 (MPD = 0.04%) and benzene at temperature 303 (MPD = 11.62%). The overall MPD of the correlated data points was 3.48% ($N = 146$). Equation (6) is valid for interpolation purposes in all temperatures and for extrapolation purposes in a narrow range of temperatures.

Previous studies have shown the importance of Abraham solvation parameters in calculating the surface tension of the mono-solvents [12]. A comparison between surface tension prediction for mono-solvents with our proposed model and Freitas study at 20 °C ($\sigma_{i,20^\circ\text{C}}$) is shown in Figure 1. Moreover, the MPD for a previous model by our group was 11%. It can be clearly understood that considering the Catalan and Hansen parameters, the prediction ability of the model has been improved in comparison to previous models. An important distinction between the current method and the earlier method of Freitas et al. is that Equation (3) used the solute descriptors of the organic solvents as input parameters. The current treatment uses the Abraham model equation coefficients for each solvent as the input parameters for Equation (2). Solvent coefficients, rather than solute descriptors, are likely the more appropriate parameter to use when dealing with properties such as surface tension. While both types of parameters can be used in describing molecular interactions, their numerical values are determined under a different set of experimental conditions. In the case of solute descriptors, the measurements are normally performed at low concentrations where the dissolved solute is completely surrounded by solvent molecules. Such measurements would not capture the effects of self-association. Solvent parameters, on the other hand, would include effects arising from self-association, as well as any special structural features resulting from “solvent stacking”. We recognize that the limited availability of solvent coefficients does make it appealing to use the more readily available solute parameters when developing predictive expressions. Experimental-based solute descriptors are known for more than 8000 different organic and organometallic compounds [40]. Abraham model solvent coefficients, on the other hand, have been determined for only 130 different organic molecules and a few binary aqueous-alcoholic mixtures [41].

In order to validate the model, each solvent was sorted based on the temperature and was divided into training and test sets one by one in order to have different solvents containing various physicochemical properties with different temperatures in both test and training sets. The temperature values of the used training data points are listed in the second column of Table 1 using bold font. The proposed model was trained using the training data points, and the rest of the data points were predicted by the trained model. The obtained overall MPD value was 4.01% ($N = 118$). The results confirm the validity of the model.

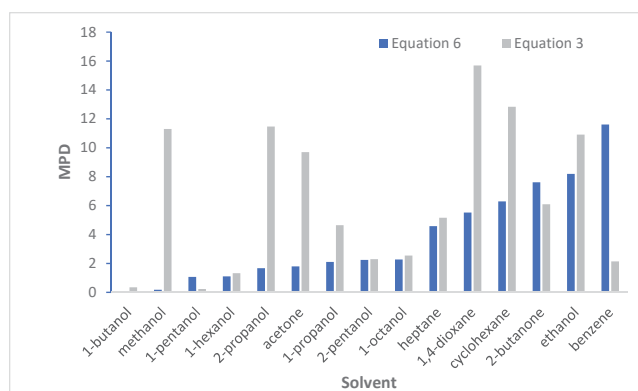


Figure 1. Comparison of MPD values for the calculated surface tension of studied solvents at 293 K by combination of van't Hoff type model and the solvation parameters (Equation (6)) and the reported model by Freitas et al. (Equation (3)).

4. Conclusions

A van't Hoff type-mathematical expression was developed for predicting the surface tension of both water and 27 different organic mono-solvents as a function of temperature using only Abraham solvation parameters, Hansen solubility parameters, and Catalan parameters as input values. The derived mathematical expression described the experimental surface tension data within an overall MPD of the model was 3.48%. The minimum and maximum MPD between predicted and observed values were 0.04% and 11.62%, respectively. The predictive model reported in the current study could help researchers to estimate the surface tension of mono-solvents at different temperatures and identify possible outlier values in need of re-measurement. The availability of needed solvation parameters currently limits the applicability of the proposed model; however, progress is being made to estimate Abraham model solvent coefficients using functional group additivity and machine learning methods [42–44].

Author Contributions: N.K.; data collection and curation, writing—original draft preparation, A.S.; methodology, writing—review, W.E.A.J.; writing—review and editing, A.J.; conceptualization, data collection, and curation, writing—review and editing. All authors have read and agreed to the published version of the manuscript.

Funding: This research received a small grant from the Student Research Committee, Tabriz University of Medical Sciences (grant No. # 70194).

Data Availability Statement: Data used in this study are available from the published literature [16–39].

Conflicts of Interest: The authors declare no conflict of interest.

References

- Lee, Y.C.; Simamora, P.; Pinsuwan, S.; Yalkowsky, S.H. Review on the systemic delivery of insulin via the ocular route. *Int. J. Pharm.* **2002**, *233*, 1–18. [\[CrossRef\]](#)
- Khattab, I.S.; Bandarkar, F.; Fakhree, M.A.A.; Jouyban, A. Density, viscosity, and surface tension of water+ ethanol mixtures from 293 to 323K. *Korean J. Chem. Eng.* **2012**, *29*, 812–817. [\[CrossRef\]](#)
- Fathi Azarbayjani, A.; Jouyban, A.; Chan, S.Y. Impact of surface tension in pharmaceutical sciences. *J. Pharm. Pharm. Sci.* **2009**, *12*, 218–228. [\[CrossRef\]](#) [\[PubMed\]](#)
- Fathi-Azarbayjani, A.; Jouyban, A. Surface tension in human pathophysiology and its application as a medical diagnostic tool. *Bioimpacts* **2015**, *5*, 29–44. [\[CrossRef\]](#)
- Jouyban, A.; Fathi Azarbayjani, A. Experimental and computational methods pertaining to surface tension of pharmaceutical. In *Toxicity and Drug Testing*; Acree, W.E., Jr., Ed.; IntechOpen: London, UK, 2012; pp. 47–70.
- Khoubnasabjafari, M.; Jouyban, V.; Azarbayjani, A.F.; Jouyban, A. Application of Abraham solvation parameters for surface tension prediction of mono-solvents and solvent mixtures at various temperatures. *J. Mol. Liq.* **2013**, *178*, 44–56. [\[CrossRef\]](#)
- Lee, G.; Che, M.; Qian, E.; Wang, L.; Gupta, A.; Neal, R.; Yue, D.; Downs, S.; Mayes, T.; Rose, O. Determination of Abraham model solute descriptors for o-acetoacetanilide based on experimental solubility data in organic mono-solvents. *Phys. Chem. Liq.* **2019**, *57*, 528–535. [\[CrossRef\]](#)
- Hansen, C.M. *Hansen Solubility Parameters: A User's Handbook*; CRC Press: New York, NY, USA, 1998.
- Catalán, J. Toward a generalized treatment of the solvent effect based on four empirical scales: Dipolarity (SdP, a new scale), polarizability (SP), acidity (SA), and basicity (SB) of the medium. *J. Phys. Chem. B* **2009**, *113*, 5951–5960. [\[CrossRef\]](#)
- Calvo, E.; Pintos, M.; Amigo, A.; Bravo, R. Thermodynamic analysis of surface formation of [1,4-dioxane + 1-alkanol] mixtures. *J. Colloid Interface Sci.* **2002**, *253*, 203–210. [\[CrossRef\]](#)
- Vijande, J.; Pineiro, M.M.; García, J.; Valencia, J.L.; Legido, J.L. Density and surface tension variation with temperature for heptane + 1-alkanol. *J. Chem. Eng. Data* **2006**, *51*, 1778–1782. [\[CrossRef\]](#)
- Segade, L.; Jiménez de Llano, J.; Domínguez-Pérez, M.; Cabeza, Ó.; Cabanas, M.; Jiménez, E. Density, surface tension, and refractive index of octane + 1-alkanol mixtures at T = 298.15 K. *J. Chem. Eng. Data* **2003**, *48*, 1251–1255. [\[CrossRef\]](#)
- Azizian, S.; Bashavard, N. Surface tension of dilute solutions of linear alcohols in benzyl alcohol. *J. Chem. Eng. Data* **2005**, *50*, 1303–1307. [\[CrossRef\]](#)
- Vazquez, G.; Alvarez, E.; Navaza, J.M. Surface tension of alcohol water + water from 20 to 50. degree. C. *J. Chem. Eng. Data* **1995**, *40*, 611–614. [\[CrossRef\]](#)
- Yaws, C.L. *Thermophysical Properties of Chemicals and Hydrocarbons*; William Andrew: Norwich, NY, USA, 2008.
- Bermúdez-Salguero, C.; Gracia-Fadrique, J.; Calvo, E.; Amigo, A. Densities, refractive indices, speeds of sound, and surface tensions for dilute aqueous solutions of 2-methyl-1-propanol, cyclopentanone, cyclohexanone, cyclohexanol, and ethyl acetoacetate at 298.15 K. *J. Chem. Eng. Data* **2011**, *56*, 3823–3829. [\[CrossRef\]](#)

17. Enders, S.; Kahl, H.; Winkelmann, J. Surface tension of the ternary system water + acetone + toluene. *J. Chem. Eng. Data* **2007**, *52*, 1072–1079. [[CrossRef](#)]
18. Howard, K.S.; McAllister, R. Surface tension of acetone–water solutions up to their normal boiling points. *AIChE J.* **1957**, *3*, 325–329. [[CrossRef](#)]
19. Jasper, J.J. The surface tension of pure liquid compounds. *J. Phys. Chem. Ref. Data* **1972**, *1*, 841–1010. [[CrossRef](#)]
20. Wanchoo, R.; Narayan, J.; Raina, G.; Rattan, V. Excess properties of (2-propanol + ethyl acetate or benzene) binary liquid mixture. *Chem. Eng. Commun.* **1989**, *81*, 145–156. [[CrossRef](#)]
21. Washburn, E.R.; Shildneck, C.H. Surface tension studies with n-butyl acetate. *J. Am. Chem. Soc.* **1933**, *55*, 2354–2357. [[CrossRef](#)]
22. Kahl, H.; Wadewitz, T.; Winkelmann, J. Surface tension and interfacial tension of binary organic liquid mixtures. *J. Chem. Eng. Data* **2003**, *48*, 1500–1507. [[CrossRef](#)]
23. Gómez-Díaz, D.; Mejuto, J.C.; Navaza, J.M. Physicochemical properties of liquid mixtures. 1. Viscosity, density, surface tension and refractive index of cyclohexane + 2, 2, 4-trimethylpentane binary liquid systems from 25 C to 50 C. *J. Chem. Eng. Data* **2001**, *46*, 720–724. [[CrossRef](#)]
24. Bagheri, A.; Abolhasani, A.; Moghadas, A.; Nazari-Moghaddam, A.; Alavi, S. Study of surface tension and surface properties of binary systems of DMSO with long chain alcohols at various temperatures. *J. Chem. Thermodyn.* **2013**, *63*, 108–115.
25. Álvarez, E.; Correa, A.; Correa, J.M.; García-Rosello, E.; Navaza, J.M. Surface tensions of three amyl alcohol + ethanol binary mixtures from (293.15 to 323.15) K. *J. Chem. Eng. Data* **2011**, *56*, 4235–4238. [[CrossRef](#)]
26. Azizian, S.; Hemmati, M. Surface tension of binary mixtures of ethanol+ ethylene glycol from 20 to 50 C. *J. Chem. Eng. Data* **2003**, *48*, 662–663. [[CrossRef](#)]
27. Tsierkezos, N.G.; Molinou, I.E. Thermodynamic properties of water+ ethylene glycol at 283.15, 293.15, 303.15, and 313.15 K. *J. Chem. Eng. Data* **1998**, *43*, 989–993. [[CrossRef](#)]
28. Rolo, L.L.; Caco, A.I.; Queimada, A.J.; Marrucho, I.M.; Coutinho, J.A. Surface tension of heptane, decane, hexadecane, eicosane, and some of their binary mixtures. *J. Chem. Eng. Data* **2002**, *47*, 1442–1445. [[CrossRef](#)]
29. Bermúdez-Salguero, C.; Gracia-Fadrique, J.S.; Amigo, A. Surface tension data of aqueous binary mixtures of methyl, ethyl, propyl, and butyl acetates at 298.15 K. *J. Chem. Eng. Data* **2010**, *55*, 2905–2908. [[CrossRef](#)]
30. García-Abuín, A.; Gómez-Díaz, D.; Navaza, J.M.; Vidal-Tato, I. Surface tension of aqueous solutions of short n-alkyl-2-pyrrolidones. *J. Chem. Eng. Data* **2008**, *53*, 2671–2674. [[CrossRef](#)]
31. Hoke, B.C., Jr.; Patton, E.F. Surface tensions of propylene glycol + water. *J. Chem. Eng. Data* **1992**, *37*, 331–333. [[CrossRef](#)]
32. Vargaftik, N.; Volkov, B.; Voljak, L. International tables of the surface tension of water. *J. Phys. Chem. Ref. Data* **1983**, *12*, 817–820. [[CrossRef](#)]
33. Markarian, S.A.; Terzyan, A.M. Surface tension and refractive index of dialkylsulfoxide + water mixtures at several temperatures. *J. Chem. Eng. Data* **2007**, *52*, 1704–1709. [[CrossRef](#)]
34. Abraham, M.H.; Smith, R.E.; Luchtfeld, R.; Boorem, A.J.; Luo, R.; Acree, W.E., Jr. Prediction of solubility of drugs and other compounds in organic solvents. *J. Pharm. Sci.* **2010**, *99*, 1500–1515. [[CrossRef](#)] [[PubMed](#)]
35. Jouyban, A.; Acree, W.E., Jr.; Michael, H. Abraham and his developed parameters: Various applications in medicine, chemistry and biology. *Pharm. Sci.* **2022**, *28*, 170–173. [[CrossRef](#)]
36. Freitas, A.A.; Quina, F.H.; Carroll, F.A. A linear free energy analysis of the surface tension of organic liquids. *Langmuir* **2000**, *16*, 6689–6692. [[CrossRef](#)]
37. Acree, J.; William, E.; Abraham, M.H. Solubility predictions for crystalline nonelectrolyte solutes dissolved in organic solvents based upon the Abraham general solvation model. *Can. J. Chem.* **2001**, *79*, 1466–1476. [[CrossRef](#)]
38. Abraham, M.H.; Ibrahim, A.; Zissimos, A.M. Determination of sets of solute descriptors from chromatographic measurements. *J. Chromatogr. A* **2004**, *1037*, 29–47. [[CrossRef](#)]
39. Abraham, M.H.; McGowan, J. The use of characteristic volumes to measure cavity terms in reversed phase liquid chromatography. *Chromatographia* **1987**, *23*, 243–246. [[CrossRef](#)]
40. Ulrich, N.; Endo, S.; Brown, T.N.; Watanabe, N.; Bronner, G.; Abraham, M.H.; Goss, K.-U. UFZ-LSER Database v 3.2.1. Available online: <http://www.ufz.de/lserd> (accessed on 10 October 2022).
41. Sinha, S.; Yang, C.; Wu, E.; Acree, W.E., Jr. Abraham solvation parameter model: Examination of possible intramolecular hydrogen-bonding using calculated solute descriptors. *Liquids* **2022**, *2*, 131–146. [[CrossRef](#)]
42. Brown, T.N. Empirical regressions between system parameters and solute descriptors of polyparameter linear free energy relationships (PPLFRs) for predicting solvent-air partitioning. *Fluid Phase Equilib.* **2021**, *540*, 113035. [[CrossRef](#)]
43. Grubbs, L.M.; Saifullah, M.; Nohelli, E.; Ye, S.; Achi, S.S.; Acree, W.E., Jr.; Abraham, M.H. Mathematical correlations for describing solute transfer into functionalized alkane solvents containing hydroxyl, ether, ester or ketone solvents. *Fluid Phase Equilib.* **2010**, *298*, 48–53. [[CrossRef](#)]
44. Bradley, J.-C.; Abraham, M.H.; Acree, W.E.; Lang, A.S. Predicting Abraham model solvent coefficients. *Chem. Cent. J.* **2015**, *9*, 12. [[CrossRef](#)]

Article

The Solubility of Ethyl Candesartan in Mono Solvents and Investigation of Intermolecular Interactions

Cunbin Du

School of Pharmaceutical Sciences, TaiZhou University, Taizhou 318000, China; cbd@tzc.edu.cn

Abstract: In this work, the experimental solubility of ethyl candesartan in the selected solvents within the temperature ranging from 278.15 to 318.15 K was studied. It can be easily found that the solubility of ethyl candesartan increases with the rising temperature in all solvents. The maximum solubility value was obtained in *N,N*-dimethylformamide (DMF, 7.91×10^{-2}), followed by cyclohexanone (2.810×10^{-2}), 1,4-dioxanone (2.69×10^{-2}), acetone (7.04×10^{-3}), ethyl acetate (4.20×10^{-3}), *n*-propanol (3.69×10^{-3}), isobutanol (3.38×10^{-3}), methanol (3.17×10^{-3}), *n*-butanol (3.03×10^{-3}), ethanol (2.83×10^{-3}), isopropanol (2.69×10^{-3}), and acetonitrile (1.15×10^{-2}) at the temperature of 318.15 K. Similar results of solubility sequence from large to small were also obtained in other temperatures. The X-ray diffraction analysis illustrates that the crystalline forms of all samples were consistent, and no crystalline transformation occurred during the dissolution process. In aprotic solvents, except for individual solvents, the solubility data decreases with the decreasing values of hydrogen bond basicity (β) and dipolarity/polarizability (π^*). The largest average relative deviation (ARD) data in the modified Apelblat equation is 1.9% and observed in isopropanol; the maximum data in λh equation is 4.3% and found in *n*-butanol. The results of statistical analysis show that the modified Apelblat equation is the more suitable correlation of experimental data for ethyl candesartan in selected mono solvents at all investigated temperatures. In addition, different parameters were used to quantify the solute–solvent interactions that occurred in the dissolution process including Abraham solvation parameters (AP_i), Hansen solubility parameters (HP_i), and Catalan parameters (CP_i).

Keywords: ethyl candesartan; solubility; model correlation; intermolecular interactions

Citation: Du, C. The Solubility of Ethyl Candesartan in Mono Solvents and Investigation of Intermolecular Interactions. *Liquids* **2022**, *2*, 404–412. <https://doi.org/10.3390/liquids2040023>

Academic Editors: William E. Acree, Jr. and Juan Ortega Saavedra

Received: 17 October 2022
Accepted: 10 November 2022
Published: 17 November 2022

Publisher's Note: MDPI stays neutral with regard to jurisdictional claims in published maps and institutional affiliations.



Copyright: © 2022 by the author. Licensee MDPI, Basel, Switzerland. This article is an open access article distributed under the terms and conditions of the Creative Commons Attribution (CC BY) license (<https://creativecommons.org/licenses/by/4.0/>).

1. Introduction

Candesartan (CNS) is a highly effective, long-acting, and selective angiotensin II type 1 receptor antagonist [1]. Candesartan cilexetil is a prodrug of candesartan, which can be completely hydrolyzed in the gastrointestinal tract and transformed into candesartan with antihypertensive activity [2]. At present, according to the different key intermediates in the synthesis process, there are many literature reports on the synthesis methods of candesartan cilexetil [3–7]. Among them, candesartan cilexetil is widely used by using 2-tert-butoxycarbonylamino-3-nitrobenzoate ethyl ester as a raw material through nine steps. However, in the process of triphenyl removal, due to the existence of multiple chemical sensitive groups in trityl candesartan cilexetil, impurities such as ethyl candesartan and incomplete materials will be produced. The purity of the product is low, and it needs to be purified many times to obtain candesartan ester with high purity [3]. EP 0720982 discloses a method for preparing candesartan cilexetil by deprotection of triphenylmethane in the presence of methanol and hydrochloric acid. The disadvantage of this process is that the yield is very low, and the product needs to be purified by chromatography [4].

In the process development and research of candesartan cilexetil, ethyl candesartan (Figure 1, chemical formula, $C_{26}H_{24}N_6O_3$, CAS No. 139481-58-6) is one of the important impurities in the preparation, and there is little literature on it. As we all know, the impurity profile of active pharmaceutical ingredients (API) and the evaluation of their toxic effects are necessary steps in the development of effective drugs, which is very important for

medical safety. Therefore, the basic knowledge required for any drug is its impurities and possible degradation products [8]. Solvent crystallization is a common method for the separation and purification step during the production process. The solubility of impurities in different solvents plays an important role for understanding the phase equilibrium in the development of the crystallization process [9–12]. Moreover, the solubility of a substance is determined by both the solid state (crystal lattice energy) and the interaction with the solvent (solvation) [9–12].

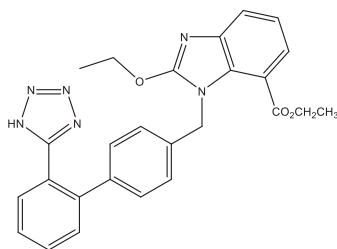


Figure 1. The chemical structure of ethyl candesartan.

Therefore, the proposed research work was performed to study the solubilization behavior of ethyl candesartan in some different pure solvents. The solubility data was correlated by a modified Apelblat equation and λh equation. The crystal form before and after dissolution was characterized using X-ray powder diffractometer. Moreover, the solubilization behavior was discussed by using the solvent properties. The solute–solvent interactions that occurred in the dissolution process were quantified by Abraham solvation parameters (AP_i), Hansen solubility parameters (HP_i), and Catalan parameters (CP_i). The physicochemical data obtained would be useful in purification, recrystallization, and formulation development of ethyl candesartan in pharmaceutical industries.

2. Experimental Section

2.1. Materials and Apparatus

Raw ethyl candesartan was recrystallized by ethanol; the final mass fraction purity was 0.992 (determined by the High Performance Liquid Chromatograph, HPLC, Agilent 1260, Beijing, China), provided by Zhejiang Junfeng Technology Co., Ltd., Taizhou, China. During the experiment, all pure organic solvents with analytical grade were purchased from Sinopharm Chemical Reagent Co., Ltd., Beijing, China, and used without any additional purification. The purity of the solvent was provided by the supplier. The detailed information is listed in Table 1.

Table 1. Source and purity of the materials used in this work.

Chemicals	CAS Number	Molar Mass g·mol ⁻¹	Source	Mass Fraction Purity	Analysis Method
Ethyl Candesaratan	139481-58-6	468.51	Zhejiang Junfeng Technology Co., Ltd. China	0.992	HPLC ^b
Methanol	67-56-1	32.04	Sinopharm Chemical Reagent Co., Ltd., China	0.995 ^a	None
Ethanol	64-17-5	46.07		0.996 ^a	
<i>n</i> -Propanol	71-23-8	60.10		0.995 ^a	
Isopropanol	67-63-0	60.10		0.996 ^a	
<i>n</i> -Butanol	71-36-3	74.12		0.995 ^a	
Isobutanol	78-83-1	74.12		0.996 ^a	
Acetonitrile	75-05-8	41.05		0.996 ^a	
Ethyl Acetate	141-78-6	88.11		0.995 ^a	
DMF	68-12-2	73.09		0.995 ^a	
Acetone	67-64-1	58.08		0.996 ^a	
Cyclohexanone	108-94-1	98.14	0.995 ^a		
1,4-Dioxane	123-91-1	88.11	0.996 ^a		

^a the purity was obtained from chemical reagent Co., Ltd., ^b determined by HPLC.

2.2. X-ray Diffraction Analysis

The crystals from raw ethyl candesartan and the recovered equilibrated samples from each solvent were analyzed by using X-ray powder diffractometer with an X-ray generator of Cu-K α radiation (1.5405 Å). The experimental tube voltage and current were 40 kV and 30 mA. The data collection was performed at 2θ of 5–60° in steps of 0.02°.

2.3. Measurement Experiment

In this work, the isothermal saturation method [13–19] was used to determine the solubility data of ethyl candesartan in each solvent in the temperature ranging from 278.15 K to 318.15 K under atmospheric pressure. For solubility measurement, a jacketed glass vessel with a magnetic stirrer was used, and the temperature maintained by a thermostatic bath with an accuracy of 0.01 K.

Excess mL of ethyl candesartan and 30 mL of solvent were added into the jacketed glass vessel. The actual temperature in solution was displayed by a mercury glass micro thermometer. A magnetic stirrer was used to mix continuously for 24 h to achieve phase equilibrium state. Then, the magnetic stirrer was stopped, and solution was settled for 2 h before sampling. Equilibrium liquor with the amount of 2 mL was taken out using a syringe attached with a 0.2 μm pore filter and transferred into a 25 mL pre-weighted flask covered with a rubber stopper, then weighed again by the analytical balance. After that, the concentration of ethyl candesartan was determined by HPLC. Each analysis was repeated three times at all temperatures. The mobile phase was methanol/water = (2:1) at a flow rate of 1.0 mL·min⁻¹. A reverse phase column LP-C18 (250 mm \times 4.6 mm), with a column temperature of 303.15 K, and a UV detector, with the wavelength of 270 nm, were applied.

3. Results and Discussion

3.1. X-ray Diffraction Analysis

Figure 2 presents the XRD patterns of the crystals from raw ethyl candesartan and the recovered equilibrated samples from each solvent. The peaks in the raw material match well with the recovered equilibrated samples, which illustrates that the crystalline forms of all samples were consistent, and no crystalline transformation occurred during the dissolution process.

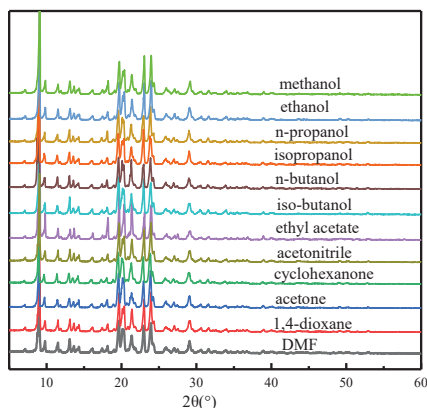


Figure 2. The XRD curves of ethyl candesartan recrystallized from each solvent.

3.2. Experimental Solubility Data

Through a search of related literature, we have found that previous studies mainly focused on the synthesis of ethyl candesartan. The quantitative solubility values in any of the investigated organic solvents are not reported yet. Therefore, the experimental solubility of ethyl candesartan in the selected solvents within the temperature range of

278.15 to 318.15 K was studied, and the solubility data together with the calculated values on the basis of correlation equation were tabulated in Table 2.

Table 2. Experimental and calculated solubility in mole fraction of ethyl candesartan in solvent at the temperature range of $T = (278.15 \text{ to } 318.15) \text{ K}$ under 101.1 kPa^a.

T/K	Solvent											
	x^{exp}	x^{AP}	x^{Lh}	x^{exp}	x^{AP}	x^{Lh}	x^{exp}	x^{AP}	x^{Lh}	x^{exp}	x^{AP}	x^{Lh}
	Methanol			Ethanol			<i>n</i>-Propanol			Isopropanol		
278.15	3.81×10^{-4}	3.66×10^{-4}	3.98×10^{-4}	3.25×10^{-4}	3.28×10^{-4}	3.44×10^{-4}	5.17×10^{-4}	5.06×10^{-4}	5.27×10^{-4}	3.10×10^{-4}	2.87×10^{-4}	3.14×10^{-4}
283.15	5.24×10^{-4}	5.23×10^{-4}	5.37×10^{-4}	4.64×10^{-4}	4.59×10^{-4}	4.64×10^{-4}	6.67×10^{-4}	6.89×10^{-4}	6.95×10^{-4}	4.18×10^{-4}	4.14×10^{-4}	4.28×10^{-4}
288.15	7.04×10^{-4}	7.28×10^{-4}	7.16×10^{-4}	6.24×10^{-4}	6.29×10^{-4}	6.20×10^{-4}	9.04×10^{-4}	9.19×10^{-4}	9.07×10^{-4}	5.59×10^{-4}	5.81×10^{-4}	5.76×10^{-4}
293.15	9.80×10^{-4}	9.85×10^{-4}	9.46×10^{-4}	8.36×10^{-4}	8.44×10^{-4}	8.21×10^{-4}	1.22×10^{-3}	1.20×10^{-3}	1.17×10^{-3}	7.76×10^{-4}	7.94×10^{-4}	7.68×10^{-4}
298.15	1.32×10^{-3}	1.30×10^{-3}	1.24×10^{-3}	1.12×10^{-3}	1.11×10^{-3}	1.08×10^{-3}	1.58×10^{-3}	1.55×10^{-3}	1.51×10^{-3}	1.06×10^{-3}	1.06×10^{-3}	1.01×10^{-3}
303.15	1.68×10^{-3}	1.68×10^{-3}	1.61×10^{-3}	1.45×10^{-3}	1.44×10^{-3}	1.40×10^{-3}	1.97×10^{-3}	1.97×10^{-3}	1.92×10^{-3}	1.40×10^{-3}	1.38×10^{-3}	1.33×10^{-3}
308.15	2.11×10^{-3}	2.12×10^{-3}	2.07×10^{-3}	1.82×10^{-3}	1.83×10^{-3}	1.81×10^{-3}	2.44×10^{-3}	2.46×10^{-3}	2.43×10^{-3}	1.76×10^{-3}	1.76×10^{-3}	1.72×10^{-3}
313.15	2.61×10^{-3}	2.61×10^{-3}	2.65×10^{-3}	2.27×10^{-3}	2.29×10^{-3}	2.31×10^{-3}	3.01×10^{-3}	3.02×10^{-3}	3.05×10^{-3}	2.19×10^{-3}	2.20×10^{-3}	2.22×10^{-3}
318.15	3.17×10^{-3}	3.17×10^{-3}	3.37×10^{-3}	2.83×10^{-3}	2.82×10^{-3}	2.94×10^{-3}	3.69×10^{-3}	3.69×10^{-3}	3.81×10^{-3}	2.69×10^{-3}	2.69×10^{-3}	2.84×10^{-3}
	<i>n</i>-Butanol			Isobutanol			Ethyl Acetate			Acetonitrile		
278.15	3.43×10^{-4}	3.36×10^{-4}	3.69×10^{-4}	4.24×10^{-4}	4.17×10^{-4}	4.47×10^{-4}	7.90×10^{-4}	7.69×10^{-4}	7.68×10^{-4}	1.63×10^{-4}	1.57×10^{-4}	1.69×10^{-4}
283.15	4.88×10^{-4}	4.89×10^{-4}	5.00×10^{-4}	5.73×10^{-4}	5.88×10^{-4}	5.98×10^{-4}	9.67×10^{-4}	9.70×10^{-4}	9.72×10^{-4}	2.17×10^{-4}	2.18×10^{-4}	2.22×10^{-4}
288.15	6.72×10^{-4}	6.88×10^{-4}	6.72×10^{-4}	8.07×10^{-4}	8.08×10^{-4}	7.92×10^{-4}	1.20×10^{-3}	1.21×10^{-3}	1.22×10^{-3}	2.87×10^{-4}	2.94×10^{-4}	2.90×10^{-4}
293.15	9.39×10^{-4}	9.40×10^{-4}	8.93×10^{-4}	1.09×10^{-3}	1.08×10^{-3}	1.04×10^{-3}	1.51×10^{-3}	1.51×10^{-3}	1.52×10^{-3}	3.90×10^{-4}	3.89×10^{-4}	3.75×10^{-4}
298.15	1.26×10^{-3}	1.25×10^{-3}	1.18×10^{-3}	1.42×10^{-3}	1.42×10^{-3}	1.35×10^{-3}	1.87×10^{-3}	1.88×10^{-3}	1.88×10^{-3}	5.04×10^{-4}	5.02×10^{-4}	4.82×10^{-4}
303.15	1.62×10^{-3}	1.61×10^{-3}	1.54×10^{-3}	1.82×10^{-3}	1.81×10^{-3}	1.75×10^{-3}	2.32×10^{-3}	2.31×10^{-3}	2.32×10^{-3}	6.37×10^{-4}	6.36×10^{-4}	6.14×10^{-4}
308.15	2.03×10^{-3}	2.04×10^{-3}	1.99×10^{-3}	2.27×10^{-3}	2.27×10^{-3}	2.24×10^{-3}	2.86×10^{-3}	2.84×10^{-3}	2.84×10^{-3}	7.90×10^{-4}	7.89×10^{-4}	7.76×10^{-4}
313.15	2.50×10^{-3}	2.51×10^{-3}	2.56×10^{-3}	2.79×10^{-3}	2.80×10^{-3}	2.84×10^{-3}	3.45×10^{-3}	3.46×10^{-3}	3.45×10^{-3}	9.60×10^{-4}	9.63×10^{-4}	9.75×10^{-4}
318.15	3.03×10^{-3}	3.02×10^{-3}	3.27×10^{-3}	3.39×10^{-3}	3.38×10^{-3}	3.59×10^{-3}	4.20×10^{-3}	4.21×10^{-3}	4.19×10^{-3}	1.15×10^{-3}	1.15×10^{-3}	1.22×10^{-3}
	Cyclohexanone			Acetone			1,4-Dioxane			DMF		
278.15	7.92×10^{-3}	7.99×10^{-3}	7.88×10^{-3}	2.01×10^{-3}	2.03×10^{-3}	2.01×10^{-3}				1.07×10^{-2}	1.08×10^{-2}	1.09×10^{-2}
283.15	9.41×10^{-3}	9.41×10^{-3}	9.37×10^{-3}	2.39×10^{-3}	2.39×10^{-3}	2.38×10^{-3}				1.45×10^{-2}	1.45×10^{-2}	1.45×10^{-2}
288.15	1.11×10^{-2}	1.10×10^{-2}	1.11×10^{-2}	2.82×10^{-3}	2.80×10^{-3}	2.81×10^{-3}	6.42×10^{-3}	6.44×10^{-3}	6.38×10^{-3}	1.93×10^{-2}	1.92×10^{-2}	1.91×10^{-2}
293.15	1.31×10^{-2}	1.30×10^{-2}	1.30×10^{-2}	3.29×10^{-3}	3.28×10^{-3}	3.30×10^{-3}	8.34×10^{-3}	8.27×10^{-3}	8.27×10^{-3}	2.54×10^{-2}	2.51×10^{-2}	2.49×10^{-2}
298.15	1.52×10^{-2}	1.52×10^{-2}	1.53×10^{-2}	3.84×10^{-3}	3.83×10^{-3}	3.86×10^{-3}	1.06×10^{-2}	1.06×10^{-2}	1.06×10^{-2}	3.24×10^{-2}	3.24×10^{-2}	3.20×10^{-2}
303.15	1.77×10^{-2}	1.77×10^{-2}	1.79×10^{-2}	4.46×10^{-3}	4.47×10^{-3}	4.49×10^{-3}	1.33×10^{-2}	1.34×10^{-2}	1.35×10^{-2}	4.11×10^{-2}	4.12×10^{-2}	4.09×10^{-2}
308.15	2.07×10^{-2}	2.07×10^{-2}	2.08×10^{-2}	5.19×10^{-3}	5.21×10^{-3}	5.22×10^{-3}	1.70×10^{-2}	1.70×10^{-2}	1.71×10^{-2}	5.15×10^{-2}	5.18×10^{-2}	5.16×10^{-2}
313.15	2.41×10^{-2}	2.41×10^{-2}	2.41×10^{-2}	6.07×10^{-3}	6.06×10^{-3}	6.05×10^{-3}	2.15×10^{-2}	2.14×10^{-2}	2.14×10^{-2}	6.45×10^{-2}	6.43×10^{-2}	6.46×10^{-2}
318.15	2.81×10^{-2}	2.81×10^{-2}	2.78×10^{-2}	7.04×10^{-3}	7.03×10^{-3}	6.99×10^{-3}	2.69×10^{-2}	2.69×10^{-2}	2.67×10^{-2}	7.91×10^{-2}	7.91×10^{-2}	8.01×10^{-2}

^a Standard uncertainties u are $u(T) = 0.02 \text{ K}$, $u(p) = 400 \text{ Pa}$, the relative standard uncertainty of mole solubility u_r is $u_r(x) = 0.06$.

It can be easily found that the mole fraction solubility of ethyl candesartan increases with the rising temperature in all solvents. The solubility values of ethyl candesartan were found to be maximum in DMF (7.91×10^{-2}), followed by cyclohexanone (2.81×10^{-2}), 1,4-dioxanone (2.688×10^{-2}), acetone (7.04×10^{-3}), ethyl acetate (4.20×10^{-3}), *n*-propanol (3.69×10^{-3}), isobutanol (3.38×10^{-3}), methanol (3.17×10^{-3}), *n*-butanol (3.03×10^{-3}), ethanol (2.83×10^{-3}), isopropanol (2.69×10^{-3}), and acetonitrile (1.15×10^{-2}) at a temperature of 318.15 K. Similar results of solubility sequence from large to small were also obtained in other temperatures.

In alcohols, there is no obvious regularity in the order of molar fraction solubility. However, the mass fraction solubility shows a certain degree of trend at 318.15 K; the maximum data was observed in methanol, and the minimum was found in *n*-butanol. As can be seen from Table 2, there is little difference in the solubility of mole fractions in alcohols, and the trend of solubility curve is affected by the molecular weight of the solvent. The order of mole fraction solubility values in non-alcoholic solvents, from large to small, is DMF > cyclohexanone > 1,4-dioxanone > acetone > ethyl acetate > acetonitrile. Through the analysis of solvent properties in non-protonic select solvents, it was found that the order of solubility is consistent with the sequence of hydrogen bond basicity (β) with the exception of 1,4-dioxane and acetone ($\beta_{\text{DMF}} = 0.69$, $\beta_{\text{cyclohexanone}} = 0.53$, $\beta_{1,4\text{-dioxane}} = 0.37$, $\beta_{\text{acetone}} = 0.43$, $\beta_{\text{ethyl acetate}} = 0.45$ and $\beta_{\text{acetonitrile}} = 0.40$). This phenomenon could also be observed with the values of dipolarity/polarizability (π^*) except in 1,4-dioxane and acetonitrile ($\pi^*_{\text{DMF}} = 0.88$, $\pi^*_{\text{cyclohexanone}} = 0.76$, $\pi^*_{1,4\text{-dioxane}} = 0.55$, $\pi^*_{\text{acetone}} = 0.71$, $\pi^*_{\text{ethyl acetate}} = 0.55$ and $\pi^*_{\text{acetonitrile}} = 0.75$) [20]. In aprotic solvents, except for individual solvents, the solubility data decreases with the decreasing values of β and π^* , which indicates that the dissolution process of ethyl candesartan in selected pure solvents is complicated, which may be caused by some combination of multiple factors. By ana-

lyzing the molecular structure of the solute, it can be found that the -NH structure on the heterocycle, as the only hydrogen proton donor, forms a hydrogen bond with the solvent molecule. Especially in polar aprotic solvents, solute molecules play the role of Lewis acid.

3.3. Correlation Section

Based on the non-ideal solution, the modified Apelblat equation, Equation (1), has already been one of the most commonly and widely used models in solubility correlation, especially in engineering applications. It has a high accuracy to describe the function between the solubility data and temperature in Kelvin, which can be expressed as follows [21–25]:

$$\ln x_{w,T} = A + \frac{B}{T} + C \ln T \quad (1)$$

where $x_{w,T}$ is the mole fraction solubility of ethyl candesartan in different solvents at temperature T in Kelvin. A , B , and C refer to the equation parameters.

The λh equation is another semi-empirical equation, which can also provide a good description of the solid–liquid equilibrium in different solvents, as presented in Equation (2) [26–28]:

$$\ln \left[1 + \frac{\lambda(1-x)}{x} \right] = \lambda h \left(\frac{1}{T} - \frac{1}{T_m} \right) \quad (2)$$

where λ and h are equation parameters, and T_m is the melting temperature of ethyl candesartan, 432.15 K, cited from ref. [29].

In order to evaluate the fitting accuracy and applicability of the selected two models and for ethyl candesartan, the average relative deviation (ARD) was proposed to compare the correlation results and is shown in Equation (3):

$$ARD = \frac{1}{N} \sum_{i=1}^N \left| \frac{x_i^e - x_i^c}{x_i^e} \right| \quad (3)$$

In Equation (3), N is the number of experimental points in each solvent. x_i^e and x_i^c refer to the experimental and calculated mole fraction solubility values. The values of ARD along with model parameters are listed in Table 3. All values of ARD in the modified Apelblat equation are smaller than that in the λh equation. Moreover, the largest ARD data in the modified Apelblat equation is 1.9% and observed in isopropanol; the maximum data in the λh equation is 4.3% and found in *n*-butanol. The results may indicate two selected models can provide a satisfactory correlation solubility of ethyl candesartan as crucial data and model parameters in the industrial production process, while the modified Apelblat equation shows the more suitable correlation with experimental data of ethyl candesartan in selected pure solvents at all investigated temperatures.

Table 3. The results of model parameters along with ARD values.

Solvent	Modified Apelblat Equation			λh Equation			
	A	B	C	$10^2 ARD$	100λ	h	$10^2 ARD$
Methanol	358.1	−20,259.5	−52.1	1.1	16.2	28,930.2	3.6
Ethanol	226.9	−14,430.3	−32.5	0.7	14.5	32,637.8	2.5
<i>n</i> -Propanol	193.6	−12,615.4	−27.7	1.3	13.5	32,011.2	2.5
Isopropanol	340.4	−19,633.8	−49.4	1.9	15.5	31,305.1	2.9
<i>n</i> -Butanol	428.4	−23,457.7	−62.6	0.8	17.2	27,923.4	4.3
Isobutanol	320.3	−18,454.9	−46.5	0.6	15.6	29,266.2	3.8
Ethyl Acetate	−37.3	−1822.6	6.5	0.7	8.4	43,701.2	0.9
Acetonitrile	295.4	−17,202.8	−43.0	0.9	4.3	101,448.0	3.1
Cyclohexanone	−78.8	945.9	12.5	0.3	22.9	11,560.7	0.5
Acetone	−79.8	958.6	12.5	0.4	5.2	49,105.4	0.5
1,4-Dioxane	−75.2	−522.7	12.7	0.5	100.5	4352.1	0.7
DMF	113.4	−8933.7	−15.2	0.5	359.8	1255.3	1.0

3.4. Quantitative Analysis of Interactions

The solute–solvent interactions are important parameters for the estimation of the solubility of the solute in a given solvent system. In this work, different parameters were used to quantify the solute–solvent interactions that occurred in the dissolution process, including Abraham solvation parameters (AP_i), Hansen solubility parameters (HP_i), and Catalan parameters (CP_i). [30,31] The numerical values of AP_i , HP_i , and CP_i for the investigated solvents were tabulated in Table 4 [30–33]. The combined model could be presented as:

$$\ln x = \left(\alpha_0 + \sum_{i=1}^5 \alpha_{i,Ab} AP_i + \sum_{i=1}^3 \alpha_{i,HP} HP_i + \sum_{i=1}^4 \alpha_{i,CP} CP_i \right) + \left(\frac{\beta_0 + \sum_{i=1}^5 \beta_{i,Ab} AP_i + \sum_{i=1}^3 \beta_{i,HP} HP_i + \sum_{i=1}^4 \beta_{i,CP} CP_i}{T} \right) \quad (4)$$

where α and β terms are the model parameters computed using regression analysis. Equation (4) was obtained from combining the van't Hoff model and the AP_i , HP_i , and CP_i parameters. The significant ($p < 0.05$) variables which are obtained from the regression analysis of solubility data in mono solvents at various temperatures is:

$$\ln x = (-23.416(\pm 4.851) + 6.22(\pm 1.075)v + 0.528(\pm 0.062)\delta_h - 2.02(\pm 0.345)SA) + \left(\frac{5111.558(\pm 1460.518) - 662.582(\pm 69.119)c + 279.251(\pm 13.462)s - 128.103(\pm 6.114)b - 2514.547(\pm 325.425)v - 142.667(\pm 18.05)\delta_h + 3594.333(\pm 224.505)SP}{T} \right) \quad (5)$$

where c , s , and v are AP_i parameters, δ_h is the HP_i parameter, and SA and SP are CP_i parameters. The quantitative analysis of solvent–solute interactions is presented in Equation (5) with $R = 0.995$ ($N = 106$). The resulted ARD values for back-calculated solubility data using Equation (5) are listed in Table 5; moreover, the predicted values are presented as well. The maximum (20.6%) and minimum (3.3%) ARD values were observed for *n*-propanol and isopropanol data sets. The reasons for large ARD data could be related to the error in the experimental solubility determinations, inaccurate values of AP_i , HP_i , and CP_i parameters, and some other undefined errors. In addition, the proposed model possesses some weakness in cross validation, since it employs lots of model parameters; however, it is a starting point to model the solubility data in mono solvents at various temperatures using a single linear model.

Table 4. The numerical values of Abraham solvation parameters (AP_i), Hansen solubility parameters (HP_i), and Catalan parameters ^a.

Solvent	Abraham					Hansen			Catalan				
	<i>c</i>	<i>e</i>	<i>s</i>	<i>a</i>	<i>b</i>	<i>v</i>	δ_d	δ_p	δ_h	<i>SP</i>	<i>SdP</i>	<i>SA</i>	<i>SB</i>
Methanol	0.28	0.33	−0.71	0.24	−3.32	3.55	15.10	12.30	22.3	0.61	0.9	0.61	0.55
Ethanol	0.22	0.47	−1.04	0.33	−3.6	3.86	15.75	8.90	19.61	0.64	0.78	0.4	0.66
<i>n</i> -Propanol	0.13	0.38	−0.92	0.42	−3.49	3.82	16.00	6.80	17.40	0.66	0.75	0.37	0.78
Isopropanol	0.10	0.34	−1.05	0.41	−3.83	4.03	15.8	6.10	16.40	0.63	0.81	0.28	0.83
<i>n</i> -Butanol	0.17	0.40	−1.01	0.06	−3.96	4.04	16.00	5.70	15.80	0.67	0.66	0.34	0.81
Isobutanol	0.19	0.35	−1.13	0.02	−3.57	3.97	15.80	5.70	14.50	0.66	0.71	0.22	0.89
Ethyl Acetate	0.33	0.37	−0.45	−0.70	−4.90	4.15	15.80	5.30	7.20	0.66	0.60	0.00	0.54
Acetonitrile	0.41	0.08	0.33	−1.57	4.39	3.36	11.59	12.95	16.34	0.65	0.97	0.04	0.29
Cyclohexanone	0.04	0.23	0.06	−0.98	−4.84	4.32	17.80	6.30	5.10	0.77	0.75	0.00	0.48
Acetone	0.31	0.31	−0.12	−0.61	−4.75	3.94	15.50	10.40	7.00	0.65	0.91	0.00	0.48
1,4-Dioxane	0.10	0.35	−0.08	−0.56	−4.83	4.17	19.00	1.80	7.40	0.74	0.31	0.00	0.44
<i>N,N</i> -Dimethylformamide	−0.31	−0.06	0.34	0.36	−4.87	4.49	17.4	13.70	11.3	0.76	0.98	0.03	0.61

^a cited from Refs. [30–33].

Table 5. The values of back-calculated logarithmic solubility data using Equation (5) along with ARD results.

T	Solvent							
	lnx	lnx (Pred)	lnx	lnx (Pred)	lnx	lnx (Pred)	lnx	lnx (Pred)
	Methanol		Ethanol		<i>n</i> -Propanol		Isopropanol	
278.15	-7.87	-7.91	-8.03	-8.08	-7.57	-7.39	-8.08	-8.11
283.15	-7.55	-7.61	-7.67	-7.75	-7.31	-7.11	-7.78	-7.79
288.15	-7.26	-7.32	-7.38	-7.44	-7.01	-6.83	-7.49	-7.49
293.15	-6.93	-7.04	-7.09	-7.14	-6.71	-6.56	-7.16	-7.19
298.15	-6.63	-6.76	-6.8	-6.85	-6.45	-6.31	-6.85	-6.91
303.15	-6.39	-6.50	-6.53	-6.57	-6.23	-6.06	-6.57	-6.64
308.15	-6.16	-6.25	-6.31	-6.3	-6.01	-5.82	-6.34	-6.37
313.15	-5.95	-6.00	-6.09	-6.04	-5.81	-5.58	-6.12	-6.11
318.15	-5.75	-5.76	-5.87	-5.78	-5.6	-5.36	-5.92	-5.86
ARD	7.0%		5.3%		20.6%		3.3%	
	<i>n</i> -Butanol		Isobutanol		Ethyl Acetate		Acetonitrile	
278.15	-7.98	-7.82	-7.76	-7.87	-7.14	-7.09	-8.72	-8.62
283.15	-7.62	-7.51	-7.46	-7.58	-6.94	-6.85	-8.44	-8.36
288.15	-7.31	-7.22	-7.12	-7.31	-6.73	-6.62	-8.16	-8.11
293.15	-6.97	-6.94	-6.82	-7.04	-6.5	-6.41	-7.85	-7.87
298.15	-6.68	-6.66	-6.56	-6.78	-6.28	-6.19	-7.59	-7.63
303.15	-6.42	-6.4	-6.31	-6.52	-6.07	-5.99	-7.36	-7.41
308.15	-6.2	-6.14	-6.09	-6.28	-5.86	-5.79	-7.14	-7.19
313.15	-5.99	-5.9	-5.88	-6.04	-5.67	-5.6	-6.95	-6.98
318.15	-5.8	-5.66	-5.69	-5.82	-5.47	-5.42	-6.76	-6.77
ARD	8.4%		15.7%		8.1%		4.8%	
	Cyclohexanone		Acetone		1,4-Dioxane		<i>N,N</i> -Dimethylformamide	
278.15	-4.84	-5	-6.21	-6.32			-4.54	-4.45
283.15	-4.67	-4.8	-6.04	-6.12			-4.23	-4.18
288.15	-4.5	-4.61	-5.87	-5.93	-5.05	-4.81	-3.95	-3.93
293.15	-4.34	-4.43	-5.72	-5.75	-4.79	-4.62	-3.67	-3.69
298.15	-4.18	-4.25	-5.56	-5.57	-4.55	-4.44	-3.43	-3.45
303.15	-4.04	-4.08	-5.41	-5.4	-4.32	-4.26	-3.19	-3.22
308.15	-3.88	-3.91	-5.26	-5.23	-4.07	-4.08	-2.97	-3
313.15	-3.72	-3.75	-5.1	-5.07	-3.84	-3.92	-2.74	-2.79
318.15	-3.57	-3.6	-4.96	-4.92	-3.62	-3.75	-2.54	-2.58
ARD	7.3%		4.3%		12.0%		3.9%	

4. Conclusions

The mole fraction solubility of ethyl candesartan in selected mono solvents within the temperature range of 278.15 to 318.15 K was measured. The largest solubility data of ethyl candesartan were found in DMF, followed by cyclohexanone, 1,4-dioxanone, acetone, ethyl acetate, *n*-propanol, isobutanol, methanol, *n*-butanol, ethanol, isopropanol, and acetonitrile at each temperature. In aprotic solvents, except for individual solvents, the solubility data decreases with the decreasing values of hydrogen bond basicity (β) and dipolarity/polarizability (π^*). The results of statistical analysis show that the modified Apelblat equation is the more suitable correlation of experimental data for ethyl candesartan in selected mono solvents at all investigated temperatures. Moreover, the results may indicate the selected two models can provide satisfactory correlation solubility of ethyl candesartan as crucial data and model parameters in the industrial production process

Funding: This research received no external funding.

Data Availability Statement: Data are contained within the article.

Acknowledgments: This paper is in memory of the first anniversary of the death of my grandfather (Fangshan Du). As time flies, you have been away for a year. I miss you very much and wish you all the best in heaven.

Conflicts of Interest: The author declares no conflict of interest.

References

1. Troficiuk, E.; Wielgat, P.; Braszko, J.J. Candesartan, angiotensin II type 1 receptor blocker is able to relieve age-related cognitive impairment. *Pharmacol. Rep.* **2018**, *70*, 87–92. [[CrossRef](#)] [[PubMed](#)]
2. Usama, F.A.; Hatem, A.S.; Taha, F.S.A.; Hosny, A.E.S. Applying different techniques to improve the bioavailability of candesartan cilexetil antihypertensive drug. *Drug Des. Dev. Ther.* **2020**, *14*, 1851–1865.
3. Qin, H.L.; Liu, J.; Fan, X.Q. Synthesis Process for Candesartan Cilexetil. Chinese Patent Application No. 113,912,588, 11 January 2022.
4. Naka, T.; Nishikawa, K.; Kato, T. Benzimidazole Derivatives, Their Production and Use and Use as Angiotensin II Antagonists. European Patent Application No. 0720982, 10 July 1996.
5. Wang, P.; Zheng, G.; Wang, Y.; Wang, X.J.; Li, Y.; Xiang, W.S. A novel and practical synthesis of substituted 2-ethoxy benzimidazole: Candesartan cilexetil. *Tetrahedron* **2010**, *66*, 5402–5406. [[CrossRef](#)]
6. Kocienski, P. Synthesis of Candesartan Cilexetil. *Synfacts* **2013**, *9*, 0006. [[CrossRef](#)]
7. Wang, Y.P.; Li, Y.G.; Li, Y.L.; Zheng, G.J.; Li, Y.; Koecher, S. Process for the Production of Candesartan. U.S. Patent Application No. 2,008,114,045, 15 May 2008.
8. Rahman, N.; Azmi, S.N.H.; Wu, H.F. The importance of impurity analysis in pharmaceutical products: An integrated approach. *Accredit. Qual. Assur.* **2006**, *11*, 69–74. [[CrossRef](#)]
9. Capellades, G.; Bonsu, J.O.; Myerson, A.S. Impurity incorporation in solution crystallization: Diagnosis, prevention and control. *CrystEngComm* **2022**, *24*, 1989–2001. [[CrossRef](#)]
10. Shakeel, F.; Haq, N.; Alanazi, F.K.; Alanazi, S.A.; Alsarra, I.A. Solubility of sinapic acid in various (Carbitol + water) systems: Computational modeling and solution thermodynamics. *J. Therm. Anal. Calorim.* **2020**, *142*, 1437–1446. [[CrossRef](#)]
11. Alshehri, S.; Shakeel, F.; Alam, P.; Pena, A.; Jouyban, A.; Martinez, F. Effect of temperature and polarity on the solubility and preferential solvation of sinapic acid in aqueous mixtures of DMSO and Carbitol. *J. Mol. Liq.* **2021**, *340*, 117268. [[CrossRef](#)]
12. Shakeel, F.; Haq, N.; Alam, P.; Jouyban, A.; Ghoneim, M.M.; Alshehri, S.; Martine, F. Solubility of sinapic acid in some (ethylene glycol + water) mixtures: Measurement, computational modeling, thermodynamics and preferential solvation. *J. Mol. Liq.* **2022**, *348*, 118057. [[CrossRef](#)]
13. Chen, Y.H.; Luo, Z.Y.; Ren, Z.X.; Shen, L.B.; Li, R.R.; Chen, L.; Du, C.B. The interactions and thermodynamic parameters of lenvatinib mesylate in pure and mixed solvents at several temperatures. *J. Chem. Thermodyn.* **2022**, *176*, 106922. [[CrossRef](#)]
14. Shakeel, F.; Haq, N.; Alanazi, F.K.; Alsarra, I.A. Solubility and thermodynamics of apremilast in different mono solvents: Determination, correlation and molecular interactions. *Int. J. Pharm.* **2017**, *523*, 410–417. [[CrossRef](#)] [[PubMed](#)]
15. Li, R.R.; Jin, Y.X.; Yu, B.B.; Xu, Q.Q.; Chen, X.L.; Han, D.M. Solubility determination and thermodynamic properties calculation of macitentan in mixtures of ethyl acetate and alcohols. *J. Chem. Thermodyn.* **2021**, *156*, 106344. [[CrossRef](#)]
16. Du, C.B.; Luo, Y.L.; Huang, C.Y.; Li, R.R. The solubility measurement and thermodynamic models correlation of baclofen in twelve pure organic solvents. *J. Chem. Eng. Data* **2022**, *67*, 2655–2661. [[CrossRef](#)]
17. Li, R.R.; Tang, T.; Yin, X.F.; Yao, L.S.; Lin, Z.P.; Zhang, L.; Gao, X.; Xu, X.J.; Zhao, J.; Han, D.M. Solubility of Naftopidil in pure and mixed solvents at 273.15 to 313.15 K and its correlation with the Jouyban-Acree and CNIBS/R-K models. *J. Chem. Thermodyn.* **2020**, *145*, 105969. [[CrossRef](#)]
18. Li, R.R.; Yin, X.F.; Jin, Y.X.; Chen, X.L.; Zhao, B.; Wang, W.; Zhong, S.Y.; Han, D.M. The solubility profile and dissolution thermodynamic properties of minocycline hydrochloride in some pure and mixed solvents at several temperatures. *J. Chem. Thermodyn.* **2021**, *157*, 106399. [[CrossRef](#)]
19. Du, C.B.; Li, R.R.; Chen, L. Dissolution thermodynamic properties calculation and intermolecular interaction analysis of diacerein in different pure and mixed solvents. *J. Chem. Thermodyn.* **2022**, *173*, 106850. [[CrossRef](#)]
20. Marcus, Y. The properties of organic liquids that are relevant to their use as solvating solvents. *Chem. Soc. Rev.* **1993**, *22*, 409–416. [[CrossRef](#)]
21. Apelblat, A.; Manzurola, E. Solubilities of L-aspartic, DL-aspartic, DL-glutamic, p-hydroxybenzoic, o-anisic, p-anisic and itaconic acids in water from T = 278 K to T = 345 K. *J. Chem. Thermodyn.* **1997**, *29*, 1527–1533. [[CrossRef](#)]
22. Apelblat, A.; Manzurola, E. Solubilities of o-acetylsalicylic, 4-aminosalicylic, 3,5-dinitrosalicylic, and p-toluic acid and magnesium-DL-aspartate in water from T = (278 to 348) K. *J. Chem. Thermodyn.* **1999**, *31*, 85–91. [[CrossRef](#)]
23. Li, R.R.; Wang, W.; Chen, X.L.; Chen, H.; Bao, H.H.; Zhu, Y.W.; Zhao, J.; Han, D.M. Equilibrium solubility determination and correlation of monobenzene in fifteen monosolvents at a series of temperatures. *J. Chem. Eng. Data* **2020**, *65*, 2300–2309. [[CrossRef](#)]
24. Yu, S.; Cheng, Y.; Feng, W.; Xing, W.; Li, H.; Xue, F. Solid-liquid phase equilibrium and thermodynamic properties analysis of 2,4,5-trimethoxybenzaldehyde in mono-solvents. *J. Chem. Thermodyn.* **2021**, *163*, 106609. [[CrossRef](#)]
25. Tian, N.; Yu, C.; Du, S.; Lin, B.; Gao, Y.; Gao, Z. Solubility Measurement and Data Correlation of Isatoic Anhydride in 12 Pure Solvents at Temperatures from 288.15 to 328.15 K. *J. Chem. Eng. Data* **2020**, *65*, 2044–2052. [[CrossRef](#)]
26. Buchowski, H.; Ksiazczak, A.; Pietrzyk, S. Solvent activity along a saturation line and solubility of hydrogen-bonding solids. *J. Phys. Chem.* **1980**, *84*, 975–979. [[CrossRef](#)]
27. Buchowski, H.; Khaiat, A. Solubility of solids in liquids: One-parameter solubility equation. *Fluid Phase Equilib.* **1986**, *25*, 273–278. [[CrossRef](#)]

28. He, Z.C.; Zhang, J.Y.; Gao, X.; Tang, T.; Yin, X.F.; Zhao, J.; Li, R.R.; Han, D.M. Solubility Determination, Correlation, and Solute-Solvent Molecular Interactions of 5-Aminotetrazole in Various Pure Solvents. *J. Chem. Eng. Data* **2019**, *64*, 3988–3993. [[CrossRef](#)]
29. Cao, R.H.; Zhong, Q.H.; Peng, W.L.; Xu, A.L. Synthesis of candesartan axetil. *Chin. J. Pharm.* **2003**, *34*, 425–427.
30. Jouyban, A.; Rahimpour, E.; Karimzadeh, Z. A new correlative model to simulate the solubility of drugs in mono-solvent systems at various temperatures. *J. Mol. Liq.* **2021**, *343*, 117587. [[CrossRef](#)]
31. Catalán, J. Toward a generalized treatment of the solvent effect based on four empirical scales: Dipolarity (SdP, a new scale), polarizability (SP), acidity (SA), and basicity (SB) of the medium. *J. Phys. Chem. B* **2009**, *113*, 5951–5960. [[CrossRef](#)]
32. Hansen, C.M. *Hansen Solubility Parameters: A User's Handbook*; CRC Press: Boca Raton, FL, USA, 2007.
33. Chen, L.; Shen, L.B.; Chen, Y.H.; Luo, Z.Y.; Ren, Z.X.; Li, R.R.; Du, C.B. The solubility profile and intermolecular force analysis of nimesulide (form I) in mono and mixed solvents at several temperatures. *J. Chem. Eng. Data*, 2022; *accepted*. [[CrossRef](#)]

Article

Using Two Group-Contribution Methods to Calculate Properties of Liquid Compounds Involved in the Cyclohexanone Production Operations

Luis Fernández ¹, Juan Ortega ^{1,*}, Leandro Domínguez ¹, David Lorenzo ², Aurora Santos ^{2,*} and Arturo Romero ²

¹ Thermal Engineering & Instrumentation Division (IDeTIC), Universidad de Las Palmas de Gran Canaria, 35017 Las Palmas de Gran Canaria, Spain

² Chemical Engineering and Materials Department, Universidad Complutense de Madrid, 28040 Madrid, Spain

* Correspondence: juan.ortega@ulpgc.es (J.O.); aurasan@ucm.es (A.S.)

Abstract: A numerical application has been carried out to determine the thermophysical properties of more than fifty pure liquid compounds involved in the production process of cyclohexanone, whose real values are unknown, in many cases. Two group-contribution methods, the Joback and the Marrero–Gani methods, both used in the fields of physicochemistry and engineering, are employed. Both methods were implemented to evaluate critical properties, phase transition properties, and others, which are required for their use in industrial process simulation/design. The quality of the estimates is evaluated by comparing them with those from the literature, where available. In general, both models provide acceptable predictions, although each of them shows improvement for some of the properties considered, recommending their use, when required.

Keywords: cyclohexanone; group-contribution methods; Joback method; Marrero–Gani method

Citation: Fernández, L.; Ortega, J.; Domínguez, L.; Lorenzo, D.; Santos, A.; Romero, A. Using Two Group-Contribution Methods to Calculate Properties of Liquid Compounds Involved in the Cyclohexanone Production Operations. *Liquids* **2022**, *2*, 413–431. <https://doi.org/10.3390/liquids2040024>

Academic Editor: Enrico Bodo

Received: 31 October 2022

Accepted: 18 November 2022

Published: 23 November 2022

Publisher's Note: MDPI stays neutral with regard to jurisdictional claims in published maps and institutional affiliations.



Copyright: © 2022 by the authors. Licensee MDPI, Basel, Switzerland. This article is an open access article distributed under the terms and conditions of the Creative Commons Attribution (CC BY) license (<https://creativecommons.org/licenses/by/4.0/>).

1. Introduction

In a previous work [1], an exhaustive analysis was carried out on the possibilities of the separation of a set of substances generated in the production process of cyclohexanone, the base compound for the manufacture of nylon-6, used in the textile industry. However, the indicated process is not direct, intermediate processes being necessary to obtain ϵ -caprolactam, a precursor of nylon-6. Therefore, the production of cyclohexanone as a raw material for different industrial processes, including different types of nylon, is high, currently at approximately 6 MTm/year [2]. In addition, the quality requirements of the cyclic ketone are also high, and the purification process from cyclohexane is complex, as shown in Figure 1. This makes it necessary to optimize the different separation stages, both technically and economically, whose performance represents an important area of work in the field of chemical engineering, requiring an appropriate modeling with the support of the mathematics-thermodynamics binomial.

According to Figure 1, cyclohexanone is obtained by the oxidation of cyclohexane, producing, in addition to cyclohexanone, cyclohexanol, cyclohexyl hydroperoxide, and many other compounds, in smaller proportion. The last-mentioned compound is recon-verted (after washing with water and alkalis) into the first two, after removing undesirable compounds by decantation. The resulting solution is subjected to distillation, separating the unreacted cyclohexane in the first unit and recycled into the initial process unit, while the cyclohexanol is dehydrogenated to convert it to cyclohexanone. The aforementioned operations, as defined, suggest a simple development of the global process; however, the current development of the process is quite different due to the formation, during the different stages, of many compounds (more than fifty, although they are considered secondary) that are produced from the beginning with the oxidation of cyclohexane, and in varying quantities, some of them unidentified up until now [3–10].

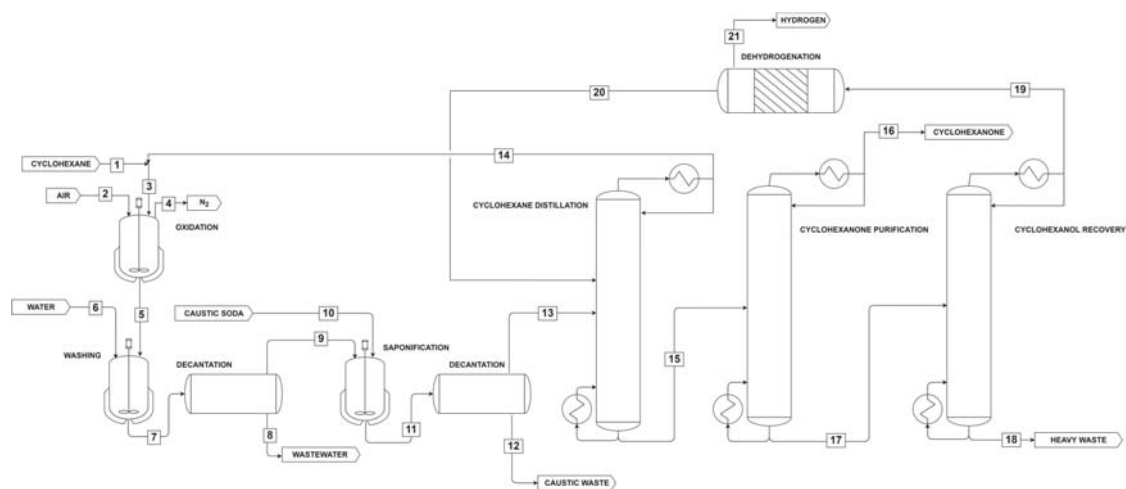


Figure 1. Scheme indicating the different operation units existing in the cyclohexanone production process.

Many of the compounds discovered in various cyclohexanone production plants are shown in Appendix A, indicating the process streams in which they are found. Some of these substances do not pose a problem for the quality of cyclohexanone, either because they are easy to separate, e.g., cyclohexane (streams 1, 3, 5, 7, 9, 11) or cyclohexylidene-cyclohexanone (stream 16), see Figure 1, or because they are only present when the process operates outside its normal conditions, such as 5-hexenal (stream 19 in Figure 1). However, other substances are likely to contaminate cyclohexanone, creating the need to design appropriate separation operations to remove the most undesirable substances. Appendix B shows a list of substances that influence the global process, including some common substances, such as phenol and toluene, as well as many others that are unusual and little studied, whose properties are unknown. In any case, the design of separation processes depends on the availability of the physicochemical information for the substances involved, as well as their solutions. The most important information required, such as boiling temperatures, enthalpies of change of state, thermal capacities, and critical properties, among others, are used to define the corresponding operation units.

The necessary information is obtained through direct experimentation and with appropriate equipment; however, these actions are costly, both in terms of money and time. Without ignoring the importance of experimental work, in the chemical engineering field, the theoretical estimation methods are sometimes used to generate approximate values of the properties involved in the design of operations. In the literature [11–15], there are many methods for estimating the thermophysical properties of pure substances and solutions; of these, the so-called “group contribution methods” (GCM) prove to be useful and easy to use in practical engineering cases. A GCM is generated as a mathematical tool that combines the particular contributions of each of the functional groups present in the molecules of a compound/system to the calculation of a given thermophysical property. In a previous work [1], the Joback method [14] was used to discriminate between positional isomers, but an exhaustive assessment of the reliability of the estimates was not performed.

Once the necessity of certain properties of a large number of substances—more than fifty involved in the global process, shown in Figure 1—is known, the goal of this work is to estimate these requirements to achieve the process design. For this, two GCM procedures were used: the Joback, previously mentioned, and the Marrero–Gani [15], checking the results to determine their reliability given the different levels of theory of both methodolo-

gies, which will be quantified by comparing the predicted results with the values available in the literature.

2. Two Group-Contribution Methods for Estimating Properties of Pure Substances

The GCMs are based on the assumption that the properties of a chemical compound can be calculated by combining, by means of certain procedures (differing according to the method), the contribution to that property of the different “fragments” that make up its molecule. To do this, the molecule is broken down using “standardized” entities or “groups”, varying depending on the method. To each group (see Figures 2 and 3) is assigned a numerical parameter that quantifies its contribution to the studied property. This approach makes it possible to calculate the properties of a substance by determining the number of groups of each type present in the molecule and then applying a simple calculation defined by the corresponding method. In the first-order GCMs, the contribution of each group is assumed to be independent of its environment and of other groups. Therefore, by using experimental data of the compounds containing that group, the contribution of the parameter associated with it can be determined. In this way, the values obtained can be used to estimate the properties of other substances for which experimental information is not available.

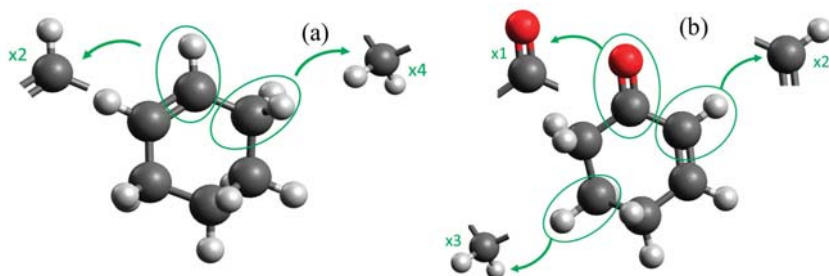


Figure 2. Decomposition of molecules according to the Joback method [14]. (a) Cyclohexene, (b) 2-cyclohexen-1-one.

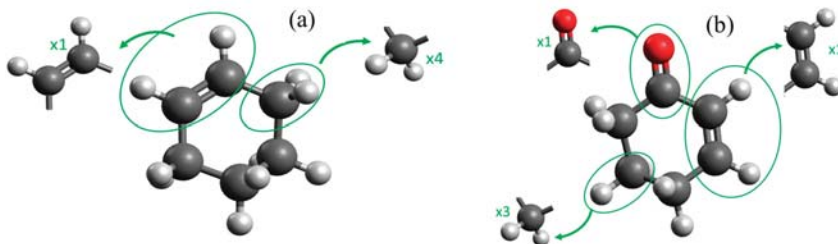


Figure 3. Decomposition of molecules according to Marrero–Gani method [15]. (a) Cyclohexene, (b) 2-cyclohexen-1-one.

One of the best known first-order methods for estimating the properties of pure substances is the Joback [14] method used in this work, since it has been shown to produce estimates with acceptable accuracy and, in addition, it can be applied to a wide variety of groups and properties, characteristics that justify its relevance as a tool in chemical engineering calculations.

The major drawback of the Joback method, and also of others classified as first-order methods, is that they do not differentiate the calculation for the case of molecules constituting the so-called position isomers. These methods are also unsuitable for complex molecules for which the chemical environment significantly influences the thermophysical behavior. These deficiencies are corrected by the higher-order qualified methods, as they

include additional groups produced by combinations of lower-order groups, and whose parameters take into account the effect caused by the chemical environment. Marrero and Gani [15] developed a method that includes groups of several levels (specifically three), producing acceptable results. Therefore, this method, along with the Joback method, is used in this work to determine the properties of the selected compounds, as described briefly in the following section, with examples illustrating the specific calculation procedures.

2.1. The Joback Method

In this procedure, the contributions of the groups generate a parameter in a characteristic equation defined for each property with which the estimation is achieved. The authors [14] provide equations for different thermophysical quantities, such as boiling temperatures T_b^o , melting temperatures T_m^o , enthalpies of changes of state, vaporization enthalpies Δh_v^o , melting enthalpies Δh_m^o , enthalpies of formation Δh_f^o , Gibbs energy formation Δg_f^o , isobaric thermal capacities, c_p , and critical properties; p_c , v_c , T_c . Table A1 of Appendix C compiles the calculation equations for each of these properties, showing the characteristic parameters of the groups of each property in the second column of the table, whose values are quantified [14]. To estimate the molecule's properties, it is broken down into the groups identified by Joback [14], as shown in Figure 2, with two specific cases taken as examples: cyclohexene and 2-cyclohexen-1-one. Once the groups have been identified and quantified, this method multiplies the parameter of each group by adding the value obtained for all the groups. With these values, the property is estimated using the expressions shown in the third column of Table A1. Table 1 shows the values obtained for the critical properties of the two species chosen in Figure 2, comparing the results with those from the literature, as indicated.

Table 1. Groups for cyclohexene and 2-cyclohexen-1-one, according to Joback method [14], and the contribution terms for critical properties. N_k is the number of groups in the molecules; $\tau_{c,k}$, $\pi_{c,k}$, $v_{c,k}$ are the contributing parameters corresponding to T_c , p_c , and v_c , respectively. The calculated values and those estimated by the procedure are shown.

Compounds	Groups	N_k	$\tau_{c,k}$	$\pi_{c,k}$	$v_{c,k}$
Cyclohexene	–CH ₂ –	4	0.0100	0.0025	48
	=CH–	2	0.0082	0.0011	41
	total:		0.0564	0.0122	274
	estimated → from ref. [16]		$T_c/K = 567$ $T_c/K = 560.4$	$p_c/\text{bar} = 43.3$ $p_c/\text{bar} = 48.41$	$v_c/\text{cm}^3 \cdot \text{mol}^{-1} = 291$ $v_c/\text{cm}^3 \cdot \text{mol}^{-1} = 377.4$
2-Cyclohexen-1-one	–CH ₂ –	3	0.0100	0.0025	48
	=CH–	2	0.0082	0.0011	41
	>C=O	1	0.0284	0.0028	55
	total:		0.0784	0.0125	281
	estimated → from ref. [17]		$T_c/K = 655$ $T_c/K = 685.0$	$p_c/\text{bar} = 45.3$ $p_c/\text{bar} = 45.30$	$v_c/\text{cm}^3 \cdot \text{mol}^{-1} = 298$ $v_c/\text{cm}^3 \cdot \text{mol}^{-1} = 304.9$

2.2. Marrero–Gani Method

This procedure [15], pointed out in the previous section as of higher order, uses groups in three different orders. The first-order groups correspond to those with a single functional group and divide the molecule into fragments similar to those used in the Joback method, e.g., linear alkanes and monofunctional compounds. Second-order groups are used to improve the estimation of branched and polyfunctional compounds, with a maximum of one aromatic ring; these groups are established by combining two or more functional groups. Lastly, third-order groups are used to represent polycyclic compounds and specific combinations of functional groups, allowing the method to make satisfactory estimates of complex molecules. As in the Joback method, the Marrero–Gani method allows the same properties to be estimated, with the exception of the isobaric thermal capacity. The corresponding mathematical equations of this procedure are presented in Appendix D.

The application of the method to the same compounds chosen as examples in Section 2.1 requires the generation of the groups in the molecules. Figure 3a shows that those with first-order groups corresponding to cyclohexene coincide with those in the Joback method (Figure 2a), with the addition of the second-order groups. However, 2-cyclohexen-1-one is a polyfunctional compound, containing both first- and second-order groups, as shown in Figure 2b. Table 2 shows the results obtained with the application of the Marrero–Gani method to the estimation of the critical properties of the two selected molecules, comparing the results with those from the literature.

Table 2. Groups for cyclohexene and 2-cyclohexen-1-one, according to Marrero–Gani method [15], and contribution parameters for critical properties. N_k is the number of groups in the molecules, and j is the group order. Calculated values and those estimated by the procedure are shown.

Compounds	Groups	j	N_k	$T_{c,i,j}$	$p_{c,i,j}$	$v_{c,i,j}$
Cyclohexene	CH ₂ (cyc)	1°	4	1.8815	0.009884	49.24
	CH=CH (cyc)	1°	1	3.6426	0.013815	83.91
	total:			11.1686	0.053351	280.87
	estimated→ from ref. [16]			$T_c/K = 558$ $T_c/K = 560.4$	$p_c/\text{bar} = 43.9$ $p_c/\text{bar} = 48.41$	$v_c/\text{cm}^3 \cdot \text{mol}^{-1} = 289$ $v_c/\text{cm}^3 \cdot \text{mol}^{-1} = 377.4$
2-Cyclohexen-1-one	CH ₂ (cyc)	1°	3	1.8815	0.009884	49.24
	CH=CH (cyc)	1°	1	3.6426	0.013815	83.91
	CO (cyc)	1°	1	12.6396	−0.000207	57.38
	total:			21.9267	0.043260	289.01
	estimated→ from ref. [17]			$T_c/K = 714$ $T_c/K = 685.0$	$p_c/\text{bar} = 49$ $p_c/\text{bar} = 45.30$	$v_c/\text{cm}^3 \cdot \text{mol}^{-1} = 297$ $v_c/\text{cm}^3 \cdot \text{mol}^{-1} = 304.9$

3. Evaluation of Estimates for the Selected Substances

The numerical results obtained for the different properties for all the compounds selected, estimated with the Joback and Marrero–Gani methods, are given in Appendix C (Table A2) and Appendix D (Table A5), respectively. A comparison with the values available in the literature is made in this section.

3.1. Evaluation of Temperatures and Enthalpies of Phase Transition

Figure 4a compares the values found [16–30] for the boiling temperatures, T_b^o , and the estimates obtained by both methods, showing the existence of a direct correlation. The Joback method produces greater dispersion in the results than does the Marrero–Gani method, which is reflected in a lower R^2 coefficient. The residuals yield an average error of 2.2% for the Joback method, and a slightly lower average error of 0.6% for the Marrero–Gani method, the average standard deviation of the former, 12.5 K, being higher than that of the latter, 4.5 K.

Figure 4b shows the comparison of the estimates made using both methods for the melting temperatures, T_m^o , in relation to the values found in the literature [16,23,24,29–40]. In general, both methods present estimates with a lower order than the T_b^o , the average errors for both methods being close to 9%, with average standard deviations of 32 K for the Joback method and 25 K for the Marrero–Gani method.

Figure 5a compares the estimates of enthalpies of vaporization, Δh_v^o with the literature values [16,20,24,41–48]. Both methods yield similar results, with average errors of 15.3%, for the Joback method, and 19.7%, for the Marrero–Gani method. The similarity is greater for the case of melting enthalpies, Δh_m^o [16,30,31,46–50], Figure 5b, yielding average error values of 15.9%, with Marrero–Gani method, and 16.9%, with the Joback method. However, in both cases, the determination coefficient for the melting enthalpy is very small.

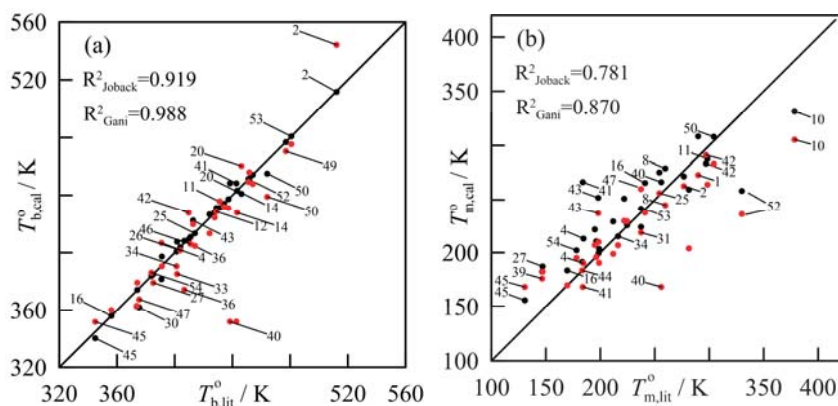


Figure 4. (a) Comparison between the boiling temperatures, $T_{b,lit}^0$, from literature and those estimated, $T_{b,calc}^0$, by the methods of Joback (●) and Marrero–Gani (●). (b) Analogous comparison for the melting temperatures. Labels correspond to the order of compounds established in Appendix B.

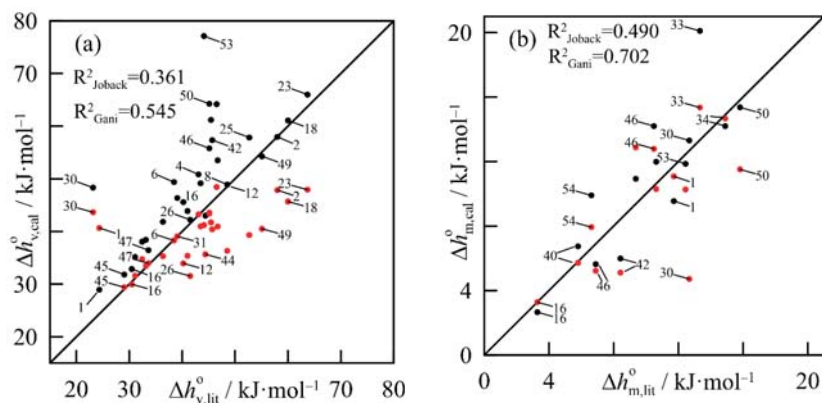


Figure 5. Comparison between the enthalpies of phase transition obtained by the methods of Joback (●) and Marrero–Gani (●) and those from the literature: (a) vaporization enthalpies; (b) melting enthalpies. Labels correspond to the order of compounds, as shown in Appendix B.

3.2. Critical Properties

Comparison with literature data [16,17,24,39,51–57] of the critical temperatures, T_c , is shown in Figure 6a–c, and the estimates are considered acceptable. The two methods show good experimental vs. model correlations; those of the Marrero–Gani method rise to an average error of 3.5%, compared to 2.9% according to the Joback method. In contrast, the critical pressure p_c is slightly better represented by the Marrero–Gani method (5.7%) than by the Joback method (6.2%). The results for the critical volume, v_c , yield errors of 5.9% (Marrero–Gani) and 4.6% (Joback), although the information for this property is currently scarce. Numerical values of all those properties are shown in Tables A2 and A5 of the Appendices C and D.

3.3. Estimation of Enthalpies of Formation and Thermal Capacities

The amount of information available for the enthalpies of formation, Δh_f^0 [16,24,58–67], and thermal capacities, c_p [16,50,64,68–73], is reduced for the set of selected compounds; therefore, the comments made in this work on these properties cannot be assessed generi-

cally. The estimation of Δh_f^0 is acceptable using both models, as shown in Figure 7a. The average errors are around 12% for the Joback method and much higher—21%—for the Marrero–Gani method. The estimation of the c_p s is only conducted using the Joback method (Figure 7b), with a systematic deviation that underestimates the value of the property with respect to the experimental values, showing an average error of more than 32%.

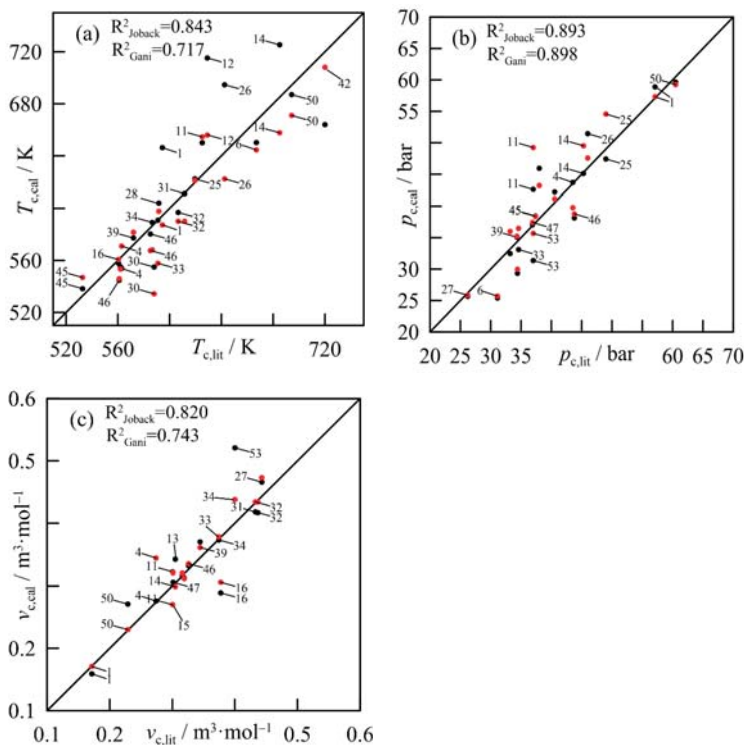


Figure 6. Comparison between the critical properties obtained from the literature and those calculated by the methods of Joback (●) and Marrero–Gani (●): (a) critical temperature; (b) critical pressure; (c) critical volume. Labels correspond to the order of compounds, as shown in Appendix B.

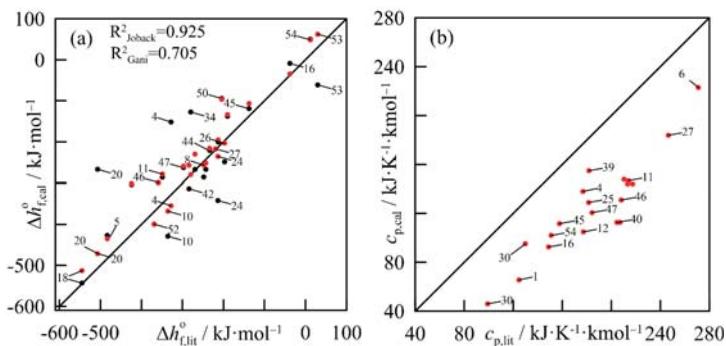


Figure 7. (a) Comparison between the enthalpies of formation obtained from literature and those calculated by the methods of Joback (●) and Marrero–Gani (●). (b) Comparison between the thermal capacities obtained from literature and those calculated by the Joback method. Labels correspond to the order of compounds, as shown in Appendix B.

4. Conclusions

Estimates are presented for different properties of a set of substances involved in the cyclohexanone production process, as obtained using two group-contribution methods: the Joback method [14] and the Marrero–Gani method [15]. The predictions made are evaluated by comparing the results with those available in the experimental research. The latter does not lead to a clear choice of one method over the other, as the comparisons made do not sufficiently clarify the preference.

The Marrero–Gani method has a higher level of theory, since it uses groups of different orders, which allows it to be used for isomeric compounds. In general, it produces better results for most properties, with the exception of the melting enthalpy, critical temperature, and critical volume, which are better represented by the Joback method. The latter can also be used to estimate thermal capacities. Despite these differences and the assessment of the small errors obtained with both methods, at least statistically, it is acceptable to use either of the two procedures. The major advantage of using the Joback method is that it is simpler, where appropriate.

In summary, the use of any of these methods provides a rapid and reasonably reliable approximation of the different properties required to address a given analysis or simulation in order to optimize the cyclohexanone production process. For a practical case, the methods used have served to estimate boiling temperatures and critical properties, which are important for evaluating the distillation process of the towers shown in Figure 1. Likewise, the approximation obtained for the enthalpies of phase change, especially those of vaporization and thermal capacities, facilitates the design of the heat exchangers, such as the reboilers and condensers of the towers mentioned. The properties corresponding to the enthalpies of formation and the Gibbs energies are involved in the prediction of the complex reactions that take place in the different stages of the global process.

Author Contributions: Conceptualization, J.O., L.F. and A.S.; methodology, L.F. and J.O.; software, L.F.; validation, J.O., A.S., A.R. and D.L.; formal analysis, L.D. and J.O.; investigation, J.O. and L.F.; resources, J.O. and L.F.; data curation, L.F.; writing—original draft preparation, L.F. and J.O.; writing—review and editing, J.O., D.L. and L.F.; visualization, L.F., J.O., L.D., A.S., D.L. and A.R.; supervision, J.O.; project administration, J.O.; funding acquisition, J.O. All authors have read and agreed to the published version of the manuscript.

Funding: This research received no external funding.

Data Availability Statement: The data used and presented in this work were calculated according to Appendices C and D.

Conflicts of Interest: The authors declare no conflict of interest.

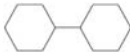
Appendix A. Compounds Present in the Streams of the Cyclohexanone Production Process

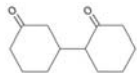
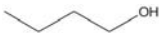
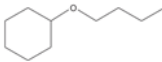
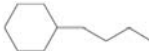
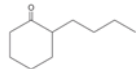
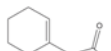
1. Cyclohexane feeding; cyclohexane, hydrocarbons.
2. Oxidant supply; air.
3. Entrance to oxidation; cyclohexane, hydrocarbons, cyclohexanone, cyclohexanol, light oxides.
4. Nitrogen.
5. Oxidation effluent; cyclohexane, cyclohexanone, cyclohexanol, light and heavy oxidized, peroxides, formic acid, acetic acid, other monocarboxylic acids, dicarboxylic acids, esters, butanol, pentanol, cyclopentanone, cyclopentanol, 2-pentanone, 2-cyclohexen-1-one, cyclohexene, 2-methylcyclopentanone, methylcyclopentanol, heptanones, 2-methyl-3-heptanone, 1,3-cyclohexanedione, 1,2-cyclohexanediol, methylcyclohexanols, ethers.
6. Washing water; water.
7. Washing emulsion; water, cyclohexane, cyclohexanone, cyclohexanol, light and heavy oxidized, peroxides, formic acid, acetic acid, other monocarboxylic acids, dicarboxylic acids, esters, butanol, pentanol, cyclopentanone, cyclopentanol, 2-pentanone, 2-cyclo-

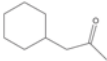
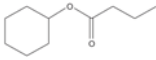
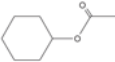
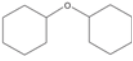
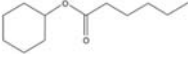
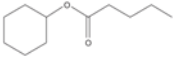
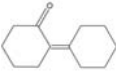
- hexen-1-one, cyclohexene, 2-methylcyclopentanone, 1-methylcyclopentanol, heptanones, 2-methyl-3-heptanone, 1,3-cyclohexanedione, 1,2-cyclohexanediol, methylcyclohexanols, ethers.
8. Acid water; water, formic acid, acetic acid, other monocarboxylic acids.
 9. Oxidized product; cyclohexane, cyclohexanone, cyclohexanol, light and heavy oxidized, peroxides, monocarboxylic acids, dicarboxylic acids, esters, butanol, pentanol, cyclopentanone, cyclopentanol, 2-pentanone, 2-cyclohexen-1-one, cyclohexene, 2-methyl cyclopentanone, 1-methylcyclopentanol, heptanones, 2-methyl-3-heptanone, 1,3-cyclohexanedione, 1,2-cyclohexanediol, methylcyclohexanols, ethers.
 10. Alkali; water, sodium hydroxide.
 11. Saponification emulsion; water, sodium hydroxide, cyclohexane, cyclohexanone, cyclohexanol, light and heavy oxidized, peroxides, monocarboxylic acids, dicarboxylic acids, esters, butanol, pentanol, cyclopentanone, cyclopentanol, 2-pentanone, cyclohexenone, cyclohexene, methylcyclopentanone, methylcyclopentanol, heptanones, methylheptanone, cyclohexanedione, cyclohexanediol, methylcyclohexanols, ethers.
 12. Sodium salts; sodium hydroxide, sodium salts.
 13. Saponified product; sodium hydroxide, cyclohexanone, cyclohexanol, light oxidized.
 14. Cx I recycle; cyclohexanone, cyclohexanol, light oxides.
 15. KA-Oil; cyclohexanone, cyclohexanol, oxides, alcohols, aldehydes and ketones.
 16. Purified cyclohexanone; butanol, pentanol, cyclopentanol, cyclopentanone, 5-hexenal, hexanal, 2-hexanone, cyclohexanone, cyclohexanol, 2-cyclohexen-1-one, heptanones, methylcyclohexanones, butylcyclohexane, cyclohexyl-butyl-ether.
 17. Residue from the purification of cyclohexanone; cyclohexanol, 2-cyclohexen-1-one, 2-cyclohexen-1-ol, heptanones, methylcyclohexanones, butylcyclohexane, cyclohexyl-butyl-ether, cyclohexene oxides, cyclohexylidene-cyclohexanone, cyclohexanone oligomers, pentylcyclohexane, cyclohexyl acetate, other light/heavy condensation products.
 18. Heavy-residue; cyclohexylidene-cyclohexanone, cyclohexanone oligomers, heavy condensation products.
 19. Cyclohexanol for dehydrogenation; cyclohexanone, cyclohexanol, 2-cyclohexen-1-one, 2-cyclohexen-1-ol, heptanones, methylcyclohexanones, butylcyclohexane, cyclohexyl-butyl-ether, cyclohexene oxides, cyclohexylidene-cyclohexanone, cyclohexanone oligomers, n-pentylcyclohexane, cyclohexyl acetate, other light/heavy condensation products.
 20. Cyclohexanol recycle; cyclopentanol, hexanal, 2-hexanone, cyclohexanone, cyclohexanol, cyclohexenone, cyclohexenol, heptanones, methylcyclohexanone, cyclohexyl-butyl ether.
 21. Hydrogen.

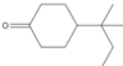
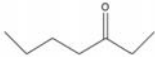
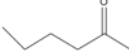
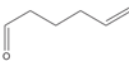
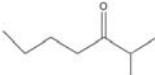
Appendix B. Compounds Involved in the Production Process of Cyclohexanone

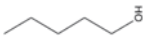
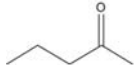
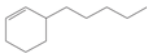
Order number, compound, empirical formula, structure, and CAS number are indicated.

No.	Compound	Formula	Chemical Structure	CAS#
1	acetic acid	$C_2H_4O_2$		64-19-7
2	1,1'-bicyclohexyl	$C_{12}H_{22}$		92-51-3

No.	Compound	Formula	Chemical Structure	CAS#
3	[1,1'-bicyclohexyl]-2,3'-dione	C ₁₂ H ₁₈ O ₂		55265-34-4
4	1-butanol	C ₄ H ₁₀ O		71-36-3
5	butoxycyclohexane	C ₁₀ H ₂₀ O		24072-44-4
6	butylcyclohexane	C ₁₀ H ₂₀		1678-93-9
7	2-butylcyclohexanone	C ₁₀ H ₁₈ O		1126-18-7
8	cycloheptanone	C ₇ H ₁₂ O		502-42-1
9	1,2-cyclohexanediol	C ₆ H ₁₂ O ₂		931-17-9
10	1,3-cyclohexanedione	C ₆ H ₈ O ₂		504-02-9
11	cyclohexanol	C ₆ H ₁₂ O		108-93-0
12	cyclohexanone	C ₆ H ₁₀ O		108-94-1
13	2-cyclohexen-1-ol	C ₆ H ₈ O		822-67-3
14	2-cyclohexen-1-one	C ₆ H ₈ O		930-68-7
15	1-(1-cyclohexen-1-yl)-2-propanone	C ₉ H ₁₄ O		768-50-3

No.	Compound	Formula	Chemical Structure	CAS#
16	cyclohexene	C ₆ H ₁₀		110-83-8
17	cyclohexyl acetone	C ₉ H ₁₆ O		103-78-6
18	cyclohexyl butanoate	C ₁₀ H ₁₈ O ₂		1551-44-6
19	cyclohexyl ethanone	C ₈ H ₁₄ O		823-76-7
20	cyclohexyl ethanoate	C ₈ H ₁₄ O ₂		622-45-7
21	cyclohexyl ether	C ₁₂ H ₂₂ O		4645-15-2
22	cyclohexyl hexanoate	C ₁₂ H ₂₂ O ₂		6243-10-3
23	cyclohexyl pentanoate	C ₁₁ H ₂₀ O ₂		1551-43-5
24	2-cyclohexylidencyclohexanone	C ₁₂ H ₁₈ O		1011-12-7
25	cyclopentanol	C ₅ H ₁₀ O		96-41-3
26	cyclopentanone	C ₇ H ₈ O		120-92-3
27	3,3-dimethylhexane	C ₈ H ₁₈		563-16-6

No.	Compound	Formula	Chemical Structure	CAS#
28	4-(1,1-dimethylpropyl)cyclohexanone	C ₁₁ H ₂₀ O		16587-71-6
29	2-ethylidenecyclohexanone	C ₈ H ₁₂ O		1122-25-4
30	formic acid	CH ₂ O ₂		64-18-6
31	2-heptanone	C ₇ H ₁₄ O		110-43-0
32	3-heptanone	C ₇ H ₁₄ O		106-35-4
33	hexanal	C ₆ H ₁₂ O		66-25-1
34	2-hexanone	C ₆ H ₁₂ O		591-78-6
35	5-hexenal	C ₆ H ₁₀ O		764-59-0
36	1-methoxycyclohexane	C ₇ H ₁₄ O		931-56-6
37	5-methyl-2-isopropylidenecyclohexanone	C ₁₀ H ₁₆ O		15932-80-6
38	2-methyl-3-heptanone	C ₈ H ₁₆ O		13019-20-0
39	methylcyclohexane	C ₇ H ₁₄		108-87-2

No.	Compound	Formula	Chemical Structure	CAS#
40	2-methylcyclohexanone	C ₇ H ₁₂ O		583-60-8
41	3-methylcyclohexanone	C ₇ H ₁₂ O		591-24-2
42	methylcyclopentane	C ₆ H ₁₂		96-37-7
43	1-methylcyclopentanol	C ₆ H ₁₂ O		1462-03-9
44	(1-methylethyl)cyclohexane	C ₉ H ₁₈		696-29-7
45	2-methylcyclopentanone	C ₆ H ₁₀ O		1120-72-5
46	1-pentanol	C ₅ H ₁₂ O		71-41-0
47	2-pentanone	C ₅ H ₁₀ O		107-87-9
48	3-pentyl-1-cyclohexene	C ₁₁ H ₂₀		15232-92-5
49	pentylcyclohexane	C ₁₁ H ₂₂		4292-92-6
50	phenol	C ₆ H ₆ O		108-95-2
51	p-tert-butylcyclohexanol	C ₁₀ H ₂₀ O		98-52-2

No.	Compound	Formula	Chemical Structure	CAS#
52	2-tetrahydrofurylmethanol	C ₅ H ₁₀ O ₂		97-99-4
53	1,2,3,4-tetrahydronaphthalene	C ₁₀ H ₁₂		119-64-2
54	toluene	C ₇ H ₈		108-88-3

Appendix C. Mathematics of the Joback Method

Equations used to estimate the thermophysical properties of pure substances by the Joback method are compiled in Table A1. The estimated values for the selected compounds in this work are shown in Table A2.

Table A1. Parameters and equations used in the Joback method.

Property	Parameter	Equation
Boiling temperature/K	$\tau_{b,k}$	$T_b^0 = 198.2 + \sum_k N_k \tau_{b,k}$
Melting temperature/K	$\tau_{f,k}$	$T_m^0 = 122.5 + \sum_k N_k \tau_{f,k}$
Critical temperature/K	$\tau_{c,k}$	$T_c = T_b \left[0.584 + 0.965 \sum_k N_k \tau_{c,k} - \left(\sum_k N_k \tau_{c,k} \right)^2 \right]^{-1}$
Critical pressure/bar	$\pi_{c,k}$	$p_c = \left(0.113 + 0.0032 N_{atoms} - \sum_k N_k \pi_{c,k} \right)^{-2}$
Critical volume/cm ³ ·mol ⁻¹	$v_{c,k}$	$v_c = 17.5 + \sum_k N_k v_{c,k}$
Gibbs energy of formation/kJ·kmol ⁻¹	$\Delta g_{f,k}^0$	$\Delta g_f^0 = 53.88 + \sum_k N_k \Delta g_{f,k}^0$
Enthalpy of formation/kJ·kmol ⁻¹	$\Delta h_{f,k}^0$	$\Delta h_f^0 = 68.29 + \sum_k N_k \Delta h_{f,k}^0$
Enthalpy of vaporization/kJ·kmol ⁻¹	$\Delta h_{v,k}^0$	$\Delta h_v^0 = 15.3 + \sum_k N_k \Delta h_{v,k}^0$
Enthalpy of melting/kJ·kmol ⁻¹	$\Delta h_{m,k}^0$	$\Delta h_m^0 = -0.88 + \sum_k N_k \Delta h_{m,k}^0$
Isobaric thermal capacity/kJ·kmol ⁻¹ ·K ⁻¹	$c_{p,k}^A; c_{p,k}^B; c_{p,k}^C; c_{p,k}^D$	$c_p^0 = \sum_k N_k c_{p,k}^A - 37.93 + T \left(\sum_k N_k c_{p,k}^B + 0.210 \right) + T^2 \left(\sum_k N_k c_{p,k}^C - 3.91 \cdot 10^{-4} \right) + T^3 \left(\sum_k N_k c_{p,k}^D + 2.06 \cdot 10^{-7} \right)$

where N_k is the number of groups of type “k” in the molecule whose properties are to be calculated and N_{atoms} is the total number of atoms in it. The parameters $\tau_{b,k}$, $\tau_{f,k}$, $\tau_{c,k}$, and $\pi_{c,k}$ are the group contributions for the boiling, melting, and critical temperatures, respectively; $\pi_{c,k}$ is the contribution parameter for the critical pressure, $v_{c,k}$ is that of the critical volume, $\Delta g_{f,k}^0$ is the group contribution parameter for the Gibbs energy of formation, and $\Delta h_{f,k}^0$, $\Delta h_{v,k}^0$, $\Delta h_{m,k}^0$ are those corresponding to the enthalpies of formation, vaporization and melting, respectively; $c_{p,k}^A$, $c_{p,k}^B$, $c_{p,k}^C$, $c_{p,k}^D$ are the group contributions to calculate the thermal capacities.

Table A2. Properties estimated by the Joback method [14] for the selected compounds in this work.

No.	Compound	T_b^0 K	T_m^0 K	T_c K	p_c bar	v_c m ³ /kmol	Δh_f^0 kJ/mol	Δg_f^0 kJ/mol	Δh_v^0 kJ/mol	Δh_m^0 kJ/mol	c_p (298 K) J/(molK)
1	acetic acid	390.7	272.9	587.3	57.31	0.171	-434.8	-377.9	40.67	11.08	65.7
2	1,1'-bicyclohexyl	544.3	262.8	782.6	27.35	0.587	-320.5	0.8	47.85	16.39	275.0
3	[1,1'-bicyclohexyl]-2,3'-dione	648.7	376.2	909.1	27.99	0.588	-457.8	-146.1	63.11	9.53	219.2
4	1-butanol	406.7	190.1	571.1	39.76	0.344	-354.6	-198.0	43.25	12.87	138.0
5	butoxycyclohexane	470.2	232.1	665.9	25.25	0.547	-327.6	-47.2	40.69	14.68	238.0
6	butylcyclohexane	447.8	209.8	644.6	25.69	0.529	-195.4	57.8	38.28	13.49	223.0
7	2-butylcyclohexanone	515.6	278.1	729.1	26.63	0.536	-333.1	-64.8	42.53	13.00	228.0
8	cycloheptanone	455.9	245	689.2	39.46	0.361	-257.0	-94.5	36.33	2.06	123.0
9	1,2-cyclohexanediol	502.8	358.9	720.4	34.8	0.342	-464.9	-273.6	53.77	16.55	195.0

Table A2. Cont.

No.	Compound	T_b^o K	T_m^o K	T_c K	p_c bar	v_c m ³ /kmol	Δh_f^o kJ/mol	Δg_f^o kJ/mol	Δh_v^o kJ/mol	Δh_m^o kJ/mol	C_p (298 K) J/(molK)
10	1,3-cyclohexanedione	496.5	305.4	743.3	45.29	0.319	-367.9	-213.3	48.19	1.08	114.7
11	cyclohexanol	431.9	264	654.6	49.25	0.270	-278.7	-120.9	41.73	9.30	147.0
12	cyclohexanone	428.7	237.2	656.0	43.23	0.313	-230.2	-90.8	33.94	1.57	105.0
13	2-cyclohexen-1-ol	431.0	264.7	656.2	62.89	0.257	-220.9	-90.9	42.02	10.53	140.0
14	2-cyclohexen-1-one	427.9	238	654.8	45.35	0.299	-172.4	-60.8	34.23	2.79	97.5
15	1-(1-cyclohexen-1-yl)-2-propanone	488.6	271.8	707.4	34.04	0.458	-180.8	12.0	43.46	14.40	190.0
16	cyclohexene	360.1	169.8	566.9	43.28	0.292	-34.7	61.8	29.98	3.28	92.6
17	cyclohexylacetone	478.7	248.5	689.0	30.39	0.479	-287.4	-79.6	42.80	12.50	201.0
18	cyclohexyl butanoate	506.0	252.2	708.4	25.82	0.555	-512.7	-252.6	45.69	17.86	239.0
19	cyclohexylethanone	455.9	237.2	669.2	33.88	0.423	-266.7	-88.0	40.58	9.91	178.0
20	cyclohexyl ethanoate	460.2	229.1	668.4	41.52	0.443	-471.4	-269.4	40.94	14.44	169.0
21	cyclohexyl ether	544.3	262.8	782.6	26.46	0.587	-320.5	0.8	47.85	16.39	275.0
22	cyclohexyl hexanoate	551.7	274.7	748.6	21.43	0.667	-554.0	-235.8	50.14	23.04	285.0
23	cyclohexyl pentanoate	528.9	263.4	728.5	23.47	0.611	-533.3	-244.2	47.92	20.45	262.0
24	2-cyclohexylidencyclohexanone	621.1	362.1	872.0	27.33	0.606	-235.8	43.5	59.44	11.56	220.1
25	cyclopentanol	404.7	256.2	621.0	54.55	0.223	-251.9	-117.2	39.33	8.81	129.0
26	cyclopentanone	401.6	229.5	622.3	47.56	0.265	-203.4	-87.1	31.54	1.08	87.0
27	3,3-dimethylhexane	379.2	182.3	553.4	25.85	0.473	-217.2	19.3	34.77	14.67	184.0
28	4-(1,1-dimethylpropyl)cyclohexanone	535.2	291.8	758.9	24.63	0.581	-362.5	-53.6	46.13	13.79	251.0
29	2-ethylidencyclohexanone	481.1	270.1	709.8	35.26	0.408	-195.5	-28.5	39.62	7.07	142.0
30	formic acid	363.1	203.8	534.4	75.88	0.127	-301.8	-278.6	43.65	4.72	46.1
31	2-heptanone	413.4	218.58	590.0	29.96	0.434	-300.4	-120.9	39.08	15.49	167.3
32	3-heptanone	413.4	218.58	590.0	29.96	0.434	-300.4	-120.9	39.08	15.49	167.3
33	hexanal	385.3	198.9	557.8	36.47	0.389	-252.8	-99.9	35.37	15.35	148.0
34	2-hexanone	390.6	206.8	568.1	35.99	0.378	-279.8	-129.3	35.30	14.66	144.0
35	5-hexenal	382.0	197.1	558.1	35.52	0.370	-127.3	-12.0	34.70	14.07	137.0
36	1-Methoxycyclohexane	374.4	190.5	569.6	33.53	0.331	-238.9	-68.8	31.62	6.42	151.0
37	5-methyl-2-isopropylidencyclohexanone	522.1	274.5	755.1	27.58	0.520	-266.9	-27.9	43.40	12.01	219.0
38	2-methyl-3-heptanone	435.8	214.8	615.2	27.27	0.483	-326.3	-114.8	40.96	14.55	189.2
39	Methylcyclohexane	379.1	176	581.6	35.22	0.361	-133.5	32.5	31.61	5.72	155.0
40	2-methylcyclohexanone	352.0	168.28	546.9	38.39	0.313	-106.7	36.2	29.40	5.23	112.6
41	3-methylcyclohexanone	352.0	168.28	546.9	38.39	0.313	-106.7	36.2	29.40	5.23	112.6
42	1-methylcyclopentanol	427.8	291.4	651.6	50.66	0.277	-257.3	-114.3	40.41	5.11	121.0
43	2-methylcyclopentanone	419.8	236.5	637.4	40.11	0.320	-244.4	-86.4	37.61	4.74	117.5
44	(1-methylethyl)cyclohexane	424.4	183.6	628.2	28.63	0.467	-180.1	46.9	35.67	7.38	200.0
45	methylcyclopentanone	351.9	168.2	546.9	38.39	0.312	-106.6	36.1	29.40	5.23	111.7
46	1-pentanol	406.0	206.9	567.6	38.77	0.335	-298.8	-145.6	43.40	12.79	131.0
47	2-pentanol	367.6	196	545.9	37.41	0.321	-259.1	-137.7	33.96	10.30	120.7
48	3-pentyl-1-cyclohexene	469.8	221.9	666.3	24.19	0.571	-158.3	96.2	40.80	17.30	239.0
49	pentylcyclohexane	470.6	221.1	665.2	23.36	0.585	-216.1	66.2	40.51	16.08	246.0
50	phenol	439.0	283	671.0	59.26	0.230	-96.5	-32.9	43.58	11.51	95.2
51	p-tert-butylcyclohexanol	523.6	271.8	729.8	25.77	0.576	-270.8	-32.7	50.04	18.90	214.3
52	2-tetrahydrofurylmethanol	449.3	235.8	635.2	48.29	0.315	-399.6	-227.7	48.45	14.06	125.0
53	1,2,3,4-tetrahydronaphthalene	475.5	260.1	708.1	35.69	0.438	62.3	192.5	41.19	10.27	144.0
54	toluene	386.2	195.1	597.8	41.14	0.320	48.7	120.5	33.45	7.93	102.0

Appendix D. Mathematics of the Marrero–Gani Method

The Marrero–Gani method estimates the same properties as the Joback method, with the exception of the thermal capacity. The combination of groups of different order is performed in the same way for each property, following Equation (A1):

$$f = \sum_i N_i A_i^1 + \sum_j M_j A_j^2 + \sum_k O_k A_k^3 \quad (\text{A1})$$

where N_i , M_j , and O_k are, respectively, the number groups of first, second, or third order for a given type present in the molecule, and A_i^1 , A_j^2 , and A_k^3 are the characteristic parameters of the corresponding group. The function f varies according to the property to be estimated, as shown in Table A3. The constants used for that function are presented in Table A4. Results obtained from the application of the method for the selected compounds are shown in Table A5.

Table A3. Equations used in the Marrero–Gani method [15] for estimating the different thermophysical properties.

Property	$f =$	Right-Hand Side of Equation (A1)
Melting temperature/K	$\exp(T_m^o / T_{m,0}^o)$	$\sum_i N_i T_{m,i}^o + \sum_j M_j T_{m,j}^o + \sum_k O_k T_{m,k}^o$
Boiling temperature/K	$\exp(T_b^o / T_{b,0}^o)$	$\sum_i N_i T_{b,i}^o + \sum_j M_j T_{b,j}^o + \sum_k O_k T_{b,k}^o$

Table A3. Cont.

Property	$f=$	Right-Hand Side of Equation (A1)
Critical temperature/K	$\exp(T_c/T_{c0})$	$\sum_i N_i T_{c1i} + \sum_j M_j T_{c2j} + \sum_k O_k T_{c3k}$
Critical pressure/bar	$(p_c - p_{c1})^{-0.5} - p_{c2}$	$\sum_i N_i p_{c1i} + \sum_j M_j p_{c2j} + \sum_k O_k p_{c3k}$
Critical volume/cm ³ ·mol ⁻¹	$v_c - v_{c0}$	$\sum_i N_i v_{c1i} + \sum_j M_j v_{c2j} + \sum_k O_k v_{c3k}$
Gibbs energy of formation/kJ·kmol ⁻¹	$\Delta g_f^0 - \Delta g_{f0}^0$	$\sum_i N_i g_{f1i}^0 + \sum_j M_j g_{f2j}^0 + \sum_k O_k g_{f3k}^0$
Enthalpy of formation/kJ·kmol ⁻¹	$\Delta h_f^0 - \Delta h_{f0}^0$	$\sum_i N_i h_{f1i}^0 + \sum_j M_j h_{f2j}^0 + \sum_k O_k h_{f3k}^0$
Enthalpy of vaporization/kJ·kmol ⁻¹	$\Delta h_v^0 - \Delta h_{v,0}^0$	$\sum_i N_i h_{v1i}^0 + \sum_j M_j h_{v2j}^0 + \sum_k O_k h_{v3k}^0$
Enthalpy of melting/kJ·kmol ⁻¹	$\Delta h_m^0 - \Delta h_{m,0}^0$	$\sum_i N_i h_{m1i}^0 + \sum_j M_j h_{m2j}^0 + \sum_k O_k h_{m3k}^0$

Table A4. Generic constants used in the Marrero–Gani method [15] for equations shown in Table A3.

Generic Constants	
$T_{m,0}^0/K$	147.450
$T_{b,0}^0/K$	222.543
T_{c0}/K	231.239
p_{c1}/bar	5.9827
$p_{c2}/\text{bar}^{-0.5}$	0.108998
$v_{c0}/\text{cm}^3 \cdot \text{mol}^{-1}$	7.95
$\Delta g_{f0}^0/\text{kJ} \cdot \text{mol}^{-1}$	-34.967
$\Delta h_{f0}^0/\text{kJ} \cdot \text{mol}^{-1}$	5.549
$\Delta h_{v,0}^0/\text{kJ} \cdot \text{mol}^{-1}$	11.733
$\Delta h_{m,0}^0/\text{kJ} \cdot \text{mol}^{-1}$	-2.806

Table A5. Properties estimated by the Marrero–Gani method [15] for the selected compounds used in this work.

No.	Compound	T_b^0/K	T_m^0/K	T_c/K	p_c/bar	$v_c/\text{m}^3/\text{kmol}$	$\Delta g_f^0/\text{kJ/mol}$	$\Delta h_f^0/\text{kJ/mol}$	$\Delta h_v^0/\text{kJ/mol}$	$\Delta h_m^0/\text{kJ/mol}$
1	acetic acid	397.3	308.4	646.20	58.88	0.159	-369.2	-426.9	28.95	9.55
2	1,1'-bicyclohexyl	511.7	271.7	727.00	25.60	0.598	42.6	-272.0	57.98	12.91
3	[1,1'-bicyclohexyl]-2,3'-dione	579.8	354.2	867.22	30.29	0.599	-528.3	-229.8	85.54	23.04
4	1-butanol	381.7	213.0	553.80	43.70	0.276	-277.8	-151.9	50.83	10.93
5	Butoxycyclohexane	464.5	231.5	676.94	22.89	0.610	-40.9	-357.0	59.80	19.52
6	butylcyclohexane	454.1	199.4	650.20	25.40	0.533	70.0	-200.3	49.37	13.49
7	2-Butylcyclohexanone	493.3	286.4	762.27	27.58	0.544	-105.3	-366.3	63.58	19.70
8	cycloheptanone	451.7	278.9	734.20	41.37	0.361	-111.9	-286.1	48.90	9.75
9	1,2-cyclohexanediol	504.2	349.0	714.14	44.00	0.341	-263.8	-466.5	90.63	16.06
10	1,3-cyclohexanedione	493.4	331.6	807.20	51.56	0.312	-295.2	-429.1	58.73	13.74
11	cyclohexanol	434.0	287.8	650.00	42.60	0.322	-109.5	-286.2	61.20	9.84
12	cyclohexanone	431.2	265.7	715.26	45.93	0.312	-125.2	-267.5	45.56	8.68
13	2-cyclohexen-1-ol	437.2	288.9	648.32	45.39	0.307	-49.6	-189.2	62.29	8.88
14	2-cyclohexen-1-one	443.2	267.8	714.00	49.12	0.297	-59.2	-183.0	53.06	10.23
15	1-(1-cyclohexen-1-yl)-2-propanone	470.7	262.3	685.83	31.52	0.460	-27.4	-205.9	52.37	14.73
16	cyclohexene	356.1	183.6	558.00	43.92	0.289	104.7	-8.9	32.86	2.66
17	cyclohexylacetone	473.7	266.4	679.01	29.83	0.483	-75.0	-301.2	54.96	15.75
18	cyclohexyl butanoate	486.2	237.2	683.41	25.83	0.545	-245.5	-543.1	61.08	18.83
19	cyclohexylethanone	453.7	278.5	662.05	33.33	0.427	-83.1	-280.4	49.43	13.11
20	cyclohexyl ethanoate	441.0	225.4	639.90	31.20	0.448	-481.9	-267.1	53.53	12.88
21	cyclohexyl ether	515.7	281.6	732.56	26.16	0.608	-3.9	-342.5	64.85	16.71
22	cyclohexyl hexanoate	515.7	257.9	727.13	20.21	0.713	-221.3	-605.5	75.81	26.75
23	cyclohexyl pentanoate	497.7	244.4	698.92	23.63	0.601	-237.4	-563.9	65.99	21.47
24	2-cyclohexylidencyclohexanone	565.4	323.2	783.20	31.56	0.501	-72.1	-341.8	58.93	12.95
25	cyclopentanol	413.4	275.3	622.23	47.41	0.273	-122.8	-267.6	57.86	11.73
26	cyclopentanone	403.8	251.1	694.64	51.44	0.262	-138.5	-248.9	42.22	7.61
27	3,3-dimethylhexane	385.1	187.3	555.14	25.68	0.466	17.2	-217.9	38.06	10.52
28	4-(1,1-dimethylpropyl)cyclohexanone	503.9	298.3	776.91	27.06	0.575	-90.3	-392.6	65.55	16.86
29	2-ethylidencyclohexanone	478.4	276.7	737.22	33.74	0.448	-47.1	-211.7	63.55	11.38
30	formic acid	362.8	259.4	554.90	83.20	0.102	-279.9	-303.6	48.32	13.31
31	2-heptanone	426.7	223.8	611.13	29.34	0.417	-300.8	-122.0	46.38	17.58
32	3-heptanone	417.1	227.2	596.91	29.44	0.418	-305.0	-125.4	46.29	17.26
33	hexanal	407.6	228.8	591.00	33.10	0.373	-251.1	-100.7	43.90	20.10
34	2-hexanone	400.8	215.1	589.20	32.47	0.373	-278.6	-127.6	41.82	14.20
35	5-hexenal	405.6	232.5	594.10	34.76	0.359	-128.8	-14.9	42.80	17.07
36	1-Methoxycyclohexane	408.2	203.4	607.23	32.33	0.406	-63.2	-279.8	37.51	10.73

Table A5. Cont.

No.	Compound	T_b^o K	T_m^o K	T_c K	p_c bar	v_c m ³ /kmol	Δg_f^o kJ/mol	Δh_f^o kJ/mol	Δh_g^o kJ/mol	Δh_m^o kJ/mol
37	5-methyl-2-isopropylidencyclohexanone	497.2	299.0	753.09	28.05	0.558	−33.8	−255.2	77.19	11.98
38	2-methyl-3-heptanone	431.2	233.0	613.20	26.78	0.470	−122.8	−334.2	49.16	16.81
39	Methylcyclohexane	374.2	182.4	577.23	35.07	0.370	44.6	−137.8	35.17	6.74
40	2-methylcyclohexanone	448.3	266.3	723.99	38.52	0.370	−299.4	−125.3	48.95	11.81
41	3-methylcyclohexanone	448.3	266.3	723.99	38.52	0.370	−299.4	−125.3	48.95	11.81
42	1-methylcyclopentanol	409.2	283.5	580.05	44.29	0.325	−142.0	−313.4	57.35	5.99
43	2-methylcyclopentanone	422.4	251.8	704.16	42.52	0.321	−280.8	−138.6	45.61	10.74
44	(1-methylethyl)cyclohexane	427.9	191.4	621.05	28.42	0.481	57.3	−196.4	43.00	11.32
45	methylcyclopentanone	340.4	155.8	538.30	38.44	0.313	31.3	−119.2	31.83	5.64
46	1-pentanol	410.9	221.5	580.32	38.12	0.332	−143.9	−298.6	55.80	14.20
47	2-pentanone	362.1	210.4	544.80	37.06	0.306	−141.6	−263.3	36.47	11.98
48	3-pentyl-1-cyclohexene	473.2	180.7	652.99	25.51	0.559	128.8	−109.7	59.95	16.49
49	pentylcyclohexane	476.9	208.7	668.01	23.27	0.590	78.0	−221.2	54.28	16.13
50	phenol	455.0	308.0	687.06	59.65	0.271	−32.6	−94.3	64.25	15.36
51	p-tert-butylcyclohexanol	494.8	240.6	694.60	24.12	0.595	216.4	−43.5	58.23	13.72
52	2-tetrahydrofurfylmethanol	451.2	258.3	641.69	48.15	0.305	−239.0	−399.2	64.17	14.14
53	1,2,3,4-tetrahydronaphthalene	480.8	241.7	664.03	31.37	0.521	110.1	−61.3	77.10	11.86
54	toluene	383.8	202.1	604.05	42.18	0.317	123.6	50.6	38.43	9.90

References

- Sosa, A.; Ortega, J.; Fernández, L.; Romero, A.; Santos, A.; Lorenzo, D. Evaluation of VLEs for Binary Compounds Involved in the Production Process of Cyclohexanone. *ChemEngineering* **2022**, *6*, 42. [\[CrossRef\]](#)
- Ritz, J.; Fuchs, H.; Kieczka, H.; Moran, W.C. Caprolactam. In *Ullmann's Encyclopedia of Industrial Chemistry*; Cambell, F.T., Pfefferkorn, R., Rounsaville, J.R., Eds.; Wiley-VCH: Weinheim, Germany, 1986; Volume A5, pp. 31–50.
- Zhu, Z.; Li, G.; Yang, J.; Dai, Y.; Cui, P.; Wang, Y.; Xu, D. Improving the energy efficiency and production performance of the cyclohexanone ammoxidation process via thermodynamics, kinetics, dynamics, and economic analyses. *Energy Convers. Manag.* **2019**, *192*, 100–113. [\[CrossRef\]](#)
- Matshwele, J.; Mmusi, K.; Vishwanathan, V. A single step low cost production of cyclohexanone from phenol hydrogenation. *Sreyas Int. J. Sci. Technol.* **2019**, *3*, 1–6. [\[CrossRef\]](#)
- Jodra, L.G.; Romero, A.; García-Ochoa, F.; Aracil, J. Analysis of the Impurities in Industrial Epsilon-Caprolactam—Hypothesis of Formation. *J. Appl. Polym. Sci.* **1981**, *26*, 3271–3282. [\[CrossRef\]](#)
- Jodra, L.G.; Romero, A.; García-Ochoa, F.; Aracil, J. Impurity Content and Quality Definition of Commercial Epsilon-Caprolactam. *Ind. Eng. Chem. Prod. Res. Dev.* **1981**, *20*, 562–566. [\[CrossRef\]](#)
- Romero, A.; Yustos, P.; Santos, A. Dehydrogenation of cyclohexanol to cyclohexanone: Influence of methylcyclopentanols on the impurities obtained in epsilon-caprolactam. *Ind. Eng. Chem. Res.* **2003**, *42*, 3654–3661. [\[CrossRef\]](#)
- Romero, A.; Yustos, P.; Santos, A.; Rodríguez, S. Kinetic study of the oxidation of epsilon-caprolactam impurities with permanganate for PZ estimation. *J. Ind. Eng. Chem.* **2005**, *11*, 88–95.
- Romero, A.; Santos, A.; Escrig, D.; Simón, E. Comparative dehydrogenation of cyclohexanol to cyclohexanone with commercial copper catalysts: Catalytic activity and impurities formed. *Appl. Cat. A Gen.* **2011**, *392*, 19–27. [\[CrossRef\]](#)
- Lorenzo, D.; Santos, A.; Simon, E.; Romero, A. Kinetics of Alkali-Catalyzed Condensation of Impurities in the Cyclohexanone Purification Process. *Ind. Eng. Chem. Res.* **2013**, *52*, 15780–15788. [\[CrossRef\]](#)
- Lydersen, A.L.; Greenkorn, R.A.; Hougen, O.A. *Generalized Thermodynamic Properties of Pure Fluids*; Engineering Experiment Station Report 4; University of Wisconsin: Madison, WI, USA, 1955.
- Poling, B.E.; Prausnitz, J.M.; O'Connell, J.P. *The Properties of Gases and Liquids*, 5th ed.; McGraw-Hill: New York, NY, USA, 2001.
- Simmrock, K.H.; Janowsky, R.; Ohnsorge, A. *Critical Data of Pure Substances*; Chemistry Data Series; DECHEMA: Frankfurt, Germany, 1986; Volume II.
- Joback, K.G.; Reid, R.C. Estimation of pure-component properties from group-contributions. *Chem. Eng. Commun.* **1987**, *57*, 233–243. [\[CrossRef\]](#)
- Marrero, J.; Gani, R. Group-contribution based estimation of pure component. *Fluid Phase Equilib.* **2001**, *183–184*, 183–208. [\[CrossRef\]](#)
- Riddick, J.A.; Bunger, W.B.; Sakano, T.K. *Organic Solvents: Physical Properties and Methods of Purification*, 4th ed.; Wiley-Interscience: New York, NY, USA, 1986.
- Steele, W.V.; Chirico, R.D.; Knipmeyer, S.E.; Nguyen, A. Vapor Pressure, Heat Capacity, and Density along the Saturation Line, Measurements for Cyclohexanol, 2-Cyclohexen-1-one, 1,2-Dichloropropane, 1,4-Di-tert-butylbenzene, (±)-2-Ethylhexanoic Acid, 2-(Methylamino)ethanol, Perfluoro-n-heptane, and Sulfolane. *J. Chem. Eng. Data* **1997**, *42*, 1021–1036. [\[CrossRef\]](#)
- Weast, R.C.; Grasselli, J.G. (Eds.) *CRC Handbook of Data on Organic Compounds*, 2nd ed.; CRC Press: Boca Raton, FL, USA, 1989; Volume 1.
- Forziati, A.F.; Rossini, F.D. Physical properties of sixty API-NBS hydrocarbons. *J. Res. Natl. Bur. Stand.* **1949**, *43*, 473–476. [\[CrossRef\]](#)

20. Markovnik, V.S.; Sachek, A.I.; Peshchenko, A.D.; Shvaro, O.V.; Andreevskii, D.N.; Olizarevich, N.M. Temperature Dependence of Pressure for a Few Aldehydes. *Termodin. Org. Soedin.* **1979**, *8*, 107–110.
21. Mears, T.W.; Stanley, C.L.; Compere, E.L.; Howard, F.L. Synthesis, purification, and physical properties of seven twelve-carbon hydrocarbons. *J. Res. Natl. Bur. Stand. A Phys. Chem.* **1963**, *67*, 475–479. [[CrossRef](#)]
22. Moshkin, P.A. Vpr. Izolz. Pentozansoderzh. Syrya. *Tr. Vses. Soveshch. Riga* **1958**, *1955*, 225.
23. Olson, W.T.; Hipsher, H.F.; Buess, C.M.; Goodman, I.A.; Hart, I.; Lamneck, J.H.; Gibbons, L.C. The Synthesis and Purification of Ethers. *J. Am. Chem. Soc.* **1947**, *69*, 2451–2454. [[CrossRef](#)]
24. Reid, R.C.; Prausnitz, J.M.; Sherwood, T.K. *The Properties of Gases and Liquids*, 3rd ed.; McGraw-Hill: New York, NY, USA, 1977.
25. Sayar, A.A.; Tatli, B.; Dramur, U. Liquid-Liquid Equilibria of the Water + Acetic Acid + Cyclohexyl Acetate Ternary. *J. Chem. Eng. Data* **1991**, *36*, 378–382. [[CrossRef](#)]
26. Smith, H.A.; Pennekamp, E.F.H. The Catalytic Hydrogenation of the Benzene Nucleus II. The Hydrogenation of Benzene and Mono-alkylbenzenes. *J. Am. Chem. Soc.* **1945**, *67*, 276–278. [[CrossRef](#)]
27. Timmermans, J.; Hennaut-Roland, M. Works from International Bureau at Physical-Chemical Standards. VIII. Physical constants of 20 organic compounds. *J. Chim. Phys. Phys.-Chim. Biol.* **1937**, *34*, 693–735. [[CrossRef](#)]
28. Walling, C.; Padwa, A. Positive Halogen Compounds. VI. Effects of Structure and Medium on the β -Scission of Alkoxy Radicals. *J. Am. Chem. Soc.* **1963**, *85*, 1593–1597. [[CrossRef](#)]
29. White, A.H.; Bishop, W.S. Dielectric Evidence of Molecular Rotation in the Crystals of Certain Non-aromatic Compounds. *J. Am. Chem. Soc.* **1940**, *62*, 8–16. [[CrossRef](#)]
30. Bridson-Jones, F.S.; Buckley, G.D.; Cross, L.H.; Driver, A.P. Oxidation of organic compounds by nitrous oxide: Part I. *J. Chem. Soc.* **1951**, 2999–3008. [[CrossRef](#)]
31. Adkins, H.; Pavlic, A.A. Hydrogenation of Esters to Alcohols over Raney Nickel. I. *J. Am. Chem. Soc.* **1947**, *69*, 3039–3041. [[CrossRef](#)] [[PubMed](#)]
32. Gonthier-Vassal, A.; Szwarc, H. Thermodynamic properties of cycloketones: A DSC study. *Thermochim. Acta* **1998**, *320*, 141–154. [[CrossRef](#)]
33. Kabo, G.J.; Kozyro, A.A.; Frenkel, M.; Blokhin, A.V. Solid Phase Transitions of the Cyclohexane Derivatives and the Model of Energy States of Molecules in Plastic Crystals. *Mol. Cryst. Liq.* **1999**, *326*, 333–355. [[CrossRef](#)]
34. Streiff, A.J.; Hulme, A.R.; Cowie, P.A.; Krouskop, N.C.; Rossini, F.D. Purification, Purity, and Freezing Points of Sixty-four American Petroleum Institute Standard and Research Hydrocarbons. *Anal. Chem.* **1955**, *27*, 411–415. [[CrossRef](#)]
35. Timmermans, J. Freezing points of organic compounds. VVI New determinations. *Bull. Soc. Chim. Belg.* **1952**, *61*, 393–402. [[CrossRef](#)]
36. Timmermans, J. *Physical Constants of Crystalline Organic Compounds*; Mass on & Cie: Paris, France, 1953.
37. Timmermans, J.; Mattaar, J.F. The Freezing Points of Organic Substances IV. New Exp. Determinations. *Bull. Soc. Chim. Belg.* **1921**, *30*, 62–71.
38. Fiege, C.; Joh, R.; Petri, M.; Gmehling, J. Solid-Liquid Equilibria for Different Heptanones with Benzene, Cyclohexane, and Ethanol. *J. Chem. Eng. Data* **1996**, *41*, 1431–1433. [[CrossRef](#)]
39. Wibaut, J.P.; Hoog, H.; Langedijk, S.L.; Overhoff, J.; Smittenberg, J. A study on the preparation and the physical constants of a number of alkanes and cycloalkanes. *Recl. Trav. Chim. Pays-Bas* **1939**, *58*, 329–377. [[CrossRef](#)]
40. Wolfrom, M.L.; Bobbitt, J.M. Periodate Oxidation of Cyclic 1,3-Diketones. *J. Am. Chem. Soc.* **1956**, *78*, 2489–2493. [[CrossRef](#)]
41. Ambrose, D.; Ghiassee, N.B. Vapour pressures and critical temperatures and critical pressures of C5 and C6 cyclic alcohols and ketones. *J. Chem. Thermodyn.* **1987**, *19*, 903–909. [[CrossRef](#)]
42. Fuchs, R.; Peacock, L.A. Heats of vaporization of monoalkylcyclohexanes by the gas chromatography-calorimetry method. *Can. J. Chem.* **1978**, *56*, 2493–2498. [[CrossRef](#)]
43. Landrieu, P.; Baylocq, F.; Johnson, J.R. Etude thermochimique dans la serie furanique. *Bull. Soc. Chim. France* **1929**, *45*, 36–49.
44. Lee, C.H.; Dempsey, D.M.; Mohamed, R.S.; Holder, G.D. Vapor-liquid equilibria in the systems of n-decane/tetralin, n-hexadecane/tetralin, n-decane/1-methylnaphthalene, and 1-methylnaphthalene/tetralin. *J. Chem. Eng. Data* **1992**, *37*, 183–186. [[CrossRef](#)]
45. Majer, V.; Svoboda, V. *Enthalpies of Vaporization of Organic Compounds: A Critical Review and Data Compilation*; Blackwell Scientific Publications: Oxford, UK, 1985.
46. Paulechka, Y.U.; Zaitsau, D.H.; Kabo, G.J. On the difference between isobaric and isochoric heat capacities of liquid cyclohexyl esters. *J. Mol. Liq.* **2004**, *115*, 105–111. [[CrossRef](#)]
47. Stephenson, R.M.; Malanowski, S. *Handbook of the Thermodynamics of Organic Compounds*, 1st ed.; Springer: Dordrecht, The Netherlands, 1987.
48. Teodorescu, M.; Barhala, A.; Dragoescu, D. Isothermal (vapour+liquid) equilibria for the binary (cyclopentanone or cyclohexanone with 1,1,2,2-tetrachloroethane) systems at temperatures of (343.15, 353.15, and 363.15) K. *J. Chem. Thermodyn.* **2006**, *38*, 1432–1437. [[CrossRef](#)]
49. Domalski, E.S.; Hearing, E.D. Heat Capacities and Entropies of Organic Compounds in the Condensed Phase. Volume III. *J. Phys. Chem. Ref. Data* **1996**, *25*, 1–523. [[CrossRef](#)]

50. McCullough, J.P.; Finke, H.L.; Messerly, J.F.; Kincheloe, T.C.; Waddington, G. The low temperature thermodynamic properties of naphthalene, 1-methylnaphthalene, 2-methylnaphthalene, 1,2,3,4-tetrahydronaphthalene, trans-decahydronaphthalene and cis-decahydronaphthalene. *J. Phys. Chem.* **1957**, *61*, 1105–1116. [[CrossRef](#)]
51. Verevkin, S.P.; Krasnykh, E.L.; Vasil'tsova, T.V.; Koutek, B.; Doubtsky, J.; Heintz, A. Vapor pressures and enthalpies of vaporization of a series of the linear aliphatic aldehydes. *Fluid Phase Equilib.* **2003**, *206*, 331–339. [[CrossRef](#)]
52. Wiberg, K.B.; Wasserman, D.J.; Martin, E.J.; Murcko, M.A. Enthalpies of hydration of alkenes. 3. Cycloalkenes. *J. Am. Chem. Soc.* **1985**, *107*, 6019–6022. [[CrossRef](#)]
53. Pulliam, M.K.; Gude, M.T.; Teja, A.S. The Critical Properties of Twelve Isomeric n-Alkanones with Six to Nine Carbon Atoms. In *Experimental Results for DIPPR 1990–91 Projects on Phase Equilibria and Pure Component Properties*; DIPPR Data Series; American Institute of Chemical Engineers: New York, NY, USA, 1994; pp. 184–187.
54. Teja, A.S.; Rosenthal, D.J. The critical pressures and temperatures of twelve substances using a low residence time flow apparatus. *AIChE Symp. Ser.* **1990**, *86*, 133–137.
55. Tsonopoulos, C.; Ambrose, D. Vapor-Liquid Critical Properties of Elements and Compounds. 3. Aromatic Hydrocarbons. *J. Chem. Eng. Data* **1995**, *40*, 547–558. [[CrossRef](#)]
56. Ambrose, D.; Broderick, B.E.; Townsend, R. The Critical Temperatures and Pressures of Thirty Organic Compounds. *J. Appl. Chem. Biotechnol.* **1974**, *24*, 359–372. [[CrossRef](#)]
57. Wilson, L.C.; Wilson, H.L.; Wilding, W.V.; Wilson, G.M. Critical Point Measurements for Fourteen Compounds by a Static Method and a Flow Method. *J. Chem. Eng. Data* **1996**, *41*, 1252–1254. [[CrossRef](#)]
58. Prosen, E.J.; Johnson, W.H.; Rossini, F.D. Heats of formation and combustion of the normal alkylcyclopentanes and cyclohexanes and the increment per CH₂ group for several homologous series of hydrocarbons. *J. Res. Natl. Bur. Stand.* **1946**, *37*, 51–56. [[CrossRef](#)]
59. Wiberg, K.B.; Crocker, L.S.; Morgan, K.M. Thermochemical studies of carbonyl compounds. 5. Enthalpies of reduction of carbonyl groups. *J. Am. Chem. Soc.* **1991**, *113*, 3447–3450. [[CrossRef](#)]
60. Verevkin, S.P.; Beckhaus, H.D.; Belen'kaja, R.S.; Rakus, K.; Rüchardt, C. Geminal substituent effects Part 9. Standard enthalpies of formation and strain free increments of branched esters and ethers. *Thermochim. Acta* **1996**, *279*, 47–64. [[CrossRef](#)]
61. Blokhin, A.V.; Kabo, G.J.; Kozyro, A.A.; Ivashkevich, L.S.; Krasulin, A.P.; Diky, V.V.; Maksimuk, Y.V. Thermodynamic properties of 1-methylcyclopentanol and 1-chloro-1-methylcyclopentane in the ideal gas state. *Thermochim. Acta* **1997**, *292*, 19–29. [[CrossRef](#)]
62. Wolf, G. Thermochemische Untersuchungen an cyclischen Ketonen. *Helv. Chim. Acta* **1972**, *55*, 1446–1459. [[CrossRef](#)]
63. Good, W.D.; Lee, S.H. The enthalpies of formation of selected naphthalenes, diphenylmethanes, and bicyclic hydrocarbons. *J. Chem. Thermodyn.* **1976**, *8*, 643–650. [[CrossRef](#)]
64. Harrop, D.; Head, A.J.; Lewis, G.B. Thermodynamic properties of organic oxygen compounds. 22. Enthalpies of combustion of some aliphatic ketones. *J. Chem. Thermodyn.* **1970**, *2*, 203–210. [[CrossRef](#)]
65. Simirskii, V.V.; Kozyro, A.A.; Kabo, G.Y.; Yursha, I.A.; Marachuk, L.I. Thermodynamic properties and saponification kinetics of cyclohexyl acetate. *J. Appl. Chem. USSR* **1993**, *65*, 1348–1353.
66. Pilcher, G.; Parchment, O.G.; Hillier, I.H.; Heatley, F.; Fletcher, D.; Ribeiro da Silva, M.A.V.; Ferrao, M.L.C.C.H.; Monte, M.J.S.; Jiye, F. Thermochemical and theoretical studies on cyclohexanediones. *J. Phys. Chem.* **1993**, *97*, 243–247. [[CrossRef](#)]
67. Marachik, L.I.; Kozyro, A.A.; Simirskii, V.V.; Kabo, G.Y.; Yursha, I.A.; Krasulin, A.P.; Sevruk, V.M. Thermodynamic characteristics of by-products from caprolactam synthesis. *J. Appl. Chem. USSR* **1992**, *65*, 710–715.
68. Benson, G.C.; D'Arcy, P.J. Excess isobaric heat capacities of some binary mixtures: (a C₅-alkanol + n-heptane) at 298.15 K. *J. Chem. Thermodynam.* **1986**, *18*, 493–498. [[CrossRef](#)]
69. Finke, H.L.; Messerly, J.F.; Todd, S.S. Thermodynamic properties of n-propyl-, n-butyl-, and n-decyl-substituted cyclohexane from 10 to 370 K. *J. Phys. Chem.* **1965**, *69*, 2094–2100. [[CrossRef](#)]
70. Mayer, J.; Rachwalska, M.; Sciesinska, E.; Sciesinski, J. On the polymorphism of solid cyclohexanol by adiabatic calorimetry and far infrared methods. *J. Phys. France* **1990**, *51*, 857–867. [[CrossRef](#)]
71. Nakamura, N.; Suga, H.; Seki, S. Calorimetric study on orientationally disordered crystals. Cyclohexene oxide and cyclohexanone. *Bull. Chem. Soc. Japan* **1980**, *53*, 2755–2761. [[CrossRef](#)]
72. Osborne, N.S.; Ginnings, D.C. Measurements of heat of vaporization and heat capacity of a number of hydrocarbons. *J. Res. Natl. Bur. Stand.* **1947**, *39*, 453–477. [[CrossRef](#)] [[PubMed](#)]
73. Siddiqi, M.A.; Svejda, P.; Kohler, F. A generalized van der Waals equation of state II. Excess heat capacities of mixtures containing cycloalkanes (C₅,C₆), methylcycloalkanes (C₅,C₆) and n-decane. *Ber. Bunsenges. Phys. Chem.* **1983**, *87*, 1176–1181. [[CrossRef](#)]

Article

Density and Refractive Index of Binary Ionic Liquid Mixtures with Common Cations/Anions, along with ANFIS Modelling

G. Reza Vakili-Nezhaad ^{1,*}, Morteza Mohammadzaheri ², Farzaneh Mohammadi ^{3,*} and Mohammed Humaid ¹¹ Petroleum & Chemical Engineering Department, College of Engineering, Sultan Qaboos University, Muscat 123, Oman² School of Engineering and the Built Environment, Birmingham City University, Birmingham B4 7XG, UK³ School of Health, Isfahan University of Medical Sciences (MUI), Isfahan 81746-73461, Iran

* Correspondence: vakili@squ.edu.om (G.R.V.-N.); fm_1363@hlth.mui.ac.ir (F.M.)

Abstract: Ionic liquids have many interesting properties as they share the properties of molten salts as well as organic liquids, such as low volatility, thermal stability, electrical conductivity, non-flammability, and much more. Ionic liquids are known to be good solvents for many polar and nonpolar solutes. Combined with their special properties, ionic liquids are good replacements for the conventional toxic and volatile organic solvents. Each ionic liquid has different properties than others. In order to alter, tune, and enhance the properties of ionic liquids, sometimes, it is necessary to mix different ionic liquids to achieve the desired properties. However, using mixtures of ionic liquids in chemical processes requires reliable estimations of the mixtures' physical properties such as refractive index and density. The ionic liquids used in this work are 1-butyl-3-methylimidazolium thiocyanate ([BMIM][SCN]), 1-butyl-3-methylimidazolium tetrafluoroborate ([BMIM][BF₄]), 1-hexyl-3-methylimidazolium tetrafluoroborate ([HMIM][BF₄]), and 1-hexyl-3-methylimidazolium hexafluorophosphate ([HMIM][PF₆]). These ionic liquids were supplied by Io-li-tec and used as received. However, new measurements for the density and refractive index were taken for the pure ionic liquids to be used as reference. In the present work, the densities and refractive indices of four different binary mixtures of ionic liquids with common cations and/or anions have been measured at various compositions and room conditions. The accuracy of different empirical mixing rules for calculation of the mixtures refractive indices was also studied. It was found that the overall absolute average percentage deviation from the ideal solution in the calculation of the molar volume of the examined binary mixtures was 0.78%. Furthermore, all of the examined mixing rules for the calculation of the refractive indices of the mixtures were found to be accurate. However, the most accurate empirical formula was found to be Heller's relation, with an average percentage error of 0.24%. Furthermore, an artificial intelligence model, an adaptive neuro-fuzzy inference system (ANFIS), was developed to predict the density and refractive index of the different mixtures studied in this work as well as the published literature data. The predictions of the developed model were analyzed by various methods including both statistical and graphical approaches. The obtained results show that the developed model accurately predicts the density and refractive index with overall R^2 , RMSE, and AARD% values of 0.968, 7.274, 0.368% and 0.948, 7.32×10^{-3} and 0.319%, respectively, for the external validation dataset. Finally, a variance-based global sensitivity analysis was formed using extended the Fourier amplitude sensitivity test (EFAST). Our modelling showed that the ANFIS model outperforms the best available empirical models in the literature for predicting the refractive index of the different mixtures of ionic liquids.

Keywords: refractive index; density; ionic liquids; mixtures; ANFIS

Citation: Vakili-Nezhaad, G.R.; Mohammadzaheri, M.; Mohammadi, F.; Humaid, M. Density and Refractive Index of Binary Ionic Liquid Mixtures with Common Cations/Anions, along with ANFIS Modelling. *Liquids* **2022**, *2*, 432–444. <https://doi.org/10.3390/liquids2040025>

Academic Editors: William E. Acree, Jr. and Juan Ortega Saavedra

Received: 12 October 2022

Accepted: 26 November 2022

Published: 5 December 2022

Publisher's Note: MDPI stays neutral with regard to jurisdictional claims in published maps and institutional affiliations.



Copyright: © 2022 by the authors. Licensee MDPI, Basel, Switzerland. This article is an open access article distributed under the terms and conditions of the Creative Commons Attribution (CC BY) license (<https://creativecommons.org/licenses/by/4.0/>).

1. Introduction

Ionic liquids are salts in the liquid state. Due to the strong ionic bond between the cation and the anion, most ionic compounds exist in the form of crystal lattice (solid state) at room temperature. However, many asymmetric organic based ionic liquids appear in liquid

form at room temperature due to the weaker ionic bonding between the cation and anion. Ionic liquids have many interesting properties, as they share the properties of molten salts as well as organic liquids, such as low volatility, thermal stability, electrical conductivity, non-flammability, and much more. Ionic liquids are known to be good solvents for many polar and nonpolar solutes. Combined with their special properties, ionic liquids are good replacements for the conventional toxic and volatile organic solvents. Each ionic liquid has different properties to others. In order to alter, tune, and enhance the properties of ionic liquids, sometimes, it is necessary to mix different ionic liquids to achieve the desired properties.

However, using mixtures of ionic liquids in chemical processes requires the reliable estimations of the mixtures' physical properties, such as refractive index and density. Many general mixing rules for liquids have been proposed so far, which describe specific types of systems. This emphasizes the need to examine these mixing rules with respect to ionic liquid mixtures and to determine the best mixing rule for each physical property. Furthermore, assuming ideal behavior for the mixtures simplifies their complexity. Hence, the validity and accuracy of an ideal mixture assumption are uncertain and need to be examined. This will give a clearer picture in the design stage about the uncertainty of the calculations and in estimating the safety factor required for the design.

In addition to the existing empirical rules for the estimation of the different properties of the ionic liquid mixtures, such as refractive index, artificial intelligence (AI) models such as artificial neural networks (ANNs), regression models, fuzzy logic, support vector machine (SVM), and neural-based fuzzy interference system (ANFIS), can be used to predict the behavior of such complex systems. Different techniques have already been applied for the calculation of the various thermophysical properties of ionic liquid mixtures. Among various AI techniques, ANN alone or along with evolutionary algorithms such as genetic algorithms (GAs) and particle swarm optimization (PSO) has been used effectively to predict the properties of ionic liquid binary mixtures [1–4]. These techniques can predict responses with high accuracy, regardless of variation in input parameters. Very few studies have assessed the ability of the ANFIS model for this purpose [5]. ANFIS, however, is a potential soft computational modelling technique that combines the power of ANN with fuzzy logic [6–8]. ANFIS, as with the ANN, learns from training data with any complex relationships, then implements the solutions on a fuzzy inference system (FIS). ANFIS can use FIS to define hidden layers and to improve its predictive ability; thus, it eliminates the difficulty of defining the hidden layers that often exist in ANN; however, the number of membership functions (MFs) should be defined per input. The number of MFs depends on the number of the existing dataset. Their ability to overcome problems with experimental and deterministic models makes them ideal for complex chemical processes. However, determining the structure of ANN has become a major challenge in developing a highly accurate model [9]. Consequently, Hosoz et al. [10] pointed out that ANFIS, according to other studies, can predict more accurately than ANN. However, in other studies, it has been stated that the accuracy of these techniques depends on how they are implemented and their applications [11]. Considering all the aforementioned facts, in the present study, we have made an attempt to develop and examine an ANFIS model to predict the properties of ionic liquid binary mixtures. Our measured density and refractive index of binary ionic liquid mixtures as well as the available published data on these properties have been used in this work.

2. Properties of Binary Liquid Mixtures

2.1. Molar Volume

For ideal liquid mixtures, the molar volume is defined as:

$$v_{ideal\ mix} = \sum x_i v_i \quad (1)$$

where v_{mix} is the molar volume of the mixture, v_i is the individual molar volume of component i , and x_i is mole fraction of component i . Many liquids do not form ideal

mixtures and hence do not show volume additivity. The deviation from ideality can be calculated by introducing excess molar volume term to the previous equation. Hence, the equation is written as:

$$v_{real\ mix} = v_{ideal\ mix} + v^{excess} \quad (2)$$

2.2. Mixture Density

The density of a mixture can be defined as the overall mass of mixture occupying one unit volume. It can be calculated by:

$$\rho_{mix} = \frac{m_{total}}{V_{total}} \quad (3)$$

where ρ_{mix} is the mixture density, m_{total} is the total mass of mixture, and V_{total} is the total volume of mixture. For ideal liquid mixtures, using volume additivity, this equation can be written in terms of an individual component's densities as follows:

$$\frac{1}{\rho_{ideal\ mix}} = \sum \frac{x_i}{\rho_i} \quad (4)$$

where ρ_i is the density of component i and x_i is the mass fraction of component i . The average absolute relative difference percent (AARD%) is a good statistical parameter for analyzing the success of the proposed correlations for different properties such as density, which is defined as:

$$AARD\% = \frac{100 \sum \left| \frac{\rho_{ideal\ mix} - \rho_{mix, exp}}{\rho_{mix, exp}} \right|}{n} \quad (5)$$

2.3. Refractive Index

There are several mixing rules for the refractive index of mixtures in the literature. The most well-known correlations which have been used in this work are the following:

- Lorentz–Lorenz relation (L–L)

$$\frac{n_{mix}^2 - 1}{n_{mix}^2 + 2} = \sum \frac{n_i^2 - 1}{n_i^2 + 2} \phi_i \quad (6)$$

where n_{mix} is the refractive index of the mixture, n_i is the refractive index of pure component i , and ϕ_i is the volume fraction of component i in the mixture.

- Gladstone–Dale (G–D)

$$n_{mix} - 1 = \phi_1(n_1 - 1) + \phi_2(n_2 - 1) + \dots + \phi_n(n_n - 1) \quad (7)$$

- Arago–Biot (A–B)

$$n_{mix} = \phi_1 n_1 + \phi_2 n_2 + \dots + \phi_n n_n \quad (8)$$

- Weiner's relation (W)

$$\frac{n_{mix}^2 - n_1^2}{n_{mix}^2 + 2n_1^2} = \sum_{i \neq 1} \frac{n_i^2 - n_1^2}{n_i^2 + 2n_1^2} \phi_i \quad (9)$$

- Heller's relation (H)

$$\frac{n_{mix} - n_1}{n_1} = \frac{3}{2} \sum_{i \neq 1} \frac{m_i^2 - 1}{m_i^2 + 2} \phi_i \quad (10)$$

where $m_i = \frac{n_i}{n_1}$.

3. Materials and Experiments

The ionic liquids used in this work are 1-butyl-3-methylimidazolium thiocyanate ([BMIM][SCN]), 1-butyl-3-methylimidazolium tetrafluoroborate ([BMIM][BF₄]), 1-hexyl-3-methylimidazolium tetrafluoroborate ([HMIM][BF₄]), and 1-hexyl-3-methylimidazolium hexafluorophosphate ([HMIM][PF₆]). These ionic liquids were supplied by Io-li-tec and used as received. However, new measurements for the density and refractive index were taken for the pure ionic liquids to be used as reference. Table 1 shows the purity of each ionic liquid reported by Io-li-tec and their molecular weights.

Table 1. Purity of the ionic liquids used in this work.

Ionic Liquid	Molecular Weight	Purity
[BMIM][SCN]	197.30	≥98%
[BMIM][BF ₄]	226.03	≥99%
[HMIM][BF ₄]	254.08	≥99%
[HMIM][PF ₆]	312.24	≥99%

A pipette was used to transfer exact amounts of ionic liquids in a graduated cylinder to measure the total volume, each with uncertainty of 0.05 and 0.1 cm³, respectively. A mass balance of an uncertainty of 1×10^{-4} g was used to measure the mass of the samples. The refractive index was measured using a programmable digital KEM Refractometer (Kyoto Electronics Manufacturing Co., LTD., Model RA 620, Kyoto, Japan) connected to a water bath to maintain constant temperature. The uncertainty in the refractive index measurement is 1×10^{-5} , and the uncertainty in the temperature measurement is 0.1 K. The density was measured using an Anton Paar U-tube Densitometer (Model DMA 4500 M, Anton Paar GmbH, Graz, Austria) connected to a water bath. The uncertainty in the density measurement is 5×10^{-5} g cm⁻³, while the uncertainty in the temperature measurement was 0.1 K.

The density and refractive index of all samples were measured at 20 °C for the pure ionic liquids using an Anton Paar U-tube Densitometer and a Programmable Digital KEM Refractometer, respectively. The temperature was constantly maintained at 20 °C by connecting both the densitometer and the refractometer to a water bath set to a temperature of 20 °C. Binary mixtures of different ionic liquids were prepared from different volume compositions. The mass of each ionic liquid as well as the total mass of the mixture were measured before transfer to the graduated cylinder. A droplet was taken to be used in the refractometer to measure the refractive index. The remainder of the mixture was used to measure the mixture density using the density meter.

4. The Developed ANFIS Model and EFAST Sensitivity Analysis

Fuzzy logic is an appropriate technique for solving complex and nonlinear problems. ANNs have a strong ability to learn from existing data. Fuzzy logic theory is a powerful tool to deal with uncertainty. In general, fuzzy logic is an approach to calculate the degree of accuracy instead of using two-state true or false logic. Therefore, combining fuzzy logic theory with ANNs could provide great results for describing complex patterns, which is called ANFIS modelling. FIS assigns fuzzy rules and a membership function (MF) which ANN can optimize. Takagi–Sugeno and Mamdani are two well-known structures of FISs. Each FIS consists of a number of fuzzy rules, and each fuzzy rule has an antecedent and a consequent. In Mamdani-type FISs, both antecedents and consequents include fuzzy values; however, in Takagi–Sugeno-type FISs, the consequent of fuzzy rules are in the form of a fixed number (for zero type Takagi–Sugeno FISs) or a linear combination of inputs; this type of FISs are often used in ANFIS modelling. In this study, an ANFIS model was developed using the Takagi–Sugeno structure with the Neuro-Fuzzy Designer app in MATLAB 2017a software [9]. The ANFIS structure comprises four layers, which are fuzzy, product, consequent calculation, and output layer. The first layer includes antecedent

fuzzy values (also known as membership functions), the inputs enter these fuzzy values, and a membership grade is produced for each fuzzy value in each rule. In layer 2, the product of membership grades in a fuzzy rule is used as the firing strength of the rule in this research. Then, in layer 4 (in parallel with layers 1 and 2), the output of each rule is calculated using the input values. In the last layer, the output of the FIS is calculated by the output values and firing strengths of all rules. In this research, the weighted sum of outputs was used, where the weight of each rule output is the firing strength of the same rule. The unknowns of this modelling problem were the number of rules and fuzzy values (membership functions) of rules and consequent parameters. These were identified by using the experimental data.

In this study, various membership functions were investigated for their use in the rules' antecedents, such as the triangular-shaped membership function (trimf) and others, for which the details can be found elsewhere [12]. The result of this comparison is given in Section 6.

To estimate the density parameter using ANFIS, 1670 datasets were collected from the literature, which were applied for model training and cross validation. Cross validation partition defines a random partition on a dataset. This partition is used to define training and validation sets for validating a model. In this study, the early stopping method was used for preventing overfitting and the total dataset partitioned into training (85%) and holdout cross validation (15%) partitions. The holdout cross validation method creates a random nonstratified partition for holdout validation on n observations. Then, to determine the predictive power of the model, the measured data from this study (16 samples) were introduced to the model as external validation or a test dataset. The same procedure was followed for modelling the refractive index parameter, in which 149 data were collected and utilized from the published data for training and validation. Finally, 16 new measured data from this study were entered into the model for external validation. The hybrid-learning algorithm (as detailed in [13]) was used for parameter estimation, and the validity of the optimized ANFIS model was evaluated using experimental test data. The coefficient of determination (R^2), the root-mean-squared error (RMSE), and average absolute relative deviation (AARD%) were calculated to evaluate the model's performance [14,15].

$$R^2 = \frac{1 - \sum_{i=1}^n (Y_p - Y_e)^2}{\sum_{i=1}^n (Y_p - \underline{Y}_e)^2} \quad (11)$$

$$RMSE = \sqrt{\frac{1}{n} \sum_{i=1}^n (Y_e - Y_p)^2} \quad (12)$$

$$AARD\% = \frac{100}{n} \sum_{i=1}^n \frac{|Y_e - Y_p|}{Y_e} \quad (13)$$

where Y_e , Y_p , and \underline{Y}_e show the actual response, predicted response, and the average of the actual response, respectively, and n is the number of datasets.

For complex nonlinear models, such as the artificial intelligence models, global sensitivity analysis (GSA) techniques are able to provide appropriate information about parameter sensitivity. In the present study, the extended Fourier amplitude sensitivity test (EFAST), which is one of the efficient and well-known GSA methods, was applied for sensitivity analysis in MATLAB 2017 software. FAST is a variance-based global sensitivity analysis technique, which is based on conditional variances, indicating the individual or interaction effects of the uncertain inputs on the response parameter [16].

5. Experiments

5.1. Pure Ionic Liquids

Density and refractive index of the pure ionic liquids measured at 20 °C are shown in Table 2.

Table 2. Density and refractive index of the pure ionic liquids at 20 °C.

Ionic Liquid	Refractive Index	Density (g/cm ³)
[HMIM][BF ₄]	1.43940	1.14859, 1.14511 ^a
[HMIM][PF ₆]	1.42257	1.29544, 1.29145 ^a
[BMIM][SCN]	1.54543	1.07254, 1.06954 ^a
[BMIM][BF ₄]	1.43223	1.20447, 1.20085 ^a

^a Literature data at 298.15 K [17].

These values are used as references for the pure components in the analysis. Ionic liquid mixtures prepared for the experiments were labeled, and their measured masses and volumes at 20 °C are shown in Table 3.

Table 3. Measured volume and mass of prepared ionic liquid mixtures.

Mole Fraction (x_1)	Components		Mass (g)		Total
	1	2	1	2	
0.813			13.78308	3.88632	17.66940
0.620	[HMIM][BF ₄]	[HMIM][PF ₆]	10.33731	7.77264	18.10995
0.421			6.89154	11.65896	18.55050
0.214			3.44577	15.54528	18.99105
0.769			13.78308	3.21762	17.00070
0.555	[HMIM][BF ₄]	[BMIM][SCN]	10.33731	6.43524	16.77255
0.357			6.89154	9.65286	16.54440
0.172			3.44577	12.87048	16.31625
0.772			13.78308	3.61341	17.39649
0.560	[HMIM][BF ₄]	[BMIM][BF ₄]	10.33731	7.22682	17.56413
0.361			6.89154	10.84023	17.73177
0.175			3.44577	14.45364	17.89941
0.753			15.54528	3.21762	18.76290
0.534	[HMIM][PF ₆]	[BMIM][SCN]	11.65896	6.43524	18.09420
0.337			7.77264	9.65286	17.42550
0.160			3.88632	12.87048	16.75680

Table 3 shows the volume and mass of each component in the mixture. The mass of each component was used to calculate the mass fraction and mole fraction needed for the rest of calculations.

5.2. Mixtures of Ionic Liquids

5.2.1. Molar Volume and Density of Ionic Liquid Mixtures

Table 4 shows the measured mixture density, ideal mixture density, AARD%, measured mixture molar volume, ideal mixture molar volume, excess molar volume, and AARD% of the prepared ionic liquids.

Table 4. Measured and calculated volumetric data for the ionic liquid mixtures studied in this work.

Mixture	ρ_{mix} (g/cm ³)	$\rho_{ideal\ mix}$ (g/cm ³)	v_{mix} (cm ³ /mol)	$v_{ideal\ mix}$ (cm ³ /mol)	v^{excess} (cm ³ /mol)
[HMIM][BF4] + [HMIM][PF6]					
0.813	1.18620	1.17796	223.34763	224.90918	−1.56154
0.620	1.21185	1.20733	227.88141	228.73380	−0.85239
0.421	1.23965	1.2367	232.13618	232.69074	−0.55456
0.214	1.27477	1.26607	235.17064	236.78701	−1.61637
[HMIM][BF4] + [BMIM][SCN]					
0.769	1.13934	1.13338	211.48711	212.59928	−1.11218
0.555	1.11587	1.11817	205.05542	204.63350	0.42191
0.357	1.09203	1.10296	199.21668	197.24310	1.97359
0.172	1.10823	1.08775	186.84919	190.36790	−3.51871
[HMIM][BF4] + [BMIM][BF4]					
0.772	1.14710	1.159766	215.93122	213.57352	2.35771
0.560	1.15424	1.170942	209.43286	206.44638	2.98648
0.361	1.17505	1.182118	200.98041	199.77956	1.20086
0.175	1.18286	1.193294	195.23652	193.52985	1.70667
[HMIM][PF6] + [BMIM][SCN]					
0.753	1.25270	1.25086	226.61410	226.94751	−0.33341
0.534	1.20984	1.20628	213.78904	214.41969	−0.63065
0.337	1.16933	1.1617	201.87652	203.20263	−1.32611
0.160	1.13755	1.11712	189.63286	193.10083	−3.46797
AARD% = 0.78058%			AARD% = 0.78264%		

5.2.2. Refractive Index of Ionic Liquid Mixtures

Table 5 shows the experimental refractive indices of the ionic liquid mixtures and the calculated values using different empirical mixing rules.

Table 5. Experimental refractive indices of the ionic liquid mixtures and the calculated values using different empirical mixing rules.

Binary Mixtures	Refractive Index (n)					
	Experimental	L–L	G–D	A–B	W	H
[HMIM][BF4]+[HMIM][PF6]						
0.813	1.43831	1.43599	1.43604	1.43604	1.43603	1.43603
0.620	1.43745	1.43267	1.43267	1.43267	1.43267	1.43266
0.421	1.42883	1.42932	1.42931	1.42931	1.42930	1.42929
0.214	1.42408	1.42598	1.42594	1.42594	1.42594	1.42592
[HMIM][BF4]+[BMIM][SCN]						
0.769	1.46016	1.45955	1.46061	1.46061	1.46038	1.46033
0.555	1.46524	1.48088	1.48182	1.48182	1.48145	1.48125
0.357	1.50059	1.50209	1.50302	1.50302	1.50266	1.50217
0.172	1.52000	1.52364	1.52423	1.52423	1.52395	1.52309
[HMIM][BF4]+[BMIM][BF4]						
0.772	1.43918	1.43801	1.43798	1.43797	1.43797	1.43797
0.560	1.43767	1.43655	1.43654	1.43654	1.43654	1.43654
0.361	1.43475	1.43513	1.43511	1.43511	1.43511	1.43510
0.175	1.43288	1.43372	1.43367	1.43367	1.43367	1.43367
[HMIM][PF6]+[BMIM][SCN]						
0.753	1.45442	1.44636	1.44715	1.44715	1.44683	1.44676
0.534	1.47034	1.47048	1.47172	1.47172	1.47123	1.47094
0.337	1.50643	1.49504	1.49629	1.49629	1.49579	1.49512
0.160	1.51558	1.52005	1.52086	1.52086	1.52053	1.51930
	ARD (%)	0.24810	0.25711	0.25711	0.25190	0.24188

As we can see from Table 5, the refractive index of the ionic liquid mixtures can be confidently estimated using any of the discussed empirical formulae since the average relative error is around 0.25% for each correlation. However, Heller's relation (H) best estimates the refractive index of these ionic liquid mixtures with an average relative error of 0.242%.

6. ANFIS Modelling

The ANFIS models, developed to predict the density and refractive index of ionic liquid mixtures, are shown in Figures 1A and 2A. In this structure, we have employed the Takagi–Sugeno-type FIS with Gaussian curve membership functions. The ANFIS model has seven inputs of temperature (T), pressure (P), BMIM (mole fraction of BMIM ion), HMIM (mole fraction of HMIM ion), BF4 (mole fraction of BF4 ion), PF6 (mole fraction of PF6 ion), and SCN (mole fraction of SCN ion) for density and refractive index prediction. The grid partition technique is used to generate the rules for the model. The obtained results showed that the Gaussian membership function (gaussmf), compared to other membership functions, has less prediction errors in both models. Figures 1B and 2B illustrate the RMSE of the models' training and validation stages. During the training and validation process of the ANFIS model, the RMSEs were plotted versus the number of epochs. The RMSE reduces and then remains constant after some epochs. The RMSE values of the validation step for the density and refractive index models were equal to 8.730 and 7.45×10^{-3} , respectively. The regression curves plotted in Figures 1C and 2C display the model outputs, which show a very satisfactory performance. This comparison showed a good consistency between the predicted and actual responses of the ANFIS models.

We have used some statistical parameters as shown in Table 6 to examine the performance of the developed models.

Table 6. The performance of the statistical parameters for the proposed models.

Parameters	ANFIS (Density)			ANFIS (Refractive index)		
	Train	Validation	Test	Train	Validation	Test
R^2	0.992	0.985	0.968	0.988	0.972	0.948
RMSE	6.035	8.730	7.274	4.47×10^{-3}	7.45×10^{-3}	7.32×10^{-3}
AARD%	0.437	0.649	0.368	0.242	0.444	0.319

It is noteworthy that the ranges of error parameters for two responses (density and refractive index) are suitable at the training, validation, and test stages. The use of more data in the training and validation stages for density resulted in high predictive power, therefore the test data that were externally validated (not used in the training stage) resulted in predictions with higher accuracy. Moreover, a variance-based global analysis was performed using an extended EFAST method to determine which parameter had the greatest effect on the density and refractive index [18]. According to Figure 3A, the first three main factors affecting density are PF6, SCN, and pressure. In addition, according to Figure 3B, the most effective input parameters for the refractive index were SCN, pressure, and PF6. The coefficient values of different parameters are given in Figure 3.

Figures 4 and 5 show the three-dimensional plots of the developed models for the density and refractive index (n). As shown in Figure 4A,B, the density parameter often decreases with increasing temperature and increases with increasing pressure. In addition, an increase in parameters BMIM and SCN lead to a decrease in density (Figure 4B,E). BF4 has very little effect on density (Figure 4D). HMIM and PF6 have a positive correlation with density, as shown in Figure 4C,E. It is evident from Figure 5A that temperature has a negative effect on refractive index, and pressure has shown a non-uniform effect on it. However, the effect of the temperature on the refractive index is very small compared to the effect of pressure. In addition, an increase in parameters BMIM, BF4, and SCN leads to a decrease in the refractive index (Figure 5B–D). HMIM has very little effect on

the refractive index (Figure 5C). PF6 has a positive correlation with the refractive index, which is shown in Figure 5D. The model dataset contains 1670 density values over a temperature range of 220–472 K and a pressure range of 100–300,000 kPa collected from the NIST ILThermo database [19]. The model dataset contains 1670 density values over a temperature range of 220–472 K and a pressure range of 100–300,000 kPa collected from the NIST ILThermo database [19]. Our dataset for the refractive index which contains 149 values also has been collected from the NIST ILThermo database [19] in the range of 280–353 K for temperature, and the range of 81–116 kPa for pressure. This collected database is available in the Supplementary file in excel.

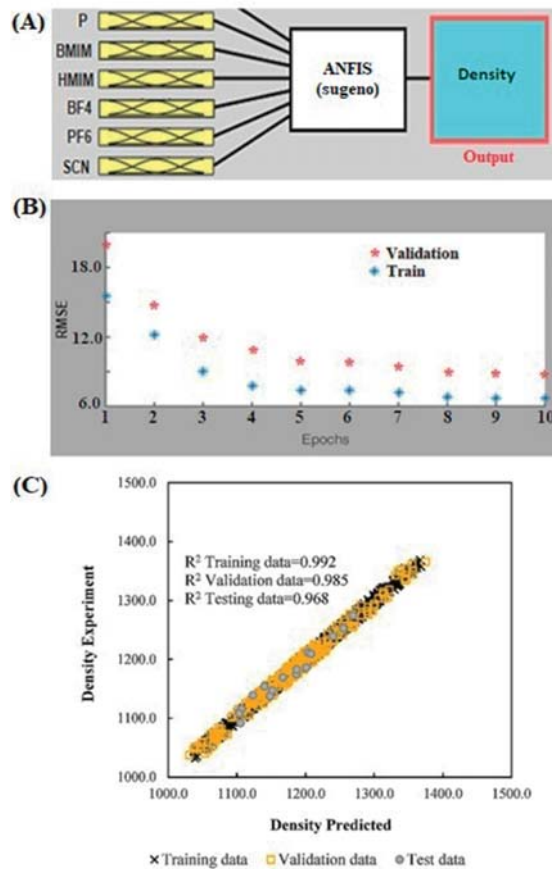


Figure 1. (A) Developed ANFIS structure, (B) training error curve, (C) regression between ANFIS predictions, and experimental results for density.

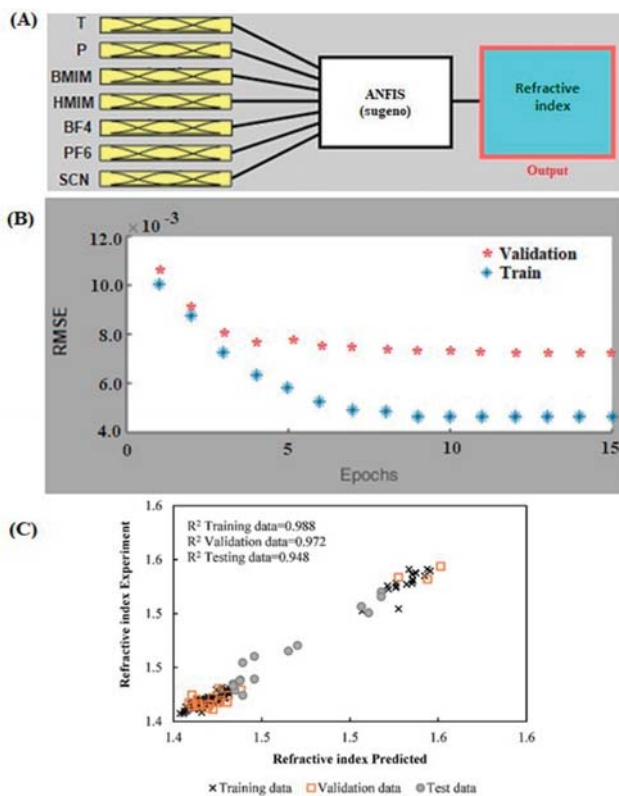


Figure 2. (A) Developed ANFIS structure, (B) training error curve, (C) regression between ANFIS predictions, and experimental results for refractive index.

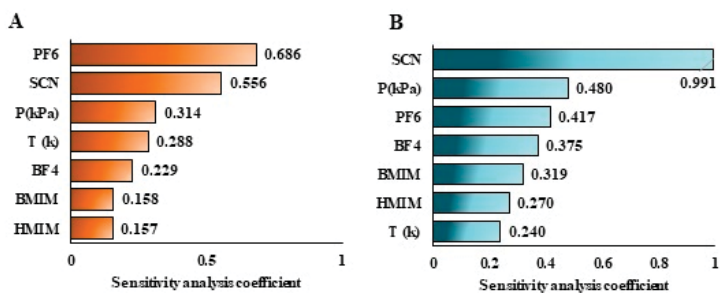


Figure 3. Relative importance of the input parameters on (A): density and (B): refractive index (n).

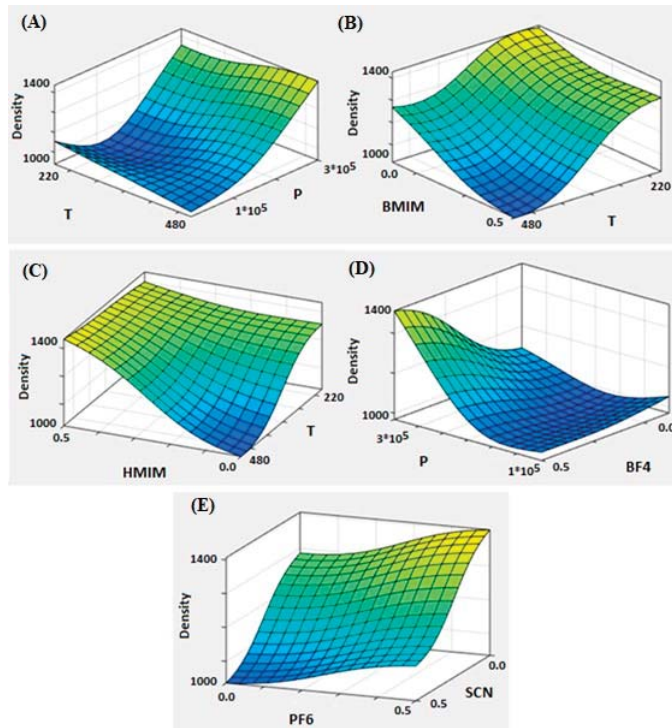


Figure 4. Three-dimensional mesh plot of the density variation using ANFIS model versus (A)–Temperature and Pressure, (B)–BMIM and Temperature, (C)–HMIM and Temperature, (D)–Pressure and BF4 and (E)–PF6 and SCN.

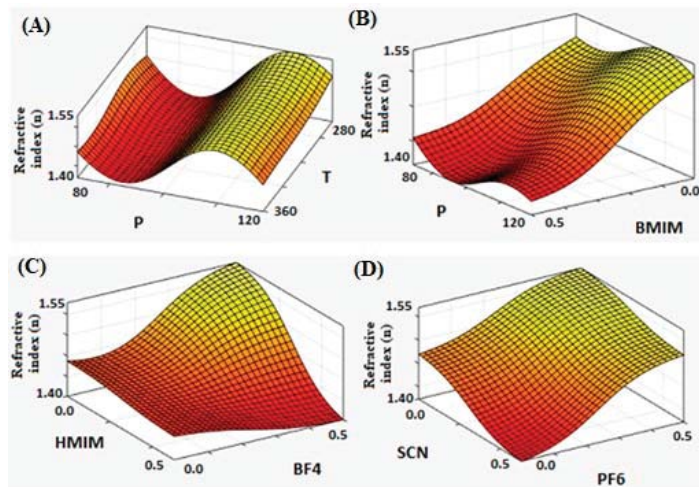


Figure 5. Three-dimensional mesh plot of the refractive index (n) variation using ANFIS model Versus, (A)–Pressure and Temperature, (B)–Pressure and BMIM, (C)–HMIM and BF4 and (D)–SCN and PF6.

7. Conclusions

Density and refractive index of different binary mixtures of ionic liquids were studied in this work. Some data were generated experimentally in this work and the rest of required data were collected from the literature. The effects of different variables such as temperature, pressure, and the molar concentrations of different functional groups in the ionic liquids were investigated. For analyzing the data, we first examined different models including empirical models for these properties. The deviation from the ideal mixture volume was calculated and found to be 0.78%. Therefore, it is a very accurate assumption to assume an ideal mixture and apply a volume additivity rule. Furthermore, the refractive indices of the binary ionic liquid mixtures were measured and compared with the estimated values using different empirical mixing rules. All of the empirical rules showed good performance for estimation of the refractive index of the binary ionic liquid mixtures, with an average percentage error around 0.25%. However, Heller's relation was found to be the best model to estimate these mixtures' refractive index with an average relative error of only 0.242%. For gaining a deep understanding of the effects of the different parameters on the density and refractive index of the studied mixtures, we have also developed artificial intelligence models. An ANFIS model was developed to predict a density and refractive index, and the grid partition technique was implemented. Our results showed that the Gaussian membership function, compared to other membership functions, has a low prediction error. Based on obtained results, the developed model showed excellent performance for predicting the density and refractive index of various mixtures, with overall R^2 , RMSE, and AARD% values of 0.985, 8.730, 0.649%, and 0.972, 7.45×10^{-3} , and 0.444%, in cross validation, and 0.968, 7.274, 0.368%, and 0.948, 7.32×10^{-3} , and 0.319% in the external validation stages, respectively. According to the sensitivity analysis using the EFAST method, the most effective input parameters for both properties were found to be SCN, pressure, and PF6.

Supplementary Materials: Supplementary data associated with this article can be found at: <https://www.mdpi.com/article/10.3390/liquids2040025/s1>.

Author Contributions: Conceptualization, G.R.V.-N.; methodology, G.R.V.-N.; software, F.M.; formal analysis, G.R.V.-N. and F.M.; resources, G.R.V.-N.; data curation, M.H.; writing—original draft preparation, G.R.V.-N., F.M. and M.H.; writing—review and editing, F.M., M.M. and G.R.V.-N.; project administration, G.R.V.-N.; funding acquisition, G.R.V.-N. and M.M. All authors have read and agreed to the published version of the manuscript.

Funding: The authors are thankful to Sultan Qaboos University for the financial support through the internal grant project number IG/ENG/PCED/22/02.

Data Availability Statement: Not applicable.

Conflicts of Interest: The authors declare no conflict of interest.

References

- Hemmati-Sarapardeh, A.; Tashakkori, M.; Hosseinzadeh, M.; Mozafari, A.; Hajirezaie, S. On the evaluation of density of ionic liquid binary mixtures: Modeling and data assessment. *J. Mol. Liq.* **2016**, *222*, 745–751. [[CrossRef](#)]
- Astray Dopazo, G.; González-Temes, M.; Larios López, D.; Mejuto, J.C. Density, viscosity and refractive index prediction of binary and ternary mixtures systems of ionic liquid. *Mediterr. J. Chem.* **2014**, *3*, 972–986. [[CrossRef](#)]
- Ornedo-Ramos, K.F.P.; Muriel, C.A.M.; Adornado, A.P.; Soriano, A.N.; Bungay, V.C. Prediction of density of binary mixtures of ionic liquids with alcohols (methanol/ethanol/1-propanol) using artificial neural network. *ASEAN J. Chem. Eng.* **2015**, *15*, 33–50. [[CrossRef](#)]
- Movagharnjad, K.; Vafaei, N. A Comparison Between GA and PSO Algorithms in Training ANN to Predict the Refractive Index of Binary Liquid Solutions. *J. Chem. Pet. Eng.* **2018**, *52*, 125–135.
- Barati-Harooni, A.; Najafi-Marghmaleki, A.; Mohammadi, A.H. ANFIS modeling of ionic liquids densities. *J. Mol. Liq.* **2016**, *224*, 965–975. [[CrossRef](#)]
- Mehrabi, D.; Mohammadzaheri, M.; Firoozfar, A.; Emadi, M. A fuzzy virtual temperature sensor for an irradiative enclosure. *J. Mech. Sci. Technol.* **2017**, *31*, 4989–4994. [[CrossRef](#)]

7. Mohammadzaheri, M.; Grainger, S.; Bazghaleh, M. Fuzzy modeling of a piezoelectric actuator. *Int. J. Precis. Eng. Manuf.* **2012**, *13*, 663–670. [CrossRef]
8. Mohammadzaheri, M.; Al Qallaf, A.; Ghodsi, M.; Ziaiefar, H. Development of a Fuzzy Model to Estimate the Head of Gaseous Petroleum Fluids Driven by Electrical Submersible Pumps. *Fuzzy Inf. Eng.* **2018**, *10*, 99–106. [CrossRef]
9. Ibrahim, K.S.M.H.; Huang, Y.F.; Ahmed, A.N.; Koo, C.H.; El-Shafie, A. A review of the hybrid artificial intelligence and optimization modelling of hydrological streamflow forecasting. *Alex. Eng. J.* **2022**, *61*, 279–303. [CrossRef]
10. Hosoz, M.; Ertunc, H.M.; Bulgurcu, H. An adaptive neuro-fuzzy inference system model for predicting the performance of a refrigeration system with a cooling tower. *Expert Syst. Appl.* **2011**, *38*, 14148–14155. [CrossRef]
11. Gill, J.; Singh, J.; Ohunakin, O.S.; Adelekan, D.S. Artificial neural network approach for irreversibility performance analysis of domestic refrigerator by utilizing LPG with TiO₂-lubricant as replacement of R134a. *Int. J. Refrig.* **2018**, *89*, 159–176. [CrossRef]
12. Marjani, A.; Babanezhad, M.; Shirazian, S. Application of adaptive network-based fuzzy inference system (ANFIS) in the numerical investigation of Cu/water nanofluid convective flow. *Case Stud. Therm. Eng.* **2020**, *22*, 100793. [CrossRef]
13. Mohammadzaheri, M.; Amouzadeh, A.; Doustmohammadi, M.; Emadi, M.; Jamshidi, E.; Ghodsi, M.; Soltani, P. Fuzzy Analysis of Resonance Frequencies for Structural Inspection of an Engine Cylinder Block. *Fuzzy Inf. Eng.* **2021**, *13*, 266–276. [CrossRef]
14. Deng, Y.; Xiao, H.; Xu, J.; Wang, H. Prediction model of PSO-BP neural network on coliform amount in special food. *Saudi J. Biol. Sci.* **2019**, *26*, 1154–1160. [CrossRef] [PubMed]
15. Jahangir, M.H.; Mousavi Reineh, S.M.; Abolghasemi, M. Spatial predication of flood zonation mapping in Kan River Basin, Iran, using artificial neural network algorithm. *Weather Clim. Extrem.* **2019**, *25*, 100215. [CrossRef]
16. Ebert, N.; Goos, J.C.; Kirschbaum, F.; Yildiz, E.; Koch, T. Methods of sensitivity analysis in model-based calibration. *Automot. Engine Technol.* **2020**, *5*, 45–56. [CrossRef]
17. Vakili-Nezhaad, G.R.; Vatani, M.; Asghari, M.; Ashour, I. Effect of temperature on the physical properties of 1-butyl-3-methylimidazolium based ionic liquids with thiocyanate and tetrafluoroborate anions, and 1-hexyl-3-methylimidazolium with tetrafluoroborate and hexafluorophosphate anions. *J. Chem. Thermodyn.* **2012**, *54*, 148–154. [CrossRef]
18. Mohammadi, F.; Bina, B.; Karimi, H.; Rahimi, S.; Yavari, Z. Modeling and sensitivity analysis of the alkylphenols removal via moving bed biofilm reactor using artificial neural networks: Comparison of Levenberg Marquardt and particle swarm optimization training algorithms. *Biochem. Eng. J.* **2020**, *161*, 107685. [CrossRef]
19. Ionic Liquids Database—ILThermo (v2.0). Available online: <https://ilthermo.boulder.nist.gov/> (accessed on 23 July 2022).

Article

Application of Solution Calorimetry to Determining the Fusion Enthalpy of an Arylaliphatic Compound at 298.15 K: *n*-Octadecanophenone

Mikhail I. Yagofarov *, Ilya S. Balakhontsev, Andrey A. Sokolov and Boris N. Solomonov

Department of Physical Chemistry, Kazan Federal University, Kremlevskaya Str. 18, 420008 Kazan, Russia

* Correspondence: miyagofarov@kpfu.ru

Abstract: Evaluating the temperature dependence of the fusion enthalpy is no trivial task, as any compound melts at a unique temperature. At the same time, knowledge of the fusion enthalpies under some common conditions, particularly at the reference temperature of 298.15 K, would substantially facilitate the comparative analysis and development of the predictive schemes. In this work, we continue our investigations of the temperature dependence of the fusion enthalpy of organic non-electrolytes using solution calorimetry. As an object of study, *n*-octadecanophenone, an arylaliphatic compound was chosen. The solvent appropriate for evaluating the fusion enthalpy at 298.15 K from the solution enthalpy of crystal was selected: *p*-xylene. The heat capacity and fusion enthalpy at the melting temperature were measured by differential scanning calorimetry to derive the fusion enthalpy at 298.15 K from the Kirchhoff's law of Thermochemistry. An agreement between the independently determined values was demonstrated. This particular result opens a perspective for further studies of the fusion thermochemistry of arylaliphatic compounds at 298.15 K by solution calorimetry.

Keywords: solution calorimetry; fusion enthalpy; differential scanning calorimetry; alkanophenones

Citation: Yagofarov, M.I.; Balakhontsev, I.S.; Sokolov, A.A.; Solomonov, B.N. Application of Solution Calorimetry to Determining the Fusion Enthalpy of an Arylaliphatic Compound at 298.15 K: *n*-Octadecanophenone. *Liquids* **2023**, *3*, 1–6. <https://doi.org/10.3390/liquids3010001>

Academic Editors: William E. Acree, Jr. and Juan Ortega Saavedra

Received: 27 November 2022

Accepted: 19 December 2022

Published: 21 December 2022



Copyright: © 2022 by the authors. Licensee MDPI, Basel, Switzerland. This article is an open access article distributed under the terms and conditions of the Creative Commons Attribution (CC BY) license (<https://creativecommons.org/licenses/by/4.0/>).

1. Introduction

The studies of phase transition thermodynamics of organic non-electrolytes have more than a 150-year-old history. A lot of efforts have been paid to develop increasingly precise experimental techniques [1], as well as predictive methods. Quantitative structure-property relationships proposed so far to characterize the fusion process, particularly its enthalpy, remain relatively less accurate [2–7], compared with the vaporization and sublimation [7–12]. Among the obstacles to establishing the relationships of the fusion enthalpy with the molecular structure and descriptors, one can distinguish the fact that it is measured at the melting point (T_m), which is unique for each compound. This impedes the comparative analysis, in contrast with the vaporization and sublimation processes, whose thermodynamic parameters can be determined under the common conditions (e.g., 298.15 K) for numerous systems. Adjustment of the fusion enthalpies (Δ_{cr}^1H) to 298.15 K would require knowledge of its temperature dependence. The temperature dependence of the fusion enthalpy is also of interest when applying the ideal solubility equation [13–17], and analyzing nucleation and crystallization kinetics [18,19].

Δ_{cr}^1H at 298.15 K can be found from Kirchhoff's law of Thermochemistry (Equation (1)):

$$\Delta_{cr}^1H(298.15\text{ K}) = \Delta_{cr}^1H(T_m) + \int_{T_m}^{298.15\text{ K}} \Delta_{cr}^1C_{p,m}dT \quad (1)$$

where $\Delta_{cr}^1C_{p,m}$ is the heat capacity change on melting. Generally speaking, it also depends on temperature and this dependence can sometimes significantly contribute to $\Delta_{cr}^1H(298.15\text{ K})$ [20].

Experimental determination of this value below T_m would require supercooling the melt, which is rarely possible.

In a recent cycle of works [21,22] we proposed a method for determining the fusion enthalpies of organic non-electrolytes based on solution calorimetry, based on Hess's law (Equation (2)):

$$\Delta_{\text{soln}}H(\text{cr}, 298.15 \text{ K}) = \Delta_{\text{cr}}^1H(298.15 \text{ K}) + \Delta_{\text{soln}}H(\text{l}, 298.15 \text{ K}) \quad (2)$$

According to Equation (2), the solution enthalpy of the crystal in a certain solvent $\Delta_{\text{soln}}H(\text{cr}, 298.15 \text{ K})$ is equal to a sum of $\Delta_{\text{cr}}^1H(298.15 \text{ K})$ and the solution enthalpy of the quasi-equilibrium melt in the same solvent at 298.15 K. In many solute-solvent systems (e.g., aromatic compounds incapable of self-association in benzene [21] or alkanes in heptane [23]) the latter is nearly 0, so $\Delta_{\text{cr}}^1H(298.15 \text{ K})$ can be found directly from $\Delta_{\text{soln}}H(\text{cr}, 298.15 \text{ K})$.

Combining Equations (1) and (2), we independently tracked the temperature dependence of the supercooled liquid heat capacity between 298.15 K and T_m :

$$\Delta_{\text{cr}}^1H(T_m) + \int_{T_m}^{298.15 \text{ K}} \Delta_{\text{cr}}^1C_{p,m}dT = \Delta_{\text{soln}}H(\text{cr}, 298.15 \text{ K}) - \Delta_{\text{soln}}H(\text{l}, 298.15 \text{ K}) \quad (3)$$

Analyzing the relationship between the enthalpies of fusion and solution, we established that an agreement between the left and right sides of Equation (3) is achieved when the temperature dependence of the heat capacity of the liquid determined above T_m is extrapolated down to 298.15 K as a linear function of temperature [21].

Equation (2) provides a useful alternative to Equation (1), replacing a laborious procedure of heat capacity measurement with solution calorimetry. However, it requires searching for the solvent, in which $\Delta_{\text{soln}}H(\text{l}, 298.15 \text{ K})$ can be accurately evaluated based on the molecular structure. Previously we mainly focused on aromatic (both hydrogen-bonded [22] and non-hydrogen-bonded [21]) and aliphatic [23] systems but did not concern alkylaromatic compounds. For alkylarenes, the solution enthalpy in benzene significantly grows with the chain length increase, while the solution enthalpy in heptane can be significantly influenced by the presence of any substituent, except for the alkyl group. In this work we tested if *p*-xylene, which contains both aromatic core and alkyl groups, can be used as an "athermal" solvent for a long-chain alkylaromatic solute, *n*-octadecanophenone, to determine its fusion enthalpy at 298.15 K.

2. Materials and Methods

2.1. Materials

p-Xylene (CAS № 106-42-3, C₈H₁₀, Acros, Thermo Fisher Scientific, Waltham, MA, USA), *n*-octanophenone (CAS № 1674-37-9, C₁₄H₂₀O, TCI Chemicals, Tokyo, Japan), and *n*-octadecanophenone (CAS № 6786-36-3, C₂₄H₄₀O, Alfa Aesar, Haverhill, MA, USA) were of commercial origin with a purity more than 0.99 (mole fraction), as it was stated in the certificate of analysis (determined by gas chromatography). Water content in *p*-xylene was determined by Fischer titration and equaled 0.01% (mole fraction). Before the measurements, *n*-octanophenone and *n*-octadecanophenone were dried *in vacuo* to remove any traces of moisture.

The samples were used without further purification.

2.2. Differential Scanning Calorimetry

The specific heat capacity of crystal, enthalpy, and temperature of fusion of *n*-octadecanophenone were measured using DSC 8500 (Perkin Elmer, Waltham, MA, USA). Prior to the experiment, aluminum crucibles were annealed at 200 °C. DSC was calibrated according to the manufacturer's recommendation using the standard samples of Indium and Zinc. Each value (onset temperature and area of the peak) was determined three times. The reproducibilities of heat flow and temperature calibration (0.95 level of confidence,

coverage factor 2.0) were equal to 1% and 0.1 K, respectively. The correctness of the determination of the heat capacity and heat effects was checked as previously [24]. The agreement with the reference values was within 2%.

The samples were placed in a 50 μL aluminum crucible in an inert atmosphere. Two samples were studied to determine each value. Experiments were performed in a nitrogen dynamic atmosphere (30 mL min^{-1}) with a heating/cooling rate of 5 K min^{-1} . Two cycles of "heating-cooling" from room temperature to a temperature 40 K higher than the melting point were carried out to determine the enthalpy and temperature of fusion. The samples crystallized completely on cooling. Experimental results from DSC measurements are presented in Table 1. An exemplary melting peak of *n*-octadecanophenone obtained by DSC is shown in Figure 1. An agreement between the fusion enthalpies obtained in each experiment was within a typical reproducibility of the DSC technique (2–3%).

Table 1. The enthalpies and temperatures of fusion of *n*-octadecanophenone determined in this work by DSC at 0.1 MPa ^a.

<i>m</i> /mg	T_m /K	$\Delta_{cr}^1 H(T_m)/(\text{kJ}\cdot\text{mol}^{-1})$
8.54	337.6	70.65
8.54	337.6	70.84
10.31	337.5	71.82
10.31	337.5	71.95
Average ^b	337.6 ± 0.1	71.3 ± 2.1

^a The standard uncertainty $u(p) = 5 \text{ kPa}$. ^b The uncertainty includes the standard deviation of the mean and the standard calibration uncertainty both multiplied by the coverage factor $k \approx 2.0$ (expanded uncertainty of the mean U ; 0.95 level of confidence).

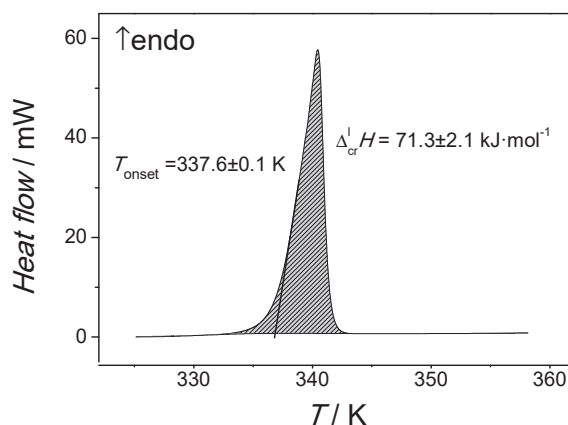


Figure 1. Melting peak of *n*-octadecanophenone obtained by DSC in this work.

The measurement of specific heat capacity was performed according to the isothermal step method as previously [25]. The procedure included three steps. First, the baseline was determined using empty crucibles. Then, using the baseline, a standard sample (sapphire) with a weight of 33.79 mg and a sample of *n*-octadecanophenone were each measured in the same crucible. This procedure was repeated twice for two samples of *n*-octadecanophenone, whose fusion enthalpies were measured. The temperature program included a dynamic segment between 320 K and 325 K and two isothermal segments at 320 K and 325 K. The resulting heat capacity of solid *n*-octadecanophenone at 322.5 K was $622 \pm 18 \text{ J}\cdot\text{K}^{-1}\cdot\text{mol}^{-1}$ (the uncertainty includes the standard deviation of the mean and the standard calibration uncertainty both multiplied by the coverage factor $k \approx 2.0$ (expanded uncertainty of the mean U ; 0.95 level of confidence)).

2.3. Solution Calorimetry

The solution enthalpies of *n*-octadecanophenone and *n*-octanophenone in *p*-xylene were measured at 298.15 K in the concentration range from 1.39 to 6.37 mmol kg⁻¹ using TAM III precision solution calorimeter (TA Instruments, New Castle, DE, USA). Crystal *n*-octadecanophenone was dissolved by breaking a glass ampule filled with ~50 mg of the studied sample in a glass cell containing 90 mL of the pure solvent. Liquid *n*-octanophenone was injected in ~50 μL portions using an electronically operated syringe equipped with a long gold cannula immersed in the solvent. The details of the solution calorimetry procedure have been described elsewhere [26]. The conditions corresponding to an infinite dilution, which was confirmed by an absence of the concentration dependence of the solution enthalpy. The experimental values are provided in Table 2.

Table 2. The solution enthalpies of phenones in *p*-xylene measured in this work at 298.15 K and 0.1 MPa^a.

Compound	<i>m</i> /mg ^b	<i>b</i> /(mmol·kg ⁻¹) ^c	Δ _{soln} <i>H</i> /(kJ·mol ⁻¹) ^d
<i>n</i> -Octanophenone	49.8	3.15	−0.28
	50.6	3.20	−0.48
	51.0	6.37	−0.34
	49.7	6.34	−0.51
	Average^e		−0.40 ± 0.11
<i>n</i> -Octadecanophenone	37.2	1.39	71.54
	48.9	1.83	70.78
	43.8	3.03	71.07
	43.9	3.48	70.72
	Average^e		71.0 ± 0.5

^a Standard uncertainties *u* are *u*(*T*) = 0.01 K, *u*(*p*) = 5 kPa. ^b Mass of the solute sample which was added in each dissolution experiment. ^c Molality of solute in solution after experiments. Standard uncertainty *u*(*b*) = 0.01 mmol·kg⁻¹. ^d Enthalpy of solution of each experiment. ^e Average enthalpy of solution. The uncertainty includes the standard deviation of the mean and the standard calibration uncertainty both multiplied by the coverage factor *k* ≈ 2.0 (expanded uncertainty of the mean *U*; 0.95 level of confidence).

3. Results

In Ref. [27] the molar heat capacity of liquid *n*-octadecanophenone was determined as a function of temperature between 373 and 418 K with an uncertainty of 2% (Equation (4)):

$$C_{p,m}/(\text{J}\cdot\text{K}^{-1}\cdot\text{mol}^{-1}) = 297.5 + 1.238 \cdot (T/K) \quad (4)$$

In this work, $C_{p,m}(\text{cr}, 322.5 \text{ K}) = 622 \pm 18 \text{ J}\cdot\text{K}^{-1}\cdot\text{mol}^{-1}$ was determined. The extrapolated $C_{p,m}(\text{l}, 322.5 \text{ K})$ value equals $697 \pm 30 \text{ J}\cdot\text{K}^{-1}\cdot\text{mol}^{-1}$ (uncertainty evaluated according to Ref. [20]). Thus, $\Delta_{\text{cr}}^{\text{l}}C_{p,m}(322.5 \text{ K}) = 75 \pm 35 \text{ J}\cdot\text{K}^{-1}\cdot\text{mol}^{-1}$. Within the temperature range of Equation (4) (298.15–337.6 K), it is reasonable to assume that $\Delta_{\text{cr}}^{\text{l}}C_{p,m}$ slightly depends on temperature. Then $\int_{T_m}^{298.15 \text{ K}} \Delta_{\text{cr}}^{\text{l}}C_{p,m} dT = \Delta_{\text{cr}}^{\text{l}}C_{p,m} \cdot (298.15 \text{ K} - T_m) = -3.0 \pm 1.4 \text{ kJ}\cdot\text{mol}^{-1}$. Therefore, from Equation (1) one can obtain $\Delta_{\text{cr}}^{\text{l}}H(298.15 \text{ K}) = 68.3 \pm 2.5 \text{ kJ}\cdot\text{mol}^{-1}$.

Evaluation of $\Delta_{\text{cr}}^{\text{l}}H(298.15 \text{ K})$ is also possible using the experimental value of $\Delta_{\text{soln}}H$ of crystal *n*-octadecanophenone ($71.0 \pm 0.5 \text{ kJ}\cdot\text{mol}^{-1}$) and Equation (2). The solution enthalpies of liquid alkanes in *p*-xylene are notably less than in benzene, which has been previously used as a solvent for aromatic compounds. For example, $\Delta_{\text{soln}}H(\text{l}, 298.15 \text{ K})$ of hexadecane in benzene is equal to $11.3 \text{ kJ}\cdot\text{mol}^{-1}$ [28] and in *p*-xylene to $3.1 \text{ kJ}\cdot\text{mol}^{-1}$ [29]. Those of heptane equal 5.6 [28] and $1.4 \text{ kJ}\cdot\text{mol}^{-1}$ [29], respectively. $\Delta_{\text{soln}}H(\text{l}, 298.15 \text{ K})$ of *n*-octanophenone in *p*-xylene determined in this work equaled $-0.4 \text{ kJ}\cdot\text{mol}^{-1}$. Thus, it is reasonable to assume that $\Delta_{\text{soln}}H(\text{l}, 298.15 \text{ K})$ of *n*-octadecanophenone in *p*-xylene is in the range from -0.4 to $3.1 \text{ kJ}\cdot\text{mol}^{-1}$, or $1.4 \pm 1.8 \text{ kJ}\cdot\text{mol}^{-1}$, which is not quite wide, taking in mind the absolute values of $\Delta_{\text{soln}}H(\text{cr}, 298.15 \text{ K})$ and $\Delta_{\text{cr}}^{\text{l}}H(T_m)$. Further elaboration of this value is possible if additional measurements of the solution enthalpies of alkylarenes is

performed to understand the regularities met in this series. Then, from Equation (2), one obtains $\Delta_{cr}^1H(298.15\text{ K}) = 69.6 \pm 1.9\text{ kJ}\cdot\text{mol}^{-1}$.

4. Discussion

The above-obtained $\Delta_{cr}^1H(298.15\text{ K})$ values of 68.3 ± 2.5 and $69.6 \pm 1.9\text{ kJ}\cdot\text{mol}^{-1}$ agree within the limits of the propagated errors. Such an agreement confirms the validity of the assumptions made during the $\Delta_{soln}H(l, 298.15\text{ K})$ evaluation. Thus, the fusion enthalpies of alkylarenes and their derivatives can actually be determined using solution calorimetry and *p*-xylene as an “athermal” solvent. It is worth noting that, due to an extrapolation uncertainty, the error of the enthalpy correction to 298.15 K according to Kirchhoff’s law may attain ~50% of its value. In this paper, this error was comparable with the fusion and solution enthalpies uncertainties. However, when the temperature range of adjustment and heat capacity integral increase, its contribution can become crucial. This highlights the advantages of the solution calorimetry approach, which enables to evaluation of the fusion enthalpy directly at 298.15 K, with an uncertainty independent of the melting temperature and tendency to supercooling.

Further quantification of the regularities, especially tracking the effects of the chain length, branching, and substituents on $\Delta_{soln}H(l, 298.15\text{ K})$ in *p*-xylene is anticipated to obtain more accurate results for a wider range of compounds. This finding echoes with the previously denoted “molecule-additivity” of the vaporization enthalpies of alkylaromatic compounds [30], which can be associated with instantaneous nanoheterogeneities in such systems, i.e., aromatic-aromatic and aliphatic-aliphatic interactions are more frequent than aromatic-aliphatic ones. Such distinction can be enough to minimize the significant endothermic effects met when studying benzene-alkanes systems under infinite dilution conditions [28].

Author Contributions: Conceptualization, M.I.Y.; methodology, M.I.Y.; investigation, I.S.B. and A.A.S.; writing—original draft preparation, M.I.Y.; writing—review and editing, B.N.S. All authors have read and agreed to the published version of the manuscript.

Funding: This paper has been supported by the Kazan Federal University Strategic Academic Leadership Program (‘PRIORITY-2030’).

Data Availability Statement: Not applicable.

Conflicts of Interest: The authors declare no conflict of interest.

References

1. Weir, R.D.; de Loos, T.W. *Measurement of the Thermodynamic Properties of Multiple Phases*; Gulf Professional Publishing: Woburn, MA, USA, 2005.
2. Dannenfelser, R.-M.; Yalkowsky, S.H. Estimation of Entropy of Melting from Molecular Structure: A Non-Group Contribution Method. *Ind. Eng. Chem. Res.* **1996**, *35*, 1483–1486. [[CrossRef](#)]
3. Jain, A.; Yang, G.; Yalkowsky, S.H. Estimation of Melting Points of Organic Compounds. *Ind. Eng. Chem. Res.* **2004**, *43*, 7618–7621. [[CrossRef](#)]
4. Wu, M.; Yalkowsky, S. Estimation of the molar heat capacity change on melting of organic compounds. *Ind. Eng. Chem. Res.* **2008**, *48*, 1063–1066. [[CrossRef](#)]
5. Chickos, J.S.; Acree, W.E. Total phase change entropies and enthalpies. An update on fusion enthalpies and their estimation. *Thermochim. Acta* **2009**, *495*, 5–13. [[CrossRef](#)]
6. Bondi, A. A Correlation of the Entropy of Fusion of Molecular Crystals with Molecular Structure. *Chem. Rev.* **1967**, *67*, 565–580. [[CrossRef](#)]
7. Naef, R.; Acree, W.E. Calculation of five thermodynamic molecular descriptors by means of a general computer algorithm based on the group-additivity method: Standard enthalpies of vaporization, sublimation and solvation, and entropy of fusion of ordinary organic molecules and total phase-change entropy of liquid crystals. *Molecules* **2017**, *22*, 1059. [[PubMed](#)]
8. Gharagheizi, F.; Babaie, O.; Mazdeyasna, S. Prediction of vaporization enthalpy of pure compounds using a group contribution-based method. *Ind. Eng. Chem. Res.* **2011**, *50*, 6503–6507. [[CrossRef](#)]
9. Mulero, A.; Cachadina, I.; Parra, M.I. Comparison of corresponding-states-based correlations for the prediction of the vaporization enthalpy of fluids. *Ind. Eng. Chem. Res.* **2008**, *47*, 7903–7916. [[CrossRef](#)]

10. Solomonov, B.N.; Yagofarov, M.I. An approach for the calculation of vaporization enthalpies of aromatic and heteroaromatic compounds at 298.15 K applicable to supercooled liquids. *J. Mol. Liq.* **2020**, *319*, 114330. [[CrossRef](#)]
11. Solomonov, B.N.; Yagofarov, M.I. Compensation relationship in Thermodynamics of solvation and vaporization: Features and applications. I. Non-hydrogen-bonded systems. *J. Mol. Liq.* **2022**, submitted. [[CrossRef](#)]
12. Abraham, M.H.; Acree Jr, W.E. Estimation of enthalpies of sublimation of organic, organometallic and inorganic compounds. *Fluid Phase Equilibria* **2020**, *515*, 112575. [[CrossRef](#)]
13. Bustamante, P.; Peña, M.A.; Barra, J. Partial-solubility Parameters of Naproxen and Sodium Diclofenac. *J. Pharm. Pharmacol.* **2011**, *50*, 975–982. [[CrossRef](#)] [[PubMed](#)]
14. Cheuk, D.; Svård, M.; Rasmuson, Å.C. Thermodynamics of the Enantiotropic Pharmaceutical Compound Benzocaine and Solubility in Pure Organic Solvents. *J. Pharm. Sci.* **2020**, *109*, 3370–3377. [[CrossRef](#)] [[PubMed](#)]
15. Neau, S.H.; Bhandarkar, S.V.; Hellmuth, E.W. Differential molar heat capacities to test ideal solubility estimations. *Pharm. Res.* **1997**, *14*, 601–605. [[CrossRef](#)] [[PubMed](#)]
16. Schwartz, P.A.; Paruta, A.N. Solution thermodynamics of alkyl p-aminobenzoates. *J. Pharm. Sci.* **1976**, *65*, 252–257. [[CrossRef](#)]
17. Pappa, G.D.; Voutsas, E.C.; Magoulas, K.; Tassios, D.P. Estimation of the differential molar heat capacities of organic compounds at their melting point. *Ind. Eng. Chem. Res.* **2005**, *44*, 3799–3806. [[CrossRef](#)]
18. Hoffman, J.D. Thermodynamic driving force in nucleation and growth processes. *J. Chem. Phys.* **1958**, *29*, 1192–1193. [[CrossRef](#)]
19. Huang, C.; Chen, Z.; Gui, Y.; Shi, C.; Zhang, G.G.; Yu, L. Crystal nucleation rates in glass-forming molecular liquids: D-sorbitol, d-arabitol, d-xylitol, and glycerol. *J. Chem. Phys.* **2018**, *149*, 054503. [[CrossRef](#)]
20. Yagofarov, M.I.; Solomonov, B.N. Calculation of the fusion enthalpy temperature dependence of polyaromatic hydrocarbons from the molecular structure: Old and new approaches. *J. Chem. Thermodyn.* **2021**, *152*, 106278. [[CrossRef](#)]
21. Yagofarov, M.I.; Nagrimanov, R.N.; Solomonov, B.N. New aspects in the thermochemistry of solid-liquid phase transitions of organic non-electrolytes. *J. Mol. Liq.* **2018**, *256*, 58–66. [[CrossRef](#)]
22. Yagofarov, M.I.; Lapuk, S.E.; Mukhametzyanov, T.A.; Ziganshin, M.A.; Valiakhmetov, T.F.; Solomonov, B.N. The fusion thermochemistry of self-associated aromatic compounds at 298.15 K studied by solution calorimetry. *J. Chem. Thermodyn.* **2019**, *137*, 43–47. [[CrossRef](#)]
23. Nagrimanov, R.N.; Samatov, A.A.; Solomonov, B.N. Additive scheme of solvation enthalpy for linear, cyclic and branched-chain aliphatic compounds at 298.15 K. *J. Mol. Liq.* **2019**, *292*, 111365. [[CrossRef](#)]
24. Yagofarov, M.I.; Sokolov, A.A.; Gerasimov, A.V.; Solomonov, B.N.; Stepurko, E.N.; Yurkshovich, Y.N. Thermodynamic Properties of Thioxanthone between 80 and 540 K. *J. Chem. Eng. Data* **2022**, in press. [[CrossRef](#)]
25. Yagofarov, M.I.; Bolmatenkov, D.N.; Solomonov, B.N. Relationship between the vaporization enthalpies of aromatic compounds and the difference between liquid and ideal gas heat capacities. *J. Chem. Thermodyn.* **2021**, *158*, 106443. [[CrossRef](#)]
26. Solomonov, B.N.; Varfolomeev, M.A.; Nagrimanov, R.N.; Novikov, V.B.; Zaitsau, D.H.; Verevkin, S.P. Solution calorimetry as a complementary tool for the determination of enthalpies of vaporization and sublimation of low volatile compounds at 298.15 K. *Thermochim. Acta* **2014**, *589*, 164–173. [[CrossRef](#)]
27. Bolmatenkov, D.N.; Notfullin, A.A.; Yagofarov, M.I.; Nagrimanov, R.N.; Italmasov, A.R.; Solomonov, B.N. Vaporization thermodynamics of normal alkyl phenones. *J. Mol. Liq.* **2023**, *370*, 121000. [[CrossRef](#)]
28. Lu, J.Z.; Acree, W.E.; Abraham, M.H. Updated Abraham model correlations for enthalpies of solvation of organic solutes dissolved in benzene and acetonitrile. *Phys. Chem. Liq.* **2019**, *57*, 84–99. [[CrossRef](#)]
29. Varfolomeev, M.A.; Rakupov, I.T.; Acree, W.E., Jr.; Brumfield, M.; Abraham, M.H. Examination of hydrogen-bonding interactions between dissolved solutes and alkylbenzene solvents based on Abraham model correlations derived from measured enthalpies of solvation. *Thermochim. Acta* **2014**, *594*, 68–79. [[CrossRef](#)]
30. Solomonov, B.N.; Yagofarov, M.I.; Nagrimanov, R.N. Additivity of vaporization enthalpy: Group and molecular contributions exemplified by alkylaromatic compounds and their derivatives. *J. Mol. Liq.* **2021**, *342*, 117472. [[CrossRef](#)]

Disclaimer/Publisher's Note: The statements, opinions and data contained in all publications are solely those of the individual author(s) and contributor(s) and not of MDPI and/or the editor(s). MDPI and/or the editor(s) disclaim responsibility for any injury to people or property resulting from any ideas, methods, instructions or products referred to in the content.

Article

Thermodynamic Analysis of the Solubility of Sulfadiazine in (Acetonitrile + 1-Propanol) Cosolvent Mixtures from 278.15 K to 318.15 K

Carlos Francisco Trujillo-Trujillo ^{1,2}, Fredy Angarita-Reina ³, Mauricio Herrera ¹, Claudia Patria Ortiz ⁴, Rossember Edén Cardenas-Torres ⁵, Fleming Martínez ⁶ and Daniel Ricardo Delgado ^{1,*}

- ¹ Programa de Ingeniería Civil, Grupo de Investigación de Ingenierías UCC-Neiva, Facultad de Ingeniería, Universidad Cooperativa de Colombia, Sede Neiva, Neiva 410001, Colombia
 - ² Maestría en Gestión de Tecnologías de la Información, Facultad de Ingeniería, Universidad Cooperativa de Colombia, Sede Bucaramanga, Bucaramanga 680001, Colombia
 - ³ Programa de Ingeniería de Sistemas, Grupo de Investigación en Tecnologías de la Información GITI, Facultad de Ingeniería, Universidad Cooperativa de Colombia, Sede Bucaramanga, Bucaramanga 680001, Colombia
 - ⁴ Programa de Administración en Seguridad y Salud en el Trabajo, Grupo de Investigación en Seguridad y Salud en el Trabajo, Corporación Universitaria Minuto de Dios-UNIMINUTO, Neiva 410001, Colombia
 - ⁵ Grupo de Físicoquímica y Análisis Matemático, Facultad de Ciencias y Humanidades, Fundación Universidad de América, Avenida Circunvalar No. 20-53, Bogotá 110321, Colombia
 - ⁶ Grupo de Investigaciones Farmacéutico-Físicoquímicas, Departamento de Farmacia, Facultad de Ciencias, Universidad Nacional de Colombia, Sede Bogotá, Carrera 30 No. 45-03, Bogotá 110321, Colombia
- * Correspondence: danielr.delgado@campusucc.edu.co ; Tel.: +57-3219104471

Abstract: Drug solubility is one of the most significant physicochemical properties as it is related to drug design, formulation, quantification, recrystallization, and other processes, so understanding it is crucial for the pharmaceutical industry. In this context, this research presents the thermodynamic analysis of the solubility of sulfadiazine (SD) in cosolvent mixtures {acetonitrile + 1-propanol} at 9 temperatures (278.15 K–318.15 K), which is a widely used drug in veterinary therapy, and two solvents of high relevance in the pharmaceutical industry, respectively. The solubility of SD, in cosolvent mixtures {acetonitrile + 1-propanol} is an endothermic process where the maximum solubility was reached in pure acetonitrile at 318.15 K and the minimum in 1-propanol at 278.15 K. Although the solubility parameters of acetonitrile and propanol were similar, the addition of acetonitrile to the cosolvent mixture leads to a positive cosolvent effect on the solubility of SD. As for the thermodynamic functions of the solution, the process is strongly influenced by enthalpy, and according to the enthalpy–entropy compensation analysis, the process is enthalpy-driven in intermediate to rich mixtures in 1-propanol and entropy-driven in mixtures rich in acetonitrile.

Keywords: sulfadiazine; solubility; cosolvent; thermodynamics; acetonitrile; 1-propanol

Citation: Trujillo-Trujillo, C.F.; Angarita-Reina, F.; Herrera, M.; Ortiz, C.P.; Cardenas-Torres, R.E.; Martínez, F.; Delgado, D.R. Thermodynamic Analysis of the Solubility of Sulfadiazine in (Acetonitrile + 1-Propanol) Cosolvent Mixtures from 278.15 K to 318.15 K. *Liquids* **2023**, *3*, 7–18. <https://doi.org/10.3390/liquids3010002>

Academic Editors: William E. Acree, Jr. and Juan Ortega Saavedra

Received: 26 November 2022

Revised: 15 December 2022

Accepted: 17 December 2022

Published: 22 December 2022



Copyright: © 2022 by the authors. Licensee MDPI, Basel, Switzerland. This article is an open access article distributed under the terms and conditions of the Creative Commons Attribution (CC BY) license (<https://creativecommons.org/licenses/by/4.0/>).

1. Introduction

Sulfadiazine (SD, C₁₀H₁₀N₄O₂S, CAS Number: 68-35-9, Figure 1) is a broad-spectrum, fast-acting, synthetic bacteriostatic agent effective against most gram-positive and many gram-negative bacteria; it is used in human and veterinary therapy for the treatment of infections [1,2].

Since one of the main difficulties in developing drugs made with SD is the low aqueous solubility of this [3–10], solubility studies in cosolvent systems are highly relevant as they allow for the identification of the most suitable solvents or solvent mixtures to improve the solubility of the drug [11]. The solubility of SD in different cosolvent mixtures of pharmaceutical interest has been reported, such as: acetonitrile+methanol [2], ethanol+water [3,12], methanol+water [13], 1,4-dioxane+water [4], propylene glycol+water [14], ethylene glycol+water [15], N-methyl-2-pyrrolidone+water [5], and water-N,N-dimethylformamide [7].

In addition, experimental solubility data have been correlated with some mathematical models, which have allowed one to optimize processes [6,16–18].

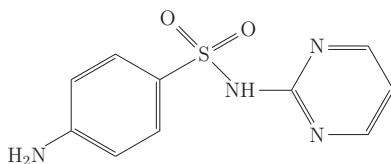


Figure 1. Molecular structure of the sulfadiazine.

Although a large number of solubility data have been reported for SD in different cosolvent mixtures, the generation of new data allows one to understand the possible mechanisms involved in the dissolution process, as well as to compare and identify which factors improve drug solubility.

In this context, the solubility data of SD in cosolvent mixtures acetonitrile (1) + 1-propanol (2), two solvents with a similar solubility parameter, are reported ($\delta_1 = 24.8 \text{ MPa}^{1/2}$ and $\delta_2 = 24.9$ [19]). Both acetonitrile (MeCN) and 1-propanol (n-PrOH) are solvents widely used in the industry; acetonitrile is an aprotic solvent used in the pharmaceutical industry in the manufacture of pharmaceutical products and in analytical processes (HPLC). On the other hand, 1-propanol is an alcohol miscible with water and is classified as a class 3 residual solvent, i.e., it has a low toxic potential for humans [20]. Solubility studies in these pure solvents and their cosolvent mixtures would provide useful information in industrial processes.

In addition, a thermodynamic analysis and the enthalpic-entropic compensation of the SD solution process in MeCN + nPrOH mixtures is performed.

2. Materials and Methods

2.1. Reagents

Table 1 reports the reagents used in the development of this research.

Table 1. Source and purities of the compounds used in this research.

Chemical Name	CAS ^a	Source	Purity in Mass Fraction	Analytic Technique ^b
Sufadiazine	57-83-0	Sigma-Aldrich, Burlington, MA, USA	>0.990	HPLC
Acetonitrile	75-05-8	Merck Millipore, Burlington, MA, USA	0.998	GC
1-Propanol	71-23-8	Merck Millipore, Burlington, MA, USA	0.998	GC
Ethanol	64-17-5	Merck Millipore, Burlington, MA, USA	0.998	GC

^a Chemical Abstracts Service Registry Number. ^b HPLC is high-performance liquid chromatography; GC is gas chromatography.

2.2. Preparation of Solvent Mixtures

Nineteen cosolvent mixtures of acetonitrile + 1-propanol from 0.05 through 0.95 in mass fraction were prepared using an analytical balance (RADWAG AS 220.R2, Torun, Poland) of 4 decimal places (sensitivity $\pm 0.0001 \text{ g}$). Samples were prepared in amber glass vials with a capacity of 15 mL. For each concentration, 3 samples of approximately $10.00 \pm 0.00 \text{ g}$ each were prepared.

2.3. Solubility Determination

The procedure of the flask agitation method proposed by Higuchi and Connors was followed [21–23]. Initially, the pure solvents or cosolvent mixtures were saturated by adding sufficient SD to each flask (see previous section) to obtain two phases. Subsequently, each solution was deposited in a thermostatted circulation bath at each of the 9 study temperatures

(278.15 K, 283.15 K, 288.15 K, 293.15 K, 298.15 K, 303.15 K, 308.15 K, 313.15 K, and 318.15 K) during 48 h. Later, an aliquot of each sample was taken and filtered through a 0.45 μm membrane; then, a gravimetric dilution was performed with absolute ethanol, and the concentration of the solution was measured by UV/Vis spectrophotometry (UV/VIS EMC-11-UV spectrophotometer, Dresden, Germany) at 268 nm (wavelength of maximum absorbance).

2.4. Calorimetric Study

The enthalpy and melting temperature of four SD samples were determined by differential scanning calorimetry (DSC 204 F1 Phoenix, Dresden, Germany). A mass of approximately 10.0 mg of each sample was deposited in an aluminum crucible and placed in the calorimeter under a nitrogen flow of 10 mL·min⁻¹. The heating cycle was developed from 300 to 575 K, with a heating ramp of 10 K·min⁻¹.

3. Results and Discussion

3.1. Experimental Mole Fraction Solubility (x_3)

Table 2 reports the mole fraction solubility of SD in cosolvent mixtures {MeCN + 1-PrOH} at nine temperatures (278.15 K, 283.15 K, 288.15 K, 293.15 K, 298.15 K, 303.15 K, 308.15 K, 313.15 K, and 318.15 K). With increasing temperature, the solubility of SD increases, indicating an endothermic dissolution process. Concerning the cosolvent effect, solubility usually depends on the polarity of the solvent, so the maximum solute solubility is reached in the solvent or cosolvent mixture with a solubility parameter similar to the solute.

In this case, the solubility parameter of MeCN and PrOH are similar, so it is complex to elucidate the relationship between the polarity of the solvent medium (the quasi-constant solubility parameter, between 24.8 and 24.9 MPa^{1/2}) and the SD (28.89 MPa^{1/2} [3]). Therefore, regarding the solubility parameter, one alternative is to consider the three-dimensional solubility parameter [24], which means the dispersion force (d), polar force (p), and hydrogen-bonding force (h). In this way, PrOH ($\delta_d = 14.1$ MPa^{1/2}, $\delta_p = 10.1$ MPa^{1/2}, and $\delta_h = 17.1$ MPa^{1/2} [19]) differs the most from MeCN ($\delta_d = 10.3$ MPa^{1/2}, $\delta_p = 11.1$ MPa^{1/2}, and $\delta_h = 19.6$ MPa^{1/2} [19]) in δ_d , so the increase in SD solubility with increasing PrOH concentration in the cosolvent mixture is possibly due to the increase in non-polar interactions between PrOH and SD.

On the other hand, when evaluating the solubility behavior of SD considering the Kamlet–Taft acidity scale α [25], SD behaves as an acid against MeCN ($\alpha = 0.29 \pm 0.06$ [25]), which is a more basic solvent than 1-PrOH ($\alpha = 0.766 \pm 0.013$ [25]).

An important factor to consider is the possible formation of polymorphs since this phenomenon affects drug solubility [26]. For this purpose, the solid phases of the original sample and the phases in the equilibrium with pure MeCN, pure 1-PrOH, and in the cosolvent mixture $w_{0.50}$ were evaluated (Figure 2).

Table 3 shows the experimental values of the enthalpy and fusion temperatures of the samples evaluated and some of the values taken from the literature. It is observed that the values from the original sample and those from the solid phase in equilibrium were similar, indicating that there were no polymorphic changes; furthermore, the results agree with those reported by other authors.

Table 2. Experimental solubility of sulfadiazine (3) in {acetonitrile (1) + 1-propanol (2)} cosolvent mixtures expressed in mole fraction ($10^4 x_3$) at different temperatures and $p = 96$ kPa ^{ac}.

w_1^b	Temperature/K								
	278.15	283.15	288.15	293.15	298.15	303.15	308.15	313.15	318.15
0.00	0.152	0.210	0.275	0.388	0.471	0.587	0.721	0.913	1.097
0.05	0.179	0.228	0.288	0.394	0.490	0.588	0.740	0.938	1.187
0.10	0.203	0.254	0.326	0.407	0.518	0.650	0.821	1.038	1.303
0.15	0.226	0.285	0.362	0.455	0.577	0.720	0.907	1.140	1.431
0.20	0.250	0.317	0.401	0.503	0.635	0.789	0.990	1.241	1.543
0.25	0.281	0.346	0.435	0.536	0.675	0.843	1.055	1.310	1.642
0.30	0.312	0.389	0.486	0.599	0.744	0.926	1.144	1.424	1.753
0.35	0.353	0.433	0.538	0.662	0.816	0.992	1.242	1.520	1.875

Table 2. Cont.

w_1^b	Temperature/K								
	278.15	283.15	288.15	293.15	298.15	303.15	308.15	313.15	318.15
0.40	0.407	0.495	0.603	0.731	0.890	1.093	1.324	1.614	1.974
0.45	0.472	0.572	0.699	0.837	1.011	1.211	1.461	1.760	2.092
0.50	0.562	0.661	0.791	0.941	1.126	1.326	1.577	1.871	2.253
0.55	0.679	0.804	0.949	1.106	1.292	1.523	1.783	2.085	2.402
0.60	0.900	1.035	1.189	1.363	1.572	1.792	2.073	2.384	2.716
0.65	1.021	1.168	1.343	1.535	1.731	1.982	2.250	2.556	2.890
0.70	1.269	1.440	1.611	1.795	2.032	2.279	2.560	2.859	3.208
0.75	1.585	1.743	1.946	2.161	2.404	2.636	2.977	3.286	3.655
0.80	1.916	2.098	2.316	2.554	2.833	3.062	3.422	3.754	4.198
0.85	2.306	2.525	2.783	3.024	3.382	3.684	4.055	4.446	4.946
0.90	2.673	2.964	3.314	3.671	4.037	4.468	4.945	5.427	5.972
0.95	2.966	3.279	3.696	4.126	4.615	5.139	5.818	6.518	7.442
1.00	3.162	3.849	4.653	5.323	6.022	6.663	7.748	8.649	9.352

^a p is the atmospheric pressure in Neiva, Colombia. ^b w_1 is the mass fraction of acetonitrile (1) in the acetonitrile (1) + 1-propanol (2) mixtures free of sulfadiazine (3). ^c Standard uncertainty in p is $u(p) = 3.0$ kPa. Average relative standard uncertainty in w_1 is $u_r(w_1) = 0.0008$. Standard uncertainty in T is $u(T) = 0.10$ K. Average relative standard uncertainties in x_3 is $u_r(x_{3(1+2)}) = 0.025$.

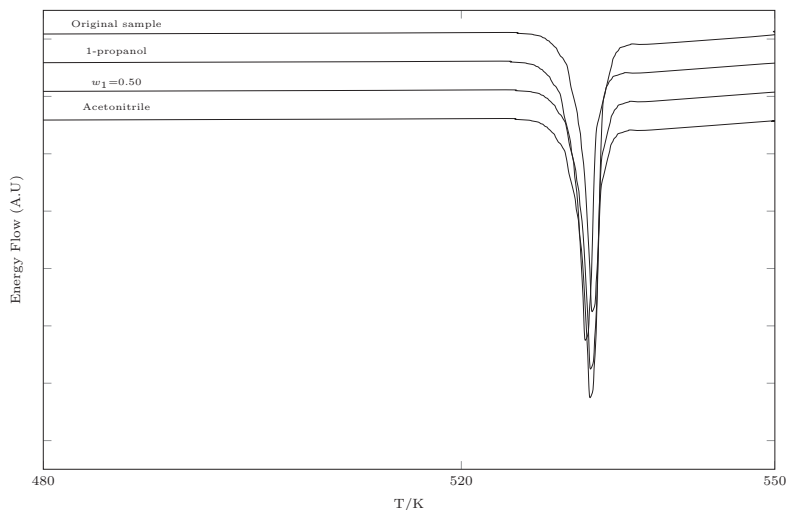


Figure 2. DSC thermograms of sulfadiazine.

Table 3. The thermophysical properties of SD obtained by the DSC.

Sample	Enthalpy of Fusion, $\Delta_{fus}H/kJ \cdot mol^{-1}$	Melting Point T_{fus}/K	Ref.
Original sample	44.36 ± 0.5	532.6 ± 0.5	This work
	44.352	532.7	[27]
	44.35	520.4	[28]
	31.21	538.7	[29]
		538.8	[29]
		534.0	[30]
		531.0	[30]
1-Propanol	44.23 ± 0.5	533.1 ± 0.5	This work
$w_{0.50}$	44.45 ± 0.5	531.8 ± 0.5	This work
Acetonitrile	44.63 ± 0.5	532.4 ± 0.5	This work

3.2. Ideal Solubility and Activity Coefficients

The possible molecular interactions that occur during the SD dissolution process in MeCN + 1-PrOH cosolvent mixtures can be evaluated through the activity coefficients.

Firstly, the ideal solubility is calculated by the Equation (1) [31], where T and T_m (in K), $\Delta_m H$ is the solute enthalpy of fusion (in kJ mol^{-1}), R is the gas constant (in $\text{kJ}\cdot\text{mol}^{-1}\cdot\text{K}^{-1}$), and ΔC_p is the differential heat capacity of fusion (in $\text{kJ}\cdot\text{K}^{-1}\cdot\text{mol}^{-1}$) [10]. Some researchers such as Hildebrand et al. [32], Neau and Flynn [33], Neau et al. [34], and Opperhuizen et al. [35] assume ΔC_p as the entropy of fusion ($\Delta_m S$), which is calculated as $\Delta_m H/T_m$

$$\ln x_3^{id} = -\frac{\Delta_m H}{R} \left(\frac{T_m - T}{T_m T} \right) + \frac{\Delta C_p}{R} \left(\frac{T_m - T}{T} \right) - \frac{\Delta C_p}{R} \ln \left(\frac{T_m}{T} \right) \tag{1}$$

Once the ideal solubility has been calculated, Equation (2) is used to calculate the activity coefficient (γ_3) from the experimental solubility (x_3) data [32,36].

$$\gamma_3 = \frac{x_3^{id}}{x_3} \tag{2}$$

Finally, from Equation (3), γ_3 can be interpreted in terms of molecular interactions [37,38]. Then, e_{11} and e_{33} represent the solvent–solvent and solute–solute interaction energy, respectively, where e_{11} is related to the MeCN–MeCN, 1-PrOH–1-PrOH, and MeCN–PrOH interactions. On the other hand, e_{13} represents the solute–solvent interaction energy, i.e., MeCN–SD, 1-PrOH–SD, and MeCN–SD–1-PrOH.

When the solution process behaves ideally $e_{11} = e_{22} = e_{33}$, the values of γ_3 greater than 1 indicate that e_{11} and e_{22} control the solution process [39,40].

$$\ln \gamma_3 = (e_{11} + e_{33} - 2e_{13}) \frac{V_3 \phi_1^2}{RT} \tag{3}$$

Table 4. Activity coefficient of sulfadiazine (3) in {acetonitrile (1) + 1-propanol (2)} cosolvent mixtures at different temperatures and pressure $p = 0.096 \text{ MPa}^a$.

w_1^b	Temperature/K									
	278.15	283.15	288.15	293.15	298.15	303.15	308.15	313.15	318.15	
0.00	99.13	85.70	77.99	65.65	63.99	60.63	58.11	53.93	52.59	
0.05	84.04	78.98	74.30	70.00	65.49	60.58	56.63	52.48	48.61	
0.10	74.19	70.73	65.77	62.60	58.24	54.78	51.08	47.46	44.28	
0.15	66.68	63.11	59.26	55.88	52.23	49.44	46.24	43.21	40.34	
0.20	60.09	56.77	53.50	50.63	47.48	45.10	42.33	39.70	37.40	
0.25	53.51	52.02	49.28	47.50	44.62	42.21	39.74	37.59	35.15	
0.30	48.31	46.26	44.09	42.45	40.53	38.44	36.65	34.59	32.92	
0.35	42.63	41.53	39.84	38.45	36.92	35.87	33.75	32.41	30.78	
0.40	37.01	36.33	35.54	34.82	33.87	32.58	31.66	30.51	29.23	
0.45	31.92	31.45	30.65	30.42	29.82	29.40	28.70	27.98	27.59	
0.50	26.79	27.22	27.07	27.04	26.77	26.84	26.59	26.32	25.62	
0.55	22.16	22.36	22.57	23.00	23.33	23.37	23.51	23.62	24.03	
0.60	16.72	17.38	18.02	18.67	19.17	19.87	20.22	20.66	21.25	
0.65	14.74	15.40	15.95	16.58	17.41	17.96	18.63	19.27	19.97	
0.70	11.86	12.49	13.30	14.18	14.83	15.62	16.38	17.23	17.99	
0.75	9.49	10.32	11.01	11.78	12.54	13.50	14.08	14.99	15.79	
0.80	7.85	8.57	9.25	9.96	10.64	11.62	12.25	13.12	13.74	
0.85	6.53	7.12	7.70	8.42	8.91	9.66	10.34	11.08	11.67	
0.90	5.63	6.07	6.47	6.93	7.47	7.97	8.48	9.07	9.66	
0.95	5.07	5.49	5.80	6.17	6.53	6.93	7.21	7.56	7.75	
1.00	4.76	4.67	4.60	4.78	5.00	5.34	5.41	5.69	6.17	

^a p is the atmospheric pressure in Neiva, Colombia. ^b w_1 is the mass fraction of acetonitrile (1) in the {acetonitrile (1) + 1-propanol (2)} mixtures free of sulfadiazine (3).

According to the data reported in Table 4, the increase in temperature favors the solute–solvent interactions in general. Moreover, when analyzing the influence of cosolvent

composition, it is deduced that MeCN-SD interactions are more favorable than 1-PrOH-SD interactions.

3.3. Thermodynamic Functions of Solution

The thermodynamic solution functions (Table 5), enthalpy ($\Delta_{\text{soln}}H^\circ$), Gibbs energy ($\Delta_{\text{soln}}G^\circ$), and entropy of solution ($\Delta_{\text{soln}}S^\circ$) (in $\text{kJ}\cdot\text{mol}^{-1}$) were calculated by the Gibbs–van't Hoff–Krug model from the SD experimental solubility data (Table 2) [41,42] by means of the Equations (4)–(6).

$$\Delta_{\text{soln}}H^\circ = -R \left(\frac{\partial \ln x_3}{\partial (T^{-1} - T_{\text{hm}}^{-1})} \right)_p \quad (4)$$

$$\Delta_{\text{soln}}G^\circ = -RT_{\text{hm}} \cdot \text{intercept} \quad (5)$$

$$\Delta_{\text{soln}}S^\circ = (\Delta_{\text{soln}}H^\circ - \Delta_{\text{soln}}G^\circ) T_{\text{hm}}^{-1} \quad (6)$$

where T_{hm} is the harmonic temperature (in K) and R is the gas constant ($\text{kJ}\cdot\text{mol}^{-1}\cdot\text{K}^{-1}$).

The contributions of enthalpy and entropy to the Gibbs energy ζ_H and ζ_{TS} were calculated using the Equations (7) and (8)

$$\zeta_H = |\Delta_{\text{soln}}H^\circ| / (|\Delta_{\text{soln}}H^\circ| + |\Delta_{\text{soln}}S^\circ|) \quad (7)$$

$$\zeta_{TS} = 1 - \zeta_H \quad (8)$$

Table 5. Thermodynamic functions of the solution process of sulfadiazine (3) in (acetonitrile (1) + 1-propanol (2)) co-solvent mixtures at $T_{\text{hm}} = 297.6 \text{ K}$ ^a.

w_1 ^b	$\Delta_{\text{soln}}G^\circ /$ ($\text{kJ}\cdot\text{mol}^{-1}$)	$\Delta_{\text{soln}}H^\circ$ ($\text{kJ}\cdot\text{mol}^{-1}$)	$\Delta_{\text{soln}}S^\circ$ ($\text{J}\cdot\text{mol}^{-1}\cdot\text{K}^{-1}$)	$T_{\text{hm}}\Delta_{\text{soln}}S^\circ$ ($\text{kJ}\cdot\text{mol}^{-1}$)	ζ_H ^c	ζ_{TS} ^c
0.00	24.79	36.09	37.94	11.29	0.76	0.24
0.05	24.70	34.77	33.83	10.07	0.78	0.22
0.10	24.43	34.27	33.07	9.84	0.78	0.22
0.15	24.17	33.95	32.85	9.77	0.78	0.22
0.20	23.94	33.43	31.89	9.49	0.78	0.22
0.25	23.76	32.56	29.56	8.80	0.79	0.21
0.30	23.52	31.76	27.69	8.24	0.79	0.21
0.35	23.30	30.71	24.89	7.41	0.81	0.19
0.40	23.07	29.03	20.05	5.97	0.83	0.17
0.45	22.78	27.41	15.58	4.64	0.86	0.14
0.50	22.51	25.50	10.03	2.99	0.90	0.10
0.55	22.15	23.28	3.79	1.13	0.95	0.05
0.60	21.68	20.37	−4.40	−1.31	0.94	0.06
0.65	21.43	19.14	−7.71	−2.29	0.89	0.11
0.70	21.04	17.00	−13.58	−4.04	0.81	0.19
0.75	20.62	15.43	−17.47	−5.20	0.75	0.25
0.80	20.23	14.33	−19.83	−5.90	0.71	0.29
0.85	19.79	13.97	−19.56	−5.82	0.71	0.29
0.90	19.34	14.79	−15.29	−4.55	0.76	0.24
0.95	18.99	16.82	−7.29	−2.17	0.89	0.11
1.00	18.43	19.73	4.34	1.29	0.94	0.06

^a Average relative standard uncertainty in w_1 is $u_r(w_1) = 0.0008$. Standard uncertainty in T is $u(T) = 0.10 \text{ K}$. Average relative standard uncertainty in apparent thermodynamic quantities of real dissolution processes are $u_r(\Delta_{\text{soln}}G^\circ) = 0.015$, $u_r(\Delta_{\text{soln}}H^\circ) = 0.019$, $u_r(\Delta_{\text{soln}}S^\circ) = 0.024$, and $u_r(T\Delta_{\text{soln}}S^\circ) = 0.024$. ^b w_1 is the mass fraction of acetonitrile (1) in the (acetonitrile (1) + 1-propanol (2)) mixtures free of sulfadiazine (3). ^c ζ_H and ζ_{TS} are the relative contributions by enthalpy and entropy toward the apparent Gibbs energy of dissolution.

As the concentration of MeCN in the cosolvent mixtures increases, the solution Gibbs energy decreases from pure 1-PrOH to pure MeCN. The solution enthalpy decreases from pure 1-PrOH to $w_{0.85}$, and from this mixture to pure MeCN, the enthalpy of the solution increases. The enthalpy decrease in 1-PrOH-rich and intermediate mixtures is probably due

to solvent–solvent bond breaking, which agrees with the increase in solubility. However, in MeCN-rich mixtures, the enthalpy increases possibly due to the MeCN tendency to form micro-cluster [43], which leads to the formation of MeCN–MeCN bonds and increases the enthalpy of the solution.

The solution entropy follows a similar pattern as the enthalpy of the solution, decreasing from pure 1-PrOH to $w_{0.85}$ and then increasing to pure MeCN. Finally, when analyzing the solution enthalpy and entropy contribution to the Gibbs energy, the energetic component, i.e., the solution enthalpy, is the main source (>71%). This was verified by Perlovich’s analysis (Figure 3) since when plotting $\Delta_{\text{soln}}H^\circ$ vs. $T\Delta_{\text{soln}}S^\circ$, all of the values were recorded in the sector I ($\Delta_{\text{soln}}H^\circ > T\Delta_{\text{soln}}S^\circ$) and the sector VIII ($\Delta_{\text{soln}}H^\circ > 0$, $T\Delta_{\text{soln}}S^\circ < 0$, $|\Delta_{\text{soln}}H^\circ| > |T\Delta_{\text{soln}}S^\circ|$), indicating an enthalpic conduction of the dissolution process [44,45].

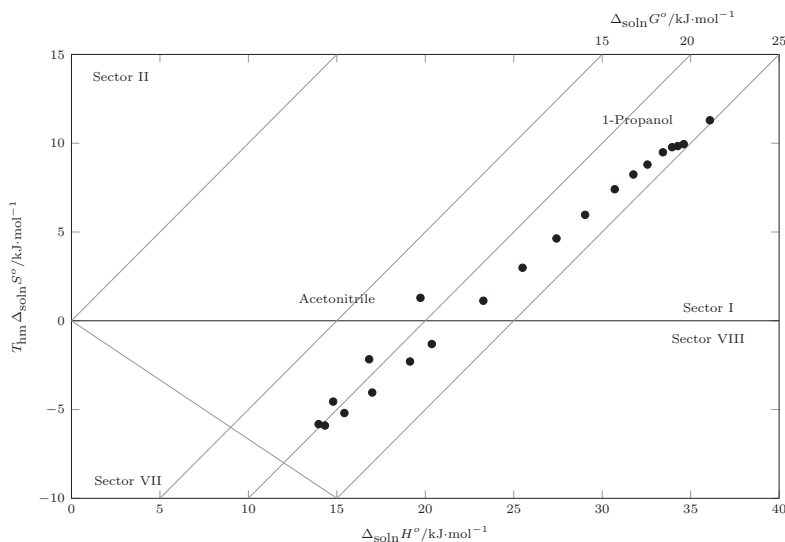


Figure 3. Relation between enthalpy ($\Delta_{\text{soln}}H^\circ$) and entropy ($T_{\text{hm}}\Delta_{\text{soln}}S^\circ$) in terms of the process of sulfadiazine (3) solution in {MeCN (1) + 1-PrOH (2)} cosolvent mixtures at 297.6 K. The isoenergetic curves for $\Delta_{\text{soln}}G^\circ$ are represented by dotted lines.

3.4. Thermodynamic Functions of Mixing

The solution process involves the change of state of the solute ($\text{Solute}_{\text{solid},T} \rightarrow \text{Solute}_{\text{solid},T_m} \rightarrow \text{Solute}_{\text{liquid},T_m} \rightarrow \text{Solute}_{\text{liquid},T}$); the molecular reorganization of the solvent to form a cavity to house the solute; and the mixing process (Table 6), which involves the molecular interaction between the solute and the solvent to form the solution ($\text{Solute}_{\text{liquid},T} \rightarrow \text{Solute}_{\text{soln}}$) [31,46,47]. The solution process can be described by Equation (9)

$$\Delta_{\text{sol}}f^\circ = \Delta_{\text{mix}}f^\circ + \Delta_{\text{m}}f^\circ \quad (9)$$

Clearing $\Delta_{\text{mix}}f^\circ$ Equation (9), we obtain:

$$\Delta_{\text{mix}}f^\circ = \Delta_{\text{soln}}f^\circ - \Delta_{\text{m}}f^\circ \quad (10)$$

The mixing Gibbs energy was positive in each case and decreased from pure 1-PrOH to pure MeCN. This indicates that as the concentration of MeCN in the cosolvent mixtures increases, lower energy is required to generate the cavity where the solute is accommodated. The enthalpy of mixing decreases from 1-PrOH to $w_{0.85}$, and from this cosolvent composition to pure MeCN it increases. Similarly, the entropy of mixing was negative in each case and behaved similarly to the enthalpy of mixing. In general, from 1-PrOH up to

$w_{0.50}$, the solution process is disfavored by the thermodynamic mixing functions, and from $w_{0.55}$ up to MeCN, the solution process is favored by the mixing enthalpy.

According to Perlovich’s analysis (Figure 4) from 1-PrOH up to $w_{0.30}$, the mixing process is driven by the enthalpy of mixing (Sector VIII: $\Delta_{\text{mix}}H^\circ > 0, T\Delta_{\text{mix}}S^\circ < 0, |\Delta_{\text{mix}}H^\circ| > |T\Delta_{\text{mix}}S^\circ|$); from $w_{0.30}$ to $w_{0.50}$ (Sector VII: $\Delta_{\text{mix}}H^\circ > 0, T\Delta_{\text{mix}}S^\circ < 0, |\Delta_{\text{mix}}H^\circ| < |T\Delta_{\text{mix}}S^\circ|$) and from $w_{0.50}$ to pure MeOH (Sector VI: $\Delta_{\text{mix}}H^\circ < 0, T\Delta_{\text{mix}}S^\circ < 0, |\Delta_{\text{mix}}H^\circ| < |T\Delta_{\text{mix}}S^\circ|$), the process is driven by the entropy of mixing [44,45].

Table 6. Thermodynamic functions relative to mixing processes of sulfadiazine (3) in {acetonitrile (1) + 1-propanol (2)} co-solvent mixtures at $T_{\text{hm}} = 297.6 \text{ K}$ ^a.

w_1 ^b	$\Delta_{\text{mix}}G^\circ$ ($\text{kJ}\cdot\text{mol}^{-1}$)	$\Delta_{\text{mix}}H^\circ$ ($\text{kJ}\cdot\text{mol}^{-1}$)	$\Delta_{\text{mix}}S^\circ$ ($\text{J}\cdot\text{mol}^{-1}\cdot\text{K}^{-1}$)	$T\Delta_{\text{mix}}S^\circ$ ($\text{kJ}\cdot\text{mol}^{-1}$)
0.00	13.51	11.24	-7.62	-2.27
0.05	13.41	9.92	-11.74	-3.49
0.10	13.14	9.42	-12.50	-3.72
0.15	12.88	9.10	-12.72	-3.78
0.20	12.65	8.58	-13.67	-4.07
0.25	12.47	7.71	-16.00	-4.76
0.30	12.23	6.91	-17.88	-5.32
0.35	12.01	5.86	-20.67	-6.15
0.40	11.78	4.18	-25.51	-7.59
0.45	11.49	2.57	-29.99	-8.92
0.50	11.22	0.65	-35.53	-10.57
0.55	10.86	-1.57	-41.77	-12.43
0.60	10.39	-4.48	-49.96	-14.87
0.65	10.14	-5.71	-53.27	-15.85
0.70	9.75	-7.85	-59.15	-17.60
0.75	9.33	-9.42	-63.03	-18.76
0.80	8.94	-10.52	-65.39	-19.46
0.85	8.50	-10.88	-65.13	-19.38
0.90	8.05	-10.06	-60.86	-18.11
0.95	7.70	-8.02	-52.85	-15.73
1.00	7.14	-5.12	-41.22	-12.27

^a Average relative standard uncertainty in w_1 is $u_r(w_1) = 0.0008$. Standard uncertainty in T is $u(T) = 0.10 \text{ K}$. Average relative standard uncertainties in apparent thermodynamic quantities of real dissolution processes are $u_r(\Delta_{\text{mix}}G^\circ) = 0.015$, $u_r(\Delta_{\text{mix}}H^\circ) = 0.019$, $u_r(\Delta_{\text{mix}}S^\circ) = 0.024$, and $u_r(T\Delta_{\text{mix}}S^\circ) = 0.024$. ^b w_1 is the mass fraction of acetonitrile (1) in the {acetonitrile (1) + 1-propanol (2)} mixtures free of sulfadiazine (3).

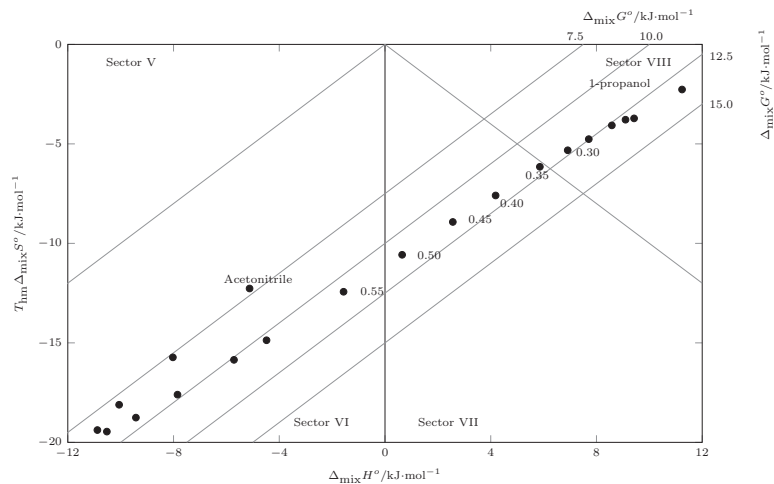


Figure 4. Relation between enthalpy ($\Delta_{\text{mix}}H^\circ$) and entropy ($T\Delta_{\text{mix}}S^\circ$) of the process mixing of sulfadiazine (3) in {MeCN (1) + 1-PrOH (2)} cosolvent mixtures at 297.6 K. The isoenergetic curves for $\Delta_{\text{mix}}G^\circ$ are represented by dotted lines.

3.5. Enthalpy–Entropy Compensation Analysis

Enthalpy–entropy compensation is defined by Ryde as the cancellation of an entropy increase, generated by the non-covalent interaction of two molecules (solute–solvent), by a simultaneous decrease in enthalpy [48]. This phenomenon creates a linear enthalpy–entropy relationship when changes in solubility occur as a consequence of changes in cosolvent composition (Figure 5). Therefore, an adverse enthalpy change is compensated for by a favorable entropy change that allows for the process to occur.

According to Sharp, when $\Delta_{\text{soln}}G^\circ$ changes are present, there is a linear relationship between $\Delta_{\text{soln}}H^\circ$ and $T\Delta_{\text{soln}}S^\circ$, which is a strong enthalpy–entropy compensation indicator [49].

Following this, by analyzing the enthalpic–entropic compensation of the drug solution process in cosolvent mixtures, the mechanisms involved in the solution process can be identified. This can be done by evaluating the thermodynamic effects of the solute–solvent molecular interactions, such as the formation of hydrogen bonds [6,50,51].

The enthalpy–entropy compensation can be evaluated through two graphic models: (i) $\Delta_{\text{soln}}H^\circ$ vs. $\Delta_{\text{soln}}G^\circ$, where negative slopes indicate entropic driving and positive slopes enthalpy driving; and (ii) $\Delta_{\text{soln}}H^\circ$ vs. $T\Delta_{\text{soln}}S^\circ$, where slopes >1.0 indicate enthalpy driving and slopes <1.0 indicate entropic driving. Hence, according to Figures 5 and 6, from 1-PrOH to $w_{0.85}$, the process is driven by the enthalpy of solution, and from $w_{0.85}$ to pure MeCN, the process is driven by entropy.

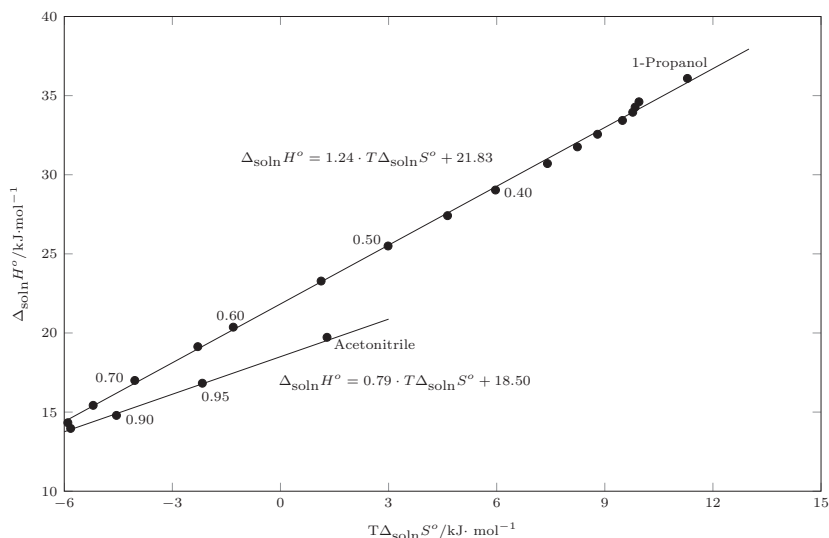


Figure 5. Enthalpy–entropy compensation plot for the solubility of SD (3) in {MeCN(1) + 1-PrOH(2)} mixtures at $T_{\text{hm}} = 297.6$ K.

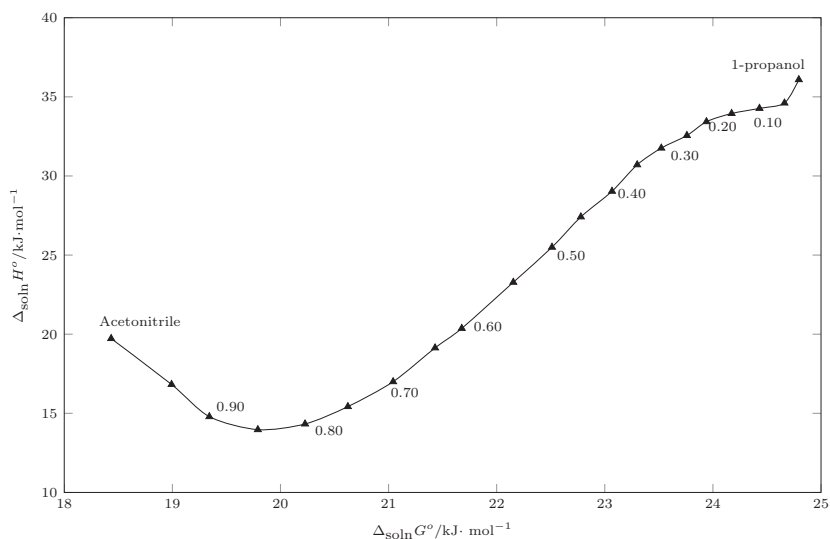


Figure 6. Enthalpy–entropy compensation plot for the solubility of SD (3) in {MeCN(1) + 1-PrOH (2)} mixtures at $T_{hm} = 297.6$ K.

4. Conclusions

The solubility of sulfadiazine in acetonitrile + 1-propanol cosolvent mixtures is an endothermal process, and it is dependent on the cosolvent composition. Sulfadiazine tends to present an acidic character relative to acetonitrile, increasing its solubility as the concentration of acetonitrile increases. In the latter, the lowest values of the activity coefficient were obtained, indicating quasi-ideal behavior in MeCN-rich mixtures.

Regarding the thermodynamic functions of solution, the solution Gibbs energy is highly dependent on the enthalpy values, and overall the solution process is favored by entropy in 1-propanol-rich mixtures. The mixing process is driven by the enthalpy in 1-propanol-rich and intermediate mixtures, and in acetonitrile-rich mixtures, the mixing process is driven by the entropy.

Finally, according to the enthalpy–entropy compensation analysis, the process is driven by the enthalpy in acetonitrile-rich and intermediate mixtures and by the entropy in 1-propanol-rich mixtures.

Author Contributions: Conceptualization, C.F.T.-T. and D.R.D.; methodology, F.A.-R., D.R.D. and C.P.O.; software, R.E.C.-T.; validation, F.M. and D.R.D.; formal analysis, F.A.-R.; investigation, F.A.-R. and C.P.O.; resources, C.F.T.-T. and D.R.D.; data curation, D.R.D.; writing—original draft preparation, F.A.-R.; writing—review and editing, M.H., C.F.T.-T., D.R.D. and F.M.; visualization, D.R.D.; supervision, F.M.; project administration, D.R.D.; and funding acquisition, D.R.D. All authors have read and agreed to the published version of the manuscript.

Funding: This research was funded by Universidad Cooperativa de Colombia grant number INV2976.

Institutional Review Board Statement: Not applicable for studies not involving humans or animals.

Informed Consent Statement: Not applicable for studies not involving humans.

Data Availability Statement: Data is contained within the article.

Acknowledgments: We thank the National Directorate of Research and National Committee for Research Development of the Universidad Cooperativa de Colombia for the financial support of the Project “Análisis matemático y termodinámico de la solubilidad algunas sustancias antimicrobianas de uso industrial en mezclas cosolventes” with code INV2976. We also thank the Universidad Cooperativa de Colombia, Sede Neiva for facilitating the laboratories and equipment used.

Conflicts of Interest: The authors declare no conflict of interest.

References

- Feng, Y.; Wu, D.; Liao, C.; Deng, Y.; Zhang, T.; Shih, K. Red mud powders as low-cost and efficient catalysts for persulfate activation: Pathways and reusability of mineralizing sulfadiazine. *Sep. Purif. Technol.* **2016**, *167*, 136–145. [[CrossRef](#)]
- Delgado, D.R.; Bahamón-Hernandez, O.; Cerquera, N.E.; Ortiz, C.P.; Martínez, F.; Rahimpour, E.; Jouyban, A.; Acree, W.E. Solubility of sulfadiazine in (acetonitrile + methanol) mixtures: Determination, correlation, dissolution thermodynamics and preferential solvation. *J. Mol. Liq.* **2021**, *322*, 114979. [[CrossRef](#)]
- Delgado, D.R.; Martínez, F. Solution thermodynamics of sulfadiazine in some ethanol+water mixtures. *J. Mol. Liq.* **2013**, *187*, 99–105. [[CrossRef](#)]
- Jiménez, D.M.; Cárdenas, Z.J.; Delgado, D.R.; Peña, M.A.; Martínez, F. Solubility temperature dependence and preferential solvation of sulfadiazine in 1,4-dioxane+water co-solvent mixtures. *Fluid Phase Equilibria* **2015**, *397*, 26–36. [[CrossRef](#)]
- Osorio, I.P.; Martínez, F.; Peña, M.A.; Jouyban, A.; Acree, W.E. Solubility, dissolution thermodynamics and preferential solvation of sulfadiazine in (N-methyl-2-pyrrolidone+water) mixtures. *J. Mol. Liq.* **2021**, *330*, 115693. [[CrossRef](#)]
- Bustamante, P.; Escalera, B.; Martín, A.; Selles, E. A modification of the extended Hildebrand approach to predict the solubility of structurally related drugs in solvent mixtures. *J. Pharm. Pharmacol.* **2011**, *45*, 253–257. [[CrossRef](#)] [[PubMed](#)]
- Elworthy, P.H.; Worthington, H.E.C. The solubility of sulphadiazine in water-dimethylformamide mixtures. *J. Pharm. Pharmacol.* **2011**, *20*, 830–835. [[CrossRef](#)]
- Zhang, C.L.; Wang, F.A.; Wang, Y. Solubilities of sulfadiazine, sulfamethazine, sulfadimethoxine, sulfamethoxydiazine, sulfamonomethoxine, sulfamethoxazole, and sulfachloropyrazine in water from (298.15 to 333.15) K. *J. Chem. Eng. Data* **2007**, *52*, 1563–1566. [[CrossRef](#)]
- Yalkowsky, S.H. *Solubility and Solubilization in Aqueous Media*; American Chemical Society: Washington, DC, USA, 1999.
- Yalkowsky, S.H.; Wu, M. Estimation of the ideal solubility (crystal-liquid fugacity ratio) of organic compounds. *J. Pharm. Sci.* **2010**, *99*, 1100–1106. [[CrossRef](#)]
- Mauger, J.W.; Paruta, A.N.; Gerraughty, R.J. Solubilities of sulfadiazine, sulfisomidine, and sulfadimethoxine in several normal alcohols. *J. Pharm. Sci.* **1972**, *61*, 94–97. [[CrossRef](#)]
- Delgado, D.R.; Martínez, F. Preferential solvation of sulfadiazine, sulfamerazine and sulfamethazine in ethanol+water solvent mixtures according to the IKBI method. *J. Mol. Liq.* **2014**, *193*, 152–159. [[CrossRef](#)]
- Delgado, D.R.; Martínez, F. Solubility and preferential solvation of sulfadiazine in methanol+water mixtures at several temperatures. *Fluid Phase Equilibria* **2014**, *379*, 128–138. [[CrossRef](#)]
- Muñoz, M.M.; Delgado, D.R.; Peña, M.A.; Jouyban, A.; Martínez, F. Solubility and preferential solvation of sulfadiazine, sulfamerazine and sulfamethazine in propylene glycol+water mixtures at 298.15K. *J. Mol. Liq.* **2015**, *204*, 132–136. [[CrossRef](#)]
- Cruz-González, A.M.; Vargas-Santana, M.S.; Ortiz, C.P.; Cerquera, N.E.; Delgado, D.R.; Martínez, F.; Jouyban, A.; Acree, W.E., Jr. Solubility of sulfadiazine in (ethylene glycol+water) mixtures: Measurement, correlation, thermodynamics and preferential solvation. *J. Mol. Liq.* **2021**, *323*, 115058. [[CrossRef](#)]
- Blanco-Márquez, J.H.; Quigua-Medina, Y.A.; García-Murillo, J.D.; Castro-Camacho, J.K.; Ortiz, C.P.; Cerquera, N.E.; Delgado, D.R. Thermodynamic analysis and applications of the Abraham solvation parameter model in the study of the solubility of some sulfonamides. *Rev. Colomb. Cienc. Químico-Farm.* **2020**, *49*, 234–255. [[CrossRef](#)]
- Delgado, D.R.; Peña, M.; Martínez, F. Extended Hildebrand solubility approach applied to some structurally related sulfonamides in ethanol + water mixtures. *Rev. Colomb. Química* **2016**, *45*, 34–43. [[CrossRef](#)]
- Delgado, D.R.; Martínez, F. Preferential solvation of some structurally related sulfonamides in 1-propanol + water co-solvent mixtures. *Phys. Chem. Liq.* **2015**, *53*, 293–306. [[CrossRef](#)]
- Barton, A.F.M. *Handbook of Solubility Parameters and Other Cohesion Parameters*, 2nd ed.; CRC Press: Boca Raton, FL, USA, 1991.
- Witschi, C.; Doelker, E. Residual solvents in pharmaceutical products: Acceptable limits, influences on physicochemical properties, analytical methods and documented values. *Eur. J. Pharm. Biopharm.* **1997**, *43*, 215–242. [[CrossRef](#)]
- Higuchi, T.; Connors, K. *Advances in Analytical Chemistry and Instrumentation*; Interscience Publishers, Inc.: New York, NY, USA, 1965.
- Dittert, L.W.; Higuchi, T.; Reese, D.R. Phase solubility technique in studying the formation of complex salts of triamterene. *J. Pharm. Sci.* **1964**, *53*, 1325–1328. [[CrossRef](#)]
- Mader, W.J.; Higuchi, T. Phase solubility analysis. *Crit. Rev. Anal. Chem.* **1970**, *1*, 193–215. [[CrossRef](#)]
- Crowley, J.; Teague, G., Jr.; Lowe, J., Jr. A three-dimensional approach to solubility. *Chem. Mater. Sci.* **1966**, *38*, 269–280.
- Taft, R.W.; Kamlet, M.J. The solvatochromic comparison method. 2. The .alpha.-scale of solvent hydrogen-bond donor (HBD) acidities. *J. Am. Chem. Soc.* **1976**, *98*, 2886–2894. [[CrossRef](#)]
- Hilfiker, R.; Blatter, F.; Raumer, M.V. Relevance of solid-state properties for pharmaceutical products. In *Polymorphism*; John Wiley & Sons, Ltd.: New York, NY, USA, 2006; Chapter 1, pp. 1–19. [[CrossRef](#)]
- Martínez, F.; Ávila, C.M.; Gómez, A. Thermodynamic study of the solubility of some sulfonamides in cyclohexane. *J. Braz. Chem. Soc.* **2003**, *14*, 803–808. [[CrossRef](#)]
- Martin, A.; Wu, P.; Velasquez, T. Extended Hildebrand solubility approach: Sulfonamides in binary and ternary solvents. *J. Pharm. Sci.* **1985**, *74*, 277–282. [[CrossRef](#)] [[PubMed](#)]
- Sunwoo, C.; Eisen, H. Solubility parameter of selected sulfonamides. *J. Pharm. Sci.* **1971**, *60*, 238–244. [[CrossRef](#)]

30. Kofler, L.; Sitte, H.Z. Zur Schmelzpunktbestimmung von Substanzen, die unter Zersetzung schmelzen. *Monatshefte Chem.* **1950**, *81*, 619–626. [[CrossRef](#)]
31. Ortiz, C.P.; Cardenas-Torres, R.E.; Martínez, F.; Delgado, D.R. Solubility of sulfamethazine in the binary mixture of acetonitrile + methanol from 278.15 to 318.15 K: Measurement, dissolution thermodynamics, preferential solvation, and correlation. *Molecules* **2021**, *26*, 588. [[CrossRef](#)]
32. Hildebrand, J.H.; Prausnitz, J.M.; Scott, R.L. *Regular and Related Solutions: The Solubility of Gases, Liquids, and Solids*; Van Nostrand Reinhold: New York, NY, USA, 1970.
33. Neau, S.H.; Flynn, G.L. Solid and liquid heat capacities of n-Alkyl para-aminobenzoates near the melting point. *Pharm. Res.* **1990**, *7*, 157–1162 [[CrossRef](#)]
34. Neau, S.H.; Bhandarkar, S.V.; Hellmuth, E.W. Differential molar heat capacities to test ideal solubility estimations. *Pharm. Res.* **1997**, *14*, 601–605 [[CrossRef](#)]
35. Opperhuizen, A.; Gobas, F.A.P.C.; Van der Steen, J.M.D.; Hutzinger, O. Aqueous solubility of polychlorinated biphenyls related to molecular structure. *Environ. Sci. Technol.* **1988**, *22*, 638–646. [[CrossRef](#)]
36. Holguín, A.R.; Rodríguez, G.A.; Cristancho, D.M.; Delgado, D.R.; Martínez, F. Solution thermodynamics of indomethacin in propylene glycol+water mixtures. *Fluid Phase Equilibria* **2012**, *314*, 134–139. [[CrossRef](#)]
37. Delgado, D.R.; Martínez, F. Solubility and solution thermodynamics of sulfamerazine and sulfamethazine in some ethanol+water mixtures. *Fluid Phase Equilibria* **2013**, *360*, 88–96. [[CrossRef](#)]
38. Delgado, D.R.; Martínez, F. Solubility and solution thermodynamics of some sulfonamides in 1-propanol + water mixtures. *J. Solut. Chem.* **2014**, *43*, 836–852. [[CrossRef](#)]
39. Delgado, D.R.; Almanza, O.A.; Martínez, F.; Peña, M.A.; Jouyban, A.; Acree, W.E. Solution thermodynamics and preferential solvation of sulfamethazine in (methanol + water) mixtures. *J. Chem. Thermodyn.* **2016**, *97*, 264–276. [[CrossRef](#)]
40. Delgado, D.R.; Martínez, F. Solution thermodynamics and preferential solvation of sulfamerazine in methanol + water mixtures. *J. Solut. Chem.* **2015**, *44*, 360–377. [[CrossRef](#)]
41. Krug, R.R.; Hunter, W.G.; Grieger, R.A. Enthalpy–entropy compensation. 1. Some fundamental statistical problems associated with the analysis of van't Hoff and Arrhenius data. *J. Phys. Chem.* **1976**, *80*, 2335–2341. [[CrossRef](#)]
42. Krug, R.R.; Hunter, W.G.; Grieger, R.A. Enthalpy–entropy compensation. 2. Separation of the chemical from the statistical effect. *J. Phys. Chem.* **1976**, *80*, 2341–2351. [[CrossRef](#)]
43. Nagasaka, M.; Yuzawa, H.; Kosugi, N. Microheterogeneity in aqueous acetonitrile solution probed by Soft X-ray absorption spectroscopy. *J. Phys. Chem. B* **2020**, *124*, 1259–1265. [[CrossRef](#)]
44. Perlovich, G.L.; Tkachev, V.V.; Strakhova, N.N.; Kazachenko, V.P.; Volkova, T.V.; Surov, O.V.; Schaper, K.; Raevsky, O.A. Thermodynamic and structural aspects of sulfonamide crystals and solutions. *J. Pharm. Sci.* **2009**, *98*, 4738–4755. [[CrossRef](#)]
45. Perlovich, G.L.; Strakhova, N.N.; Kazachenko, V.P.; Volkova, T.V.; Tkachev, V.V.; Schaper, K.J.; Raevsky, O.A. Sulfonamides as a subject to study molecular interactions in crystals and solutions: Sublimation, solubility, solvation, distribution and crystal structure. *Int. J. Pharm.* **2008**, *349*, 300–313. [[CrossRef](#)]
46. Torres-Cardozo, A.; Cerquera, N.E.; Ortiz, C.P.; Osorio-Gallego, J.; Cardenas-Torres, R.E.; Angarita-Reina, F.; Martinez, F.; Delgado, D.R. Thermodynamic analysis of the solubility of progesterone in 1-octanol+ethanol cosolvent mixtures at different temperatures. *Alex. Eng. J.* **2022**, *in press*. [[CrossRef](#)]
47. Baracaldo-Santamaría, D.; Calderon-Ospina, C.A.; Ortiz, C.P.; Cardenas-Torres, R.E.; Martinez, F.; Delgado, D.R. Thermodynamic analysis of the solubility of isoniazid in (PEG 200 + water) cosolvent mixtures from 278.15 K to 318.15 K. *Int. J. Mol. Sci.* **2022**, *23*, 10190. [[CrossRef](#)] [[PubMed](#)]
48. Ryde, U. A fundamental view of enthalpy–entropy compensation. *Med. Chem. Commun.* **2014**, *5*, 1324–1336. [[CrossRef](#)]
49. Sharp, K. Entropy–enthalpy compensation: Fact or artifact? *Protein Sci.* **2001**, *10*, 661–667. [[CrossRef](#)] [[PubMed](#)]
50. Bustamante, P.; Romero, S.; Peña, A.; Escalera, B.; Reillo, A. Enthalpy–entropy compensation for the solubility of drugs in solvent mixtures: Paracetamol, acetanilide, and nalidixic acid in dioxane–water. *J. Pharm. Sci.* **1998**, *87*, 1590–1596. [[CrossRef](#)]
51. Peña, M.; Escalera, B.; Reillo, A.; Sánchez, A.; Bustamante, P. Thermodynamics of cosolvent action: Phenacetin, salicylic acid and probenecid. *J. Pharm. Sci.* **2009**, *98*, 1129–1135. [[CrossRef](#)]

Disclaimer/Publisher's Note: The statements, opinions and data contained in all publications are solely those of the individual author(s) and contributor(s) and not of MDPI and/or the editor(s). MDPI and/or the editor(s) disclaim responsibility for any injury to people or property resulting from any ideas, methods, instructions or products referred to in the content.

Communication

Density and Dynamic Viscosity of Perfluorodecalin-Added *n*-Hexane Mixtures: Deciphering the Role of Fluorous Liquids

Deepika and Siddharth Pandey *

Department of Chemistry, Indian Institute of Technology Delhi, Hauz Khas, New Delhi 110016, India

* Correspondence: sipandey@chemistry.iitd.ac.in; Tel.: +91-11-26596503; Fax: +91-11-26581102

Abstract: Fluorous solvents are deputed as prominent solvent systems owing to their salient features, unique physical properties, and ecological importance. In this study, the temperature- and composition-dependence of physical properties, density ($\rho/g\cdot\text{cm}^{-3}$), and dynamic viscosity ($\eta/\text{mPa}\cdot\text{s}$), of neat perfluorodecalin (PFD) and PFD-added *n*-hexane mixtures with select compositions are reported. Density follows a linear decrease with temperature and a quadratic increase with the mole fraction of PFD. The sensitivity or dependence of density on temperature increases with an increase in PFD mole fraction. The temperature-dependence of the dynamic viscosity of the investigated mixtures follows the Arrhenius-type expression from which the resultant activation energy of the viscous flow ($E_{a,\eta}$) is determined. Interestingly, the composition-dependence of dynamic viscosity shows exponential growth with an increase in PFD mole fraction. Excess molar volumes (V^E) and deviation in the logarithmic viscosities $\Delta(\ln \eta)$ of the mixtures are calculated to highlight the presence of strong repulsive interactions between the two mixture components.

Keywords: fluorous solvents; perfluorodecalin; *n*-hexane; density; dynamic viscosity; excess molar volume; excess logarithmic viscosity

Citation: Deepika; Pandey, S. Density and Dynamic Viscosity of Perfluorodecalin-Added *n*-Hexane Mixtures: Deciphering the Role of Fluorous Liquids. *Liquids* **2023**, *3*, 48–56. <https://doi.org/10.3390/liquids3010005>

Academic Editors: Juan Ortega Saavedra and William E. Acree, Jr.

Received: 21 November 2022

Revised: 26 December 2022

Accepted: 29 December 2022

Published: 4 January 2023



Copyright: © 2023 by the authors. Licensee MDPI, Basel, Switzerland. This article is an open access article distributed under the terms and conditions of the Creative Commons Attribution (CC BY) license (<https://creativecommons.org/licenses/by/4.0/>).

1. Introduction

The solvent media is crucial in defining chemical reactivity, molecular associations, and catalytic properties of any chemical reaction. Fluorous chemistry employing perfluorinated hydrocarbons as solvent systems opens new avenues as alternative solvent media to highly toxic, flammable, non-biodegradable, and environmentally-persistent conventional organic solvents and ionic liquids (ILs) [1–5]. Perfluorinated solvents are designated as “fluorous” solvents, analogous to the term aqueous, and are widely accepted as highly non-polar and solvophobic in nature. Fluorinated solvents exhibit temperature-dependent solubility with organic solvents [6,7]. This unique thermomorphic effect enables switching between heterogeneous and homogeneous phases of fluorous solvents with organic liquids and subsequent mass transfer. The unique solvophobicity of fluorous solvents enables their use in biphasic catalysis and separation techniques [8,9].

Fluorous solvents are used in numerous applications, including the synthesis of nanoparticles [10], in enzymatic and homogeneous catalysis [11], biomolecular separations, microfluidic devices, components of artificial blood, and green chemistry [12]. Cyclic perfluorinated solvents are used as substitutes for blood plasma due to their remarkable stability; capability of dissolving two biologically important gases, oxygen and carbon dioxide; and their nontoxic nature [13]. Toxicity associated with fluorous solvents, in general, is a topic of intense research [14,15]. Despite having a plethora of applications and unique properties as a solvent medium, studies including fluorous solvents are scarce. Physical properties like dynamic viscosity, density, refractive index, and surface tension play a crucial role in developing typical applications of a solvent and help expand its application potential.

In this work, we have reported the temperature and composition dependence of two crucial thermophysical properties—density and dynamic viscosity—of a mixture consisting

of a fluoruous solvent shown in Figure 1, octadecafluorodecahydronaphthalene (commonly known as perfluorodecalin, PFD), and a common and popular organic solvent, *n*-hexane. PFD is a stable, colorless perfluorinated derivative of decalin and is chemically and biologically inert. It can exist in two isomeric forms, *cis*-isomer and *trans*-isomer. Due to its remarkable capacity to dissolve oxygen, it is used in several medical applications, including storing organs and tissues, an ingredient in fluosol, and in liquid breathing [13,16]. Interestingly, the two non-polar solvents, one hydrocarbon and one fluorocarbon, show complete miscibility at each composition investigated and at every temperature ≥ 288 K (standard uncertainty: $u(T) = \pm 0.05$ K). In addition, the easy tunability of the composition of two mixture components allows us to study the composition-dependence of the investigated thermophysical properties as well; consequently, molar excess properties are also evaluated.

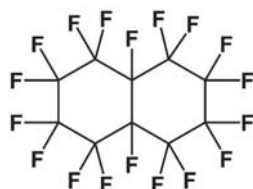


Figure 1. Structure of perfluorodecalin (PFD).

2. Materials and Methods

The investigated mixtures were prepared by mixing PFD (>95.0% from Tokyo Chemicals Industry Co. Ltd., Tokyo, Japan) and *n*-hexane ($\geq 99.0\%$ from Sigma-Aldrich, St. Louis, Missouri, MO, USA) in their respective pre-calculated amount using a Denver Instrument balance having a precision of ± 0.1 mg. Neat PFD, neat *n*-hexane, and three stable and homogeneous solutions having mole fraction ratio: $x_{\text{PFD}}/x_{\text{Hex}} = 0.2/0.8; 0.5/0.5; 0.8/0.2$ were used for physical property determination. Densities (ρ) of the neat components, as well as of the (PFD + *n*-hexane) mixtures, were measured using a Mettler Toledo, DE45 delta range density meter. The density measurement with the above-mentioned density meter was based on the electromagnetically induced oscillations of a U-shaped glass tube. The standard deviations associated with the density measurement are ± 0.0001 $\text{g}\cdot\text{cm}^{-3}$. The measurements were performed in a temperature range (293 to 333 K). The dynamic viscosities (η) were measured with a Peltier-based (resolution of 0.01 K and accuracy < 0.05 K) automated Anton Paar microviscometer (model AMVn) having calibrated glass capillaries of different diameters (1.6, 1.8, 3.0, and 4.0 mm). This instrument is based on the rolling-ball principle, wherein a steel ball rolls down the inside of inclined, sample-filled calibrated glass capillaries. The deviation in η was ± 0.001 mPa·s.

3. Results and Discussion

The two non-polar hydrocarbons, PFD and *n*-hexane, have an atmospheric boiling point of 415 K and 342 K, respectively. The density and dynamic viscosity of neat PFD (1.917 $\text{g}\cdot\text{cm}^{-3}$ and 5.412 mPa·s, respectively) and neat *n*-hexane (0.6593 $\text{g}\cdot\text{cm}^{-3}$ and 0.300 mPa·s, respectively) at 298 K are reported in the literature [17,18]. These reported values are in good agreement with our measured values (*vide infra*). The slight disparities in the values may be attributed to the differences in the instrumentation used, the purity of the chemicals, and the source of the compounds.

3.1. Density of PFD and (PFD + *n*-Hexane) Mixtures

Experimentally measured densities of PFD and (PFD + *n*-hexane) mixtures as a function of temperature in the range (293 to 333) K at select compositions are reported in Table 1. As expected, with increase in temperature, the densities of PFD, *n*-hexane, and

their mixtures were found to decrease primarily due to thermal expansion and follow a linear dependence according to the equation:

$$\rho = \rho_{0,T} + aT \quad (1)$$

where $\rho/\text{g}\cdot\text{cm}^{-3}$ is the density of (PFD + *n*-hexane) mixtures. The values of the parameters $\rho_{0,T}$ (representing density at $T = 0$ K) and the slope a along with the standard deviation of the fits are listed in Table 2 (measured densities of (PFD + *n*-hexane) mixtures along with the fits to a linear expression are presented in Figure 2).

Table 1. Densities ^a ($\rho/\text{g}\cdot\text{cm}^{-3}$) of the investigated mixtures of PFD and *n*-hexane at different mole fraction ratios at pressure $p^b = (0.1 \text{ MPa})$ and temperature $T^c = (293 \text{ K to } 333 \text{ K})$.

x_{PFD}^d	T/K					
	293	298	303	313	323	333
0.0	0.6596	0.6553	0.6515	0.6413	0.6320	0.6219
0.2	1.0433	1.0355	1.0298	1.0134	0.9983	0.9835
0.5	1.4735	1.4633	1.4553	1.4332	1.4127	1.3943
0.8	1.7855	1.7750	1.7661	1.7420	1.7199	1.7015
1.0	1.9412	1.9303	1.9212	1.8961	1.8733	1.8468

^a Standard uncertainty: $u(\rho) = \pm 0.0001 \text{ g}\cdot\text{cm}^{-3}$; ^b Standard uncertainty: $u(p) = \pm 0.005 \text{ MPa}$; ^c Standard uncertainty: $u(T) = \pm 0.05 \text{ K}$; ^d Standard uncertainty: $u(x) = \pm 0.01$.

Table 2. Result of the regression analysis of density ($\rho/\text{g}\cdot\text{cm}^{-3}$) versus temperature (T/K) data according to equation: $\rho/(\text{g}\cdot\text{cm}^{-3}) = \rho_{0,T}/(\text{g}\cdot\text{cm}^{-3}) + a(T/\text{K})$ for the investigated mixtures at different mole ratios over the temperature range 293 K to 333 K. ^a

x_{PFD}^b	$\rho_{0,T} (\text{g}\cdot\text{cm}^{-3})$	$a \cdot 10^{-3} (\text{g}\cdot\text{cm}^{-3}\cdot\text{K}^{-1})$	R^2
0.0	0.9379 ± 0.0048	$-0.9 \pm 0.0_1$	0.9990
0.2	1.4839 ± 0.0064	$-1.5 \pm 0.0_2$	0.9993
0.5	2.0610 ± 0.0094	$-2.0 \pm 0.0_3$	0.9991
0.8	2.4134 ± 0.0134	$-2.1 \pm 0.0_4$	0.9984
1.0	2.6338 ± 0.0154	$-2.4 \pm 0.0_5$	0.9982

^a Standard uncertainties u are, $u(T) = \pm 0.05 \text{ K}$, $u(\rho) = \pm 0.0001 \text{ g}\cdot\text{cm}^{-3}$; ^b Standard uncertainty: $u(x) = \pm 0.01$; Standard deviations are given with \pm sign.

A careful examination of the density data presented in Tables 1 and 2, along with Figure 2, indicates the density of PFD to be not only higher than that of water but also that it is significantly higher than that of *n*-hexane (almost 3-fold) at all temperatures. It is inferred that biphasic aqueous extractions using PFD would have PFD as the lower phase and water as the higher phase, as opposed to several organic non-polar solvents that have densities lower than that of water. It is also interesting to note that the density of the PFD is much more sensitive to temperature variation compared to the density of *n*-hexane (the slope of ρ vs. T is $-2.4 (\pm 0.0_5) \times 10^{-3} \text{ g}\cdot\text{cm}^{-3}\cdot\text{K}^{-1}$ for PFD as opposed to only $-0.9 (\pm 0.0_1) \times 10^{-3} \text{ g}\cdot\text{cm}^{-3}\cdot\text{K}^{-1}$ for *n*-hexane). Such a high sensitivity of density on temperature for PFD may find uses in several industrial applications and processes and also as temperature sensors based on physical property changes [19].

As expected, the density of *n*-hexane increases monotonically as PFD is gradually added to it (Figure 3). The increase in density with increasing PFD mole fraction in the mixture is not linear, and it rather shows a downward curvature and best fits a quadratic expression:

$$\rho = \rho_{0,x_{\text{PFD}}} + bx_{\text{PFD}} + cx_{\text{PFD}}^2 \quad (2)$$

where x_{PFD} is the mole fraction of PFD in the (PFD + *n*-hexane) mixtures, and values of parameters $\rho_{0,x_{\text{PFD}}}$, b , and c are listed in Table 3, while the fits are represented with dark curves in Figure 3. Quadratic dependence of the density on PFD mole fraction of the (PFD + *n*-hexane) mixtures is clearly established. Excess molar volume (V^E) was

estimated using equation 3 to assess the extent of molecular-level interactions within (PFD + *n*-hexane) mixtures.

$$V^E = \frac{(x_{\text{PFD}}M_{\text{PFD}} + x_{n\text{-hexane}} M_{n\text{-hexane}})}{\rho_m} - \left(\frac{x_{\text{PFD}}M_{\text{PFD}}}{\rho_{\text{PFD}}} + \frac{x_{n\text{-hexane}}M_{n\text{-hexane}}}{\rho_{n\text{-hexane}}} \right) \quad (3)$$

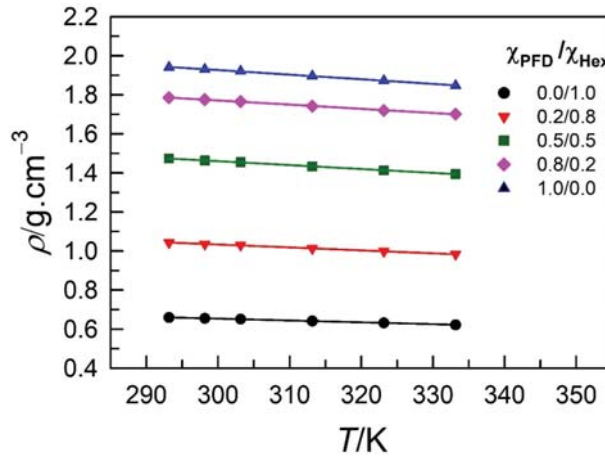


Figure 2. Variation in densities of the investigated mixtures with temperature at different mole fraction ratios and at pressure $p = 0.1$ MPa. The solid line represents fit to the equation $\rho/(g \cdot cm^{-3}) = \rho_{0,T}/(g \cdot cm^{-3}) + a(T/K)$. Parameters $\rho_{0,T}$ and a , along with R^2 are provided in Table 2.

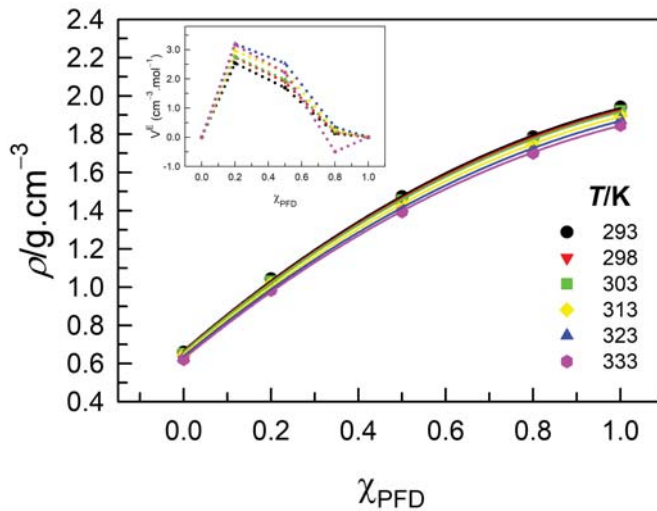


Figure 3. Variation in densities of the investigated mixtures with varying mole ratios of the constituents at different temperatures ($T = 293$ to 333 K) and at pressure $p = 0.1$ MPa. The solid line represents fit to the equation $\rho/(g \cdot cm^{-3}) = \rho_{0,\chi_{\text{PFD}}}/(g \cdot cm^{-3}) + b(\chi_{\text{PFD}}) + c(\chi_{\text{PFD}}^2)$. Parameters $\rho_{0,\chi_{\text{PFD}}}$, b , and c , along with R^2 , are provided in Table 3.

Table 3. Result of the regression analysis of density ($\rho/\text{g}\cdot\text{cm}^{-3}$) versus mole fraction of PFD (x_{PFD}) data according to equation: $\rho/(\text{g}\cdot\text{cm}^{-3}) = \rho_{0,x_{\text{PFD}}}/(\text{g}\cdot\text{cm}^{-3}) + b(x_{\text{PFD}}) + c(x_{\text{PFD}}^2)$ for the investigated mixtures over the temperature range 293 K to 333 K. ^a

T/K	$\rho_{0,x_{\text{PFD}}} (\text{g}\cdot\text{cm}^{-3})$	b	c	R^2
293	0.6661 ± 0.0107	1.9682 ± 0.0548	-0.6984 ± 0.0529	0.9998
298	0.6616 ± 0.0102	1.9521 ± 0.0526	-0.6883 ± 0.0508	0.9998
303	0.6578 ± 0.0103	1.9409 ± 0.0527	-0.6824 ± 0.0509	0.9998
313	0.6474 ± 0.0099	1.9091 ± 0.0507	-0.6650 ± 0.0489	0.9998
323	0.6378 ± 0.0095	1.8789 ± 0.0487	-0.6478 ± 0.0471	0.9998
333	0.6267 ± 0.0076	1.8682 ± 0.0392	-0.6507 ± 0.0379	0.9999

^a Standard uncertainties u are, $u(T) = \pm 0.05$ K, $u(\rho) = \pm 0.0001$ $\text{g}\cdot\text{cm}^{-3}$, $u(x) = \pm 0.01$. Standard deviations are given with \pm sign.

Here, x_{PFD} , $x_{n\text{-hexane}}$, and ρ_{PFD} , $\rho_{n\text{-hexane}}$ refer to the mole fractions and densities, respectively, of PFD and n -hexane at a given temperature, and ρ_m is the density of the mixture. M_{PFD} and $M_{n\text{-hexane}}$ are the molecular weights of PFD and n -hexane, respectively. The V^E at each investigated temperature for (PFD + n -hexane) mixtures are presented as a function of x_{PFD} in the inset of Figure 3. It is clear that, irrespective of the T , V^E are mostly positive and have maxima at ca. $x_{\text{PFD}} = 0.2$. The positive V^E points to volume expansion on mixing PFD and n -hexane and thus hints more at the presence of repulsive interaction (s) between PFD and n -hexane or weaker interactions between them than the interactions present within neat PFD and n -hexane, respectively. It may be inferred that the incompatibility of fluoruous solvents with most non-fluorous substances brings in the repulsive interaction when the two substances are mixed.

3.2. Dynamic Viscosity of PFD and (PFD + n -Hexane) Mixtures

Experimentally measured dynamic viscosities ($\eta/\text{mPa}\cdot\text{s}$) of PFD and (PFD + n -hexane) mixtures in the temperature range (293 to 333) K are reported in Table 4. It is to be noted that η of PFD is much higher than that of n -hexane and is comparable to 2-ethyl-1-hexanol and other mid-chain alkyl alcohols. While in such alcohols, H-bonding usually gives rise to higher η ; in PFD the interaction between fluorine atoms may cause similar η values [20].

Table 4. Dynamic viscosity ^a ($\eta/\text{mPa}\cdot\text{s}$) of the investigated mixtures of PFD and n -hexane at different mole fraction ratios at pressure $p^b = (0.1$ MPa) and temperature $T^c = (293$ K to 333 K).

x_{PFD}^d	T/K					
	293	298	303	313	323	333
0.0	0.349	0.322	0.317	0.291	0.271	0.255
0.2	0.572	0.536	0.509	0.458	0.420	0.387
0.5	1.271	1.173	1.060	0.892	0.768	0.669
0.8	3.179	2.816	2.524	2.050	1.703	1.435
1.0	6.535	5.647	4.925	3.815	3.152	2.446

^a Standard uncertainty: $u(\eta) = \pm 0.001$ $\text{mPa}\cdot\text{s}$. ^b Standard uncertainty: $u(p) = \pm 0.005$ MPa. ^c Standard uncertainty: $u(T) = \pm 0.05$ K. ^d Standard uncertainty: $u(x) = \pm 0.01$.

As expected, with an increase in temperature from (293 to 333) K, a monotonic decrease in η is observed for a given composition of (PFD + n -hexane) mixture (Table 4). The temperature dependence of η follows the most simplistic Arrhenius-like behavior:

$$\ln \eta = \ln A_\eta + \frac{E_{a,\eta}}{RT} \quad (4)$$

where A_η is a parameter, and $E_{a,\eta}$ is the activation energy of the viscous flow.

Figure 4 demonstrates the plots of $\ln \eta$ versus $1/T$ for (PFD + n -hexane) mixtures. The best fit lines are according to Arrhenius expression and the recovered parameters $\ln A_\eta$

and $E_{a,\eta}$ along with goodness-of-fit are presented in Table 5. As expected, $E_{a,\eta}$ increases monotonically as the concentration of the component with higher η PFD is increased in the mixture; neat PFD has the highest $E_{a,\eta}$. It is established that fluororous liquid, PFD, possesses relatively high activation energy of viscous flow compared to the organic solvent *n*-hexane.

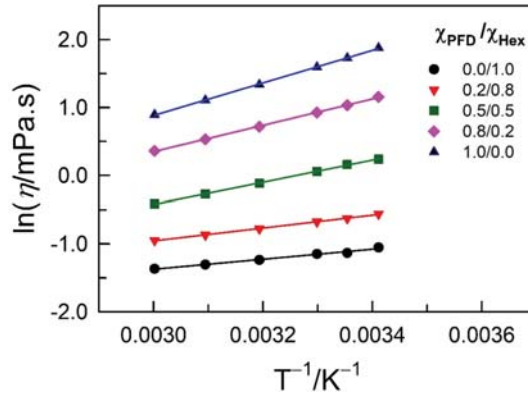


Figure 4. Variation in $\ln \eta$ of the investigated mixtures with T^{-1} at different mole fraction ratios and at pressure $p = 0.1$ MPa. The solid curves represent the best fit to the Arrhenius model: $\ln(\eta/\text{mPa}\cdot\text{s}) = \ln(A_\eta) + \frac{E_{a,\eta}}{RT}$. Parameters $\ln(A_\eta)$, and $E_{a,\eta}$, along with R^2 are reported in Table 5.

Table 5. Summary of parameters associated with dynamic viscosity of the investigated mixtures according to the Arrhenius model using the equation: $\ln \eta = \ln A_\eta + Ea/RT$.

x_{PFD}	$\ln A_\eta$	$E_{a,\eta}/\text{kJ}\cdot\text{mol}^{-1}$	R^2
0.0	-3.589 ± 0.130	6.14 ± 0.33	0.9883
0.2	-3.794 ± 0.062	7.87 ± 0.16	0.9983
0.5	-5.275 ± 0.055	13.45 ± 0.14	0.9996
0.8	-5.465 ± 0.065	16.12 ± 0.17	0.9999
1.0	-6.303 ± 0.066	19.92 ± 0.17	0.9999

Standard deviations are given with \pm sign.

The increase in η with the increasing mole fraction of PFD in the (PFD + *n*-hexane) mixture is found to be exponential, as per the equation:

$$\eta = \eta_0 + d \exp(f x_{\text{PFD}}) \quad (5)$$

Fits are presented in Figure 5, whereas the recovered parameters η_0 , d , and f , along with the goodness-of-the-fit in terms of R^2 , are given in Table 6. In order to assess the interactions within (PFD + *n*-hexane) mixtures, deviation in logarithmic viscosities, $\Delta(\ln \eta)$, are estimated from the equation [21],

$$\Delta(\ln \eta) = \ln \eta_m - [x_{\text{PFD}} \ln \eta_{\text{PFD}} + x_{n\text{-hexane}} \ln \eta_{n\text{-hexane}}] \quad (6)$$

where η_m is the dynamic viscosity of the (PFD + *n*-hexane) mixture, and x_{PFD} , $x_{n\text{-hexane}}$, and η_{PFD} , $\eta_{n\text{-hexane}}$ refer to the mole fractions and dynamic viscosities, respectively, of PFD and *n*-hexane at a given temperature. Plots of $\Delta(\ln \eta)$ versus for (PFD + *n*-hexane) mixtures in a temperature range (293 to 333 K) are presented in the inset of Figure 5. A careful examination of Figure 5 reveals that, irrespective of the T , $\Delta(\ln \eta)$ are negative and that no clear trend exists with variation in T . The negative $\Delta(\ln \eta)$ further emphasizes the lack of attractive interaction within the (PFD + *n*-hexane) mixture; it rather indicates that repulsive interactions are present between PFD and *n*-hexane within the mixture, leading

to lower viscosities than expected ideally. In this context, the negative $\Delta(\ln \eta)$ corroborates and complements the positive V^E .

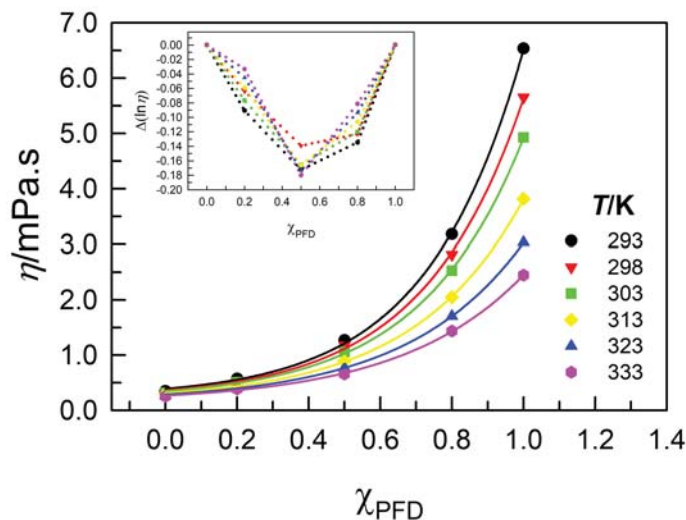


Figure 5. Variation in dynamic viscosities of the investigated mixtures with varying mole ratios of the constituents at different temperatures ($T = 293$ to 333 K) and at pressure $p = 0.1$ MPa. The solid line represents fit to the equation $\eta / (\text{mPa}\cdot\text{s}) = \eta_0 / (\text{mPa}\cdot\text{s}) + d \cdot e^{f(\chi_{\text{PFD}})}$. Parameters η_0 , d , and f , along with R^2 , are provided in Table 6.

Table 6. Result of the regression analysis of dynamic viscosity ($\eta / \text{mPa}\cdot\text{s}$) versus mole fraction of PFD (χ_{PFD}) data according to equation: $\eta / (\text{mPa}\cdot\text{s}) = \eta_0 / (\text{mPa}\cdot\text{s}) + d \cdot e^{f(\chi_{\text{PFD}})}$ for the investigated mixtures over the temperature range 293 K to 333 K. ^a

T/K	η_0 (mPa·s)	d	f	R^2
293	0.238 ± 0.060	0.151 ± 0.020	3.726 ± 0.130	0.9997
298	0.212 ± 0.063	0.151 ± 0.023	3.583 ± 0.149	0.9996
303	0.201 ± 0.041	0.145 ± 0.016	3.482 ± 0.107	0.9998
313	0.174 ± 0.028	0.137 ± 0.012	3.275 ± 0.084	0.9999
323	0.156 ± 0.024	0.130 ± 0.012	3.093 ± 0.085	0.9999
333	0.142 ± 0.031	0.124 ± 0.016	2.924 ± 0.121	0.9997

^a Standard uncertainties u are $u(T) = \pm 0.05$ K, $u(\eta) = \pm 0.001$ mPa·s, $u(x) = \pm 0.01$; Standard deviations are given with \pm sign.

It is clear from the density and dynamic viscosity of the (PFD + *n*-hexane) mixtures that unfavorable interactions exist between PFD and *n*-hexane within the mixture, as documented by the nature of the fluoruous solvents in general. The fact that the fluoruous solvents exhibit contrast in properties as compared to the common organic solvents is established nonetheless.

4. Conclusions

Fluorous solvents are notorious for their immiscibility with organic solvents and ILs. PFD shows complete miscibility with only a few organic solvents, especially short-chain hydrocarbons. The extreme non-polarity and the presence of the most electronegative fluorine atom play a key role in determining their properties. The density and dynamic viscosity of *n*-hexane show greater sensitivity towards temperature with an increase in PFD composition in the mixture. The contrasting behavior of PFD as compared to *n*-hexane

is demonstrated. Both V^E and $\Delta(\ln \eta)$ hint at the repulsive interactions between PFD and *n*-hexane. The stark differences in the molecular architecture and the size of the two components might be responsible for such interactions. The work suggests that fluororous liquids may be used to effectively modulate the physical properties of common organic solvents. The data presented in this work is the beginning of physicochemical data on fluororous solvents as these solvents may afford a link between the interactions present in the gas phase and in the condensed phase.

Author Contributions: Conceptualization, methodology, visualization, writing—original draft, D.; writing—review and editing, supervision, resources, project administration, S.P. All authors have read and agreed to the published version of the manuscript.

Funding: This work is generously supported by the Science & Engineering Research Board (SERB), Government of India, through a grant to Siddharth Pandey (grant number CRG/2021/000602).

Data Availability Statement: Not applicable.

Acknowledgments: Deepika would like to acknowledge the Ministry of Education (MoE), Government of India, for her Prime Minister Research Fellowship (PMRF).

Conflicts of Interest: There are no conflict to declare.

References

- Sheldon, R.A. Green solvents for sustainable organic synthesis: State of the art. *Green Chem.* **2005**, *7*, 267–278. [[CrossRef](#)]
- Capello, C.; Fischer, U.; Hungerbühler, K. What is green solvent? A comprehensive framework for the environmental assessment of solvents. *Green Chem.* **2007**, *9*, 927–934. [[CrossRef](#)]
- Clark, J.H.; Tavener, S.J. Alternative solvents: Shades of green. *Org. Process Res. Dev.* **2007**, *11*, 149–155. [[CrossRef](#)]
- Horváth, I.T. Solvents from nature. *Green Chem.* **2008**, *10*, 1024–1028. [[CrossRef](#)]
- Anastas, P.T.; Warner, J.C. *Green Chemistry: Theory and Practice*; Oxford University Press: Oxford, UK, 1998.
- Gładysz, J.A.; Curran, D.P.; Horváth, I.T. *Handbook of Fluororous Chemistry*; Wiley-VCH Verlag GmbH & Co. KGaA: Weinheim, Germany, 2004.
- Horváth, I.T.; Rábai, J. Facile catalyst separation without water: Fluororous biphasic hydroformylation of olefins. *Science* **1994**, *266*, 72–75. [[CrossRef](#)] [[PubMed](#)]
- Wolf, E.; van Koten, G.; Deelman, B.-J. Fluororous phase separation techniques in catalysis. *Chem. Soc. Rev.* **1999**, *28*, 37–41. [[CrossRef](#)]
- Barthel Rosa, L.P.; Gladysz, J.A. Chemistry in fluororous media: A user's guide to practical considerations in the application of fluororous catalysts and reagents. *Coord. Chem. Rev.* **1999**, *190–192*, 587–605. [[CrossRef](#)]
- Zhang, W.; Cai, C. New chemical, and biological applications of fluororous technologies. *Chem. Commun.* **2008**, 5686–5694. [[CrossRef](#)] [[PubMed](#)]
- Horvath, I.T. Fluororous biphasic chemistry. *Acc. Chem. Res.* **1998**, *31*, 641–650. [[CrossRef](#)]
- Zhang, W.; Soloshonok, V.A.; Mikami, K.; Yamazaki, T.; Welch, J.T.; Honek, J. *Current Fluoroorganic Chemistry: New Synthetic Directions, Technologies, Materials and Biological Applications*; Oxford University Press: Oxford, UK, 2006; pp. 207–220.
- Lowe, K.C. Engineering blood: Synthetic substitutes from fluorinated compound. *Tissue Eng.* **2003**, *9*, 389–399. [[CrossRef](#)] [[PubMed](#)]
- Khalil, M.A.K.; Rasmussen, R.A.; Culbertson, J.A.; Prins, J.M.; Grimsrud, E.P.; Shearer, M.J. Atmospheric perfluorocarbons. *Environ. Sci. Technol.* **2003**, *37*, 4358–4361. [[CrossRef](#)] [[PubMed](#)]
- Kennedy, G.L.; Butenhoff, J.L.; Olsen, G.W.; O'Connor, J.C.; Seacat, A.M.; Perkins, R.G.; Biegel, L.B.; Murphy, S.R.; Farrar, D.G. The toxicology of perfluorooctanoate. *Crit. Rev. Toxicol.* **2004**, *34*, 351–384. [[CrossRef](#)] [[PubMed](#)]
- Stephan, C.; Schlawne, C.; Grass, S.; Waack, I.N.; Ferenz, K.B.; Bachmann, M.; Barnert, S.; Schubert, R.; Bastmeyer, M.; De Groot, H.; et al. Artificial oxygen carriers based on perfluorodecalin-filled poly(*n*-butyl-cyanoacrylate) nanocapsules. *J. Microencapsul.* **2014**, *31*, 284–292. [[CrossRef](#)] [[PubMed](#)]
- Rumble, J.R.; Bruno, T.J.; Doa, M.J. *CRC Handbook of Chemistry and Physics: A Ready Reference Book of Chemical and Physical Data*, 102nd ed.; CRC Press: Boca Raton, FL, USA, 2021.
- Freire, M.G.; Ferreira, A.G.M.; Fonseca, I.M.A.; Marrucho, I.M.; Coutinho, J.A.P. Viscosities of liquid fluorocompounds. *J. Chem. Eng. Data* **2008**, *53*, 538–542. [[CrossRef](#)]
- Fehlauer, H.; Wolf, H. Density reference liquids certified by the Physikalisch-Technische Bundesanstalt. *Meas. Sci. Technol.* **2006**, *17*, 2588–2592. [[CrossRef](#)]

20. Sulthana, S.P.; Gowrisankar, M.; Babu, S.; Rao, P.V. Binary mixtures of 2-ethyl-1-hexanol with various functional groups (benzyl chloride, 3-methylaniline, 3-methoxyaniline and 2,6-dimethylcyclohexanone). *SN Appl. Sci.* **2020**, *2*, 960. [[CrossRef](#)]
21. Heintz, A.; Klasen, D.; Lehmann, J.K. Excess molar volumes and viscosities of binary mixtures of methanol and the ionic liquid 4-Methyl-N-butylpyridinium Tetrafluoroborate at 25, 40, and 50±C. *J. Solut. Chem.* **2002**, *31*, 467–476. [[CrossRef](#)]

Disclaimer/Publisher's Note: The statements, opinions and data contained in all publications are solely those of the individual author(s) and contributor(s) and not of MDPI and/or the editor(s). MDPI and/or the editor(s) disclaim responsibility for any injury to people or property resulting from any ideas, methods, instructions or products referred to in the content.

Review

The Relevance of Cavity Creation for Several Phenomena Occurring in Water

Giuseppe Graziano

Dipartimento di Scienze e Tecnologie, Università degli Studi del Sannio, Via Francesco de Sanctis, Snc, 82100 Benevento, Italy; graziano@unisannio.it; Tel.: +39-0824-305133

Abstract: The solvent-excluded volume effect is an under-appreciated general phenomenon occurring in liquids and playing a fundamental role in many cases. It is quantified and characterized by means of the theoretical concept of cavity creation and its Gibbs free energy cost. The magnitude of the reversible work of cavity creation proves to be particularly large in water, and this fact plays a key role for, among other things, the poor solubility of nonpolar species, the formation of host–guest complexes, and the folding of globular proteins. An analysis of some examples is provided in the present review.

Keywords: cavity creation; solvent-excluded volume effect; hydration of noble gases; host–guest complexes; folding of globular proteins

1. Introduction

The starting point of any theory able to describe processes occurring in liquids (i.e., pure liquids or solutions) is the recognition that a suitable void space, a cavity, has to be created to allow solute insertion [1–21]. This is the simple consequence of the fact that liquids are a condensed state of matter and each molecule possesses its own body. Cavity creation leads to a decrease in the number of configurations accessible to liquid molecules and thus leads to a solvent-excluded volume effect [22–25]. These words are right, but the matter has to be spelled out in more detail to reach a correct understanding (note that cavity creation is a theoretical concept and cannot be studied by performing experiments). Keeping a constant temperature and pressure, the creation of a cavity leads to an increase in liquid volume by the partial molar volume of the cavity itself. This volume increase does not cancel the solvent-excluded volume effect. If the cavity is to exist, the center of liquid molecules (assumed to be spherical) cannot go beyond the solvent-accessible surface area, SASA, and WASA in water [26], of the cavity itself. This means that the shell between the cavity van der Waals surface and the SASA is excluded to liquid molecules, causing a decrease in accessible configurations for basic geometric reasons. The latter constraint does affect the translational motion of all the liquid molecules, not solely the ones in the first solvation shell of the cavity (i.e., of the solute molecule to be hosted).

The solvent-excluded volume effect can be measured by calculating the reversible work of cavity creation, ΔG_C , by means of analytical theories or computer simulations. Classic scaled particle theory, SPT [23–25,27–29], is a simple, geometry-based statistical mechanical model providing analytical formulas to calculate ΔG_C for cavities of simple shape (i.e., a sphere, a prolate spherocylinder, and others) in liquids made up of hard particles. Its use in the case of water may appear strange, but it works well because the real liquid density is used as input in classic SPT calculations (i.e., density provides indirect information on the strength of the intermolecular attractions existing among liquid molecules; in addition, on the H-bonds between water molecules [30,31]). The classic SPT

Citation: Graziano, G. The Relevance of Cavity Creation for Several Phenomena Occurring in Water. *Liquids* **2023**, *3*, 57–65. <https://doi.org/10.3390/liquids3010006>

Academic Editor: Enrico Bodo

Received: 14 December 2022

Revised: 30 December 2022

Accepted: 1 January 2023

Published: 9 January 2023



Copyright: © 2023 by the author. Licensee MDPI, Basel, Switzerland. This article is an open access article distributed under the terms and conditions of the Creative Commons Attribution (CC BY) license (<https://creativecommons.org/licenses/by/4.0/>).

formulas to create a spherical cavity in a liquid (neglecting the pressure–volume term for its smallness at $P = 1$ atm) are:

$$\Delta G_C = RT \cdot \{-\ln(1 - \xi) + [3\xi/(1 - \xi)] \cdot x + [3\xi/(1 - \xi)] \cdot x^2 + [9\xi^2/2(1 - \xi)^2] \cdot x^2\} \quad (1)$$

$$\Delta H_C = [RT^2 \cdot \xi \cdot \alpha_P / (1 - \xi)^3] \cdot [(1 - \xi)^2 + 3(1 - \xi) \cdot x + 3(1 + 2\xi) \cdot x^2] \quad (2)$$

where R is the gas constant, α_P is the isobaric thermal expansion coefficient of the liquid, ξ is the volume packing density of the liquid, which is defined as the ratio of the physical volume of a mole of liquid molecules over the liquid molar volume, v_1 (i.e., $\xi = \pi \cdot \sigma_1^3 \cdot N_{Av} / 6 \cdot v_1$); $x = \sigma_C / \sigma_1$, and σ_1 is the hard sphere diameter of liquid molecules; σ_C is the cavity diameter, defined as the diameter of the spherical region from which any part of liquid molecules is excluded. The ΔG_C (SPT) magnitude depends upon the volume packing density of the liquid, ξ , that is, the fraction of the total liquid volume really occupied by liquid molecules, and the effective hard sphere diameter, σ_1 , of liquid molecules [25,31]. On increasing ξ , the void volume decreases and ΔG_C increases; on decreasing σ_1 , the void volume is partitioned into smaller pieces and ΔG_C increases (i.e., a significant fraction of the liquid volume is void, but most of these voids are too small to host an atom or a molecule). This implies that the effective diameter of liquid molecules is a fundamental length-scale for the liquid itself. The validity of these arguments has been verified and confirmed in several cases over the years [31].

2. Solvation of Noble Gases

A further test is provided here, by analyzing the solvation (i.e., the transfer from a fixed position in the gas phase to a fixed position in the liquid phase) of noble gases in water, carbon tetrachloride, CCl_4 , and benzene, C_6H_6 . Experimental thermodynamic data at 25 °C and 1 atm [32–34], reported in Table 1, emphasize that: (1) noble gases are poorly soluble in water, with them being characterized by large positive ΔG° values, caused by large negative entropy changes; (2) Ar is characterized by positive ΔG° values also in CCl_4 and C_6H_6 , while Xe is characterized by a negative ΔG° value in benzene. The ΔG_C (SPT) values calculated for noble gases in the three liquids, whose molecules are assumed to be spherical, at 25 °C and 1 atm, are listed in the eighth column of Table 1. They prove to be largely positive in all cases. Actually, they are significantly larger in water with respect to the other two liquids (see the trends reported in Figure 1).

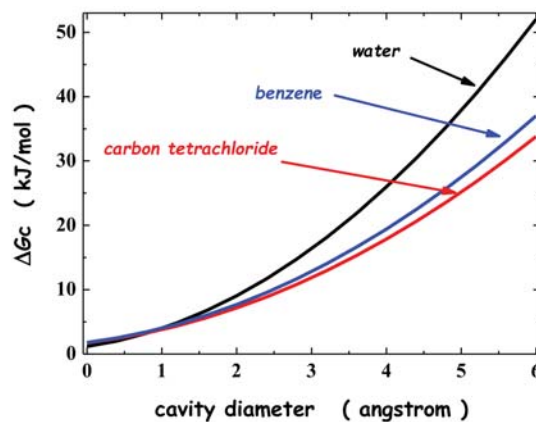


Figure 1. Trend of ΔG_C versus the cavity diameter for water, CCl_4 , and C_6H_6 calculated by means of classic SPT, at 25 °C and 1 atm. The data necessary to perform the calculations are reported in the notes of Table 1.

Table 1. Experimental thermodynamic data for the solvation [32–34], according to the Ben–Naim standard (i.e., the transfer from a fixed position in the gas phase to a fixed position in the liquid phase), at 25 °C and 1 atm, of noble gases in water (a), CCl₄ (b), and C₆H₆ (c); the values of the hard sphere diameter and the Lennard–Jones energy parameter come from [35,36] with small modifications; the values of ΔG_C are calculated by means of classic SPT analytical formulas [27,28]; those of E_a are calculated by means of Pierotti’s analytical formula [29].

		σ Å	ϵ/k K	ΔH kJ mol ^{−1}	ΔS J K ^{−1} mol ^{−1}	ΔG kJ mol ^{−1}	ΔG_C kJ mol ^{−1}	E_a kJ mol ^{−1}	$\Delta G_C + E_a$ kJ mol ^{−1}
a	He	2.6	6	1.8	−32.5	11.5	13.2	−1.6	11.6
	Ne	2.8	28	−1.3	−41.9	11.2	14.7	−3.9	10.8
	Ar	3.4	125	−9.6	−60.4	8.4	20.0	−11.3	8.7
	Kr	3.7	175	−13.0	−66.7	6.9	22.9	−15.4	7.5
	Xe	4.0	230	−16.8	−74.8	5.5	26.0	−20.2	5.8
b	Ar	3.4	110	2.1	−2.0	2.7	14.1	−11.7	2.4
c	Ar	3.4	110	2.8	−2.3	3.5	15.3	−12.3	3.0
	Kr	3.7	165	−0.2	−3.0	0.7	17.3	−16.6	0.7
	Xe	3.4	240	−5.5	−8.7	−2.9	19.4	−22.1	−2.7

Additional data used to perform the calculations [37]. Water: $\sigma_1 = 2.8$ Å; $v_1 = 18.07$ cm³·mol^{−1}; $\xi = 0.383$; $\alpha_P = 0.257 \cdot 10^{-3} \cdot K^{-1}$; $\epsilon/k = 120$ K. Carbon tetrachloride: $\sigma_1 = 5.37$ Å; $v_1 = 97.09$ cm³·mol^{−1}; $\xi = 0.503$; $\alpha_P = 1.226 \cdot 10^{-3} \cdot K^{-1}$; $\epsilon/k = 530$ K. Benzene: $\sigma_1 = 5.26$ Å; $v_1 = 89.41$ cm³·mol^{−1}; $\xi = 0.513$; $\alpha_P = 1.22 \cdot 10^{-3} \cdot K^{-1}$; $\epsilon/k = 530$ K.

This holds because, even though the volume packing density of water is the smallest, $\xi = 0.383$ for water versus 0.503 for CCl₄, and 0.513 for C₆H₆, the water molecules are the smallest, $\sigma = 2.80$ Å for water, 5.37 Å for CCl₄, and 5.26 Å for C₆H₆ [35–37]. In this respect, it is important to underscore that the effective hard sphere diameter assigned to water molecules is physically reliable because it corresponds to the location of the first peak in the oxygen–oxygen radial distribution function of water [38], the distance between two H-bonded water molecules. The size effect prevails because it is the molecular cause of the markedly larger number density of water: at 25 °C and 1 atm, ρ (in moles per liter) = 55.3 for water, 10.3 for CCl₄, and 11.2 for benzene [37]. The magnitude of the solvent-excluded volume effect associated with cavity creation depends strongly upon the liquid number density: the entropy loss is larger with the greater the number of affected molecules. This is why the size is so important. The reliability of using classic SPT for water has been further confirmed recently by the agreement between the ΔG_C (SPT) values and those obtained by computer simulations in detailed water models [39].

Moreover, a simple formula devised by Pierotti [29] allows for the calculation of the interaction energy E_a between the noble gases and the three liquids. The Pierotti’s formula is:

$$E_a = -(64/3) \cdot \xi \cdot \epsilon_{12} \cdot (\sigma_{12}/\sigma_1)^3 \quad (3)$$

where $\sigma_{12} = (\sigma_1 + \sigma_2)/2$ and $\epsilon_{12} = (\epsilon_1 \epsilon_2)^{1/2}$, and where ϵ_1 and ϵ_2 are the Lennard–Jones parameters for the liquid and solute, respectively. The E_a estimates, listed in the ninth column of Table 1, are negative and, when added to the ΔG_C (SPT) values, produce numbers that are close to the experimental ΔG ones for all of the three liquids. The success is mainly because the solvent-excluded volume effect associated with solute insertion in a liquid is correctly accounted for by calculating the reversible work of cavity creation.

Estimates of the enthalpy change associated with cavity creation, ΔH_C (SPT), calculated by means of Equation (2) and listed in the third column of Table 2, are positive in all of the three liquids and are close to the values of the $\Delta H - E_a$ difference, listed in the fourth column of Table 2. This suggests that the structural reorganization of liquid molecules upon noble gas insertion is an endothermic process at 25 °C and 1 atm (i.e., in the case of water, there is no indication of iceberg formation [40–43]). Actually, the ΔH_C (SPT) values of water are significantly smaller than those of the other two liquids [37]; this is a consequence

of the smaller isobaric thermal expansion coefficient α_P of water with respect to those of the other two liquids [37] (look at the values reported in the notes of Table 1). The latter quantity, present in the classic SPT formula of ΔH_C [29], is a measure of the ensemble correlation between fluctuations in volume and fluctuations in enthalpy, and so it can account for the liquid structural reorganization upon cavity creation. The smallness of the α_P of water is due to the strength of water–water H-bonds, in comparison to the weakness of van-der-Waals-type interactions occurring among benzene and carbon tetrachloride molecules [37]. Therefore, the ΔH_C (SPT) values indicate that cavity creation does not cause the breakage of water–water H-bonds [30,31], but a significant breakage of van der Waals interactions occurs in the other two liquids [37].

Table 2. Enthalpy and entropy changes associated with cavity creation in water (a), CCl₄ (b), and C₆H₆ (c), calculated by means of the classic SPT relationships at 25 °C and 1 atm, to be compared with the reorganization enthalpy change and the total solvation entropy change, respectively.

		ΔH_C kJ·mol ⁻¹	$\Delta H^* - E_a$ kJ·mol ⁻¹	ΔS_C J·K ⁻¹ ·mol ⁻¹	ΔS^* J·K ⁻¹ ·mol ⁻¹
a	He	2.1	3.4	-37.2	-32.5
	Ne	2.3	2.6	-41.6	-41.9
	Ar	3.2	2.1	-56.0	-60.4
	Kr	3.7	2.4	-64.1	-66.7
	Xe	4.3	3.4	-72.8	-74.8
b	Ar	13.4	13.8	-2.3	-2.0
c	Ar	14.9	15.1	-1.3	-2.3
	Kr	17.1	16.4	-0.7	-3.0
	Xe	19.5	16.6	0.3	-8.7

Estimates of the entropy change associated with cavity creation, ΔS_C (SPT), listed in the fifth column of Table 2, are close to the total solvation entropy changes, listed in the last column of Table 2, in all of the three considered liquids. This finding indicates that the process of cavity creation is the main process responsible of the negative solvation entropy change [31,37]. In water, the ΔS_C (SPT) values are largely negative, increasing in magnitude with the solute diameter [37]. This entropy loss cannot be due to an increase in water structural order [44,45], because it comes from a hard sphere approach. It is due to the decrease in the number of accessible configurations for water molecules because of cavity creation (i.e., the solvent-excluded volume effect). Such a decrease in the number of accessible configurations also occurs in the other two liquids, but it is masked by a largely positive entropy change due to the structural reorganization upon cavity creation [25,37]. The latter structural reorganization, however, has a markedly different magnitude in water and the two organic liquids; it is also characterized by a complete enthalpy-entropy compensation in all liquids [31,46] and does not affect the ΔG_C magnitude.

3. Formation of Host–Guest Complexes

It is interesting that noble gases are able to bind macrocyclic hosts in aqueous solutions. In particular, thanks to specialized NMR experiments, it has been possible to measure the binding constants of noble gases to cucurbit[5]uril, a rigid, synthetic, and water-soluble macrocyclic host [47]. Specifically, at 22 °C, K_b (in M⁻¹) = 87 for He, 72 for Ne, 360 for Ar, 2390 for Kr and 8700 for Xe. These numbers imply that the binding process is spontaneous, and thus, there is the need to identify the driving force of this host–guest recognition [47–49]. It is important to underscore that the inner part of cucurbit[5]uril proved not to be filled by water molecules, on the basis of both specialized NMR measurements and MD simulations [47] (note that the inner part of cucurbit[5]uril has a volume of 68 Å³ and can host very few water molecules, considering that the van der Waals volume of a water molecule is 11.5 Å³). Researchers calculated with great accuracy, at DFT level, the dispersion energetic attractions of noble gases in bulk water and in the inner part of cucurbit[5]uril. The unexpected result

was that the magnitude of attractive dispersion interactions was larger in bulk water than in the inner part of the rigid macrocyclic host [47]. As a consequence, researchers turned their attention to the reversible work of cavity creation. The transfer of a noble gas atom from water to the inner part of cucurbit[5]uril implies the following steps: the switching-off of the energetic dispersion attractions with water, the closure of the cavity in water, the creation of the cavity in the macrocyclic host interior, and the switching-on of the energetic dispersion attractions with the host.

However, the reversible work to create a cavity in the inner part of cucurbit[5]uril is zero because this region does not contain water molecules (i.e., it is empty); in addition, as a first approximation, the magnitude of the energetic dispersion attractions of a noble gas atom in bulk water and in the host interior can be assumed to be equal. This implies $\Delta G(\text{binding}) \approx -\Delta G_C(\text{H}_2\text{O})$, and the driving force is given by the decrease in solvent-excluded volume for cavity closure in water (i.e., leading to a gain in configurational- translational entropy of water molecules).

The experimental $\Delta G(\text{binding})$ values of noble gases to cucurbit[5]uril are reported in Figure 2, together with the values of minus $\Delta G_C(\text{H}_2\text{O})$, calculated via classic SPT formulas and listed in Table 1. One could say that the agreement between the two sets of numbers is better than expected, considering their totally different origin. In the original article, the authors calculated $\Delta G_C(\text{H}_2\text{O})$ by means of computer simulations, they also considered the contribution of the difference in energetic dispersion attractions between the bulk water and the host interior, and obtained a good agreement with the experimental data [47]. This example demonstrates the pivotal role played by the reversible work of cavity creation in driving host-guest recognition phenomena in water [50–52].

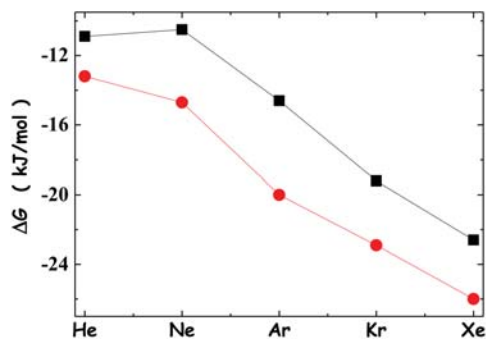


Figure 2. Experimental $\Delta G(\text{binding})$ values of noble gases to cucurbit[5]uril, measured via NMR at 22 °C (black filled squares) [47], contrasted with minus the ΔG_C values for noble gases in water, calculated via classic SPT analytical formulas, and listed in column eight of Table 1 (red filled circles).

4. Conformational Stability of Globular Proteins

The geometric explanation for the solvent-excluded volume effect implies that the ΔG_C magnitude has to increase if the cavity shape is changed, by keeping its van der Waals volume fixed, V_{vdW} , and increasing its WASA. This is a fundamental point. Passing from a spherical cavity to several prolate spherocylinders with the same V_{vdW} of the sphere, it is possible to test the rightness of the geometric arguments. Classic SPT analytical formulas allow for the calculation of ΔG_C for both spherical and prolate spherocylindrical cavities. Therefore, the test can readily be completed and the results have confirmed that ΔG_C increases with cavity WASA, even though V_{vdW} is fixed [24,53]. This holds true also with ΔG_C calculated by means of computer simulations [54,55]. The results of classic SPT calculations in water, at 25 °C and 1 atm, for two sets of cavities, the first starting with a sphere of 6 Å radius and the second starting with a sphere of 9 Å radius, are listed in Table 3. It is evident that on lengthening the prolate spherocylinder, WASA increases and ΔG_C also increases. The plot of ΔG_C versus WASA, constructed with the numbers of Table 3, is

shown in Figure 3. The ΔG_C values scale linearly with cavity WASA, but the line slope is not unique; the slope magnitude depends upon the V_{vdW} of the cavity. In fact, the largest spherocylinder of the first set has a WASA larger than that of the smallest spherocylinder of the second set, but the order is reversed in the case of ΔG_C values (see Table 3 and Figure 3). This means also that the cavity V_{vdW} plays a role [53,56–58].

Table 3. ΔG_C estimates associated with the creation of prolate spherocylindrical cavities, at 25 °C and 1 atm, in a hard sphere fluid, with the experimental density of water and particle diameter $\sigma = 2.8 \text{ \AA}$. By keeping the cavity V_{vdW} fixed at the volume of 6 \AA and 9 \AA radius spheres, respectively (i.e., 904.8 \AA^3 and 3053.6 \AA^3 , respectively), the ΔG_C numbers have been calculated on varying the cylindrical length by means of the classic SPT analytic formulas. The first row of the A and B sections contains the numbers for the two spherical cavities.

	a \AA	l \AA	WASA _C \AA^2	ΔG_C kJ mol^{-1}
A	6.0	--	688.1	184.7
	5.0	4.85	709.7	190.5
	4.0	12.67	796.3	212.8
	3.0	28.00	1017.4	266.1
	2.8	33.00	1092.5	283.4
	2.5	42.75	1238.7	316.1
	2.3	51.37	1366.3	343.9
	2.0	69.31	1625.9	398.3
B	9.0	--	1359.2	399.3
	7.0	10.50	1440.9	422.9
	6.0	19.00	1571.5	459.6
	5.0	32.21	1810.0	524.2
	4.0	55.41	2246.5	636.9
	3.5	74.69	2601.2	724.5
	3.0	104.01	3118.7	847.3
	2.5	152.15	3919.5	1028.3

The geometric formulas for a prolate spherocylinder of radius a and cylindrical length l are: $V_{vdW} = (4/3)\pi a^3 + \pi \cdot l \cdot a^2$ and $WASA = 4\pi(a + r_w)^2 + 2\pi \cdot l \cdot (a + r_w)$, where r_w is the radius of water molecules, fixed at 1.4 \AA ; by setting $l = 0$, such formulas become right for a sphere of radius a .

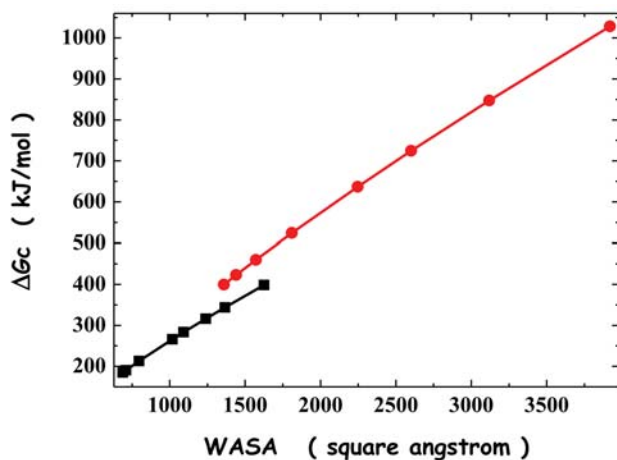


Figure 3. Plot of ΔG_C versus WASA for the two sets of cavities listed in Table 3 (in each set, all of the cavities have the same van der Waals volume). The two lines simply connect the points; they are not the result of a linear regression.

Anyway, the trend of ΔG_C versus cavity WASA is important to shed light on the driving force of protein folding and on the main factor responsible for the conformational stability of globular proteins. Experimental measurements have proved that the difference in molecular volume between the folded state and the unfolded state ensemble is negligibly small [59,60]. Thus, the folding process can be viewed as a collapse from a set of elongated conformations toward a compact, almost spherical one, keeping the volume occupied by the polypeptide chain fixed [24,25]. Such a collapse is characterized by a large WASA decrease; that means a large ΔG_C decrease, which corresponds to a significant gain in the configurational–translational entropy of water molecules. The numbers listed in the last column of Table 3 indicate that a large negative Gibbs free energy change is associated, at 25 °C and 1 atm, with the collapse from the longest spherocylinder to the sphere. Polypeptide chains are flexible and can populate different conformations, producing markedly different solvent-excluded volume effects. Water molecules push these chains to assume compact conformations in order to gain configuration–translational entropy. This is the geometric-molecular basis of what is called the hydrophobic effect, considered to be the main determinant of the conformational stability of globular proteins [24,25].

5. Conclusions

In the present article, I have tried to show that the solvent-excluded volume effect associated with cavity creation in all liquids (that are a condensed state of the matter) allows one to devise a common and general theoretical approach to rationalize several disparate phenomena occurring in liquids. In particular, the ΔG_C (SPT) values are able to rationalize the low solubility of noble gases in water and its entropic origin, the driving force of the recognition between noble gases and cucurbit[5]uril in water, and, last but not least, a reliable driving force for protein folding and stability.

Funding: This research was funded by Università degli Studi del Sannio, FRA 2022.

Conflicts of Interest: The author declares no conflict of interest.

References

1. Ben-Naim, A. *Water and Aqueous Solutions*; Springer US: Boston, MA, USA, 1974.
2. Pratt, L.R.; Chandler, D. Theory of the hydrophobic effect. *J. Chem. Phys.* **1977**, *67*, 3683–3704. [[CrossRef](#)]
3. Lee, B. The physical origin of the low solubility of nonpolar solutes in water. *Biopolymers* **1985**, *24*, 813–823. [[CrossRef](#)]
4. Ben-Naim, A. *Solvation Thermodynamics*; Plenum Press: New York, NY, USA, 1987.
5. Yu, H.; Karplus, M. A thermodynamic analysis of solvation. *J. Chem. Phys.* **1988**, *89*, 2366–2379. [[CrossRef](#)]
6. Pohorille, A.; Pratt, L.R. Cavities in molecular liquids and the theory of hydrophobic solubilities. *J. Am. Chem. Soc.* **1990**, *112*, 5066–5074. [[CrossRef](#)]
7. Blokzijl, W.; Engberts, J.B.F.N. Hydrophobic Effects. Opinions and Facts. *Angew. Chem. Int. Ed.* **1993**, *32*, 1545–1579. [[CrossRef](#)]
8. Guillot, B.; Guissani, Y. A computer simulation study of the temperature dependence of the hydrophobic hydration. *J. Chem. Phys.* **1993**, *99*, 8075–8094. [[CrossRef](#)]
9. Tomasi, J.; Persico, M. Molecular Interactions in Solution: An Overview of Methods Based on Continuous Distributions of the Solvent. *Chem. Rev.* **1994**, *94*, 2027–2094. [[CrossRef](#)]
10. Beutler, T.C.; Béguelin, D.R.; van Gunsteren, W.F. Free energy of cavity formation in solvent: Computational, methodological, and physical aspects. *J. Chem. Phys.* **1995**, *102*, 3787–3793. [[CrossRef](#)]
11. Hummer, G.; Garde, S.; García, A.E.; Paulaitis, M.E.; Pratt, L.R. Hydrophobic Effects on a Molecular Scale. *J. Phys. Chem. B* **1998**, *102*, 10469–10482. [[CrossRef](#)]
12. Lum, K.; Chandler, D.; Weeks, J.D. Hydrophobicity at Small and Large Length Scales. *J. Phys. Chem. B* **1999**, *103*, 4570–4577. [[CrossRef](#)]
13. Lazaridis, T. Solvent Size vs Cohesive Energy as the Origin of Hydrophobicity. *Acc. Chem. Res.* **2001**, *34*, 931–937. [[CrossRef](#)]
14. Southall, N.T.; Dill, K.A.; Haymet, A.D.J. A View of the Hydrophobic Effect. *J. Phys. Chem. B* **2002**, *106*, 521–533. [[CrossRef](#)]
15. Pratt, L.R.; Pohorille, A. Hydrophobic Effects and Modeling of Biophysical Aqueous Solution Interfaces. *Chem. Rev.* **2002**, *102*, 2671–2692. [[CrossRef](#)]
16. Benzi, C.; Cossi, M.; Imbrota, R.; Barone, V. Building cavities in a fluid of spherical or rod-like particles: A contribution to the solvation free energy in isotropic and anisotropic polarizable continuum model. *J. Comput. Chem.* **2005**, *26*, 1096–1105. [[CrossRef](#)]
17. Chandler, D. Interfaces and the driving force of hydrophobic assembly. *Nature* **2005**, *437*, 640–647. [[CrossRef](#)]

18. Ashbaugh, H.S.; Pratt, L.R. Contrasting Nonaqueous against Aqueous Solvation on the Basis of Scaled-Particle Theory. *J. Phys. Chem. B* **2007**, *111*, 9330–9336. [[CrossRef](#)]
19. Ben-Amotz, D.; Underwood, R. Unraveling Water's Entropic Mysteries: A Unified View of Nonpolar, Polar, and Ionic Hydration. *Acc. Chem. Res.* **2008**, *41*, 957–967. [[CrossRef](#)]
20. Otto, S. The role of solvent cohesion in nonpolar solvation. *Chem. Sci.* **2013**, *4*, 2953–2959. [[CrossRef](#)]
21. Ben-Amotz, D. Water-Mediated Hydrophobic Interactions. *Annu. Rev. Phys. Chem.* **2016**, *67*, 617–638. [[CrossRef](#)]
22. Soda, K. Solvent Exclusion Effect Predicted by the Scaled Particle Theory as an Important Factor of the Hydrophobic Effect. *J. Phys. Soc. Jpn.* **1993**, *62*, 1782–1793. [[CrossRef](#)]
23. Tang, K.E.; Bloomfield, V.A. Excluded Volume in Solvation: Sensitivity of Scaled-Particle Theory to Solvent Size and Density. *Biophys. J.* **2000**, *79*, 2222–2234. [[CrossRef](#)] [[PubMed](#)]
24. Merlino, A.; Pontillo, N.; Graziano, G. A driving force for polypeptide and protein collapse. *Phys. Chem. Chem. Phys.* **2017**, *19*, 751–756. [[CrossRef](#)]
25. Graziano, G. On the mechanism of cold denaturation. *Phys. Chem. Chem. Phys.* **2014**, *16*, 21755–21767. [[CrossRef](#)]
26. Lee, B.; Richards, F. The interpretation of protein structures: Estimation of static accessibility. *J. Mol. Biol.* **1971**, *55*, 379–IN4. [[CrossRef](#)]
27. Reiss, H. Scaled Particle Methods in the Statistical Thermodynamics of Fluids. In *Advances in Chemical Physics*; Prigogine, I., Ed.; John Wiley & Sons, Inc.: Hoboken, NJ, USA, 2007; pp. 1–84.
28. Lebowitz, J.L.; Helfand, E.; Praestgaard, E. Scaled Particle Theory of Fluid Mixtures. *J. Chem. Phys.* **1965**, *43*, 774–779. [[CrossRef](#)]
29. Pierotti, R.A. A scaled particle theory of aqueous and nonaqueous solutions. *Chem. Rev.* **1976**, *76*, 717–726. [[CrossRef](#)]
30. Gallicchio, E.; Kubo, M.M.; Levy, R.M. Enthalpy–Entropy and Cavity Decomposition of Alkane Hydration Free Energies: Numerical Results and Implications for Theories of Hydrophobic Solvation. *J. Phys. Chem. B* **2000**, *104*, 6271–6285. [[CrossRef](#)]
31. Graziano, G. Contrasting the hydration thermodynamics of methane and methanol. *Phys. Chem. Chem. Phys.* **2019**, *21*, 21418–21430. [[CrossRef](#)]
32. Wilhelm, E.; Battino, R. Thermodynamic functions of the solubilities of gases in liquids at 25. deg. *Chem. Rev.* **1973**, *73*, 1–9. [[CrossRef](#)]
33. Krause, D.; Benson, B.B. The solubility and isotopic fractionation of gases in dilute aqueous solution. IIa. solubilities of the noble gases. *J. Solut. Chem.* **1989**, *18*, 823–873. [[CrossRef](#)]
34. Graziano, G. On the temperature dependence of hydration thermodynamics for noble gases. *Phys. Chem. Chem. Phys.* **1999**, *1*, 1877–1886. [[CrossRef](#)]
35. Wilhelm, E.; Battino, R. Estimation of Lennard-Jones (6,12) Pair Potential Parameters from Gas Solubility Data. *J. Chem. Phys.* **1971**, *55*, 4012–4017. [[CrossRef](#)]
36. Graziano, G. Salting out of methane by sodium chloride: A scaled particle theory study. *J. Chem. Phys.* **2008**, *129*, 084506. [[CrossRef](#)] [[PubMed](#)]
37. Graziano, G. Scaled Particle Theory Study of the Length Scale Dependence of Cavity Thermodynamics in Different Liquids. *J. Phys. Chem. B* **2006**, *110*, 11421–11426. [[CrossRef](#)] [[PubMed](#)]
38. Head-Gordon, T.; Hura, G. Water Structure from Scattering Experiments and Simulation. *Chem. Rev.* **2002**, *102*, 2651–2670. [[CrossRef](#)] [[PubMed](#)]
39. Sedov, I.; Magsumov, T. The Gibbs free energy of cavity formation in a diverse set of solvents. *J. Chem. Phys.* **2020**, *153*, 134501. [[CrossRef](#)]
40. Buchanan, P.; Aldiwan, N.; Soper, A.; Creek, J.; Koh, C. Decreased structure on dissolving methane in water. *Chem. Phys. Lett.* **2005**, *415*, 89–93. [[CrossRef](#)]
41. Graziano, G.; Lee, B. On the Intactness of Hydrogen Bonds around Nonpolar Solutes Dissolved in Water. *J. Phys. Chem. B* **2005**, *109*, 8103–8107. [[CrossRef](#)]
42. Bowron, D.T.; Filipponi, A.; Lobban, C.; Finney, J.L. Temperature-induced disordering of the hydrophobic hydration shell of Kr and Xe. *Chem. Phys. Lett.* **1998**, *293*, 33–37. [[CrossRef](#)]
43. Kim, J.; Tian, Y.; Wu, J. Thermodynamic and Structural Evidence for Reduced Hydrogen Bonding among Water Molecules near Small Hydrophobic Solutes. *J. Phys. Chem. B* **2015**, *119*, 12108–12116. [[CrossRef](#)]
44. Irudayam, S.J.; Henschman, R. Solvation theory to provide a molecular interpretation of the hydrophobic entropy loss of noble-gas hydration. *J. Phys. Condens. Matter* **2010**, *22*, 284108. [[CrossRef](#)] [[PubMed](#)]
45. Liu, M.; Besford, Q.A.; Mulvaney, T.; Gray-Weale, A. Order and correlation contributions to the entropy of hydrophobic solvation. *J. Chem. Phys.* **2015**, *142*, 114117. [[CrossRef](#)] [[PubMed](#)]
46. Lee, B. A procedure for calculating thermodynamic functions of cavity formation from the pure solvent simulation data. *J. Chem. Phys.* **1985**, *83*, 2421–2425. [[CrossRef](#)]
47. He, S.; Biedermann, F.; Vankova, N.; Zhechkov, L.; Heine, T.; Hoffman, R.E.; De Simone, A.; Duignan, T.T.; Nau, W.M. Cavitation energies can outperform dispersion interactions. *Nat. Chem.* **2018**, *10*, 1252–1257. [[CrossRef](#)]
48. Biedermann, F.; Uzunova, V.D.; Scherman, O.A.; Nau, W.M.; De Simone, A. Release of High-Energy Water as an Essential Driving Force for the High-Affinity Binding of Cucurbit[n]urils. *J. Am. Chem. Soc.* **2012**, *134*, 15318–15323. [[CrossRef](#)] [[PubMed](#)]
49. Biedermann, F.; Nau, W.; Schneider, H.-J. The Hydrophobic Effect Revisited—Studies with Supramolecular Complexes Imply High-Energy Water as a Noncovalent Driving Force. *Angew. Chem. Int. Ed.* **2014**, *53*, 11158–11171. [[CrossRef](#)]

50. Setny, P.; Baron, R.; McCammon, J.A. How Can Hydrophobic Association Be Enthalpy Driven? *J. Chem. Theory Comput.* **2010**, *6*, 2866–2871. [[CrossRef](#)]
51. Dzubiella, J. How Interface Geometry Dictates Water’s Thermodynamic Signature in Hydrophobic Association. *J. Stat. Phys.* **2011**, *145*, 227–239. [[CrossRef](#)]
52. Graziano, G. Molecular driving forces of the pocket–ligand hydrophobic association. *Chem. Phys. Lett.* **2012**, *533*, 95–99. [[CrossRef](#)]
53. Graziano, G. The Gibbs energy cost of cavity creation depends on geometry. *J. Mol. Liq.* **2015**, *211*, 1047–1051. [[CrossRef](#)]
54. Wallqvist, A.; Berne, B.J. Molecular Dynamics Study of the Dependence of Water Solvation Free Energy on Solute Curvature and Surface Area. *J. Phys. Chem.* **1995**, *99*, 2885–2892. [[CrossRef](#)]
55. Patel, A.; Varilly, P.; Chandler, D. Fluctuations of Water near Extended Hydrophobic and Hydrophilic Surfaces. *J. Phys. Chem. B* **2010**, *114*, 1632–1637. [[CrossRef](#)]
56. Sosso, G.C.; Caravati, S.; Rotskoff, G.; Vaikuntanathan, S.; Hassanali, A. On the Role of Nonspherical Cavities in Short Length-Scale Density Fluctuations in Water. *J. Phys. Chem. A* **2016**, *121*, 370–380. [[CrossRef](#)]
57. Ansari, N.; Laio, A.; Hassanali, A.A. Spontaneously Forming Dendritic Voids in Liquid Water Can Host Small Polymers. *J. Phys. Chem. Lett.* **2019**, *10*, 5585–5591. [[CrossRef](#)]
58. Azizi, K.; Laio, A.; Hassanali, A. Model Folded Hydrophobic Polymers Reside in Highly Branched Voids. *J. Phys. Chem. Lett.* **2022**, *13*, 183–189. [[CrossRef](#)]
59. Royer, C.A. Revisiting volume changes in pressure-induced protein unfolding. *Biochim. et Biophys. Acta (BBA)—Protein Struct. Mol. Enzym.* **2002**, *1595*, 201–209. [[CrossRef](#)]
60. Chalikian, T.V. Volumetric Properties of Proteins. *Annu. Rev. Biophys. Biomol. Struct.* **2003**, *32*, 207–235. [[CrossRef](#)]

Disclaimer/Publisher’s Note: The statements, opinions and data contained in all publications are solely those of the individual author(s) and contributor(s) and not of MDPI and/or the editor(s). MDPI and/or the editor(s) disclaim responsibility for any injury to people or property resulting from any ideas, methods, instructions or products referred to in the content.

Article

Linear Solvation–Energy Relationships (LSER) and Equation-of-State Thermodynamics: On the Extraction of Thermodynamic Information from the LSER Database

Costas Panayiotou ^{1,*}, Ioannis Zuburtikudis ², Hadil Abu Khalifeh ² and Vassily Hatzimanikatis ³¹ Department of Chemical Engineering, Aristotle University of Thessaloniki, 54624 Thessaloniki, Greece² Department of Chemical Engineering, Abu Dhabi University, Abu Dhabi P.O. Box 59911, United Arab Emirates³ Laboratory of Computational Systems Biotechnology (LCSB), Swiss Federal Institute of Technology (EPFL), CH-1015 Lausanne, Switzerland

* Correspondence: cpanayio@auth.gr

Abstract: There is a remarkable wealth of thermodynamic information in freely accessible databases, the LSER database being a classical example. The LSER, or Abraham solvation parameter model, is a very successful predictive tool in a variety of applications in the (bio)chemical and environmental sector. The model and the associated database are very rich in thermodynamic information and information on intermolecular interactions, which, if extracted properly, would be particularly useful in various thermodynamic developments for further applications. Partial Solvation Parameters (PSP), based on equation-of-state thermodynamics, are designed as a versatile tool that would facilitate this extraction of information. The present work explores the possibilities of such an LSER–PSP interconnection and the challenging issues this effort is faced with. The thermodynamic basis of the very linearity of the LSER model is examined, especially, with respect to the contribution of strong specific interactions in the solute/solvent system. This is done by combining the equation-of-state solvation thermodynamics with the statistical thermodynamics of hydrogen bonding. It is verified that there is, indeed, a thermodynamic basis of the LFER linearity. Besides the provenance of the sought linearity, an insight is gained on the thermodynamic character and content of coefficients and terms of the LSER linearity equations. The perspectives from this insight for the further development of LSER and related databases are discussed. The thermodynamic LSER–PSP interconnection is examined as a model for the exchange in information between QSPR-type databases and equation-of-state developments and the associated challenges are examined with representative calculations.

Keywords: Abraham LSER model; hydrogen bonding; molecular descriptors; Partial Solvation Parameters

Citation: Panayiotou, C.; Zuburtikudis, I.; Abu Khalifeh, H.; Hatzimanikatis, V. Linear Solvation–Energy Relationships (LSER) and Equation-of-State Thermodynamics: On the Extraction of Thermodynamic Information from the LSER Database. *Liquids* **2023**, *3*, 66–89. <https://doi.org/10.3390/liquids3010007>

Academic Editors: William E. Acree, Jr. and Juan Ortega Saavedra

Received: 25 November 2022

Revised: 28 December 2022

Accepted: 3 January 2023

Published: 11 January 2023



Copyright: © 2023 by the authors. Licensee MDPI, Basel, Switzerland. This article is an open access article distributed under the terms and conditions of the Creative Commons Attribution (CC BY) license (<https://creativecommons.org/licenses/by/4.0/>).

1. Introduction

Solute–solvent interactions are, essentially, omnipresent on Earth and, as W. Ostwald mentioned in 1860, “Almost all the chemical processes, which occur in nature, whether in animal or vegetable organisms or in non-living surface of the Earth ... take place between substances in solution”. The interest, then, in solvation phenomena, solute transfer/partitioning, solvent screening, activity coefficients of solutes at infinite dilution, or in the design and development of solvent polarity scales and Quantitative Structure–Property Relationships (QSPR) and related databases is understandable. In this regard, and for decades now, the scientific community has enjoyed the remarkable success of the Abraham solvation parameter model or the linear free energy relationships (LFER) as a predictive tool for a broad variety of chemical, biomedical and environmental processes [1–18]. Numerous other Polarity or Acidity/Basicity scales and QSPR-type approaches are widely used in a variety of applications [19–24]. A very rich body of information on intermolecular interactions is, thus, available in the open literature.

To a great extent, all of the various databases and scales mentioned above were developed independently, and it is not always easy to compare their corresponding quantities. There is nothing absolute or universally accepted as regards the division of intermolecular interactions into various classes on the basis of their strength, and therefore, some degree of arbitrariness is unavoidable in and inherent to these developments. This is particularly important to keep in mind when the compared quantities are thermodynamic ones. This difficulty significantly impedes the safe exchange of the above-mentioned rich body of information between these databases and the extraction of this information for use in other developments and approaches in molecular thermodynamics [25].

In a series of papers [26–34], an effort was made to design and develop a thermodynamic framework that could facilitate the above exchange of information. This led to the concept of Partial Solvation Parameters (PSP). The development of PSPs has passed through various stages. Initially, they were heavily based on the COSMO-RS model [35–39], but since the LSER database became freely accessible [16], they have mostly been based on it and on the LSER molecular descriptors. The key feature of PSPs is their equation-of-state thermodynamic basis, which permits their estimation over a broad range of external conditions. There are two hydrogen-bonding PSPs, σ_a and σ_b , reflecting the acidity and basicity characteristics, respectively, of the molecule. The weak dispersive interactions are reflected by the dispersion PSP, σ_d , while the remaining Keesom-type and Debye-type polar interactions are, collectively, reflected by the polar PSP, σ_p . The hydrogen-bonding PSPs are used to estimate a key quantity: the free energy change upon formation of the hydrogen bond, ΔG^{hb} . Their equation-of-state characteristic permits also the estimation of the change in enthalpy, ΔH^{hb} , and the entropy change, ΔS^{hb} upon formation of the hydrogen bond.

Progress in the development of PSPs is rather slow, primarily because the corresponding information from the existing polarity scales and databases in the open literature cannot easily be used. It is not always simple and easy to reconcile information from quantum chemical (dft) calculations, molecular dynamics simulations, LSER molecular descriptors [1–18], or Gutmann donicities [20] with equation-of-state properties and solubility parameters [24].

In the LSER model [1–18], free-energy-related properties of a solute are correlated with its six molecular descriptors, V_x , L, E, S, A, and B, corresponding to the McGowan's characteristic volume V_x , the gas–liquid partition coefficient L in n-hexadecane at 298 K, the excess molar refraction E, the dipolarity/polarizability S, the hydrogen bond acidity A, and hydrogen bond basicity B, respectively. These correlations are performed, in practical applications, through two basic LFER relationships that quantify solute transfer between two phases. The first relationship, Equation (1), quantifies solute transfer between two condensed phases [2–12]:

$$\log(P) = c_p + e_p E + s_p S + a_p A + b_p B + v_p V_x \quad (1)$$

and the second LFER, Equation 2, describes solute transfer from the gas phase [2–12]:

$$\log(K^S) = c_k + e_k E + s_k S + a_k A + b_k B + l_k L \quad (2)$$

P, in Equation (1), is the water-to-organic solvent partition coefficient or alkane-to-polar organic solvent partition coefficient, and K^S is the gas-to-organic solvent partition coefficient.

The remarkable feature in Equations (1) and (2) is that the coefficients (lower-case letters) are solvent (phase or system) descriptors and are not influenced by the solute. They are referred to as LFER coefficients and are, usually, determined by fitting experimental data. They are considered to correspond to the complementary effect of the phase (solvent) on solute–solvent interactions and contain chemical information on the solvent/phase in question, and hence can be given specific physicochemical meanings [2–14]. However, their determination remains a fitting process via multiple linear regression at this point [2–18].

As a consequence, they are known only for solvents, for which extensive experimental data are available with a variety of solutes.

Solvation enthalpies are handled by LSER in a similar manner, through a linear relationship of the form [40]

$$\Delta H^S = c_H + e_H E + s_H S + a_H A + b_H B + l_H L \quad (3)$$

or with a similar equation using McGowan volume instead of the L descriptor. Only the solvent is assigned different LFER coefficients for solvation free energy (Equation (2)) and solvation enthalpy (Equation (3)), while the solute is represented by the same set of LSER molecular descriptors.

A major challenge is now to extract valid thermodynamic information on intermolecular interactions of solute/solvent systems for which both LSER descriptors and LFER coefficients are available. Equation (2), as an example, may be used to estimate the hydrogen bonding contribution to the free energy of solvation of solute (1) by solvent (2) from the products $A_1 a_2$ and $B_1 b_2$. The key question is how this "solvation" information could be used for a valid estimation of the free energy change upon formation of these acid (1)–base (2) and base (1)–acid (2) hydrogen bonds. Similar questions apply to the estimation of hydrogen bonding change in enthalpy on the basis of Equation (3), which is consistent with the information obtained from Equation (2).

Before addressing the above challenges, we must answer the question as to why free energies and free-energy-based properties obey the linear Equations (1) and (2)? The existence of such a linearity even for the strong specific hydrogen bonding or acid–base interactions is particularly puzzling [15]. The answers to the above questions are of central importance for reaching our major task: the safe extraction and transfer of information via PSPs for use in various applications of molecular thermodynamics.

Similar challenges are encountered in the transfer of thermodynamic information from other analogous QSPR databases and polarity scales [19–24,41–43]. For the LFER approach, it is worth mentioning that, in the older but still widely used Kamlet–Taft LFER version [41–43], the symbols α and β are used for the acidity and basicity molecular descriptors, respectively, of the solvent molecule, and thus there is some correlation between the two LFER sets of scales of hydrogen bonding parameters [44]. In this spirit, van Noort [13,14] developed correlations between descriptors A , B and the corresponding coefficients a , b by hypothesizing that the solvent (system) describing coefficients a and b was dependent on both Abraham solute solvation parameters, A and B , and should obey the following equations for the solvent/air partitioning:

$$a = n_1 B_{\text{solvent}}(1 - n_3 A_{\text{solvent}}) \quad (4)$$

$$b = n_2 A_{\text{solvent}}(1 - n_4 B_{\text{solvent}}) \quad (5)$$

The unknown coefficients, n_i , of these equations are determined by fitting to the available experimental data for several solutes. All of these interesting correlations are useful in practice, but do not explain, at the fundamental or thermodynamic level, the observed linearity of Equations (1)–(3) and do not facilitate the above-mentioned extraction of thermodynamically meaningful information.

From the above exposition, it is clear that the LSER database and the related work in the literature constitute a truly rich source of information that is deserving of our attention regarding its appropriate extraction and use. This is the central theme in this series of papers. In the present work, we will discuss some key aspects related to the connection of LSER and PSP approaches and will examine the basic (LFER) Equations (1) and (2) from a thermodynamic viewpoint. The solvation thermodynamics will be the basis, and the emphasis will be on the contributions of hydrogen bonding. Examples of calculations will be given in order to show what and how it may be calculated from the current LSER database, as well as what cannot be obtained from it, or which should only be obtained

with caution. These examples and the exercise with the LSER database may act as a model for analogous explorations of other databases in the literature.

2. The Thermodynamic Framework

In order to address the challenges and answer the questions mentioned in the previous section, we will need a thermodynamic framework with the quantities to be compared. For this purpose, in this section, we will recall some basic elements from solvation thermodynamics and from the equation-of-state approach explicitly handling the hydrogen bonding contribution.

2.1. Solvation Thermodynamics

In this sub-section, we will briefly recall the basics of solvation thermodynamics and the working equations, which will facilitate our discussion. Details may be found elsewhere [45–49].

The solvation free energy of a solute, i , in a mixture of composition $\{N\} = \{N_1, N_2, \dots, N_i\}$, at temperature, T , and pressure, P , is given by the following defining equation in Ben-Naim's mole/mole convention [48]:

$$\Delta G_i^S(T, P, \{N\}) = \mu_i(T, P, \{N\}) - \mu_i^{IG}(T, P, \{N\}) + RT \ln Z \quad (6)$$

where μ_i is the chemical potential of component i , superscript IG denotes the ideal gas state, and Z is the compressibility factor,

$$Z = \frac{PV}{NRT} \quad (7)$$

Equation (6) is a general one and holds true for mixtures, as well as for pure fluids (self-solvation). In the limit at infinite dilution of solute 1 in solvent 2 (subscript 1/2), Equation (6) leads to the following highly useful working equation [11,47]:

$$\frac{\Delta G_{1/2}^S}{RT} = \ln \frac{\varphi_1^0 P_1^0 V_{m2} \gamma_{1/2}^\infty}{RT} \quad (8)$$

V_{m2} in Equation (8) is the molar volume of component 2 and $\gamma_{1/2}^\infty$ is the activity coefficient of solute 1 at infinite dilution in solvent 2. P_1^0 is the vapor pressure of the solute at temperature T , and φ_1^0 its fugacity coefficient (typically set equal to 1 under ambient conditions). In order to proceed, we need an expression for $\gamma_{1/2}^\infty$ with explicit contributions from weak and strong intermolecular interactions, including hydrogen bonding ones, and this necessitates the adoption of an appropriate thermodynamic model. For this purpose, we will adopt here a statistical thermodynamic model, the basic elements of which are presented in the next sub-section.

2.2. The Equation-of-State Model

A simple equation-of-state model, meeting the above requirements, is the widely tested LFHB (Lattice Fluid with Hydrogen Bonding) model [50–53]. In this sub-section, we will confine ourselves to the essentials and the working equations of the model. Details may be found elsewhere [50–58].

In the frame of LFHB model, each fluid of molar mass, M , is characterized by two scaling constants, v_{sp}^* and ε^* , and one hydrogen bonding parameter, ΔG_{ij}^{hb} , for each type of hydrogen bond, i - j , in which it may participate. The specific hard core volume, v_{sp}^* , of the fluid provides with two key molecular parameters, the molar hard core volume, $V^* = M v_{sp}^*$, and the number, r , of molecular segments of a constant hard core volume equal to $9.75 \text{ cm}^3/\text{mol}$, or $r = V^*/9.75$. Each segment interacts with its neighbors via segmental interaction energy, ε^* . Thus, the molar interaction energy is given by $E^* = r\varepsilon^*$, while the scaling temperature, T^* , and pressure, P^* , are defined by the central lattice–fluid equation: $\varepsilon^* = RT^* = 9.75P^*$.

The reduced quantities of temperature, pressure, and volume (or density, ρ) are defined as follows:

$$\tilde{T} = \frac{T}{T^*}, \tilde{P} = \frac{P}{P^*}, \tilde{v} = \frac{v_{sp}}{v_{sp}^*} = \frac{1}{\rho v_{sp}^*} = \frac{\rho^*}{\rho} = \frac{1}{\tilde{\rho}} \tag{9}$$

When LFHB is used over a broad range of external conditions, a temperature dependence is often assumed for ϵ^* and less often for v_{sp}^* , as follows:

$$\epsilon^* = \epsilon_h^* + (T - 298.15)\epsilon_s^* \text{ and } v_{sp}^* = v_{sp0}^* + (T - 298.15)v_{sp1}^* \tag{10}$$

The fluid volume is calculated via the lattice–fluid equation of state, which, for non-hydrogen-bonded systems, is:

$$\tilde{P} + \tilde{\rho}^2 + \tilde{T} \left[\ln(1 - \tilde{\rho}) + \tilde{\rho} \left(1 - \frac{1}{r} \right) \right] = 0 \tag{11}$$

The scaling constants for pure fluids are, typically, obtained from correlation of experimental information on orthobaric densities, or on vapor pressures, heats of vaporization, supercritical-fluid densities, second virial coefficients, thermal expansivity or compressibility [50–54].

In systems interacting with strong specific intermolecular forces, such as acid/base or hydrogen-bonding interactions [31–34,45–47], one must account for the number of donor and acceptor sites, d_i and a_i , respectively, for each component i , as well as for the number of hydrogen bonds, N_{ij} , between donors i and acceptors j in the system, or for the reduced ones, $\nu_{ij} = N_{ij}/rN$. Each type of interaction i - j may be viewed as a quasi-chemical reaction of an acidic site ($Acid_i$) and a basic site ($Base_j$), of the form $Acid_i + Base_j \rightleftharpoons AB_{complex_{ij}}$, and is characterized by the corresponding free energy change upon formation of bond i - j , $\Delta G_{ij}^{hb} = -RT \ln K_{ij}$, and the equilibrium constant, K_{ij} . This free energy change may be split, in the classical manner, into enthalpic and entropic components, $\Delta G_{ij}^{hb} = \Delta H_{ij}^{hb} - T\Delta S_{ij}^{hb}$.

In a binary mixture of mole fraction, $x_1 = N_1/(N_1 + N_2) = N_1/N = 1 - x_2$, and total number of segments, $rN = r_1N_1 + r_2N_2$, in which the molecules of component i ($i = 1, 2$) have d_i donor sites and a_i acceptor sites of type 1, the reduced number of free donor sites (non-hydrogen bonded) is given by:

$$\nu_{10} = \frac{x_1 d_1}{r} - \nu_{11} - \nu_{12} \tag{12}$$

and the reduced number of free acceptor sites is given by:

$$\nu_{01} = \frac{x_1 a_1}{r} - \nu_{11} - \nu_{21} \tag{13}$$

For the purposes of the present work, we will apply the LFHB model in the limit at infinite dilution.

2.3. The Equation-of-State Model at Infinite Dilution

In hydrogen-bonded systems and in the limit at infinite dilution of solute 1 in solvent 2, LFHB leads to the following equation for the solvation free energy in the molar/molar convention [48]:

$$\frac{\Delta G_{1/2}^S}{RT} = \ln \frac{\omega_1^{IG}}{\omega_1} - r_1 \ln(1 - \tilde{\rho}_2) - 2r_1 \tilde{\rho}_2 \frac{\epsilon_{12}^*}{RT} - d_1 \ln F_{12} - a_1 \ln F_{21} \tag{14}$$

where

$$F_{12} = \lim_{x_1 \rightarrow 0} \frac{\nu_{10,0}}{\nu_{10}} = \lim_{x_1 \rightarrow 0} \frac{x_1 d_1 - r\nu_{11,0} - r\nu_{12,0}}{x_1 d_1 - r\nu_{11} - r\nu_{12}},$$

and

$$F_{21} = \lim_{x_1 \rightarrow 0} \frac{\nu_{01,0}}{\nu_{01}} = \lim_{x_1 \rightarrow 0} \frac{x_1 d_1 - r\nu_{11,0} - r\nu_{12,0}}{x_1 d_1 - r\nu_{11} - r\nu_{12}} \tag{15}$$

The reduced numbers with subscript ij,0 in Equation (15) correspond to the reference non-hydrogen-bonded system of the same composition [45,57–59]. The simple geometric mean mixing rule is used for the non-hydrogen-bonding interaction energy, or $\epsilon_{12}^* = \sqrt{\epsilon_{11}^* \epsilon_{22}^*}$.

Equation (14) may be written in the following more illustrative form:

$$\ln K^S = -\frac{\Delta G_{1/2}^S}{RT} = \ln \frac{\omega_1}{\omega_1^G} + r_1 \ln(1 - \tilde{\rho}_2) + r_1 \sqrt{\epsilon_{11}^*} \left(2\tilde{\rho}_2 \frac{\sqrt{\epsilon_{22}^*}}{RT} \right) + d_1 \ln F_{12} + a_1 \ln F_{21} \tag{16}$$

The first term on the right-hand side of Equation (16) is the *conformational* contribution term and accounts for any conformational changes and molecular restructuring on transferring the molecule from the isolated ideal gas (IG) state to the solution. It is an “internal” non-configurational term and, as such, thermodynamics cannot tell us much about it. It also accounts for conformer distribution, flexibility, symmetry, shape, or changes in the internal degrees of freedom of the solute molecule, upon solvation. Quantum mechanics calculations could be more helpful in quantifying this term [45]. Typically, this term is simply neglected in solvation thermodynamics or absorbed in cavitation terms.

The reduced density of the solvent (molecule 2), $\tilde{\rho}_2 = V_2^*/V_{m2}$, corresponds to the probability of finding a site occupied by the solvent molecule. Consequently, $1 - \tilde{\rho}_2$, is the probability of finding an empty site in the solvent phase. If the solute molecule consists of r_1 segments, the logarithm describing the probability of finding r_1 consecutive empty sites for its accommodation is given by the second term in the right-hand side of Equation (16). Thus, this second term is the *cavitation* term and reflects the difficulty of creating a cavity in the solvent volume in order to accommodate the solute molecule. The remaining terms are the *charge* terms of the solvation equation. ϵ_{ij}^* is the interaction energy for the contact of segments i and j. This refers to the non-specific or weak types of van der Waals (dispersion, and those arising from molecular polarizability and Keesom-type or Debye-type polarization) interaction. The contribution of strong specific (hydrogen bonding) interactions is accounted for by the last two terms in Equation (16).

Equation (18) can be used once for the mixture and once for the self-solvation of the solute, and the following equation can be derived for the activity coefficient at infinite dilution of solute component 1 in solvent 2, $\gamma_{1/2}^\infty$ [27–34,45–47]:

$$\ln \gamma_{1/2}^\infty = \ln \frac{\omega_1^{(1)}}{\omega_1^{(2)}} - r_1 \ln \left(\frac{1 - \tilde{\rho}_2}{1 - \tilde{\rho}_1} \right) - \ln \frac{r_2 \tilde{\rho}_1}{r_1 \tilde{\rho}_2} - 2r_1 \tilde{\rho}_2 \frac{\epsilon_{12}^*}{RT} + 2\tilde{\rho}_1 \frac{r_1}{T_1} + \{d_1 \ln F_{12} + a_1 \ln F_{21}\}_{x_1=0} - \{d_1 \ln F_{11} + a_1 \ln F_{11}\}_{x_1=1} \tag{17}$$

F_{11} in this equation is obtained from F_{12} (cf. Equation (15)) by replacing subscript 2 with 1.

Solvation studies are associated with solute transfer and partitioning between phases or with partition coefficients, which in turn are intimately associated with activity coefficients at infinite dilution. Thus, the partition coefficient of solute 1, between phases of solvent 2 and 3 at infinite dilution, is given by

$$\ln K_{32}^1 = \ln \frac{x_{1/3}}{x_{1/2}} = \ln \frac{\gamma_{1/2}^\infty}{\gamma_{1/3}^\infty} = \frac{\Delta G_{1/2}^S - \Delta G_{1/3}^S}{RT} - \ln \frac{V_{m2}}{V_{m3}} \tag{18}$$

This equation is widely used for solute partitioning in octanol–water systems (partition coefficient, K_{OW}).

Solvation enthalpy and solvation volumes may be obtained from Equation (16) for solvation free energy, through the classical defining Equations (19) and (20), respectively:

$$\Delta H_{1/2}^S = -T^2 \left(\frac{\partial (\Delta G_{1/2}^S / T)}{\partial T} \right)_P \tag{19}$$

and

$$\Delta V_{1/2}^S = \left(\frac{\partial (\Delta G_{1/2}^S)}{\partial P} \right)_T \tag{20}$$

All terms in the above equations can be calculated with the LFHB equation-of-state model, except for the terms with the ω_i s. As observed in Equation (16), the cavitation term (second term on the right-hand side of the equation) and the first charge term (third term in the equation) are “linearity” terms, that is, they are products of solute parameters with quantities (in parentheses) dependent exclusively on solvent properties. It is not clear, however, whether the two hydrogen bonding terms (last two terms in Equation (16)) are also “linearity” terms. This is examined in the next sub-section.

2.4. On the Linearity of Hydrogen Bonding Contribution to Solvation Free Energy

Now we will examine the full analytical form of the last two hydrogen bonding terms in Equation (16) at the limit of infinite dilution as described by Equation (15). The general form of the limiting Equation (15) was described recently [56], and is recalled briefly in the Supplementary Materials (SM). It should be noted also that in the LFER approach, the molecules are considered to be mono-segmental and the liquids incompressible. For the purposes of our comparison, we will also adopt these assumptions in order to make the arguments and the presentation more lucid. The full equations are provided in the SM.

At the infinite dilution limit, Equation (15) takes the following analytical form [56], SM:

$$\begin{aligned} \lim_{x_1 \rightarrow 0} \frac{v_{10,0}}{v_{10}} &= \frac{d_1 - c_{12,0}}{d_1 - c_{12}} \\ \text{and} \\ \lim_{x_1 \rightarrow 0} \frac{v_{01,0}}{v_{01}} &= \frac{a_1 - c_{21,0}}{a_1 - c_{21}} \end{aligned} \tag{21}$$

where

$$\begin{aligned} c_{12} &= d_1 \left(\frac{1/K_{22} - \sqrt{(2+1/K_{22})^2 - 4}}{1/K_{22} - \sqrt{(2+1/K_{22})^2 - 4} - 2/K_{12}} \right) \\ c_{21} &= a_1 \left(\frac{1/K_{22} - \sqrt{(2+1/K_{22})^2 - 4}}{1/K_{22} - \sqrt{(2+1/K_{22})^2 - 4} - 2/K_{21}} \right) \quad (d_i = a_i = r_i = \tilde{\rho}_i = 1) \\ c_{12,0} &= c_{21,0} = \frac{\sqrt{5}-1}{\sqrt{5}+1} \end{aligned} \tag{22}$$

In addition, for pure solvent (component 2) and, practically speaking, for our infinitely diluted solution:

$$v_{22}^0 = \frac{2 + \frac{1}{K_{22}} - \sqrt{\left(2 + \frac{1}{K_{22}}\right)^2 - 4}}{2} \tag{23}$$

Substituting in Equation (21), the contribution of hydrogen bonding to the solvation free energy is obtained as follows:

$$d_1 \ln F_{12} = \ln \frac{v_{10,0}}{v_{10}} = \ln \left(\frac{2}{1 + \sqrt{5}} + K_{12} \frac{\sqrt{(2 + 1/K_{22})^2 - 4} - 1/K_{22}}{1 + \sqrt{5}} \right) \tag{24}$$

and

$$a_1 \ln F_{21} = \ln \frac{v_{01,0}}{v_{01}} = \ln \left(\frac{2}{1 + \sqrt{5}} + K_{21} \frac{\sqrt{(2 + 1/K_{22})^2 - 4} - 1/K_{22}}{1 + \sqrt{5}} \right) \tag{25}$$

These equations may be written in the following alternative and useful form:

$$\ln \left(\frac{v_{10,0}}{v_{10}} - 0.618 \right) = \ln K_{12} + \ln \frac{\sqrt{(2 + 1/K_{22})^2 - 4} - 1/K_{22}}{1 + \sqrt{5}} = \ln K_{12} + c'_2 \tag{26}$$

and

$$\ln\left(\frac{v_{01,0}}{v_{01}} - 0.618\right) = \ln K_{21} + \ln \frac{\sqrt{(2+1/K_{22})^2 - 4} - 1/K_{22}}{1 + \sqrt{5}} = \ln K_{21} + c_2' \quad (27)$$

The constant c_2' in these equations is an exclusive property of the solvent (component 2). As can be observed, the hydrogen bonding contribution to solvation free energy depends only on the equilibrium constants K_{ij} for the quasi-chemical reactions of hydrogen bonding between the proton donor (or acidic site), i , and the proton acceptor (or basic site), j .

In the case of self-solvation, the solute is identical to the solvent, and thus $K_{12} = K_{21} = K_{22} = K$. In this case, Equations (24) and (25) become identical, and the acid–base and base–acid contributions are equal, regardless of the validity or invalidity of linearity. Whether this central result conforms with the LSER model will be determined below.

In self-solvation (one single equilibrium constant, K), the use of Equations (24) and (25) for equal acid–base and base–acid contributions gives

$$\begin{aligned} \ln \frac{v_{10,0}}{v_{10}} &= \ln \frac{v_{01,0}}{v_{01}} = \ln \frac{1+K_{22}\sqrt{(2+1/K_{22})^2-4}}{1+\sqrt{5}} \simeq \ln \frac{1+2\sqrt{K}}{1+\sqrt{5}} \quad (\text{self-solvation}) \\ &\simeq \ln \frac{2\sqrt{K}}{1+\sqrt{5}} = -0.48 + 0.5 \ln K \end{aligned} \quad (28)$$

Or

$$\begin{aligned} \ln\left(\frac{v_{10,0}}{v_{10}} - 0.31\right) &= \ln\left(\frac{v_{01,0}}{v_{01}} - 0.31\right) = \ln \frac{K_{22}\sqrt{(2+1/K_{22})^2-4}}{1+\sqrt{5}} \quad (\text{self-solvation}) \\ &\simeq \ln \frac{2\sqrt{K}}{1+\sqrt{5}} = -0.48 + 0.5 \ln K \end{aligned} \quad (29)$$

Or, alternatively:

$$\log(F_{12} - 0.31) = \log(F_{21} - 0.31) \simeq \log \frac{2\sqrt{K}}{1 + \sqrt{5}} = -0.21 + 0.5 \log K \quad (\text{self-solvation}) \quad (30)$$

The approximation in the second row of Equation (28) holds true for values of K that are not too low or for hydrogen-bonding interactions that are not too weak. It will be retained, just for the sake of discussion. We will come back to Equation (29) or to the alternative Equation (30).

The LFER approach does not provide any direct information on the equilibrium constants K_{ij} . It only gives the final form of the hydrogen bonding contribution in the form of the linearity sum (cf. Equation (2)), $A_1a_2 + B_1b_2$. If there is a thermodynamic basis to this linearity sum, Equations (24) and (25) should lead to it. The very form of the products in this sum indicates that the equilibrium constants, or the corresponding free energy changes upon hydrogen bond formation, should be expressed in terms of the acidity and basicity of the LSER molecular descriptors, A_i and B_j .

Thus, in order to proceed, we must express ΔG_{ij}^{hb} in terms of the molecular descriptors A_i and B_j . We do not know anything about this expression a priori. Common practice in solving such problems in physics is to make plausible assumptions, starting from those with the greatest simplicity, and focusing on the consistency of their implementation. Whatever assumption is made, it should also apply to self-solvation of hydrogen-bonded compounds, like alkanols, water, etc.

In LSER model, the acid (1)–base (2) interaction occurring upon self-solvation leads to the acidity–basicity product $A(1) \times a(2)$ or to the product denoted by the term A_1a_2 . Thus, apart from a constant, the $\ln K$ term in Equation (28) should be of the form $\ln K = A_1f(B_2, \dots)$, with the function f being an exclusive function of the solvent—component 2. Similarly, the acid (2)–base (1) interaction leads to the term B_1b_2 or to the product $B(1) \times b(2)$. Thus, again, apart from a constant, the $\ln K$ term in Equation (28) should be of the form $\ln K = B_1f(A_2, \dots)$, with the function f being an exclusive function of the solvent—component 2. However, upon self-solvation, $A_1 = A_2$ and $B_1 = B_2$. All of these requirements are met by the following simple and plausible assumption:

$$\frac{\Delta G_{ij}^{hb}}{RT} = -kA_i B_j \quad (31)$$

where k is a constant. Indeed, replacing in Equation (28), we obtain:

$$\ln(F_{12}) \simeq -0.48 + A(kB) = -0.48 + B(kA) \simeq \ln(F_{21}) \text{ (self – solvation)} \quad (32)$$

Equation (32) also provides important results. As can be observed, the hydrogen bonding contribution does indeed possess a linear form, $c + Aa$ or $c + Bb$, where $a = kB$ and $b = kA$. Although the essence of this result does not change, it should be recalled that Equations (29) or (30) are much better approximations than Equation 28. Based on these, Equation (32) takes the following form:

$$\ln(F_{12} - 0.31) \simeq -0.48 + A(kB) = -0.48 + B(kA) \simeq \ln(F_{21} - 0.31) \text{ (self – solvation)} \quad (33)$$

In the general solute–solvent case, substituting Equation (31) into Equations (26) and (27), we obtain:

$$\ln(F_{12} - 0.62) = A_1(kB_2) + c'_2 = A_1 a'_2 + c'_2 \quad (34)$$

and

$$\ln(F_{21} - 0.62) = B_1(kA_2) + c'_2 = B_1 b'_2 + c'_2 \quad (35)$$

It can be observed that the LFER linearity form is preserved not only for self-solvation but also for the general solute–solvent case. Thus, indeed, there is a thermodynamic basis for LFER linearity, even for strong hydrogen bonding contributions. There is, however, a noticeable difference: the hydrogen bonding functions F_{ij} are reduced by a constant, which depends on the number of donor and/or acceptor sites of the hydrogen bond (see Supplementary Materials (SM)); it is therefore indicative of these aspects of hydrogen bonding. For solute–solvent systems with one donor and one acceptor each, the constant is equal to 0.62. For the self-solvation of such compounds, the constant becomes $0.31 = 0.62/2$, indicating that acid–base interaction is indistinguishable from base–acid interaction upon self-solvation.

The linearity in Equations (33)–(35) is preserved for the logarithm of the reduced F_{ij} quantity, which is split into an LFER product ($A_1 a_2$ or $B_1 b_2$) and a solvent-dependent constant, c_2 . It should be pointed out, again, that the hydrogen bonding contribution contains a constant solvent term. This is crucial to remember if we want to extract the hydrogen bonding information from the corresponding LFER terms (disregarding the LFER constant coefficient).

2.5. The Essentials of the Partial Solvation Parameter (PSP) Approach

As mentioned in the Introduction, PSPs [26–34] were designed as a simple QSPR-type scheme to facilitate the exchange of information on intermolecular interactions between diverse polarity scales and databases rich in thermodynamic content. The initial incentive arose from a specific practical problem when modeling the equation-of-state behavior of systems of molecules interacting with strong specific forces, in a variety of applications. These studies would have been very much facilitated information being more readily available, especially information on strong acid–base or hydrogen-bonding interactions. It may appear surprising, but such thermodynamically valid information is not readily available in the open literature. As a consequence, modeling continues to be performed using the convenient engineering method with adjustable parameters of questionable physical meaning. Therefore, for historical reasons, PSPs were developed with equation-of-state applications in mind. For this purpose, it was convenient to define PSPs as cohesive-energy density or solubility parameters.

In the present work, we will confine ourselves to the interconnection between PSP and LSER approaches. The existence of such an interconnection implies that PSPs can be expressed in terms of LSER molecular descriptors. Thus, the first dispersion PSP, σ_d , reflects the weak intermolecular dispersive forces and is defined by the following equation:

$$\sigma_d = \sqrt{\tilde{\rho} \frac{E_d^*}{V_m}} = 100 \sqrt{\tilde{\rho} \frac{4V_x + E}{V_m}} = \frac{100}{V_m} \sqrt{V^*(4V_x + E)} \quad (36)$$

E_d^* in Equation (36) corresponds to the molar interaction energy resulting from dispersive forces. As can be observed, the McGowan volume, V_x , accounts for the majority of the contribution, and is weighted four times more heavily than the excess refractivity descriptor, E . The molar volume, V_m , and the hard core molar volume, V^* , are related through an LFHB-type equation (cf. Equation (9)), $V_m = V^*/\tilde{\rho}$. V^* is closely correlated with the van der Waals volume of the molecule. If the LFHB scaling constant, v_{sp}^* , is available, then $V^* = Mv_{sp}^*$. Alternatively, it may be estimated from V_x through the equation: $V^*_{new} = 11.357 + 99.492V_x$, which is a linear fit of LFHB scaling constants to V_x , with $R^2 = 0.9991$, as shown in Figure 1. At 25 °C, this PSP is very close to the dispersive Hansen solubility parameter, δ_d [24]. For non-polar compounds, this PSP is identical to the total Hildebrand solubility parameter, δ .

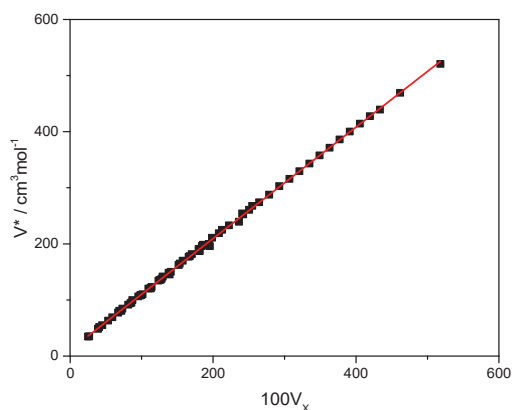


Figure 1. The hard core molar volumes of the LFHB model as a function of the corresponding McGowan volumes [16]. The straight line through the data obeys the equation $V^* = 11.357 + 99.49V_x$ with $R^2 = 0.9991$; standard errors: 0.4963 (intercept), 0.0023 (slope).

The second PSP, σ_p , reflects the weak and moderately strong polar interactions of the Keesom and the Debye types. If the molecule does not have a non-zero acidity or basicity LSER descriptor, this polar PSP is defined by the following equation:

$$\sigma_p = \sqrt{\tilde{\rho} \frac{E_p^*}{V_m}} = 100 \sqrt{\tilde{\rho} \frac{S}{V_m}} = \frac{100}{V_m} \sqrt{V^*S} \quad (37)$$

Quite often, however, polar compounds also participate in hydrogen-bonding interactions. Hydrogen-bonded compounds can be divided into two classes, the self-associated and the heterosolvated (which cross-associate only). Upon self-solvation, heterosolvated compounds do not contribute any hydrogen bonding terms to the self-solvation free energy. They do contribute with such a term when solvated by another (*heteron*, in Greek) fluid that possesses a complementary hydrogen bonding site. Obviously, these polar sites, when hydrogen bonded, are not available for ordinary polar interactions, which are reflected by the LSER polarity descriptor, S . They are available, when the compound is in its pure state, or in mixtures with compounds not possessing complementary sites. In these cases, the polarity PSP is augmented by a fraction of acidity/basicity descriptors of the compound as follows:

$$\sigma_p = 100 \sqrt{\tilde{\rho} \frac{S + \theta(A + B)}{V_m}} \quad (\text{heterosolvated compounds}) \quad (38)$$

The typical value for θ is 0.2. At 25 °C, this PSP is very close to the polar Hansen solubility parameter, δ_p , [24]. For polar and heterosolvated compounds, this PSP and the dispersion PSP are related to the total Hildebrand solubility parameter as follows:

$$\sigma_{dp}^2 = \sigma_d^2 + \sigma_p^2 = \delta^2 \text{ (polar/heterosolvated compounds)} \quad (39)$$

σ_{dp} is also referred to as non-hydrogen-bonding PSP.

With information on these PSPs, it is possible to run equation-of-state calculations. In the case of the LFHB model, the required scaling constants are V^* and E^* . V^* is obtained as shown in Figure 1. E^* has two contributing factors—dispersion and polarity—as shown in Equations (36)–(38), or $E^* = E_d^* + E_p^*$. In practice, these are estimations, at first. If several data points are available with respect to density, they are used in combination with the equation of state, Equation (11), in order to refine the estimations.

The third PSP is the hydrogen-bonding PSP, σ_{hb} , which is defined as follows:

$$\sigma_{hb} = \sqrt{\frac{-N_{hb}\Delta H_{ii}^{hb}}{V_m}} \quad (40)$$

$N_{hb} = rv_{hb}$ is the number of hydrogen bonds per mol. It is worth mentioning that σ_{hb} contains information not only for the hydrogen bonding enthalpy, ΔH_{ii}^{hb} , but also for the free energy, ΔG_{ii}^{hb} , and the entropy, ΔS_{ii}^{hb} , via the equilibrium constant, K_{ii} ($-RT \ln K_{ii} = \Delta G_{ii}^{hb}$). The equation-of-state approach, analogously to the plain Equation (23), includes information on the density of the compound, as well as on its molecular size, by means of the number of segments, r . The number of hydrogen bonds is then obtained using the following LFHB equation:

$$N_{hb} = rv_{hb} = \frac{d + a + \frac{r}{\tilde{\rho}K} - \sqrt{\left(d + a + \frac{r}{\tilde{\rho}K}\right)^2 - 4da}}{2} \quad (41)$$

This equation is made identical to Equation (23) by setting $d = a = r = \tilde{\rho} = 1$. Equation (40) calculates σ_{hb} over a broad range of external conditions. At 25 °C, this σ_{hb} PSP is often close to the Hansen solubility parameter, δ_{hb} [24].

In self-associated compounds, the total Hildebrand solubility parameter is given by the following equation:

$$\sigma_d^2 + \sigma_p^2 + \sigma_{hb}^2 = \delta^2 \text{ (self-associated compounds)} \quad (42)$$

Information on the total solubility parameter is rather easy to obtain. If the required hydrogen bonding information for ΔG_{ii}^{hb} and ΔH_{ii}^{hb} for the calculation of σ_{hb} is available from external resources, Equation (42) can be used to determine σ_p . When available, this route is preferred over that of Equations (37) and (38), since quite often the descriptor S is found to be given with relatively higher uncertainty [16].

In equation-of-state calculations, information for both ΔG_{ij}^{hb} and ΔH_{ij}^{hb} is needed. Since our interest is primarily in mixtures, it would be very much helpful to be able to obtain the acidity and basicity parameters of the pure compounds, which could be combined to give the required ΔG_{ij}^{hb} and ΔH_{ij}^{hb} for the mixture. To this end, two sets of hydrogen-bonding PSPs were defined. The first set of σ_{Ha} and σ_{Hb} is used to obtain the change in enthalpy upon formation of the hydrogen bond, as follows:

$$\Delta H_{ij}^{hb} = -\sigma_{Ha,i}\sigma_{Hb,j}\sqrt{V_{m,i}V_{m,j}} \quad (43)$$

$V_{m,i}$ is the molar volume of compound i with the acidic site and $V_{m,j}$ is the molar volume of compound j with the basic site.

The second set of σ_{Ga} and σ_{Gb} , or simply, σ_a and σ_b , is used to obtain the free energy change upon formation of the hydrogen bond, as follows:

$$\Delta G_{ij}^{hb} = -\sigma_{a,i}\sigma_{b,j}\sqrt{V_{m,i}V_{m,j}} \quad (44)$$

An interconnection of these hydrogen-bonding PSPs with the corresponding LSER molecular descriptors runs as follows:

$$\sigma_{a,i} = \sqrt{k\frac{A_i^2}{V_m}RT} = A_i\sqrt{k\frac{RT}{V_m}} \quad (45)$$

and

$$\sigma_{b,j} = \sqrt{k\frac{B_j^2}{V_m}RT} = B_j\sqrt{k\frac{RT}{V_m}} \quad (46)$$

Combining the last three equations, we recover Equation (31):

$$\frac{\Delta G_{ij}^{hb}}{RT} = -kA_iB_j \quad (47)$$

If hydrogen-bonding PSPs are known from external resources, Equations (45) and (46) can reverse their role and express the corresponding LSER descriptors in terms of the PSPs, or:

$$A_i = \sigma_{a,i}/\sqrt{kRT/V_{m,i}} \text{ and } B_j = \sigma_{b,j}/\sqrt{kRT/V_{m,j}} \quad (48)$$

There are no hydrogen bonding enthalpy LSER descriptors that can be used in a similar manner to that in Equations (45) and (46). There are, however, LFER enthalpy coefficients, as shown in Equation (3). It is, then, tempting to use hydrogen bonding enthalpy PSPs and define the corresponding LSER descriptors, $A_{H,i}$ and $B_{H,j}$, via equations analogous to Equation (47). However, it should be made clear that the enthalpic descriptors are not independent, but are quantities derived from the corresponding free energy ones. The same holds true for PSPs. In essence, if ΔG_{ij}^{hb} is known over a range of temperatures, the corresponding derived quantity, ΔH_{ij}^{hb} , could be obtained from an equation entirely analogous to Equation (19). Equivalently, one may obtain the entropy change from ΔG_{ij}^{hb} , $\Delta S_{ij}^{hb} = -(\partial\Delta G_{ij}^{hb}/\partial T)$, and the change in enthalpy from the classical equation, $\Delta H_{ij}^{hb} = \Delta G_{ij}^{hb} + T\Delta S_{ij}^{hb}$. The reverse process may also be used if extensive data on enthalpic hydrogen-bonding PSPs are available.

The above constitute a thermodynamic framework that is sufficient for carrying out a coherent discussion on the exchange of information between diverse databases and, in particular, between the LSER model and PSPs. This discussion will now continue, in the next section, with some pertinent calculations.

3. Applications

A class of hydrogen-bonded compounds that has been extensively studied in the literature is alkanols. Both LSER descriptors and LFER coefficients are available for this class [16,60], and are summarized in the Supplementary Materials (SM). Thus, we may compare the LSER predictions of solvation free energy with corresponding experimental data [49], the results of which are shown in Figure 2.

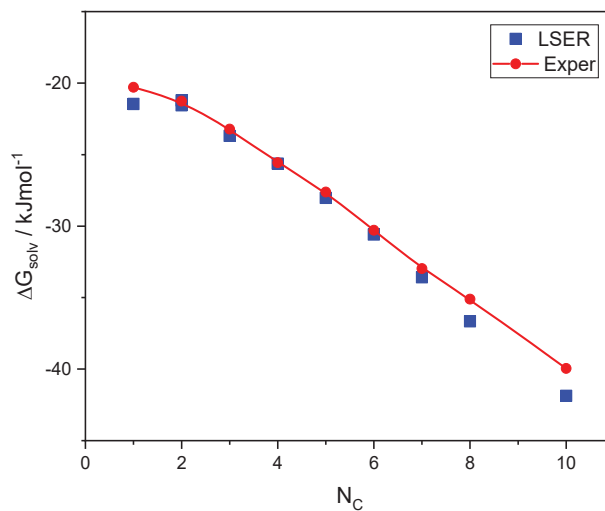


Figure 2. Comparison of the experimental [49] solvation free energies of 1-alkanols with the corresponding LSER calculations as a function of carbon atoms in the molecule.

As shown in Figure 2, there is a good agreement between the LSER predictions of solvation free energies and the experimental results. This is, then, directly exchangeable thermodynamic information. Only the experimental data [49] obtained at 298.15 K are shown in Figure 2. However, data on enthalpies and entropies of self-solvation of 1-alkanols at various temperatures are also known [49], which can be converted to the free energies of self-solvation at 298.15 K using the following equation: $\Delta G^S = \Delta H^S - 298.15\Delta S^S$. These converted data are reported in Table S5 along with the original temperature, T_{or} , for which the enthalpy and entropy data are known [49]. As shown in Table S5, the discrepancies in the experimental data regarding the free energies of self-solvation of alkanols are almost always less than 1%.

The constant LFER coefficients, c , are rather negligible for all 1-alkanols [16,60], and each of the product terms is therefore considered to reflect the full corresponding contribution to the solvation free energy. Alkanols are self-associating compounds with a significant hydrogen bonding contribution that deserve particular attention.

The five contributions to the equilibrium constant, $-\log K^S$, for the self-solvation free energy of alkanols, as given by the five products of the linearity Equation (2), are reported in Table 1. As shown, excluding cavitation contribution (lL), the main charge contribution to solvation free energy is hydrogen bonding. As observed in columns 4 and 5, the acid–base contribution, aA , is significantly different from the base–acid interaction, bB , for all alkanols. The difference (log) is 0.93 ± 0.06 for 1-alkanols and 0.65 for 2-alkanols. At present, there is no explanation for this difference. Thus, this hydrogen bonding information is not directly transferable at present.

The overall hydrogen bonding contribution, ΔG_{hb}^S , to the self-solvation free energy (calculated as $\Delta G_{hb}^S = -2.303 \times RT \times (aA + bB)$) is shown in column 7 of Table 1. In column 8, the estimated hydrogen bonding contribution to self-solvation enthalpy determined on the basis of experimental spectroscopic measurements and a set of assumptions regarding the separation of the hydrogen bonding contribution from the rest of the contributions to self-solvation enthalpy [61]. The reported values (on the order of -17 kJ/mol) are in rather considerable disagreement with the widely accepted values reported in the literature (on the order of -25 kJ/mol) [62–64]. In column 9 of the table, the hydrogen bonding entropy change with self-solvation is reported. In contrast to enthalpy, the values reported for this

change in entropy are in rather good agreement with the widely accepted values (on the order of -25 J/K mol), with the exception of methanol and ethanol [54,62–64].

Table 1. The five contributions (cf. Equation (2)) to the equilibrium constant ($-\log K^S$) for the self-solvation free energy of alkanols [16,60]: the hydrogen bonding contribution, ΔG_{hb}^S , to the solvation free energy (in kJ/mol); the experimental [61] hydrogen bonding contribution, ΔH_{hb}^S , to the self-solvation enthalpy (in kJ/mol); and the calculated hydrogen bonding contribution to the self-solvation entropy (in J/mol K) of alkanols.

Alkanol	eE	sS	aA	bB	lL	ΔG_{hb}^S	ΔH_{hb}^S	ΔS_{hb}^S
METHANOL	0.095	0.578	1.645	0.656	0.747	-13.14	-15.1	-6.58
ETHANOL	0.058	0.363	1.441	0.572	1.265	-11.49	-16.9	-18.14
1-PROPANOL	0.056	0.314	1.439	0.516	1.784	-11.16	-17.7	-21.93
1-BUTANOL	0.063	0.323	1.365	0.424	2.312	-10.21	-17.7	-25.11
1-PENTANOL	0.035	0.225	1.392	0.463	2.793	-10.59	-17.7	-23.85
1-HEXANOL	0.043	0.245	1.330	0.432	3.294	-10.06	-17.7	-25.62
1-HEPTANOL	0.045	0.234	1.323	0.388	3.837	-9.77	-17.7	-26.61
1-OCTANOL	0.043	0.236	1.283	0.364	4.349	-9.40	-17.7	-27.84
1-DECANOL	0.017	0.150	1.292	0.354	5.382	-9.40	-17.7	-27.84
2-PROPANOL	0.068	0.261	1.237	0.591	1.571	-10.43	-17.3	-23.03
2-PENTANOL	0.065	0.182	1.237	0.573	2.650	-10.34	-17.3	-23.36

The key point from the above exposition is that, even for the extensively studied alkanols, there are notorious discrepancies in the open literature regarding hydrogen bonding contribution. Since hydrogen bonding contributions constitute the main charge contributions to the solvation free energies of these systems, it would be useful to see what the above thermodynamic framework and analysis tell us.

First of all, although often minor, a distinction should be made between hydrogen bonding solvation free energy, ΔG_{hb}^S , and free energy change upon the formation of the hydrogen bond, ΔG_{ij}^{hb} , as well as for the corresponding hydrogen bonding enthalpies. The latter quantity characterizes the average strength of a specific interaction, and is well suited to carrying out modeling using explicit equations, like Equations (31) or (41). This quantity, when used in a consistent thermodynamic framework, should lead to expressions (like the above terms, F_{ij}) for the former quantity, ΔG_{hb}^S , which is part of the measurable overall solvation free energy. The same holds true for the corresponding enthalpies, although the difference in enthalpies is significantly reduced. As an example, in the case of self-solvation, we may start from the simple Equation (32) and examine the above differences.

If the logarithm of F_{ij} in Equation (30) or (32) were written without the constant term, as in the LSER model, this would imply that $\ln F_{12} = -\Delta G_{ij}^{hb}/2RT$ (cf. Equation (31)) and the hydrogen bonding equilibrium constant, K_{12} , were identical to the hydrogen bonding component of the solvation equilibrium constant, K^S , as well as, of course, with F_{12} . This would simplify things, and the differences described above would be zero. The correction constant to F_{12} , however, implies that the two K s are conceived differently by the two modeling approaches. Thus, the LSER quantity, $-2.303RT(A_1a_2 + B_1b_2) = \Delta G_{hb}^S$, cannot be considered identical to ΔG_{12}^{hb} . The way hydrogen bonding contributes to the solvation free energy depends on the nature and multiplicity of the interacting sites, and this requires some corresponding correction to the plain sum of the LFER products, $A_1a_2 + B_1b_2$. Neither should F_{12} be considered to be identical to K_{12} . Similar concerns apply to all models based on divisions of intermolecular interactions.

By combining Equation (19) with Equation (28) or with Equation (29), we obtain the following equation (the subscript 1 in Equation (49) should be taken as corresponding to the acid site, while the subscript 2 corresponds to the base site):

$$\begin{aligned} \Delta H_{hb}^S &= \Delta H_{hb,12}^S + \Delta H_{hb,21}^S = -2RT^2 \left(\frac{\partial(\Delta G_{hb,12}^S/RT)}{\partial T} \right)_P = -2RT^2 \left(\frac{\partial \ln(F_{12})}{\partial T} \right)_P \\ &= -2RT^2 \left(\frac{\partial \ln((1+2\sqrt{K})/(1+\sqrt{5}))}{\partial T} \right)_P = -2RT^2 \left(\frac{\partial \ln(1+2\sqrt{K})}{\partial T} \right)_P \\ &= -2 \frac{RT^2}{1+2\sqrt{K}} \frac{K}{\sqrt{K}} \frac{\partial}{\partial T} \left(\frac{\Delta H_{12}^{hb} - T\Delta S_{12}^{hb}}{RT} \right)_P = \frac{2K}{\sqrt{K}+2K} \Delta H_{12}^{hb} \end{aligned} \quad (49)$$

Thus, at values of K that are not very low, the hydrogen bonding solvation enthalpy may be considered to be close to the corresponding change in enthalpy upon the formation of the acid–base hydrogen bond. In alkanols in which K is greater than 350, their difference is less than 2%. Thus, information on this quantity would essentially be directly transferable. As a consequence, the enthalpy described in column 8 of Table 1 should have been nearly identical to the change in enthalpy ΔH_{12}^{hb} , which is not the case. This discrepancy highlights the problem caused by the lack of consensus in the literature on the strength of hydrogen-bonding interactions in alkanols. However, the PSP approach and the equation-of-state model permit the estimation of this change in enthalpy on the basis of other thermodynamic properties, as well.

The free energy and enthalpy data presented in Table 1 were used to correlate the basic thermodynamic quantities of alkanols (vapor pressure, vaporization heat, density, and solubility parameters) [65] with those of the LFHB and the more advanced NRHB [52–54,57,58] equation-of-state models. The LFHB scaling constants with which the best correlations were obtained are reported in the SM. In Table 2, the LFHB scaling constants are reported, along with the more widely accepted hydrogen bonding enthalpies and entropies [50–54,56–58,62–64] that were used to obtain the best correlations for the very same set of thermodynamic quantities of alkanols [65]. Two sets of scaling constants are reported for methanol, just to show how sensitive the scaling constants are to the adopted hydrogen bonding parameters.

Table 2. The scaling constants and the hydrogen bonding solubility parameters of alkanols.

Solvent	$\varepsilon^*/\text{J mol}^{-1}$	$\varepsilon_s^*/\text{JK}^{-1} \text{mol}^{-1}$	$v_{sp0}^*/\text{cm}^3 \text{mol}^{-1}$	$v_{sp1}^*/\times 10^4$	$\Delta H_{22}^{hb}/\text{kJ mol}^{-1}$	$\Delta S_{22}^h/\text{JK}^{-1} \text{mol}^{-1}$	$\Delta G_{22}^{hb}/\text{kJ mol}^{-1}$
METHANOL ¹	4609	−0.117	1.165	2.5	−23.60	−28.0	−15.25
METHANOL	4162	1.185	1.131	2	−26.00	−29.5	−17.21
ETHANOL	4134	−0.107	1.128	0	−24.05	−27.5	−15.85
1-PROPANOL	4072	0.330	1.103	−1	−23.60	−26.5	−15.70
1-BUTANOL	4092	0.610	1.097	−1	−23.40	−26.5	−15.50
1-PENTANOL	4076	0.914	1.088	−1	−23.38	−27.0	−15.33
1-HEXANOL	4058	1.090	1.079	−1	−23.08	−26.5	−15.18
1-HEPTANOL	4117	0.730	1.081	−1	−23.10	−27.0	−15.05
1-OCTANOL	4086	1.004	1.075	−1	−23.10	−27.5	−15.18
1-DECANOL	4095	1.311	1.072	−3	−23.10	−28.5	−15.05
ISOPROPANOL	3777	0.267	1.103	−1	−23.50	−26.5	−14.90
2-PENTANOL	3784	0.949	1.072	−2	−23.50	−26.5	−14.75

¹ Scaling constants for methanol accounting for δ_{hb} [24].

In Table 3, the calculated solubility parameters are compared with the two sets of hydrogen bonding parameters described in Tables 1 and 2, as well as with literature data. It can be observed that the hydrogen bonding data in Table 1 do not seem to be compatible with the experimental data regarding total solubility parameters, especially in the case of the lower (MW) alkanols, or with the Hansen solubility parameters for hydrogen bonding [24]. In fact, the large discrepancies for the later may be an explanation for the discrepancies in the former. The discrepancies were somewhat larger, when using the NRHB [57,58], rather than the LFHB, model. As shown by Equation (40), the change in enthalpy, ΔH_{12}^{hb} , strongly affects, in a direct manner, the hydrogen-bonding PSP and thus the corresponding solubility parameter, δ_{hb} . Thus, the correlation of this parameter can be considered to be a direct test of the accuracy of the proposed ΔH_{12}^{hb} values. It seems that the hydrogen bonding parameters reported in Table 1, which have apparently been adopted by the LSER model [40], are not compatible with the corresponding solubility parameter data described in the literature [24,61].

Table 3. The experimental and calculated total solubility parameters and hydrogen bonding solubility parameters of alkanols. LSER and PSP calculations were performed using the hydrogen bonding parameters presented in Tables 1 and 2, respectively.

Solvent	$\delta_t/\text{MPa}^{0.5}$			$\delta_{hb}/\text{MPa}^{0.5}$		
	LSER calc	σ	Exp [61]	LSER calc	σ_{hb}	Exp [24]
METHANOL ¹	27.8	30.2	29.4	17.9	22.8	22.3
METHANOL	27.8	30.4	29.4	17.9	24.4	22.3
ETHANOL	25.0	26.3	26.2	14.9	19.3	19.4
1-PROPANOL	23.8	24.3	24.6	13.3	16.9	17.4
1-BUTANOL	22.8	23.1	23.5	11.5	14.9	15.8
1-PENTANOL	21.9	22.6	22.4	10.5	13.6	13.9
1-HEXANOL	21.3	21.9	22.1	9.4	12.5	12.5
1-HEPTANOL	21.0	21.7	21.8	8.6	11.7	11.7
1-OCTANOL	20.5	21.0	21.0	8.6	11.0	11.9
1-DECANOL	20.1	20.4	20.2	7.0	9.8	10.0
ISOPROPANOL	22.8	23.6	23.8	12.6	16.4	16.4
2-PENTANOL	21.1	21.8	21.8	10.2	13.6	13.3

¹ With scaling constants for methanol best accounting for δ_{hb} [24].

So far, we have essentially confined ourselves to the self-solvation of alkanols. We could further test the accuracy of the proposed hydrogen bonding energies by looking at the solvation of various solutes in alkanol solvents. In this way, we could extract useful conclusions, especially from solutes that form hydrogen bonds with alkanols. In essence, if the true values of hydrogen bonding free energy and enthalpy of alkanols are significantly more negative than what is estimated by the LSER model, then, in the solvation free energies of various solutes in alkanol solvents, this would show up in the LSER model estimations by being somewhat less negative than the corresponding experimental values.

In Figure 3, the LSER estimations of the solvation free energy of a variety of solutes in 1-octanol are plotted as a function of the corresponding experimental data [49]. In the same figure, alternative predictions are also reported in which the LSER hydrogen bonding contribution to ΔG_{12}^{hb} (Table 1) is replaced with the corresponding LFHB contributions with the above, more widely used, hydrogen bonding parameters (Table 2). It can be seen that the two sets of predictions are practically identical, except for the notable case of water, where the LSER estimation is significantly less negative than the LFHB one, while being in rather good agreement with the experimental results. This picture is nearly the same for

the solvation in all alkanols as solvents. Detailed tables with the data reported in Figure 3 are provided in the Supplementary Materials (SM).

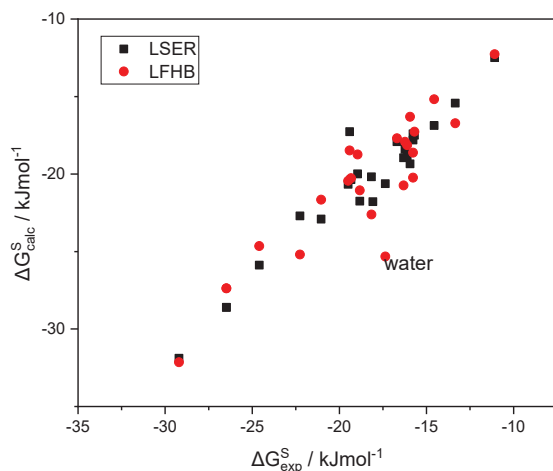


Figure 3. The LSER estimations of the solvation free energy of various solutes in 1-octanol, as a function of the corresponding experimental data [49].

As can be observed in Figure 3, the scatter of the experimental solvation free energies [49] does not permit clear judgement regarding the accuracy of the alternative sets of hydrogen bonding parameters used. The outlier in the LFHB correlation (water) is quite interesting, and will be extensively discussed in a forthcoming paper dedicated exclusively to water and aqueous systems.

All of the above indicate that the LSER estimations of hydrogen bonding contribution to solvation free energies in alkanols raise several questions, and should probably be reconsidered. However, if they were to be reconsidered, their reconsideration might affect the other products of the LFER linearity Equations (1) and (2), and such structural changes in the LSER database are not easy to make. In fact, the accuracy of the experimental results for overall solvation free energies may not always be high enough to capture the differences in hydrogen bonding parameters or, probably, the parameters of the other intermolecular interactions. These obstacles are mentioned here, just to indicate the challenges faced by PSP development. If these obstacles could be overcome, the transfer process described above might be reversed, and information from PSPs could be used to enhance the LSER database.

Assuming that the values of σ_a and σ_b are known from other sources, say, from the COSMO-RS model [35–39] or from molecular dynamics simulations, Equation (47) can be used to calculate the hydrogen bonding LSER molecular descriptors. This particular transfer, either from LSER to PSP or from PSP to LSER, is meaningful and useful when the same constant k is used in the equation. This constant may be obtained using Equation (31) if ΔC_{ij}^{hb} is known. In Table 4, the estimations of this constant are reported for alkanols based on the hydrogen bonding parameters, ΔC_{ij}^{hb} , presented in the table. It can be seen that k is nearly constant. In fact, on the basis of analogous calculations performed for other solute–solvent systems, including aqueous ones, it seems that the values of k center around $k = 33.9$ or $kR \times 298.15 = 84,000$ J/mol. The adoption of such a universal value for the constant k would greatly augment the predictive capacity of LSER and PSP, as well as other interconnected QSPR-type databases. However, the prerequisite for this remains the agreement on the values of ΔG_{12}^{hb} or ΔH_{12}^{hb} for several hydrogen-bonded compounds. In fact, the adoption of such a universal value for k would also require a rather minor change in the A and B LSER descriptors to A' and B', as reported in Table 4, in order to obtain the same solvation free energy as the product $kRTA'B'$.

Table 4. The acidity and basicity LSER descriptors, A and B [16], the free energy change upon self-association, ΔG_{ij}^{hb} , the corresponding kRT product, and the readjusted A' and B' descriptors to be used with a universal value of kRT = 84 kJ/mol.

Solvent	A	B	$-\Delta G_{ij}^{hb}/$ kJ mol ⁻¹	$-kRT/$ kJ mol ⁻¹	A'	B'
METHANOL	0.43	0.47	17.21	85.13	0.433	0.473
ETHANOL	0.37	0.48	15.85	89.25	0.381	0.495
1-PROPANOL	0.37	0.48	15.70	88.40	0.380	0.492
1-BUTANOL	0.37	0.48	15.50	87.26	0.376	0.491
1-PENTANOL	0.37	0.48	15.33	86.31	0.374	0.489
1-HEXANOL	0.37	0.49	15.18	85.15	0.370	0.489
1-HEPTANOL	0.37	0.48	15.05	84.73	0.369	0.485
1-OCTANOL	0.37	0.49	14.90	83.89	0.365	0.485
1-NONANOL	0.37	0.49	14.75	81.82	0.362	0.484
1-DECANOL	0.36	0.49	14.60	82.29	0.361	0.482
ISOPROPANOL	0.31	0.56	15.90	92.65	0.322	0.588
2-PENTANOL	0.33	0.56	15.60	85.38	0.329	0.565

Having agreed on the hydrogen bonding parameters, an agreement on the contribution of hydrogen bonding to the solvation free energy is then feasible. Once this is done, the exchange of information can be continued with the other descriptors. The contribution of non-hydrogen-bonding interactions to PSPs can easily be obtained from the equation-of-state scaling constants. Combining Equations (36)–(39), we get:

$$\sigma_d^2 + \sigma_p^2 = \tilde{\rho} \frac{E_d^* + E_p^*}{V_m} = \tilde{\rho} \frac{E^*}{V_m} \quad (50)$$

The dispersive PSP, σ_d , is mainly connected to the McGowan volume, V_x , and, to a lesser extent, to the excess refractivity descriptor, E (cf. Equation (36)). Both V_x and E are rather clearly defined, and practically speaking, Equation (36) is always considered to be valid. Since the total solubility parameter is very often known with good accuracy, Equation (42) permits the estimation of the polar PSP, σ_p , or, equivalently, the LSER polarity descriptor, S , or the interaction energy, E_d^* . The polarity descriptor S is not as clearly defined as V_x and E . Thus, the above transfer of information from σ_p may be useful for verification or for a better estimation of S .

4. Discussion

There is no doubt that the LSER approach and database [1–18] are very rich in thermodynamic content. For decades, now, the scientific community has used them in numerous applications, with remarkable success. However, the question remains as to how this content might be extracted and transferred for more extensive or specific advanced thermodynamic calculations. In response to this question, an attempt was made in the previous two sections to address some challenging issues related to the interconnection between the LSER approach and database [1–18] and the equation-of-state approach and Partial Solvation Parameters [26–34].

The three LSER molecular descriptors, V_x , E , and L , are rather clearly defined. The remaining three descriptors for the polar and strong specific interactions, S , A and B , are not as clearly defined and, to a great extent, their determination has been performed through regression and fitting to experimental data. In this regard, the more specific question is: how can hydrogen bonding or strong (Lewis) acid–base interactions, reflected by the descriptors A and B , be separated from the remaining weaker polar interactions, reflected

by the descriptor S? Furthermore, the even more specific question is: on what scale is acidity or basicity expressed? This concept of “scale” is needed whenever aiming to perform a quantitative comparison of similar properties or entities.

In the previous two sections, the focus was primarily on descriptors A and B, and indirectly on descriptor S. The basis of the discussion was the very fact that thermodynamic quantities such as solvation free energy can be estimated successfully using a simple linear equation (Equation (2)). The obvious first step was to examine the thermodynamic basis of this very linearity, especially for the hydrogen bonding contribution. The tool used for this examination was a simple statistical thermodynamic model, able to handle simple as well as complex hydrogen-bonding interactions, including intramolecular interactions, cooperativities and three-dimensional networks [50–58]. The minimal features of the model were used here, since the bulk of hydrogen-bonded solutes and solvents are attributed one donor and/or one acceptor site when using the LSER approach, while densities or external pressures are not explicitly taken into account. Even when considering temperature variations, the bulk of the data are reported at a temperature of 25 °C. Thus, hydrogen-bonding interactions could be handled as simple quasi-chemical reactions with a free energy change upon formation and an equilibrium constant. For reader convenience, a step-by-step derivation of the key equations with the corresponding assumptions is provided in the SM, along with the implementation of the central simple assumption for this (hydrogen bond) free energy change upon formation, namely, $\Delta G_{12}^{hb} = -kA_1B_2$.

With this exercise, it was verified that the hydrogen bonding contribution to solvation free energy may indeed be expressed in a linear-like manner similar to the LSER, as shown in Equation (2). This similarity is gratifying, but more interesting is the insight contained in the new equations. In the main text, above, the case of molecules with one donor and/or one acceptor was presented. The case of molecules with two donors and/or two acceptors is presented in the Supplementary Materials (SM). The acid (1)–base (2) contribution to solvation free energy is given by the following general equation:

$$\ln(F_{12} - \lambda) = A_1(kB_2) + c'_2 = A_1a'_2 + c'_2 \quad (51)$$

and the base(1)–acid(2) contribution by the following symmetric equation:

$$\ln(F_{21} - \lambda) = B_1(kA_2) + c'_2 = B_1b'_2 + c'_2 \quad (52)$$

The constant c'_2 is an exclusive property of the solvent (component 2). The constant λ reflects the character of the hydrogen-bonding interaction. In one-donor–one-acceptor solute–solvent systems, $\lambda = 2/(1 + \sqrt{5})$ and, upon self-solvation, $\lambda = 1/(1 + \sqrt{5})$. In the case of two-donor–two-acceptor solute–solvent systems, $\lambda = 2/4$ and, upon self-solvation, $\lambda = 1/4$.

Due to their symmetric character, Equations (50) and (51) indicate that, upon self-solvation, the acid–base and the base–acid contributions are identical, that is, $F_{12} = F_{21}$ and $A_1a'_2 = B_1b'_2$. What is even more interesting, though, is that both solvent coefficients, a'_2 and b'_2 , are expressed explicitly by the plain relations, $a'_2 = kB_2$ and $b'_2 = kA_2$.

It seems, however, that LSER was developed differently with respect to hydrogen-bonding interactions. Linearity is obeyed, but upon self-solvation, A_1a_2 is different from B_1b_2 . Apparently, one or both of these products also contains the information of constant c'_2 . The constant λ does not show up when using the LSER approach, since it handles solute–solvent interactions exclusively as a one-donor–one-acceptor interaction. Thus, at present, the extraction of separate information on acidity and basicity contributions is not quite straightforward. If this were possible, this information could be transferred to the corresponding PSPs via Equations (45) and (46), and practically useful equation-of-state calculations could be performed.

The overall hydrogen bonding LSER contribution seems easier to extract and transfer. Even there, however, much care must be exercised. In the previous section, the example of alkanol solvents was discussed, where the value of enthalpy-change upon the formation of

OH–OH hydrogen bonds is still controversial today. The value adopted by LSER (on the order of -17 kJ/mol) is rather drastically different from the more widely adopted value (on the order of -25 kJ/mol), and this by itself remains a challenging issue in the literature.

If the above issues were clarified, the PSP approach could facilitate the determination of the descriptor S once the hydrogen bonding contribution was known. As shown in the previous section, the solubility parameter, and especially its hydrogen bonding component, are sensitive to the value of the hydrogen bonding enthalpy. The overall solubility parameter is a rather well-defined (and measurable) quantity. Thus, once the hydrogen bonding contribution is known, it may be relatively easier to separate the remaining dispersion and polar contributions.

It should be stressed, once again, that the above analysis is not a criticism of any database or polarity scale reported in the literature. It is just an attempt to develop a thermodynamic basis for the safe exchange of information between different databases. The interconnection between LSER and PSP is just an example used to discuss some problems associated with this effort. The above discussion was not exhaustive, by any means, with respect to these problems, but their nature and key aspects have hopefully been exposed.

The calculations in the present work were confined to systems of alkanols. Water and aqueous systems will be discussed in a forthcoming manuscript. Systems of glycols will also be discussed separately, since they possess two distant donor sites and two acceptor sites in their molecules (cf. SM file). Heterosolvated compounds, possessing one type of hydrogen bonding site only—donor or acceptor—are also a separate class of compound, and will be discussed after self-associating or homosolvated compounds. These studies will contribute to our understanding of the thermodynamic content of the LSER linearity terms and the factors affecting them.

It should be stressed that the purpose of this manuscript was not to report a full new database in place of the current LSER database. The development of such a full database is not an easy task, and would require a concerted effort and wider collaboration. In this series of papers, we discuss various classes of compounds (e.g., alkanols, water and aqueous systems, heterosolvated compounds, etc.), but we are far from establishing a full database. We hope that this manuscript will stir broader interest and promote the concerted effort and collaboration required.

In summary of the key messages of this work, the LSER model with its database is not only a valuable predictive tool that is rich in thermodynamic information, the linearity of LFER indeed has a sound thermodynamic basis. It seems, however, that this thermodynamic basis was either not known, or it was disregarded, and the development of the LSER database was carried out on a more or less empirical basis using plain linear regressions and correlations of experimental data, with little interest in the thermodynamic consistency of the reported LFER parameters. As an example of this inconsistency, the acid–base interaction, aA , is often drastically different from the very same base–acid interaction, bB , upon self-solvation. This makes it difficult to extract thermodynamic information from the LSER database in its current form, in spite its remarkable potential. There is no need whatsoever to change LSER descriptors and LFER parameters for current applications of the LSER database. However, since there is now an explicitly known thermodynamic basis, the LSER database could be restructured or redesigned on this basis, if there is an interest in the exchange of thermodynamic information. With a firm thermodynamic basis, it would be meaningful to exchange information on thermodynamic quantities among a number of different databases.

5. Conclusions

The LSER model and database, which is very useful in numerous applications, are also very rich in thermodynamic information, and some key problems associated with the extraction and transfer of this information were discussed in this work. A thermodynamic basis for the linearity of the LFER/LSER approach was proposed and used to provide an

interconnection between the LSER molecular descriptors and the corresponding Partial Solvation Parameters (PSPs). It was shown that, in contrast to the well-defined thermodynamic quantities, much care must be exercised when transferring information based on the divisions of intermolecular interactions, since they necessarily have an inherently varying degree of arbitrariness. The LSER database has not been developed, to date, on the above thermodynamic basis, and some aspects of its departure from this were discussed, in an effort to recover thermodynamic information from the reported molecular descriptors and LFER coefficients. The advantages of adopting this thermodynamic basis were also indicated. This adoption is not a trivial task, and will require a concerted effort by experts in the field. It is hoped that this work will stir sufficient interest in the relevant literature, in this regard.

Supplementary Materials: The following supporting information can be downloaded at: <https://www.mdpi.com/article/10.3390/liquids3010007/s1>. In the Supplementary Materials (SM), the essentials of the derivations of the LFHB equations at infinite dilution are reported and examples are given of the use of linearity of the LSER model in practical calculations with alkanols; Table S1: The constants of equation S30–S31 for hydrogen bonding contributions to the free-energy of solvation in alkanol solvents; Table S2: The hydrogen-bonding contributions to the free-energy of solvation in alkanol solvents; Table S3: LSER descriptors and LFER coefficients for alkanols; Table S4: Experimental and calculated solvation free-energies in 1-octanol solvent; Table S5: Experimental data for the self-solvation free-energy of 1-alkanols at 298.15 K. References [2–5,16,49–53,56,60] are cited in Supplementary Materials.

Author Contributions: Conceptualization, C.P., I.Z. and V.H.; methodology, C.P.; software, V.H.; validation, C.P., I.Z. and H.A.K.; formal analysis, I.Z.; investigation, C.P.; resources, V.H.; data curation, H.A.K.; writing—original draft preparation, C.P.; writing—review and editing, V.H.; visualization, H.A.K.; supervision, C.P.; project administration, I.Z.; funding acquisition, I.Z. All authors have read and agreed to the published version of the manuscript.

Funding: This research is supported by ASPIRE, the technology program management pillar of Abu Dhabi’s Advanced Technology Research Council (ATRC), via the ASPIRE “AARE (ASPIRE Awards for Research Excellence)” and through grant no. AARE20-246 to Ioannis Zuburtikudis of Abu Dhabi University.

Institutional Review Board Statement: Not applicable.

Informed Consent Statement: Not applicable.

Data Availability Statement: Data is contained within the article and Supplementary Material.

Conflicts of Interest: The authors declare no conflict of interest.

List of Symbols

Latin letters

a_i	Number of acceptor sites of type i
a_i	LFER acidity coefficient for solvent i
A_i	LSER acidity molecular descriptor of component i
b_j	LFER basicity coefficient for solvent j
B_j	LSER basicity molecular descriptor of component j
c	LFER constant coefficient
d_i	Number of donor sites of type i
e	LFER solvent refractivity coefficient
E	Excess refractivity LSER molecular descriptors
F	Hydrogen bonding contribution term
G	Free energy
H	Enthalpy
k	Proportionality constant
K	Equilibrium constant
l	LFER coefficient for gas-to-C16 partitioning

L	LSER molecular descriptor for gas-to-C16 partitioning
N	Mole number
P	Pressure
r	Number of molecular segments
R	Gas constant
s	LFER polarity coefficient
S	Entropy
T	Temperature
v	specific volume
V	Volume
V _x	McGowan volume
x	Mole fraction
Z	Compressibility factor
Greek Letters	
γ	Activity coefficient
δ	Solubility parameter
ΔY	Change in quantity Y
ΔG _{ij} ^{hb}	Free energy change on hydrogen bond formation between donor i and acceptor j.
ε*	Interaction energy
ν	Fraction or reduced number of hydrogen bonds
ξ	Correction factor to geometric-mean interaction energy
$\tilde{\rho}$	Reduced density
σ	Partial solvation parameter
φ	Fugacity coefficient
ω	Molecular conformation parameter
Superscripts	
0	Pure component
∞	Infinite dilution
*	LFHB scaling property
hb	Hydrogen bonding quantity
IG	Ideal gas
S	Solvation quantity
Subscripts	
1/2	Property of solute (1) in solvent (2)
0i	Fraction of free acceptor sites
i0	Fraction of free donor sites
d	Dispersion quantity
hb	Hydrogen bonding quantity
i	Quantity pertaining to component i
ij	Quantity pertaining to the interacting pair i, j
m	Molar quantity
p	Polar quantity
sp	Specific

References

1. Abraham, M.H.; McGowan, J.C. The use of characteristic volumes to measure cavity terms in reversed phase liquid chromatography. *Chromatographia* **1987**, *23*, 243. [[CrossRef](#)]
2. Abraham, M.H. Scales of solute hydrogen-bonding: Their construction and application to physicochemical and biochemical processes. *Chem. Soc. Rev.* **1993**, *22*, 73. [[CrossRef](#)]
3. Abraham, M.H.; Ibrahim, A.; Zissimos, A.M. Determination of sets of solute descriptors from chromatographic measurements. *J. Chromatogr. A* **2004**, *1037*, 29. [[CrossRef](#)]
4. Poole, C.F.; Atapattu, S.N.; Poole, S.K.; Bell, A.H. Determination of solute descriptors by chromatographic methods. *Anal. Chim. Acta* **2009**, *652*, 32–53. [[CrossRef](#)] [[PubMed](#)]
5. Abraham, M.H.; Smith, R.E.; Luchtefeld, R.; Boorem, A.J.; Luo, R.; Acree, W.E., Jr. Prediction of solubility of drugs and other compounds in organic solvents. *J. Pharm. Sci.* **2010**, *99*, 1500. [[CrossRef](#)]
6. Abraham, M.H.; Whiting, G.S.; Carr, P.W.; Ouyang, H. Hydrogen bonding. Part 45. The solubility of gases and vapors in methanol at 298 K: An LFER analysis. *J. Chem. Soc. Perkin Trans.* **1998**, *2*, 1385–1390. [[CrossRef](#)]

7. Abraham, M.H.; Whiting, G.S.; Shuely, W.J.; Doherty, R.M. The solubility of gases and vapours in ethanol—The connection between gaseous solubility and water–solvent partition. *Can. J. Chem.* **1998**, *76*, 703–709. [CrossRef]
8. Abraham, M.H.; Platts, J.A.; Hersey, A.; Leo, A.J.; Taft, R.W. Correlation and estimation of gas–chloroform and water–chloroform partition coefficients by a linear free energy relationship method. *J. Pharm. Sci.* **1999**, *88*, 670–679. [CrossRef]
9. Abraham, M.H.; Le, J.; Acree, W.E., Jr.; Carr, P.W. Solubility of gases and vapors in propan-1-ol at 298 K. *J. Phys. Org. Chem.* **1999**, *12*, 675–680. [CrossRef]
10. Goss, K.-U. Predicting the equilibrium partitioning of organic compounds using just one linear solvation energy relationship (LSER). *Fluid Phase Equilib.* **2005**, *233*, 19–22. [CrossRef]
11. Acree, W.E., Jr.; Abraham, M.H. The analysis of solvation in ionic liquids and organic solvents using the Abraham linear free energy relationship. *J. Chem. Technol. Biotechnol.* **2006**, *81*, 1441–1446. [CrossRef]
12. Goss, K.-U. Using COSMO-RS for the Prediction of Vapor-Liquid Equilibria, Gas Solubilities and Partition Coefficients in Polymers. *Anal. Chem.* **2011**, *83*, 5304–5308. [CrossRef]
13. van Noort, P.C.M. Solvation thermodynamics and the physical-chemical meaning of the constant in Abraham solvation equations. *Chemosphere* **2012**, *87*, 125–131. [CrossRef] [PubMed]
14. Van Noort, P.C.M. Estimation of Abraham solvation equation coefficients for hydrogen bond formation from Abraham solvation parameters for solute acidity and basicity. *Chemosphere* **2013**, *90*, 344–348. [CrossRef] [PubMed]
15. Endo, S.; Goss, K.U. Applications of polyparameter linear free energy relationships in environmental chemistry. *Environ. Sci. Technol.* **2014**, *48*, 12477–12491. [CrossRef]
16. Ulrich, N.; Endo, S.; Brown, T.N.; Watanabe, N.; Bronner, G.; Abraham, M.H.; Goss, K.-U. UFZ-LSER database v 3.2.1, Leipzig, Germany, Helmholtz Centre for Environmental Research-UFZ. 2017. Available online: <http://www.ufz.de/lserd> (accessed on 15 December 2022).
17. Eggert, T.; Langowski, H.C. Linear Solvation Energy Relationships (LSERs) for Robust Prediction of Partition Coefficients between Low Density Polyethylene and Water Part I: Experimental Partition Coefficients and Model Calibration. *Eur. J. Pharm. Sci.* **2022**, *172*, 106137. [CrossRef] [PubMed]
18. Egert, T.; Langowski, H.C. Linear Solvation Energy Relationships (LSERs) for Accurate Prediction of Partition Coefficients between Low Density Polyethylene and Water—Part II: Model Evaluation and Benchmarking. *Eur. J. Pharm. Sci.* **2022**, *172*, 1–10.
19. Drago, R.S. A modern approach to acid–base chemistry. *J. Chem. Educ.* **1974**, *51*, 300–307. [CrossRef]
20. Gutmann, V. *The Donor–Acceptor Approach to Molecular Interactions*; Plenum Press: New York, NY, USA; London, UK, 1978.
21. Reichardt, C. *Solvents and Solvent Effect in Organic Chemistry*, 3rd ed.; Wiley-VCH: Weinheim, Germany, 2003.
22. Katritzky, D.; Fara, E.; Yang, H.; Ta^omm, K.; Tamm, T.; Karelson, M. Quantitative Measures of Solvent Polarity. *Chem. Rev.* **2004**, *104*, 175–198. [CrossRef]
23. Laurence, C.; Gal, J.-F. *Lewis Basicity and Affinity Scales: Data and Measurements*; Wiley: New York, NY, USA, 2010.
24. Hansen, C.M. *Hansen Solubility Parameters, A User’s Handbook*, 2nd ed.; CRC Press: Boca Eaton, FL, USA, 2007.
25. Prausnitz, J.M.; Lichtenthaler, R.N.; de Azevedo, E.G. *Molecular Thermodynamics of Fluid-Phase Equilibria*, 3rd ed.; Prentice-Hall PTR: Upper Saddle River, NJ, USA, 1999.
26. Panayiotou, C. Redefining solubility parameters: The partial solvation parameters. *Phys. Chem. Chem. Phys.* **2012**, *14*, 3882–3908. [CrossRef]
27. Panayiotou, C. Partial solvation parameters and mixture thermodynamics. *J. Phys. Chem. B* **2012**, *116*, 7302–7321. [CrossRef] [PubMed]
28. Panayiotou, C.; Aslanidou, D. Partial solvation parameters and the equation-of-state approach. *Fluid Phase Equilib.* **2015**, *406*, 101–115. [CrossRef]
29. Mastrogeorgopoulos, S.; Hatzimanikatis, V.; Panayiotou, C. Toward a Simple Predictive Molecular Thermodynamic Model for Bulk Phases and Interfaces. *Ind. Eng. Chem. Res.* **2017**, *56*, 10900–10910. [CrossRef]
30. Niederquell, A.; Wyttenbach, N.; Kuentz, M.; Panayiotou, C. Partial Solvation Parameters of Drugs as a New Thermodynamic Tool for Pharmaceuticals. *Pharmaceutics* **2019**, *11*, 17. [CrossRef]
31. Lazidou, D.; Mastrogeorgopoulos, S.; Panayiotou, C. Thermodynamic characterization of ionic liquids. *J. Mol. Liq.* **2019**, *277*, 10–21. [CrossRef]
32. Lazidou, D.; Teknetzi, I.; Aslanidou, D.; Papadopoulou, S.; Panayiotou, C. Partial Solvation Parameters in Conservation Science for Works of Art. *J. Cult. Heritage* **2019**, *39*, 12. [CrossRef]
33. Panayiotou, C.; Zuburtikudis, I.; Hatzimanikatis, V. 110th Anniversary: From solubility parameters to predictive equation-of-state modeling. *Ind. Eng. Chem. Res.* **2019**, *58*, 12787–12800. [CrossRef]
34. Panayiotou, C.; Hatzimanikatis, V. The solubility parameters of CO₂ and ionic liquids: Are they an enigma? *Fluid Phase Equilib.* **2021**, *527*, 112828. [CrossRef]
35. Klamt, A. *COSMO-RS from Quantum Chemistry to Fluid Phase Thermodynamics and Drug Design*; Elsevier: Amsterdam, The Netherlands, 2005.
36. COSMOlogic GmbH. *COSMObase*; Version C30_1401; COSMOlogic GmbH & Co. K.G.: Leverkusen, Germany, 2014.
37. Lin, S.T.; Sandler, S.I. A priori phase equilibrium prediction from a segment contribution solvation model. *Ind. Eng. Chem. Res.* **2002**, *41*, 899–913. [CrossRef]

38. Grensemann, H.; Gmehling, J. Performance of a conductor-like screening model for real solvents model in comparison to classical group contribution methods. *Ind. Eng. Chem. Res.* **2005**, *44*, 1610–1624. [[CrossRef](#)]
39. Pye, C.C.; Ziegler, T.; van Lenthe, E.; Louwen, J.N. An implementation of the conductor-like screening model of solvation within the Amsterdam density functional package. Part II. COSMO for real solvents. *Can. J. Chem.* **2009**, *87*, 790–797. [[CrossRef](#)]
40. Lu, J.; Acree, B.E.; Abraham, M.H. Abraham model correlations for enthalpies of solvation of organic solutes dissolved in N,N-Dimethylacetamide, 2-butanone and tetrahydrofuran (UPDATED) at 298.15 K. *Phys. Chem. Liquids* **2020**, *58*, 675–692. [[CrossRef](#)]
41. Kamlet, M.J.; Abboud, J.L.M.; Taft, R.W. An Examination of Linear Solvation Energy Relationships. *Proc. Phys. Org. Chem.* **1981**, *13*, 485–630.
42. Kamlet, M.J.; Doherty, R.M.; Abboud, J.-L.; Abraham, M.H.; Taft, R.W. Solubility: A new look. *Chemtechnology* **1986**, *16*, 566–576.
43. Abraham, M.H.; Doherty, R.M.; Kamlet, M.J.; Taft, R.W. A new look at acids and bases. *Chemical. Brit.* **1986**, *22*, 551–554.
44. Bernales, V.; Marenich, A.V.; Contreras, R.; Cramer, C.J.; Truhlar, D.G. Quantum mechanical continuum solvation models for ionic liquids. *J. Phys. Chem. B* **2012**, *116*, 9122–9129. [[CrossRef](#)]
45. Panayiotou, C.; Mastrogeorgopoulos, S.; Ataman, M.; Hadadi, N.; Hatzimanikatis, V. Molecular thermodynamics of metabolism: Hydration quantities and the equation-of-state Approach. *Phys. Chem. Chem. Phys.* **2016**, *18*, 32570–32592. [[CrossRef](#)]
46. Panayiotou, C.; Tsvintzelis, I.; Aslanidou, D.; Hatzimanikatis, V. Solvation quantities from a COSMO-RS equation of state. *J. Chem. Thermod.* **2015**, *90*, 294–309. [[CrossRef](#)]
47. Panayiotou, C.; Voutsas, E.; Hatzimanikatis, V. Solvation Gibbs Energy: The Equation of State Approach. In *Gibbs Energy and Helmholtz Energy: Liquids, Solutions and Vapors*; Wilhelm, E., Letcher, T.M., Eds.; The Royal Society of Chemistry: London, UK, 2022.
48. Ben-Naim, A. *Solvation Thermodynamics*; Plenum Press: New York, NY, USA, 1987.
49. Moine, E.; Privat, R.; Sirjean, B.; Jaubert, J.N. Estimation of Solvation Quantities from Experimental Thermodynamic Data: Development of the Comprehensive CompSol Databank for Pure and Mixed Solutes. *J. Phys. Chem. Ref. Data* **2017**, *46*, 033102. [[CrossRef](#)]
50. Panayiotou, C.; Sanchez, I.C. Hydrogen Bonding in Fluids: An Equation-of-State Approach. *J. Phys. Chem.* **1991**, *95*, 10090–10097. [[CrossRef](#)]
51. Sanchez, I.C.; Panayiotou, C. Polymer Solution Thermodynamics. In *Models for Thermodynamic and Phase Equilibria Calculations*; Sandler, S., Ed.; Dekker: New York, NY, USA, 1994.
52. Panayiotou, C. Hydrogen bonding in solutions: The equation-of-State approach. In *Handbook of Colloid and Interface Science*; Birdi, K.S., Ed.; CRC Press: Boca Raton, FL, USA, 2003.
53. Missopolinou, D.; Panayiotou, C. Hydrogen-Bonding Cooperativity and Competing Inter- and Intramolecular Associations: A Unified Approach. *J. Phys. Chem. A* **1998**, *102*, 3574–3581. [[CrossRef](#)]
54. Mensitieri, G.; Scherillo, G.; Panayiotou, C.; Musto, P. Towards a predictive thermodynamic description of sorption processes in polymers: The synergy between theoretical EoS models and vibrational spectroscopy. *Mater. Sci. Eng. R* **2020**, *140*, 100525. [[CrossRef](#)]
55. Veytsman, B.A. Are lattice models valid for fluids with hydrogen bonds? *J. Phys. Chem.* **1990**, *94*, 8499–8500. [[CrossRef](#)]
56. Baldanza, A.; Scherillo, G.; Mensitieri, G.; Panayiotou, C. Activity coefficients at infinite dilution via a perturbation method of NRHB model. *Chem. Eng. Sci.* **2022**, *262*, 118043. [[CrossRef](#)]
57. Panayiotou, C.; Pantoula, M.; Stefanis, E.; Tsvintzelis, I.; Economou, I.G. Nonrandom hydrogen-bonding model of fluids and their mixtures. 1. Pure fluids. *Ind. Eng. Chem. Res.* **2004**, *43*, 6592–6606. [[CrossRef](#)]
58. Panayiotou, C.; Tsvintzelis, I.; Economou, I.G. Nonrandom Hydrogen-Bonding Model of Fluids and their Mixtures. 2. Multicomponent Mixtures. *Ind. Eng. Chem. Res.* **2007**, *46*, 2628–2636. [[CrossRef](#)]
59. Shin, M.S.; Kim, H. A multi-fluid nonrandom associating lattice-fluid model. *Fluid Phase Equil.* **2007**, *253*, 29–35. [[CrossRef](#)]
60. Sinha, S.; Yang, C.; Wu, E.; Acree, W.E. Abraham Solvation Parameter Model: Examination of Possible Intramolecular Hydrogen-Bonding Using Calculated Solute Descriptors. *Liquids* **2022**, *2*, 131–146. [[CrossRef](#)]
61. Solomonov, B.; Novikov, V.; Mikhail, A.; Varfolomeev, M.; Klimovitskii, A. Calorimetric determination of hydrogen-bonding enthalpy for neat aliphatic alcohols. *J. Phys. Org. Chem.* **2005**, *18*, 1132–1137. [[CrossRef](#)]
62. Figueroa-Gerstenmaier, S.; Albertina Cabanas, A.; Costas, M. Self-association and complex formation in alcohol-unsaturated hydrocarbon systems. *Phys. Chem. Chem. Phys.* **1999**, *1*, 665–674. [[CrossRef](#)]
63. Provencal, R.; Casaes, R.; Roth, K.; Paul, J.; Chapo, C.; Saykally, R.; Tschumper, G.; Schaefer, H., III. Hydrogen Bonding in Alcohol Clusters: A Comparative Study by Infrared Cavity Ringdown Laser Absorption Spectroscopy. *J. Phys. Chem. A* **2000**, *104*, 1423–1429. [[CrossRef](#)]
64. Curtiss, L.A. Ab Initio Calculations on Hydrogen Bonding in Alcohols: Dimers of CH₃OH, CH₃-CH₂OH and CF₃CH₂OH. *Intern. J. Quantum Chem. Quantum Chem. Symp.* **1977**, *2*, 459–467.
65. Daubert, T.E.; Danner, R.P. (Eds.) *Data Compilation Tables of Properties of Pure Compounds*; AIChE Symp. Ser. No. 203; American Institute of Chemical Engineers: New York, NY, USA, 1985.

Disclaimer/Publisher's Note: The statements, opinions and data contained in all publications are solely those of the individual author(s) and contributor(s) and not of MDPI and/or the editor(s). MDPI and/or the editor(s) disclaim responsibility for any injury to people or property resulting from any ideas, methods, instructions or products referred to in the content.

MDPI
St. Alban-Anlage 66
4052 Basel
Switzerland
Tel. +41 61 683 77 34
Fax +41 61 302 89 18
www.mdpi.com

Liquids Editorial Office
E-mail: liquids@mdpi.com
www.mdpi.com/journal/liquids





Academic Open
Access Publishing

www.mdpi.com

ISBN 978-3-0365-8009-8